Convergent-Beam Electron Diffraction II

by

Michiyoshi Tanaka
Masami Terauchi

Department of Physics,
Faculty of Science,
Tohoku University

Toshikatsu Kaneyama

Electron Optics Technical
and Engineering Division,
JEOL Ltd.

JEOL LTD.

Published by JEOL LTD.
1-2, Musashino 3-chome, Akishima, Tokyo 196, Japan

Printed in Japan

Contents

Preface

Nearly three years have passed since the previous book, "Convergent-Beam Electron Diffraction", JEOL-Maruzen, was published in 1985. The book surveyed the CBED method using a plenty of photographs. I believe it has served as a practical guide to the CBED method and also as a source of enjoyment to many.

However, many worthwhile materials are yet to be published, which would permit a more extensive use of the CBED method. Included among these materials are those on an experimental technique to take simultaneously a zone-axis pattern and $\pm$G dark-field patterns, spurious symmetries, dynamical extinction rules for higher-order Laue-zone (HOLZ) reflections, computer simulations of CBED patterns and the identifications of the displacement vector of a stacking fault and the Burgers vector of a dislocation. The symmetry determinations of a high T_C superconductor ($La_2CuO_{4-\delta}$), magnetite, quasicrystals and incommensurate phases provide a better understanding of the practical uses of the CBED method, thereby showing its great potential. I have included many unpublished works in this issue because the results of these pioneering works should make this book fresh and unique. Crystal structure analysis or the determination of atomic positions using the CBED method will be carried in the next volume. The style of the previous book is followed also in this volume, that is, a good reproduction of photographs and short explanations of each subject.

In the previous book, we added simple personal computer programs for drawing HOLZ lines just for readers reference. However, I was surprised to have had many inquiries about these. Hence, in this volume, we present not only a program for drawing HOLZ lines with better performance, but also those for drawing Kikuchi lines and CBED patterns from dislocations and for determining specimen thickness. We also present flow charts of the methods for determining point and space groups and for identifying defects and flow charts of the experimental procedures for various CBED techniques. We hope that these things will be helpful in lowering some barriers which electron microscopists may encounter when they begin to use the CBED method.

The data shown herein was obtained with the cooperation of successive graduate students of Department of Physics, Tohoku University. These include Mr. R. Saito (presently at Hitachi Research Lab., Hitachi Ltd.), Dr. S. Matsuda (Textile Research Lab., Asahi Chemical Industry Co., Ltd.), Dr. S. Suzuki (R&D Division Asahi Glass Co., Ltd.), Mr. H. Sekii (Central R&D Lab., Omuron Tateishi Electrics Co.), Mr. T. Nagasawa, Mr. O. Ueno (Electronic Imaging and Research Lab., Fuji Xerox Co., Ltd.), Mr. H. Takayoshi (Komukai Works, Toshiba Co.), Mr. S. Ito, Mr. Y. Miyamura, Mr. A. Ishikawa and Mr. K. Tsuda (Master Course, Department of Physics, Tohoku Univ.), and Mr. M. Terauchi (Doctor Course, Department of Physics, Tohoku Univ.) and Mr. T. Kaneyama (EM Group, JEOL Ltd.), who are the co-authors of this book. I am deeply indebted to these people for their kind cooperation in the preparation of this work. The photographs included in this publication were taken with a JEM-100CX equipped with a field emission gun (FEG) and a JEM-2000FX.

I express my cordial gratitude to JEOL Ltd.' staff, especially Mr. T. Eto, Mr. Y. Harada, Mr. Y. Ishida, Mr. Y. Kokubo, Mr. M. Naruse and Mr. T. Tomita for their devoted collaboration in instrument development. I also wish to thank Mr. F. Sato for his outstanding maintenance of the JEM-100CX-FEG and the JEM-2000FX, and for his highly skilled photography. I also express my heartfelt thanks to Professor D. Watanabe for allowing me and the graduate students to concentrate on this work. Without the devoted help of Mr. A. Shoji, Mr. H. Matsuo and Mr. T. Handa of JEOL Ltd. in the compilation of the book, and of Mr. T. Takamatsu in the critical reading of the manuscript, this edition could never have been possible. It is pleasure to pay tribute also to Mr. T. Kondo of Kyoritsu Printing Co., Ltd. for the excellent printing of this book.

This work was supported financially by the Grant-in-Aid for Scientific Research (No. 142009, No. 346033, No. 57420014, No. 60420051), the Grant-in-Aid for Developmental Scientific Research (No. 56840016, No. 62880012) and the Grant-in-Aid for the Encouragement of Young Scientists (Terauchi) (No. 62790128), from the Ministry of Education, Science and Culture of Japan.

Sendai, Summer 1988

Michiyoshi Tanaka

Introduction

The standard method of point-group determination, which was given by Buxton *et al.* [1], requires that four patterns (whole, bright-field, dark-field and ±G dark-field patterns) be taken. With the ordinary experimental method, these patterns are recorded on three different films at different times and at different crystal settings. It is desirable to develop experimental techniques by which these four patterns are recorded simultaneously on a film. One of such techniques was already reported in the reference [2] and also described in the previous book [3] (hereafter referred to as book I). However, the technique needs large flat-surfaced specimen areas and brings the exact Bragg positions to off-center positions of the diffraction disks. An improved technique [4] which enables us to take the four patterns from a smaller specimen area and to set the exact Bragg positions to the disk centers is described first.

CBED can identify 32 crystal point groups unambiguously [1], [5]. However, we found that spurious symmetries arise from crystals of a certain structure type [6]. The structure is composed of two equivalent substructures which are displaced from each other by a certain vector and are each occupied by a different kind of atoms. The crystals with such a structure often exhibit a symmetry m_2 or 1_R in the dark-field pattern, or 2_R between a pair of dark-field patterns despite the fact that they do not have a horizontal twofold axis, a horizontal mirror plane, and an inversion center. These spurious symmetries are harmful to the correct determination of point-groups. Hence, it is important to know the origin of the phenomena to avoid incorrect identification of point-groups. Examples of spurious symmetries are shown and a short theoretical analysis of the phenomena is given.

We add an observation of a symmetry m_2 due to a twofold axis oblique to the specimen surface. This axis is not a symmetry element of an infinitely extending parallel sided specimen or diperiodic plane figures, which Buxton *et al.* [1] postulated in their study of point-group determination.

Concerning the dynamical extinction, there are many things to be described. The dynamical extinction rules, which were given by Gjønnes and Moodie [7], are the basis of space-group determination. The extinction appears as lines of zero intensity in kinematically forbidden reflection disks when a screw axis is set perpendicular to the incident beam or when a glide plane is set parallel to it. These dark lines, which are called GM lines after Gjønnes and Moodie, have successfully been utilized for the identification of screw axes and glide planes. Tables of dynamical extinction in which expected GM lines appearing in the 0th order Laue-zone (ZOLZ) reflections are listed for various incident-beam directions of all the space groups were given by Tanaka *et al.* [3], [8].

The dynamical extinction due to a glide plane which is set perpendicular to the incident beam has also been predicted to appear as a dark spot at the exact Bragg position of a kinematically forbidden reflection. This extinction had not been observed, however, until our investigation was made [9]. We give here examples of the extinction. On the basis of the experimental results, the extinction rule given by Gjønnes and Moodie has been modified in a practical manner.

Spurious B_3 GM lines occur as well as the spurious symmetries described in the section of point-group determination. What we call spurious B_3 GM lines are dynamical extinction lines appearing in kinematically forbidden reflections at the symmetric electron incidence and at the incidences exactly exciting kinematically allowed reflections. At these incidences there exist pairs of Umweganregung paths via higher-order Laue-zone (HOLZ) reflections to a kinematically forbidden reflection. The phases of the two beams coming through a pair of paths are different by π from each other. The two beams are different in amplitude, unlike cases of exactly exciting kinematically forbidden reflections. As a result, partial cancellation takes place between the two beams. If the difference between the amplitudes is small, the extinction line is still observed. The presence of the spurious B_3 GM lines, together with true GM lines, indicates the existence of a screw axis, unlike the spurious symmetries described in the section of point-group determination.

What will happen to GM lines when a screw axis or a glide plane is slightly destroyed by small displacements of constituent atoms, which may occur, for instance, due to a second-order phase transition? The answer is that crossed A_2 and B_2 GM lines [8] with a symmetry $2mm$ due to the interaction of ZOLZ reflections change into a pattern with a symmetry 1_R, which is expected from the horizontal mirror plane existing in the case of ZOLZ interaction. This change is worth remembering for the symmetry identification of patterns with a subtle symmetry. We give a good example of a CBED pattern for a slight breakdown of the 2_1 screw axis in Mo_2S_3, which takes place at the phase transition from the space group $P2_1/m$ to $P\bar{1}$ or $P1$. Such a change is confirmed in the section of computer simulations.

The observation of A_3 and B_3 GM lines [8] due to HOLZ interaction is sometimes difficult at room tem-

perature because of large-amplitude lattice vibration. Cooling specimens, if possible, allows unambiguous observation of these lines. It is worth while observing how the visibility of the lines is improved by cooling specimens. Distinct A_3 GM lines taken from Si at the liq.N_2 temperature have to be compared with faint ones at room temperature given in book I. A B_3 GM line from FeS_2 was clearly observed at the liq.N_2 temperature while it was not seen at room temperature.

The space-group determination method [8] uses the dynamical extinction lines (GM lines) appearing in ZOLZ reflections. The GM lines are caused by the crystal symmetry elements which act as horizontal 2_1 screw axes, vertical glide planes with horizontal translation vectors and horizontal glide planes [7].

The vertical glide planes with arbitrary translation vectors give rise to GM lines also in HOLZ reflections. It is noted that vertical glide planes whose translation vectors are perpendicular to the specimen surface (vertical translation) do not cause GM lines in ZOLZ reflections but cause them in HOLZ reflections (see page 59) [10]. Tables of GM lines appearing in HOLZ reflections at various incident beam orientations for all the space groups which have glide planes, are given in an appendix. Use of the GM lines appearing not only in ZOLZ but also in HOLZ reflections ensures unambiguous and quick identification of space groups.

The vertical glide plane whose translation vector has a vertical component is not a symmetry element of diperiodic plane figures. The assumption of the diperiodic plane figures made by Buxton *et al.* [1] is not suitable when the symmetry elements of space groups are concerned. The GM lines due to vertical screw axes are difficult to observe in usual transmission CBED, because they can be seen in backscattered reflection disks. It makes no sense to construct space groups using actually observable symmetry elements, because they do not form a complete set. CBED does not observe all the symmetry elements of crystal space groups, but observe much more than the symmetry elements of diperiodic plane figures.

Space-group determination using ZOLZ and HOLZ GM lines is demonstrated for a high T_c superconductor, $La_2CuO_{4-\delta}$, and the low temperature phase of magnetite (Fe_3O_4) in which charge ordering (Verwey order) had been believed to occur.

The repetition of a unit cell, the translational symmetry, is a characteristic feature of crystals. An exception—incommensurate structure—appears, however, in a crystal over a certain temperature range. The period of this structure does not coincide rationally with that of the protophase. The incommensurate phase occurs when two competitive interactions are present between the first and second nearest neighbouring atoms. The phase, characterized by a temperature dependent wave number vector, causes the discommensuration at its lower temperature region and transforms into a commensurate phase due to a lock-in transition. The incommensurate structure is described by a three-dimensional section of a crystal in a higher-dimensional space [11]. Whether the symmetry elements allowed in a higher-dimensional space provide new symmetries in CBED patterns has not yet been clarified. CBED, however, can reveal what symmetry element of the protophase is destroyed and what type of a wave, a transverse or a longitudinal one, is produced in the related incommensurate phase. Such information is useful for the structure analysis of the phase, like the space-group determination performed before the determination of atomic positions. The first study of an incommensurate structure was performed by Steeds *et al.* on $NiGe_{1-x}P_x$ [12]. We give two examples of studies carried out on $Sr_2Nb_2O_7$ and Mo_8O_{23}.

The discovery of an alloy of aluminum and manganese [13] which shows sharp diffraction spots with an icosahedral symmetry has had a great impact on crystallography and solid state physics. It has revealed the existence of a new structural order (quasicrystal). The quasicrystal is defined to have a quasi-periodic long-range structural order with a noncrystallographic point group and to have a self-similarity transformation. The discovery of quasicrystals has accelerated the theoretical development of the crystallography in high-dimensional spaces. CBED is definitely the best method to investigate the symmetry of this new class of structural order [14,15,16]. We shall briefly report the latest results of CBED and small-area-parallel-beam electron diffraction studies on real quasicrystals.

CBED is now entering a stage of quantitative studies. Computer simulation of CBED patterns [17] is indispensable for their quantitative analysis. We simulated several CBED patterns using the ordinary matrix-diagonalization method for the dynamical theory of electron diffraction, and utilized the simulation for the sensitivity test of CBED patterns on a slight breakdown of a glide plane and/or a screw axis. The test proved the high sensitivity of the patterns to the breakdown of the crystal symmetries and gave instructive results on how the CBED symmetries change as the degree of the breakdown increases. Using computer simulation, we are now developing a crystal

structure analysis method based upon the dynamical theory. Structure analysis using the dynamical theory has been carried out by Vincent *et al.* for AuGeAs [18].

CBED has a great potential to identify not only crystal space groups but also crystal lattice defects. In book I, we already quoted the work of Johnson on a stacking fault [19] and that of Carpenter and Spence [20] on a dislocation. Recently, detailed studies to determine the displacement vector $\boldsymbol{R}$ of a stacking fault have been carried out [21,22] by utilizing information not only from $\alpha = 2\pi \boldsymbol{g}\cdot\boldsymbol{R} = 0$ but also from finite values of α. The method using HOLZ lines allows us to know the magnitude and sign of the vector. That is, it can determine easily and unambiguously whether the fault is intrinsic or extrinsic, while the traditional electron microscope-image method is rather complicated and open to misidentification. The CBED method is of course based on dynamical diffraction but does not utilize the absorption effect unlike the method using microscope images. This indicates that the present method can apply to specimens thinner than an extinction distance.

Cherns and Preston [23] have found that the whole strain field of a dislocation must be illuminated by a convergent beam to determine the Burgers vector $\boldsymbol{b}$ of a dislocation. They have proposed a method of determining Burgers vectors. The method uses defocus illumination and consequently provides two items of information on the strain fields of dislocation—the real and reciprocal spaces. In such a CBED pattern, a reflection line across a dislocation shows n nodes at their crossing region when $\boldsymbol{g}\cdot\boldsymbol{b} = n$. The values of n's obtained for three linearly-independent reflections allow the unique determination of the Burgers vector, where the importance of the relative signs of n's should be emphasized [22]. We give a few examples of Burgers vector determination using the excellent method of Cherns and Preston. We have applied the method further to the Burgers vector determination of a partial dislocation, which is closely related to a stacking fault [21], and of a dislocation loop, which is related to the precipitation of interstitial atoms and vacancies. The method has also been applied to the investigation of particular effects due to edge and mixed dislocations, $\boldsymbol{g}\cdot\boldsymbol{b}_e$ and $\boldsymbol{g}\cdot\boldsymbol{b}\times\boldsymbol{u}$, and those due to an extended dislocation.

The need for CBED characterization of interfaces between crystal lattices is rapidly increasing, especially in the light of industrial importance of artificial super-lattice crystals. We are not concerned, however, with the matter at present. Thus, we only quote two papers dealing with the subjects presented by Maher *et al.* [24] and Eaglesham and Humphreys [25].

In the section of applications are described the development of the degree of order observed just after a second-order phase transition of $Sr_2Ta_2O_7$, and the crystallographic relation between adjoining domains revealed for TaS_3 and $Sr_2Ta_2O_7$. We hope that readers appreciate the beautiful large-angle CBED (LACBED) patterns and hollow-cone beam CBED (HCB-CBED) patterns which were chosen in accordance with the authors' taste.

We add several appendices. Firstly, flow charts of various experimental techniques, point-group and space-group determinations, and identification methods for stacking faults and dislocations are given. Secondly, tables of GM lines appearing in HOLZ reflections are given, which can be successfully used for the identification of glide planes as well as the GM line tables for ZOLZ reflections given in book I. Computer programs were prepared for the personal computer of NEC-PC9801. For printing out results, we use the printer of NEC-PC-PR201, the plotter of Roland DXY-990, and the laser printer of Canon LBP-B406. The HOLZ line program listed in this volume has much better performance than the one provided in book I. The Kikuchi line program allows drawing Kikuchi-line maps, indexing observed zone axes and measuring the angle between two zone axes. The program for thickness determination is based on the method described in book I. These three programs, saved in a diskette, are supplied from JEOL Ltd. The simulation program for the profile of a reflection crossing a dislocation is omitted, but hard copies of input data on a CRT and an obtained result are given for readers' information. The CBED users need only the results shown in the section of lattice defects; it is not necessary to recalculate the profiles. This program, however, will also be supplied from JEOL Ltd. in the near future. Readers who wish to know the details of this program are requested to contact the authors. A simplified flow chart of dynamical calculation and obtained results are added.

The reciprocal-space lines corresponding to CBED disks are illustrated, and elimination techniques for specimen contamination are described as readers' reference.

Lastly, a reference of Steeds [26] is given for a general survey of the CBED method and other references, those of Lehmpfuhl and Dowell [27] and Eades *et al.* [28] are added as important topics of reflection CBED.

References

[1] B.F. Buxton, J.A. Eades, J.W. Steeds and G.M. Rackham: *Phil. Trans. R. Soc. London*, **281** (1976) 171.

[2] M. Terauchi and M. Tanaka: *J. Electron Microsc.*, **34** (1985) 128.

[3] M. Tanaka and M. Terauchi: Convergent-Beam Electron Diffraction, JEOL-Maruzen, Tokyo, 1985.

[4] M. Terauchi and M. Tanaka: *J. Electron Microsc.*, **34** (1985) 347.

[5] M. Tanaka, R. Saito and H. Sekii: *Acta Cryst.*, **A39** (1983) 357.

[6] M. Tanaka, H. Sekii, O. Ueno and H. Takayoshi: *Acta Cryst.*, **A40** suppl. (1984) C384.

[7] J. Gjønnes and A.F. Moodie: *Acta Cryst.*, **19** (1965) 65.

[8] M. Tanaka, H. Sekii and T. Nagasawa: *Acta Cryst.*, **A39** (1983) 825.

[9] M. Tanaka, M. Terauchi and H. Sekii: *Ultramicroscopy*, **21**(1987) 245.

[10] M. Tanaka: *Acta Cryst.*, **A40** suppl. (1984) C382.

[11] P.M. de Wolff, T. Janssen and A. Janner: *Acta Cryst.*, **A37** (1981) 625.

[12] J.W. Steeds, D.M. Bird, D.J. Eaglesham, S. McKernan, R. Vincent and R.L. Withers: *Ultramicroscopy*, **18** (1985) 97.

[13] D. Shechtman, I. Blech, D. Gratias and J.W. Cahn: *Phys. Rev. Lett.*, **53** (1984) 1951.

[14] M. Tanaka, M. Terauchi, K. Hiraga and M. Hirabayashi: *Ultramicroscopy*, **17** (1985) 279.

[15] L.A. Bendersky and M.J. Kaufman: *Phil. Mag.*, **B53** (1986) L75.

[16] M. Tanaka, M. Terauchi, K. Hiraga and M. Hirabayashi: *Acta Cryst.*, **B43** (1987) 494.

[17] N.S. Blom and F.W. Schapink: *J. Appl. Cryst.*, **18** (1985) 126.

[18] R. Vincent, D.M. Bird and J.W. Steeds: *Phil. Mag.*, **A50** (1984) 745 and *ibid.* 765.

[19] A.W.S. Johnson: *Acta Crsyt.*, **A28** (1972) 89.

[20] R.W. Carpenter and J.C.H. Spence: *Acta Cryst.*, **A38** (1982) 55.

[21] M. Tanaka and T. Kaneyama: Proc. XIth Int. Congr. on Electron Microsc., Kyoto, 1986, p.203.

[22] M. Tanaka: *J. Electorn Microsc.*, **35** (1986) 314.

[23] D. Cherns and A.R. Preston: Proc. XIth Int. Congr. on Electron Microsc., Kyoto, 1986, p.721.

[24] D.M. Maher, H.L. Fraser, C.J. Humphreys, R.V. Knoell, R.D. Field, J.B. Woodhouse and J.C. Bean: Inst. Phys. Conf. Ser. No. 78, 1985, p.49.

[25] D.J. Eaglesham and C.J. Humphreys: Proc. XIth Int. Congr. on Electron Microsc., Kyoto, 1986, p.209.

[26] J.W. Steeds: in "Introduction to Analytical Electron Microscopy" eds. J.J. Hren *et al.*, Plenum Press, New York, 1979.

[27] G. Lehmpfuhl and W.C.T. Dowell: *Acta Cryst.*, **A42** (1986) 569.

[28] J.A. Eades, A.E. Smith and D.F. Lynch: G.W. Bailey Ed., Proc. of 45th Annual Meeting of Electron Microsc. Soc. America, 1987, p.30.

Abbreviations of Technical Terms

CBED	Convergent-Beam Electron Diffraction
ZAP	Zone-Axis Pattern
WP	Whole Pattern
BP	Bright-Field Pattern
DP	Dark-Field Pattern
±DP	± Dark-Field Pattern
ZOLZ	Zeroth Order Laue-Zone
H(F,S)OLZ	Higher (First, Second) Order Laue-Zone
GM Line	Gjønnes-Moodie Line = Dynamical Extinction Line
LACBED Pattern	Large-Angle CBED Pattern
HCB-CBED Pattern	Hollow-Cone Beam CBED Pattern
MB-LACBED Pattern	Many-Beam LACBED Pattern
SA-CBED Pattern	Selected-Area CBED Pattern
FEG	Field Emission Gun
CTEM	Conventional Transmission Electron Microscopy
SAMAG mode	Selected Area Magnification mode
SADIFF mode	Selected Area Diffraction mode
BFI	Bright-Field Image
DFI	Dark-Field Image
CL	Condenser Lens
OL	Objective Lens
IL	Intermediate Lens
DEF1,2	Deflector 1,2
α-selector	Convergence Angle Control of the Incident Beam
HCB generator	Hollow-Cone Beam generator
FLC mode	Free Lens Control mode
Z-control	Specimen Height control

Point-Group Determination

Simultaneous Observation of ZAP and ±G Dark-Field Patterns

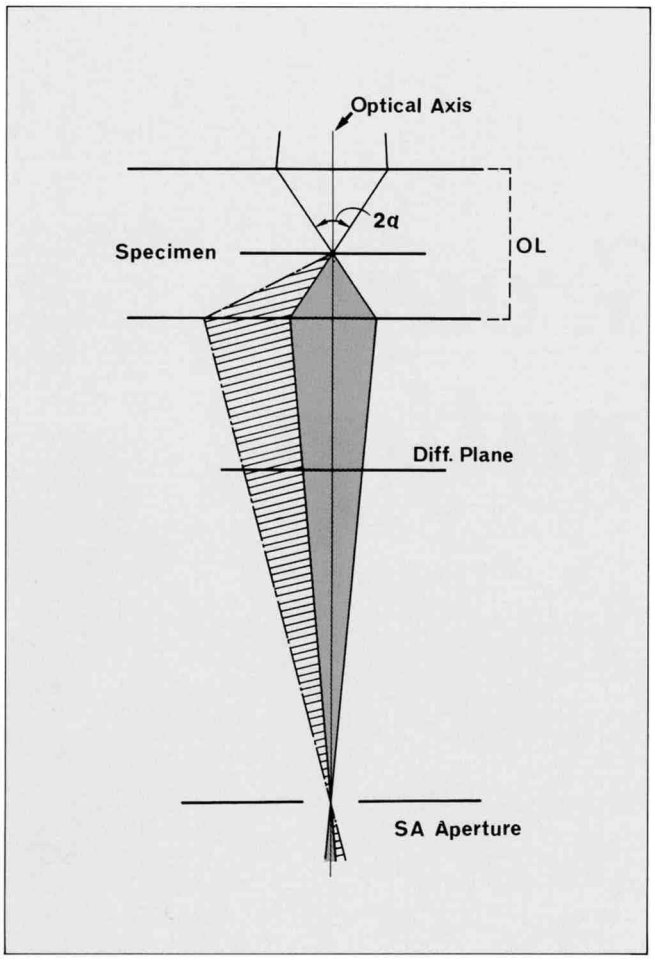

Ordinary CBED method. The convergence angle 2α is set to twice the Bragg angle of the lowest order reflection.

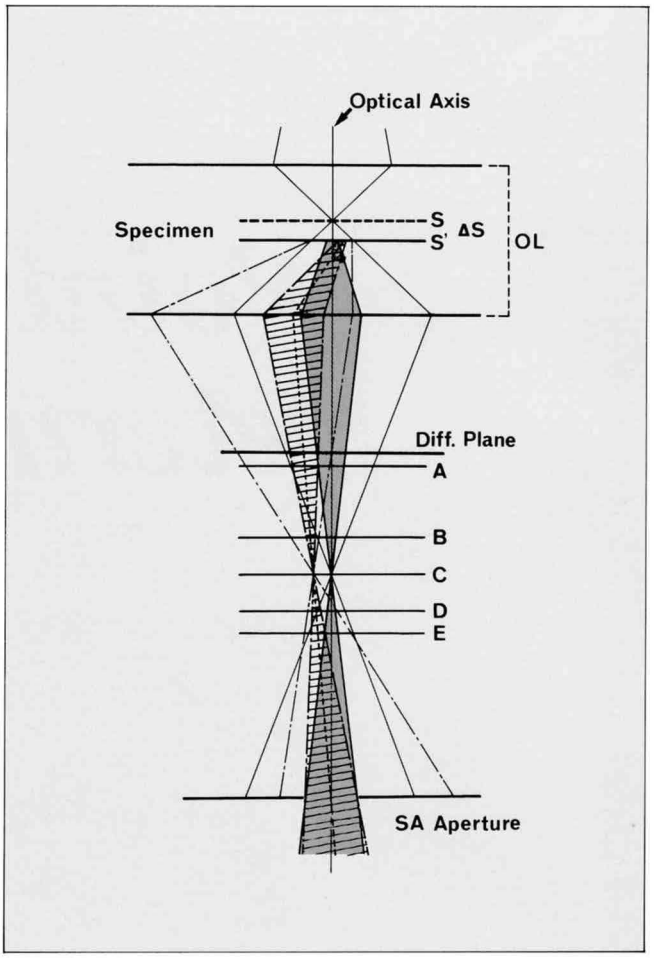

Selected area CBED (SA-CBED) method. The excitation of the objective lens is increased from the condenser-objective condition (the left diagram). The specimen receives defocused illumination. The selector aperture is used to select the convergent beam angle (and specimen area). The intermediate lens is focused on a plane between A and B.

When the standard CBED method of Buxton *et al.* [1] is used to determine point groups, the four patterns (whole, bright-field, dark-field, and ±G dark-field patterns) appearing in three photographs are needed. With the ordinary experimental method, these patterns are not obtained simultaneously, but are recorded on different films at different times and at different crystal settings. It is desirable to develop experimental techniques by which these four patterns are recorded simultaneously on a film. We already developed such a method [a] and described it in book I. However, the method requires an about 1-μm-diameter specimen area with a uniform thickness and with no bend. Exact Bragg positions are at off-centers of dark-field disks, which makes some portions of the patterns ineffective for symmetry determination.

A new method [b] can take simultaneously the four patterns from a specimen area about 100 nm in diameter with exact Bragg positions kept at the centers of dark-field disks, although the angular size of each disk is smaller than that in the previous method.

The ray path of the ordinary CBED method is shown in the left diagram. The convergence angle 2α of the incident beam is set to twice the Bragg angle of the lowest order reflection so that the CBED disks are in contact with each other. The incident beam is converged on the specimen. The image of the specimen is formed on the selector aperture, because the condenser-objective condition is satisfied for the objective lens. The intermediate lens is focused on the back focal plane of the objective lens.

The right diagram illustrates the final ray path of the new method. The incident-beam angle is set larger than that in the ordinary CBED method by removing the condenser aperture from the optical axis. The selector aperture is inserted in the optical axis. The excitation of the objective lens is increased so that the cross-over point of the incident beam is imaged above the selector aperture. As a result, the back focal plane moves from plane A to a plane written as Diff. plane, but the two planes are so near that they are not necessary to distinguish. The intermediate lens remains focused on plane A. The specimen position is shifted to a position S' with a specimen height control so that the exactly Bragg reflected beam crosses the optical axis at the selector aperture. Finally, the selector aperture size and the excitation of the objective lens are readjusted so that neighbouring disks do not overlap each other.

The maximum nonoverlapping disk size on plane A is limited to the Bragg angle of the lowest order reflection or one-half the angle obtained by the ordinary method. It is seen in the right diagram that the reflection disks are separated from each other below plane A. This indicates that disks with larger angular spreads can be obtained. CBED patterns obtained at plane B have a disk size almost twice that at plane A or the same as that in the ordinary method.

We remember that in ordinary selected area diffraction, the selector aperture selects a specimen area, because it is inserted in the image plane. Since in the present method, a defocused image is formed on the selector aperture, the aperture selects both the illuminated specimen-area size and the angular size of the incident beam. Therefore, the method is regarded as an extension of selected area diffraction. We call it selected-area CBED (SA-CBED). The specimen area selected by the disks of the transmitted beam and six 220 reflected beams was calculated to be about 100 nm in diameter for a pattern of (111) Si formed on plane B using a 5-μm-diameter selector aperture.

High resolution of the pattern formed on plane B is ensured when the incident beam impinges on a point of the specimen with an incidence angle without any divergence. Such illumination is realized only when the source size of the electron gun is sufficiently small. When only the central beam emitted from an LaB_6 cathode heated at an unsaturated condition is used, a fairly good angular and/or spatial resolution is obtained. Our JEM-100CX, equipped with a field emission gun having a virtual source diameter of about 40 nm, has been successfully used for the present purpose. In fact, the HOLZ lines in the pattern taken at plane B are seen as sharp as in the pattern taken at plane A without detectable deterioration.

The first advantage of this method is that the size of the selected area is much smaller than that needed in the previous method [a]. The second is that exact Bragg positions can be brought to the centers of diffraction disks. The third advantage is that the pattern can be observed with less contamination even for insufficiently clean specimens, because this method, as well as the LACBED method, does not use the condenser aperture but exposes the specimen to a beam shower.

References

[a] M. Terauchi and M. Tanaka: *J. Electron Microsc.*, **34** (1985) 128.

[b] M. Terauchi and M. Tanaka: *J. Electron Microsc.*, **34** (1985) 347.

Si [111]

60 kV

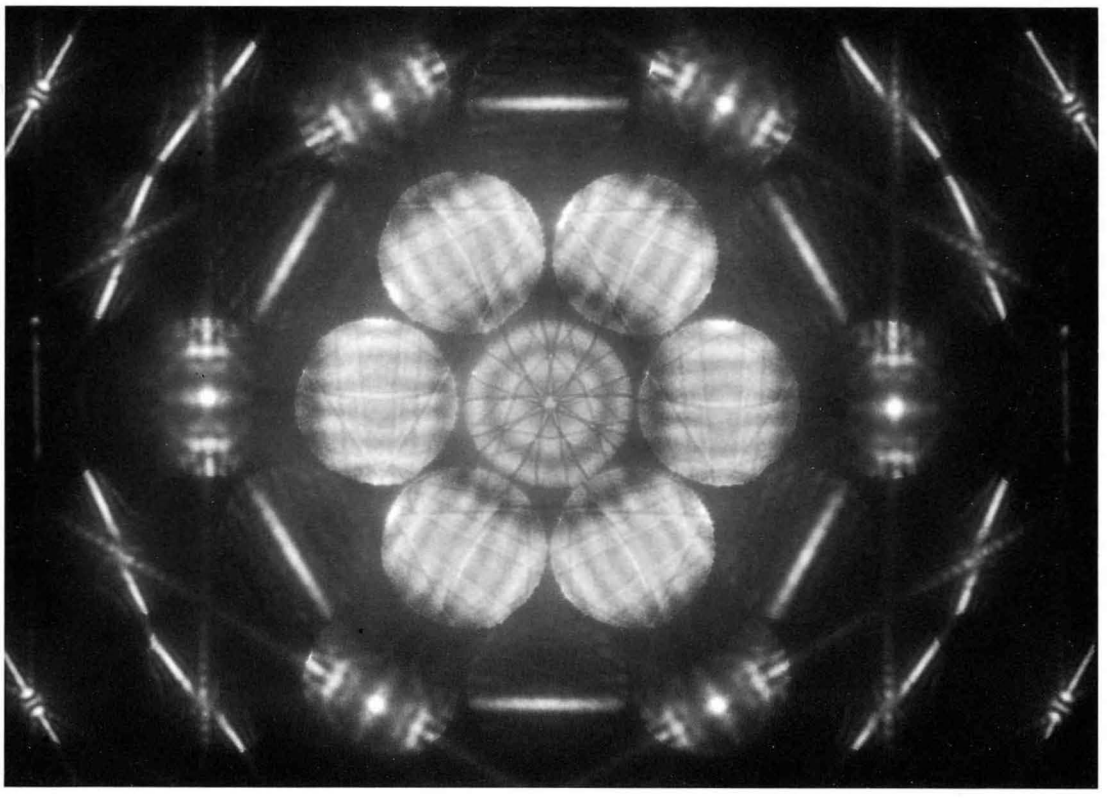

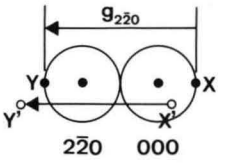

SA-CBED pattern of (111) Si. The intermediate lens was focused on plane A, which lay nearly at the same level as the back focal-plane. The angular size of the disks is the Bragg angle of the $2\bar{2}0$ reflection, 1×10^{-2} rad. The exact Bragg position is at the center of each disk.
The two schematical disks at right express the 000 and $2\bar{2}0$ CBED disks produced on the back focal-plane. The $2\bar{2}0$ beams diffracted from the 000 beams do not fall in the $2\bar{2}0$ disk but outside it. The selected specimen areas corresponding to these disks are different from each other.

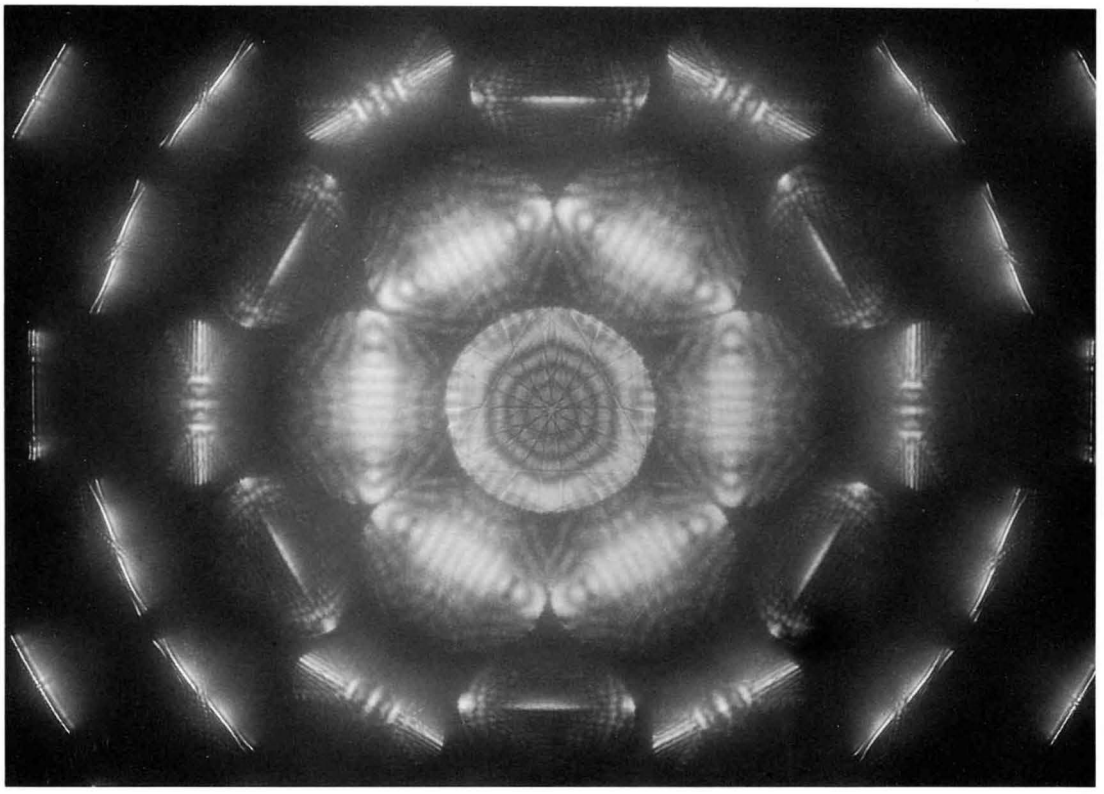

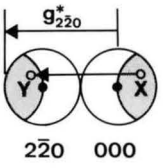

SA-CBED pattern of (111) Si. The intermediate lens was focused on plane B. The angular size of the disks is twice the Bragg angle of the $2\bar{2}0$ reflection, 2×10^{-2} rad. The exact Bragg position is at the center of each disk.

The two schematical disks at right express the 000 and $2\bar{2}0$ disks produced on plane B. The beams in the shaded area in the 000 disk are diffracted into the shaded area of the $2\bar{2}0$ disk. The illuminated specimen area corresponding to the shaded areas is the same.

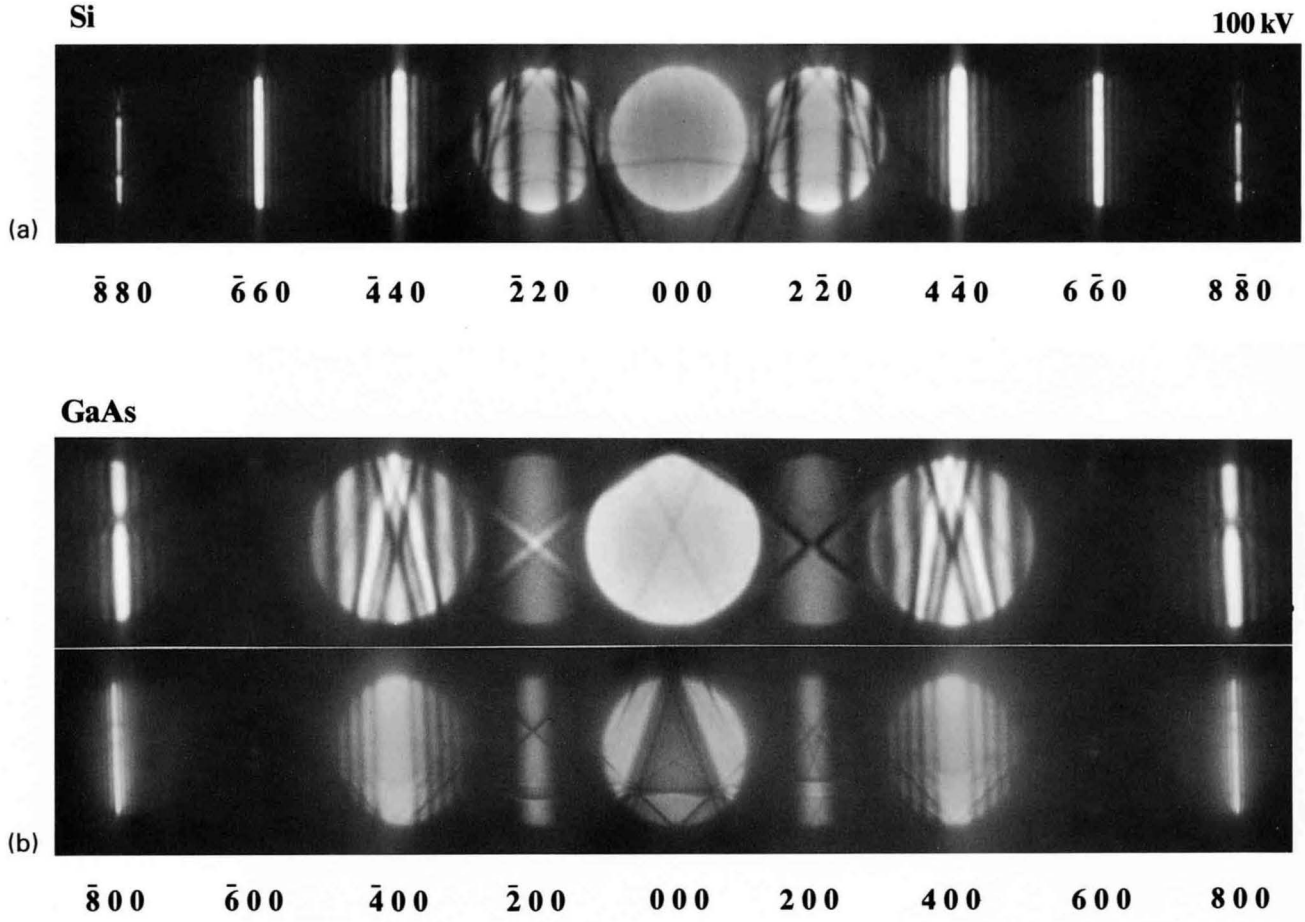

The photographs show SA-CBED patterns taken from Si(a), GaAs(b) and InP(c) by preferentially exciting the systematic reflections. The noncentrosymmetric property of GaAs and InP appears clearly as a lack of the translational symmetry in the 200 and $\bar{2}00$ reflections, whereas the $2\bar{2}0$ and $\bar{2}20$ reflections from Si which have an inversion center show the same intensity distribution. In contrast to the ordinary method, the present method can, by varying the azimuthal angle, easily find favorable crystal orientations at which the intensity difference between 200 and $\bar{2}00$ reflections from GaAs and InP is clearly observed, because the 200 and $\bar{2}00$ dark-field patterns are observed simultaneously. Consequently, a distinct lack of symmetry 2_R can be displayed for GaAs despite its slight noncentrosymmetry.

InP

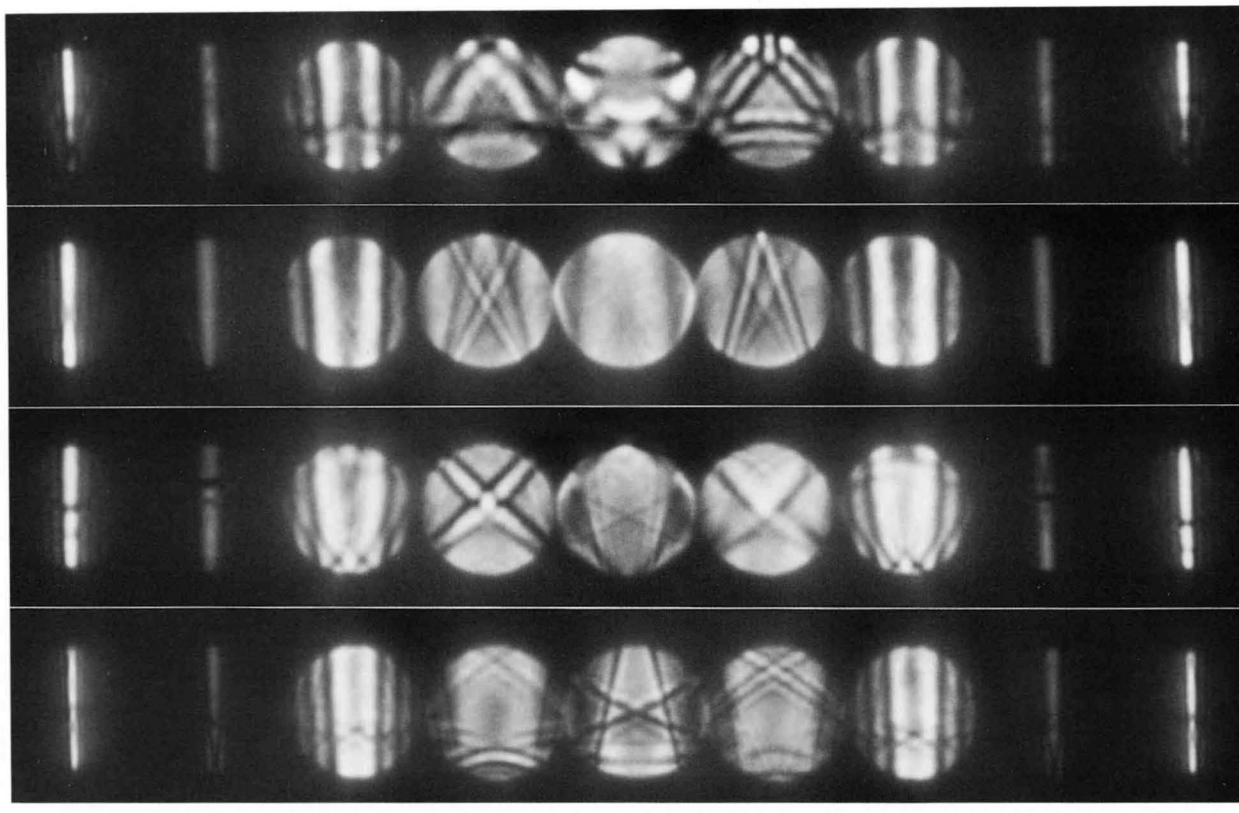

(c)

$\bar{8}00$ $\bar{6}00$ $\bar{4}00$ $\bar{2}00$ 000 200 400 600 800

CdS [$\bar{2}110$]

100 kV

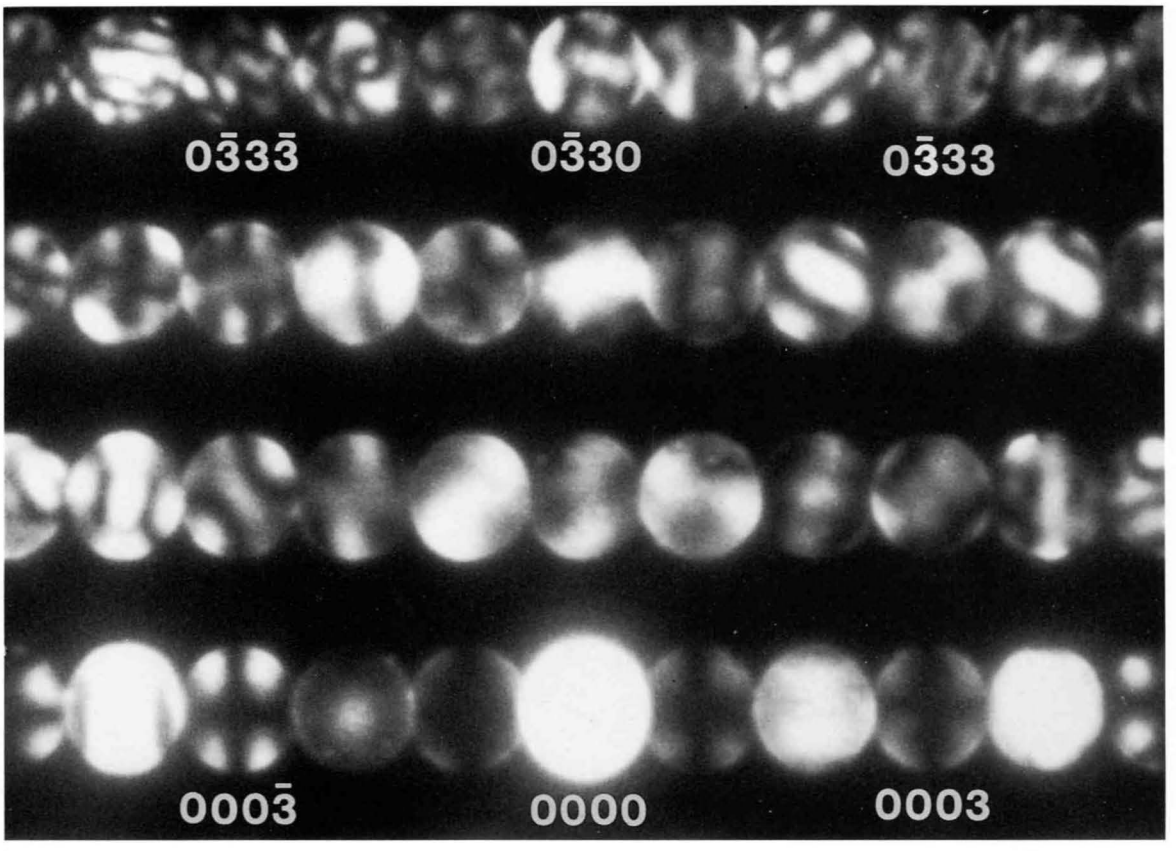

(a)

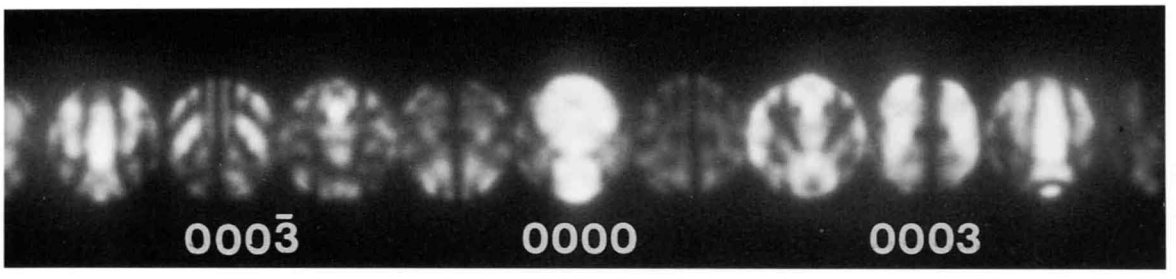

(b)

Photographs (a) and (b) show SA-CBED patterns taken from CdS belonging to the space group $P6_3mc$ at the $\bar{2}110$ zone axis setting and at a crystal setting tilted by more than a few degrees from the zone axis about the [0001] axis, respectively. Crossed dynamical extinction lines [7] (*A* and *B* GM lines[8]) are clearly seen at the centers of all the odd order 000*l* forbidden reflections in Photo (a), whereas the crossed lines are observed only in one disk by the ordinary method.

No symmetry between $\pm 000l$ disk pairs proves that the crystal is noncentrosymmetric. All the reflections of the index $k \neq 0$ show symmetries 1_R due to two-dimensional interaction. The patterns of these reflections are compared with LACBED patterns which were taken by laborious work and shown in book I.

In photograph(b), only *B* GM lines are displayed in all the odd order 000*l* disks, because the specimen was tilted from the zone axis. This is clear evidence of the fact that the lines were produced from the 6_3 screw axis. The lack of symmetries 2_R is seen more clearly than that in Photo (a).

Graphite [0001]

80 kV

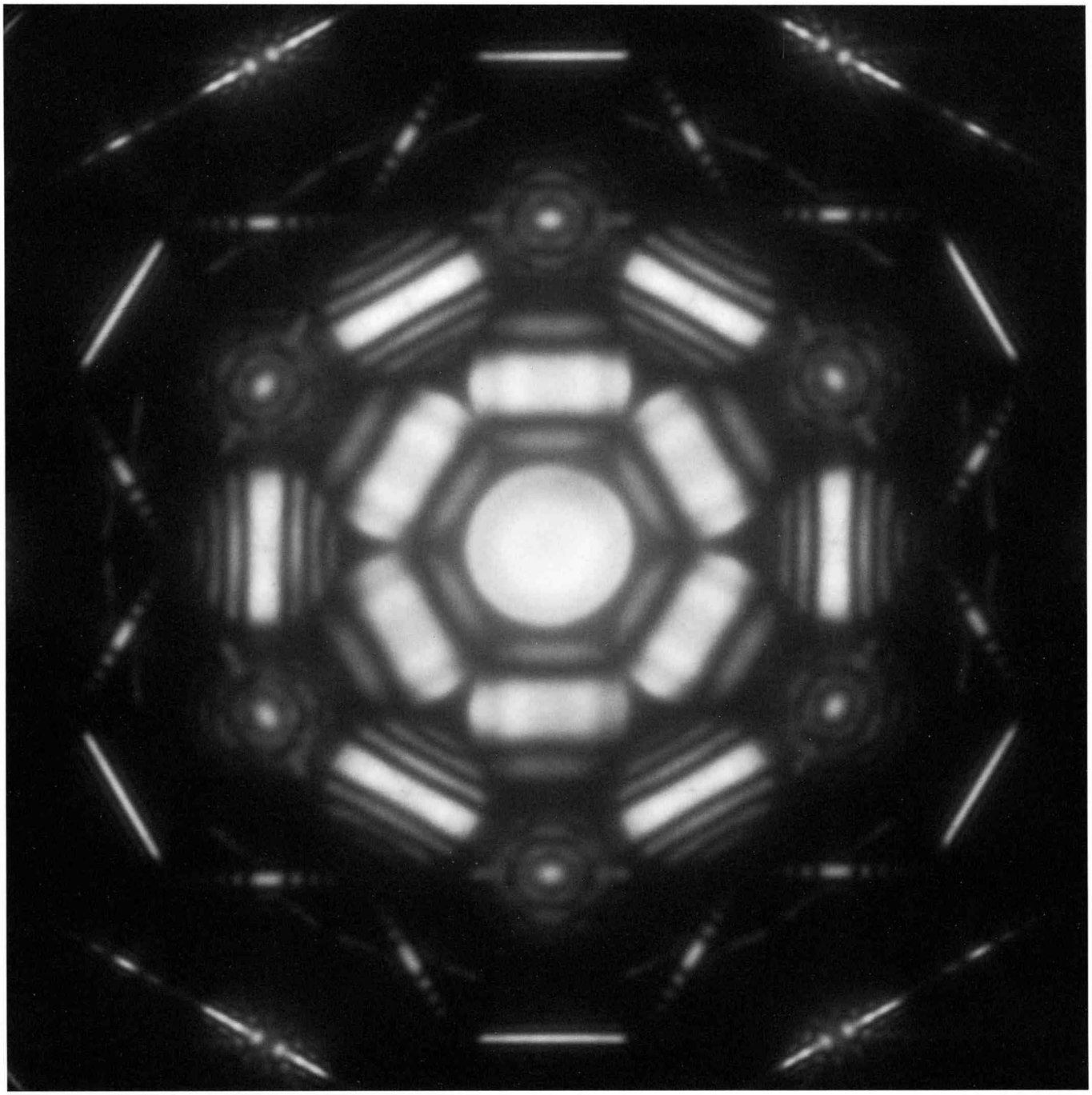

SA-CBED pattern

Ge [111]

100 kV

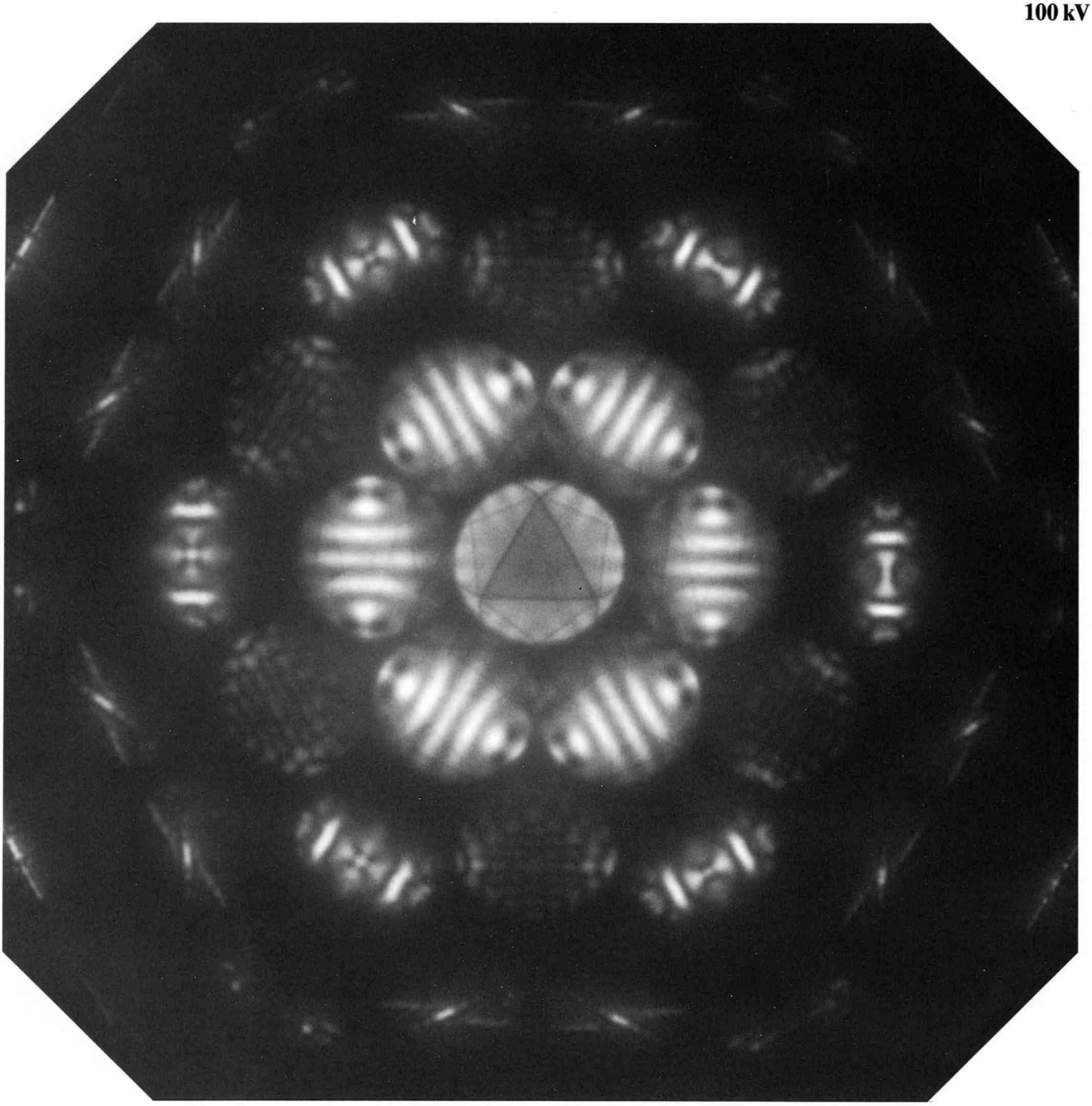

SA-CBED pattern

Spurious Symmetries

Convergent-beam electron diffraction (CBED) patterns do not always show true symmetries of a specimen crystal, but may show higher symmetries than those expected from the specimen (symmetry enhancement). If the phase of a structure factor can not be detected, symmetry enhancement or spurious symmetries can take place, like a classical example that the lack of an inversion center cannot be detected by X-ray diffraction.

When the structure factors of two reflections which are related to each other by a twofold rotation have the same amplitude but different phases, let us regard that a pseudo twofold rotation axis 2* is present between two reflections (A and B in Fig. (a)-1). A pseudo mirror plane m* is defined in a similar manner (A and C in Fig. (a)-2).

A pseudo twofold axis and a pseudo mirror plane always exist perpendicular to a true mirror plane and a true twofold axis, respectively. In these cases, two structure factors related by these pseudosymmetry elements are complex conjugate to each other. It was theoretically proved that the pseudo symmetries do not cause spurious symmetries. However, spurious symmetries m_2, 1_R and 2_R [a] have been experimentally observed in several crystals which have no horizontal twofold axis, no horizontal mirror plane and no inversion center. We investigated the origin of the observed spurious symmetries.

The crystals which caused the spurious symmetries were found to be composed of two equivalent substructures, which are displaced from each other by a certain vector and are each occupied by a different kind of atoms. We call this type of structures the AA' structure. It may safely be said that the AA' structure does not exhibit the symmetry of the whole structure but that of the substructure in the dark-field pattern. We see on pages 21 to 32 examples of spurious symmetries obtained from crystals of the zinc-blende (ZnS) type structure and polytypes of SiC, these structures actually belonging to the AA' structure (Fig. (b)).

The kinematical structure factor $F(\boldsymbol{h})$ of the AA' structure is expressed as

$$\begin{aligned} F(\boldsymbol{h}) &= (f_A + f_B \exp 2\pi i \boldsymbol{h}\cdot\boldsymbol{R}) \sum_j \exp 2\pi i \boldsymbol{h}\cdot\boldsymbol{r}_j \\ &= H(\boldsymbol{h})G(\boldsymbol{h}), \end{aligned} \tag{1}$$

where $\boldsymbol{R}$ is the displacement vector between two substructures, $H(\boldsymbol{h}) = f_A + f_B \exp 2\pi i \boldsymbol{h}\cdot\boldsymbol{R}$ and $G(\boldsymbol{h}) = \sum_j \exp 2\pi i \boldsymbol{h}\cdot\boldsymbol{r}_j$.

The crystal structure factor $F_{\boldsymbol{h}}$ which takes account of multiple reflections is written as

$$\begin{aligned} F_{\boldsymbol{h}} &= -iF(\boldsymbol{h})Z(\varrho_{\boldsymbol{h}}) - F(\boldsymbol{h}_1)F(\boldsymbol{h}-\boldsymbol{h}_1)Z'(\varrho_{\boldsymbol{h}_1}, \varrho_{\boldsymbol{h}-\boldsymbol{h}_1}) \\ &\quad + \cdots \end{aligned} \tag{2}$$

where Z and Z' are functions of the excitation errors ϱ of reflections concerned.

Substitution of eq. (1) into eq. (2) yields

$$\begin{aligned} F_{\boldsymbol{h}} &= -iH(\boldsymbol{h})G(\boldsymbol{h})Z \\ &\quad - H(\boldsymbol{h}_1)H(\boldsymbol{h}-\boldsymbol{h}_1)G(\boldsymbol{h}_1)G(\boldsymbol{h}-\boldsymbol{h}_1)Z' \\ &\quad + \cdots \\ &= -i\hat{H}_1\hat{G}_1 Z - \hat{H}_2\hat{G}_2 Z' + \cdots \end{aligned} \tag{3}$$

where $\hat{H}_1 = H(\boldsymbol{h})$, $\hat{G}_1 = G(\boldsymbol{h})$,
$\hat{H}_2 = H(\boldsymbol{h}_1)H(\boldsymbol{h}-\boldsymbol{h}_1)$, $\hat{G}_2 = G(\boldsymbol{h}_1)G(\boldsymbol{h}-\boldsymbol{h}_1)$, $\cdots$

Let us consider a spurious symmetry m_2 in the $2\bar{2}0$ dark-field pattern obtained at the [111] electron incidence from ZnS, which belongs to the space group of $F\bar{4}m$ and has no twofold rotation axis in the $[1\bar{1}0]$ direction. The substructure of ZnS is of face-centered cubic and has a twofold axis in the $[1\bar{1}0]$. The displacement vector $\boldsymbol{R}$ is 1/4 [111]. G and H are expressed as

$$\begin{aligned} G &= 4 && \text{for all of } h, k \text{ and } l : \text{even or odd} \\ H &= f_A + f_B && \text{for } h+k+l = 4n \\ &= f_A + if_B && = 4n+1 \\ &= f_A - f_B && = 4n+2 \\ &= f_A - if_B && = 4n+3 \end{aligned} \tag{4}$$

where A and B correspond to Zn and S.

Let us consider two positions in the $2\bar{2}0$ dark-field disk, which form a symmetry m_2. The first terms of eq. (3) for these positions are the same. Figure (c) shows two double reflection paths (1) and (2) falling on these positions. Let us compare the second terms of eq. (3) for these two paths. As the substructure has a twofold axis in the $[1\bar{1}0]$ direction, $\hat{G}_2^{(1)}$ is equal to $\hat{G}_2^{(2)}$. The reflection equivalent to the reflection hkl with respect to the twofold axis is $\bar{k}\bar{h}\bar{l}$. Thus,

$$\begin{aligned} H(\bar{k}\bar{h}\bar{l}) &= f_A(\bar{k}\bar{h}\bar{l}) + f_B(\bar{k}\bar{h}\bar{l}) \exp[\frac{\pi i}{2}(\bar{k}+\bar{h}+\bar{l})] \\ &= [f_A(hkl) + f_B(hkl)\exp[\frac{\pi i}{2}(h+k+l)]]^* \\ &= H^*(hkl). \end{aligned} \tag{5}$$

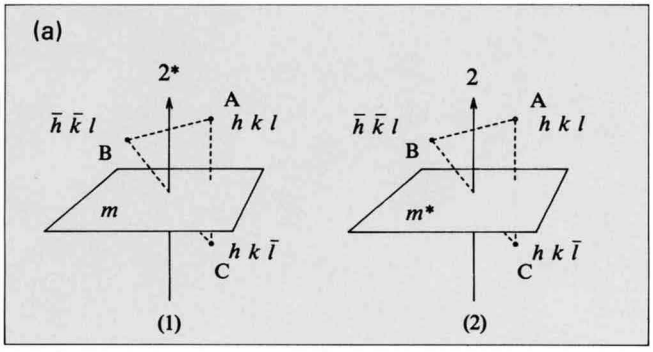

Similarly,

$$H\,(2+k,\ \bar{2}+h,l)=H^{*}\,(2-h,\ \bar{2}-k,\ \bar{l}). \tag{6}$$

$\hat{H}_2^{(1)}$ and $\hat{H}_2^{(2)}$ are written as

$$\hat{H}_2^{(1)} = H(hkl)\ H(2-h,\ \bar{2}-k,\ \bar{l})$$

and

$$\hat{H}_2^{(2)} = H\,(2+k,\ \bar{2}+h,\ l)\ H\,(\bar{k}\bar{h}\bar{l}).$$

Thus,

$$\hat{H}_2^{(2)} = (\hat{H}_2^{(1)})^{*}. \tag{7}$$

When we consider the first and second terms of eq. (3), $F_{2\bar{2}0}$ is expressed for the two paths as

$$\begin{aligned} F_{2\bar{2}0}^{(1)} &= -4i\hat{H}_1^{(1)}Z - 16\hat{H}_2^{(1)}Z' \\ F_{2\bar{2}0}^{(2)} &= -4i\hat{H}_1^{(2)}Z - 16\hat{H}_2^{(2)}Z' \\ &= -4i\hat{H}_1^{(1)}Z - 16(\hat{H}_2^{(1)})^{*}Z'. \end{aligned} \tag{8}$$

For obtaining $F_{2\bar{2}0}^{(1)} = F_{2\bar{2}0}^{(2)}$, $\hat{H}_2^{(1)}$ must be equal to $\hat{H}_2^{(2)}$. Then, from eq. (7), $\hat{H}_2^{(1)}$ must be real. As $H_2^{(1)}$ is not always real, the spurious symmetry does not occur in general.

Calculation of $\hat{H}_2^{(1)}$

At the [111] incidence, reflections in the Nth Laue zone satisfy the relation $h+k+l=N$. Thus,

$$\begin{aligned} H &= f_A + f_B \exp[\tfrac{\pi i}{2}(h+k+l)] \\ &= f_A + f_B \exp(\tfrac{\pi i}{2}N). \end{aligned} \tag{9}$$

When in the double reflection paths to the $2\bar{2}0$ reflection, $000 \rightarrow hkl \rightarrow 2\bar{2}0$, the reflection hkl belongs to a $2N$th Laue zone, a spurious symmetry m_2 is produced because H is real. When the reflection hkl belongs to a $(2N+1)$th Laue zone,

$$\begin{aligned} \hat{H}_2^{(1)} &= H(hkl)\ H(2-h,\ \bar{2}-k,\ \bar{l}) \\ &= (f_A \pm if_B)\ (f'_A \mp if'_B) \\ &= f_A f'_A + f_B f'_B \pm i(f'_A f_B - f_A f'_B) \end{aligned} \tag{10}$$

where f_A and f_B are atomic scattering factors for the reflection hkl, and f'_A and f'_B for the reflection $2\text{-}h\ \bar{2}\text{-}k\ \bar{l}$. If the relation $f'_A/f_A = f'_B/f_B$ holds, $H_2^{(1)}$ takes a real number, and then a spurious symmetry m_2 occurs. The phase of $H_2^{(1)}$ was calculated to be about 1×10^{-2} rad and 3×10^{-3} rad for several reflections of ZnS and GaAs, respectively (Tables (a) and (b)). We can safely ignore the higher order terms in eq. (3), although these terms can exhibit the true symmetry. Therefore, as a whole, an approximate spurious symmetry is produced. Figure (d) shows the atomic scattering curves of Zn and S. The spurious symmetry obtained originates from the fact that the scattering-angle dependences of the curves of Zn and S are approximately the same. This argument is a qualitative one, but not satisfactory for a quantitative account. Figure (e) shows rocking curves of the $2\bar{2}0$ reflection of ZnS obtained by dynamical calculations using 10 ZOLZ and 8 HOLZ beams. The curves are symmetric with respect to the middle point, indicating the presence of symmetries m_2. Therefore, the computer simulations have proved the occurrence of the spurious symmetry.

Spurious symmetries m_2 obtained from ZnS and GaAs at the $[33\bar{2}]$ incidence and from SiC-15R at the $[1\bar{1}0\bar{1}]$ incidence are shown on pages 24 and 25. Similar spurious symmetries were observed in $11\bar{2}0$ dark-field patterns from $LiTaO_3$ and polytypes of TaS_2.

Reference

[a] M. Tanaka, H. Sekii, O. Ueno and H. Takayoshi: *Acta Cryst.*, **A40** Suppl. (1984) C384.

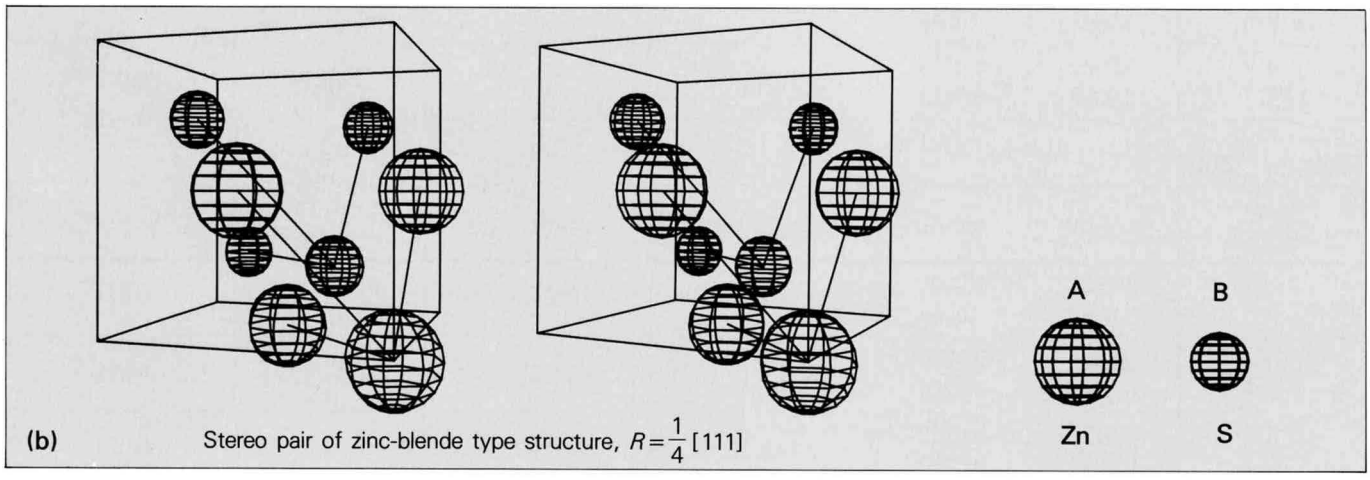

(b) Stereo pair of zinc-blende type structure, $R=\frac{1}{4}[111]$

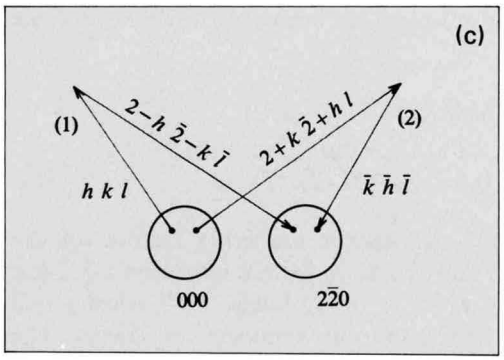

Double reflection paths forming a symmetry m_2.

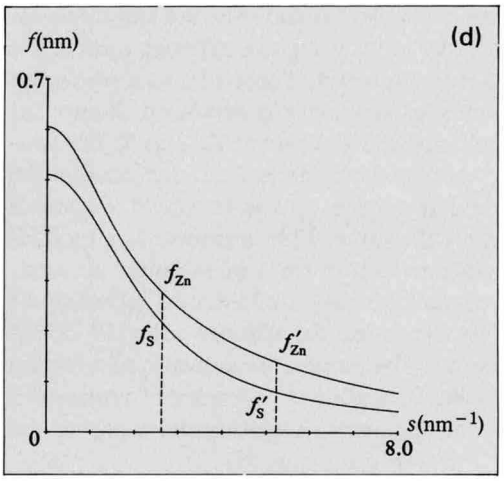

Atomic scattering curves of Zn and S.

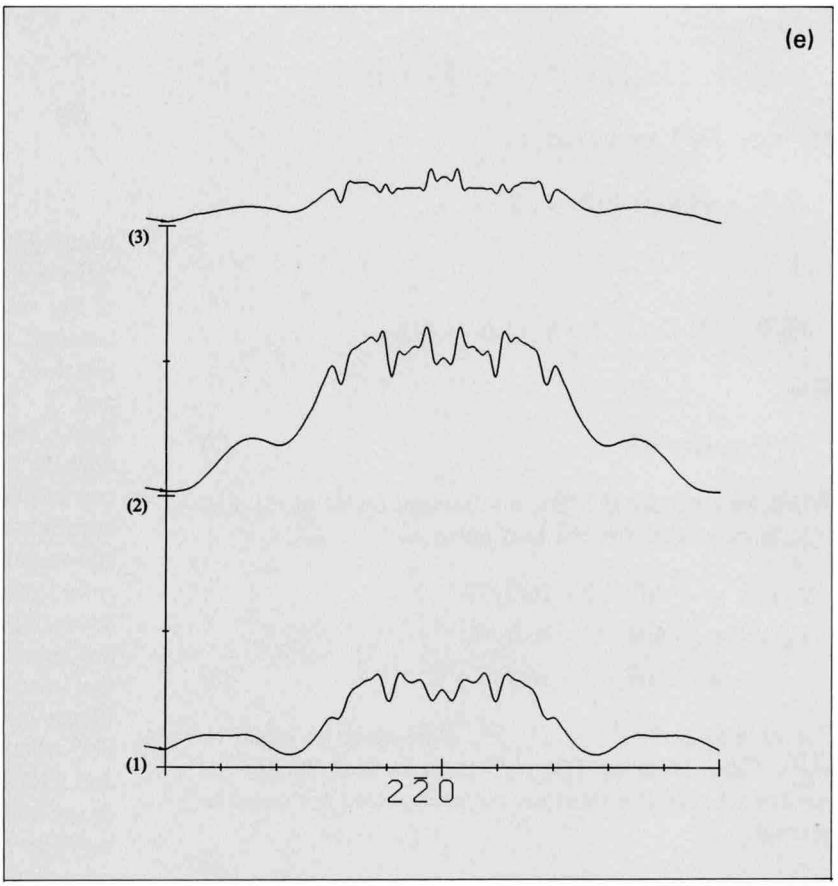

2$\bar{2}$0 rocking curves of ZnS calculated dynamically using 10 ZOLZ and 8 HOLZ reflections for three thicknesses (1) 99.9, (2) 124.8 and (3) 149.8 nm.

Table (a) GaAs

hkl $2-h, \bar{2}-k, \bar{l}$	f_{Ga}(nm)	f_{As}(nm)	$R=f_{Ga}f'_{Ga}+f_{As}f'_{As}$	$I=f'_{Ga}f_{As}-f_{Ga}f'_{As}$	$\tan^{-1}(I/R)$ (rad)	$\left\|1-\frac{f_{Ga}f'_{As}}{f'_{Ga}f_{As}}\right\|$
$5\ \bar{1}\bar{1}\ 7$ $\bar{3}\ 9\ \bar{7}$	0.0388 0.0525	0.0413 0.0555	4.33×10^{-2}	1.5×10^{-4}	3.4×10^{-3}	0.007
$7\ \bar{1}\bar{1}\ 5$ $\bar{5}\ 9\ \bar{5}$	0.0525 0.0549	0.0555 0.0580	6.10×10^{-2}	-2.0×10^{-5}	-3.2×10^{-4}	0.001
$\bar{9}\ 3\ 7$ $11\ \bar{5}\ \bar{7}$	0.0525 0.0388	0.0555 0.0413	4.30×10^{-2}	-1.5×10^{-4}	-3.4×10^{-3}	0.007

Table (b) ZnS

hkl $2-h, \bar{2}-k, \bar{l}$	f_{Zn}(nm)	f_S(nm)	$R=f_{Zn}f'_{Zn}+f_Sf'_S$	$I=f'_{Zn}f_S-f_{Zn}f'_S$	$\tan^{-1}(I/R)$ (rad)	$\left\|1-\frac{f_{Zn}f'_S}{f'_{Zn}f_S}\right\|$
$5\ \bar{1}\bar{1}\ 7$ $\bar{3}\ 9\ \bar{7}$	0.0352 0.0263	0.0200 0.0263	2.19×10^{-2}	2×10^{-4}	1×10^{-2}	0.024
$7\ \bar{1}\bar{1}\ 5$ $\bar{5}\ 9\ \bar{5}$	0.0352 0.0500	0.0200 0.0276	2.31×10^{-2}	3×10^{-4}	1×10^{-2}	0.029
$\bar{9}\ 3\ 7$ $11\ \bar{5}\ \bar{7}$	0.0474 0.0352	0.0263 0.0200	2.19×10^{-2}	-2×10^{-4}	1×10^{-2}	0.024

Spurious m_2

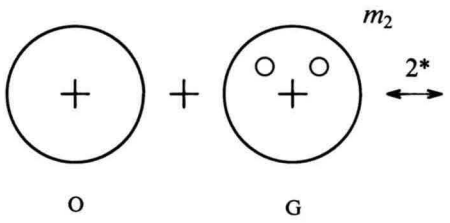

[111]

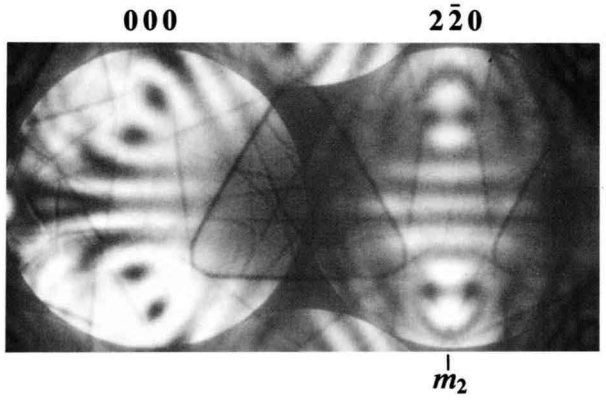

Ge

m3m

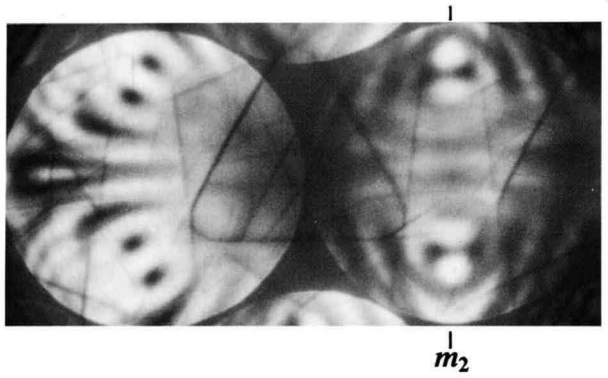

GaAs

$\bar{4}3m$

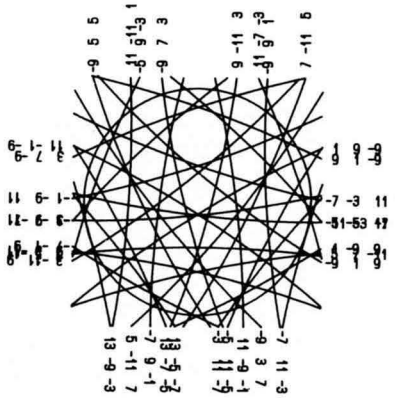

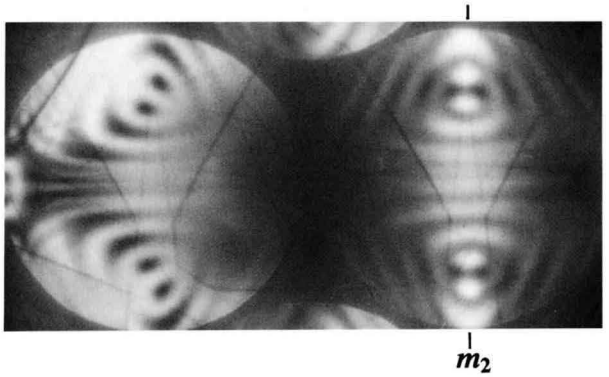

ZnS

$\bar{4}3m$

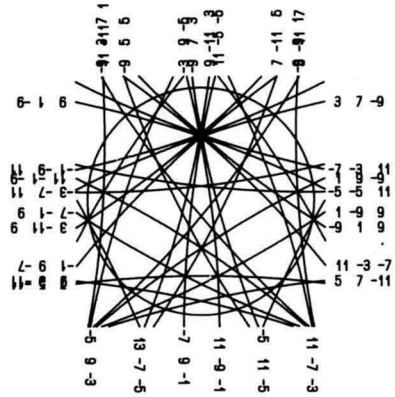

The 2$\bar{2}$0 reflection was exactly excited in each photograph.
A true symmetry m_2 from Ge is shown for comparison.

Spurious m_2

GaAs [3 3 $\bar{2}$]

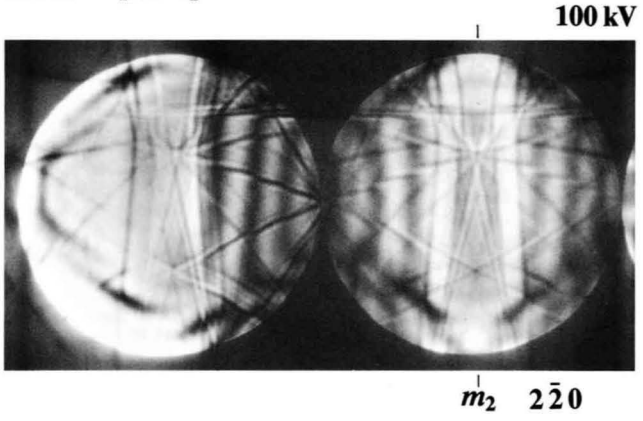

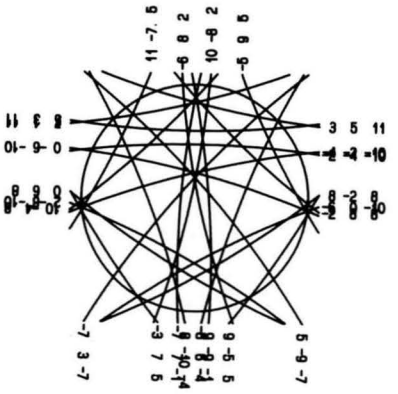

ZnS [3 3 $\bar{2}$]

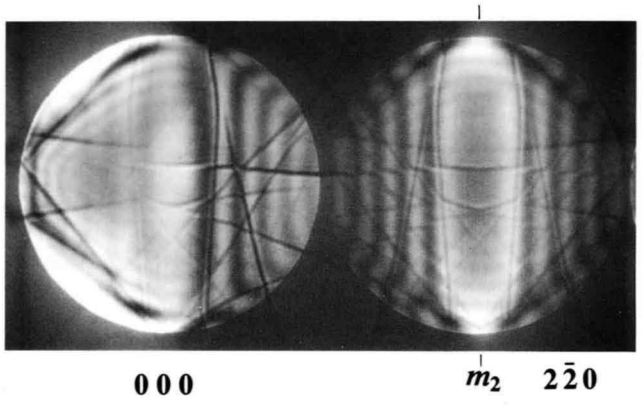

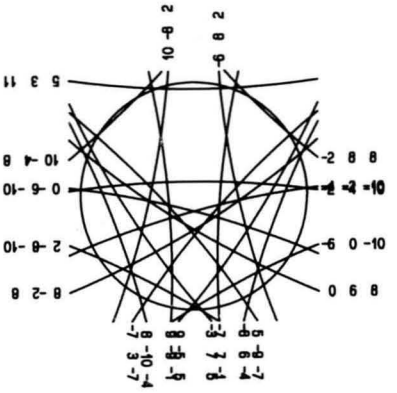

SiC-15R [1$\bar{1}$01]

100 kV

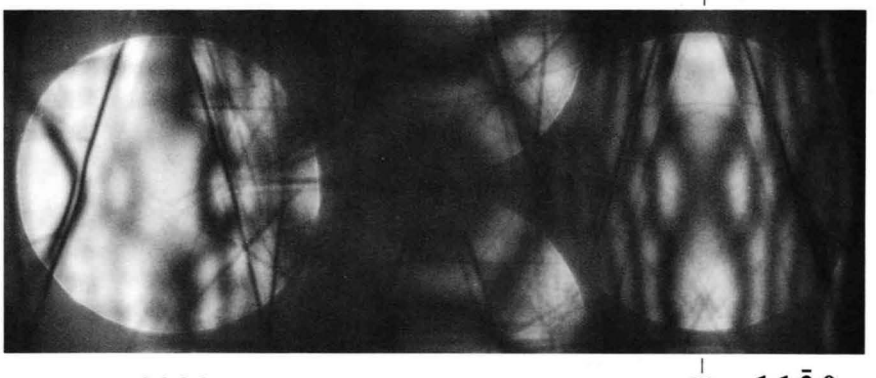

0000 m_2 **11$\bar{2}$0**

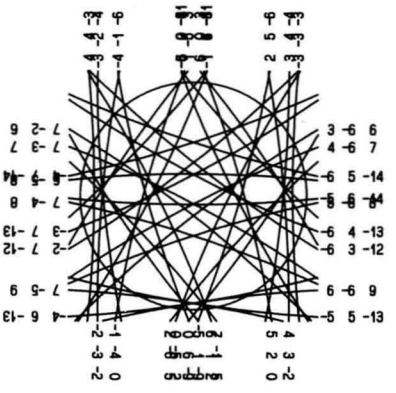

Spurious 1_R

InAs [001]

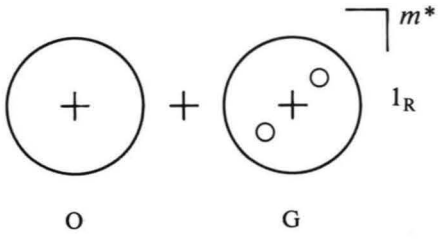

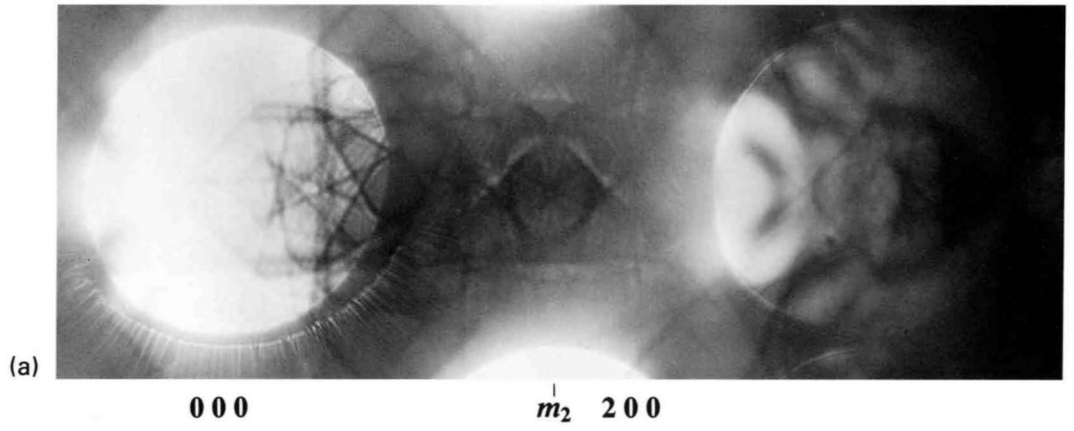

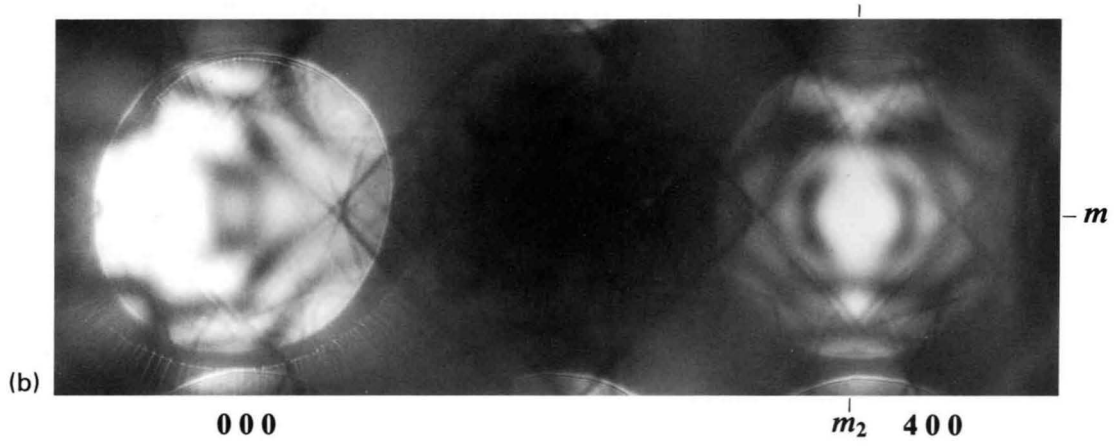

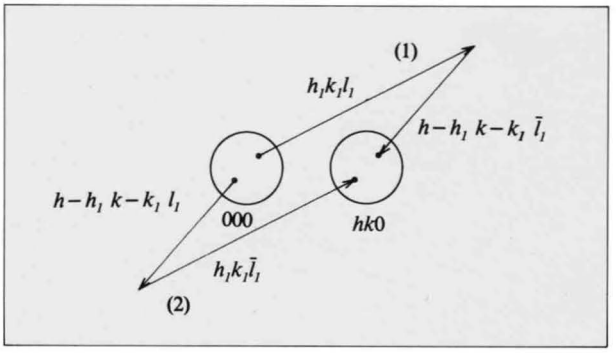

Doule reflection paths forming a symmetry 1_R

InAs also has a zinc-blende type structure. Dark-field patterns of the 200 and 400 reflections taken at the [001] incidence show symmetries m_2 and $2mm$, respectively. The symmetry m_2 is a correct symmetry expected from the twofold axis in the [100] direction. However, the symmetry $2mm$ in the 400 reflection is caused by the addition of a spurious symmetry 1_R.

Double reflection paths (1) and (2) which form a symmetry 1_R are shown in the figure. Table (a) gives the expressions of $H(h_1k_1l_1)$ and $H(h_1k_1\bar{l}_1)$ for four different cases about the sum of reflection indices. When the table is referred to by considering the lattice type of InAs to be face-centered cubic and the resultant reflection to be of $hk0$ (h,k = even), the following relations are obtained:

$$\hat{H}_2^{(1)} = \hat{H}_2^{(2)} \quad \text{for } h_1+k_1+l_1 = 4n,\ 4n+2$$

$$\hat{H}_2^{(1)} = (\hat{H}_2^{(2)})^* \quad \text{for } h_1+k_1+l_1 = 4n+1,\ 4n+3$$

As a result, a spurious symmetry 1_R occurs for the double reflection paths of 000→$2N$th Laue zone→$hk0$ ($l_1 = 2N$). It also occurs for the paths of 000→$(2N+1)$th Laue zone→$hk0$ ($l_1 = 2N+1$), if $\hat{H}_2^{(1)}$ is real.

Table (b) shows combinations of two types of reflections for each of two cases of the resultant reflection $hk0$. For $h+k=4n+2$, the imaginary part of $\hat{H}_2^{(1)}$ is neither zero nor small. Therefore, no spurious symmetry occurs, for instance, in the 200 dark-field pattern (a). For $h+k=4n$, a spurious symmetry 1_R appears when $f'_A/f_A \cong f'_B/f_B$, for instance, in the 400 reflection (b). The observation shows a good agreement with theoretical analysis. Computer simulation also proved quantitatively the occurrence of the spurious symmetry.

Table (a)

$h_1+k_1+l_1$	$H(h_1k_1l_1)$	l_1	$h_1+k_1-l_1$	$H(h_1k_1\bar{l}_1)$
$4n$	f_A+f_B	$2m$	$4n'$	f_A+f_B
$4n+1$	f_A+if_B	$2m+1$	$4n'+3$	f_A-if_B
$4n+2$	f_A-f_B	$2m$	$4n'+2$	f_A-f_B
$4n+3$	f_A-if_B	$2m+1$	$4n'+1$	f_A+if_B

Table (b)

$h+k$	$h_1+k_1+l_1$	$(h-h_1)+(k-k_1)-l_1$	$H_2=H(h_1k_1l_1)\cdot H(h-h_1,k-k_1,-l_1)$
$4n$	$4n+1$	$4n+3$	$(f_A\pm if_B)(f'_A\mp if'_B)=f_Af'_A+f_Bf'_B\pm i(f'_Af_B-f_Af'_B)$
	$4n+3$	$4n+1$	
$4n+2$	$4n+1$	$4n+1$	$(f_A\pm if_B)(f'_A\pm if'_B)=f_Af'_A-f_Bf'_B\pm i(f'_Af_B+f_Af'_B)$
	$4n+3$	$4n+3$	

Spurious 2_R

SiC-15R $[1\bar{1}0\bar{1}]$

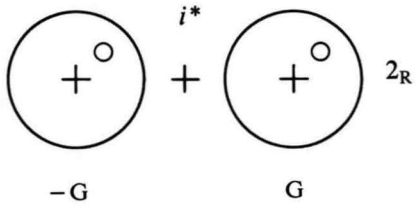

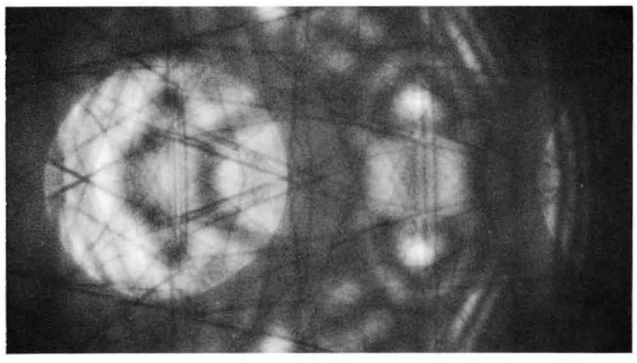

100 kV

0000 **$1\bar{1}02$**

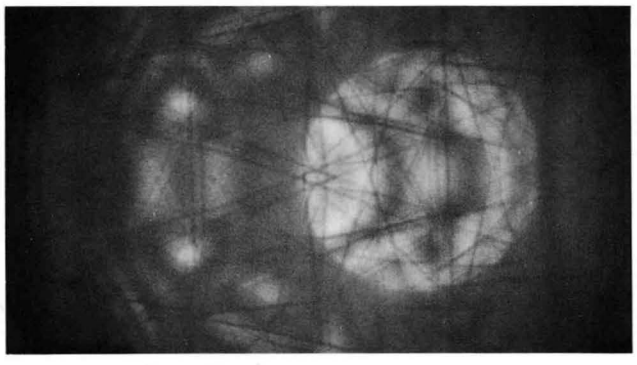

$\bar{1}10\bar{2}$ **0000**

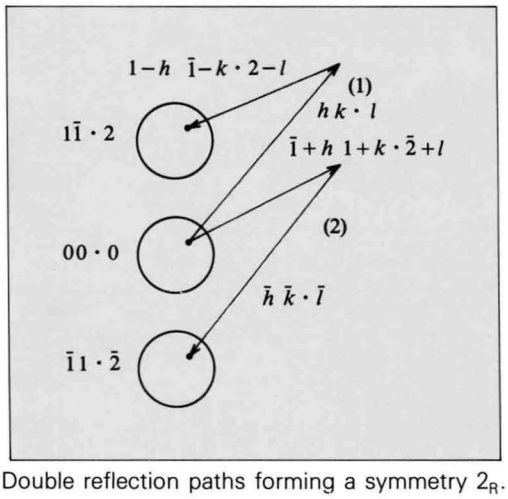

Double reflection paths forming a symmetry 2_R.

SiC-15R belongs to a noncentrosymmetric space group $R3m$. The whole structure lacks an inversion center whereas the substructure has one. No symmetry is expected between a pair of $\pm$G dark-field patterns from the whole structure. The observed symmetry 2_R between the $1\bar{1}02$ and $\bar{1}10\bar{2}$ reflections at the $[1\bar{1}0\bar{1}]$ incidence must have originated from an inversion center of the substructure.

Double reflection paths (1) and (2) which form a symmetry 2_R are shown in the figure. G, which originates from the substructure, is real. $\hat{H}_1^{(1)}$ is equal to $(\hat{H}_1^{(2)})^*$, because of the lack of centrosymmetry. $\hat{H}_2^{(1)}$ is equal to $(\hat{H}_2^{(2)})^*$ (eq. (7)). When the phases of $\hat{H}_1^{(1)}$ and $\hat{H}_2^{(1)}$ are the same, $F^{(1)}$ and $F^{(2)}$ becomes the same in their magnitudes and different only in their phases, resulting a spurious symmetry 2_R. The phase θ of $\hat{H}_1^{(1)}$ was calculated to be 0.221 rad for the $1\bar{1}02$ reflection. The table show the phase θ' of $\hat{H}_2^{(1)}$ and the phase difference $\theta' - \theta$ for several double reflections. Although the values of about 2×10^{-1} rad for the three lower cases look rather large, experimental results show a spurious symmetry 2_R. It is noted that the symmetry 2_R was not observed between the $2\bar{2}04$ and $\bar{2}20\bar{4}$ reflections at the $[1\bar{1}0\bar{1}]$ indidence, at which a pair of double reflection paths had a phase difference of about 0.6 rad. Computer simulation proved quantitatively the occurrence of the spurious symmetry between the $1\bar{1}02$ and $\bar{1}10\bar{2}$ reflections.

$\begin{matrix}h\ k\cdot l\\ 1-h\ \bar{1}-k\cdot 2-l\end{matrix}$	f_{Si}(nm)	f_C(nm)	$R=f_{Si}f'_{Si}+f_Cf'_C$	$I=f'_{Si}f_C-f_{Si}f'_C$	$\theta'=\tan^{-1}(I/R)$ (rad)	$\theta'-\theta$ (rad)
$2\ \bar{1}\cdot 3$ $\bar{1}\ 0\cdot\bar{1}$	0.1364 0.2793	0.0829 0.1541	8.20×10^{-2}	1.98×10^{-2}	0.236	0.015
$1\ 0\cdot 1$ $0\ \bar{1}\cdot 1$	0.2793 0.2793	0.1541 0.1541	1.79×10^{-1}	4.06×10^{-2}	0.223	0.001
$\bar{1}\ \bar{5}\cdot 7$ $2\ 4\cdot\bar{5}$	0.0252 0.0272	0.0109 0.0118	6.15×10^{-4}	1.8×10^{-5}	0.029	−0.192
$\bar{6}\ 2\cdot\bar{5}$ $7\ \bar{3}\cdot 7$	0.0272 0.0217	0.0118 0.0093	5.3×10^{-4}	1.3×10^{-5}	0.025	−0.196
$6\ \bar{6}\cdot 15$ $\bar{5}\ 5\cdot\bar{1}3$	0.0218 0.0293	0.0094 0.0128	5.72×10^{-4}	2.1×10^{-5}	0.037	−0.184

$\theta = 0.221$ rad

SiC-10H

The space group of SiC-10H is $P3m1$, projections of the structure being depicted schematically in Fig.(a). X-ray diffraction identified the point group of this substance to be $6/mmm$ instead of $3m$ (Fig. (b)). This phenomenon is called Ramsdell-type symmetry enhancement. From the symmetries of CBED patterns, the diffraction and point groups were identified to be $3m1_R$ and $\bar{6}m2$ at the [0001] incidence (Table (a)), and $m1_R$ and $6mm$ at the [1$\bar{1}$00] incidence (Table (b)). These inconsistent results originate from spurious symmetries. CBED symmetries expected from the true point group $3m$ are given in the tables as a reference.

H and G of SiC-10H are expressed as

$$H(\boldsymbol{h}) = f_{Si} + f_C \exp 2\pi i \left(\frac{3}{40}\right)l$$
$$G(\boldsymbol{h}) = \sum_{j}^{10} \exp 2\pi i \boldsymbol{h}\cdot\boldsymbol{r}_j, \qquad (1)$$

where $\boldsymbol{h} = hkil$.

The kinematical structure factors satisfy the relations,

$$F(hki\bar{l}) = H^*(hkil)G(hkil) \qquad (2)$$
$$F(\bar{h}\bar{k}\bar{i}l) = H(hkil)G^*(hkil) \qquad (3)$$
$$F(h+k\ \bar{k}\bar{h}\bar{l}) = H^*(hkil)G(hkil) \qquad (4)$$

Equation (2) indicates that a pseudo mirror plane m^* exists perpendicular to the [0001]. The pseudo horizontal and vertical mirror planes always produce a spurious symmetry 1_R and m_v in the bright-field pattern. These symmetries are, however, hidden in usual cases due to the existence of a true vertical and horizontal twofold rotation axes perpendicular to the corresponding pseudo mirror planes as shown in Fig. (c). In the present case, instead a true twofold axis, a pseudo twofold axis (eq. (3) and Fig. (d)) exists perpendicular to a pseudo mirror plane (eq. (2)), owing to a very special arrangement of Si and C. The symmetry due to the pseudo mirror plane causes the symmetries $6mm$ and $2mm$ in the bright-field pattern at the [0001] incidence (Photo (a)) and [1$\bar{1}$00] incidence (Photo (d)), instead of the symmetries $3m$ and m, respectively.

The substructure has a twofold axis in the [10$\bar{1}$0] direction, although the whole structure does not (eq. (4)). As a result, in the 10$\bar{1}$0 and $\bar{1}$010 dark-field patterns (b) and (c) taken at the [0001] incidence, a spurious symmetry m_2 is added perpendicular to the true symmetry m, resulting in a symmetry $2mm$. This spurious symmetry is of the same type as that observed in ZnS, GaAs and SiC-15R. The symmetry m_2 in the symmetry $2mm$ of the 0 0 0 10 and 0 0 0 $\overline{10}$ dark-field patterns (e) and (f) is also a spurious one. This spurious symmetry, however, does not originate from the symmetry of the substructure, because the substructure has no twofold axis in the [0001] direction ($G(\bar{h}\bar{k}\bar{i}l) \neq G(hkil)$ in eq. (3)). It is caused by a psudo twofold axis in the whole structure, and originates from the special atomic arrangements in SiC-10H.

The specimen was supplied by Z. Inoue of the National Institute for Research in Inorganic Materials of Japan.

References

[a] L.S. Ramsdell and J.A. Kohn: *Acta Cryst.*, **4** (1951) 111.

[b] M. Tanaka, H. Sekii, O. Ueno and H. Takayoshi: *Acta Cryst.*, **A40** Suppl. (1984) C384.

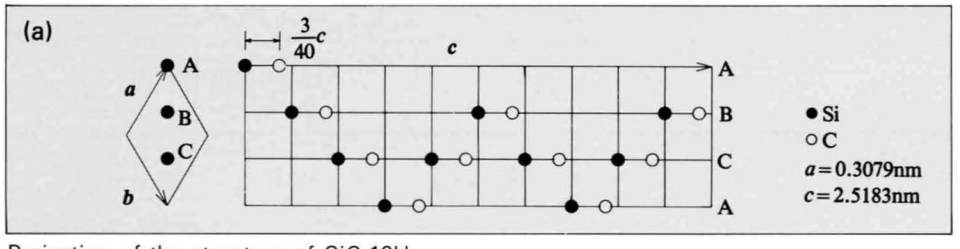

Projection of the structure of SiC-10H.

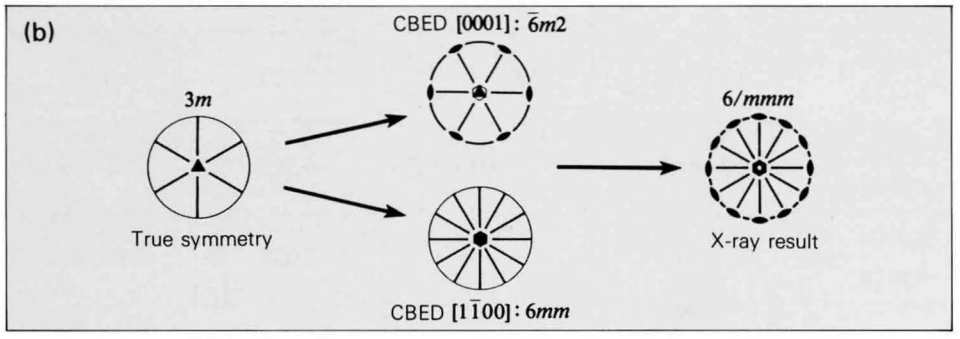

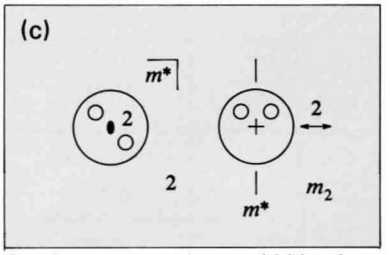

Spurious symmetries are hidden by true symmetries in BP.

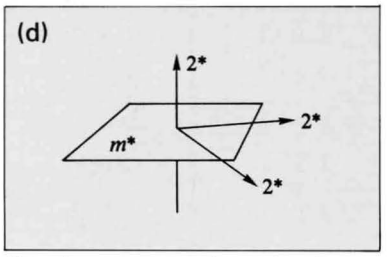

Pseudo symmetry elements of SiC-10H.

[0001]

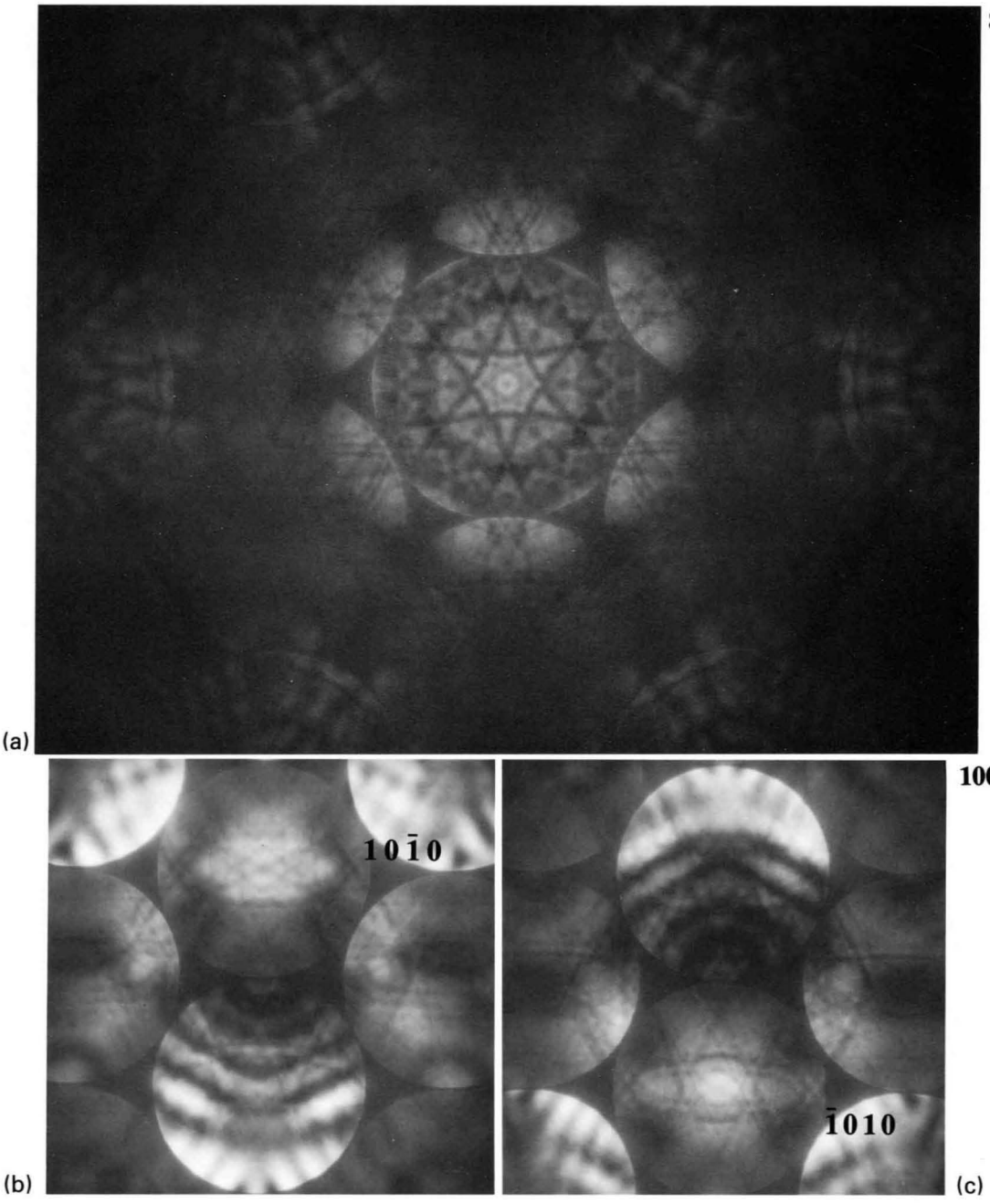

Table (a)

Incidence	Point Group	Diffraction Group	BP	WP	DP	±DP
[0001]	$\bar{6}m2$ (exp.)	$3m1_R$	$6mm$	$3m_v$	$2m_v m_2$	1
	$3m$ (true)	$3m$	$3m_v$	$3m_v$	m_v	1

SiC-10H

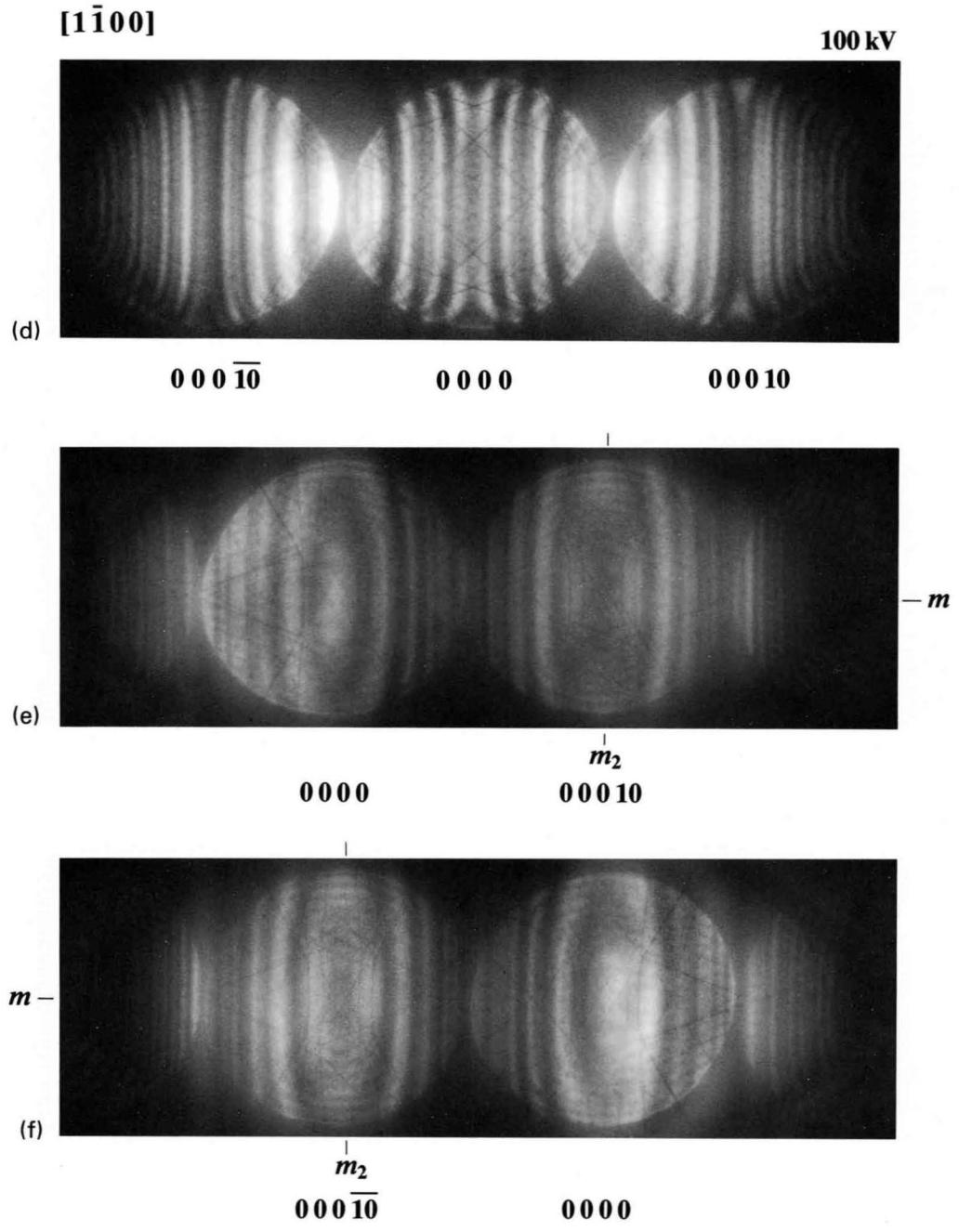

Table (b)

Incidence	Point Group	Diffraction Group	BP	WP	DP	±DP
[1$\bar{1}$00]	$6mm$ (exp.) $3m$ (true)	$m1_R$ m	$2mm$ m_v	m_v m_v	$2m_v m_2$ m_v	— 1

Symmetry Due to Twofold Axes Oblique to Specimen Surfaces

When the theory of Buxton *et at.* [1] is accepted in a strict sense, CBED observes the symmetry elements of diperiodic plane figures. Then, for example, a twofold rotation axis oblique to the specimen surface is not a symmetry element of diperiodic plane figures. The two photographs shown were taken at the 220 Bragg settings with the [111] incidence by tilting a Si film with the [100] surface normal. Symmetries of m_2 due to twofold axes are clearly seen. At least one of the twofold axes is oblique to the specimen surface. Important for CBED is that the top and bottom surfaces be parallel over a specimen area illuminated with the incident beam. It is not necessary to stick so much to whether symmetry elements of a crystal are those of diperiodic plane figures. CBED observes symmetries of a crystal, as far as the boundary condition does not break symmetries of CBED patterns. Gjønnes and Gjønnes [a] reported that the breaking of symmetries due to the surface set oblique to the incident beam is practically negligible. We can tilt a parallel-sided specimen to find crystal symmetry elements oblique to the surface.

The reader will later see on pages 51 to 61 symmetries of CBED patterns produced from crystal symmetry elements which do not belong to those of diperiodic plane figures.

Si **100 kV**

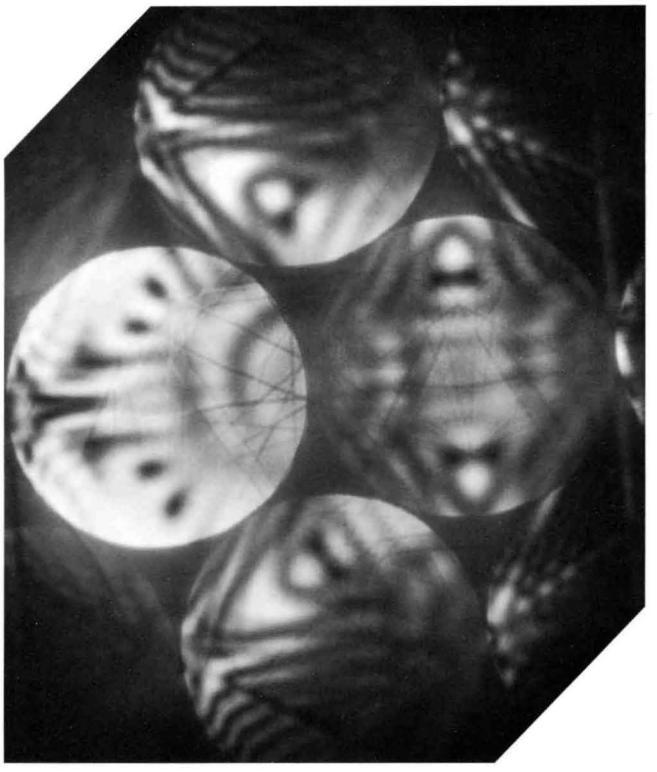

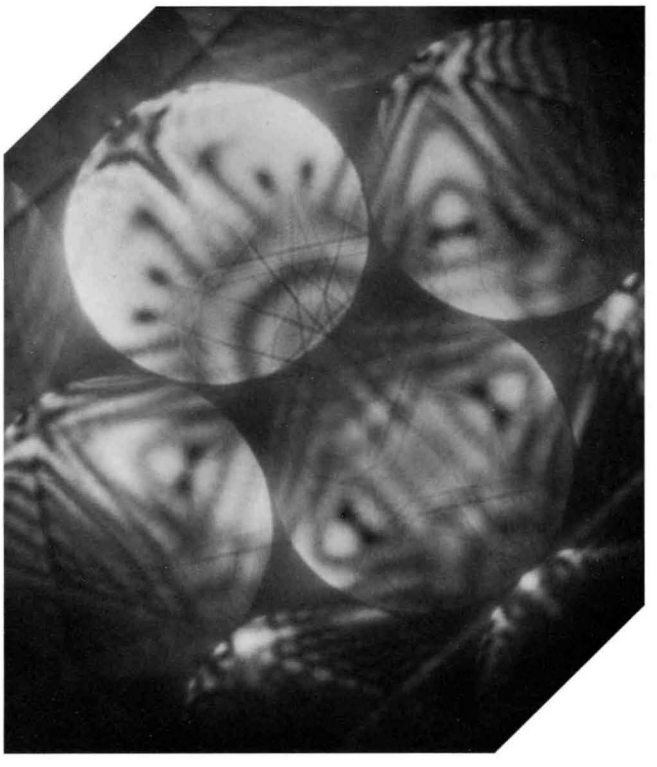

Reference

[a] J. Gjønnes and K. Gjønnes: *Ultramicroscopy,* **18** (1985) 77.

Space-Group Determination

GM Lines Due to Horizontal Glide Planes

Dynamical extinction lines or GM lines [7] have been successfully utilized for the identification of screw axes and glide planes [8]. The table on the opposite page shows the extinction rules given by Gjønnes and Moodie [7]. The dynamical extinction due to a glide plane which is set perpendicular to the incident beam has been predicted to appear as a dark spot at the exact Bragg position of a kinematically forbidden reflection. However, this extinction had not been observed until recently. The observation of the extinction was reported for the 420 reflection of spinel ($MgAl_2O_4$) and the 200 reflection of silicon (Si) [a]. On the basis of the experimental results, the extinction rule given by Gjønnes and Moodie has been modified in a practical manner.

Spinel belongs to the space group of $F4_1/d\bar{3}2/m$. The d-glide planes of this space group lie parallel to the {100} planes. Owing to the glide planes, the reflections with indices $h+k=4n+2$ (cyclic) are kinematically forbidden. The dynamical extinction due to the (001) d-glide plane set perpendicular to the incident beam is expected to appear in the 420 reflection ($n=1$).

Figure (a) schematically illustrates low-order 0th Laue-zone reflection disks and Umweganregung paths to the 420 reflection for the [001] incidence. The 020, 400 and 420 reflections are set simultaneously at the exact Bragg condition. Thus, the projection of the Laue point along the [001] direction is located at the 210 Bragg position and denoted by the letter L. The 420 reflection occurs due to Umweganregung via HOLZ reflections. The paths A and B are symmetric with respect to the point L. The two beams coming through these paths meet on the 420 reflection, and lose their intensity because of their phase difference π. To obtain a spot-shaped extinction, several pairs of HOLZ lines running in different directions have to meet near the exact Bragg position. To produce this situation, the accelerating voltage must be set to a certain value.

Figure (b) shows HOLZ reflections excited at 50.0 kV. Four pairs of Umweganregung paths are depicted. The computer simulated pattern added to Photo (a) on page 38 shows HOLZ reflection lines appearing in the 420 reflection disk. Two HOLZ lines corresponding to a pair of paths, A and B, are almost superposed in a certain angular range with the exact excitation position as the center. Such four superposed lines cross at the center of the disk.

Photograph (a) shows a CBED pattern taken from a (001) spinel specimen with an accelerating voltage of 50.0 kV at the Liq. N_2 temperature to enhance the intensity of HOLZ lines. The extinction is seen to occur not only at the exact excitation position but also in a certain angular range along the HOLZ line pairs, thus forming dark lines instead of a spot-shaped extinction at the exact excitation position [7]. This result is due to the fact that each pair of parallel lines loses its intensity in the overlapping region and other intense HOLZ lines do not intersect or disturb the pair lines over a certain angular range around the exact excitation position.

On the basis of such experimental facts, the extinction rule has been modified as follows: *The extinction occurs as dark lines crossing each other at the exact excitation position.*

When the accelerating voltage is increased by 0.5 kV to 50.5 kV, a spot-shaped extinction is seen over a small angular range with the exact excitation position as the center. This may be a direct proof of the prediction of Gjønnes and Moodie [7]. However, in order to observe a spot-shaped extinction, special attention must be paid to the very careful adjustment of the accelerating voltage.

A similar extinction is also seen in the 020 reflection. Consider two Umweganregung paths to the 020 reflection via HOLZ reflections H and H' in Fig.(a). The HOLZ line geometry in the 020 disk is the same as in the 420 disk. The phases of the two paths differ by an integral multiple of 2π from those of the paths A and B, since the two paths are created by subtracting the vector of the 400 reflection from the paths A and B. Hence, the sign of the resultant structure amplitude remains opposite between the two paths, although its magnitude is now different between the two. Therefore, imperfect cancellation still takes place between the two beams. If the difference between the magnitudes is small, an extinction similar to that in the 420 disk also occurs in the 020 disk. This is the origin of the extinction observed in the 020 reflection. The reader is referred to the section of spurious B_3 GM lines.

Reference

[a] M. Tanaka, M. Terauchi and H. Sekii: *Ultramicroscopy*, **21** (1987) 245.

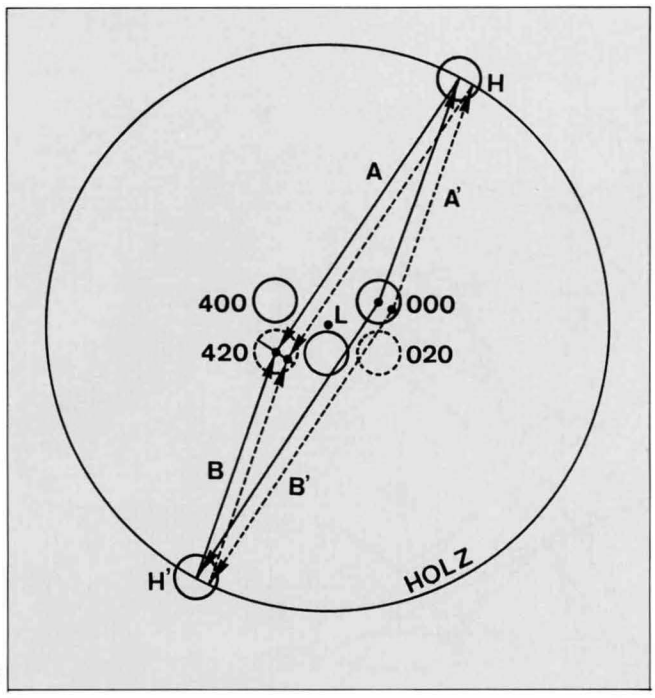

(a)

The 420 reflection occurs due to Umweganregung via HOLZ reflections. The paths A and B are symmetric with respect to the point L.

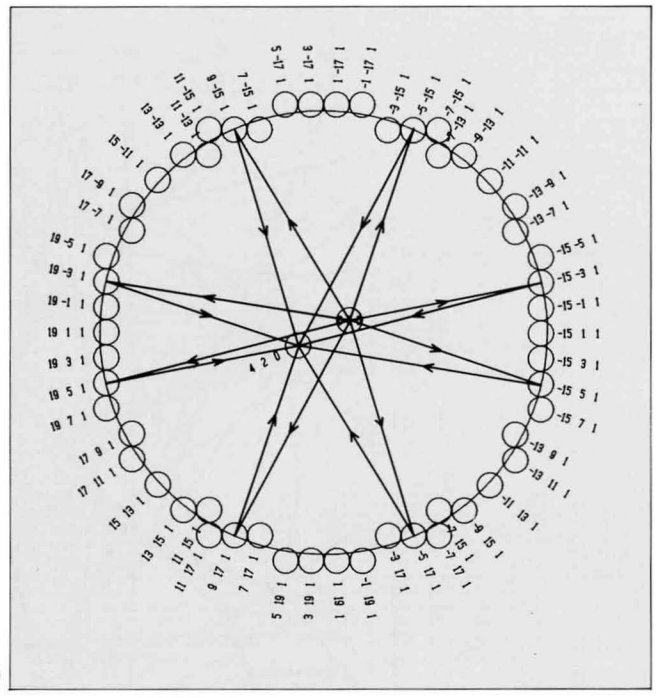

(b)

Simulation of HOLZ reflections of spinel excited at [001] electron incidence and 50.0 kV accelerating voltage. Four pairs of Umweganregung paths to the 420 reflection are drawn.

Dynamical extinction rules for symmetry elements of a parallel-sided specimen

Symmetry elements of parallel-sided specimen	Orientation to specimen surface	GM lines	
		Two-dimensional (ZOLZ) interaction	Three-dimensional (HOLZ) interaction
Glide planes	Perpendicular : g	A_2 and B_2	A_3
	Parallel : g'	———	Intersection of A_3 and B_3
Twofold screw axes	Parallel : $2_1'$	A_2 and B_2	B_3

$MgAl_2O_4$ [001]

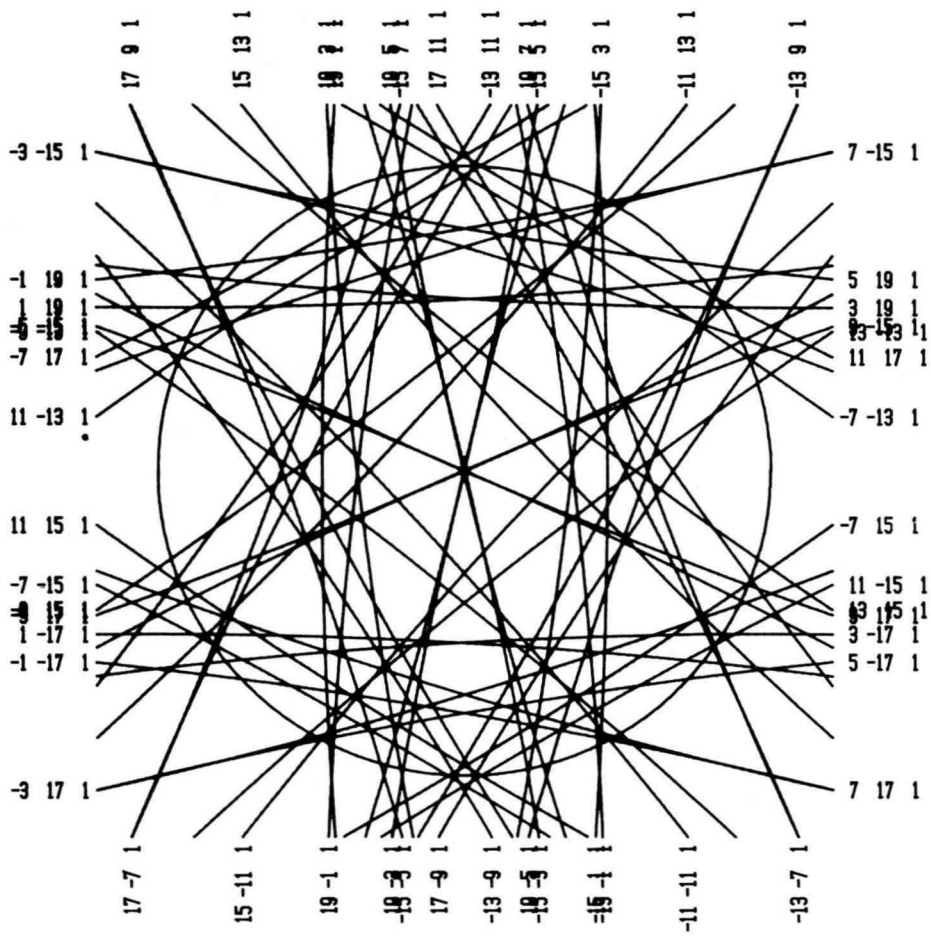

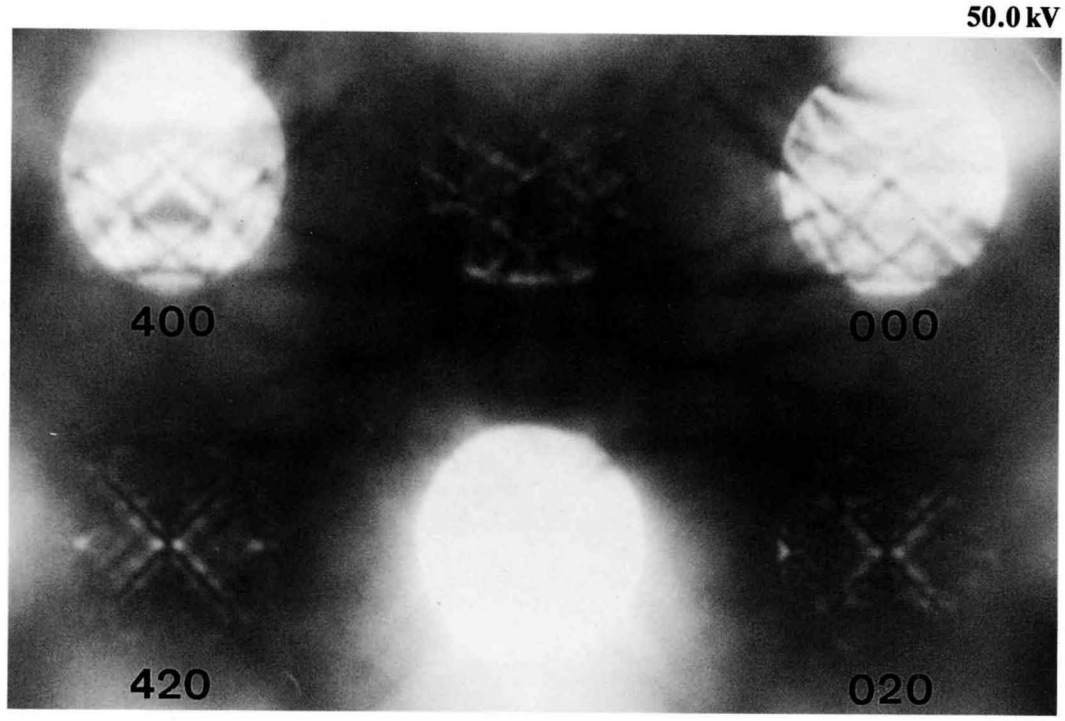

(a)

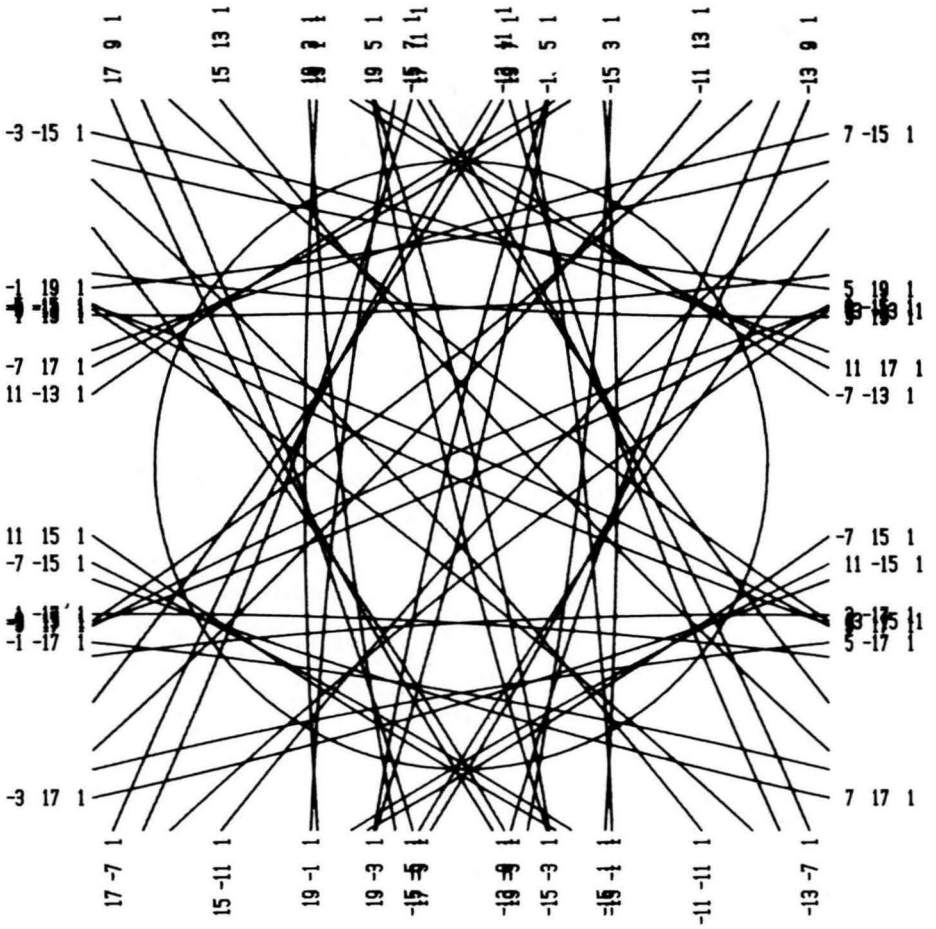

50.5 kV

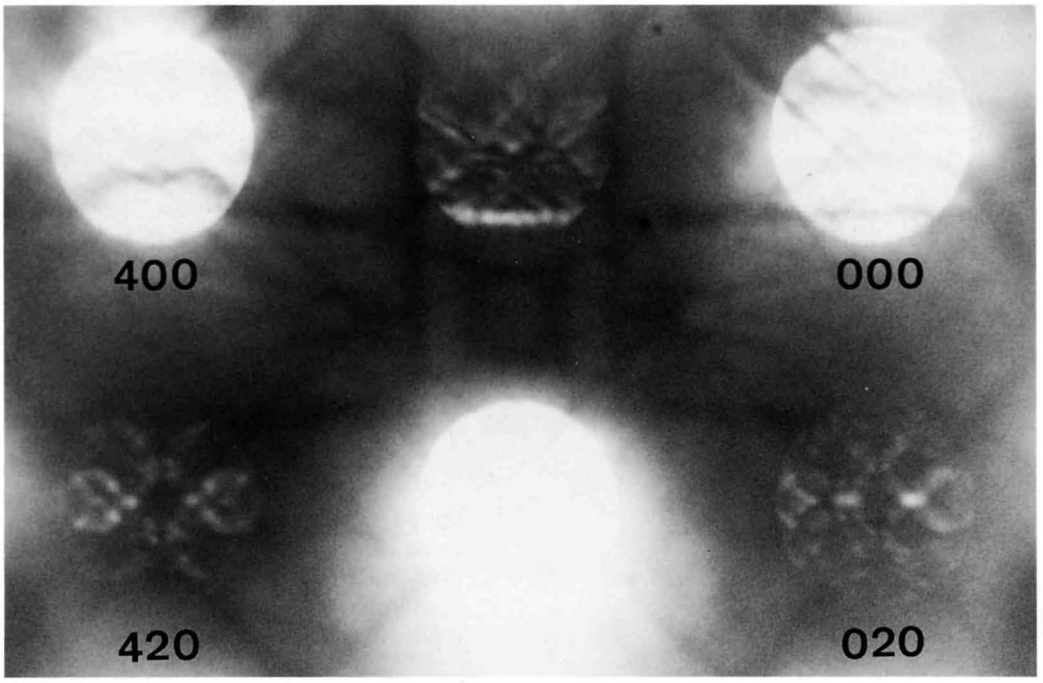

(b)

Si [001]

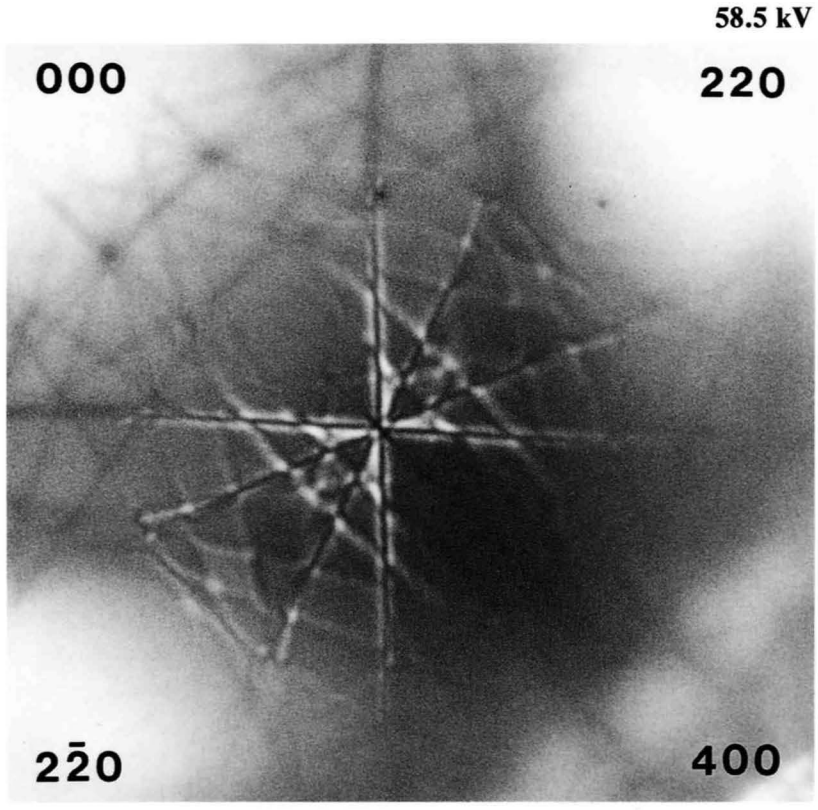

The dynamical extinction lines due to the (001) *d*-glide plane crossing at the exact 200 Bragg position.

The above photograph shows a pattern taken from (001) Si with the [001] incidence at an accelerating voltage of 58.5 kV.

The dark lines skewed to the [100] direction clearly cross at the exact excitation position of the 200 reflection. This proves the existence of the (001) *d*-glide plane.

In the reflection, an extinction due to the (010) *d*-glide plane is also expected to appear. However, the extinction line in the [100] direction due to this glide plane is not clear, because no HOLZ line appears in this direction at this accelerating voltage.

▶

A series of photographs on the opposite page shows 200 dark-field patterns taken from (001) Si with the [001] incidence at succesive accelerating voltages. Not only GM lines due to a horizontal (001) *d*-glide plane but also the lines in the [100] direction due to a vertical (010) *d*-glide plane are seen.

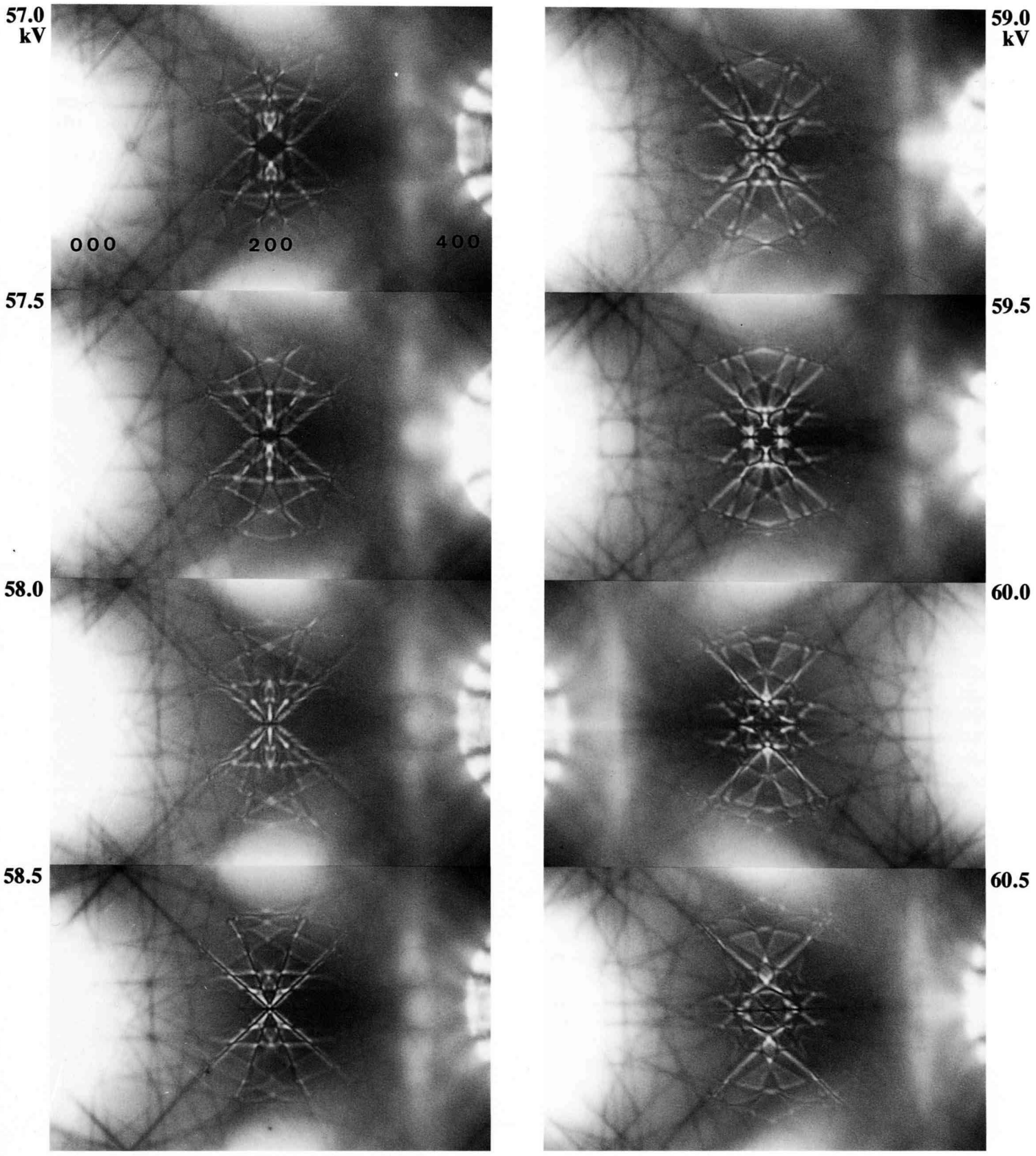

Accelerating-voltage dependence of GM lines due to a horizontal and a vertical *d*-glide plane.

Spurious B_3 GM Lines

When a 2_1 screw axis is set perpendicular to the incident beam, A_2 GM lines are observed in kinematically forbidden reflections and B_2 and B_3 GM lines in exactly excited forbidden reflections. However, extinctions similar to B_3 GM lines are sometimes observed in forbidden reflections at the symmetric incidence and at incidences exciting kinematically allowed reflections. We call these extinction lines spurious B_3 GM lines.

A series of photographs on the opposite page shows B_3 type dynamical extinction lines appearing in the 001 reflection at different crystal settings: (a) symmetric incidence, (b) 001 exact Bragg setting, (c) intermediate setting between 001 and 002 Bragg settings and (d) 002 exact Bragg setting. True GM lines are seen at the positions indicated by fine arrows in Photos (b) and (c). The spurious B_3 GM lines are seen at the centers of the 001 and $00\bar{1}$ reflections at the symmetric incidence (a), at the center of the 001 reflection at the 002 exact Bragg setting (d), and at an off-center position in the 001 reflection (c), as indicated by thick arrows.

The reason for the appearance of the spurious B_3 GM lines is as follows. A schematic diagram of Umweganregung paths via HOLZ reflections to the 001 and $00\bar{1}$ reflections is given below for the symmetric incidence. These two reflections are kinematically forbidden due to the 2_1 screw axis in the [001] direction. The path aa' is found to be equivalent to the path bb' by successively operating twofold rotation about the [001] axis and inversion. The phases of the two beams coming through these paths are different by π from each other due to the existence of the 2_1 screw axis in the [001] direction. The path b' to the 001 reflection and the path b'' to the $00\bar{1}$ reflection from the same HOLZ reflection have a phase difference of $2n\pi$, because these two reflections differ by the vector of the 002 reflection. As a result, the two beams coming through the paths aa' and bb'' still differ by $(2n+1)\pi$ in phase. The amplitudes of Umweganregung via these paths are not the same, because the paths are not equivalent with respect to the twofold rotation. However, a dynamical extinction still takes place, since a partial cancellation of the amplitudes occurs between the two paths. The spurious B_3 GM line, together with true B_2 and B_3 GM lines, indicates the existence of a 2_1 screw axis. It appears that spurious A_2 and B_2 GM lines do not occur, because a sufficient cancellation does not take place between Umweganregung-beams owing to strong scattering-angle dependences of atomic scattering factors for ZOLZ reflections.

It is noted that the dynamical extinction observed in the 020 reflection due to a horizontal glide plane in spinel described on pages 36 to 39 is also a spurious GM line in the meaning given above. Furthermore, spurious (A_3) GM lines due to vertical glide planes have been observed in 420 reflections from $MgAl_2O_4$ at the [001] zone axis incidence.

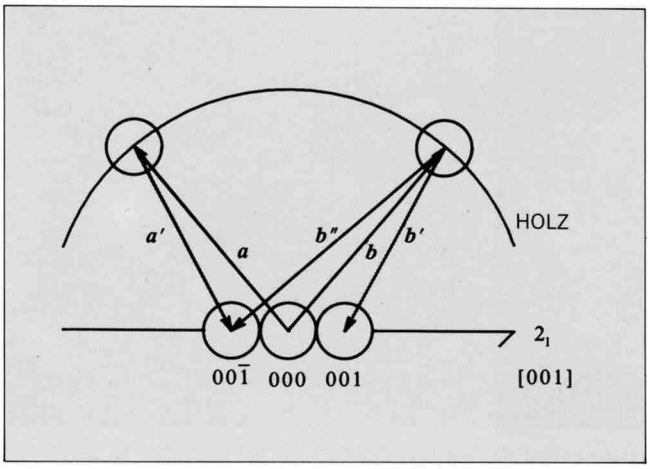

FeS_2

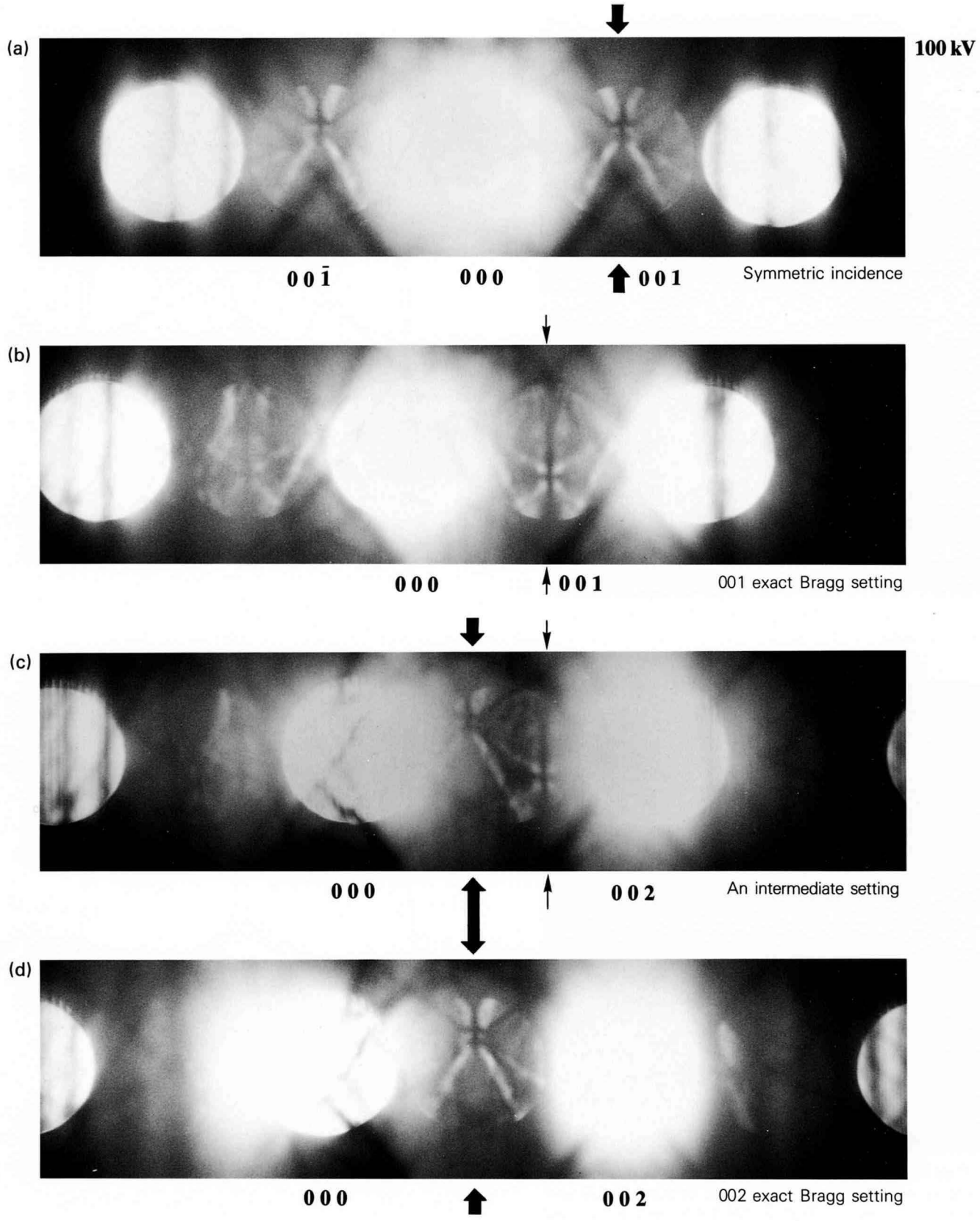
(a)
100 kV
0 0 1̄
0 0 0
0 0 1
Symmetric incidence
(b)
0 0 0
0 0 1
001 exact Bragg setting
(c)
0 0 0
0 0 2
An intermediate setting
(d)
0 0 0
0 0 2
002 exact Bragg setting

FeS_2 [210]

104 kV

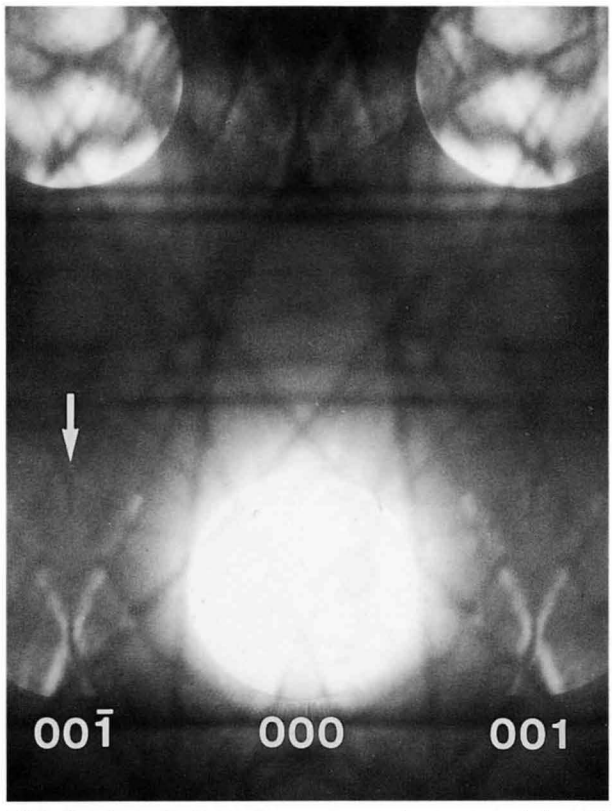

(a)

ZAP. Spurious B_3 GM lines are seen at the centers of the 001 and 00$\bar{1}$ disks.

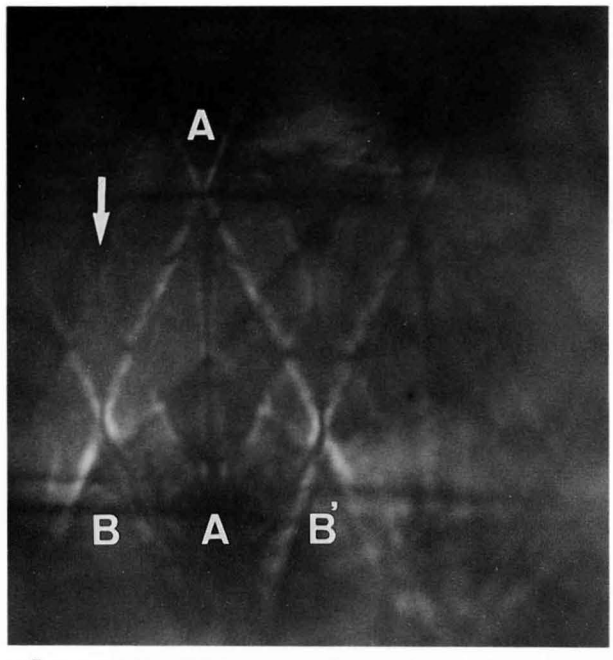

(b)

00$\bar{1}$ dark-field LACBED pattern. The angular position indicated by an arrow corresponds to that in (a). Spurious B_3 GM lines are seen at B and B'. True B_3 GM line is seen at the exact 00$\bar{1}$ Bragg position, A.

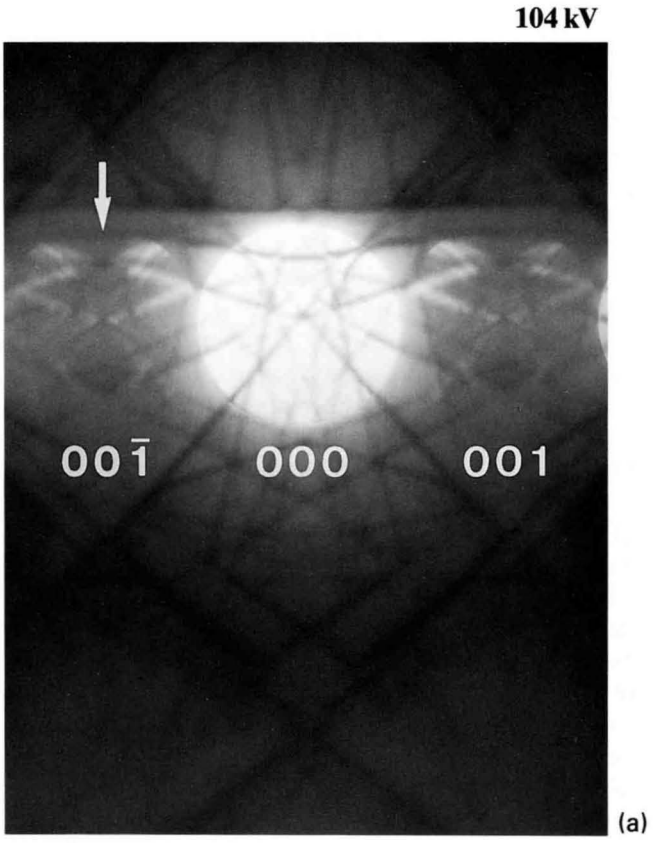

(a)

ZAP. Spurious B_3 GM lines are seen at the centers of the 001 and 00$\bar{1}$ disks.

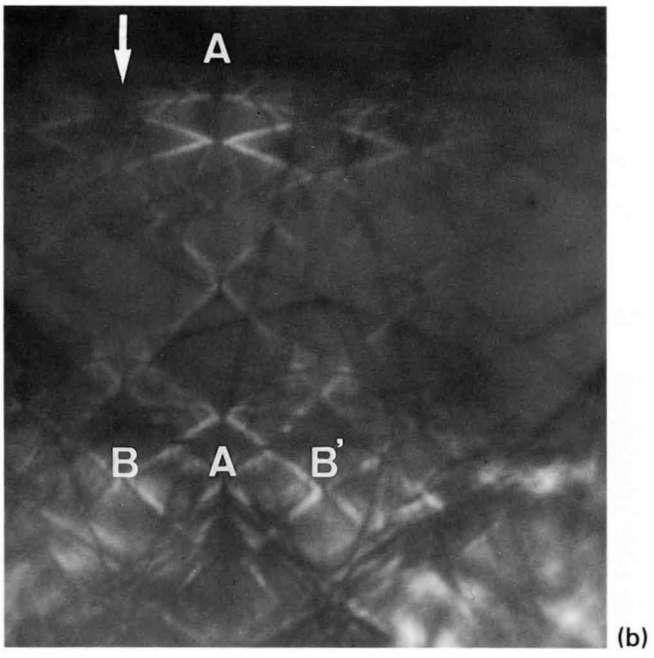

(b)

00$\bar{1}$ dark-field LACBED pattern. The angular position indicated by an arrow corresponds to that in (a). Spurious B_3 GM lines are seen at B and B'. True B_3 GM line is seen at the exact 00$\bar{1}$ Bragg position, A.

Slight Breakdown of GM Lines

Substance Mo_2S_3 belons to a space group $P2_1/m$ above approximately 150°C. The ***b*** projection of the structure of this phase is drawn in Fig. (a). After two phase transformations with decreasing temperature, it undergoes the last phase transformation at about −90°C.

Photographs (a) and (b) were taken at 155°C and −185°C, respectively. The $h\ k/2\ 0$ reflections in (b) are superlattice reflections, indicating a cell doubling in the ***b***-direction at the low temperature phase. The fundamental reflections in the CBED patterns (c) and (d) taken at −185°C exhibit a mirror symmetry perpendicular to the b^* axis to a good approximation, and the $0k0$ (k = odd) fundamental reflections in the patterns (c), (e) and (g) show GM lines due to the 2_1 screw axis. These results indicate that the fundamental structure of the high temperature phase is almost preserved in the low temperature phase. The superlattice reflections $h\ k/2\ 0$, however, have no mirror symmetry and no GM line, these results being summarized in the table below. Therefore, the space group of the low temperature phase is $P\bar{1}$ or $P1$. Figure (b) schematically shows a structural model given by Deblieck *et al.* Their model is that the fundamental structure is triclinic (△), while the superstructure is a monoclinic one composed of the twinning of two triclinic unit cells. On the other hand, our experimental result concluded that the fundamental structure is approximately monoclinic (○) and the superstructure is triclinic (Fig. (c)).

If the superlattice reflections show a symmetry expected from a triclinic structure, the fundamental reflections are more or less affected by the superlattice reflections, and therefore should have the same symmetry as that of the superlattice reflections. Actually, a detailed inspection revealed that the fundamental $0k0$ (k = odd) reflection disks did not show correct GM lines. Photographs (e) and (g) were taken at the $0\bar{3}0$ exact Bragg setting from a thin and a thick specimen area, respectively. Photographs (f) and (h) show enlarged $0\bar{3}0$ dark-field patterns. A_2 and B_2 GM lines do not form an accurate black cross in the disks. The deviation from the cross is more easily seen for the thicker specimen (h). A symmetry $2mm$ of the black cross is changed into a symmetry 1_R. The symmetry 1_R is expected in the case of the projection approximation or the 0th Laue zone interaction even if the specimen has no symmetry. It is also seen that the A_2 GM lines in the $0\bar{1}0$ reflection disks in Photos (c), (e) and (g) are not straight but of a little irregular shape owing to a slight breakdown of the 2_1 screw axis.

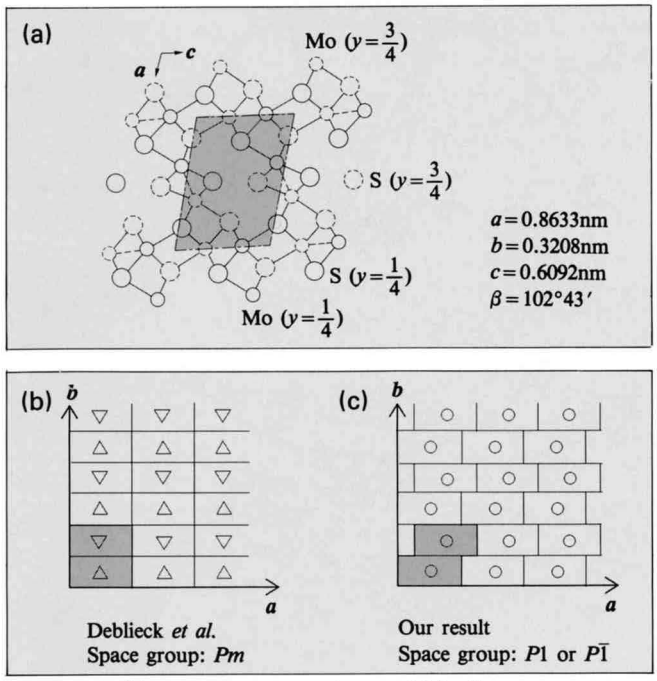

Structure of low temperature phase of Mo_2S_3

A slight breakdown of a symmetry of a crystal often occurs at a second order phase transition. In such a case crystal symmetries may be incorrectly determined. For the correct determination, it is helpful to know in advance how the symmetries of CBED patterns are changed by a slight breakdown of a crystal symmetry element. The present example provides an instructive demonstration on how a symmetry changes due to a slight breakdown of a 2_1 screw axis. That is, a pattern with crossed A_2 and B_2 GM lines having a symmetry $2mm$ changes into a pattern of a symmetry 1_R due to the breakdown of a 2_1 screw axis (or a glide plane). Such changes will be studied again in the section of computer simulations.

The specimens were supplied by Dr. N. Kobayashi and Prof. Y. Muto of the Research Institute for Iron, Steel and Other Metals, Tohoku University.

Reference

[a] R. Deblieck, G.A. Wiegers, K.D. Bronsema, D. van Dyck, G. van Tendeloo, J. van Landuyt and S. Amelinckx: *phys. stat. sol.*, **(a) 77** (1983) 249.

Mo_2S_3 [001]

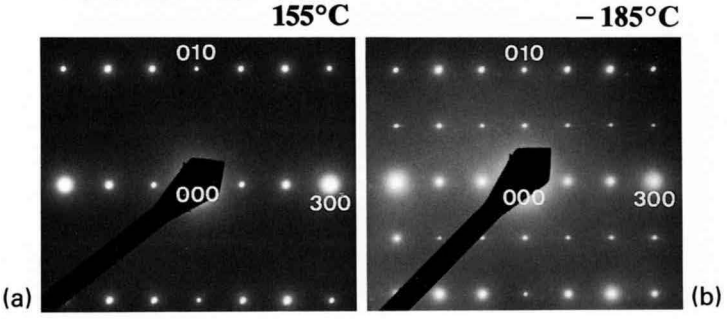

$T < -90$°C

Fundamental reflections	$\sim 2_1/m$ (approximately)
Superlattice reflections	1

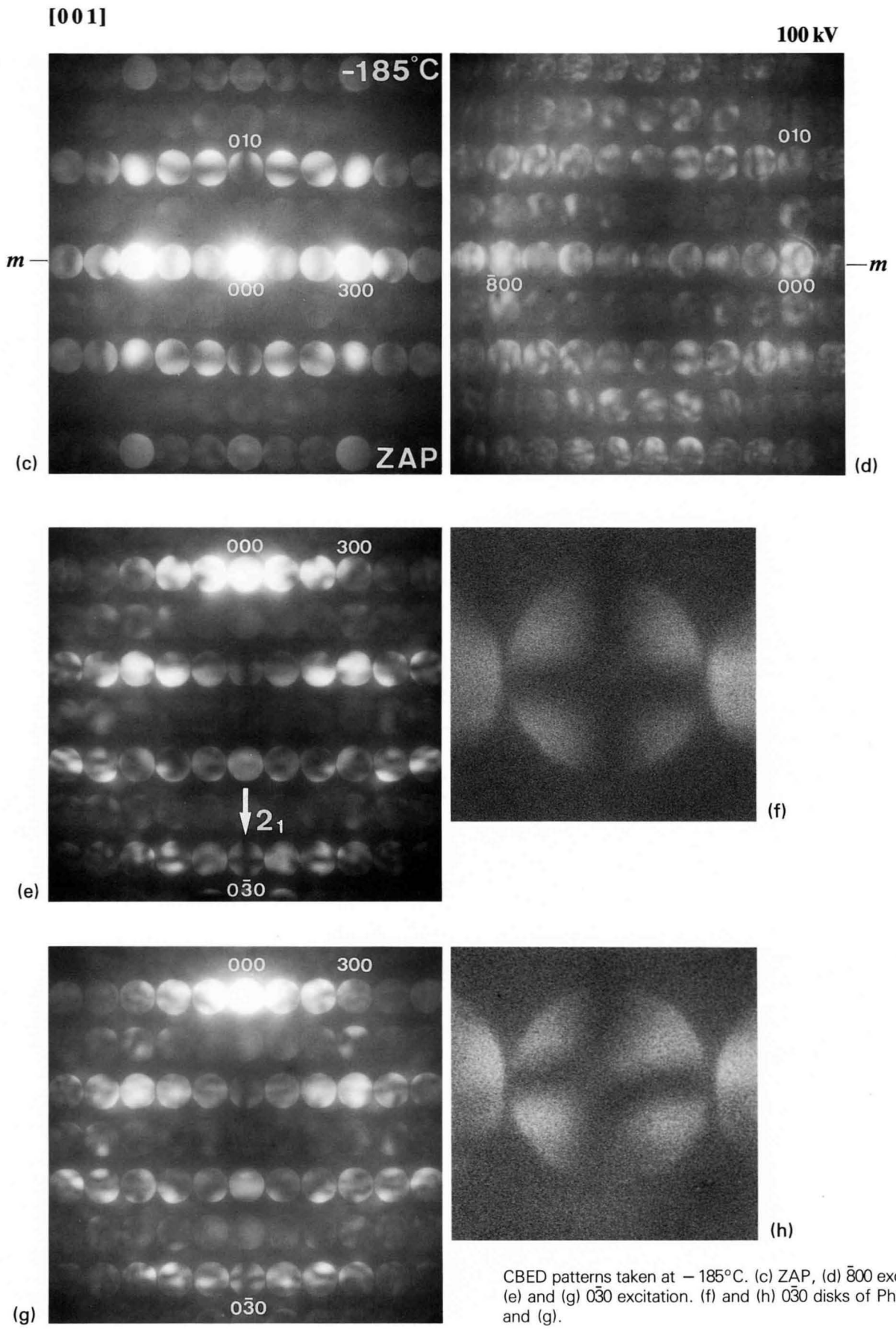

CBED patterns taken at −185°C. (c) ZAP, (d) $\bar{8}00$ excitation, (e) and (g) $0\bar{3}0$ excitation. (f) and (h) $0\bar{3}0$ disks of Photos (e) and (g).

A_3 and B_3 GM Lines from Cooled Specimens

Si [001]

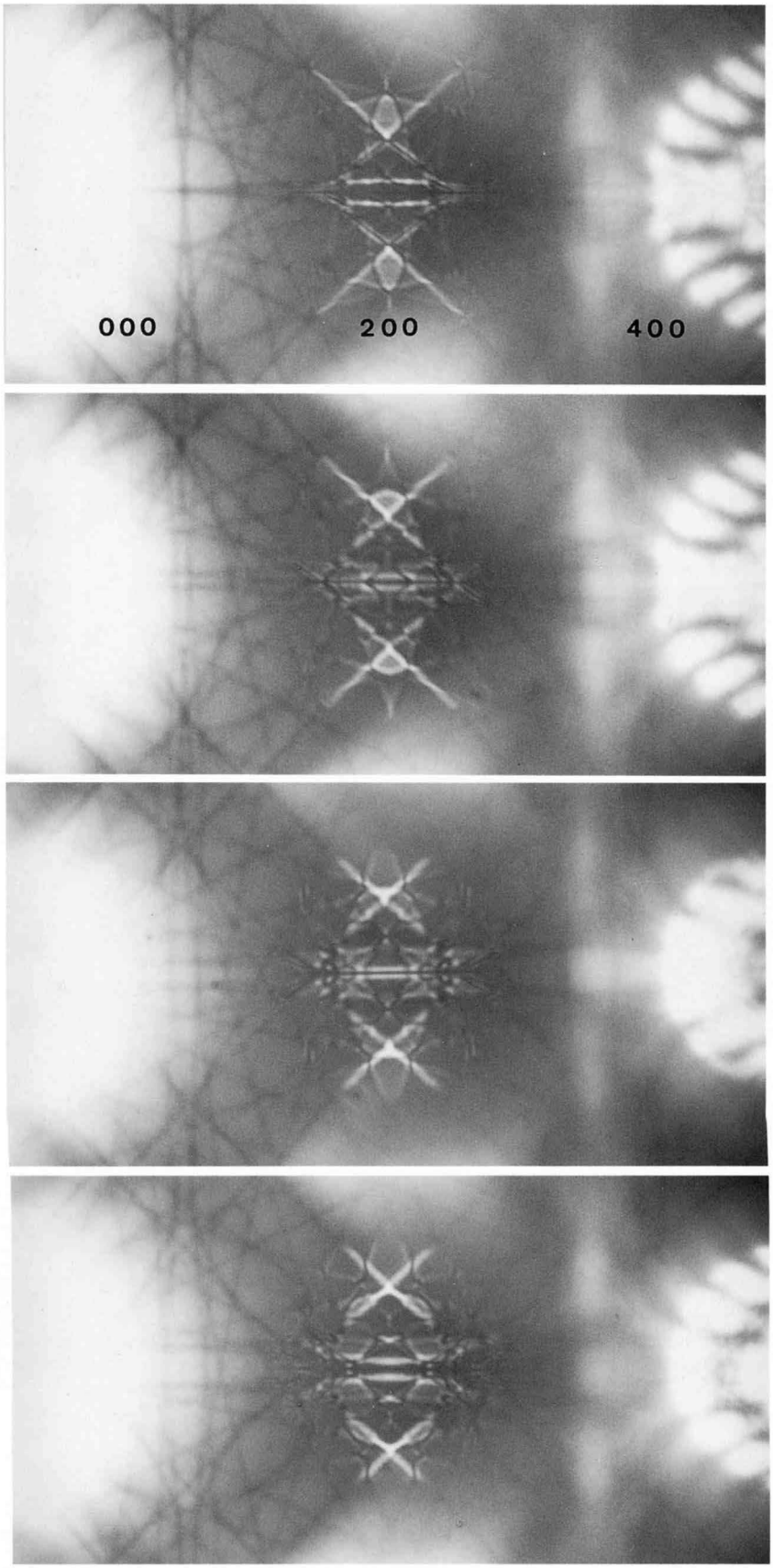

61.5 kV Cooling specimens down to the Liq.N_2 temperature, if possible, enables clear observation of A_3 and B_3 GM lines.

62.0 kV

62.5 kV

63.0 kV

A_3 GM lines appearing in the 200 reflections taken at the Liq.N_2 temperature. Compare these with faint ones taken at room temperature, which have been given in book I.

FeS_2 [001]

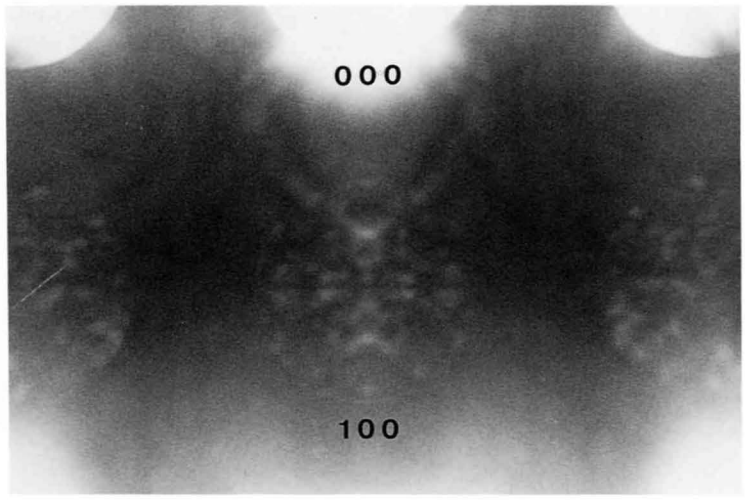

55.0 kV

A B_3 GM line in the 100 reflection is seen at the Liq.N_2 temperature, whereas it is not observed at room temperature.

$MgAl_2O_4$ [001]

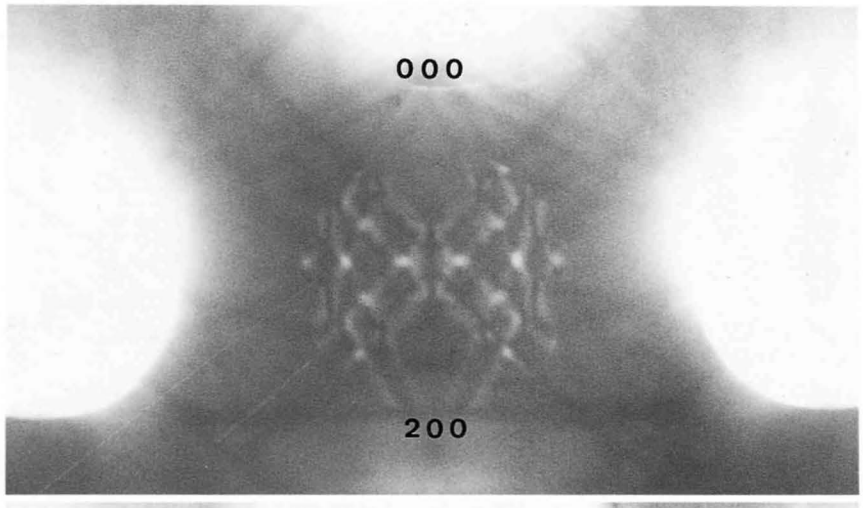

71.5 kV

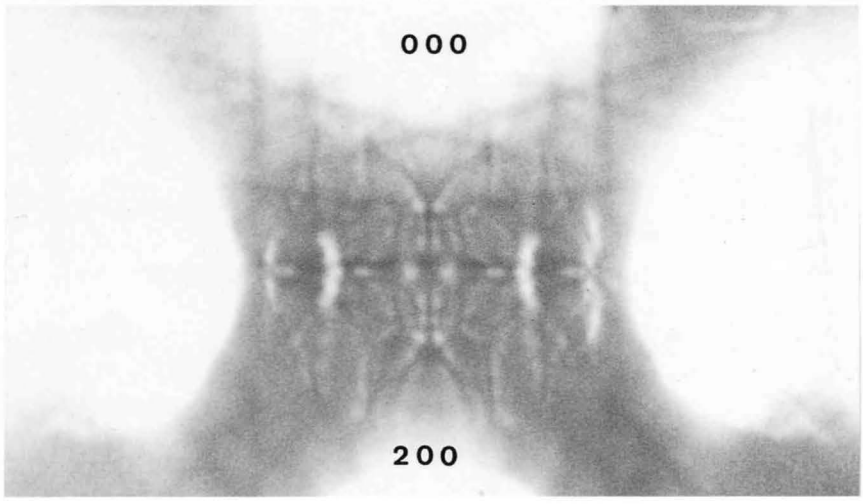

55.0 kV

A_3 GM lines in the 200 reflections are clearly seen, because many HOLZ lines appear over the whole disks at the Liq. N_2 temperature in contrast to a few weak lines at room temperature.

Space groups indistinguishable by GM lines

The table of space groups indistinguishable by GM lines given in book I is not perfect. It should be replaced by the table given here. As a result, the number of distinguishable space groups should read 181 instead of 185 in the last paragraph on page 173 of book I. In the same paragraph, the 19 sets should read 21 sets. These corrections are due to Dr. J.A. Eades.

The 49 crystal space-groups in the present table can not be identified by GM lines. Whether an axis is a rotation axis or a screw axis can be made clear by observing how the intensities of reflections which may be kinematically forbidden change when the crystal orientation is varied. If an axis is a screw axis, kinematically forbidden reflections show a sudden decrease in intensity with a rotation that causes the loss of Umweganregung paths. If the axis is a rotation axis, the intensities of the reflections are not changed conspicuously by such a rotation. By such a test, each space group in the 21 sets can be identified except the pairs in parentheses and pairs 16 and 17. The pairs in parentheses form left- and right-handed space groups. The handedness of space groups can be identified in such a way that the senses of two crystal axes are determined with the aid of crystal structure factor calculations and the sense of the third axis is determined with the aid of dynamical calculations ([a], [b] and [c]). It should be noted that two special pairs 16 and 17 ($I222$ and $I2_12_12_1$, $I23$ and $I2_13$) can not be distinguished from kinematical extinction rules, but distinguished when atomic positions are determined.

In crystal data on 5572 different inorganic materials collected by Nowacki[d], the numbers of materials belonging to a space group among the sets 1, 4, 8, 10, 12, 14, 17, 18 and 21 are less than two, those belonging to a space group among the sets 6, 9, 13, 15, 16, 19 and 20 are less than ten, and only those belonging to the sets 2, 3, 5, 7 and 11 are more than fifteen. It is emphasized that the probability to find most indistinguishable space groups is very low.

1. $P3$, ($P3_1$, $P3_2$)
2. $P312$, ($P3_112$, $P3_212$)
3. $P321$, ($P3_121$, $P3_221$)
4. $P6$, ($P6_2$, $P6_4$)
5. $P622$, ($P6_222$, $P6_422$)
6. $P6_3$, ($P6_1$, $P6_5$)
7. $P6_322$, ($P6_122$, $P6_522$)
8. $P4$, $P4_2$
9. ($P4_1$, $P4_3$)
10. $P4/m$, $P4_2/m$
11. $P4/n$, $P4_2/n$
12. $P422$, $P4_222$
13. $P42_12$, $P4_22_12$
14. $I4$, $I4_1$
15. $I422$, $I4_122$
16. $I23$, $I2_13$
17. $I222$, $I2_12_12_1$
18. $P432$, $P4_232$
19. ($P4_132$, $P4_332$)
20. $I432$, $I4_132$
21. $F432$, $F4_132$

References

[a] P. Goodman and T.W. Secomb: *Acta Cryst.*, **A33** (1977) 126.

[b] P. Goodman and A.W.S. Johnson: *Acta Cryst.*, **A33** (1977) 997.

[c] M. Tanaka, H. Takayoshi, M. Ishida and Y. Endoh: *J. Phys. Soc. Jpn.*, **54** (1985) 2970.

[d] W. Nowacki: Crystal Data, ACA Monograph No. 6, American Crystallographic Association (1967).

GM Lines in HOLZ Reflections

Space-group determination has been carried out by using GM lines appearing in ZOLZ reflections [3], [8]. The GM lines are caused by the crystal symmetry elements which act as horizontal 2_1 screw axes, vertical glide planes with horizontal translation vectors and horizontal glide planes [7]. The vertical glide planes give rise to GM lines also in HOLZ reflections. Vertical glide planes whose translation vectors are perpendicular to the specimen surface (vertical translation) do not cause GM lines in ZOLZ reflections but cause them in HOLZ reflections (see page 59). It should be noted that vertical glide planes with glide translations not-parallel to the surface are not symmetry elements of diperiodic plane figures.

Vertical screw axes also form GM lines in HOLZ reflections whose vectors are parallel to the screw axes. However, these reflections cannot be observed by usual transmission CBED. Therefore, only glide planes can be identified from GM lines in HOLZ reflections.

HOLZ GM lines

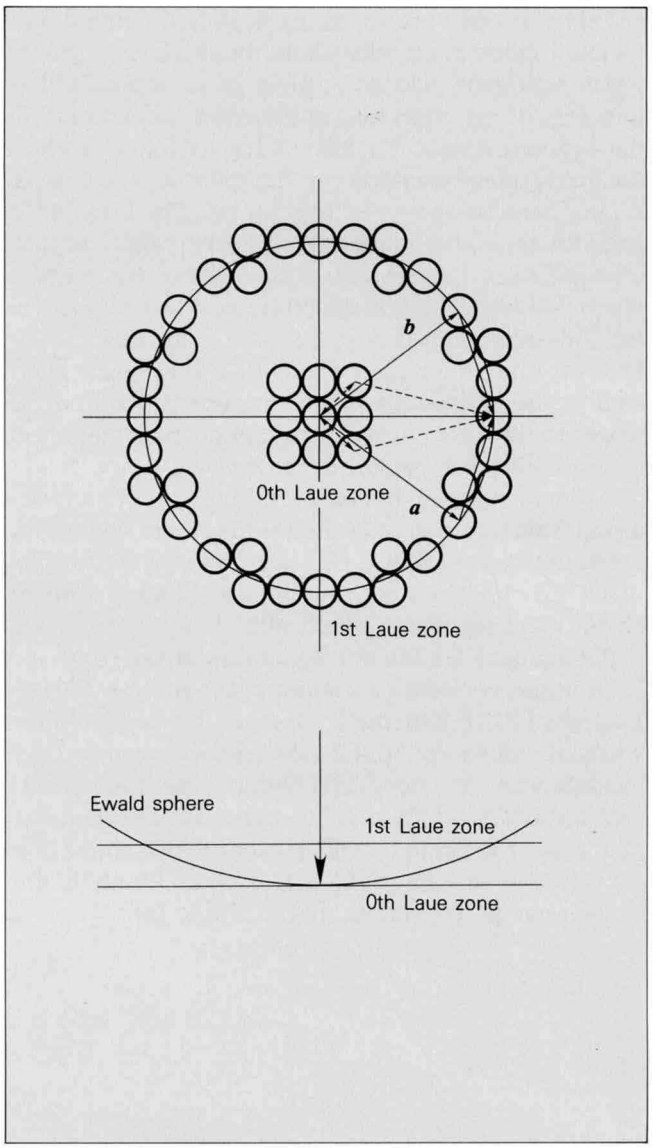

The symmetric paths ***a*** and ***b*** with respect to a vertical glide plane produce a GM line in a HOLZ reflection.

Tables of GM lines appearing in HOLZ reflections at various incident beam orientations for all the space groups which have glide planes, are given in an appendix. The meanings of the letters used in the tables are explained in the diagrams at right. The letter A is given for cases where the Ewald sphere intersects two circled-cross-reflections in a Laue zone, as shown in diagram (a). The letter A^* is given for cases where the Ewald sphere intersects a circled-cross-reflection on one side of the incident beam and a black-circle-reflection on the other, as shown in diagram (b). This case occurs only in the space group $P2_1/a\bar{3}$. The letter A_h is given for cases where the Ewald sphere intersects a circled-cross-reflection on one side but does not intersect on the other, owing to the asymmetric arrangement of reflections with respect to the incident beam.

It should be noted that HOLZ GM lines are clearly observed from specimen areas thinner than those suitable for the observation of ZOLZ GM lines, because the profiles of HOLZ reflections are concentrated in small areas of CBED disks for thicker specimens.

Photographs (a) and (b) were taken at the [100] and [110] incidences from FeS_2 whose space group is $P2_1/a\bar{3}$. Enlarged HOLZ patterns are inserted for easy viewing. The table shows the HOLZ GM lines expected in three incident beam directions. GM lines of type A are seen in two h_0k0 HOLZ reflections of Photo (a) due to the a-glide plane parallel to the (001) plane. A GM line of type A^* is seen in an h_0k0 HOLZ reflection of Photo (b) due to the same glide plane as that of Photo (a).

HOLZ GM lines

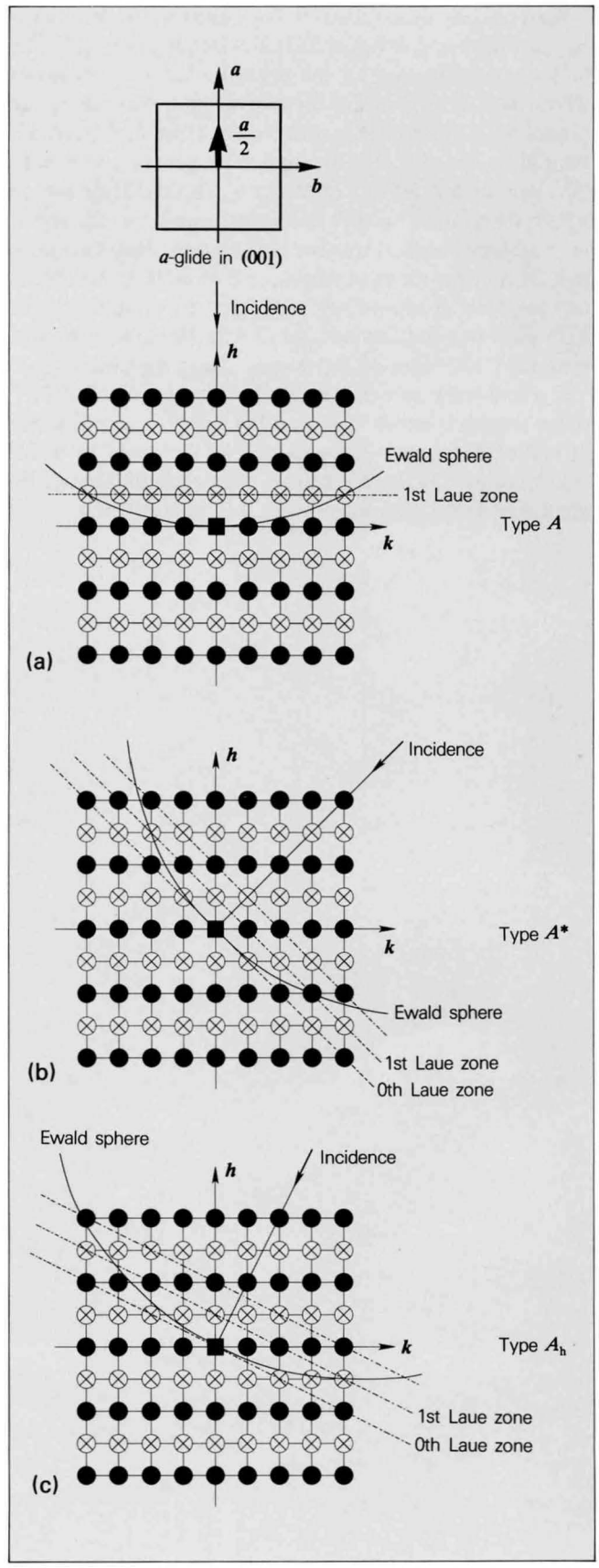

FeS_2 [100]

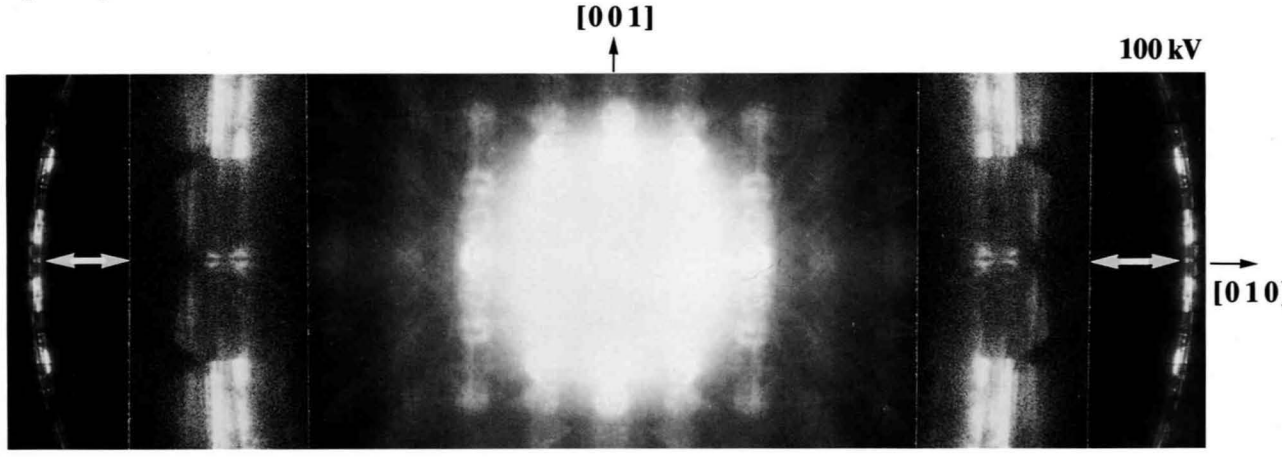

Type *A* GM line due to an *a*-glide in the (001) plane.

FeS_2 [110]

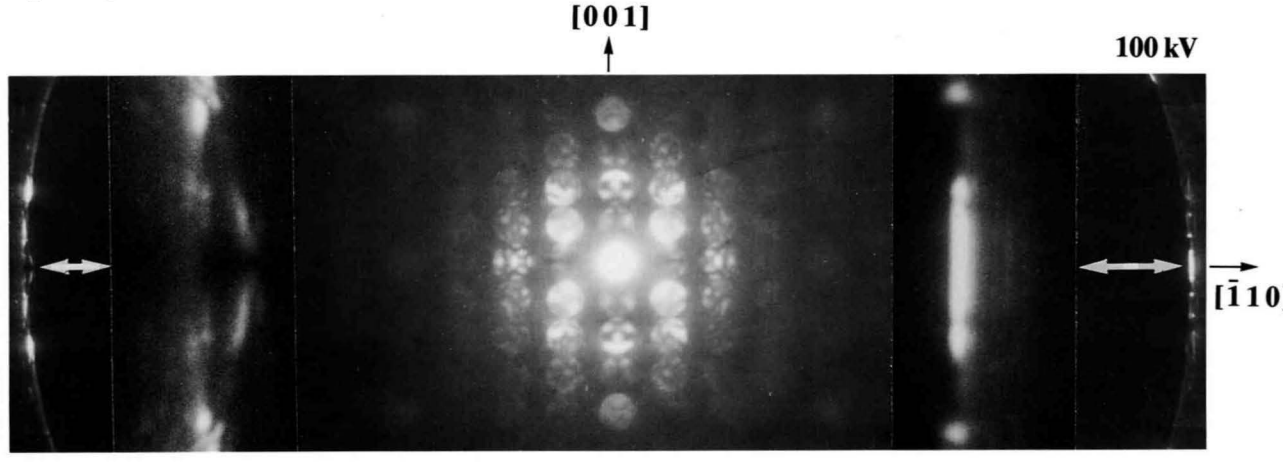

Type *A** GM line due to an *a*-glide in the (001) plane.

Point group *m*3

Incident beam direction / Space group	[100]		[110]		[*uv*0]	
205 $Pa3$ $P2_1/a\bar{3}$	$h0l_o$ c_2 h_ok0 a_3	*A*	h_ok0 a_3	*A**	h_ok0 a	A_h

1

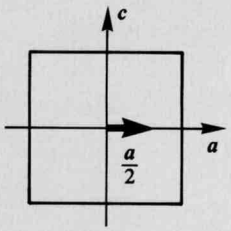

a-glide in (010)

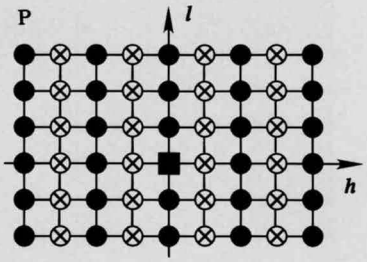

2

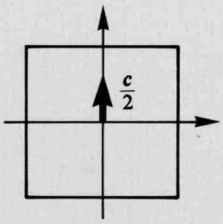

c-glide in (010)

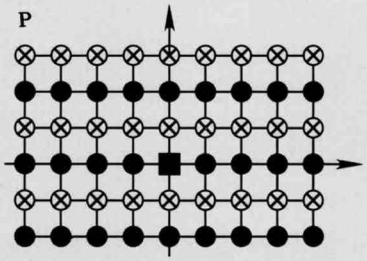

3

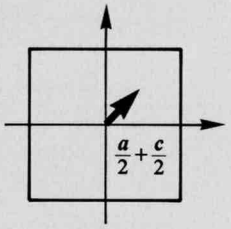

n-glide in (010)

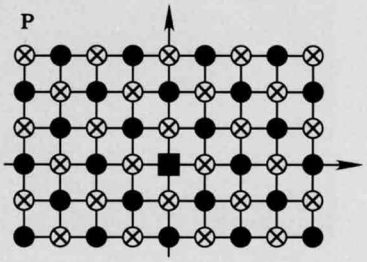

4

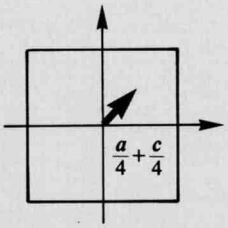

d-glide in (010)

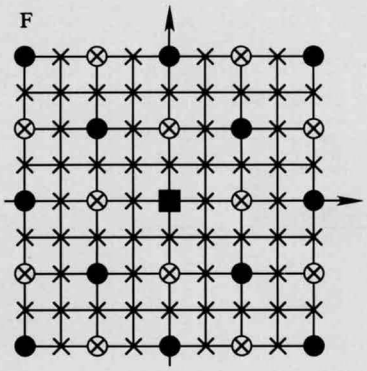

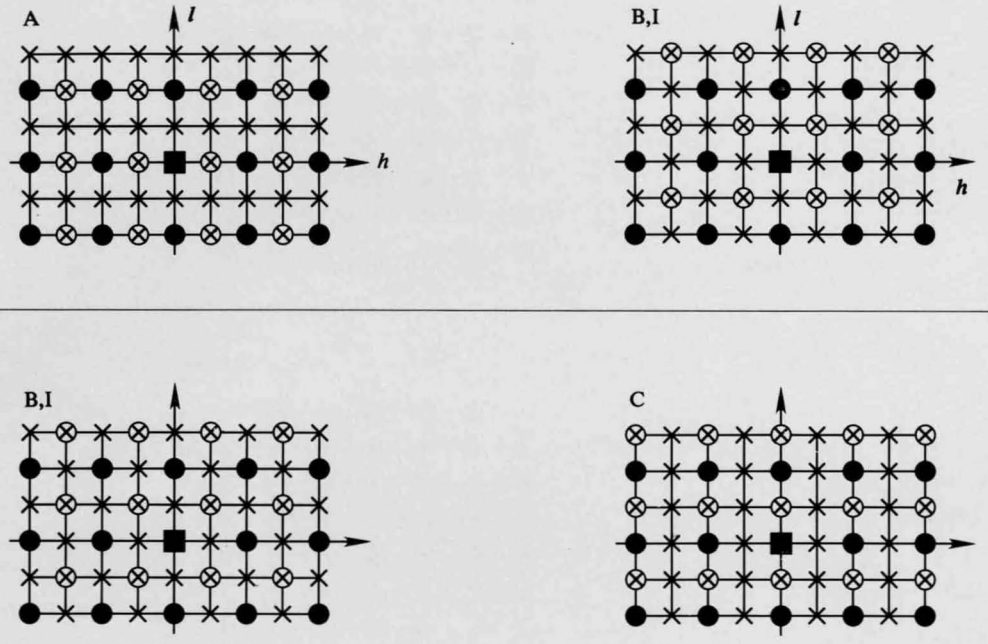

P: Primitive lattice
A, **B** and **C**: **A**, **B** and **C** centered lattices, respectively
I: Body centered lattice
F: Face centered lattice
●: Allowed reflections
×: Kinematically and dynamically forbidden reflections due to lattice types
⊗: Kinematically forbidden but dynamically allowed reflections due to glide planes

5

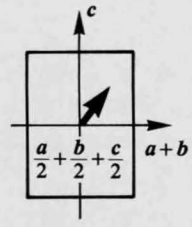

n-glide in $(1\bar{1}0)$

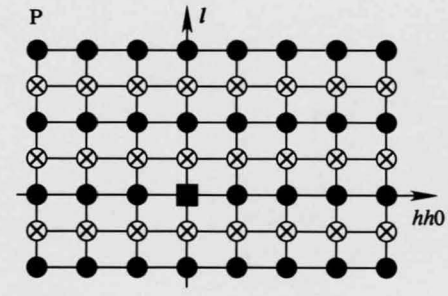

6

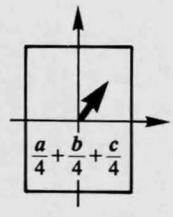

d-glide in $(1\bar{1}0)$

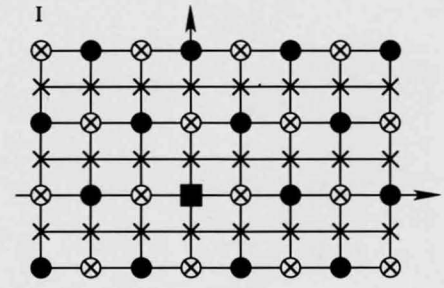

7a

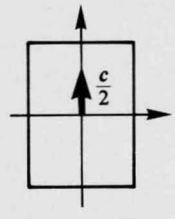

c-glide in $(1\bar{1}0)$

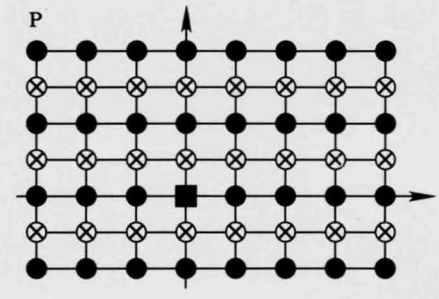

7b

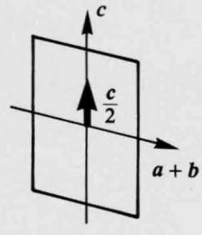

c-glide in $(1\bar{1}0)$

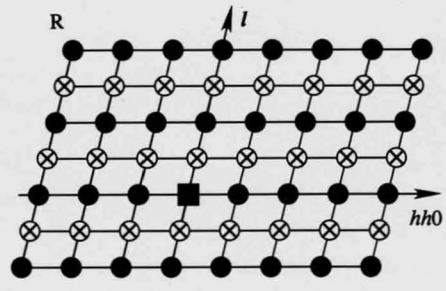

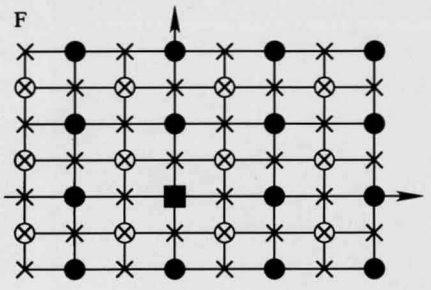

P: Primitive lattice
A, B and C: A, B and C centered lattices, respectively
I : Body centered lattice
F: Face centered lattice
R: Rhombohedral lattice
●: Allowed reflections
×: Kinematically and dynamically forbidden reflections due to lattice types
⊗: Kinematically forbidden but dynamically allowed reflections due to glide planes

Figures on pages 54 to 57 show various vertical glide planes and schematically depict the arrangements of kinematically allowed (black circles), kinematically and dynamically forbidden (crosses), and kinematically forbidden but dynamically allowed (circled crosses) reflections for possible combinations of lattice types and glide planes. When the Ewald sphere intersects HOLZ reflections designated with circled crosses, GM lines appear in the reflections.

FeS_2 [100] — Changes of excitation condition

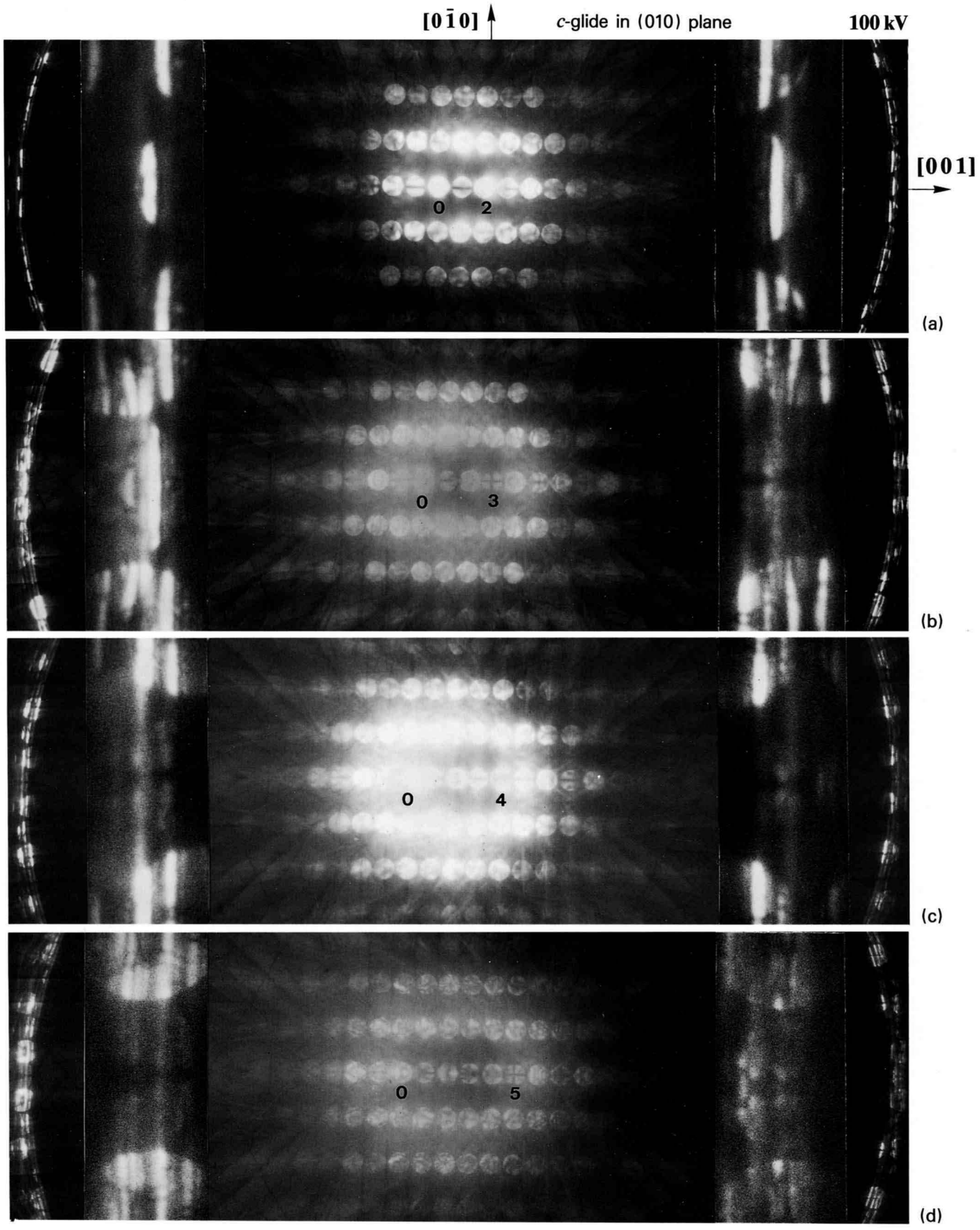

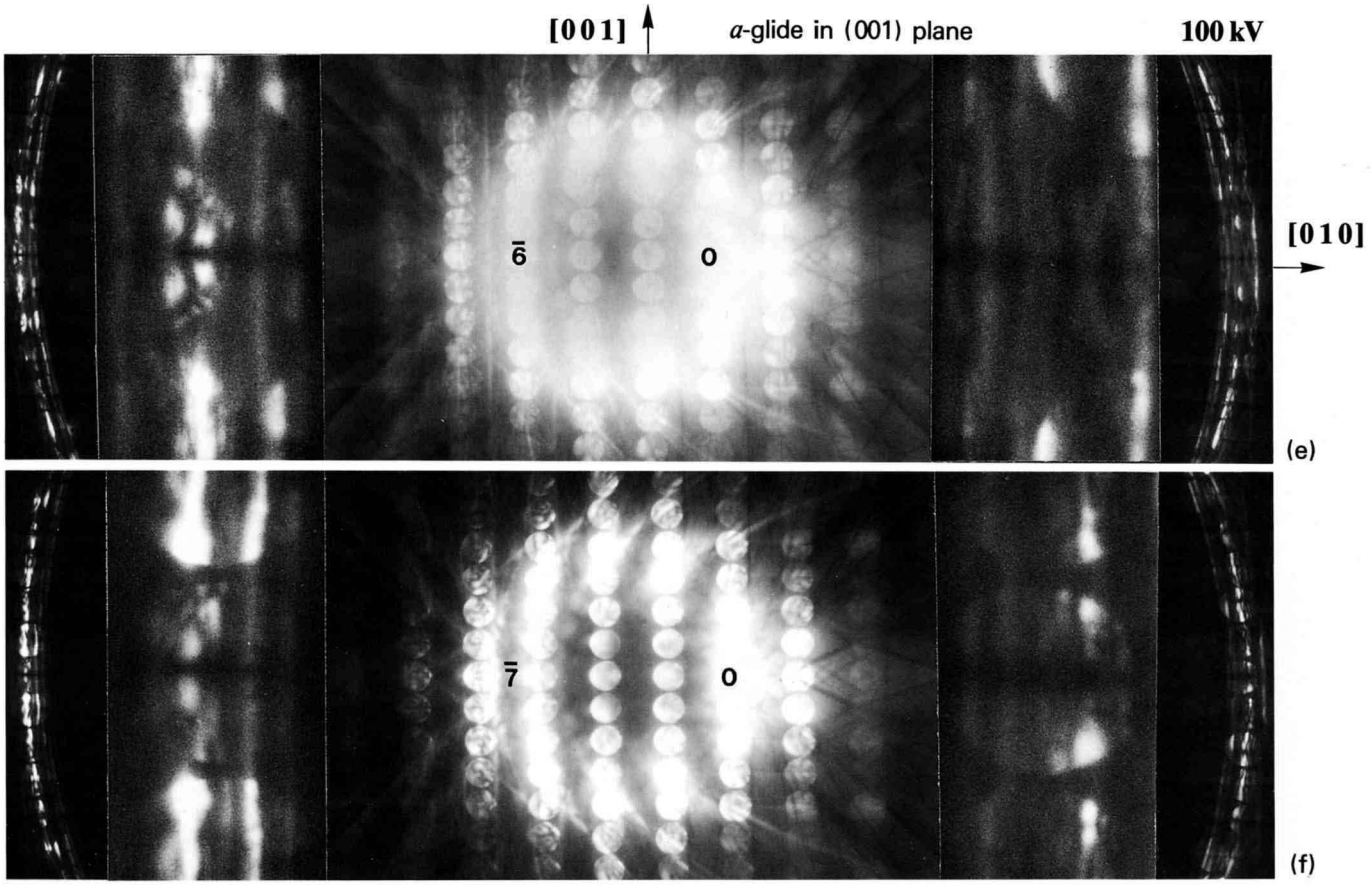

Table (a)

	Exactly excited ZOLZ reflection	GM line in $10l$ HOLZ reflection	
		left	right
(a)	002	no	no
(b)	003	no	yes
(c)	004	yes	yes
(d)	005	yes	no

Table (b)

	Exactly excited ZOLZ reflection	GM line in $1k0$ HOLZ reflection	
		left	right
(e)	$0\bar{6}0$	yes	yes
(f)	$0\bar{7}0$	yes	yes

Incident beam direction / Space group	[100]	
205 $Pa3$ $P2_1/a\bar{3}$	$h0l_o$ c_2 h_ok0 a_3	A

A series of Photos (a) to (d) and two Photos (e) and (f) show the variation of the appearance of GM lines with changes of the excitation condition. The results are summarized in Tables (a) and (b) for the former and the latter photos. The words "left" and "right" indicate left and right HOLZ reflections. The word "yes" expresses the presence of a GM line, and "no" the absence of a GM line. These results can be understood with the help of the figures below.

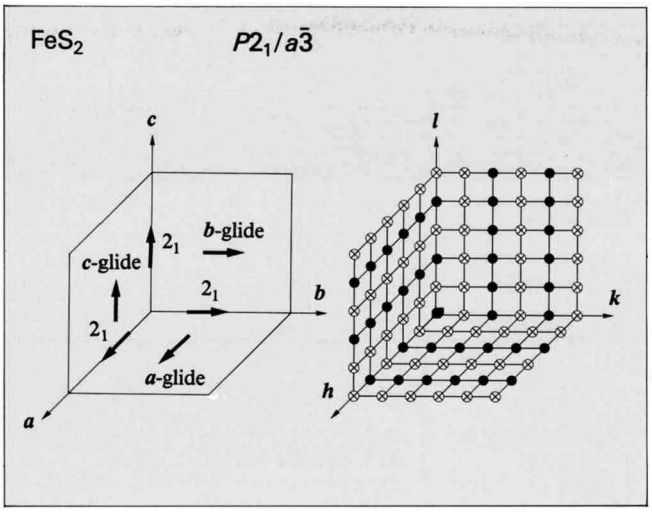

$MgAl_2O_4$ [100]

ZAP ↑ **[001]** *d*-glide in (001) plane

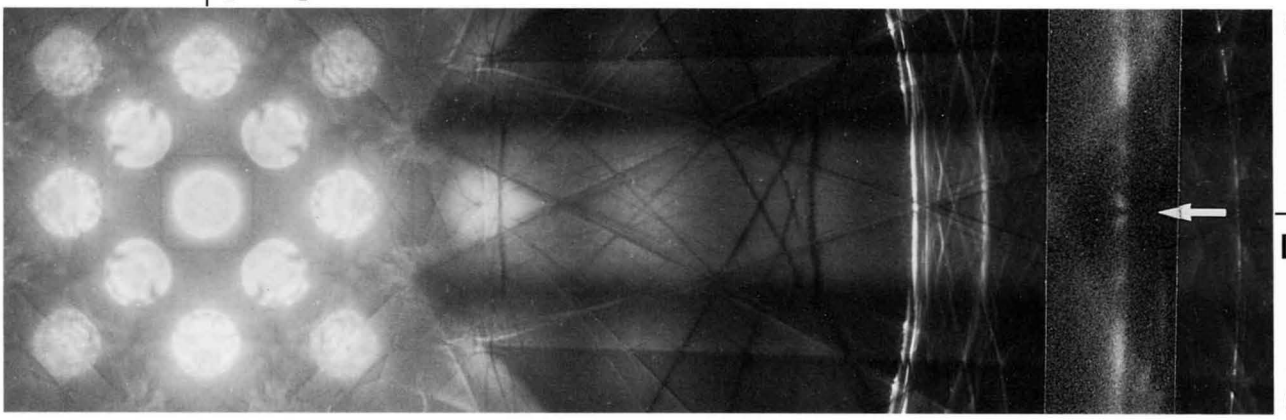

80 kV

[010]

(a)

$MgAl_2O_4$ [110]

$\bar{5}50$ excitation ↑ **[001]** *d*-glide in (001) plane

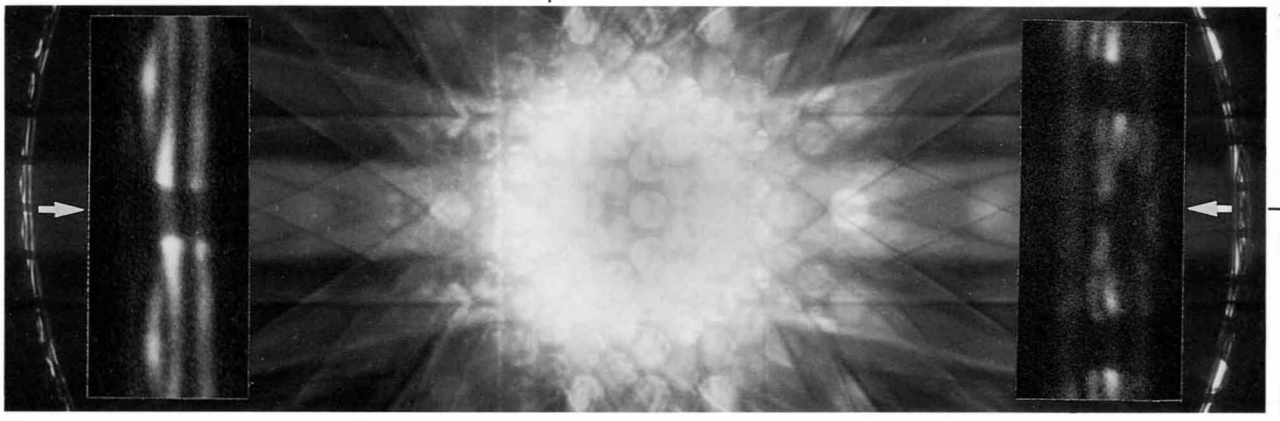

100 kV

[$\bar{1}$10]

(b)

$\bar{6}60$ excitation

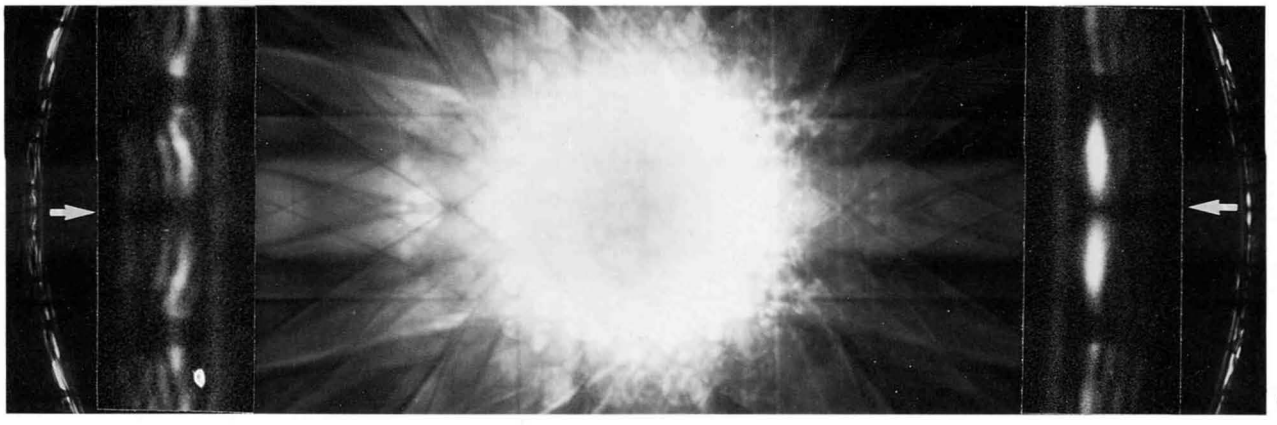

(c)

Point group $m3m$

Incident beam direction / Space group	[100]		[110]		[uv0]		[uuw]	
227 $Fd3m$ $F4_1/d\bar{3}2/m$	h_e0l_e $h_e+l_e=4n+2$ d_2 h_ek_e0 $h_e+k_e=4n+2$ d_3	A	h_ek_e0 $h_e+k_e=4n+2$ d_3	A	h_ek_e0 $h_e+k_e=4n+2$ d	A_h		

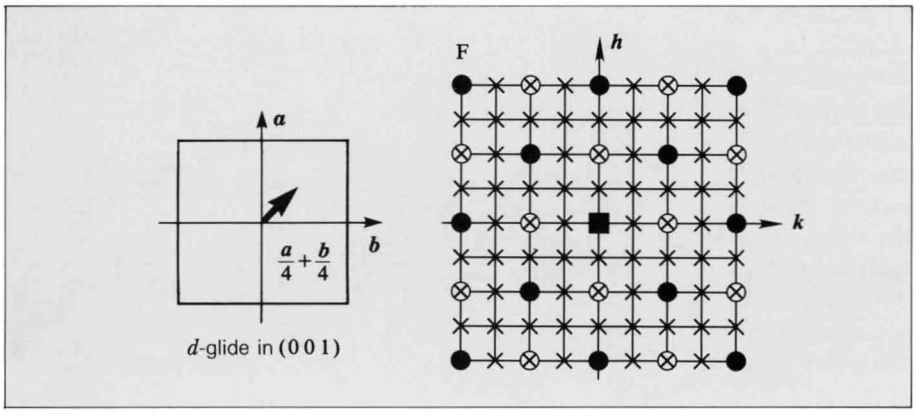
a
b
$\frac{a}{4}+\frac{b}{4}$
d-glide in (0 0 1)
F
h
k

Space-Group Determinations

$La_2CuO_{4-\delta}$

$La_{2-x}M_xCuO_{4-\delta}$ (M = Ba, Sr and Ca) is a 40 K class superconductor. Many space groups were proposed for this system: *Fmmm*, *Fmm*2, *F*222 and *Cmmm* (or *C*222) for $La_{2-x}Sr_xCuO_{4-\delta}$, *Cmca*, *Pccn* and *Pccm* for $La_{2-x}Ba_xCuO_{4-\delta}$ and *Cmca*, *Pccn* and *Cmmm* for $La_2CuO_{4-\delta}$. These controversial results may be attributed to specimen preparation, doping effects and experimental accuracy.

Figures (a) and (b) show intensity profile fits obtained by the Rietveld method for the neutron powder diffraction data from as-grown $La_2CuO_{4-\delta}$. The fits to the experimental data are excellent but show no difference for the two space groups, *Cmca* (a) and *Pccn* (b). Therefore, the space groups could not be distinguished by the powder diffraction data.

Photograph (a) shows typical twin domains of this substance. Photographs (b) to (e) show electron diffraction patterns taken at four different electron incidences. The schematic diagrams corresponding to the patterns are given in Figs. (c) to (e). The large and small black circles indicate the observed reflections. From the extinction rules for the reflections, a possible lattice type is the B-centered type. The forbidden reflections due to this lattice type are denoted by crosses. The other reflections indicated by circled crosses must vanish due to screw axes and/or glide planes. The 010 and $0\bar{1}0$ reflections are not seen in Photo (b) but seen in Photo (c). This fact means that the reflections observed in Photo (c) occurred owing to Umweganregung. From these results, we obtained a space group *Bmab*(= *Cmca*). However, we have determined the space group unambiguously by revealing the symmetry elements of the crystal using CBED.

Photograph (f) shows a CBED pattern taken at the [001] incidence, Photo (g) being the central part of Photo (f). The whole pattern has a symmetry 2*mm*. This indicates that the crystal has two mirror symmetries perpendicular to each other and that the point group is *mmm* or *mm*2. To investigate whether the third mirror plane perpendicular to these two mirror planes exists or not, a CBED pattern was taken at the [100] incidence (Photos (h) and (i)). Two mirror planes are seen, one of which being the third one. As a result, the point group was determined to be *mmm*.

Photograph (j) was taken by tilting the incident beam in the ***b**** direction from the [100] zone axis to clearly observe the GM lines. A_2 GM lines are seen in the 010 and $0\bar{5}0$ reflections. Reference to Table (a) for ZOLZ GM lines clarified that the possible space groups are *Bmab* and *Bmmb*. In Photo (h), type *A* GM lines are seen in the 10*l* and $10\bar{l}$ HOLZ reflections. Reference to Table (b) for HOLZ GM lines allowed determining the space group to be *Bmab*, which is equivalent to *Cmca* in the standard notation. For confirmation, GM lines were observed at two other incidences. That is, a B_2 GM line was observed in the 010 reflection at a [*u*0*w*] incidence (Photo (k)) and A_2 GM lines in the $2\bar{1}0$ and $\bar{2}10$ reflections at the [120] incidence (Photo (l)). These observations show a good agreement with the predictions in Table (a).

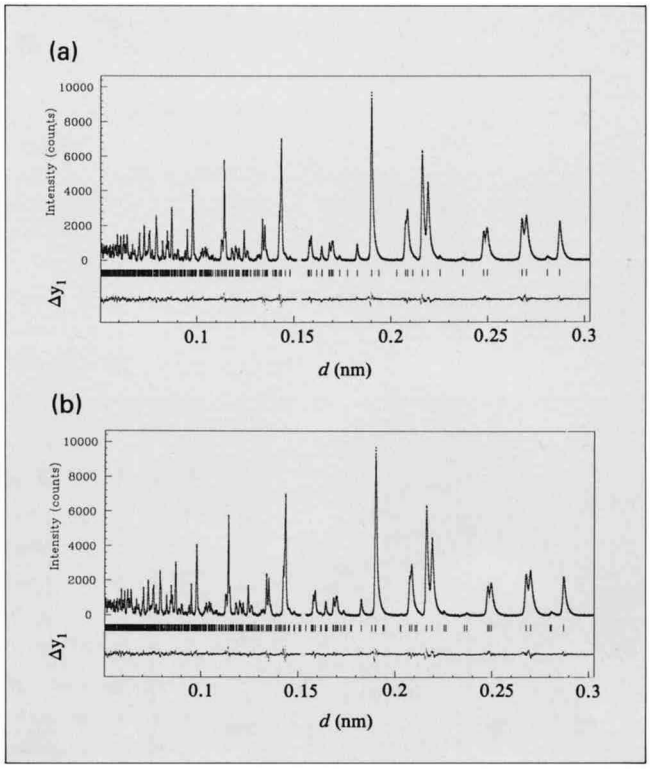

References

[a] M. Tanaka, K. Tsuda, K. Yamada, Y. Endoh, Y. Hidaka, M. Oda, M. Suzuki and T. Murakami: *Jpn. J. Appl. Phys.*, **26** (1987) L1502.

[b] K. Yamada, E. Kudo, Y. Endoh, K. Tsuda, M. Tanaka, K. Kokusho, H. Asano, F. Izumi, M. Oda, Y. Hidaka, M. Suzuki and T. Murakami: *Jpn. J. Appl. Phys.*, in the press.

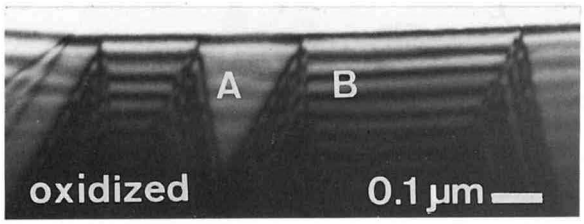

(a)

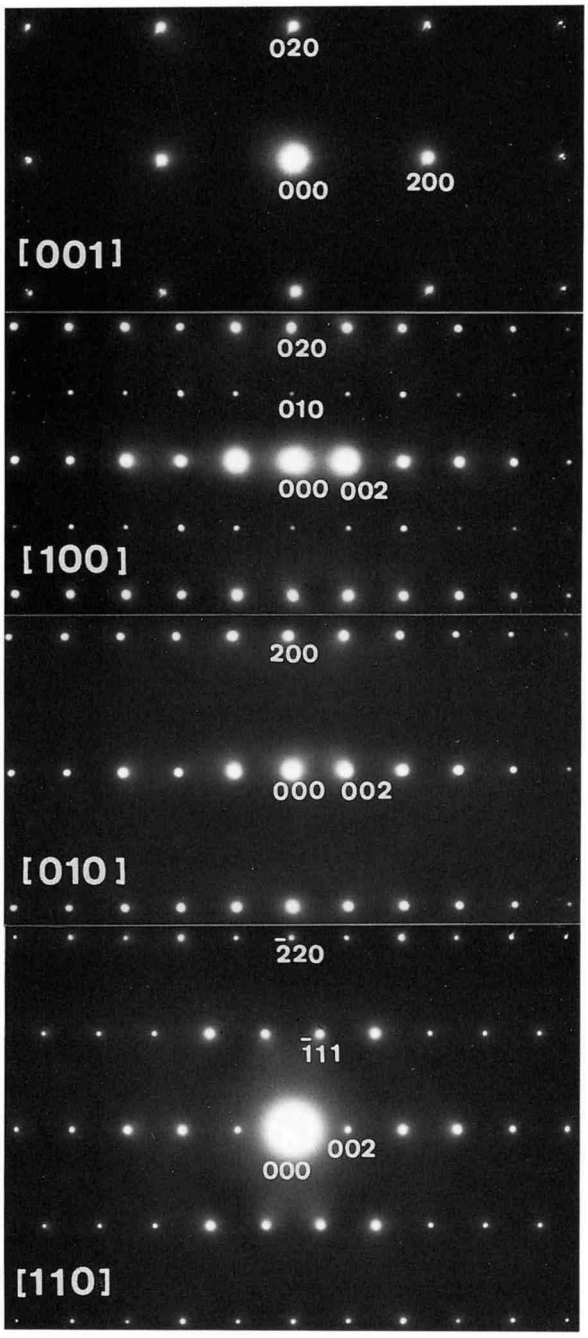

(b)

(c)

(d)

(e)

(c) [0 0 1]

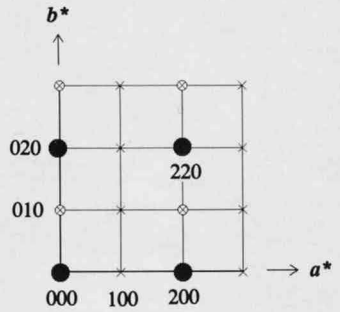

(d) [1 0 0]

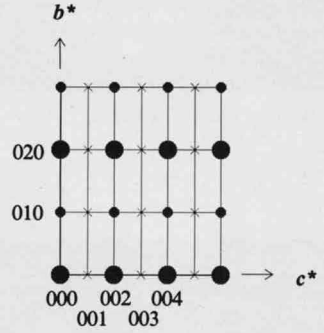

(e) [0 1 0]

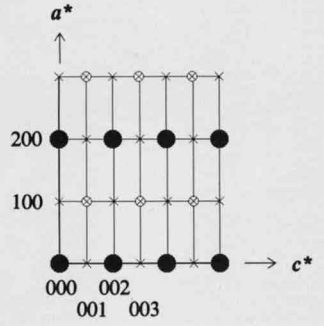

● • Observed
× Forbidden due to B-centered lattice
⊗ Forbidden due to glide plane and/or 2_1 screw axis

$La_2CuO_{4-\delta}$ 80kV

[001]

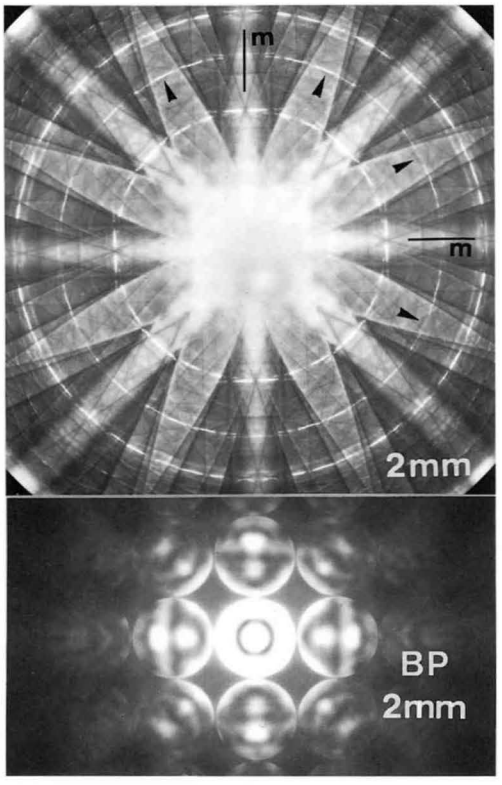

(f)

(g)

Point group: *mmm* or *mm*2

[100]

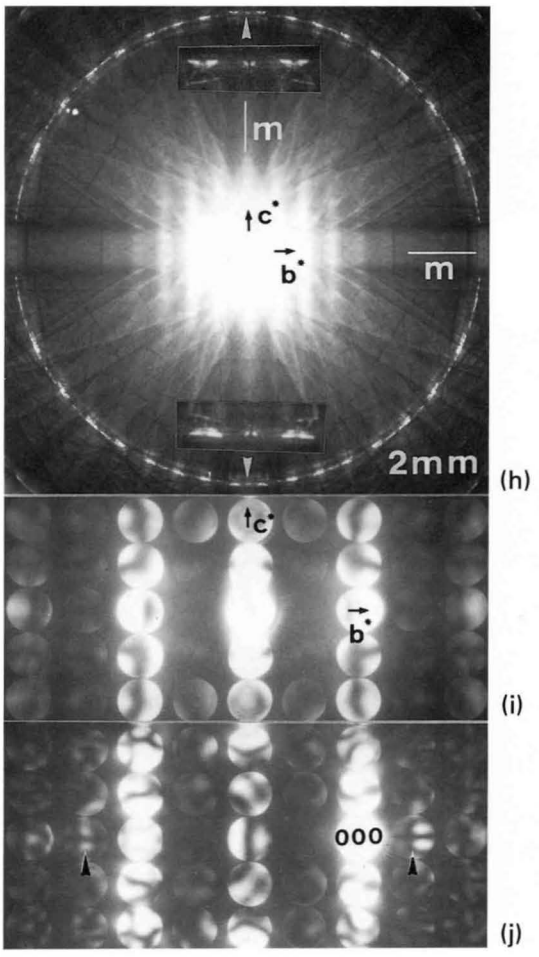

(h)

(i)

(j)

A_2 GM lines in the 010 and $0\bar{5}0$ reflections in Photo (j) indicate the presence of a 2_1 screw axis parallel to the [010] axis and/or that of a *b*-glide plane in the (001) plane. A type *A* GM line in the $10l$ and $10\bar{l}$ reflections in Photo (h) indicate the presence of an *a*- or a *c*-glide plane in the (010) plane.

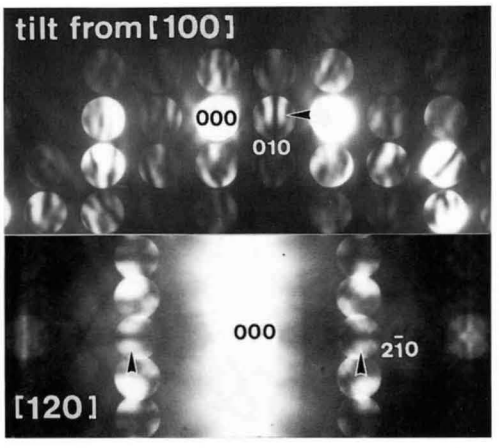

(k)

(l)

A B_2 GM line in the 010 reflection in Photo (k) indicates the presence of a 2_1 screw axis parallel to the [010] axis. A_2 GM lines in the $2\bar{1}0$ and $\bar{2}10$ reflections indicate the presence of a *b*-glide plane in the (001) plane.

Table (a) ZOLZ GM line table

Incident beam direction / Space group	[100]		[010]		[001]		[$uv0$]		[$0vw$]		[$u0w$]	
63 $B2/m2_1/m2/b$	$0k_o0$ $b, 2_1$	A_2 B_2 A_3 B_3			$0k_o0$ 2_1	B_3	h_ek_o0 b	A_2 B_2 A_3			$0k_o0$ 2_1	A_2 B_2 B_3
64 $B2/m2_1/a2/b$	$0k_o0$ $b, 2_1$	A_2 B_2 A_3 B_3			$0k_o0$ 2_1	B_3	h_ek_o0 b	A_2 B_2 A_3			h_o0l_o a $0k_o0$ 2_1	A_2 B_2 A_3 A_2 B_2 B_3
65 $B2/m2/m2/m$												
66 $B2/b2/m2/b$	$0k_o0$ b_2	A_3			$0k_o0$ b_1	A_3	h_ek_o0 b_2	A_2 B_2 A_3	$0k_ol_e$ b_1	A_2 B_2 A_3		
67 $B2/m2/a2/m$											h_o0l_o a	A_2 B_2 A_3
68 $B2/b2/a2/b$	$0k_o0$ b_2	A_3			$0k_o0$ b_1	A_3	h_ek_o0 b_2	A_2 B_2 A_3	$0k_ol_e$ b_1	A_2 B_2 A_3	h_o0l_o a	A_2 B_2 A_3

Table (b) HOLZ GM line table

Incident beam direction / Space group	[100]		[010]		[001]		[$uv0$]		[$0vw$]		[$u0w$]	
63 $B2/m2_1/m2/b$	h_ek_o0 b	A	h_ek_o0 b	A			h_ek_o0 b	A_h				
64 $B2/m2_1/a2/b$	h_ek_o0 b h_o0l_o a	A	h_ek_o0 b	A	h_o0l_o a	A	h_ek_o0 b	A_h			h_o0l_o a	A_h
65 $B2/m2/m2/m$												
66 $B2/b2/m2/b$	h_ek_o0 b_{23}	A	$0k_ol_e$ b_{11} h_ek_o0 b_{23}	A	$0k_ol_e$ b_{11}	A	h_ek_o0 b_{23}	A_h	$0k_ol_e$ b_{11}	A_h		
67 $B2/m2/a2/m$	h_o0l_o a	A			h_o0l_o a	A					h_o0l_o a	A_h
68 $B2/b2/a2/b$	h_ek_o0 b_{23} h_o0l_o a	A	$0k_ol_e$ b_{11} h_ek_o0 b_{23}	A	h_o0l_o a $0k_ol_e$ b_{11}	A	h_ek_o0 b_{23}	A_h	$0k_ol_e$ b_{11}	A_h	h_o0l_o a	A_h

These tables were rewritten to the B-centered lattice instead for the C-centered one which is used as the standard notation in the International Tables for X-ray Crystallography and in an appendix in the present book.

Fe_3O_4

Magnetite (Fe_3O_4) is of the spinel structure belonging to a space group *Fd*3*m* at room temperature. Verwey *et al.* reported that Fe_3O_4 underwent a phase transition at about $-150°C$, accompanied by the ordering of ions Fe^{+2} and Fe^{+3} [a]. This result had been believed to be correct until satellite reflections were found by X-ray and electron diffraction. Since then, a large number of studies on the phase transformation has been reported. The space group of the low temperature phase appears to have been established by Iizumi *et al.* as *Cc* [b]. An observation of the magnetoelectric effect [c], [d], however, implied that the space group must be *P*1, although the atomic displacements which violate the *c*-glide plane have been considered to be extremely small. Using CBED, we examined the space group of the low temperature phase. The crystallographic indexing was carried out using a monoclinic system, as was done by Iizumi *et al* [b].

Photograph (a) shows a $[001]_m([001]_c)$ zone-axis CBED pattern taken at the Liq.N_2 temperature. Its central part was enlarged to make clear the details of the symmetries in the weak reflection disks (Photo (b)). A mirror symmetry perpendicular to the $[010]_m$ exists in the whole pattern. Photograph (c) shows a $[110]_m([100]_c)$ zone axis CBED pattern. Seven weak reflections are seen between two strong reflections along the $[001]_m$ direction. The strong 008_m reflection is indexed as 004_c, indicating a cell doubling in the $[001]_m$ direction. A close inspection revealed that there is no symmetry in the pattern (c). Note especially that there is no mirror symmetry perpendicular to the $[001]_m$. These results indicate the point group to be *m*.

The diffraction pattern (d) was taken at the $[001]_m$ incidence, the pattern (e) being the central part of (d). It is seen that the reflections of $h+k=2n+1$ are forbidden (e). Hence, the lattice type is C-centered. As a result, the possible space groups are *Cm* and *Cc*. It is noted that there are two HOLZ rings in (d). The inner ring is characteristic of the low temperature phase and indicates again that the lattice parameter *c* is twice that at room temperature.

Photograph (f) shows CBED patterns taken with the $[100]_m$ incidence at different accelerating voltages. Clear A_2 GM lines are seen in the $00l(l=\text{odd})$ reflections of all the photographs. It is noted that the photographs needed an about 3-minute exposure even using our JEM-100CX/FEG. The result proved the existence of a *c*-glide plane. There was no indication that the *c*-glide plane was lost. Photograph (g) is a $[100]_m$ CBED pattern covering a wide angular range. GM lines due to the *c*-glide plane are seen in the HOLZ reflections of $2\,0\,\overline{43}_m$ and $2\,0\,43_m$. Thus, the space group of the low temperature phase was unambiguously determined to be *Cc*, supporting the result of Iizumi *et al.* The CBED patterns never showed a possibility of triclinic symmetry.

The specimens were supplied by Mr. S. Todo of the Institute for Solid State Physics, University of Tokyo.

References

[a] E.J. Verwey, P.W. Haayman and F.C. Romeijn: *J. Chem. Phys.*, **15** (1947) 181.

[b] M. Iizumi, T.F. Koetzle, G. Shirane, S. Chikazumi, M. Matsui and S. Todo: *Acta Cryst.*, **B38** (1982) 2121.

[c] G.T. Rado and J.M. Ferrari: *Phys. Rev.*, **B15** (1977) 290.

[d] K. Shiratori, E. Kita, G. Kaji, A. Tasaki, S. Kimura, I. Shindo and K. Kohn: *J. Phys. Soc. Jpn.*, **47** (1979) 1779.

$[0\,0\,1]_m$ $-186°C$ 60 kV

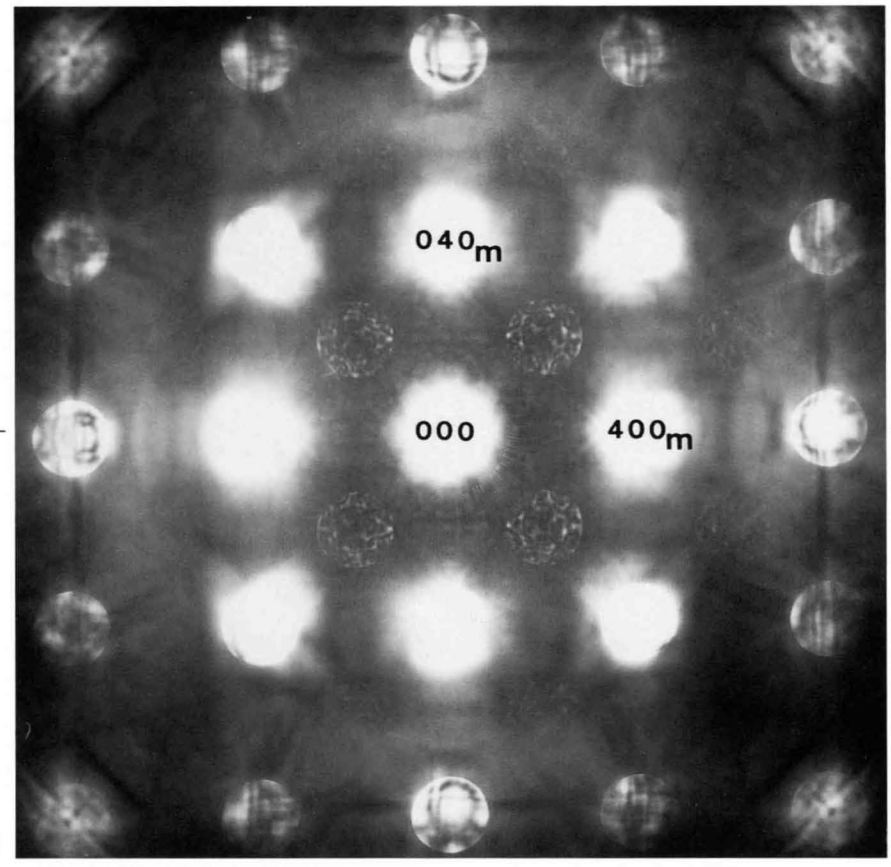

(a)

ZAP showing a mirror symmetry.

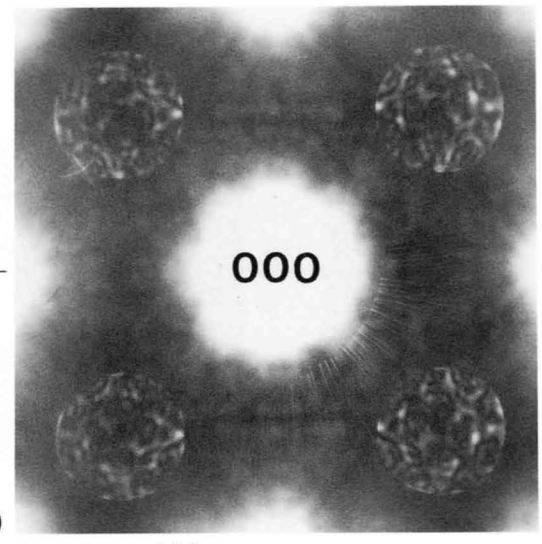

(b)

Central part of (a).

Fe_3O_4 $[1\,1\,0]_m$ −186°C 60 kV

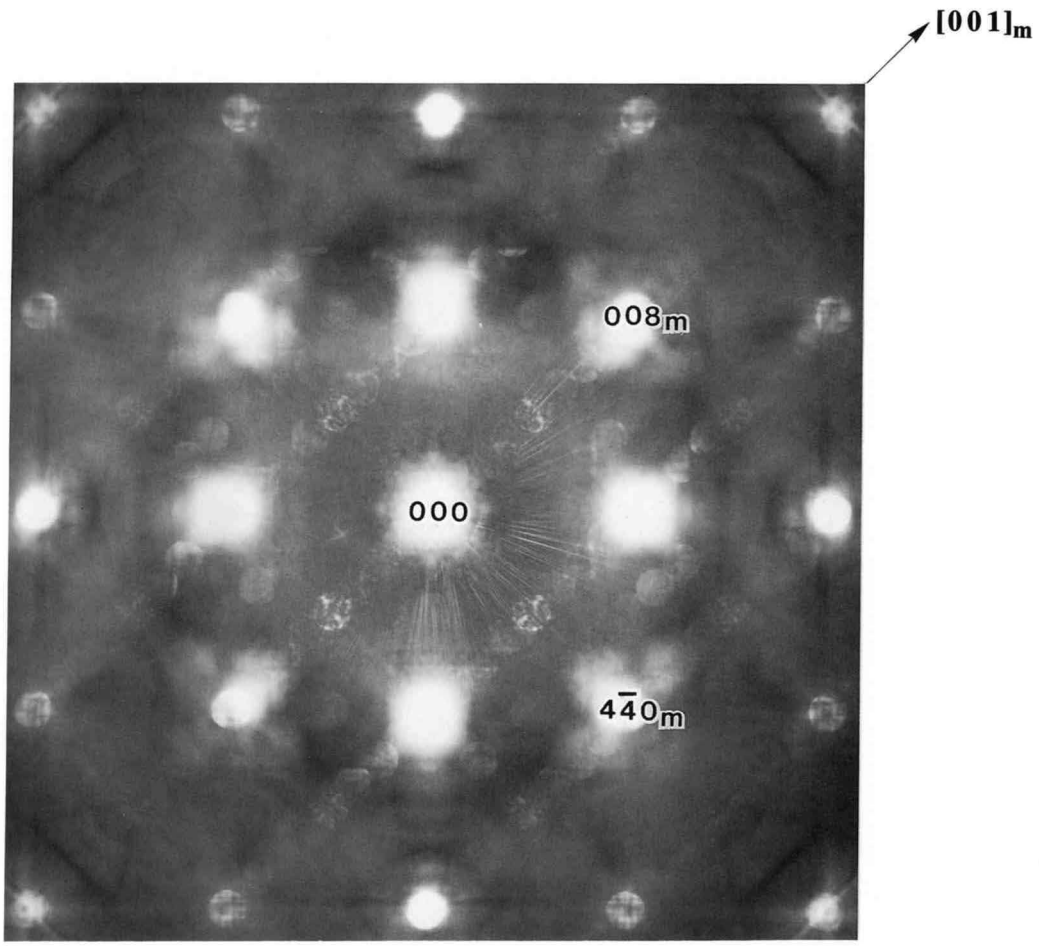

(c)

ZAP showing symmetry 1.

$[0\,0\,1]_m$

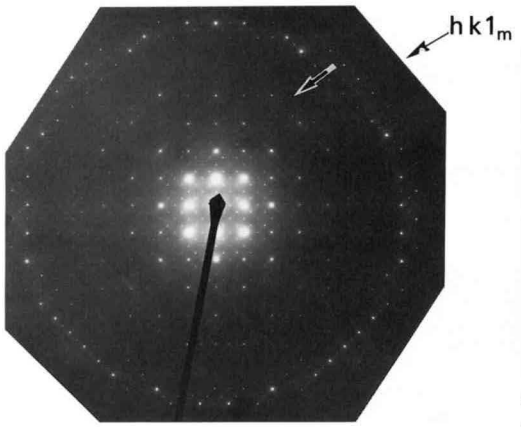

(d)

The inner weak HOLZ ring is characteristic of the low temperature phase.

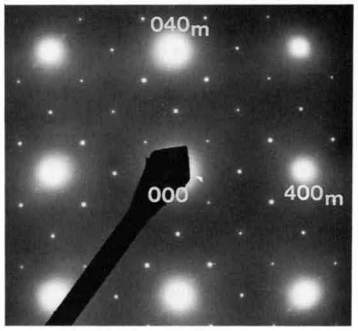

(e)

Central part of (d), indicating the crystal to be of a C-centered lattice.

$[100]_m$ $-186°C$

(f)

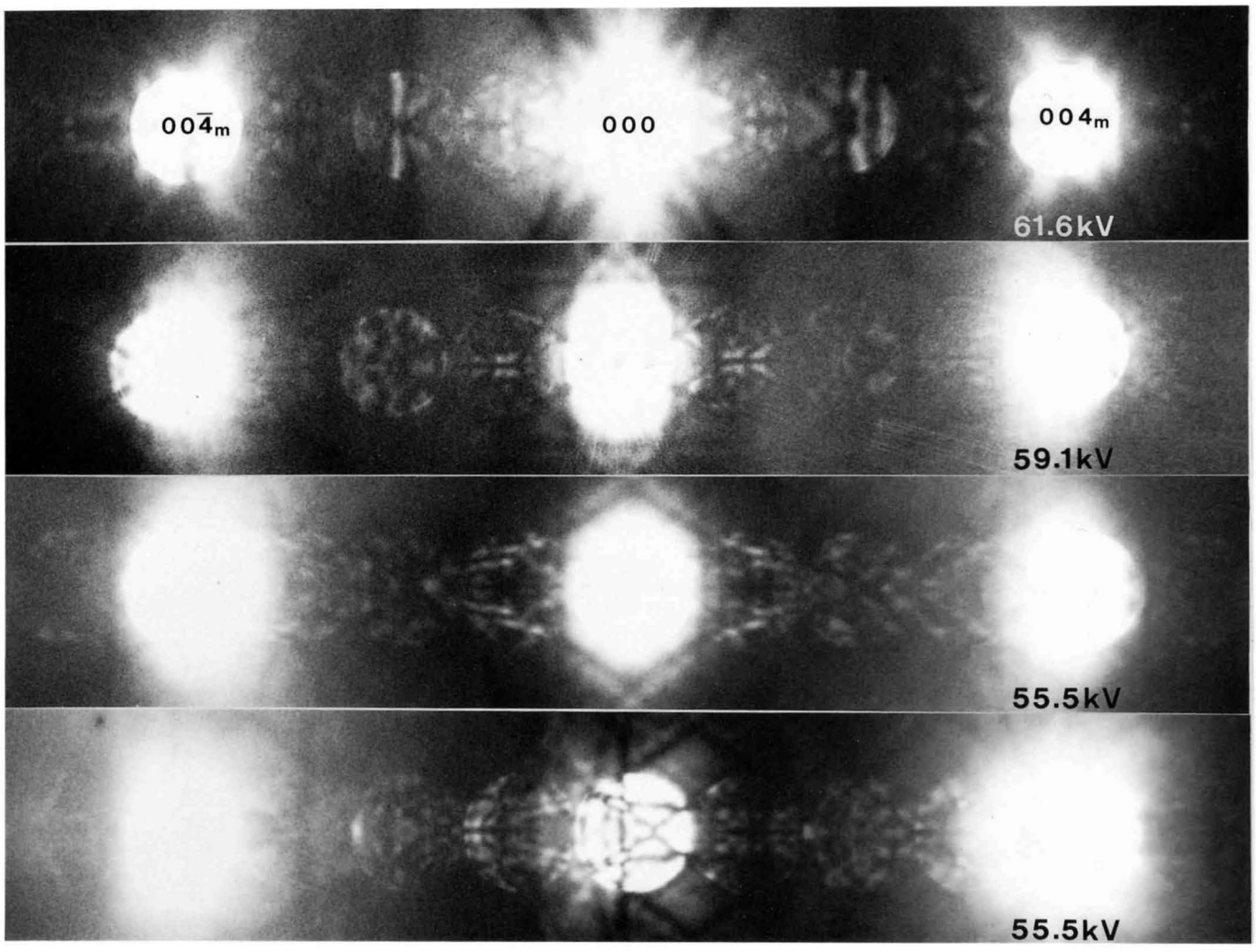

Odd order reflections are characteristic of the low temperature phase and show A_2 GM lines due to the *c*-glide plane. The upper three patterns were taken at the zone-axis incidence and the lowest pattern at the 001_m excitation.

Point group *m*

Incident beam direction / Space group	$[u0w]$	
6 *Pm*		
7 *Pc*	$h0l_o$ *c*	A_2 B_2 A_3
8 *Cm*		
9 *Cc*	h_e0l_o *c*	A_2 B_2 A_3

Fe_3O_4 $[100]_m$ −186°C

55.5kV

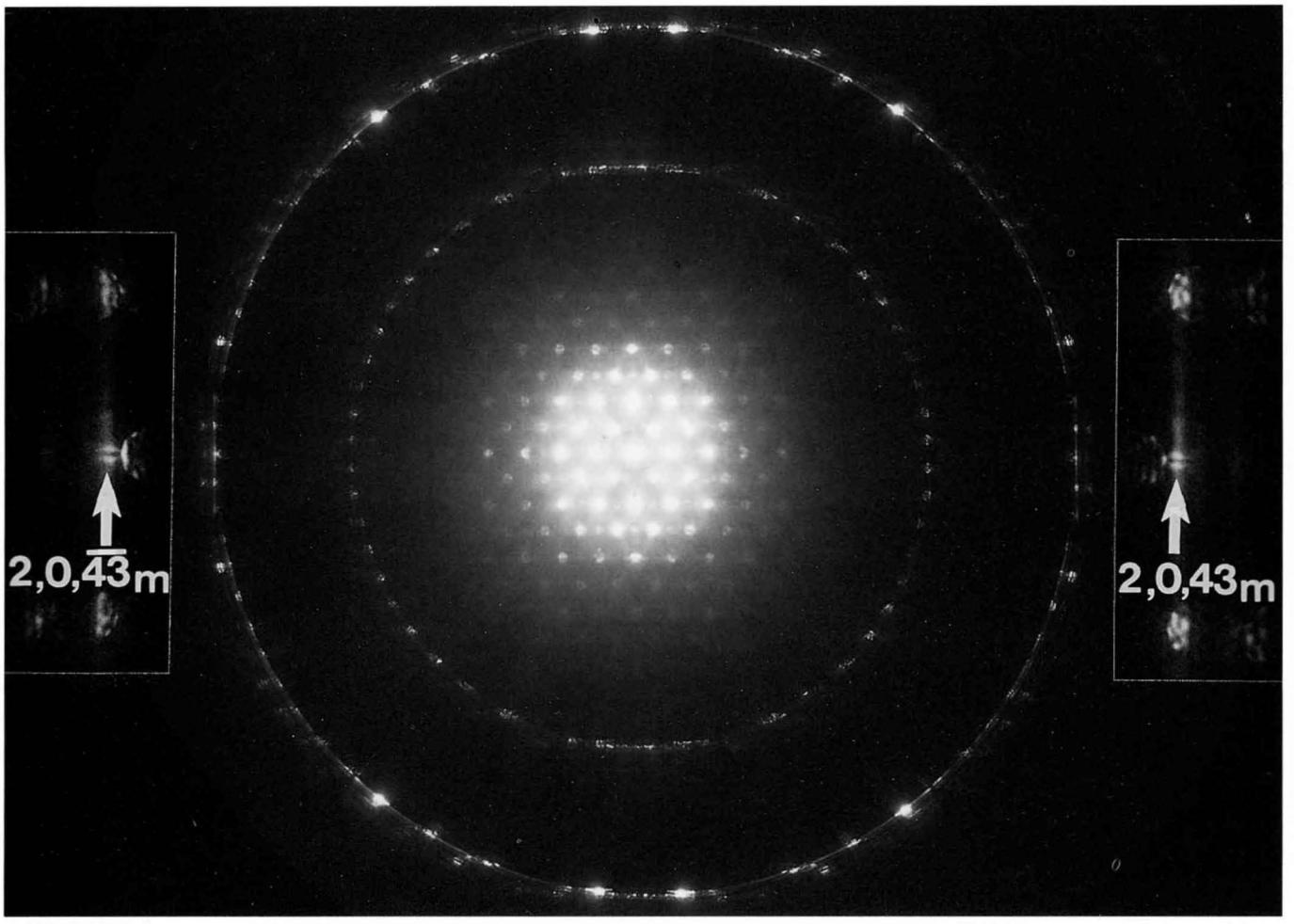

(g)

Two HOLZ reflections show a type A_h GM line due to the *c*-glide plane. The GM lines look like type *A*, owing to the *a* axis is approximately perpendicular to the *c* axis.

Point group *m*

Incident beam direction / Space group	$[u0w]$	
6 *Pm*		
7 *Pc*	$h0l_o$ *c*	A_h
8 *Cm*		
9 *Cc*	h_e0l_o *c*	A_h

Incommensurate Phases

$Sr_2Nb_2O_7$

Many materials of the $A_2B_2O_7$ family undergo phase transformations from the space group *Cmcm* to $Cmc2_1$ to $P2_1$ with decreasing temperature. The phase transformation from *Cmcm* to $Cmc2_1$ has been reported to occur due to the rotation of the oxygen octahedra about the *a* axis with a slight deformation of the octahedra. The transformation from $Cmc2_1$ to $P2_1$ has been considered to be caused by the rotation of the octahedra about the *b* axis. An incommensurate phase appears, for example, in $La_2Ti_2O_7$ [a] between the phase with the space group $Cmc2_1$ and that with $P2_1$. $Sr_2Nb_2O_7$ transforms from the phase with $Cmc2_1$ into an incommensurate phase, but does not transform into the phase with $P2_1$. No discommensuration has been observed even at lower temperatures in the incommensurate phase. It was reported by Yamamoto [b] and Yamamoto & Ishizuka [c] that the modulated structures in this phase can be explained by the rotation of the oxygen octahedra about the *b* axis. We reexamined the symmetries of the phase using CBED.

A diffraction pattern (a) shows zig-zag arrays of the incommensurate reflections in the $[0\bar{1}1]$ direction. The indexing of the observed reflections was carried out using the indices of the phase with $Cmc2_1$. CBED patterns (b) and (c) were taken at the [100] and [201] incidences. Since the pattern (b) does not have incommensurate reflections, its symmetries are produced by the average structure. The $00l$ (l = odd) reflections show A_2 GM lines, and the HOLZ ring of this pattern (not seen here) showed a mirror symmetry perpendicular to the *b* axis. These indicate the existence of a *c*-glide plane parallel to the (010) plane.

The incommensurate reflections in the CBED pattern (c) show a mirror symmetry perpendicular to the *b* axis. It is unfortunately not possible to know directly from GM lines whether the modulated structure preserves the *c*-glide plane, because no incommensurate reflections appear on the $[\bar{1}02]$ axis. If the modulation does not violate the *c*-glide plane, the glide plane gives rise to a mirror symmetry, which is observed in Photo (c). Reference to the structure of the high temperature phase with $Cmc2_1$ (see the figure) allows concluding that the modulation does not change the *c*-glide symmetry into a mirror symmetry. Therefore, the *c*-glide plane should still be preserved in the incommensurate phase.

Photograph (d) shows a [010] CBED pattern, its central part being enlarged in Photo (e). The strong fundamental reflections due to the average structure have a mirror symmetry perpendicular to the *a* axis, presumably due to little interaction between the fundamental and the incommensurate reflections. The incommensurate reflections do not have a mirror symmetry. Hence, the modurated structure violates the (100) mirror plane in the high temperature phase. If the average structure has a 2_1 screw axis parallel to the *c* axis, A_2 GM lines appear in the 001 and $00\bar{1}$ reflections. No GM lines were observed in these reflections. A plausible explanation of this fact is that the modulated structure does not have the 2_1 screw axis and violates the GM lines due to a strong dynamical diffraction effect between the weak fundamental reflections and the neighbouring incommensurate reflections.

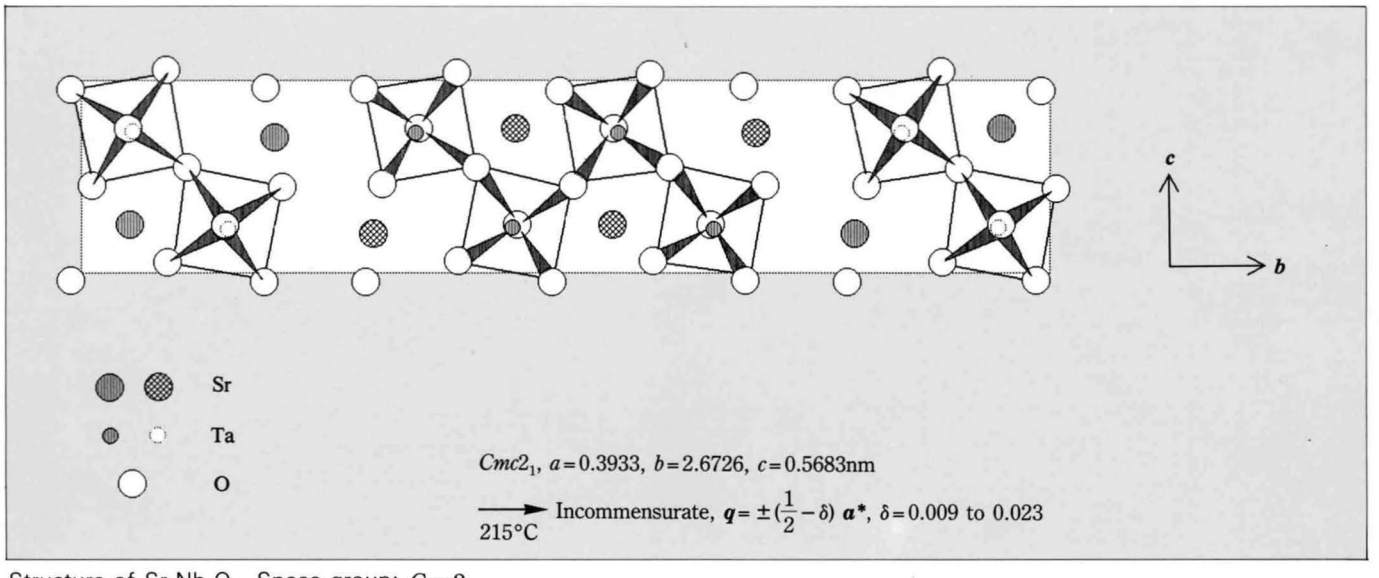

Structure of $Sr_2Nb_2O_7$. Space group: $Cmc2_1$

The CBED pattern (f) was taken by tilting the specimen a few degrees from the [110] axis about the c axis, the pattern (g) being the central part of (f). Incommensurate reflections are seen but do not strongly interact with the fundamental reflections. As a result, a B_2 GM line due to the 2_1 screw axis is clearly seen in the 001 reflection. This indicates that the average structure has a 2_1 screw axis in the c direction. These results are summarized in the table. That is, the average structure does not have the space group $P2_1$ of the expected low temperature phase but has the same space group as that of the high temperature phase. This result is acceptable from the fact that neither the lower temperature phase with $P2_1$ nor discommensuration have been observed. The modulated structure preserves only the (010) mirror plane.

The rotation of the oxygen octahedra about the b axis, which was previously proposed as a mechanism of the phase transition, preserves the 2_1 screw axis but violates the c-glide plane parallel to the (010) plane. Thus, this mechanism is incompatible with the present experimental result. A rotation about the c axis preserves the c-glide plane but loses the 2_1 screw axis, which is compatible with the present experimental result. This rotation itself introduces only the doubling of the cell parameter a, but does not produce the q value of the incommensurate phase. Thus, displacements of atoms to produce the q value must be considered additionally.

The modulation may be better explained by a sinusoidal displacement wave $\boldsymbol{u}$,

$$\boldsymbol{u} = \xi \cos 2\pi(\boldsymbol{q}\cdot\boldsymbol{r} - \nu t),$$

where ξ is the amplitude vector and $\boldsymbol{q} = (1/2\text{-}\delta)\boldsymbol{a}^*$. The intensity of the reflection $\boldsymbol{H}$ is expressed as

$$I = 2\pi \mid F \mid^2 (\xi\cdot\boldsymbol{H})^2$$

where F is the crystal structure factor of the reflection. When a longitudinal wave ($\xi//\boldsymbol{a}$) is assumed to occur, the positions of the incommensurate reflections in Photo (a) are well explained. This wave causes the (100) mirror plane and 2_1 screw axis to be lost, but preserves the c-glide plane, which is compatible with the result of our CBED experiment. Therefore, the modulated structure in the incommensurate phase may be approximated by a sinusoidal longitudinal displacement wave.

Such a CBED study of the incommensurate phase definitely gives a useful guide to the structure analysis even in the scope of three dimensional crystallography.

The specimens were supplied by N. Yamamoto of Faculty of Engineering, the Technological University of Nagaoka.

References

[a] M. Tanaka, H. Sekii and K. Oki: *Jpn. J. Appl. Phys.*, **24** (1985) Suppl. 24-2, 814.
[b] N. Yamamoto: *Acta Cryst.*, **A38** (1982) 780.
[c] N. Yamamoto and K. Ishizuka: *Acta Cryst.*, **B39** (1983) 210.

[011]

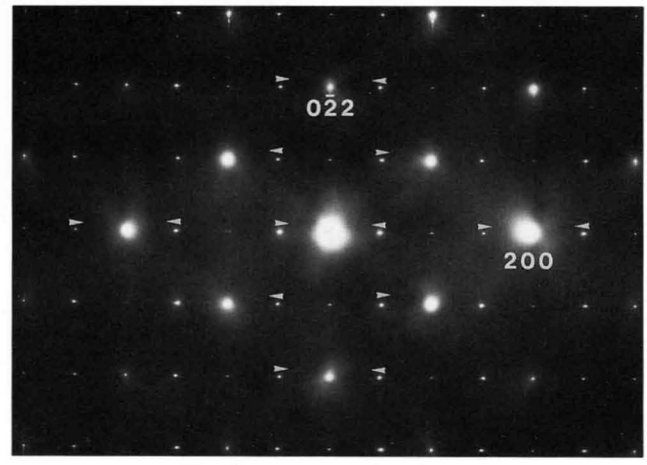

(a)

➤ Incommensurate reflections

$\boldsymbol{q} = \pm(\frac{1}{2} - \delta)\,\boldsymbol{a}^*$ $\quad \delta = 0.009$ to 0.023

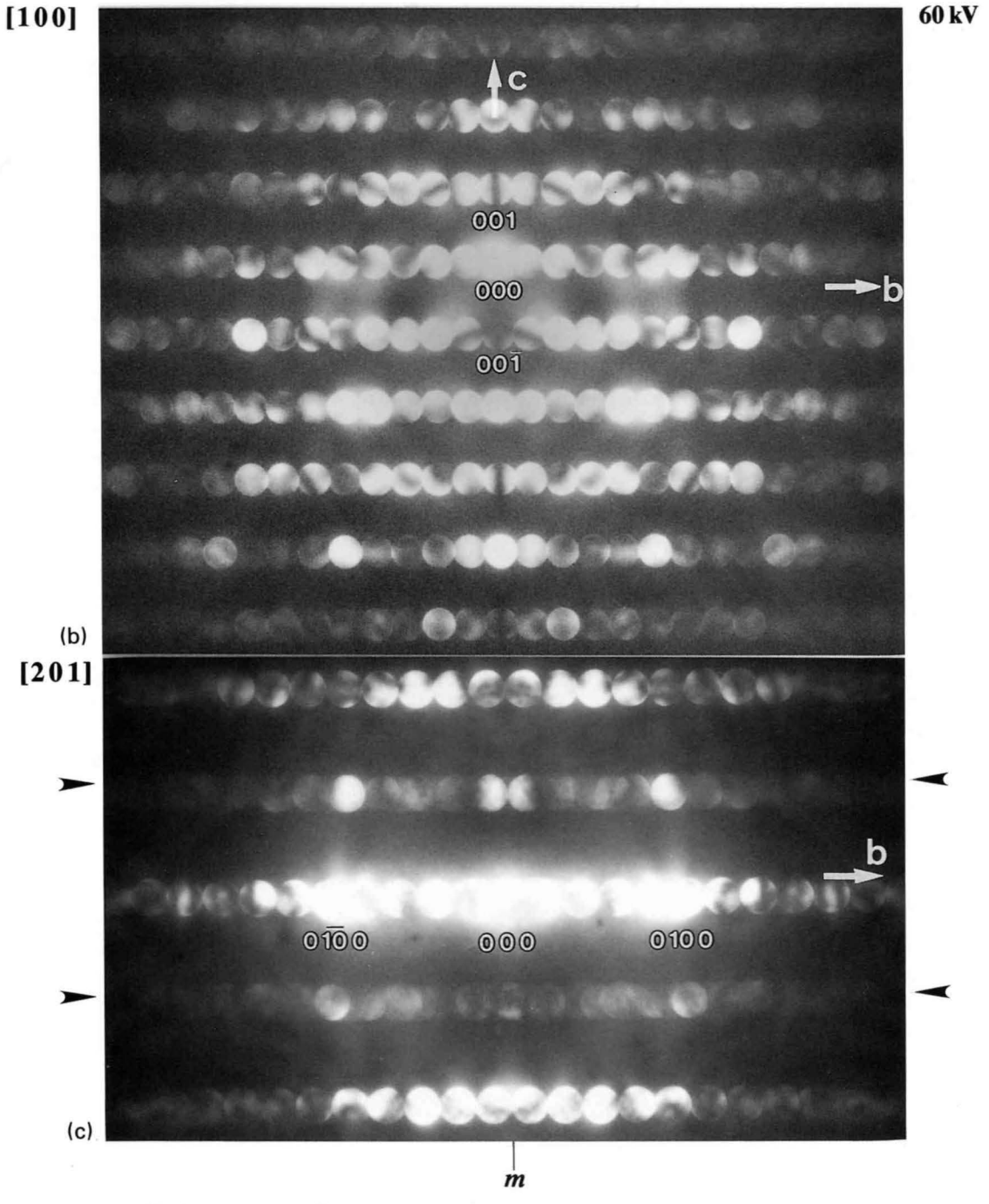

➤ Incommensurate reflections

(b) No incommensurate reflection is seen. GM lines are seen in the $00l$ (l = odd) reflections.
(c) Incommensurate reflections show a mirror symmetry.

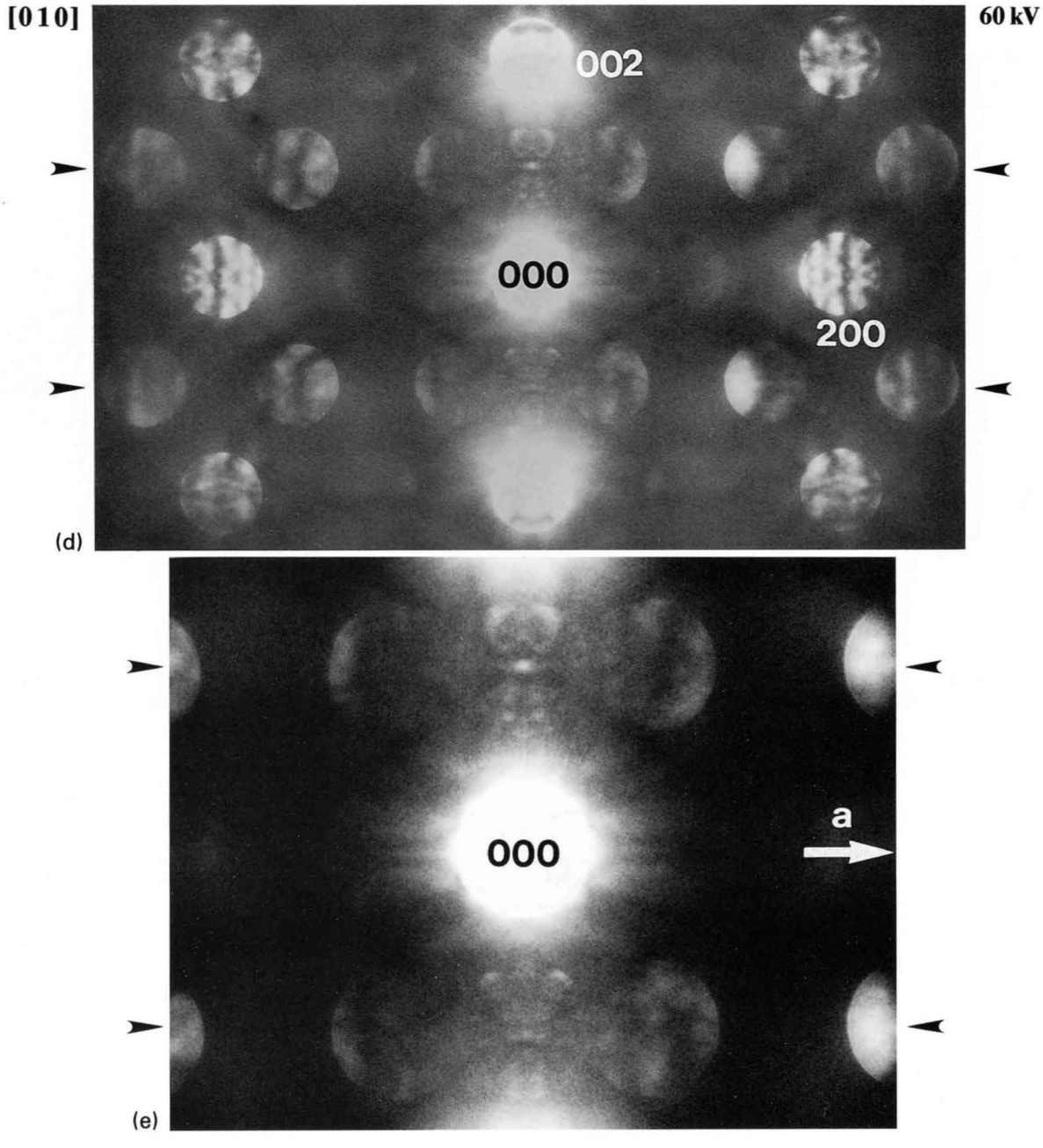

(d) Fundamental reflections show a mirror symmetry perpendicular to the *a* axis, but incommensurate reflections do not.

$Sr_2Nb_2O_7$

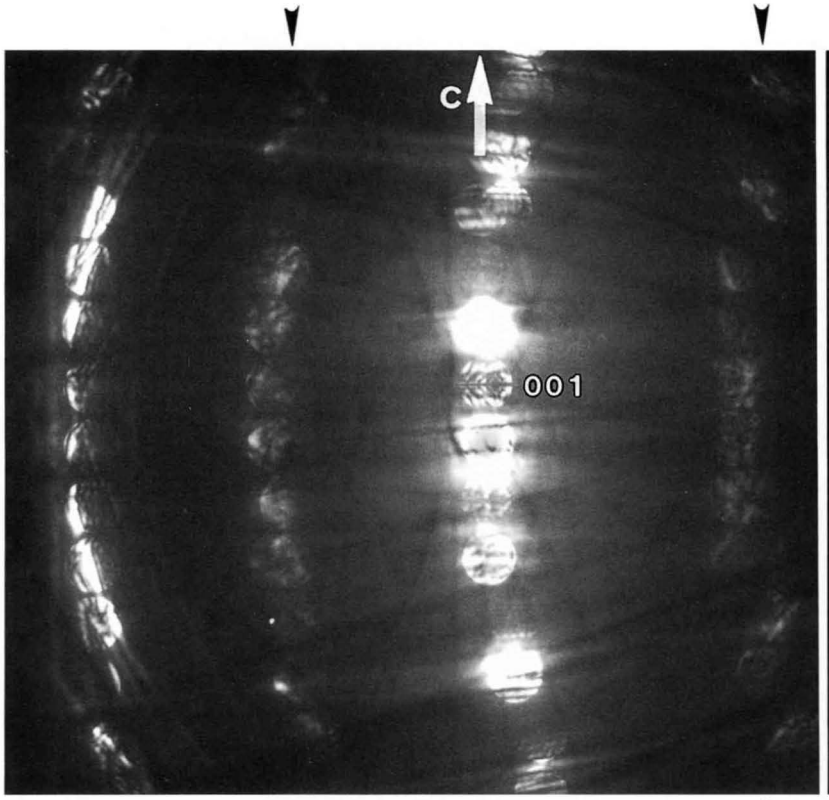

(f)

The specimen was tilted from the [110] zone axis about the [001] axis. B_2 GM line is seen in the 001 reflection.

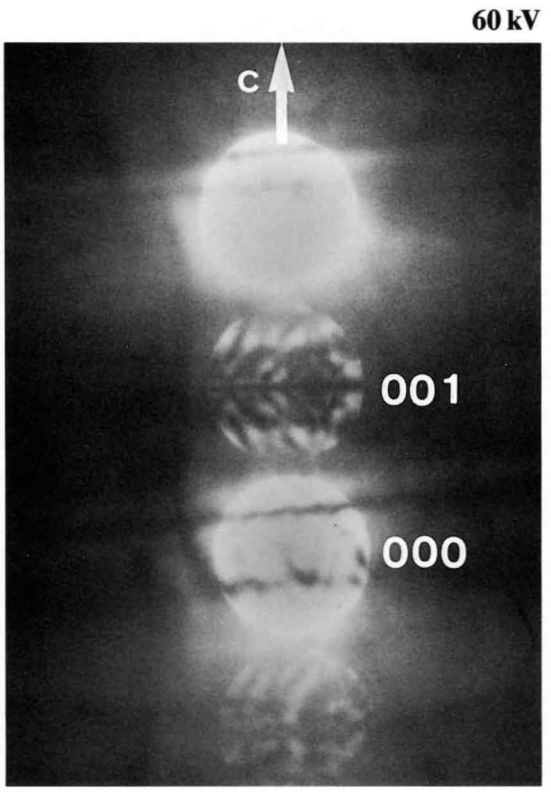

(g)

Enlarged pattern of the central part of (f).

	a	*b*	*c*
Fundamental reflections	$\sim m$	c	$\sim 2_1$
Incommensurate reflections	——	$m(c)$	——

Mo_8O_{23}

A series of transition metal oxides Mo_nO_{3n-1} ($n \geq 8$) is formed when metal-oxygen octahedra MoO_6 are combined. The figure shows a schematic diagram of the fundamental structure of Mo_8O_{23}. The high temperature form of this material belongs to a monoclinic space group $P2/c$, transforms at 42°C into an incommensurate phase characterized by a wave number vector of $\boldsymbol{q} = (0.195, 0.5, 0.120)$ and undergoes at 12°C a lock-in phase transition to a phase with a space group Pc and the $\boldsymbol{q} = (0, 0.5, 0)$. It has been reported that the phase transitions are closely related to the formation of a charge density wave [a].

The diffraction patterns (a), (b) and (c) were taken respectively at 142°C, 20°C and −173°C and at different crystal settings by tilting the specimen by a few degrees from the [100] about the [010] axis. In Photo (b), incommensurate reflections are seen on the horizontal lines indicated by the black arrows, but no such reflections in Photo (a). It should be noted that only one reflection of an incommensurate reflection pair at $\boldsymbol{q} = \pm(0.195, 0.5, 0.120)$ is seen in Photo (b) due to a nonzero value of the a^* component of $\boldsymbol{q}$. Photograph (c) shows superlattice reflections (commensurate) at $\boldsymbol{q} = (0, 0.5, 0)$.

In the [100] CBED pattern (d), incommensurate reflections are hardly seen. The presence of GM lines in the $00l$ and $10l$ (l = odd) fundamental reflections indicates that the average structure has a c-glide plane. The CBED pattern (e) shows GM lines in the $h0l$ (l = odd) fundamental reflections and exhibits a mirror symmetry between incommensurate reflections shown by the arrows. These facts indicate that the incommensurate structure preserves the c-glide plane. The [010] CBED pattern (f) shows a twofold rotation symmetry not only in the outer HOLZ ring due to the fundamental structure but also in the inner weak HOLZ ring originating from the incommensurate structure. These results are summarized in the table, and indicate that the incommensurate phase has the same symmetries as the high temperature phase.

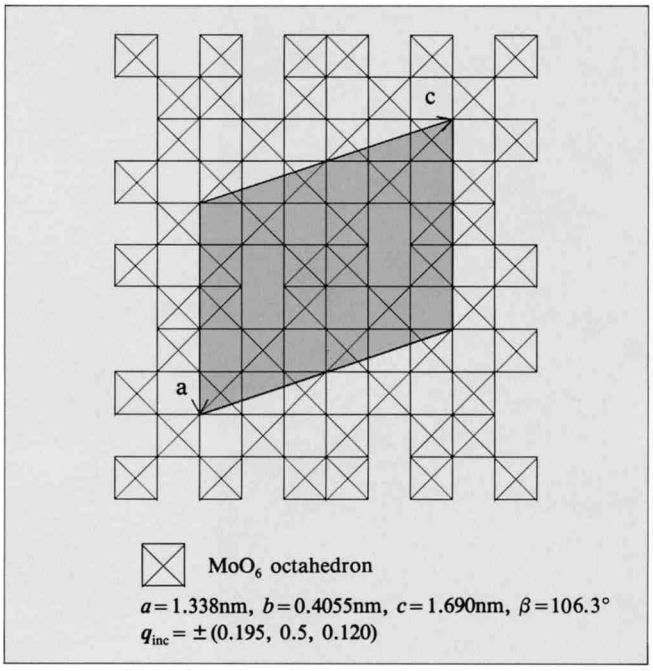

Structure of Mo_8O_{23}. Space group: $P2/c$

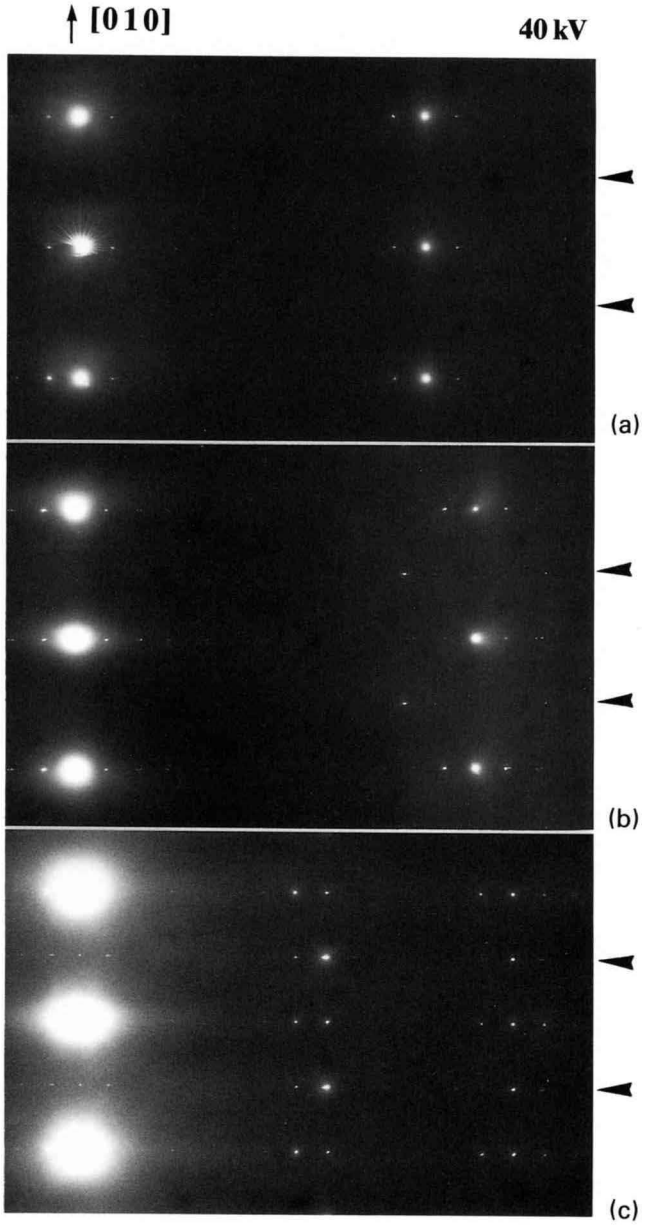

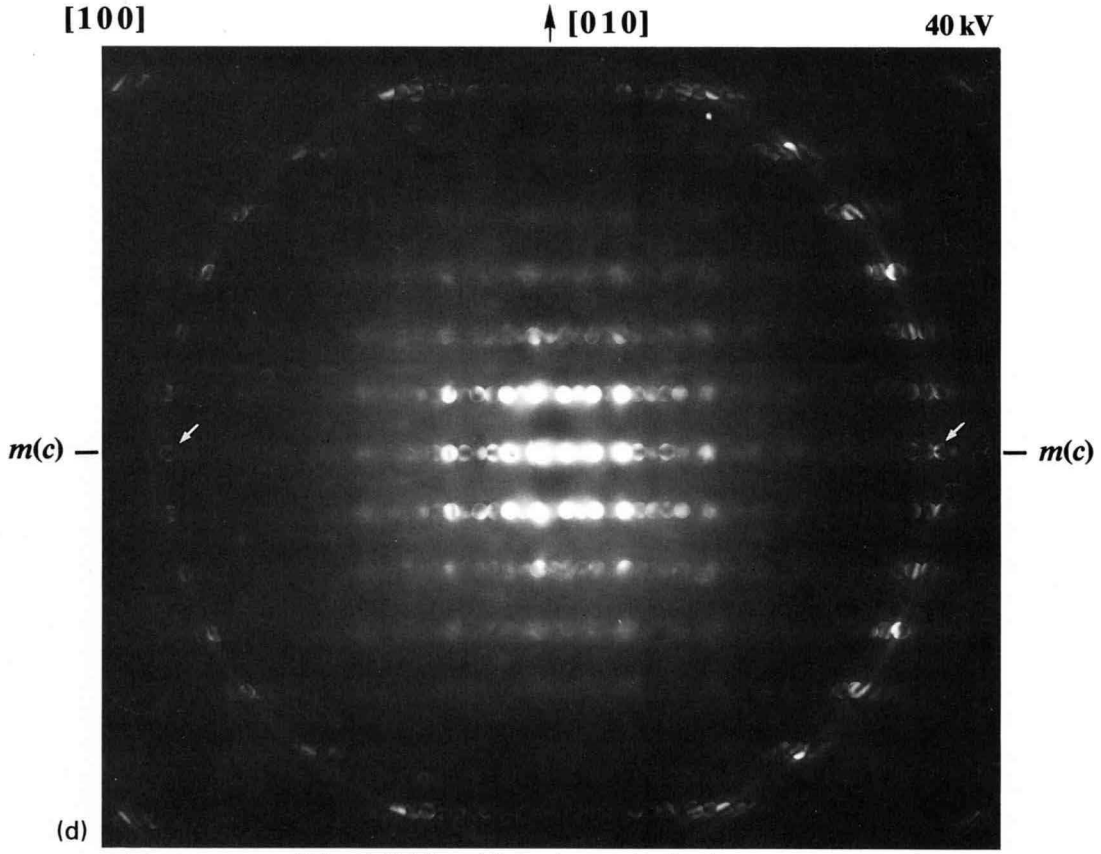

ZAP, GM lines in $00l$ and $10l$ (l = odd) fundamental reflections.

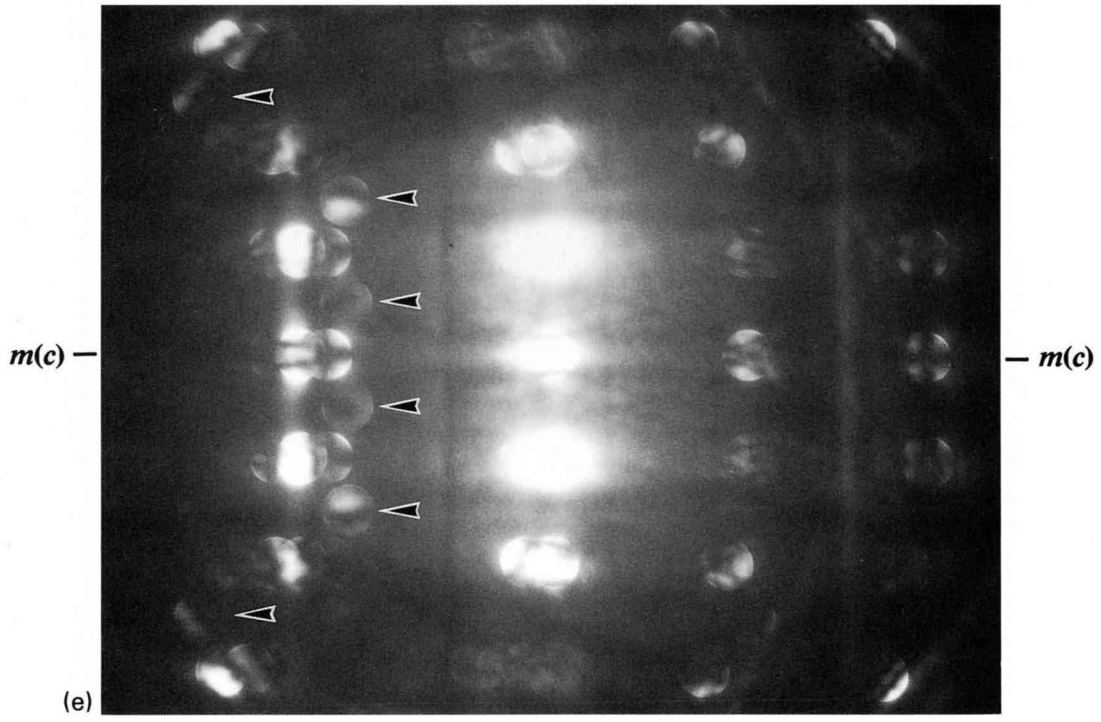

➤ Incommensurate reflections

The specimen was tilted from the [100] around the [010] axis. Incommensurate reflections showing mirror symmetry.

[0 1 0]

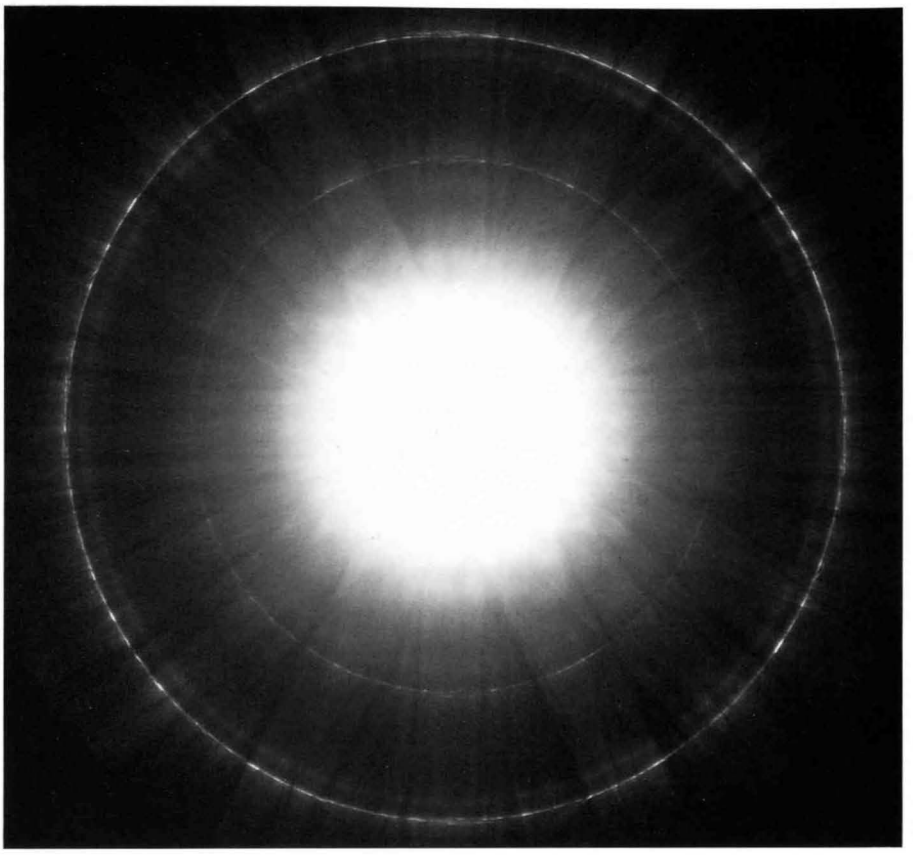

(f)

Outer and inner HOLZ rings showing symmetries 2.

It has been reported that the low temperature form with the space group *Pc* is produced by an M_3 type rotation and a deformation of MoO_6 octahedra [a]. An M_3 type rotation of the octahedra without deformation appear to preserve the space group *P*2/*c* but produce a cell doubling in the [010] direction, giving rise to superlattice reflections at $\boldsymbol{q} = (0, 0.5, 0)$. An antiphase domain structure or a long-period superlattice (LPS) in the direction of [0.195, 0, 0.120] can explain the splitting of a superlattice reflection at $\boldsymbol{q} = (0, 0.5, 0)$ into two reflections at $\boldsymbol{q} = \pm(0.195, 0.5, 0.120)$, where the incommensurate wave number is obtained by a uniform mixing of two LPSs with different but commensurate periods [b]. The LPS, which has a commensurate period, preserves twofold axes and *c*-glide planes existing in the high temperature phase. Therefore, in the incommensurate phase a long-period superlattice should be formed by an M_3 type rotation of MoO_6 octahedra without deformation accompanied by an antiphase domain structure.

The specimens were supplied by M. Sato of the Institute for Molecular Science.

	b
Fundamental reflections	2, *c*
Incommensurate reflections	2, *m*(*c*)

References

[a] M. Sato, H. Fujishita, S. Sato and S. Hoshino: *J. Phys.*, **C19** (1986) 3059.

[b] K. Fujiwara: *J. Phys. Soc. Jpn.*, **12** (1957) 7.

Quasicrystals

Icosahedral Phases

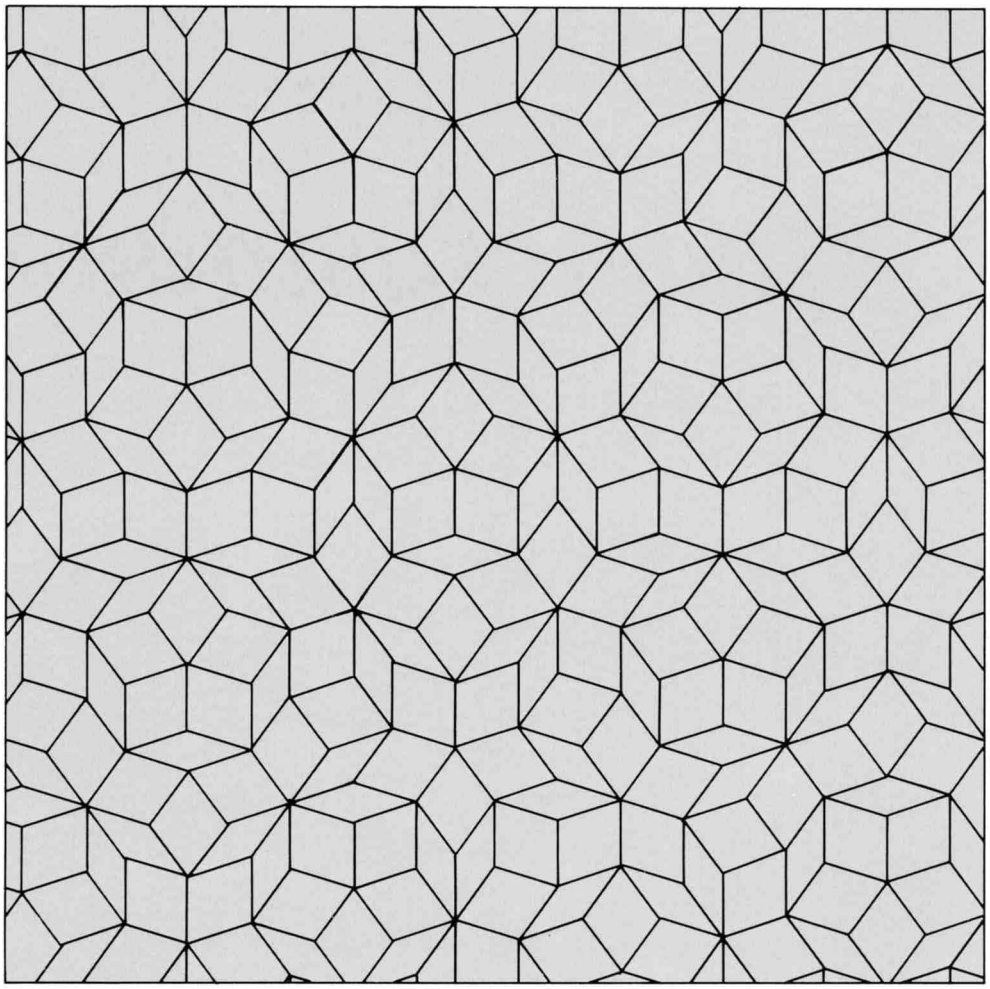

Penrose tiling

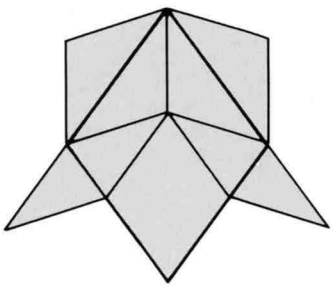

Fat rhombus

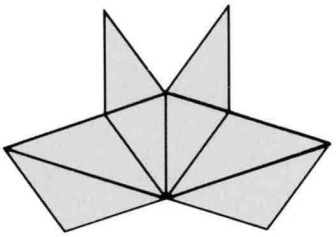

Thin rhombus

Penrose [a] demonstrated that the two dimensional plane can be tiled with thin and fat rhombi to give a pattern with local fivefold rotation symmetries but with no translational symmetry. Mackay [b] extended the tiling to three dimensions using acute and obtuse rhombohedra, which also resulted in acquisition of local fivefold symmetries and in vanishment of the translational symmetry. (The three dimensional space filling method was afterwards completed by Ogawa [c].) These, however, had remained a matter of design or amusement of geometry until Schechtman *et al.* [13] discovered an icosahedral symmetry presumably with a long-range structural order in an alloy of Al_6Mn (nominal composition), using electron diffraction. Since then, the new class of structural order, which has no translational symmetry but has a long-range structural order, has been called the "quasicrystal". Levine and Steinhardt [d] showed that the quasi-lattice produces sharp diffraction patterns, and they succeeded in reproducing almost exactly the diffraction pattern obtained by Schechtman *et al.* using the Fourier transform of a quasi-periodic icosahedral lattice. They described that one of the important properties of the quasicrystal is self-similarity transformation.

Do real quasicrystals truely have an icosahedral symmetry with a long-range structural order and self-similarity transformation? We have examined icosahedral and decagonal quasicrystals using CBED and small-area-parallel-beam electron diffraction.

References

[a] R. Penrose: *Bull. Inst. Math. and Its Appl.*, **10** (1974) 266.

[b] A.L. Mackay: *Physica*, **114A** (1982) 609.

[c] T. Ogawa: *J. Phys. Soc. Jpn.*, **54** (1985) 3205.

[d] D. Levine and P.J. Steinhardt: *Phys. Rev. Lett.*, **53** (1984) 2477.

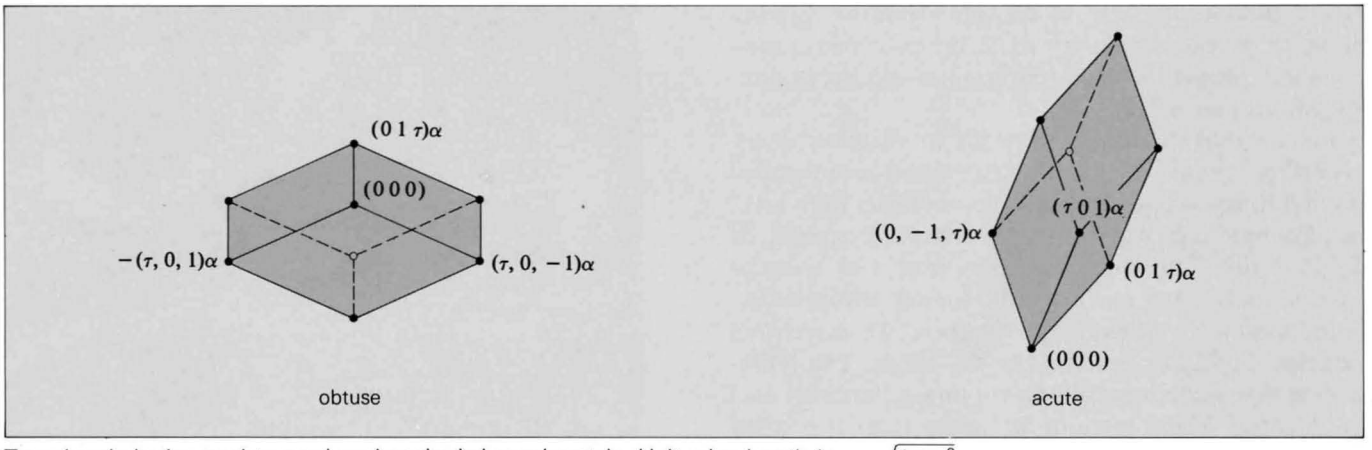

Two rhombohedra used to produce icosahedral quasicrystals. Unit edge length is $\alpha = \sqrt{1+\tau^2}$

Al_4Mn

First we investigated an alloy of the same composition [14] as that studied by Schechtman *et al.* [13], their quasicrystalline grains being later found to be of Al_4Mn. Photograph (a) shows an electron microscope image of the alloy. The grains of the quasicrystal were found to be less than 10 nm in size. All the CBED patterns obtained from an about 10 nm in diameter × 100 nm high volume did not at all exhibit any fivefold symmetry, although ordinary electron diffraction patterns showed a fivefold symmetry, as obtained by Schechtman *et al.* Small-area-parallel-beam electron diffraction patterns taken from about 100 nm diameter areas at an incidence along the fivefold axis made clear that the quasicrystal was highly strained. That is, 1) higher order Laue-zone reflections were not observed, 2) reflections due to lattice spacings greater than 1.37 nm did not appear, 3) the profiles of Kikuchi bands in five equivalent directions were not symmetric with respect to their centers, 4) each diffraction spot was composed of a number of fine spots and 5) three principal diffraction spots showed a zig-zag deviation from the radial line. Lubensky *et al.* interpreted the last result, 5), in terms of anisotropically quenched phason strains.

Reference

[a] T.C. Lubensky, J.E.S. Socolar, P.J. Steinhardt, P.A. Bancel and P.A. Heiney: *Phys. Rev. Lett.*, **57** (1986) 1440.

$Al_{74}Mn_{20}Si_6$

The addition of several percent of silicon to Al-Mn alloys causes a large increase in the degree of order of the quasicrystal. Bendersky and Kaufman [15] prepared such a less strained quasicrystalline $Al_{71}Mn_{23}Si_6$ alloy and determined its point group. They obtained fairly good zone-axis CBED patterns which showed symmetries of 10*mm*, 6*mm* and 2*mm* in ZOLZ disks and 5*m*, 3*m* and 2*mm* in HOLZ rings. From these results, they identified the point group to be centrosymmetric $m\bar{3}\bar{5}$. We examined crystallographic properties of a less strained quasicrystalline $Al_{74}Mn_{20}Si_6$ alloy [16].

Photographs (b) and (c) show 0.1 μm diameter quasicrystalline grains of $Al_{74}Mn_{20}Si_6$. Small-area-parallel-beam diffraction patterns (d) to (f) were taken from a 110 nm diameter area with an incident beam divergence of 3×10^{-5} rad. The innermost reflections with a lattice spacing of 2.27 nm in Photo (d). Among strong reflections, many weak diffraction spots appear, which were not observed in Al_4Mn and $Al_{71}Mn_{23}Si_6$ alloys. The reflections at high scattering angles have a stronger intensity than in Al_4Mn. These results indicate that the alloy $Al_{74}Mn_{20}Si_6$ has a much greater ordering than the other two.

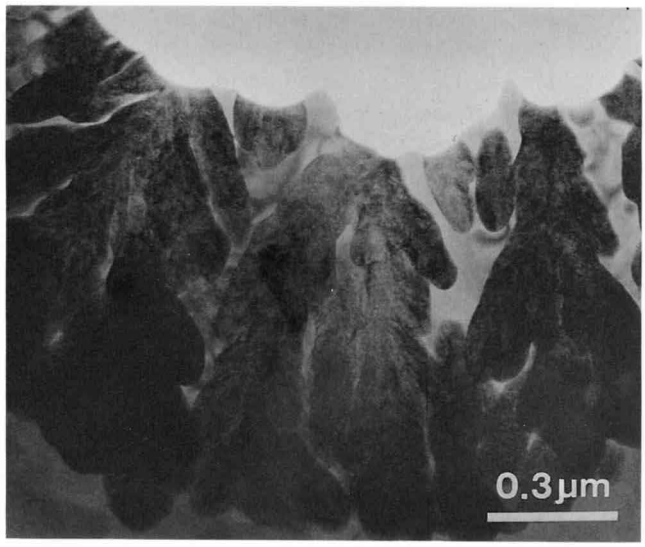

(a)

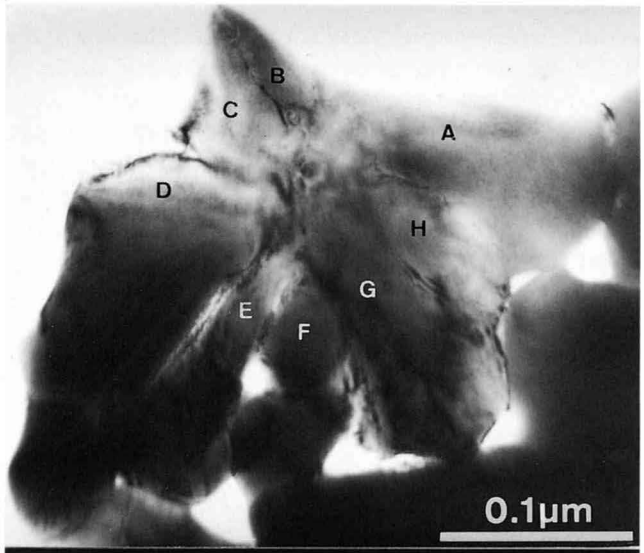

(b)

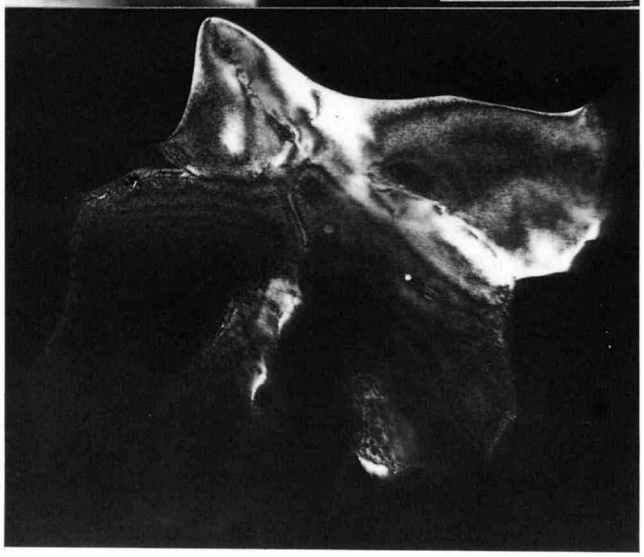

(c)

Small-area-parallel-beam electron diffraction patterns **60 kV**

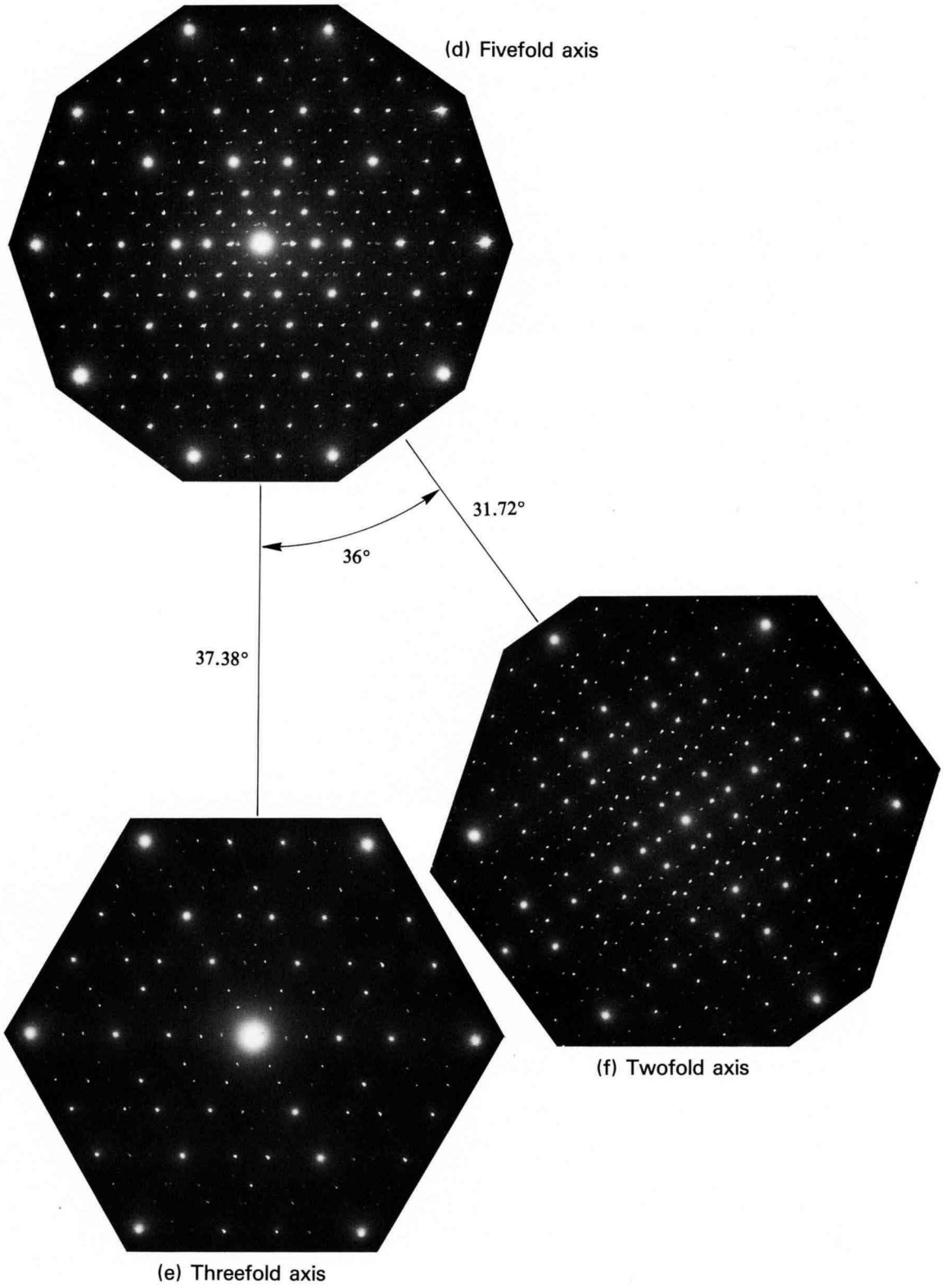

$Al_{74}Mn_{20}Si_6$

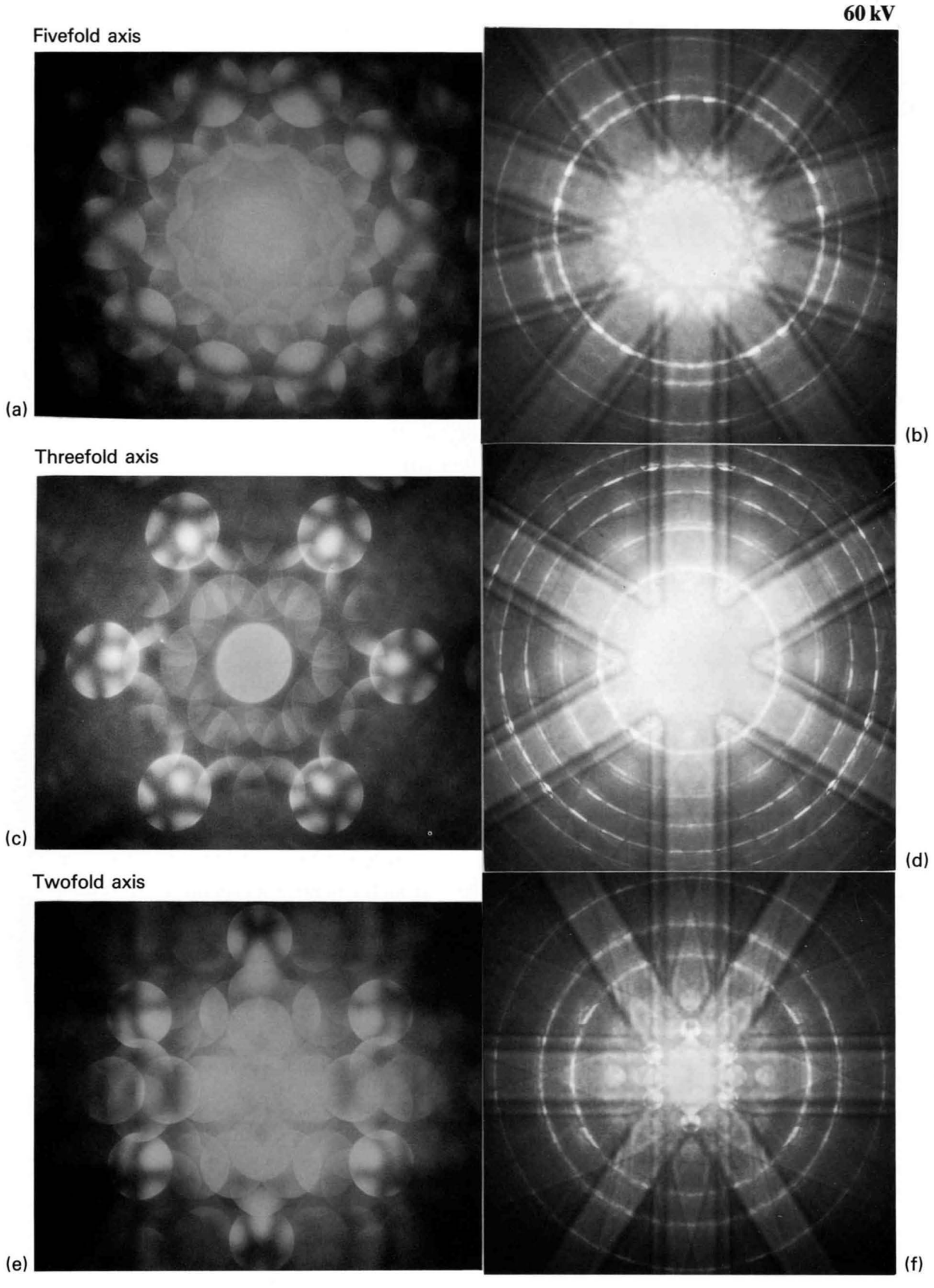

$Al_{74}Mn_{20}Si_6$ — CBED patterns —

Photographs (a) to (f) show three pairs of CBED patterns taken from an about 100 nm thick and about 3 nm diameter area of an $Al_{74}Mn_{20}Si_6$ quasicrystal at an accelerating voltage of 60 kV. Each pair consists of a ZOLZ pattern and a HOLZ pattern. The former pattern is produced almost by the interaction of ZOLZ reflections. Distinct symmetries are seen in several disks. Many HOLZ rings and Kikuchi bands are clearly seen in the HOLZ patterns. The profiles of Kikuchi bands are symmetric with respect to their centers ((b), (d) and (f)). These results contrast strongly with those of Al_4Mn, and indicate that the constituent atoms form a highly ordered arrangement of the quasicrystal.

The whole pattern (a), formed by ZOLZ reflections, exhibits a tenfold rotation and two types of mirror symmetries, the resultant symmetry being expressed as $10mm$. The whole pattern (b), formed by HOLZ reflections, is seen to show a fivefold symmetry and a type of mirror plane, the resultant symmetry being expressed as $5m$. Photographs (c) and (d) show symmetries $6mm$ and $3m$, respectively. Photographs (e) and (f) show a symmetry $2mm$.

It is known that there exist two icosahedral point groups 235 and $m\bar{3}\bar{5}$. The former is noncentrosymmetric and has no mirror symmetry, but the latter is centrosymmetric. The table in the next page shows diffraction groups expected from these point groups at an incident beam parallel to the fivefold axis and their symmetries appearing in WP, BP, DP and ± DP. Projection diffraction groups and their symmetries, in which only the interaction between ZOLZ reflections is taken into account, are written in the second row. Diffraction groups obtained at other incident beam orientations are omitted, since these have been given in the references [1] and [5]. The whole pattern symmetries observed in the present quasicrystal agree with those expected from point group $m\bar{3}\bar{5}$, which was obtained by Bendersky & Kaufman [15].

Photograph (g) shows a zone-axis CBED pattern taken at an electron incidence along the threefold axis. Photographs (h) and (i) show a pair of ± G-dark-field CBED patterns. The pattern of the + G-dark-field disk coincides with that of the − G-disk when the former is superposed on the latter with a translation of $-2\boldsymbol{G}$. This symmetry, 2_R, directly proves that the quasicrystal is centrosymmetric, again indicating the point group to be $m\bar{3}\bar{5}$.

It is noted, however, that the above symmetries are those appearing in intense reflections. To know the correct point group, the symmetries of weak reflections must be examined. Photograph (j) shows a CBED pattern taken from an area of about 3 nm diameter by tilting the specimen from the incidence along a twofold axis into a direction in which a mirror symmetry is expected to exist. Weak reflection pairs AA' and BB', for instance, show a small breakdown of a mirror symmetry. It is not clear at the present stage whether this breakdown is inherent in the quasicrystal or is attributed to residual strains of the specimen.

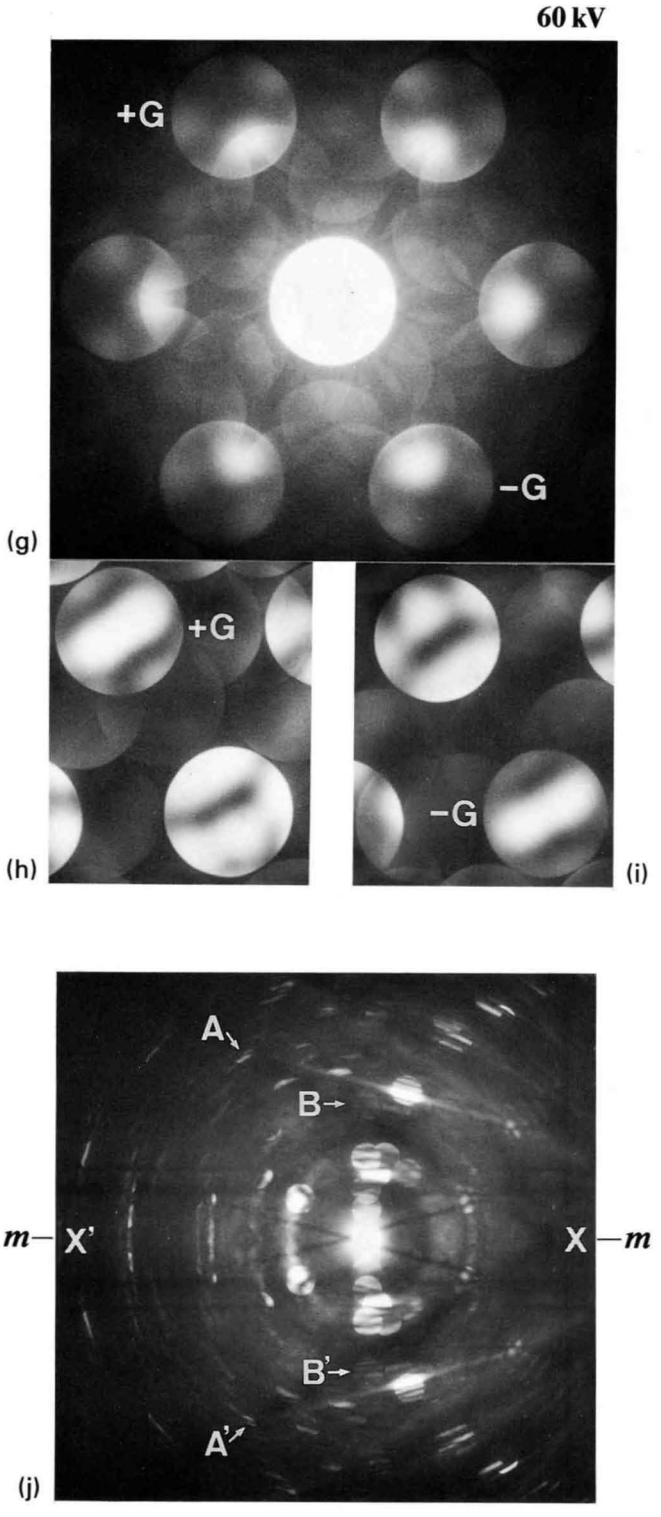

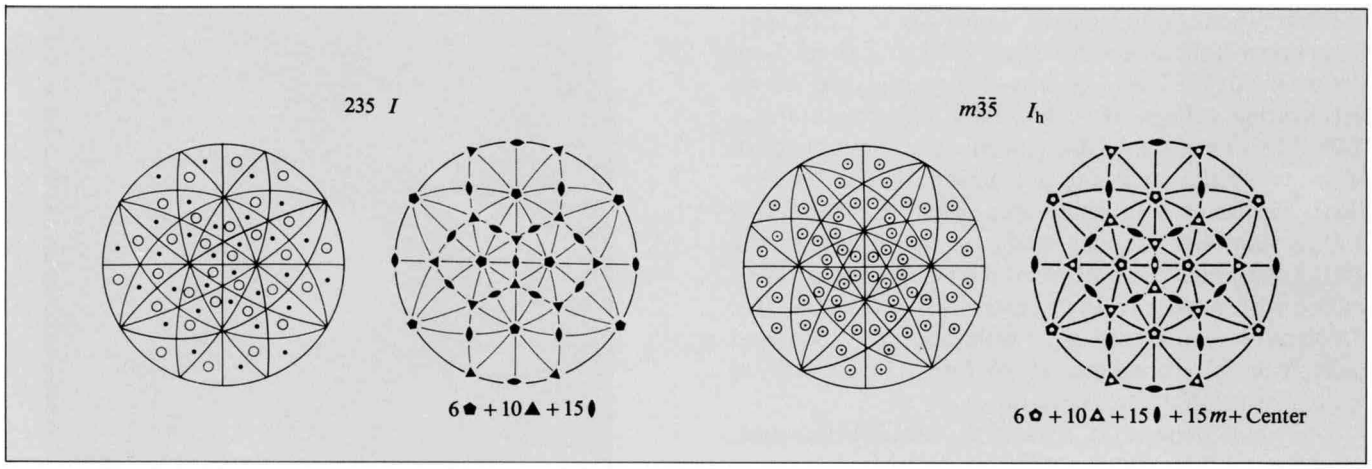

Icosahedral point groups. Quoted from International Tables for Crystallography, vol. A pp.778~779.

CBED symmetries of icosahedral phases

Point group	Diff. group	BP	WP	DP	±DP
235	$5m_R$	$5m$	5	1 m_2	1 m_R 1
	(Projection) $5m1_R$	$10mm$	$5m$	$2=1_R$ $2m_vm_2$	1 m_v1_R 1
$m\bar{3}\bar{5}$	10_Rmm_R	$10mm$	$5m$	1 m_2 m_v	2_R 2_Rm_2 2_Rm_v
	(Projection) $10mm1_R$	$10mm$	$10mm$	2 $2m_vm_2$	21_R 21_Rm_v

$Al_{74}Mn_{20}Si_6$ — Diffraction patterns —

In the previous pages, we have been concerned with symmetry determination by assuming that a quasicrystal exists. We now return to discuss the diffraction pattern which shows a fivefold symmetry. Notwithstanding a much better ordering, a zig-zag deviation of diffraction spots was still observed in $Al_{74}Mn_{20}Si_6$. The inner disks in the CBED pattern (a) are slightly overlapped to visualize the displacement of diffraction spots. It is clearly seen that the second disk in the direction *h* overlaps that in the direction *k* to a greater extent than the disks in other directions, and that the equivalent disk in the direction *m*, which is perpendicular to the direction midway between the directions *h* and *k*, radially overlaps the outer disk more than in the other directions. Close inspection of the diffraction pattern (b) on page 92, reveals the following facts. All the spots in the directions *m* and *n* line up or show almost no angular deviation. These two directions are not equivalent, because the spots S1-S6 in the direction *n* are situated at different radial positions from the spots S1'-S6' in the direction *m*. The diffraction spots in the other directions show an angular deviation. The deviated positions of the reflections in these directions can be produced by linear combinations of the reflection vectors in the directions *m* and *n*. Therefore, the two fundamental reciprocal lattice vectors can be taken in the directions *m* and *n* for the diffraction pattern (b) as in usual crystals, instead of requiring five fundamental reciprocal lattice vectors.

All the positions of the spots in the fundamental direction *n* are reproduced by the Fourier transform of a quasiperiodic array expressed by the equation

$$X_n = n + (1/\varrho)[n/\tau]. \quad (1)$$

When $\varrho = \tau = (1+\sqrt{5})/2$, the quasi-periodic array LSLLSLSLL... (Fibonacci sequence) is generated, where L and S have relative lengths of $(1+\sqrt{5})/2$ and 1, respectively. The value of ϱ determines the ratio between the lengths L and S, and that of τ the sequence of them. The Fourier transform of the array is shown in Fig. (a). The positions of the peaks F1-F3 and S1-S6 well correspond to those of the reflections indicated with the same symbols in Photo (b).

It is noted that the calculated diffraction pattern of Fig.(a) resembles that of a long-period superlattice structure in a binary alloy which consists of an ordered array two kinds of atoms and periodic antiphase domain boundaries [a]. That is, the strong reflections, F0-F3 in Fig.(a), can be regarded as the fundamental reflections of the disordered (averaged) array, and pairs of reflections, (S1,S2), (S3,S4) and (S5,S6), symmetrically situated between the fundamental reflections can be regarded as split superlattice reflections. In fact, the quasi-periodic array expressed by eq.(1) can be created to a good approximation by the introduction of the ordering of two elements (L and S) and periodic antiphase boundaries to the ordered array of L and S, although the "uniform" mixing of two long-period superlattice structures with different periods is needed to reproduce the incommensurate property of the quasilattice [b]. The meaning of the "uniform" mixing and how to produce it can be understood by the projection method [c].

The calculated diffraction pattern of a periodic array

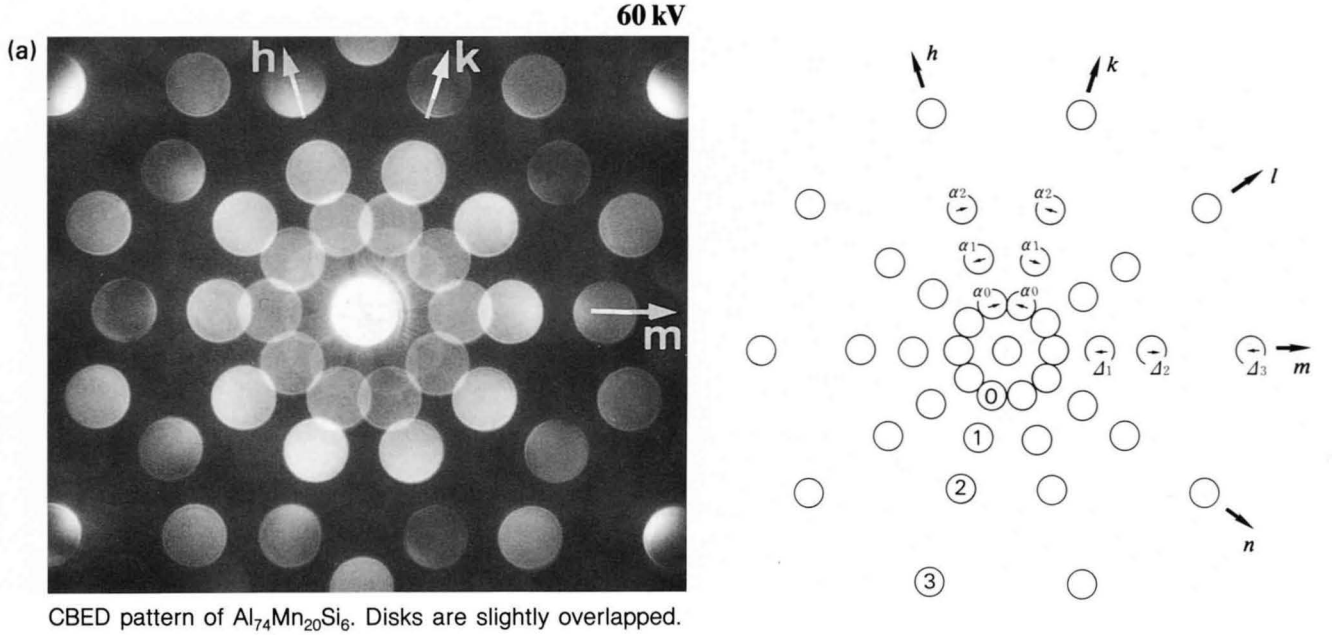

CBED pattern of $Al_{74}Mn_{20}Si_6$. Disks are slightly overlapped.

with a sequence LSLLS is shown in Fig.(b) as an approximation of the diffraction pattern of Fig.(a). These two patterns show very similar peak positions and intensities, except for very weak peaks. This indicates that the diffraction patterns obtained from the present alloy may be interpreted by a periodic array.

In contrast to the direction *n*, the coupled shifts of the pairs of split superlattice reflections are seen along the fundamental direction *m* in Photo (b). The shifts are shown schematically by arrows in the calculated pattern of Fig.(a). This suggests that there exists a change in the period of the antiphase boundaries in the language of the long-period superlattice in binary alloys. The sense of the shifts has been reproduced by a periodic array of LLLS, which can not be created by eq.(1), as shown in Fig.(c). (It is worth while to note that the opposite-sense shift to the present one is produced by a periodic array of LS. (see page 104))

As a result, the experimental diffraction pattern of the present alloy (Photo (b)) might be explained by such a crystal lattice that has tentative periodic arrays of LSLLS and LLLS in the directions *n* and *m*, respectively.

The specimens of Al_4Mn and $Al_{74}Mn_{20}Si_6$ were supplied by Dr. A. Inoue and Prof. T. Masumoto of the Research Institute for Iron, Steel and Other Metals, Tohoku University.

References

[a] C.H. Johansson and J.O. Linde: *Ann. Physik*, **25** (1936) 1.
[b] K. Fujiwara: *J. Phys. Soc. Jpn.*, **12** (1957) 7.
[c] V. Elser: *Phys. Rev.*, **B32** (1985) 4892.

(b)

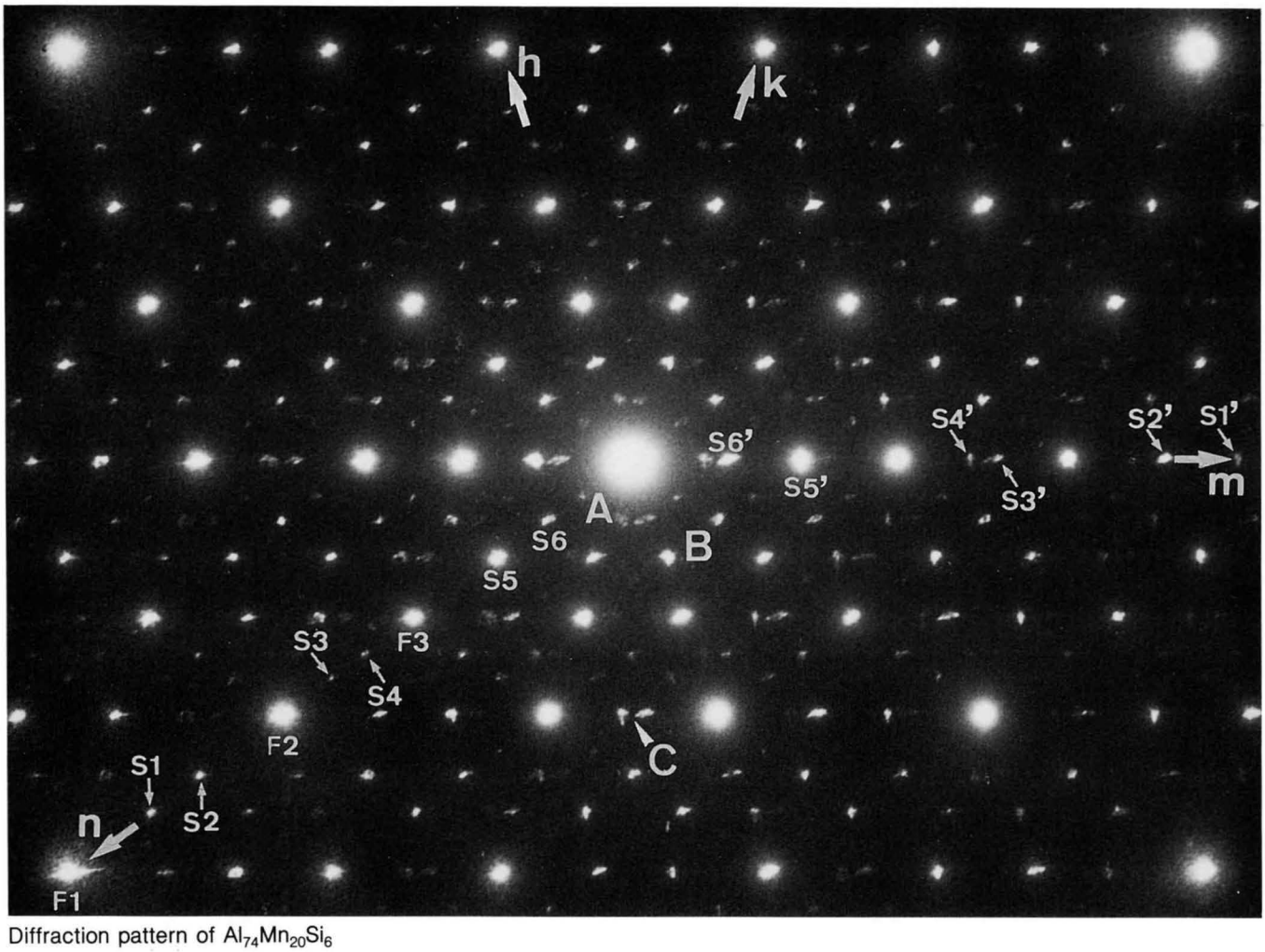

Diffraction pattern of $Al_{74}Mn_{20}Si_6$

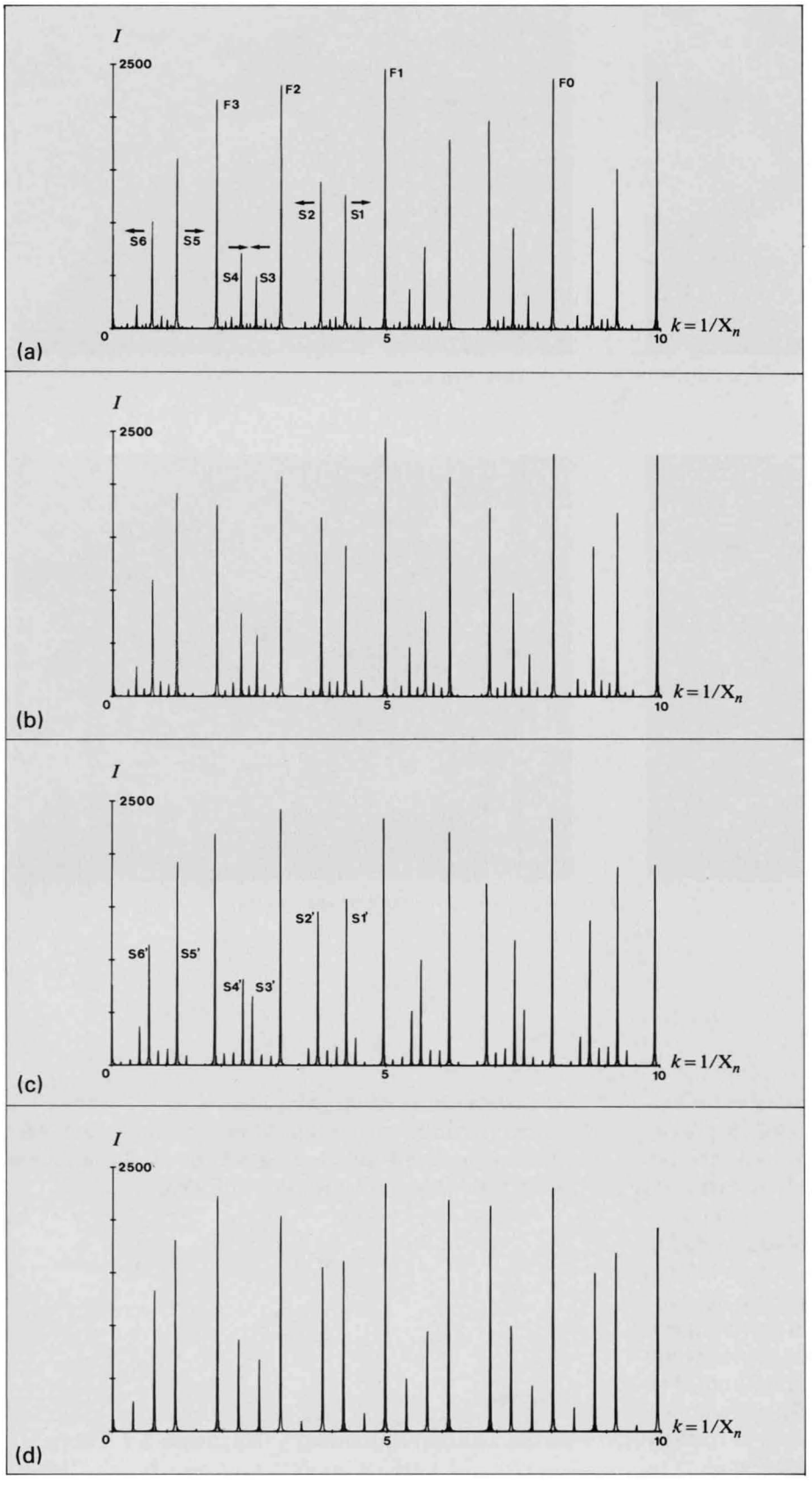

Quasi-periodic array

$X_n = n + (1/\varrho)[n/\tau]$

$\varrho = \tau = (1+\sqrt{5})/2$

Periodic array of LSLLS

Periodic array of LLLS

Periodic array of LS

$Al_{68}Mn_{20}Ru_6Si_6$

80 kV

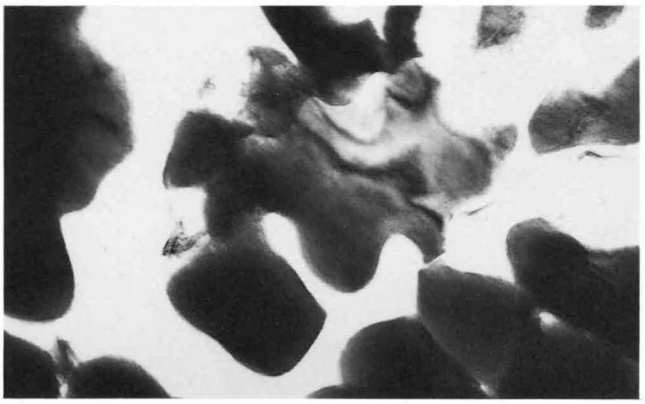

(a) Bright-field image.

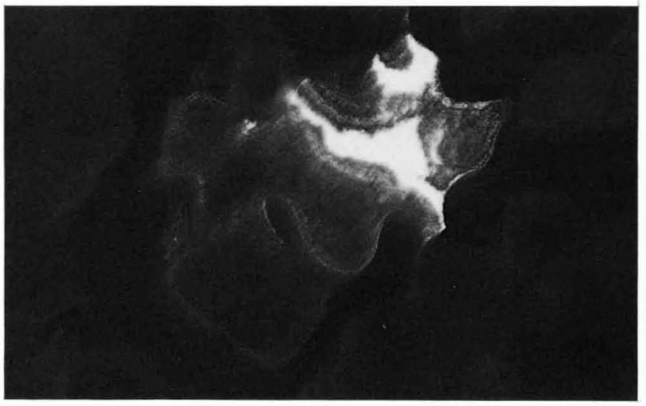

(b) Dark-field image.

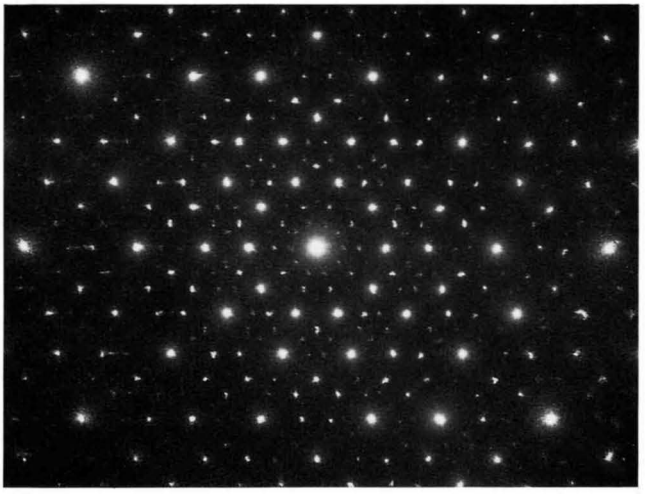

(c) Diffraction pattern of high quality.

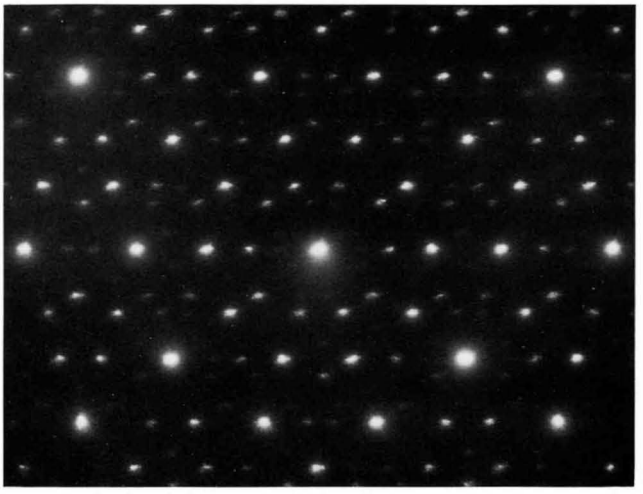

(d) Diffraction pattern of low quality.

Yamane *et al.* succeeded in growing a single-icosahedral-phase alloy of $Al_{68}Mn_{20}Ru_6Si_6$. They reported that X-ray diffraction profiles obtained from the alloy were sharper than those from other similar alloys. We have examined the alloy using CBED and small-area-parallel-beam electron diffraction. A small-area-parallel-beam electron diffraction pattern (c), which was taken from a 110 nm diameter area of Photo (a), shows very little zig-zag deviation of diffraction spots, although a low quality specimen area gave a pattern (d) with a large zig-zag deviation and no spots corresponding to the spacing 2.27 nm. The average degree of order of the phase was found to be better than that of $Al_{74}Mn_{20}Si_6$. Photographs (e) to (j) show three pairs of CBED patterns. Their quality appears to be a little inferior to that of the corresponding CBED patterns obtained from $Al_{74}Mn_{20}Si_6$.

The specimens were supplied by Dr. K. Kimura, Mr. H. Yamane and Prof. S. Takeuchi of the Institute for Solid State Physics, University of Tokyo.

Reference

[a] H. Yamane, K. Kimura, T. Shibuya and S. Takeuchi: Proc. of Inter. Workshop on Quasicrystals, Beijin, 1987

80 kV

Fivefold axis

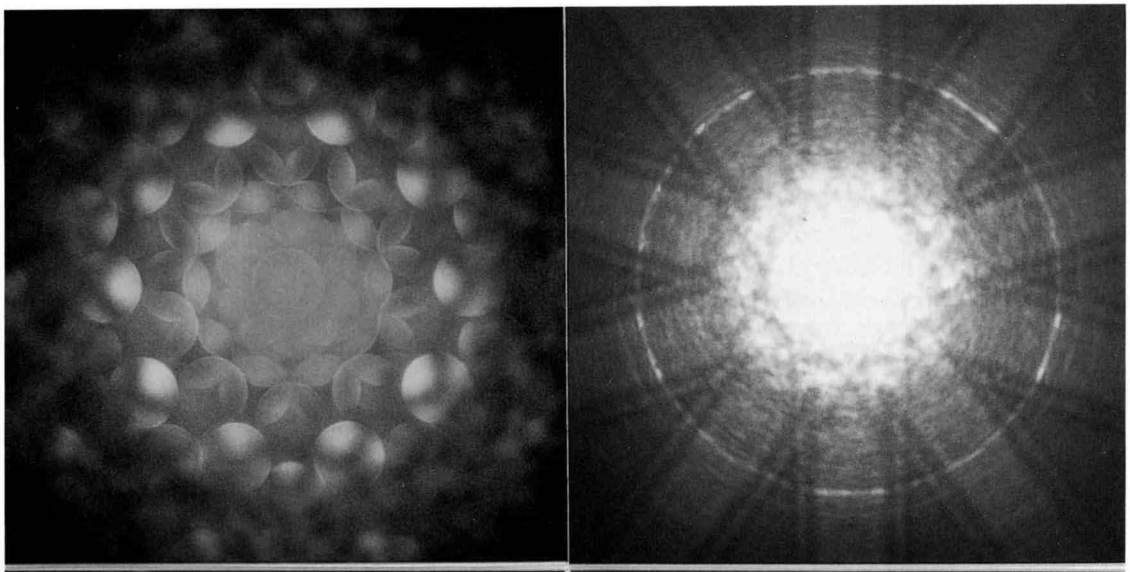

(e) (f)

Threefold axis

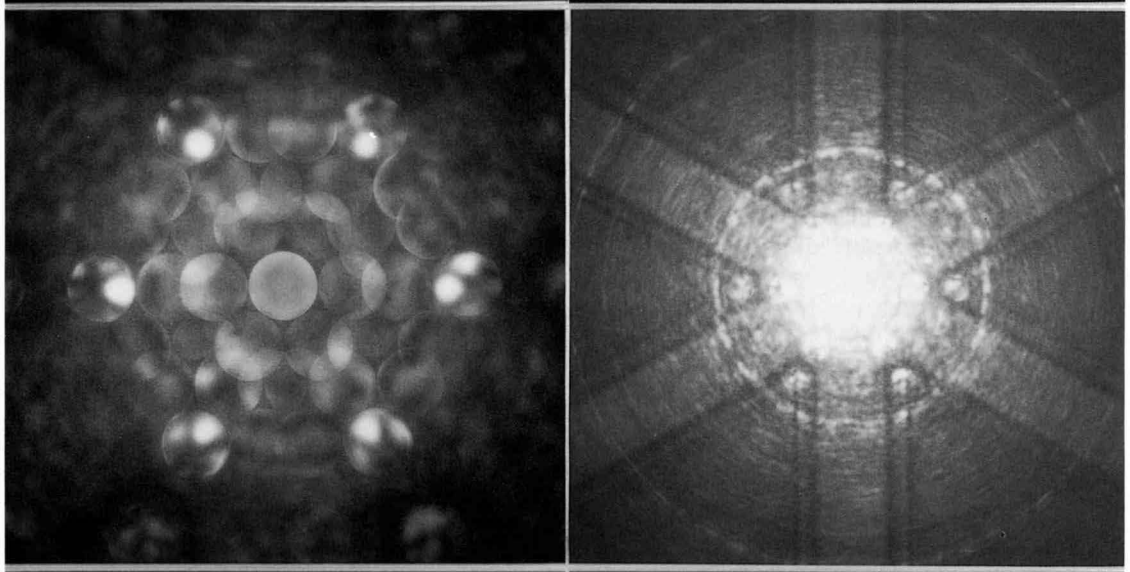

(g) (h)

Twofold axis

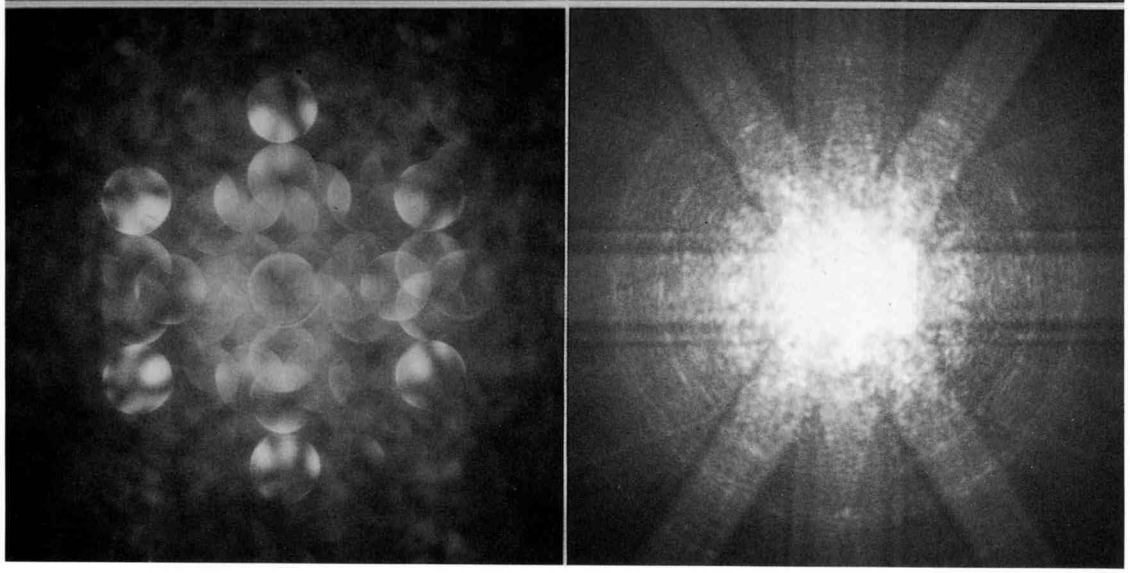

(i) (j)

$Al_{65}Cu_{20}Fe_{15}$

Tsai *et al.* have produced an alloy of $Al_{65}Cu_{20}Fe_{15}$ with a thermally stable icosahedral phase. They reported that the phase has a grain size as large as about 10 μm and is stable without phase transition up to the melting point.

Electron microscope images (Photos (a) and (b)) of $Al_{65}Cu_{20}Fe_{15}$ indicate that this alloy has the largest grain size among the quasicrystals examined so far. Almost all the specimen areas of this alloy produced a smaller zigzag deviation in small-area-parallel-beam electron diffraction patterns (Photos (c) to (e)) than $Al_{74}Mn_{20}Si_6$.

ZOLZ CBED patterns showed nearly perfect symmetries of 10*mm* (f), 6*mm* (h) and 2*mm* (j) at incidences along the fivefold, threefold and twofold axes, respectively, in contrast to slightly faulted symmetries obtained from other icosahedral alloys. The intensity distributions of HOLZ rings (g), (i) and (k) of this alloy are different from those of $Al_{74}Mn_{20}Si_6$, presumably indicating the difference between their structures. Owing to the presence of large grains, thickness changes of CBED patterns (Photos (l) and (m)) were observed. This alloy of $Al_{65}Cu_{20}Fe_{15}$ has the best qualified icosahedral phase among the alloys examined by us.

When a slightly convergent beam is used, diffraction patterns can be obtained from intermediate sized illuminated areas (approx. 20 nm in diameter) between areas needed for small-area-parallel-beam diffraction patterns (approx. 110 nm in diameter) and for CBED patterns (less than 5 nm in diameter). In Photos (n) to (p), HOLZ rings are more clearly seen and deviations of weak reflections from symmetries 5*m*, 3*m* and 2*mm* can be seen, whereas HOLZ rings are not easy to see in small-area-parallel-beam diffraction patterns (Photos (c) to (e)) and weak reflections can not be seen in CBED patterns (Photos (f) to (m)). Diffraction spots including HOLZ reflections in Photo (n) shows a very good symmetry 5*m*. Weak reflections in Photos (o) and (p), however, show deviations from symmetries 3*m* and 2*mm*, respectively. The details of the deviations are under study. This quasicrystal was found to be still insufficiently uniform, because the deviations easily changed when an illuminated area was shifted by about 50 nm.

The specimens were supplied by Dr. A. Inoue and Prof. T. Masumoto of the Research Institute for Iron, Steel and Other Metals, Tohoku University.

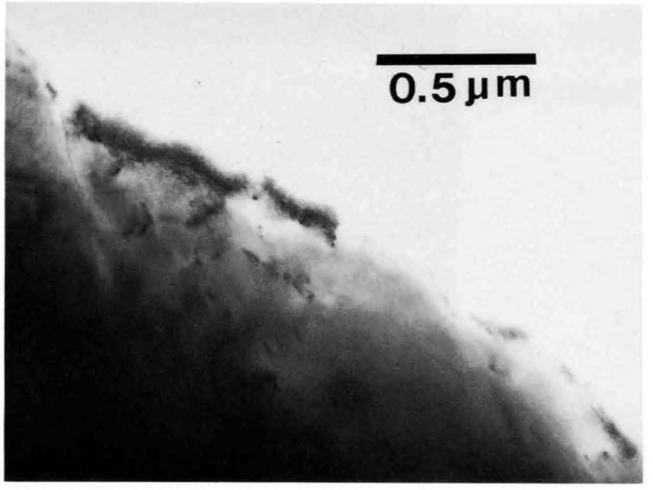

(a) Bright-field image

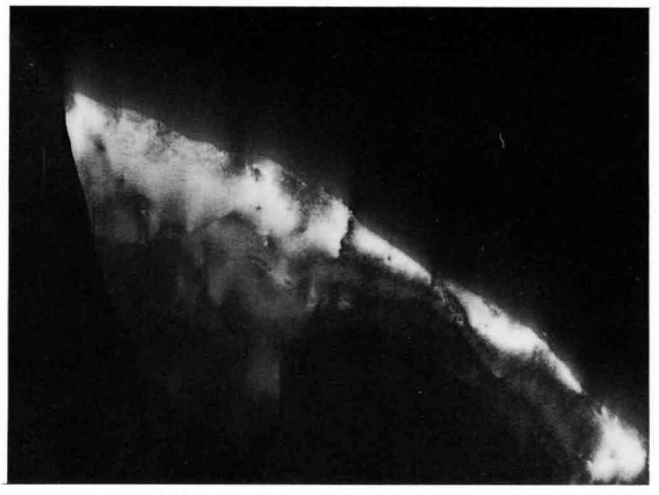

(b) Dark-field image

Reference

[a] A.P. Tsai, A. Inoue and T. Masumoto: *Jpn. J. Appl. Phys. Lett.*, **26** (1987) L1505.

Small-area-parallel-beam electron diffraction patterns **60 kV**

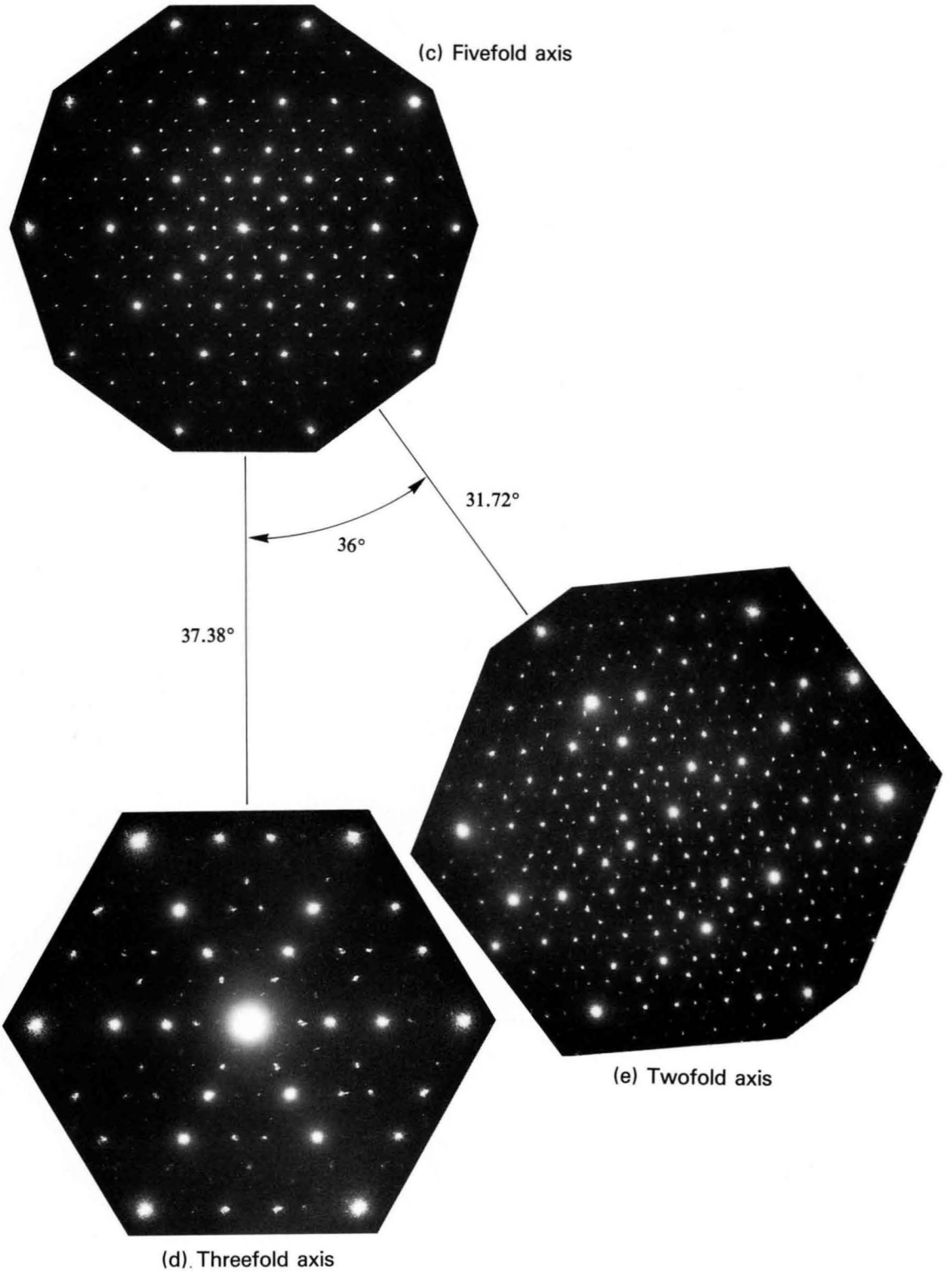

$Al_{65}Cu_{20}Fe_{15}$

60 kV

Fivefold axis

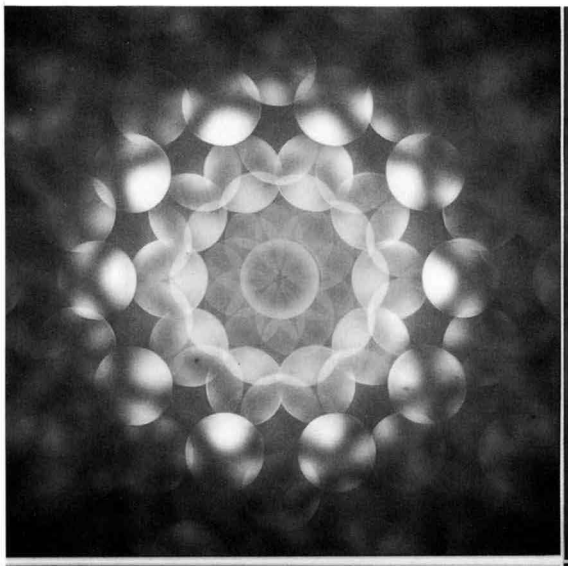

(f)

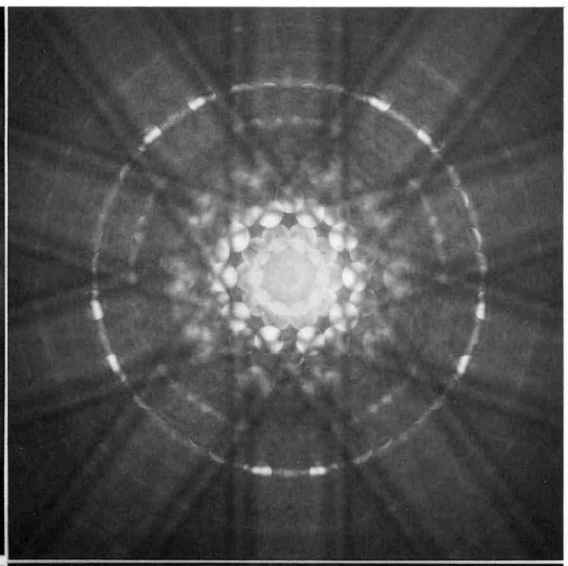

(g)

Threefold axis

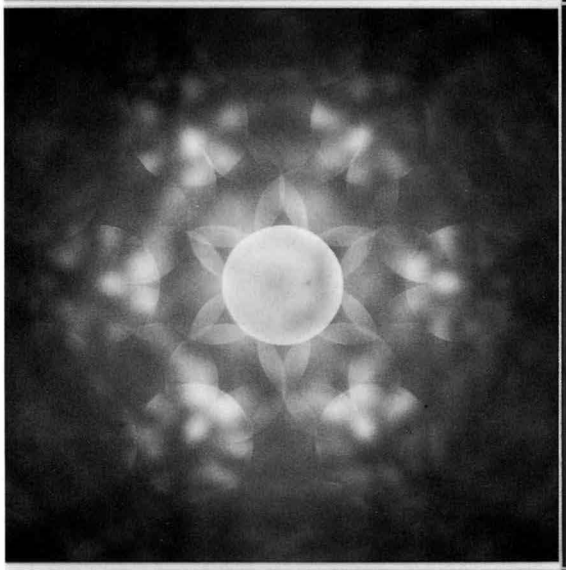

(h)

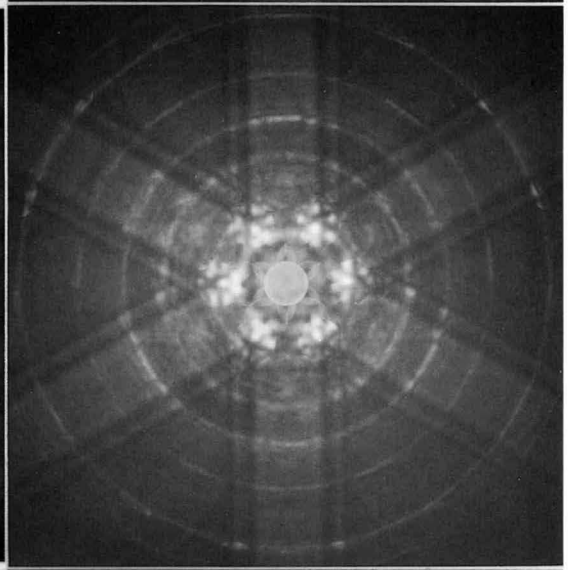

(i)

Twofold axis

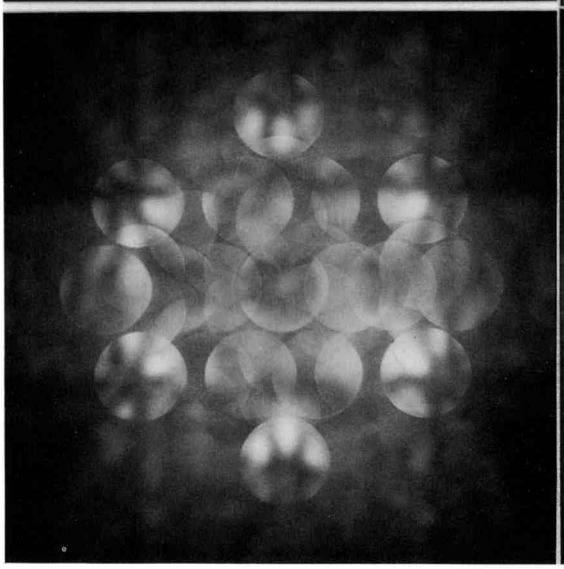

(j)

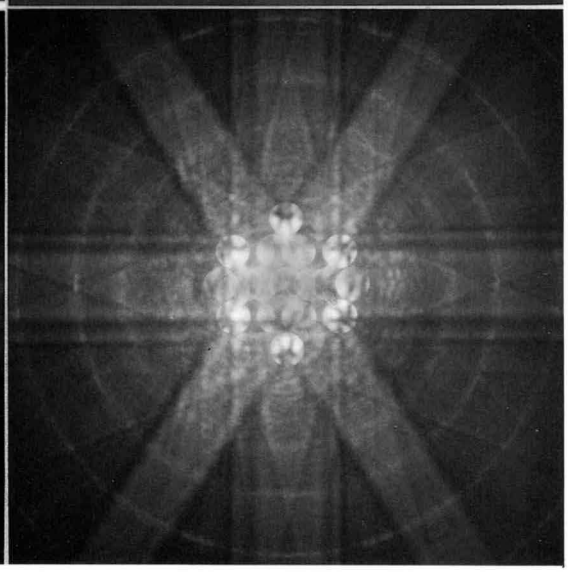

(k)

Thickness dependence of CBED pattern (fivefold axis)

60 kV

(I)

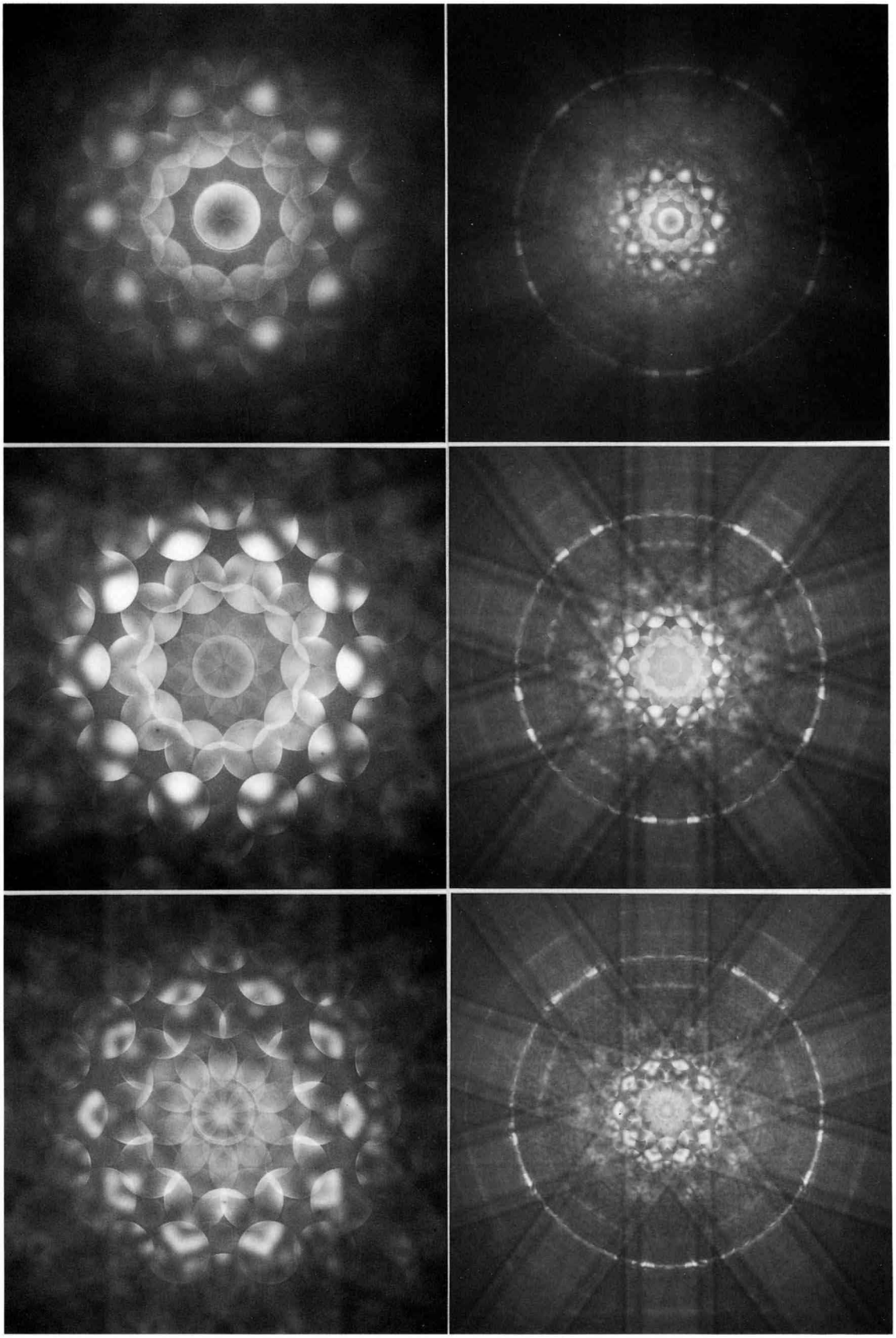

$Al_{65}Cu_{20}Fe_{15}$

Thickness dependence of CBED pattern (threefold axis)

60 kV

(m)

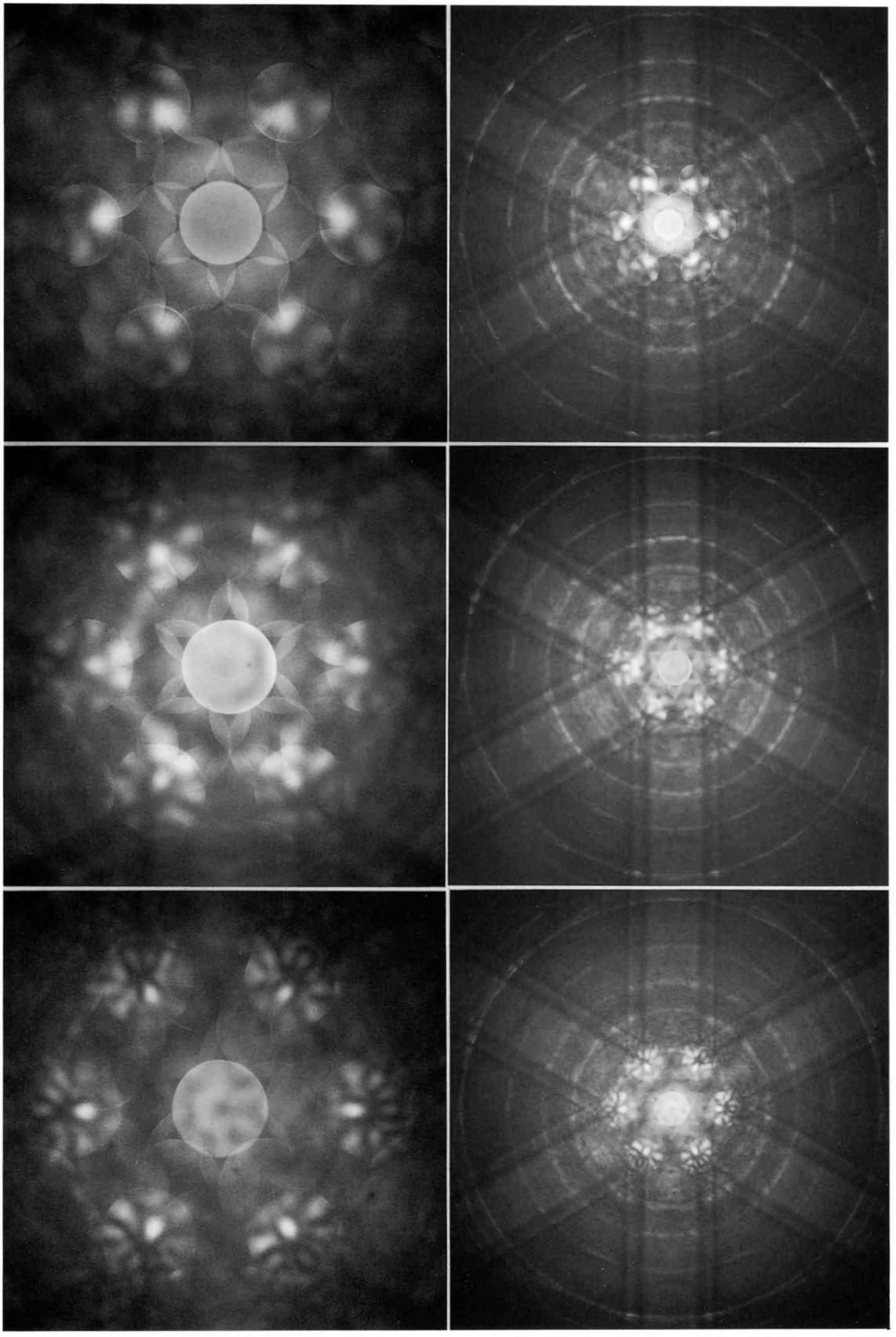

Diffraction patterns taken with slightly convergent beam

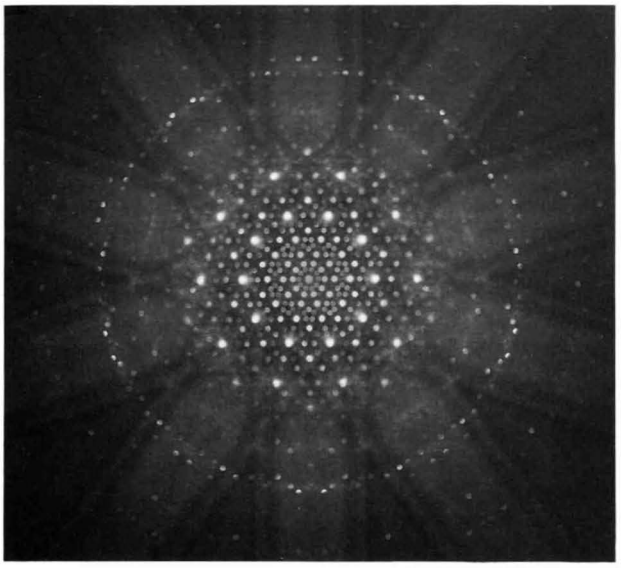

60 kV

(n) Fivefold axis

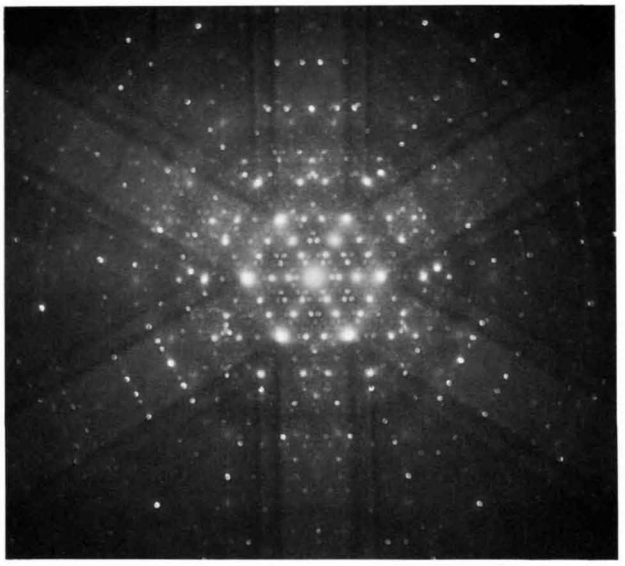

(o) Threefold axis

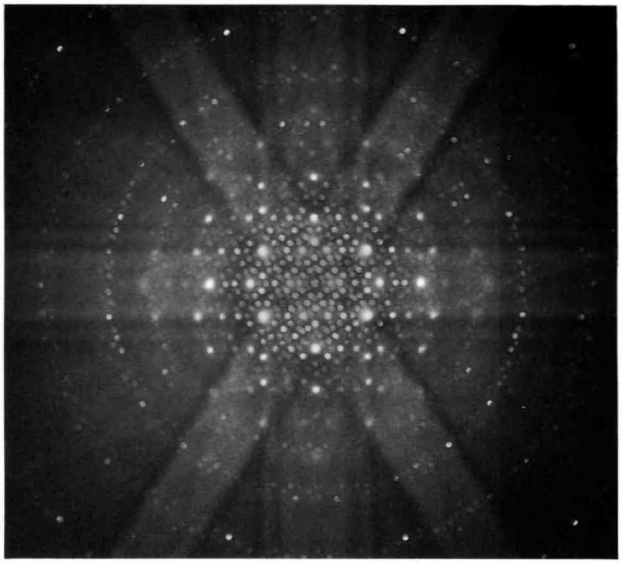

(p) Twofold axis

Decagonal Phases

Al-Mn system

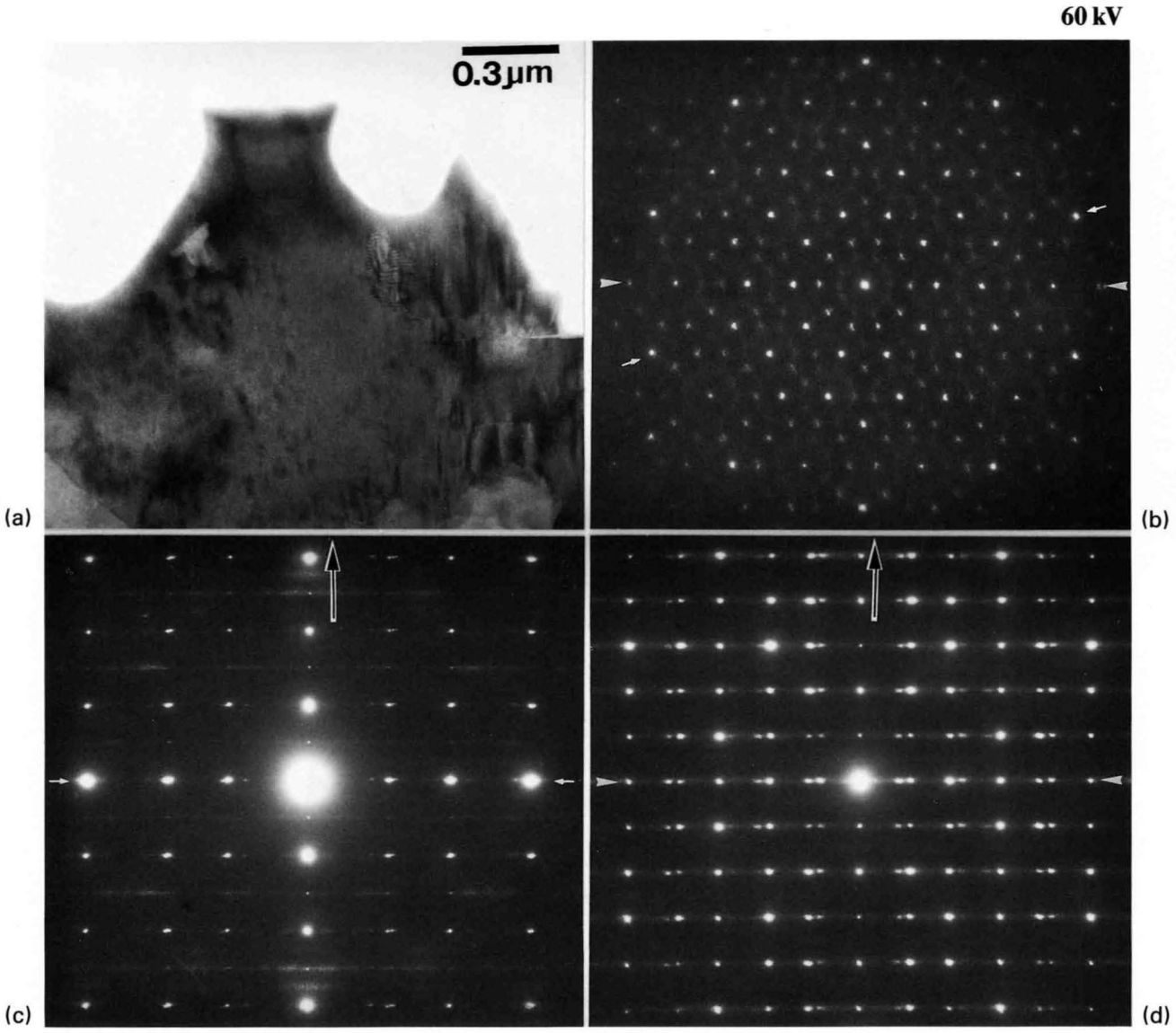

A decagonal phase found in an Al-Mn alloy has a tenfold rotation axis. The phase has a translational symmetry parallel to the tenfold axis and a quasi-periodic long-range structural order perpendicular to the axis. Two space groups, $P10_5/m$ and $P10_5/mmc$, have been proposed by Bendersky [a] and Yamamoto [b], respectively.

The diffraction pattern (b) was taken at an incidence along the tenfold axis. The diffraction patterns (c) and (d) were taken at two incidences perpendicular to the tenfold axis. The diffraction spots are periodic in the direction of the tenfold axis indicated by the black arrows. The arrays of diffraction spots indicated by two different white arrows in the two patterns (c) and (d) correspond to those indicated by the same arrows in the pattern (b). The spots are seen to be quasi-periodic along these arrays. Three pairs of CBED patterns—(e) & (f), (g) & (h) and (i) & (j)—were taken at incidences for the diffraction patterns (b), (c) and (d), respectively. The symmetries of the patterns are written beside the photographs. A tenfold axis and a mirror plane perpendicular to the axis are clearly seen. Owing to the low quality of the specimen, we could not confirm the existence of mirror planes parallel to the tenfold axis. As a result, the point group of this phase was found to be $10/m$ or $10/mmm$. Dynamical extinction was not observed in the CBED patterns.

The specimens were supplied by Dr. A. Inoue and Prof. T. Masumoto of the Research Institute of Iron, Steel and Other Metals, Tohoku University.

References

[a] L. Bendersky: *J. de Physique*, **47** (1986) C3-457.
[b] A. Yamamoto and K.N. Ishihara: *Acta Cryst.*, in the press.

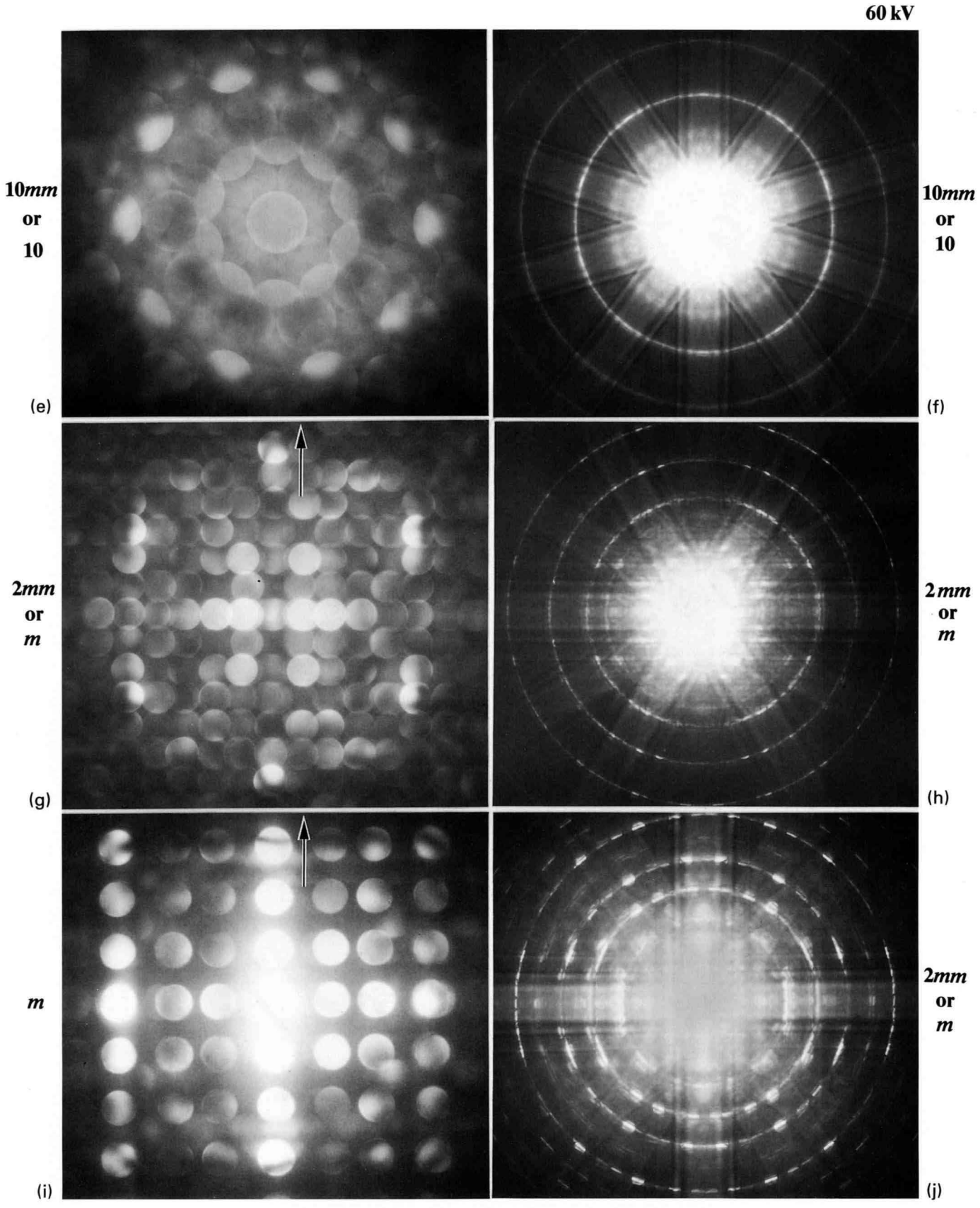
60 kV
10mm
or
10
(e)
(f)
2mm
or
m
(g)
(h)
m
(i)
(j)

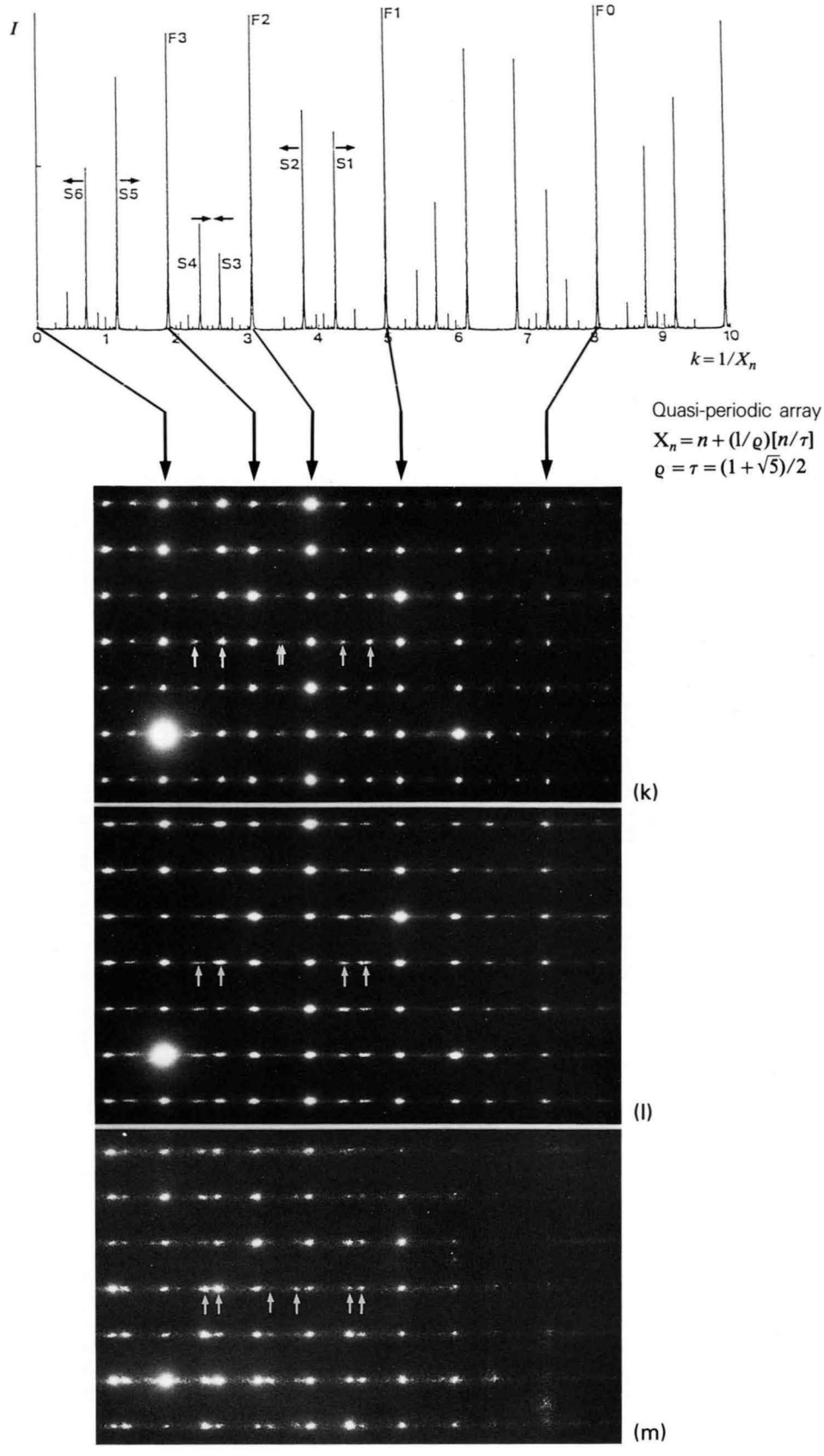
I
F3
F2
F1
F0
S6
S5
S4
S3
S2
S1
0
1
2
3
4
5
6
7
8
9
10
$k = 1/X_n$
Quasi-periodic array
$X_n = n + (1/\varrho)[n/\tau]$
$\varrho = \tau = (1+\sqrt{5})/2$
(k)
(l)
(m)

Three diffraction patterns, (k), (l) and (m), were taken from different specimen areas at the same incidence as that of Photo (c). Diffraction spots indicated by arrows in Photos (k) and (m) show deviations from the positions expected from the ideal quasi-periodic array. The positions of the spots in Photo (l) were well explained by the Fibonacci sequence (eq. (1) on page 91). The pairs of neighbouring spots indicated by arrows in (k) are displaced from the ideal positions to the sense indicated by the arrows in the above diagram. The sense of this displacement is the same as that already described in the section of the icosahedral phase of $Al_{74}Mn_{20}Si_6$. The pairs of neighbouring spots indicated by arrows in the pattern (m) are displaced from the ideal positions in the sense opposite to that in the pattern (k) (compare with Fig. (d) on page 93). These results show that the specimens did not yet form a uniform quasicrystal.

Computer Simulations

Computer simulations of CBED patterns were carried out by the usual matrix method. In our computations HOLZ reflections were taken into account automatically when their excitation errors became smaller than a given value. By considering the symmetry of a pattern, the pattern of a necessary minimum angular area was calculated and was extended to the other areas by symmetry operation. The anomalous absorpiton effect was taken into account by two ways. One is to calculate the imaginary parts of eigenvalues using the perturbation method and another is to evaluate the complex eigenvalues of the matrix which has Fourier coefficients of the absorption potential. It was found that the perturbation method worked good for obtaining the intensity profiles of reflections in a HOLZ ring, but sometimes showed an insufficient accuracy in obtaining the intensities of HOLZ lines appearing in ZOLZ reflections.

The computer used was an NEC-SX-1. Output data was transferred to a personal computer of NEC-9801, and CBED patterns were printed out with 17 grey levels using a laser printer of Canon LBP-B406. The intensities were modified by an appropriate gamma curve when necessary. For the patterns consisting of only ZOLZ reflections computation time at the NEC-SX-1 was saved by applying the Aitken-Neville interpolation method to the patterns at the NEC-9801. To reproduce HOLZ lines, one pixcel in a pattern must be taken about 1×10^{-4} rad.

Si

[111] Bright-Field Pattern

19 ZOLZ and 11 HOLZ beams, 100kV, thickness 156.8 nm

Three bright-field patterns were computed for different Debye-Waller factors of 0.0, 0.3 and 0.45. Appreciable differences are seen.

(a) Debye-Waller factor 0.0

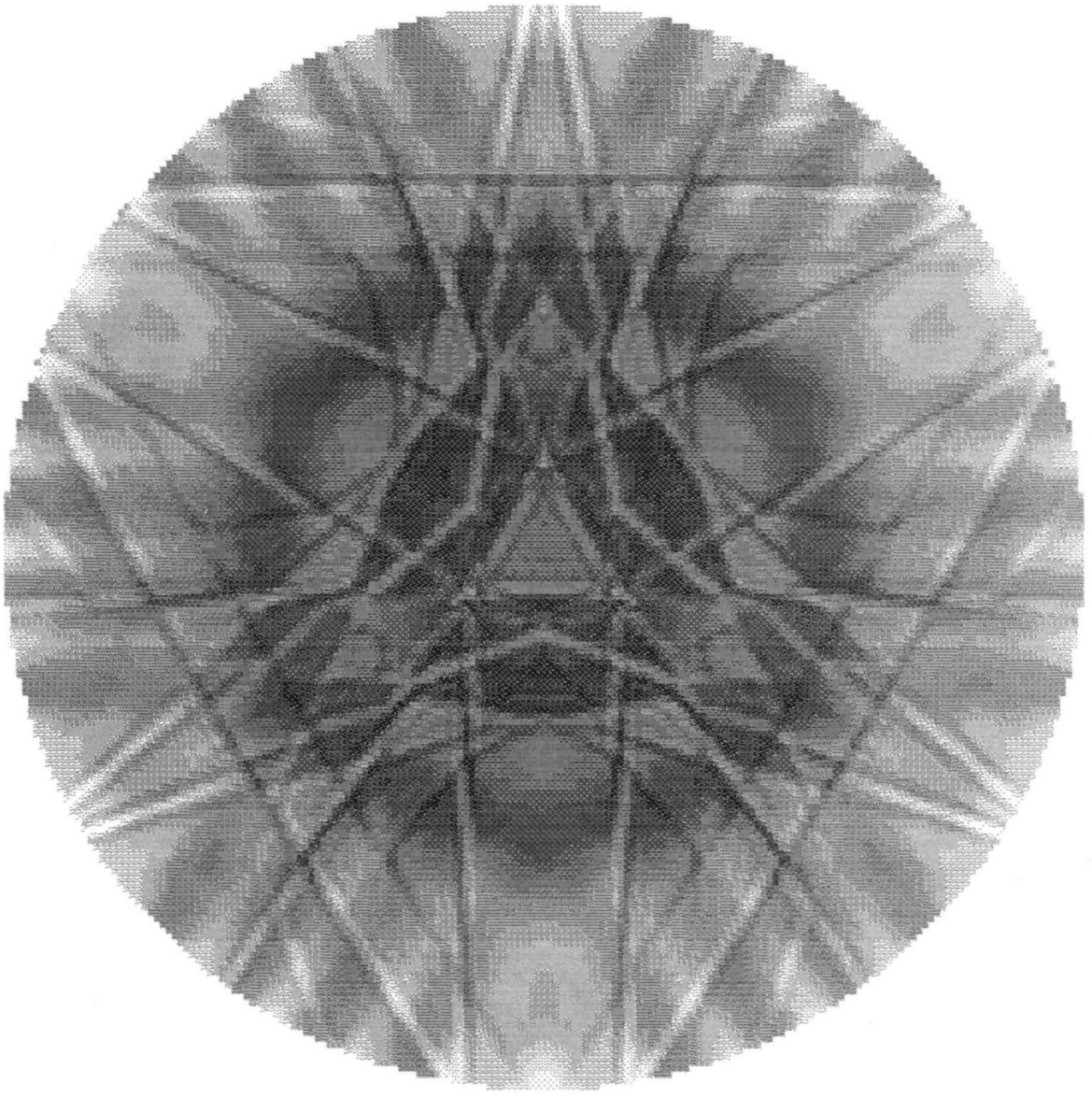

181 * 181 pixcels
type 3 enhancement curve / gamma-coef. = .5

19 ZOLZ and 11 HOLZ beams, 100kV, thickness 156.8 nm

(b) Debye-Waller factor 0.3

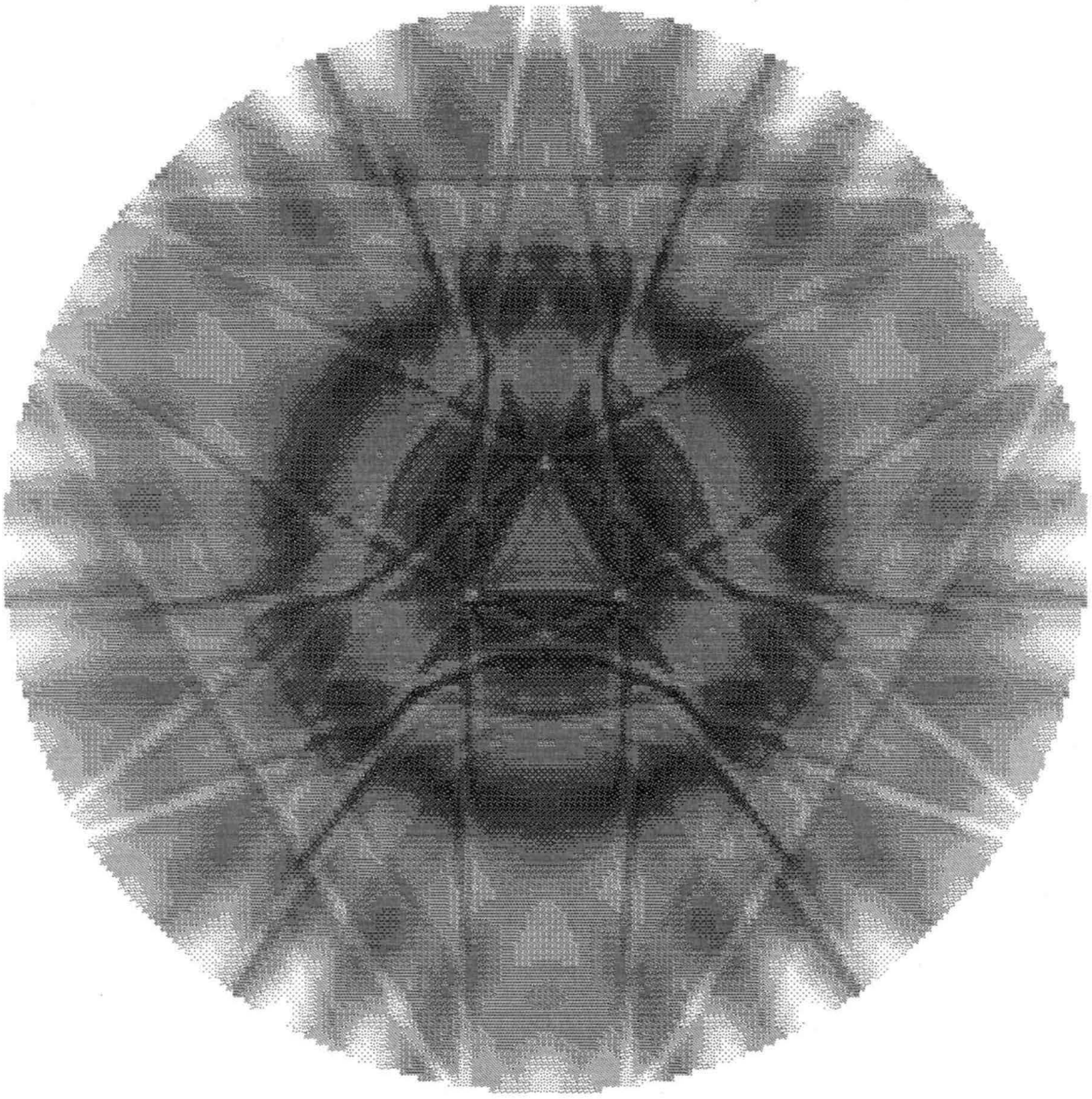

181 * 181 pixcels
type 3 enhancement curve / gamma-coef. = .5

(c) Debye-Waller factor 0.45

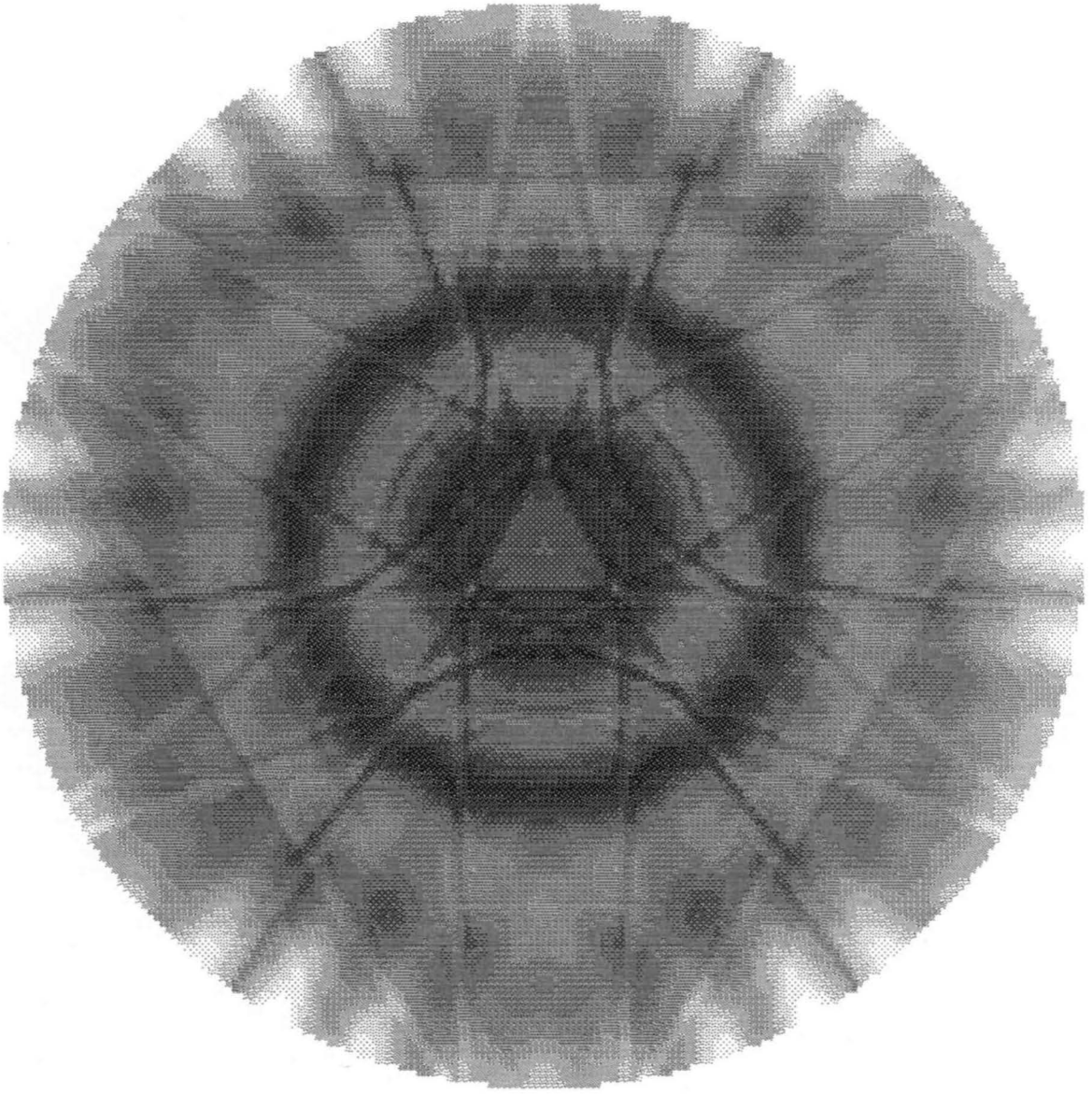

181 * 181 pixcels
type 3 enhancement curve / gamma-coef. = .5

[110] Bright-Field Pattern

23 ZOLZ beams, 100 kV

The bright-field patterns were computed for four different thicknesses at 100 kV. The patterns have no HOLZ lines.

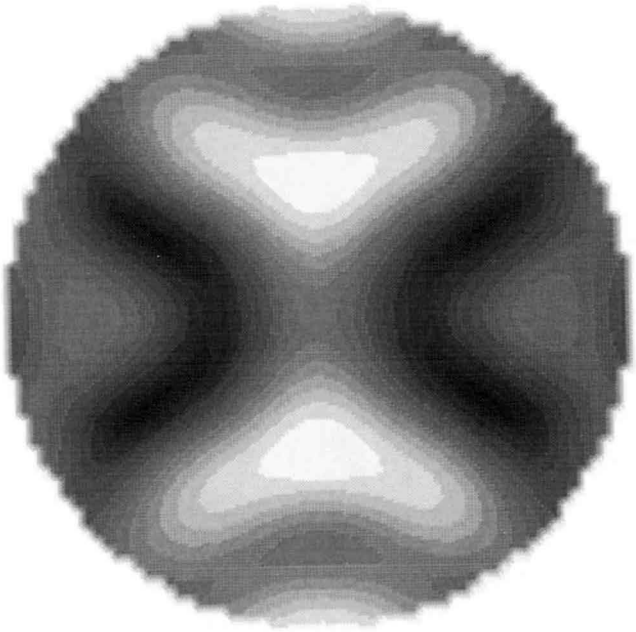

76.8 nm

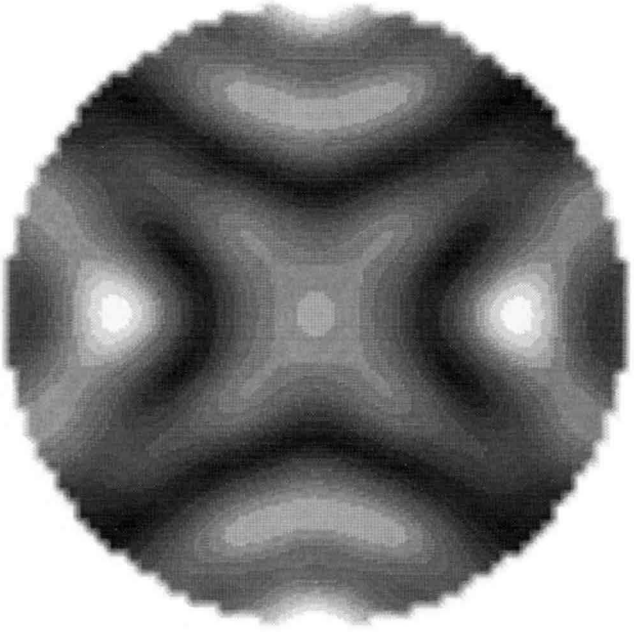

115.2 nm

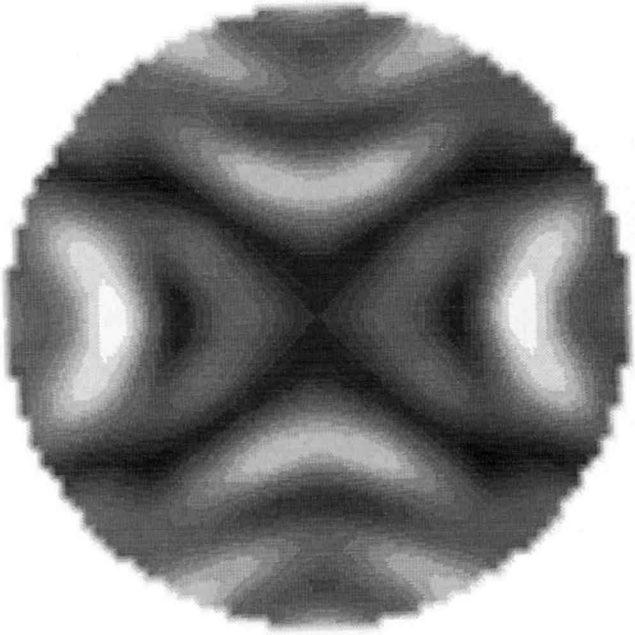

153.6 nm

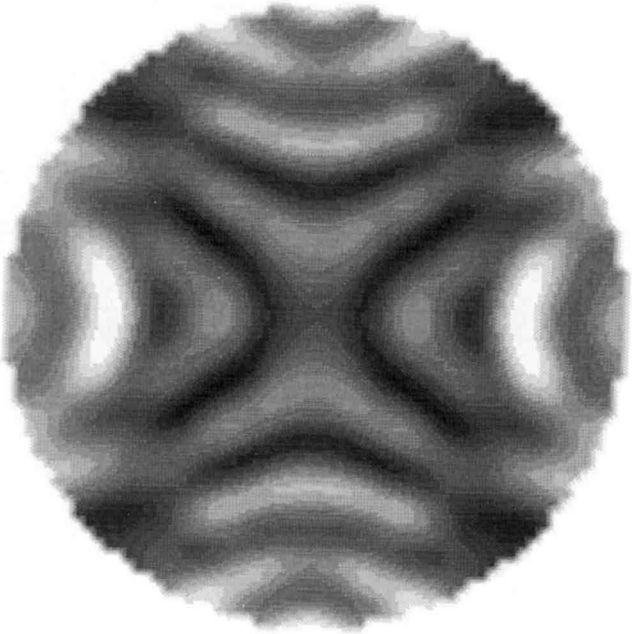

192.0 nm

original(before magnifying): 61 * 61 pixcels
magnified 3 times / 1 order interpolation
type 3 enhancement curve / gamma-coef. = .5

[001] Bright-Field Pattern

21 ZOLZ and 26 HOLZ beams, 40kV, Debye-Waller factor 0.45

The bright-field patterns were calculated for four different thicknesses at a low accelerating voltage of 40 kV to clearly see HOLZ lines.

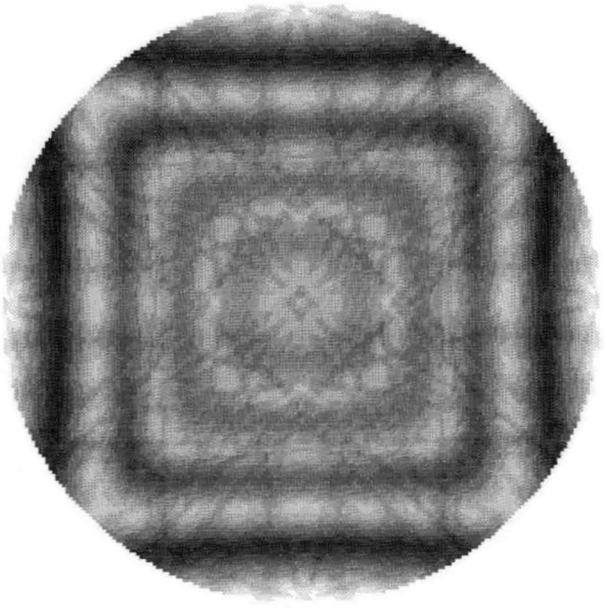

81.5 nm

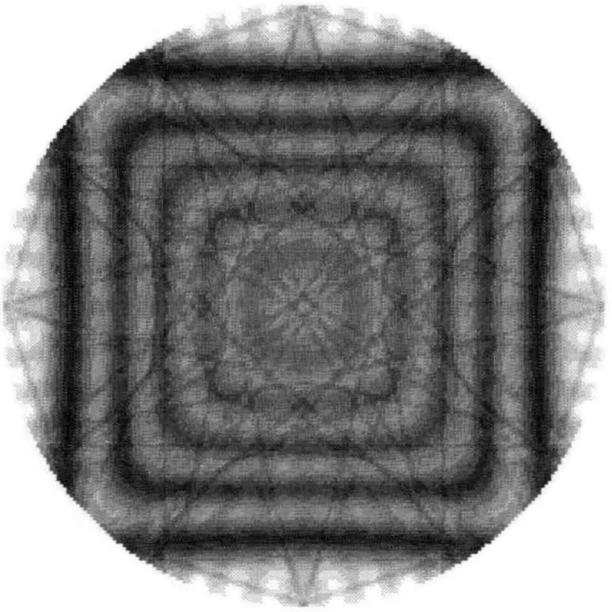

108.0 nm

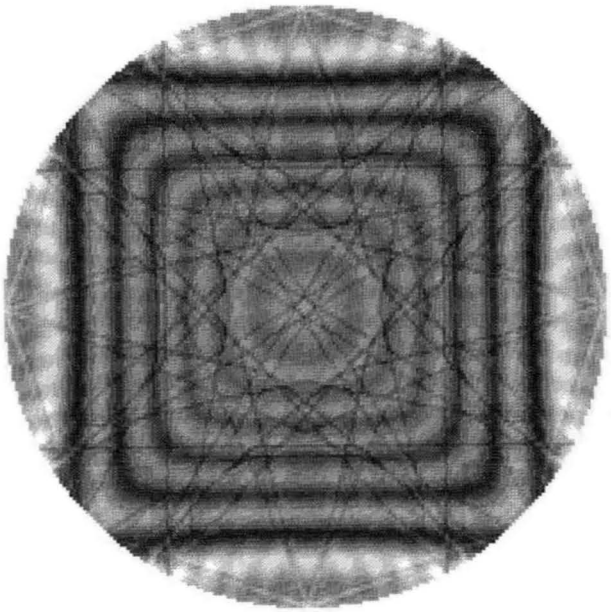

135.8 nm

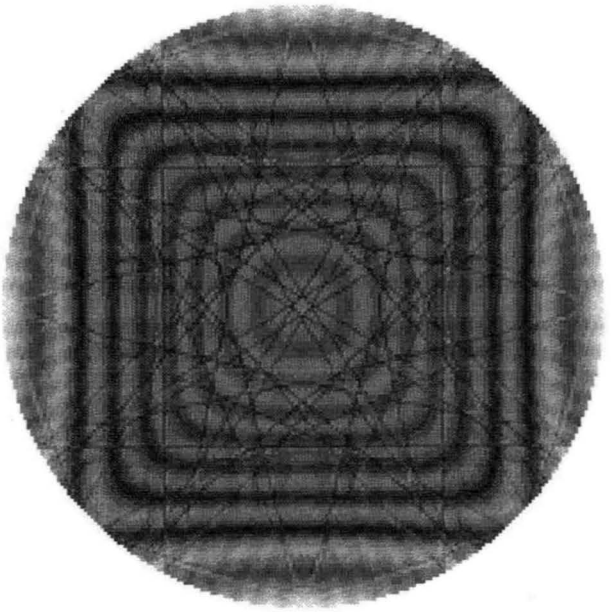

163.0 nm

181 * 181 pixcels
type 3 enhancement curve / gamma-coef. = .5

GaAs

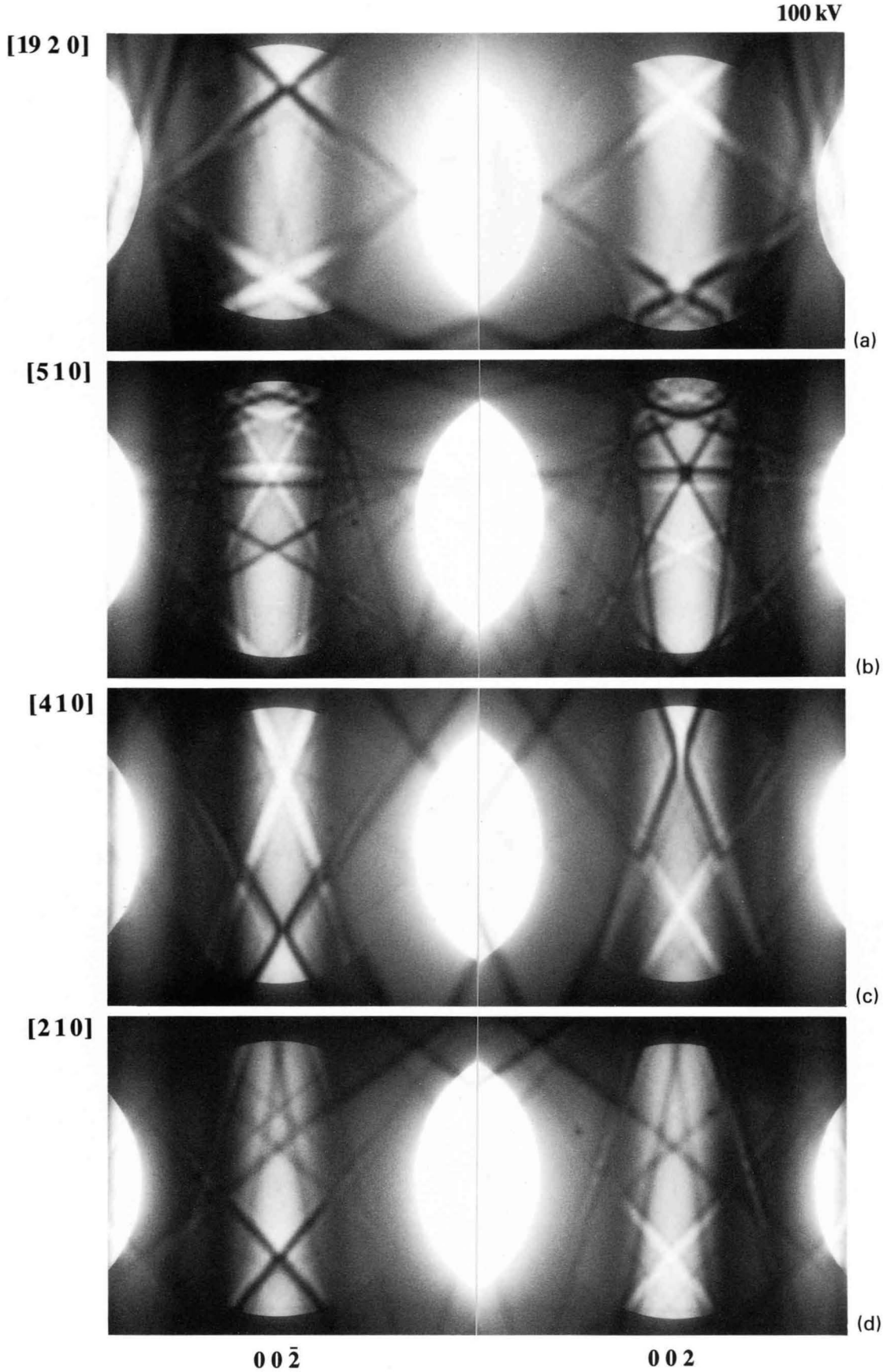

[625 262 0]

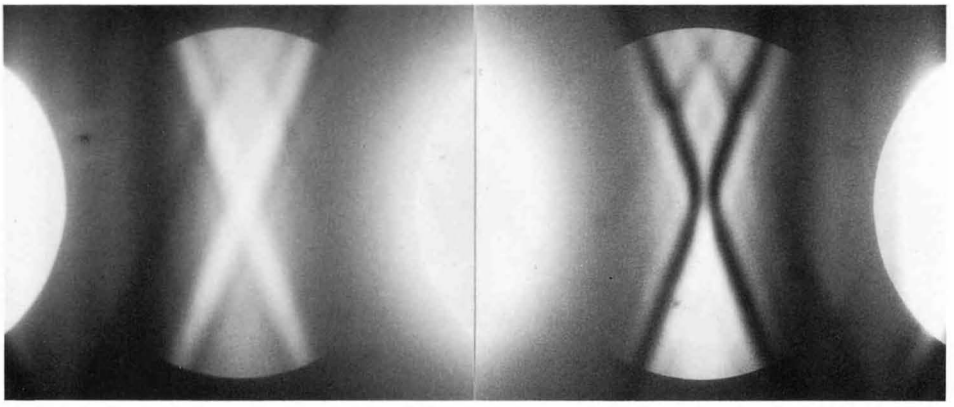

(e)

$00\bar{2}$ 002

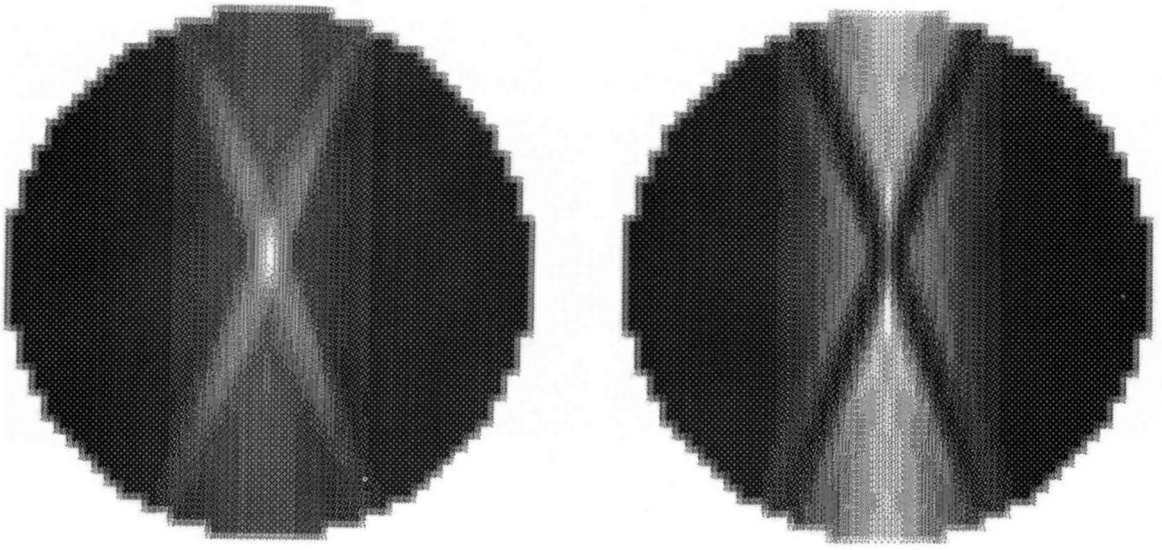

CBED patterns (a) to (e) were taken from GaAs at the settings of different azimuthal angles, clearly showing the lack of a symmetry 2_R. The simulated 002 and $00\bar{2}$ dark-field patterns at a thickness of 83.4 nm show a good agreement with Photo (e).

FeS_2

[100]

Thickness dependence of ZAP

60 kV

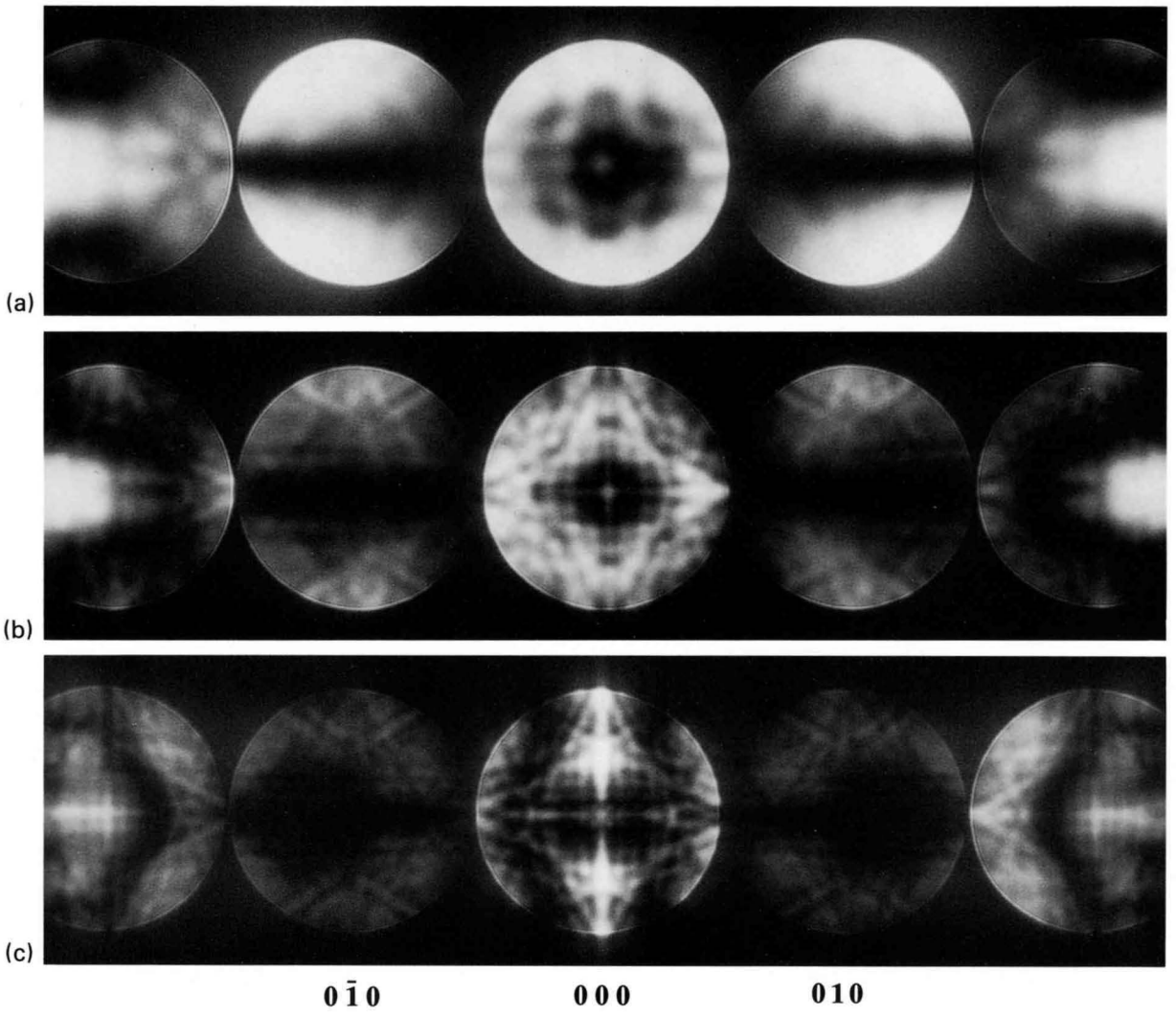

CBED patterns (a), (b) and (c) were taken from FeS_2 at the [100] incidence for three different thicknesses. The bright-field disks form light spots at their centers due to the reinforcement of the intensities of HOLZ lines. The bright-field patterns computed for three thicknesses using 37 ZOLZ and 84 HOLZ beams reproduced those light spots as shown on the opposite page.

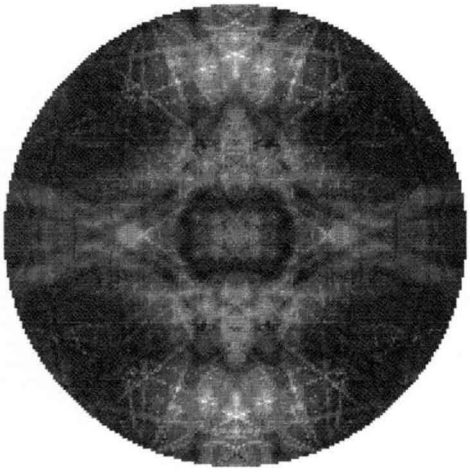

108.1 nm

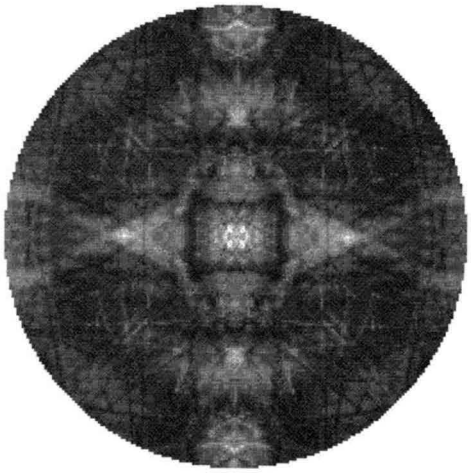

135.2 nm

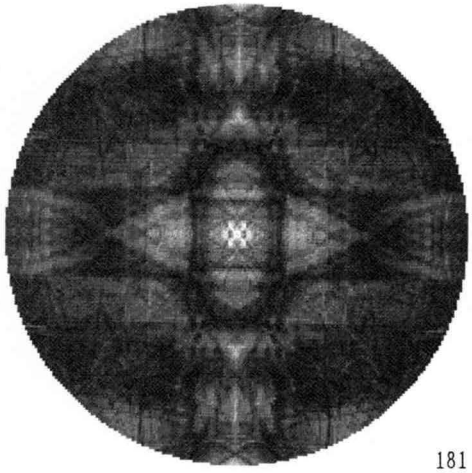

162.2 nm

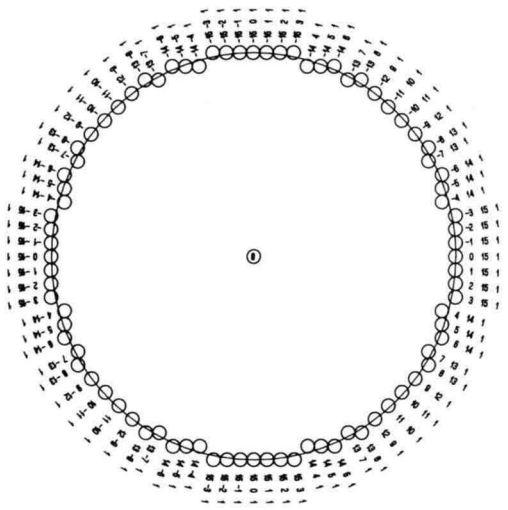

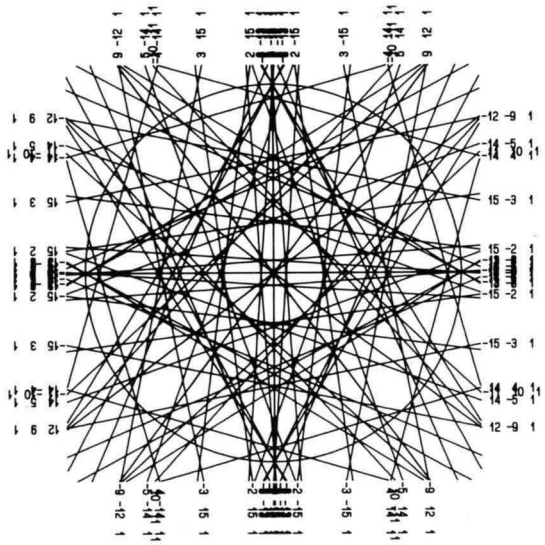

FeS2

[0 0 1]

61.9 kV

1 st Laue Zone

Holz-ring

(G= 0 0 0 excitation)

a=5.407Å
b=5.407Å
c=5.407Å
alpha=90°
beta =90°
gamma=90°

RADIUS OF HOLZRING
=2.7742 (1/A)
HORIZONTAL DIRECTION
=[0 1 0]*

181 * 181 pixcels
type 3 enhancement curve / gamma-coef. = .5

FeS_2 [001] 39 ZOLZ and 84 HOLZ beams, 61.9kV, thickness 135.2 nm

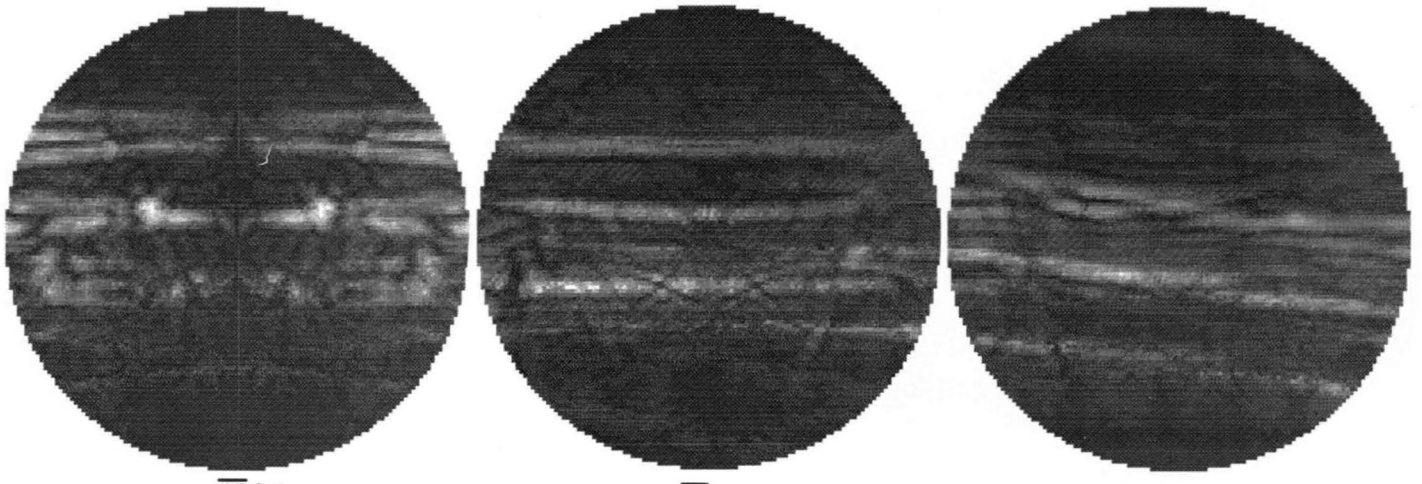

$\overline{1}501$ $\overline{1}511$ $\overline{1}521$

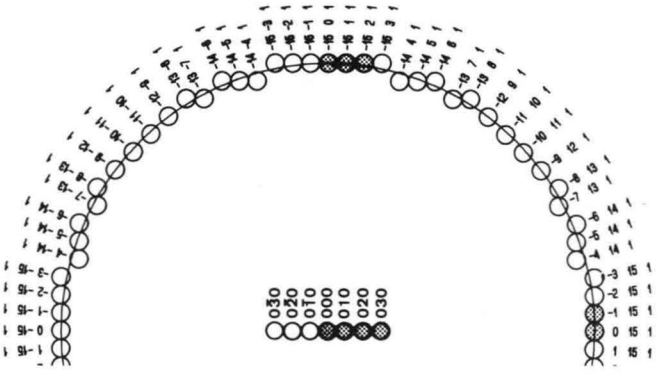

121 * 121 pixcels
type 3 enhancement curve / gamma-coef. = .5

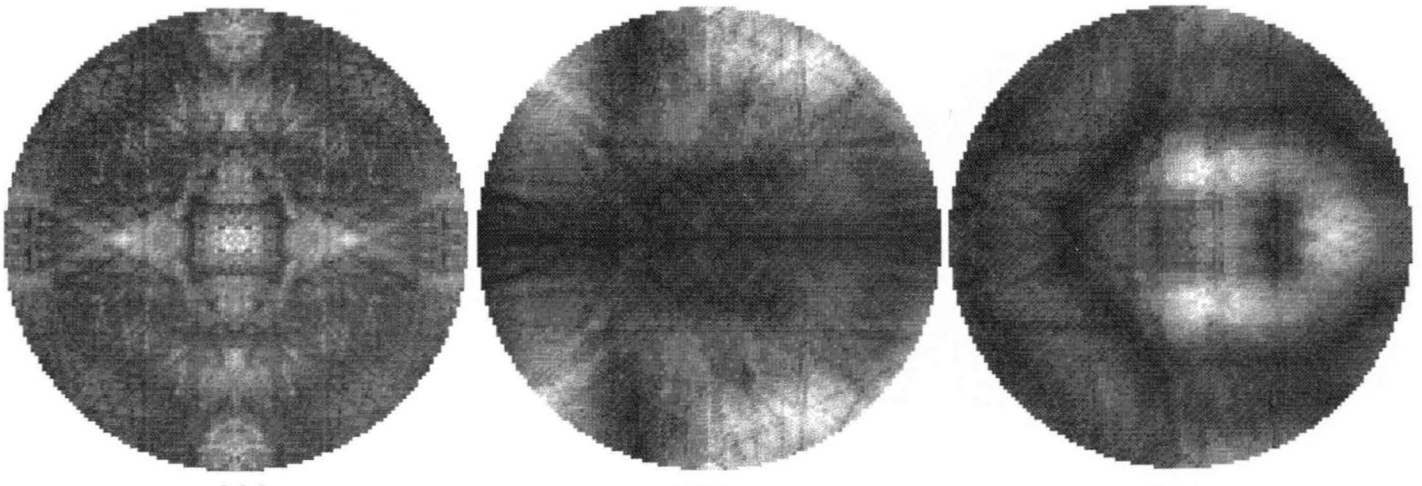

000 010 020

CBED patterns appearing not only in ZOLZ but also in HOLZ disks were simulated for FeS_2 by fully dynamical computations. Fine structures of patterns in HOLZ disks were reproduced. GM lines due to the *c*-glide plane parallel to the (010) plane and the *b*-glide plane parallel to the (100) plane are clearly seen in the $\overline{1}5\ 0\ 1$ and 0 15 1 HOLZ disks, respectively.

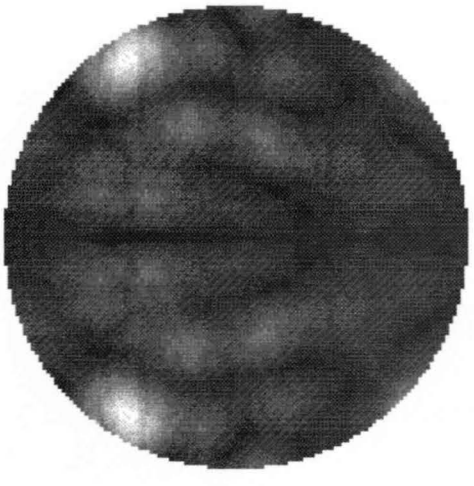

0 3 0

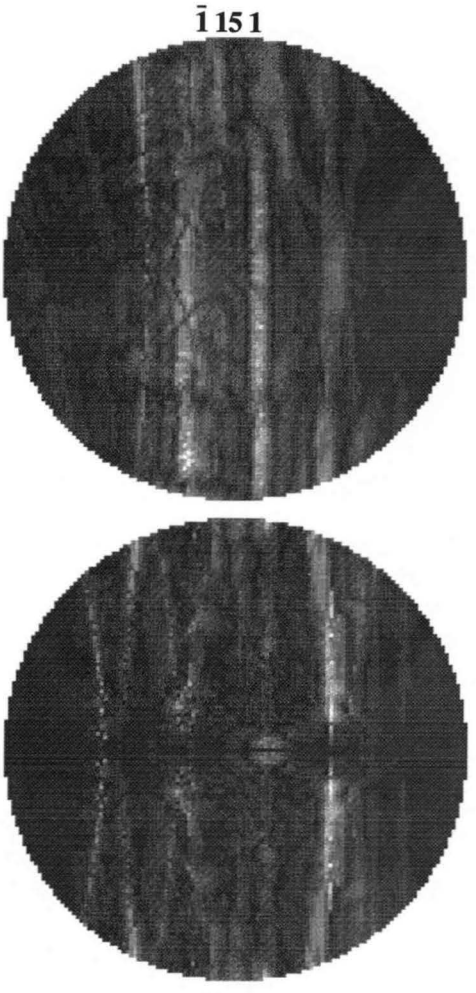

$\bar{1}$ 15 1

0 15 1

Sensitivity of CBED Patterns to the Breakdown of Symmetry Elements

CBED patterns are known to be very sensitive to crystal symmetry, but their sensitivity has not ever been discussed quantitatively. The sensitivity was studied for FeS_2 by computer simulation. The crystal structure of FeS_2 is schematically shown in Fig. (a). Its space group is $P2_1/a\bar{3}$.

Two hypothetical crystal structures were formed by displacing two sulfur atoms, A and A′ from the positions ($u=0.386$) in the real crystal. 1) The atoms A and A′ were displaced in the [111] direction to make them approach each other. The displacement caused the loss of 2_1 screw axes and a-glide planes, resulting in the space group $P\bar{3}$. 2) These atoms were displaced in the same sense in the [111] direction with their distance kept constant. The displacement caused the loss of inversion centers, resulting in the space group $P3$. The magnitude of the displacement δu was varied from -0.001 to -0.01 of the cell parameter, 0.5407 nm. Using 34-40 ZOLZ beams calculations of CBED patterns were carried out at an accelerating voltage of 60 kV and at the [001] electron incidence for three different thicknesses and for three different Bragg settings. It was studied how the CBED patterns change with gradual breakdown of crystal symmetries.

Figure (b) shows 010 dark-field CBED patterns computed at the 010 exact Bragg setting for five values of type 1) displacement. The pattern at extreme left was computed for a perfect crystal, which shows a cross of A_2 and B_2 GM lines with a symmetry $2mm$. As δu increases, the symmetry $2mm$ changes into a symmetry 1_R. The symmetry 1_R is expected from ZOLZ (projection) interaction, even if the crystal has no symmetry. The breakdown of the symmetry $2mm$ is already recognizable for $\delta u=-0.001$. For $\delta u=-0.002$, the breakdown is clearly seen as a deformed cross of the GM lines. Such deformed GM lines due to a slight breakdown of a 2_1 screw axis were already seen in the section of Mo_2S_3. The lower patterns in Fig. (b) are the difference patterns between the upper halves and lower halves of the original (upper) patterns. We define a quantitative measure of the difference, Δ, as

$$\Delta = \sum_{\text{disk}} |I_u - I_\ell| / \sum_{\text{disk}} (I_u + I_\ell),$$

where I_u and I_ℓ are the intensities at two pixcels which are related by a horizontal mirror plane passing through

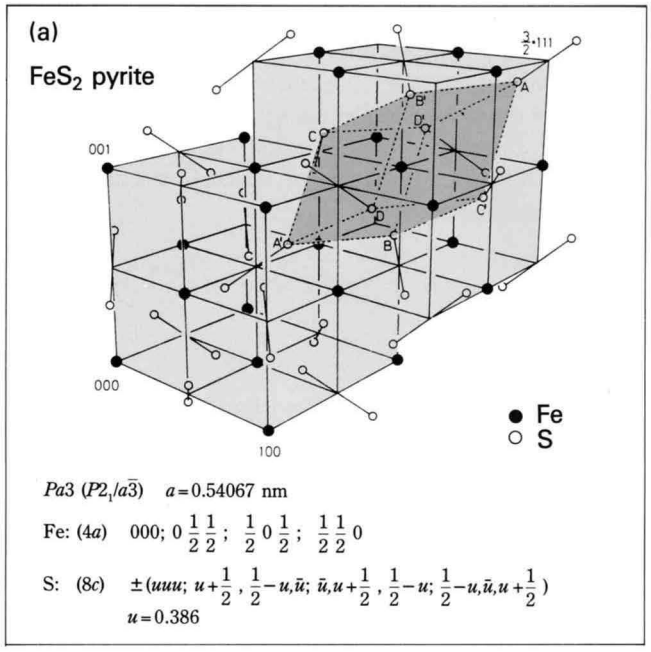

the center of the disk. The summing was carried out over the whole disk. The values of Δ are given below the patterns. It should be noted that Δ is 0.144 already for $\delta u=-0.001$ (actual displacement of 0.00054 nm) and reaches 0.71 for a displacement of 0.0054 nm.

Figure (c) shows $0\bar{1}0$ dark-field CBED patterns computed at the 010 exact Bragg setting for the same displacements of Fig. (b). The pattern at extreme left was obtained again from a perfect crystal, which shows a symmetry m with an A_2 GM line. As δu increases, the symmetry m is lost. The difference pattern is given below each original pattern. It is seen that the values of Δ are smaller than those in Fig. (b).

Figures (d), (e) and (f) are three sets of CBED patterns, all computed at the 010 exact Bragg setting for thicknesses of 54.1 nm, 108.1 nm and 162.2 nm, respectively. Changes of patterns due to both the increase of δu and thickness are obviously seen. The next three sets of CBED patterns, (g), (h) and (i), were computed at the 030 exact Bragg setting for the same thicknesses, and the last three sets, (j), (k) and (l), were computed at the 050 exact Bragg setting. It is seen that the breakdown of the symmetries is the greatest for the first set and the smallest for the last set.

FeS_2 [001]
010 excitation
60 kV

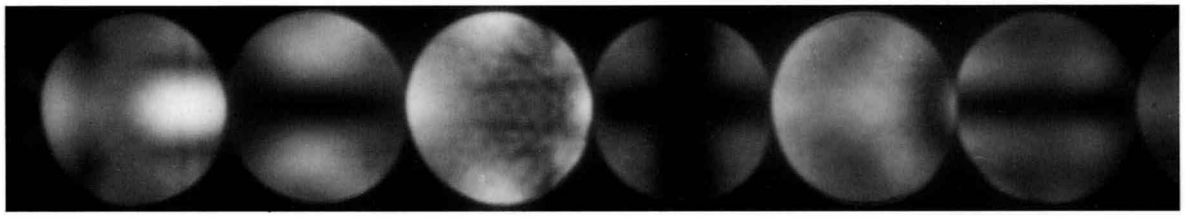

$0\bar{2}0$ $0\bar{1}0$ 000 010 020 030

Breakdown of symmetry 2*mm*

FeS_2 [0 0 1], 0 1 0 excitation, 34 ZOLZ beams, 60 kV, thickness 108.1 nm

(b) 010 reflections

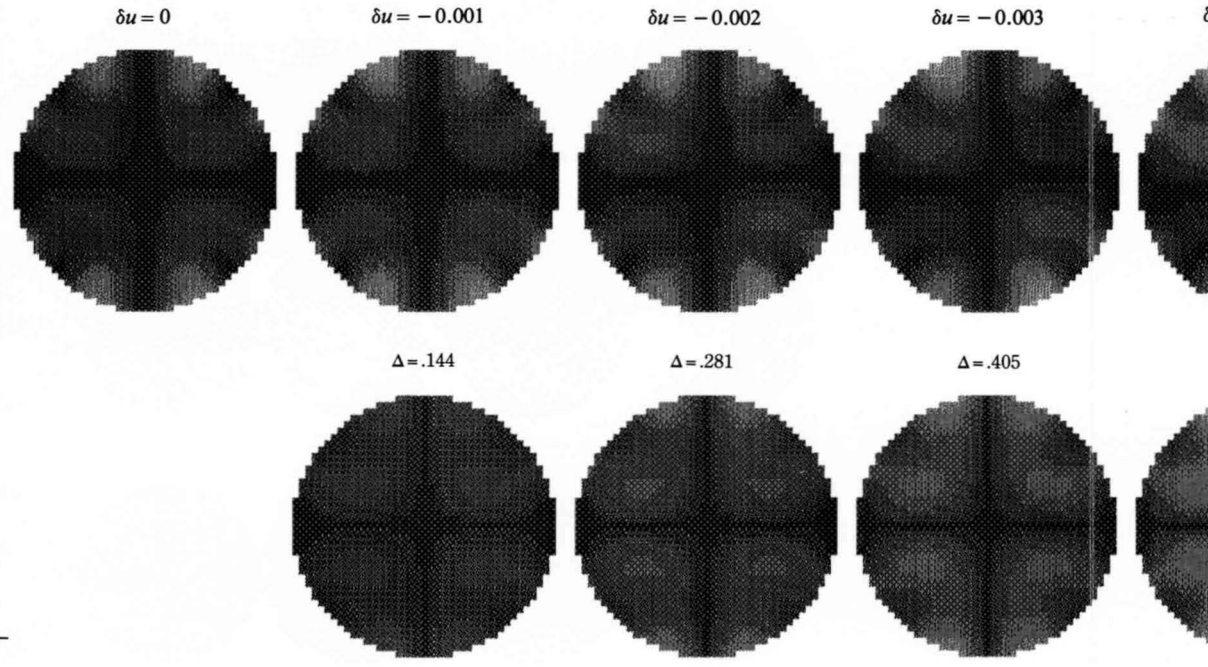

$$\Delta = \frac{\Sigma \mid I_u - I_\ell \mid}{\Sigma_{\text{disk}} (I_u + I_\ell)}$$

Breakdown of symmetry m_v

FeS_2 [0 0 1], 0 1 0 excitation, 34 ZOLZ beams, 60 kV, thickness 108.1 nm

(c) $0\bar{1}0$ reflections

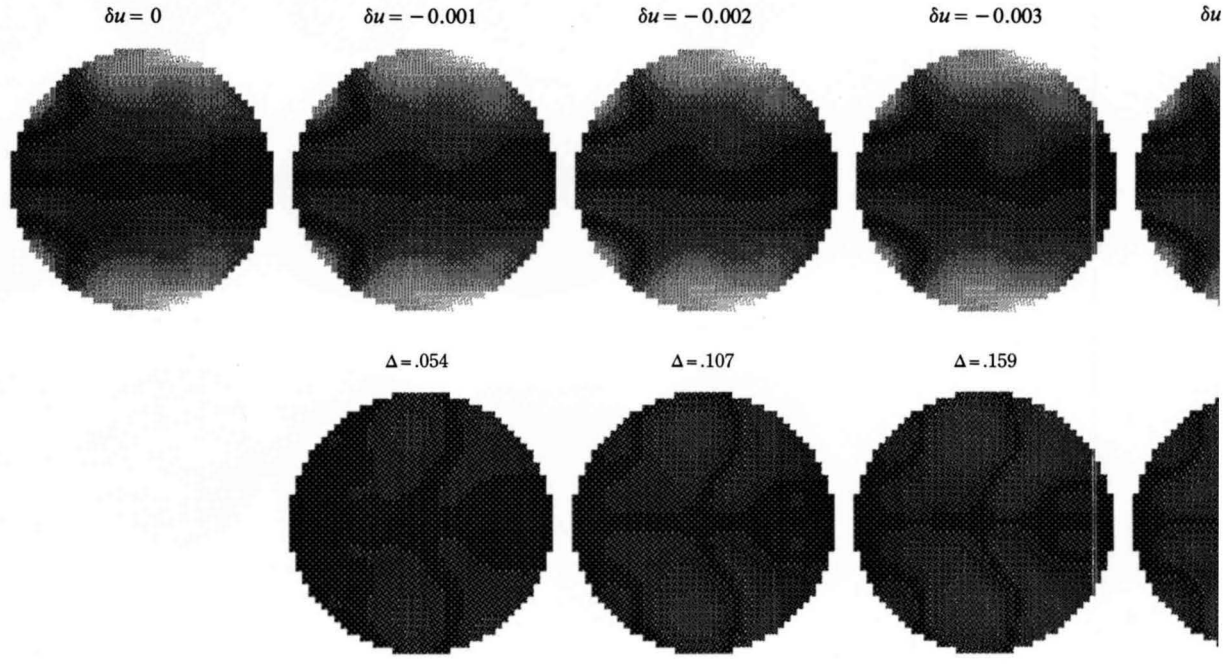

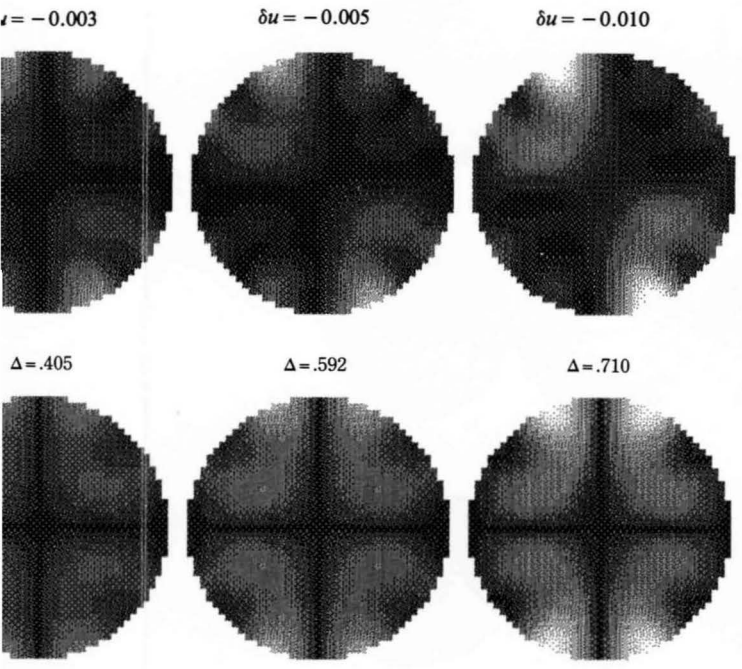

$2mm \rightarrow 1_R \quad (Pa3 \rightarrow P\bar{3})$

Difference

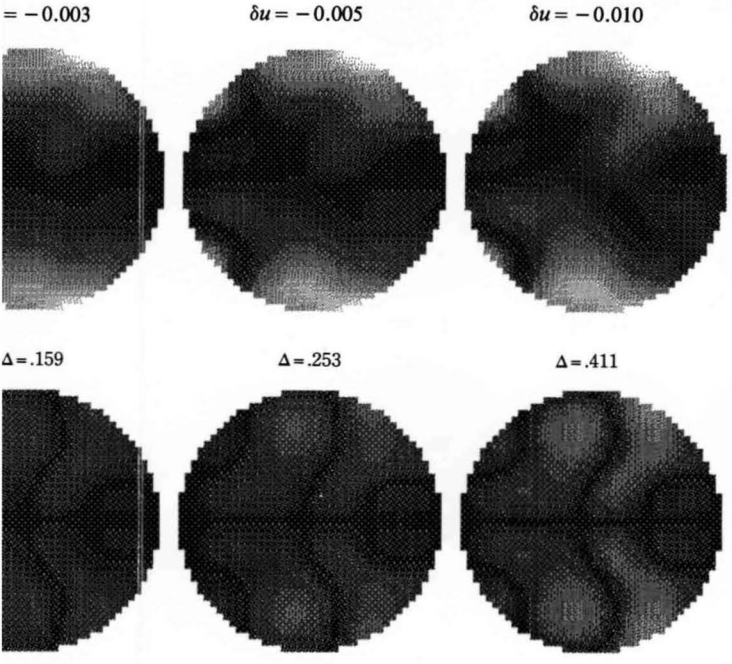

$m_v \rightarrow 1 \quad (Pa3 \rightarrow P\bar{3})$

Difference

41 * 41 pixcels
type 3 enhancement curve / gamma-coef. = .7

Breakdown of symmetry m_v

FeS_2 [001], 010 excitation, 34 ZOLZ beams, 60kV

(d) Thickness 54.1 nm

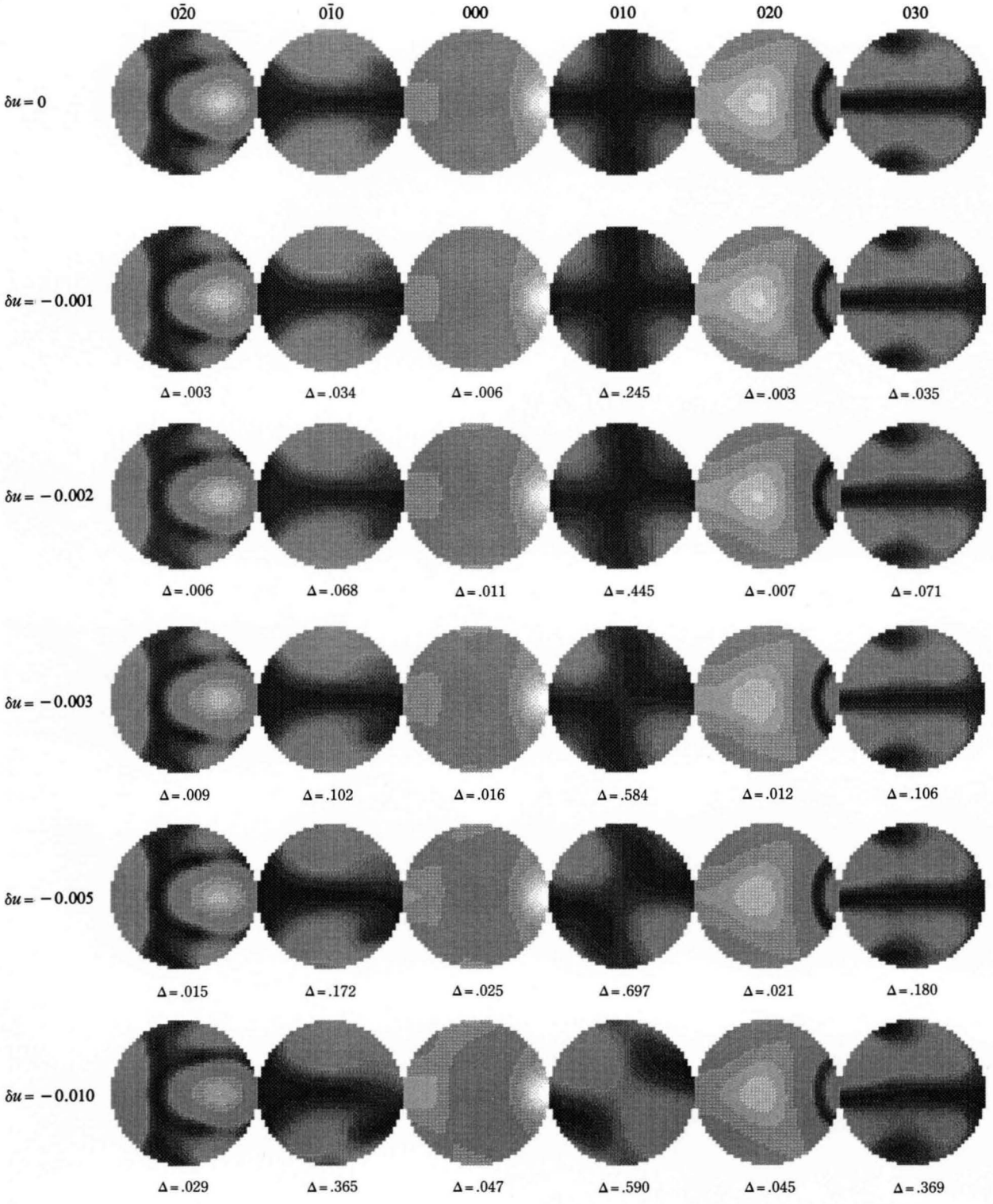

41 * 41 pixcels
type 6 enhancement curve / gamma-coef. = 1.5

(e) Thickness 108.1 nm

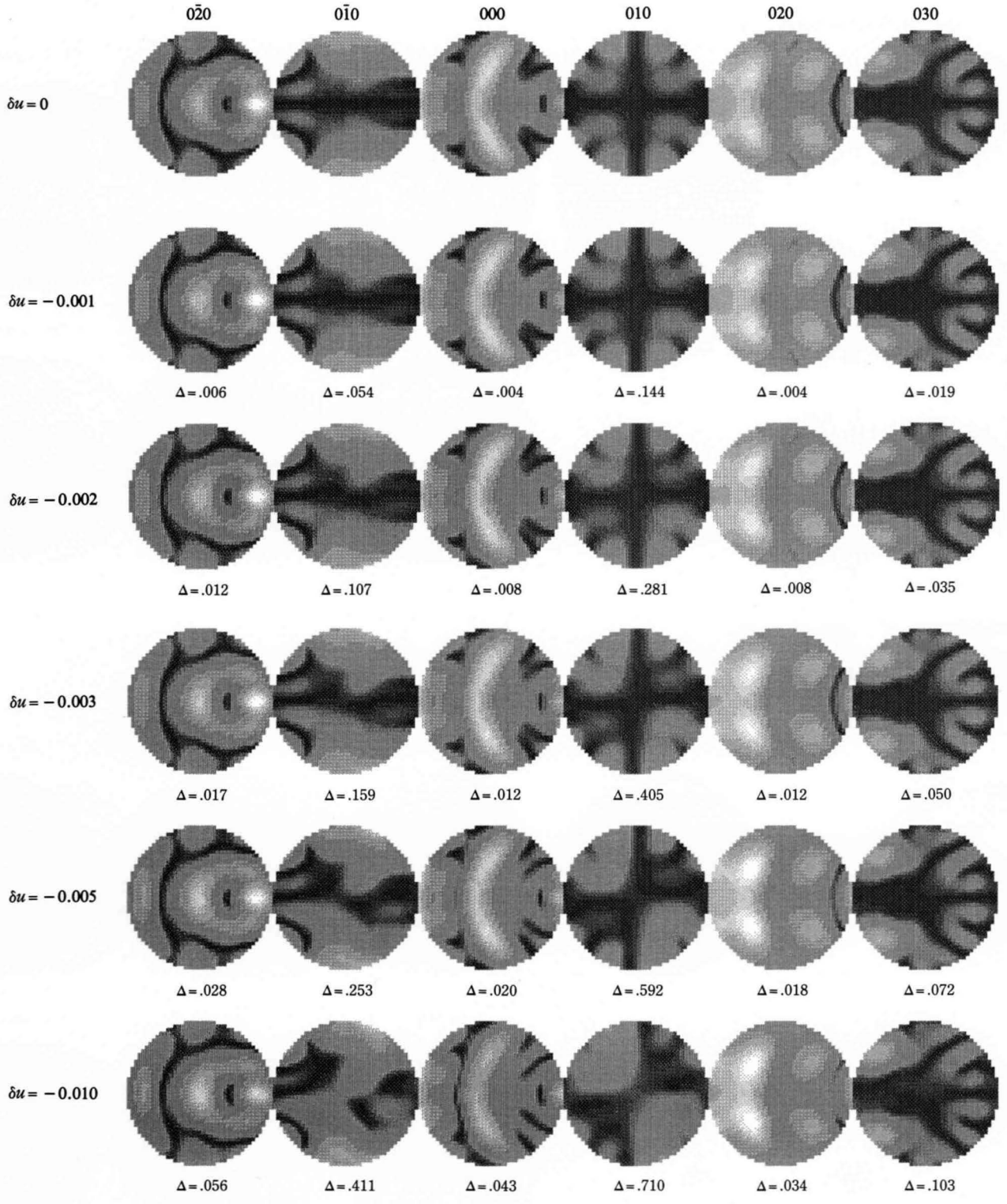

41 * 41 pixcels
type 6 enhancement curve / gamma-coef. = 1.5

(f) Thickness 162.2 nm

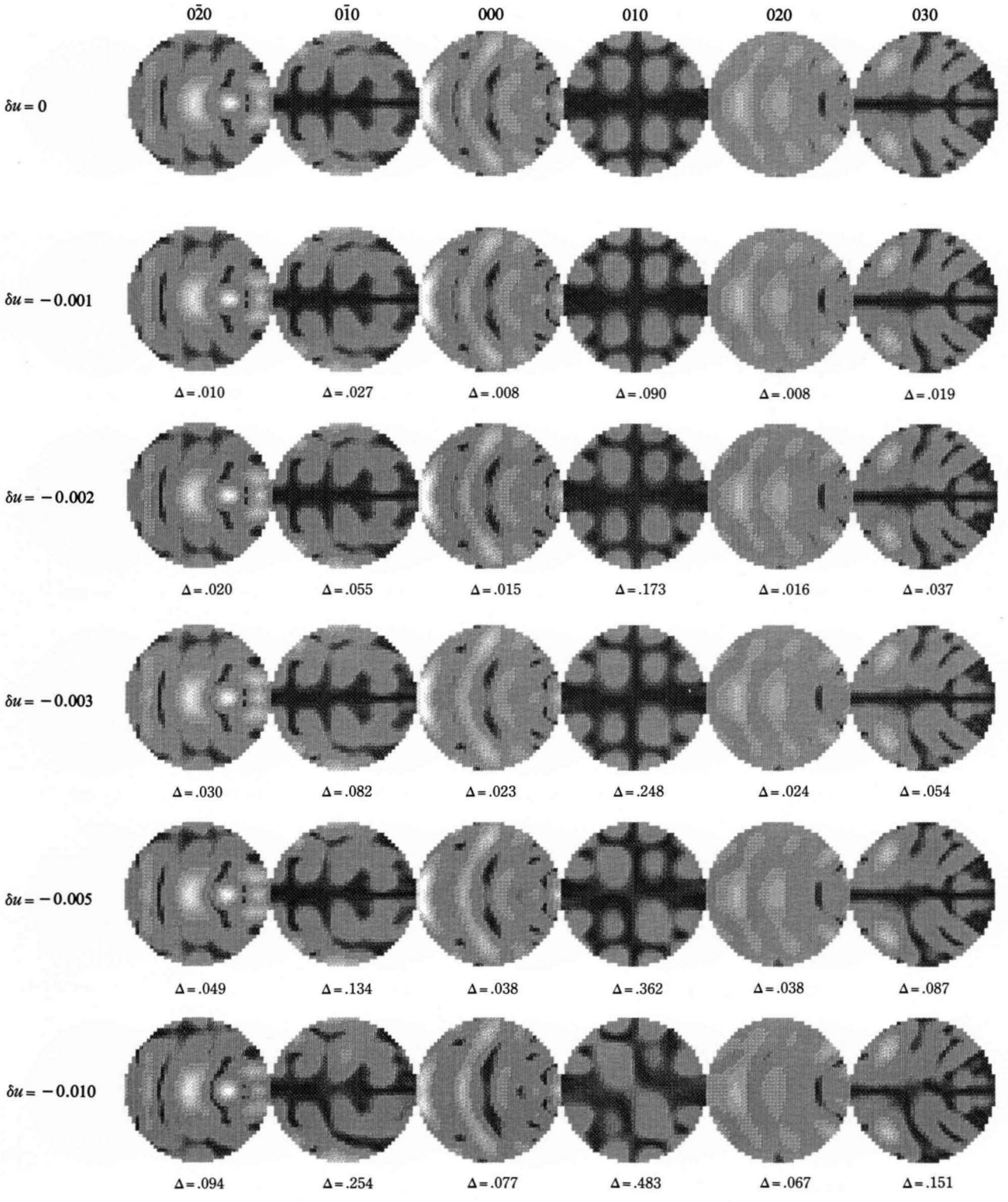

41 * 41 pixcels
type 6 enhancement curve / gamma-coef. = 1.5

Breakdown of symmetry m_v

FeS_2 [001], 030 excitation, 34 ZOLZ beams, 60kV

(g) Thickness 54.1 nm

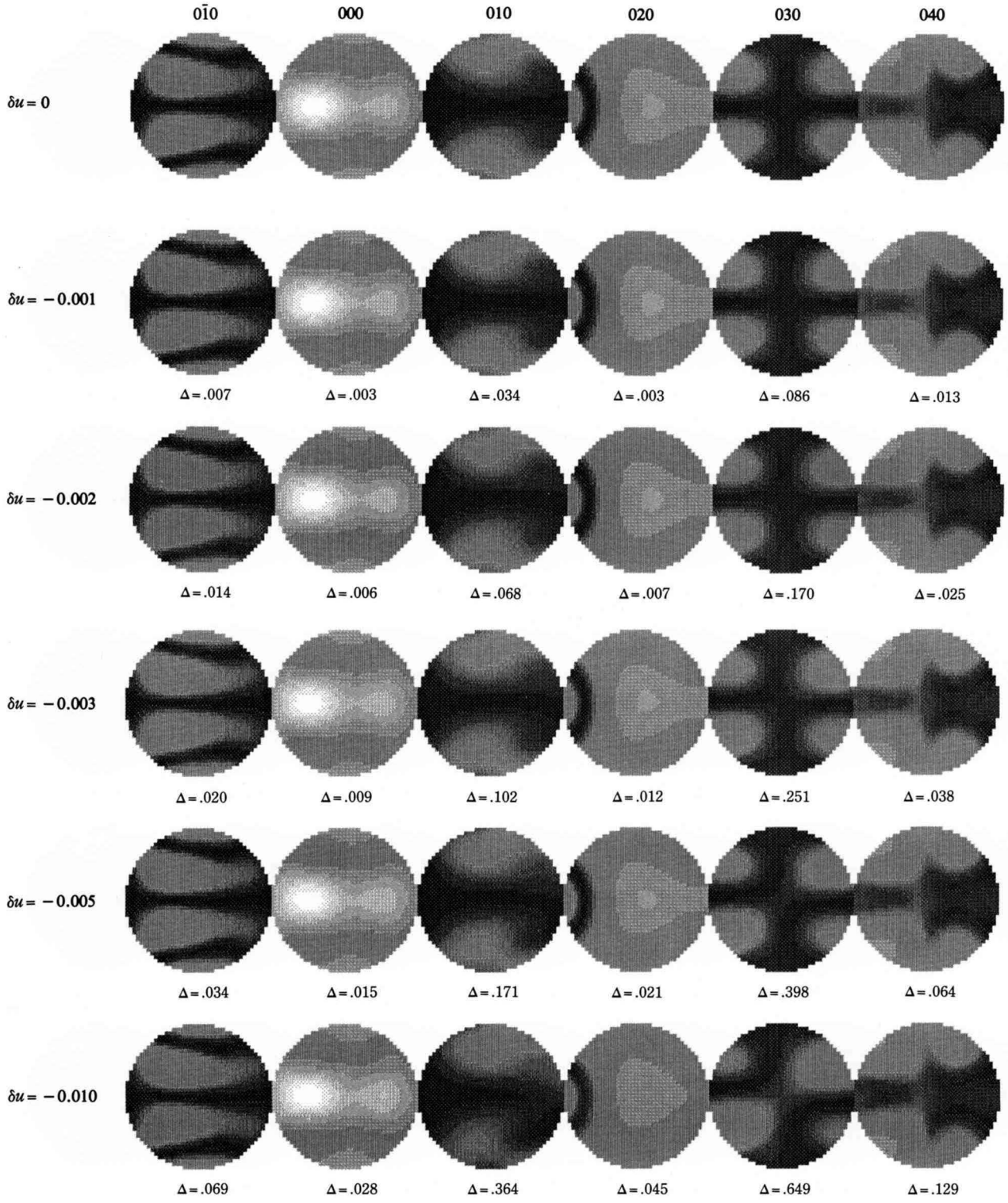

41 * 41 pixcels
type 6 enhancement curve / gamma-coef. = 1.5

(h) Thickness 108.1 nm

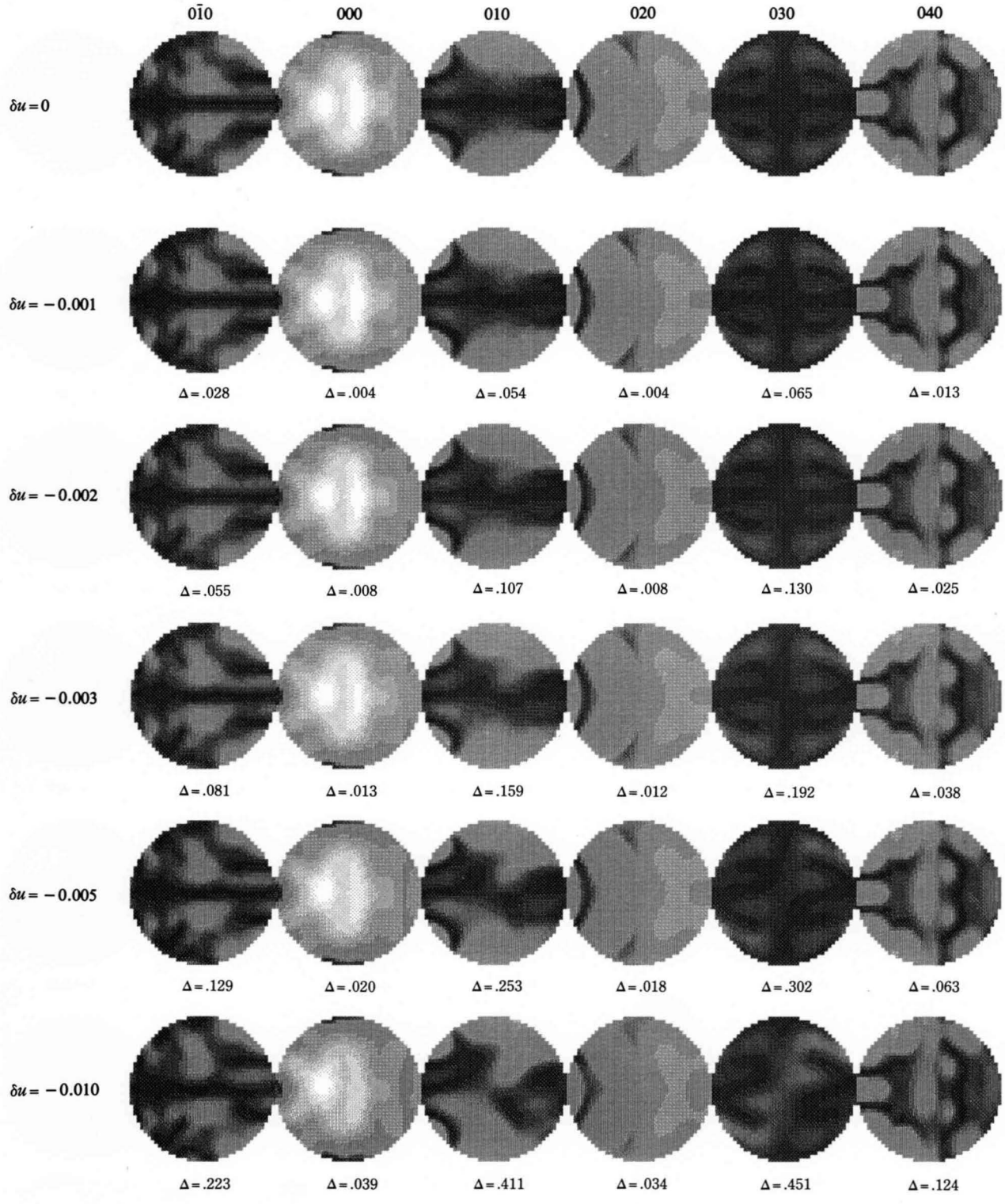

41 * 41 pixcels
type 6 enhancement curve / gamma-coef. = 1.5

(i) Thickness 162.2 nm

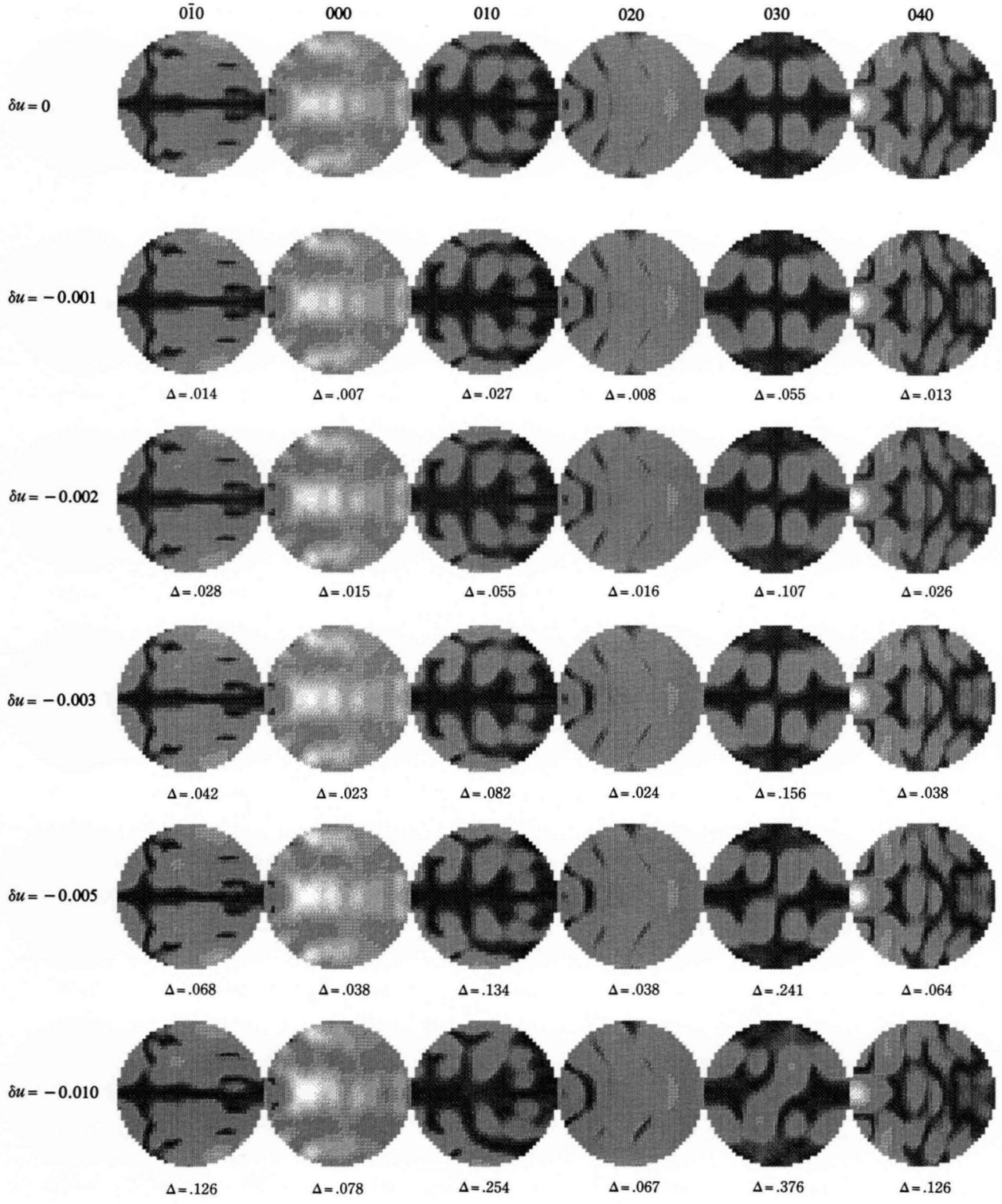

41 * 41 pixcels
type 6 enhancement curve / gamma-coef. = 1.5

Breakdown of symmetry m_v

FeS_2 [001], 050 excitation, 40 ZOLZ beams, 60kV

(j) Thickness 54.1 nm

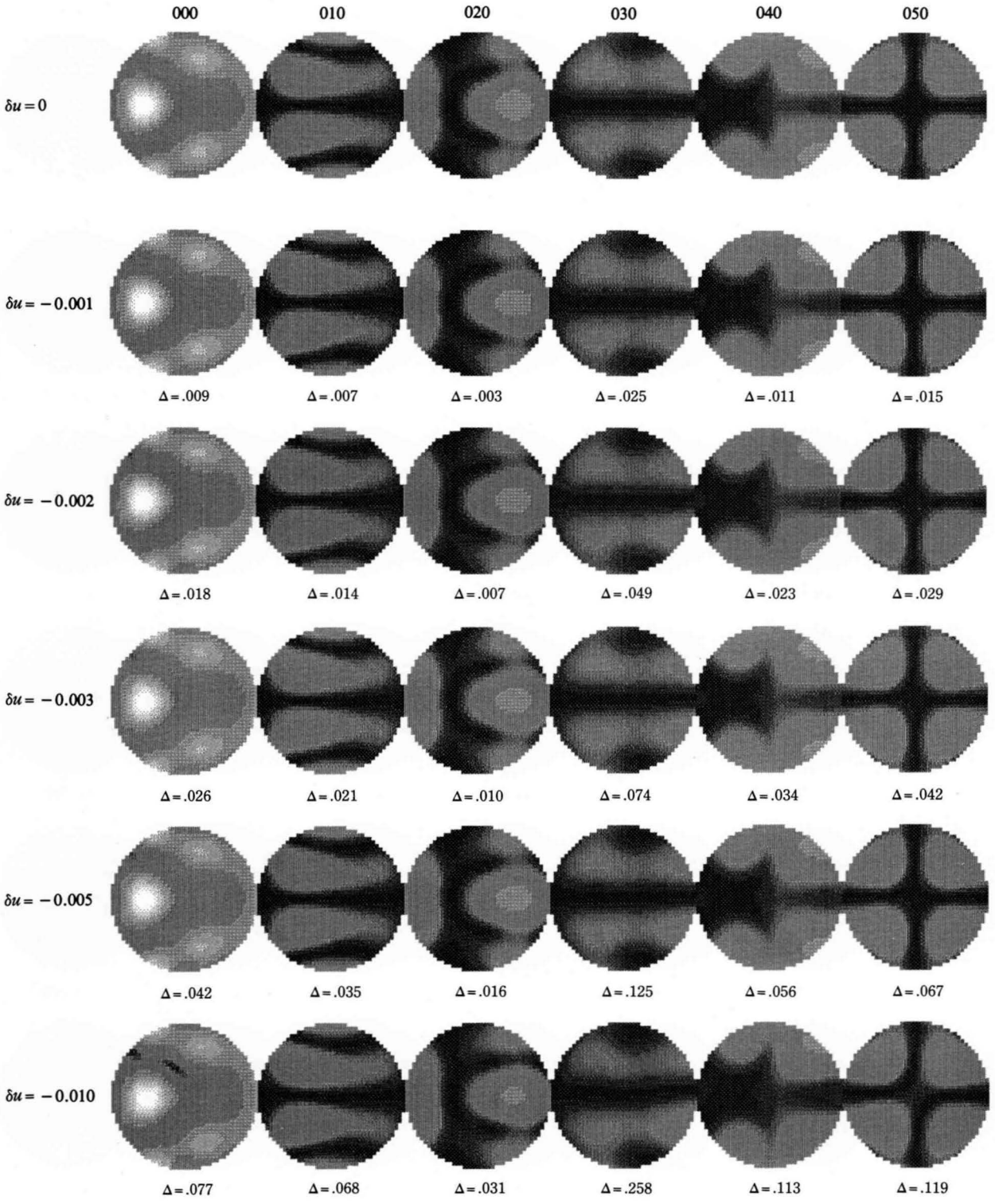

41 * 41 pixcels
type 6 enhancement curve / gamma-coef. = 1.5

(k) Thickness 108.1 nm

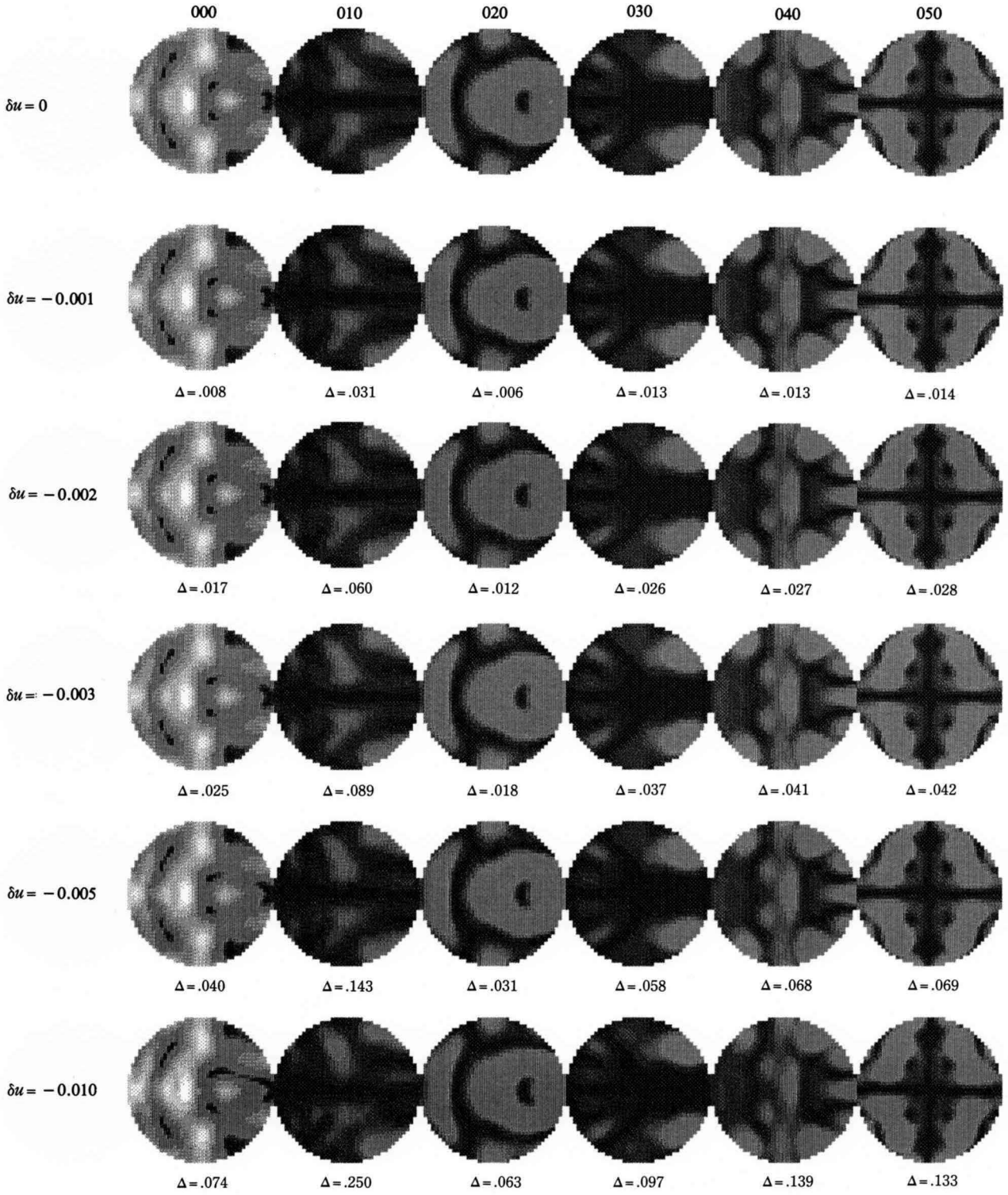

41 * 41 pixcels
type 6 enhancement curve / gamma-coef. = 1.5

(I) Thickness 162.2 nm

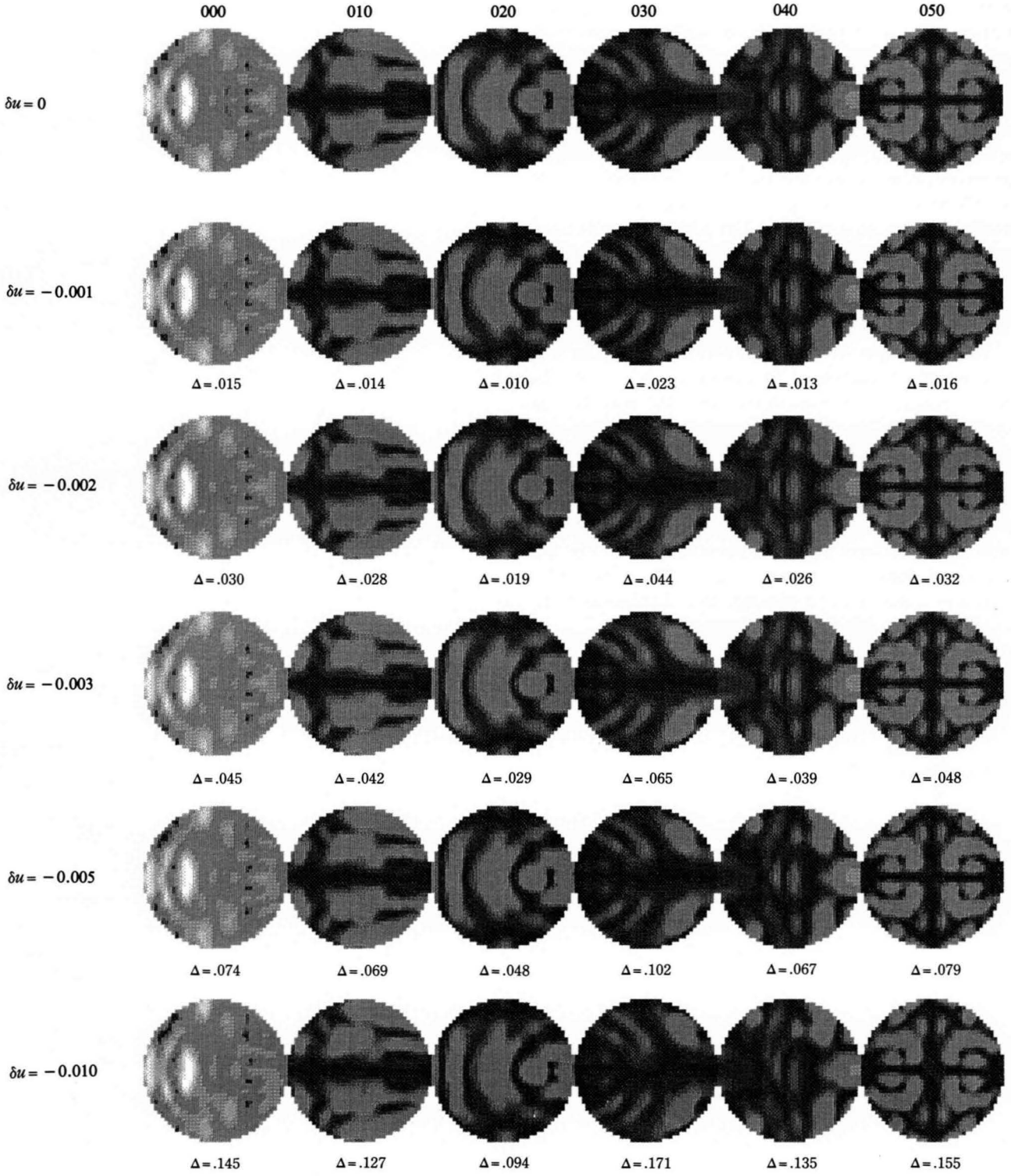

41 * 41 pixcels
type 6 enhancement curve / gamma-coef. = 1.5

The values of Δ were plotted as a function of δu, where the values of Δ for $\delta u = -0.01$ were omitted, because the measure Δ is no more suitable for correctly expressing the intensity difference for such a large value of δu. Figures (a), (b) and (c) give the results of the 010, 030 and 050 Bragg settings. The highest sensitivity was obtained for the 010 Bragg setting and the lowest one for the 050 Bragg setting. The reflections with larger excitation errors show low sensitivities. These facts indicate that the reflections which suffer from strong dynamical interaction show high sensitivity. The odd order reflections are more sensitive to the breakdown of the symmetries than the even order reflections, because the intensities of the even order (kinematically allowed) reflections are affected little by the displacements of the sulfer atoms. Thickness changes of the sensitivity is seen. The 010 reflection at a thickness of 54.1 nm (Fig. (a)) shows the highest sensitivity. It is quite sure that the sensitivity is closely related to the effective extinction distance of this reflection and is lowered with increasing thickness due to the absorption effect.

If it is assumed that a difference of $\Delta = 0.15$ is detectable in experimental patterns, which must, of course, be taken from specimens with uniform thickness, Fig. (a) indicates, at least for the present case, that CBED patterns have a potential to distinguish a displacement of less than $\delta u = 0.001$ in mean atomic positions.

Breakdown of symmetry m_v

FeS_2 [0 0 1], 34 ZOLZ beams, 60 kV

(a) 0 1 0 Bragg setting

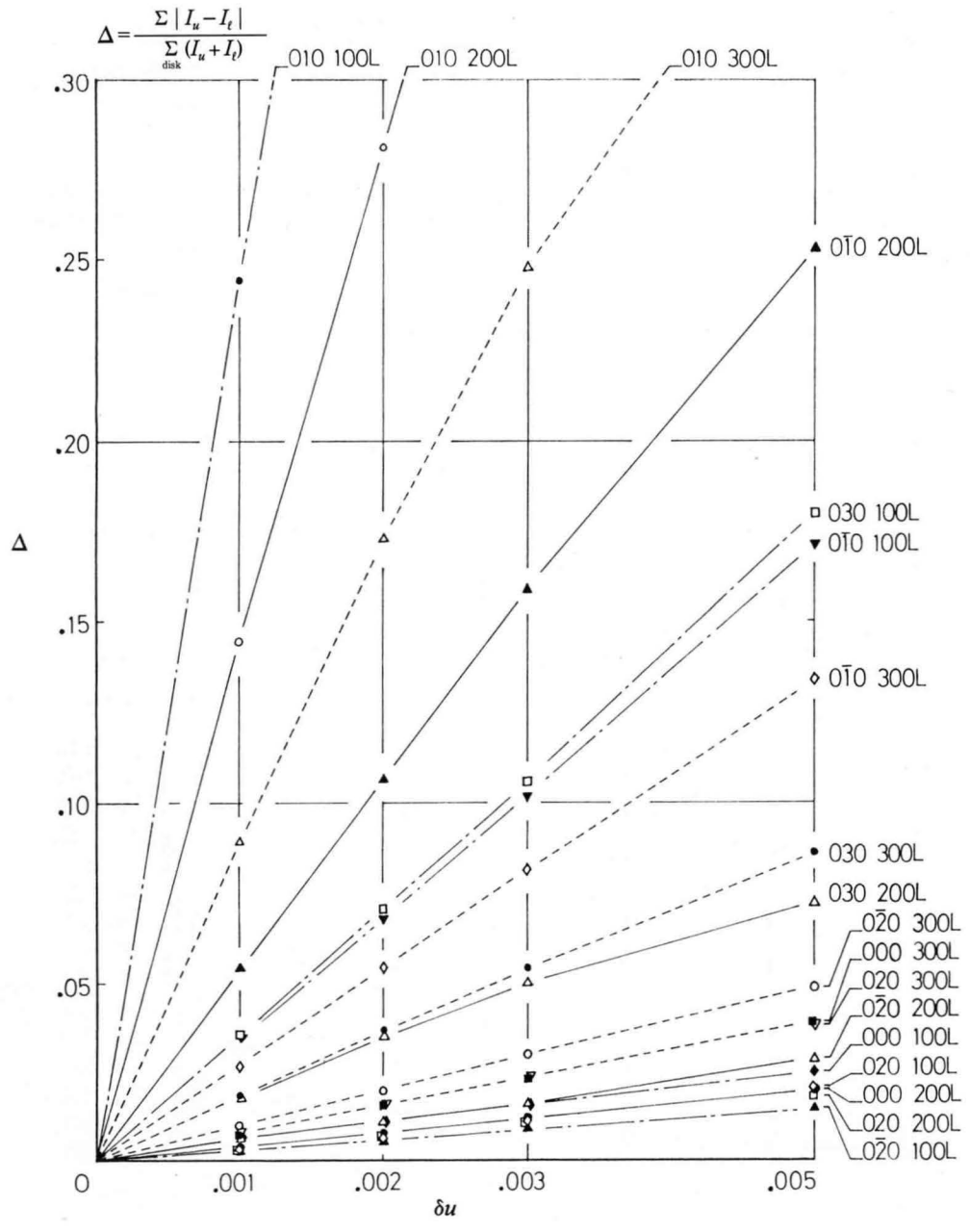

100L = 54.1nm

Breakdown of symmetry m_v

FeS_2 [0 0 1], 34 ZOLZ beams, 60 kV

(b) 0 3 0 Bragg setting

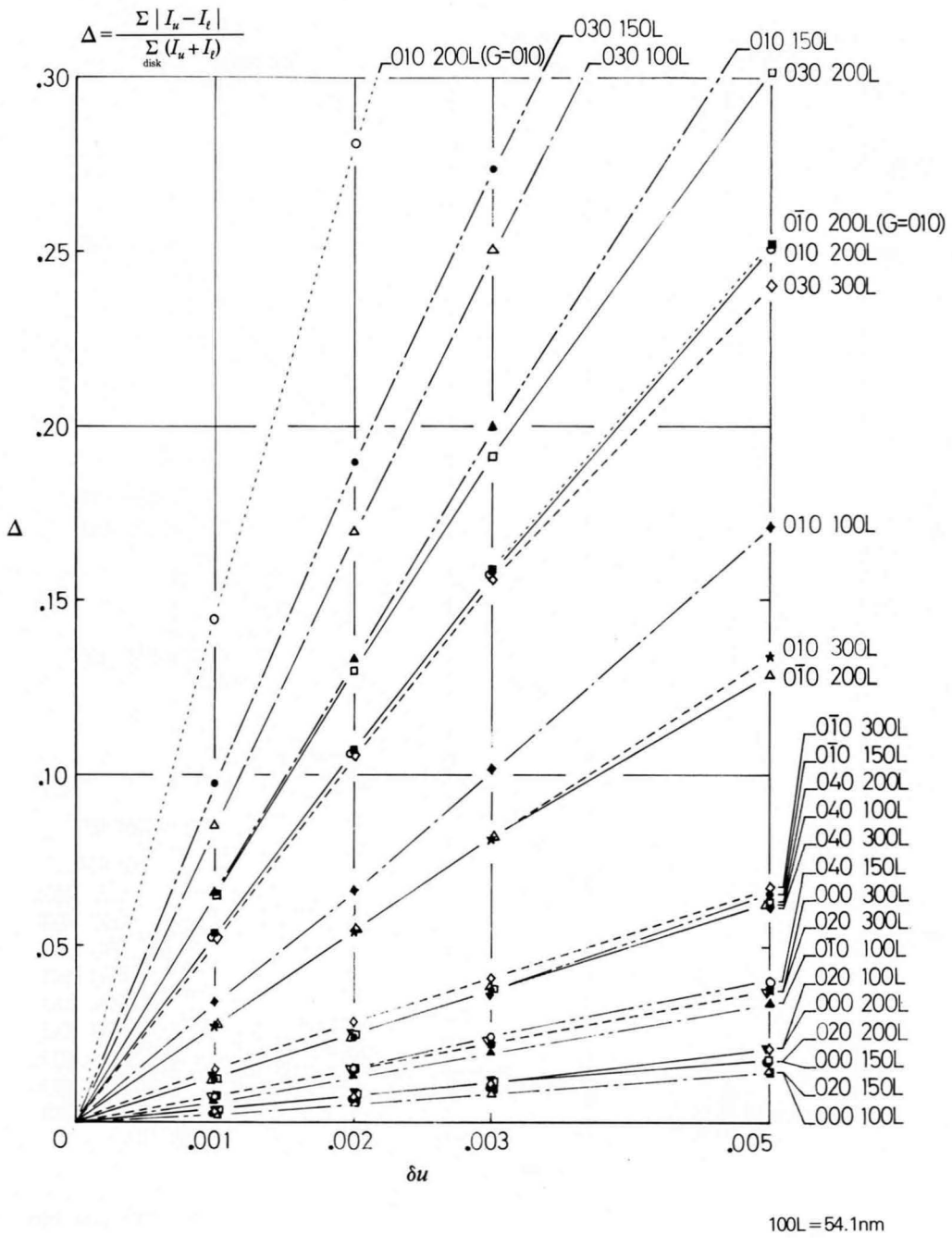

Breakdown of symmetry m_v

FeS_2 [0 0 1], 40 ZOLZ beams, 60 kV

(c) 0 5 0 Bragg setting

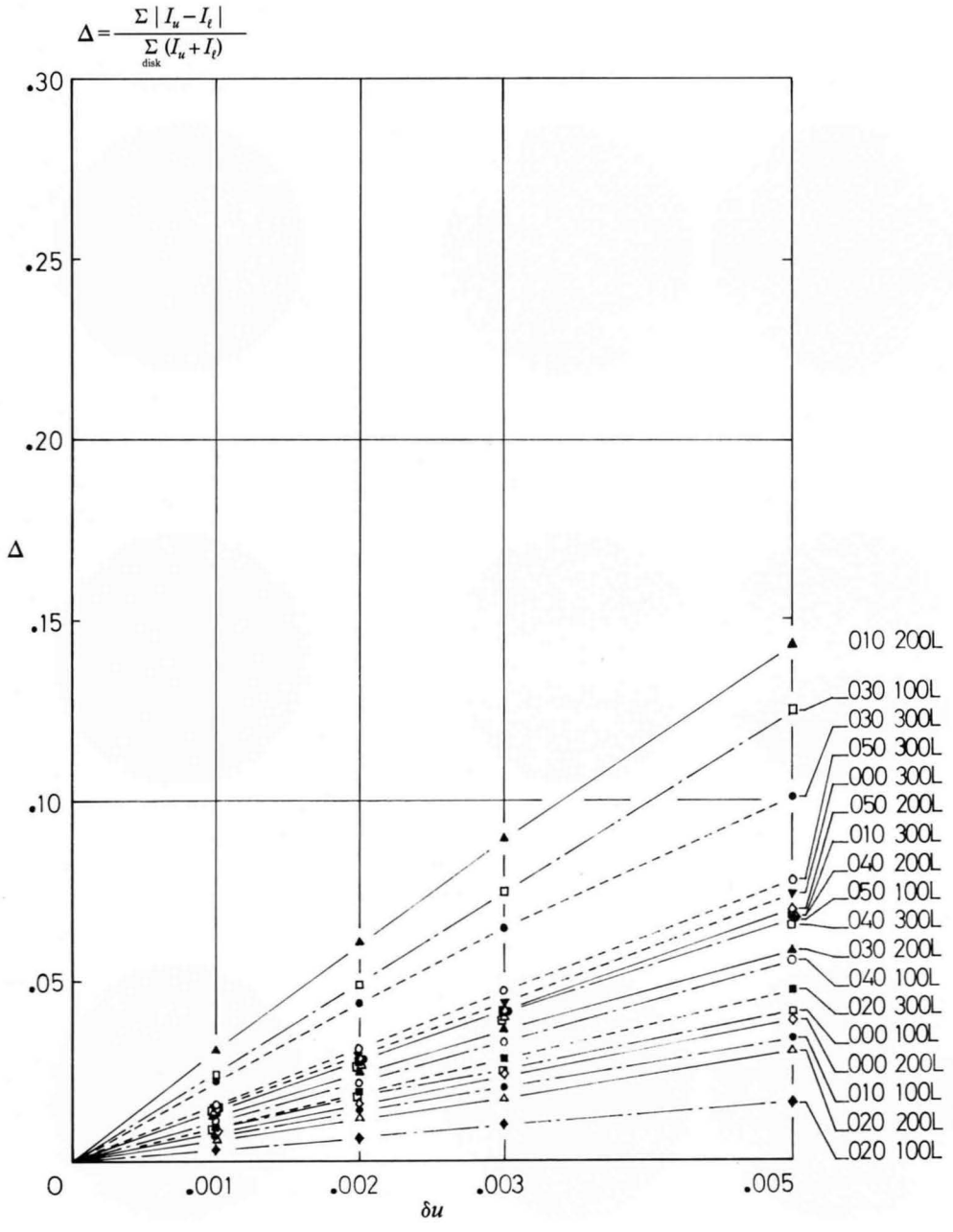

100L = 54.1nm

Breakdown of symmetry 2_R

FeS_2 [001], 34 or 37 ZOLZ beams, 60 kV

Figures (d), (e) and (f) show ±G dark-field patterns computed for the type 2) displacement with $\delta u = -0.005$ at three different thicknesses. The breakdown of a symmetry 2_R due to an inversion center is seen. The difference pattern for each pair and the value of Δ, which was defined in a similar manner to the previous case, are given. The value of Δ was plotted as a function of δu. It was found that the value of Δ varies linearly to a good approximation for the values of $|\delta u|$ smaller than 0.005. The sensitivity in this case is lower than that for the mirror symmetry. The ±030 pair shows the highest sensitivity for a thickness of 108.1 nm.

(d) Thickness 54.1 nm

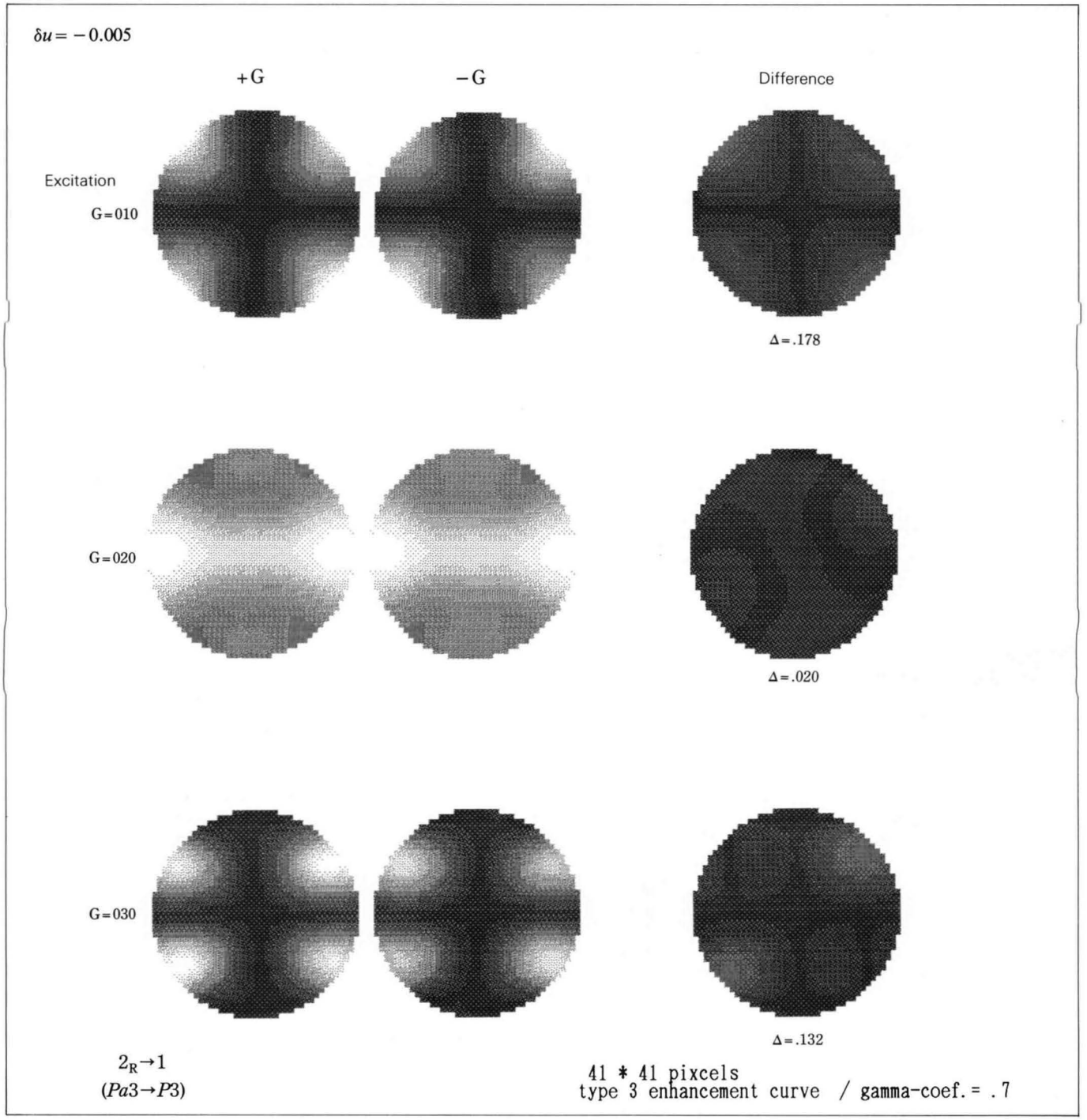

(e) Thickness 108.1 nm

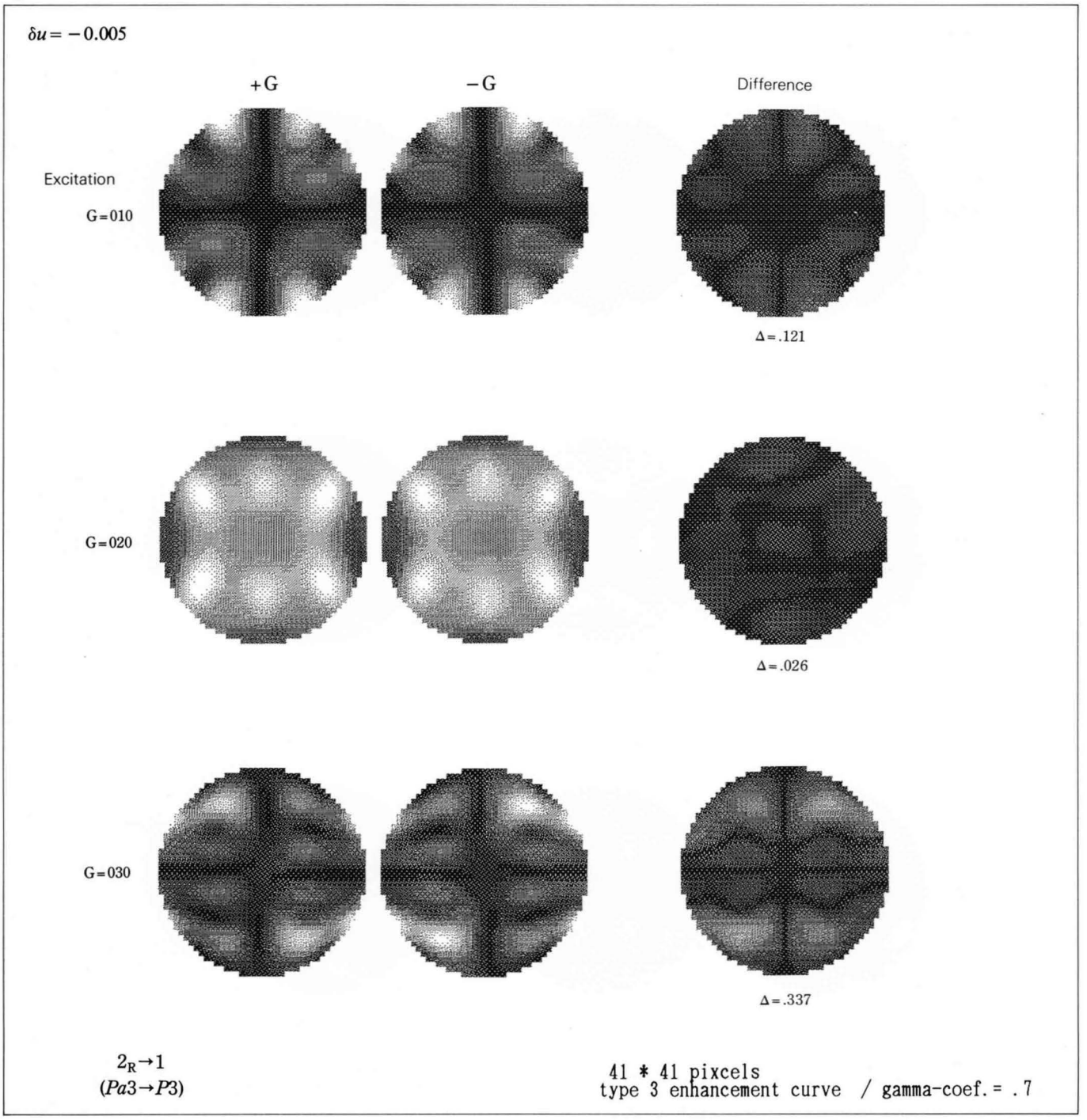

Breakdown of symmetry 2_R

FeS_2 [0 0 1], 34 or 37 ZOLZ beams, 60kV

(f) Thickness 162.2 nm

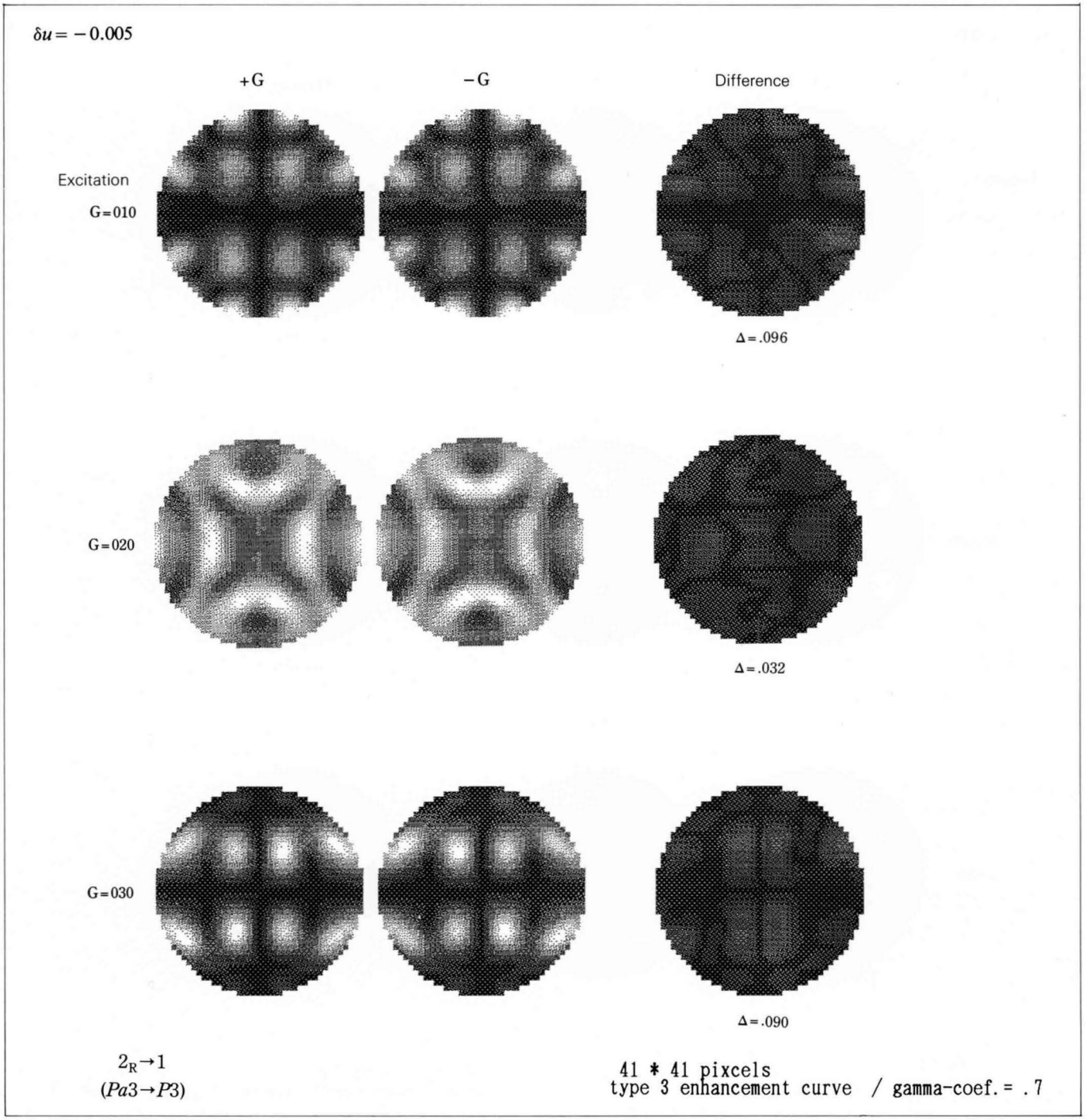

Breakdown of symmetry 2_R

FeS_2 [0 0 1], 34 or 37 ZOLZ beams, 60kV

(g) ± G Bragg setting

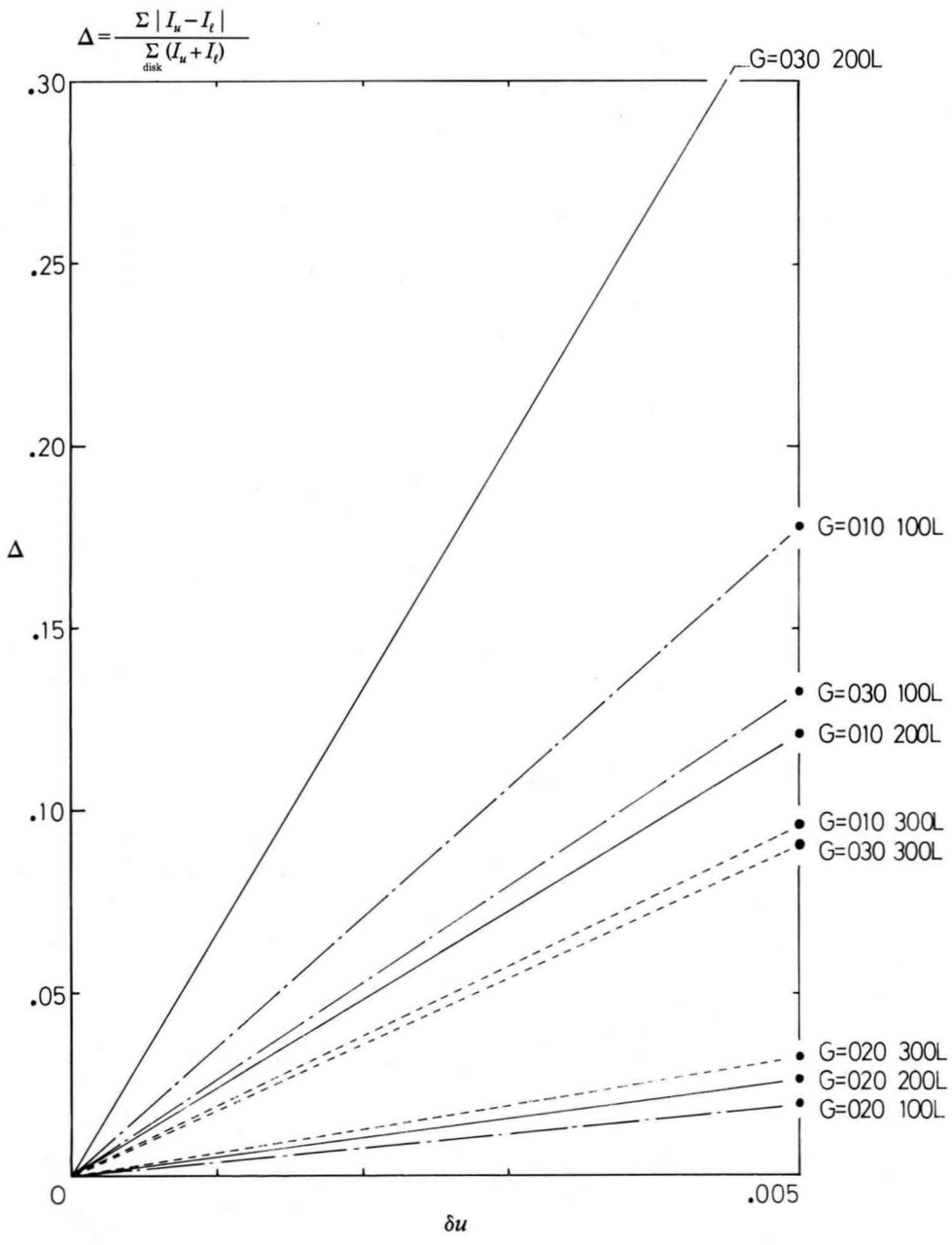

100L = 54.1nm

Lattice Defects

Stacking Faults

Electron microscopy has made a great success in the identification of lattice defects [a]. CBED also allows us to identify them. The observation of a lattice defect using CBED was first carried out by Johnson [19] for a stacking fault which lies parallel to the surface of a graphite foil, where the symmetry of a whole pattern, $6mm$, which is expected from a perfect crystal, changed into a symmetry of $3m$. Book I contains such examples. We investigated the method to determine the displacement vector of a stacking fault [21,22]. Rocking curves obtained from a faulted region are different from those of a perfect region in a manner characteristic of the displacement between two crystals at the fault. We shall describe three methods to investigate stacking faults.

The first method is to use ZOLZ reflections, which is an adaptation of the electron-microscope-image method for identifying a stacking fault. That is, the value of $\alpha = 2\pi \boldsymbol{g}\cdot\boldsymbol{R}$ is determined by the examination of rocking curves obtained from near the top and bottom edges of the fault, where $\boldsymbol{R}$ is the displacement vector for atoms at the fault and $\boldsymbol{g}$ is the reflection vector. The displacement vector $\boldsymbol{R}$ is determined with the help of the sense of tilt of the faulted plane with respect to the specimen surface. The sense of tilt must be determined by a separate method. We shall describe later a CBED method to determine this sense.

The inevitable illumination of a large specimen area in the LACBED method, the second method, is sometimes a disadvantage for the investigation of perfect crystals, but it is a great advantage for the identification of lattice defects. It is noted that the LACBED pattern is neither a pure diffraction pattern nor, of course, a microscope image. The LACBED pattern contains information on both reciprocal and real spaces, since the specimen is illuminated over a wide angular and a wide spatial spread. The LACBED method can identify the displacement vector while its sign is left undetermined.

The third method is to use HOLZ reflections, which makes the best use of the advantage of CBED. HOLZ lines obtained from a faulted area have simple and easily distinguishable profiles compared with those of ZOLZ reflections. Plural HOLZ lines appear simultaneously in one CBED pattern. These two facts enable the unambiguous determination of the displacement vector $\boldsymbol{R}$ (including its sign) without knowing the sense of tilt of the fault. Therefore, this method can easily determine whether the fault is intrinsic or extrinsic, without such complication as occurs in the electron-microscope-image method. This method is experimentally easier than the first method, since the former method allows a rough setting of the incident beam at a position around the middle of the fault, while the latter requires a rather accurate setting of the incident beam to a position in a narrow edge area. It should be noted that the CBED methods are based upon the dynamical diffraction theory but do not utilize the anomalous absorption effect. As a result, the third method has been successfully applied to the identification of a stacking fault in a thin specimen.

Figure (a) shows the side view of a specimen containing a stacking fault and a convergent beam illuminating the fault, where t is the thickness of the specimen and t_1 is that of the upper crystal, at which the incident beam meets the stacking fault. The positive direction of the excitation error w is directed from the dark-field disk to the bright-field disk. For face-centered cubic crystals, α takes a value of $+(2/3)\pi$, $-(2/3)\pi$ or 0.

Figure (b) gives a definition of the senses of the displacement vector, zone axis and incident beam. The displacement vector $\boldsymbol{R}$ is defined as the displacement of the lower crystal with respect to the upper crystal. The positive direction of the zone axis is taken upward from the specimen. The electron beam runs in the $[\bar{u}\,\bar{v}\,\bar{w}]$.

Reference

[a] P.B. Hirsch, A. Howie, R.B. Nicholson, D.W. Pashley and M.J. Whelan: Electron Microscopy of Thin Crystals, Butterworth, Sevenoaks, 1965.

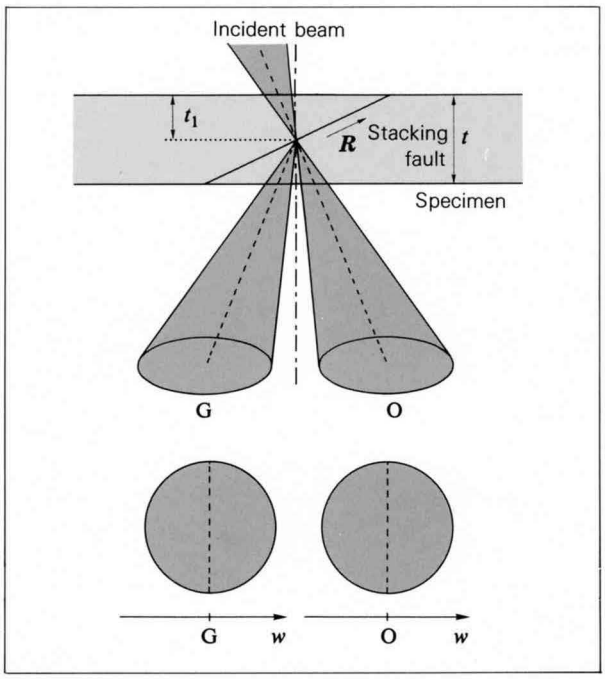

(a)

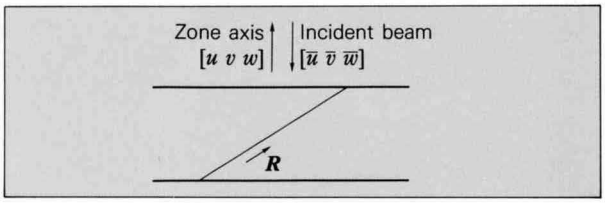

(b)

Determination of $\alpha = 2\pi \boldsymbol{g}\cdot\boldsymbol{R}$ using ZOLZ reflections

Rocking curves of a low-order ZOLZ reflection were calculated by the two beam dynamical theory. Thickness t was assumed as $t/\xi_g = 4$ in accordance with usual experimental conditions, where ξ_g is the extinction distance (e.g. $\xi_g = 30$nm, $t = 120$nm). The absorption distances ξ'_g and ξ'_0 were given as $\xi_g/\xi'_g = 1/20$ and $\xi'_0 = \xi'_g$ throughout this section. Figure (a) shows a rocking curve of a reflection for a perfect crystal, which is symmetric with respect to the exact Bragg position $w = 0$. Figure (b) shows rocking curves of a reflection for a crystal containing a stacking fault. The curves in the left column were calculated for $\alpha = 2\pi \boldsymbol{g}\cdot\boldsymbol{R} = +(2/3)\pi$ and those in the right column for $\alpha = -(2/3)\pi$. All the curves are no longer symmetric about $w = 0$. The curves for $\alpha = +(2/3)\pi$ and those for $\alpha = -(2/3)\pi$ show opposite sense asymmetries to each other. That is, for example, the curve for $\alpha = +(2/3)\pi$ and $t_1 = (1/20)t$ is identical with that for $\alpha = -(2/3)\pi$ and $t_1 = (19/20)t$, provided that the sign of w is reversed between the two curves. This relation is fully interpreted by the reciprocity theorem. For $\alpha = +(2/3)\pi$, the diffracted intensity for $w < 0$ is stronger than that for $w > 0$. For $\alpha = -(2/3)\pi$, the intensity for $w > 0$ is stronger than that for $w < 0$. The senses of asymmetry of the profiles obtained from near the top and bottom surfaces are distinguishable, while the asymmetries of other profiles are not clear.

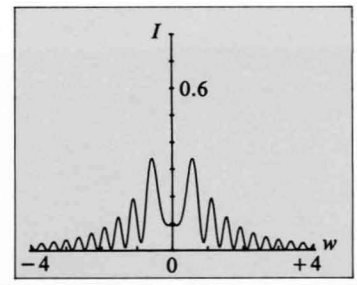

(a) Dark-field rocking curve for a perfect crystal at $t/\xi_g = 4$

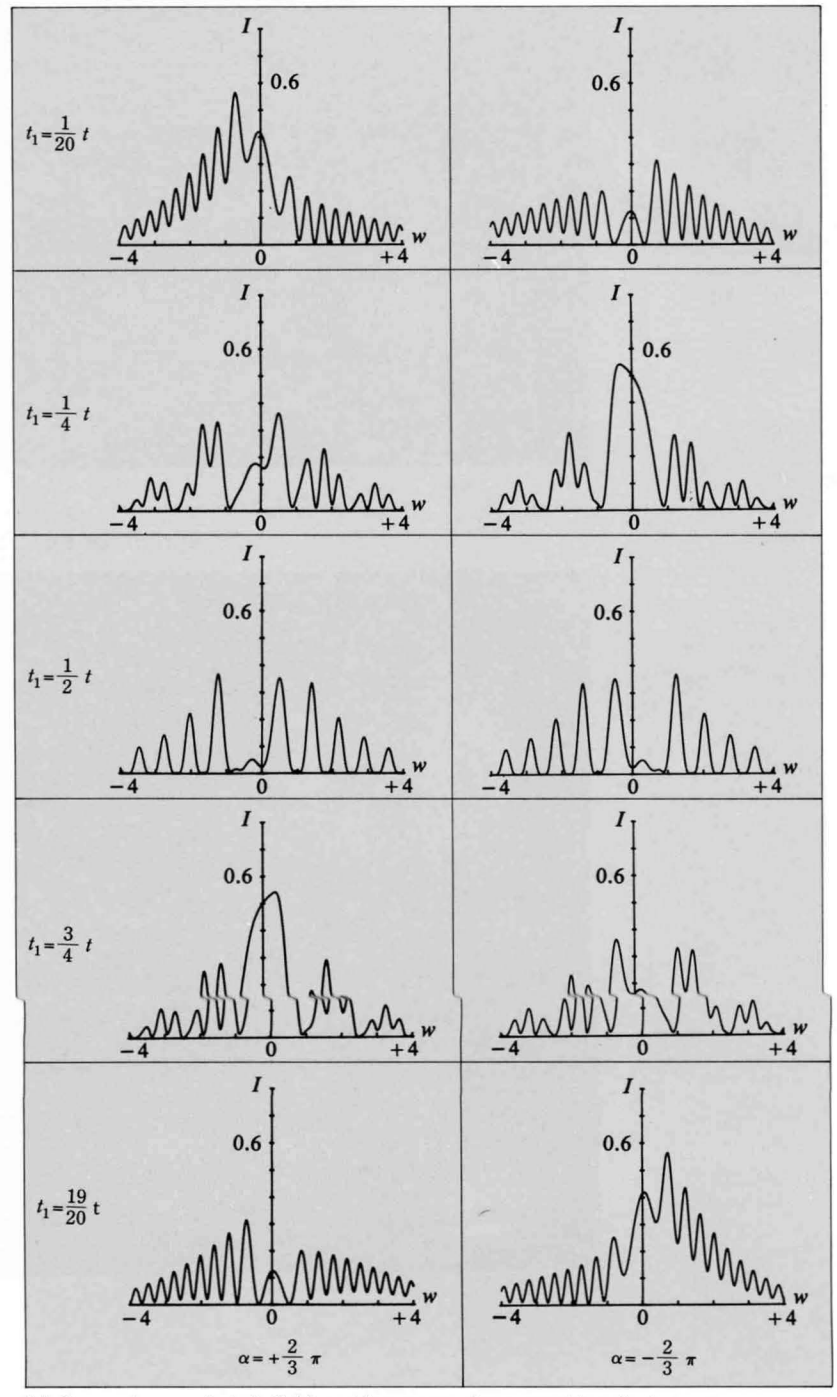

(b) Dependence of dark-field rocking curve for a stacking fault on t_1

Si [110]

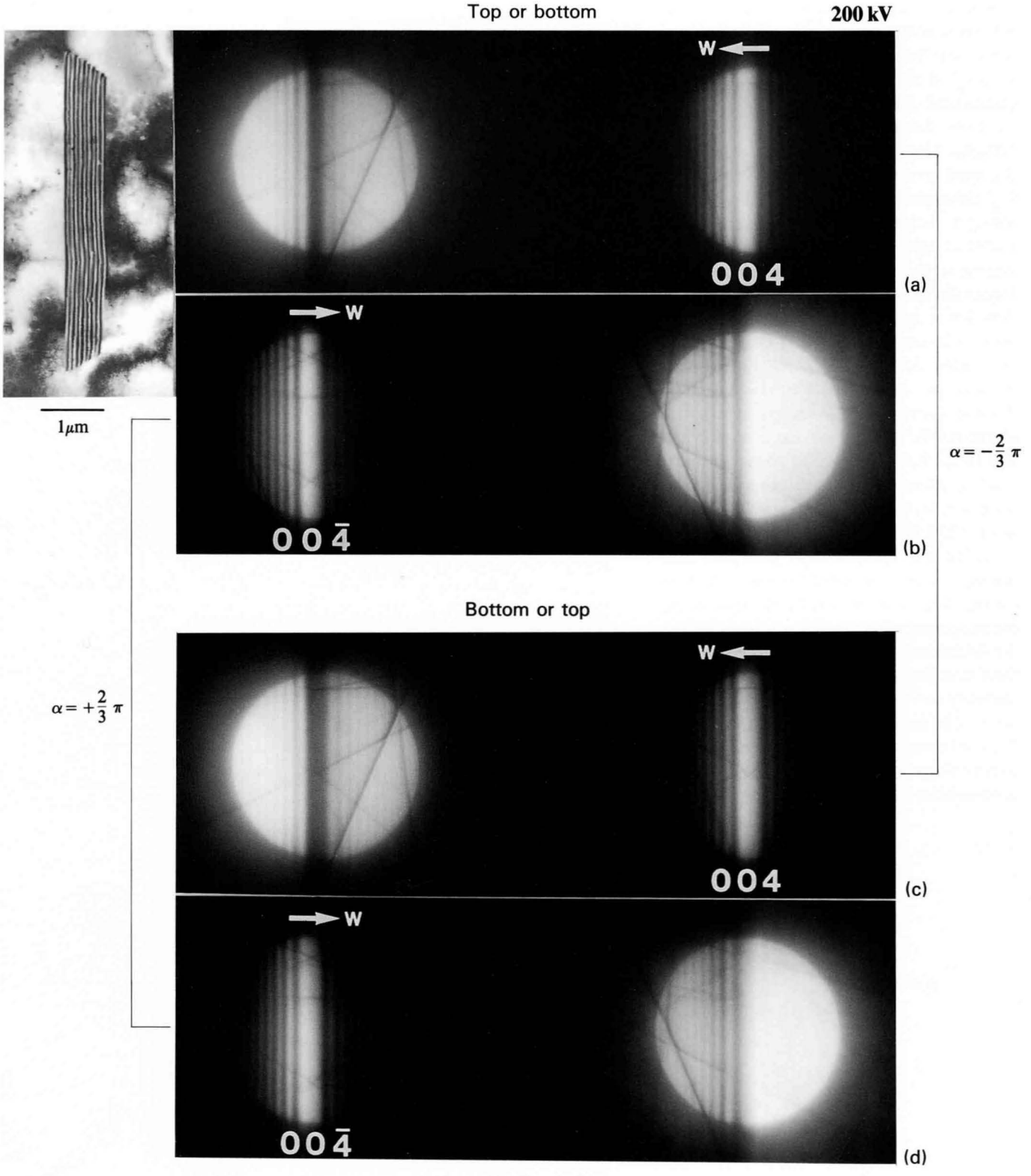
Top or bottom
200 kV
W
004
(a)
W
00$\bar{4}$
(b)
$\alpha = -\frac{2}{3}\pi$
1μm
Bottom or top
$\alpha = +\frac{2}{3}\pi$
W
004
(c)
W
00$\bar{4}$
(d)

Stacking faults of Si were formed by annealing bulk specimens at 1050°C for 10 days. Photographs (a) and (b) were taken from near the left edge of the stacking fault seen in an attached electron micrograph of (110) Si at the 004 and $00\bar{4}$ exact Bragg settings, respectively. Photographs (c) and (d) were taken from near the right edge of the fault. Figures (a), (b), (c) and (d) show microdensitometer curves of the diffracted intensities in Photos (a), (b), (c) and (d), respectively, and show a qualitatively good agreement with the calculated curves (e), (f), (g) and (h), respectively. The sign of α was determined to be negative or $-(2/3)\pi$ for the 004 reflection. Since displacement vectors $\boldsymbol{R}$ allowed for a stacking fault oblique to the (110) surface are $1/3[111]$, $1/3[\bar{1}\,\bar{1}\,\bar{1}]$, $1/3[\bar{1}\,\bar{1}\,1]$ and $1/3[11\bar{1}]$, a possible $\boldsymbol{R}$ is $1/3[\bar{1}\,\bar{1}\,\bar{1}]$ or $1/3[11\bar{1}]$. To determine which vector is the correct one, it is necessary to know whether the faulted plane is a $(\bar{1}\,\bar{1}\,\bar{1})$ plane or $(11\bar{1})$ plane. (see pages 148 and 149)

The Si specimens containing stacking faults were supplied by Dr. I. Yonenaga and Prof. K. Sumino of the Research Institute for Iron, Steel and Other Metals, Tohoku University.

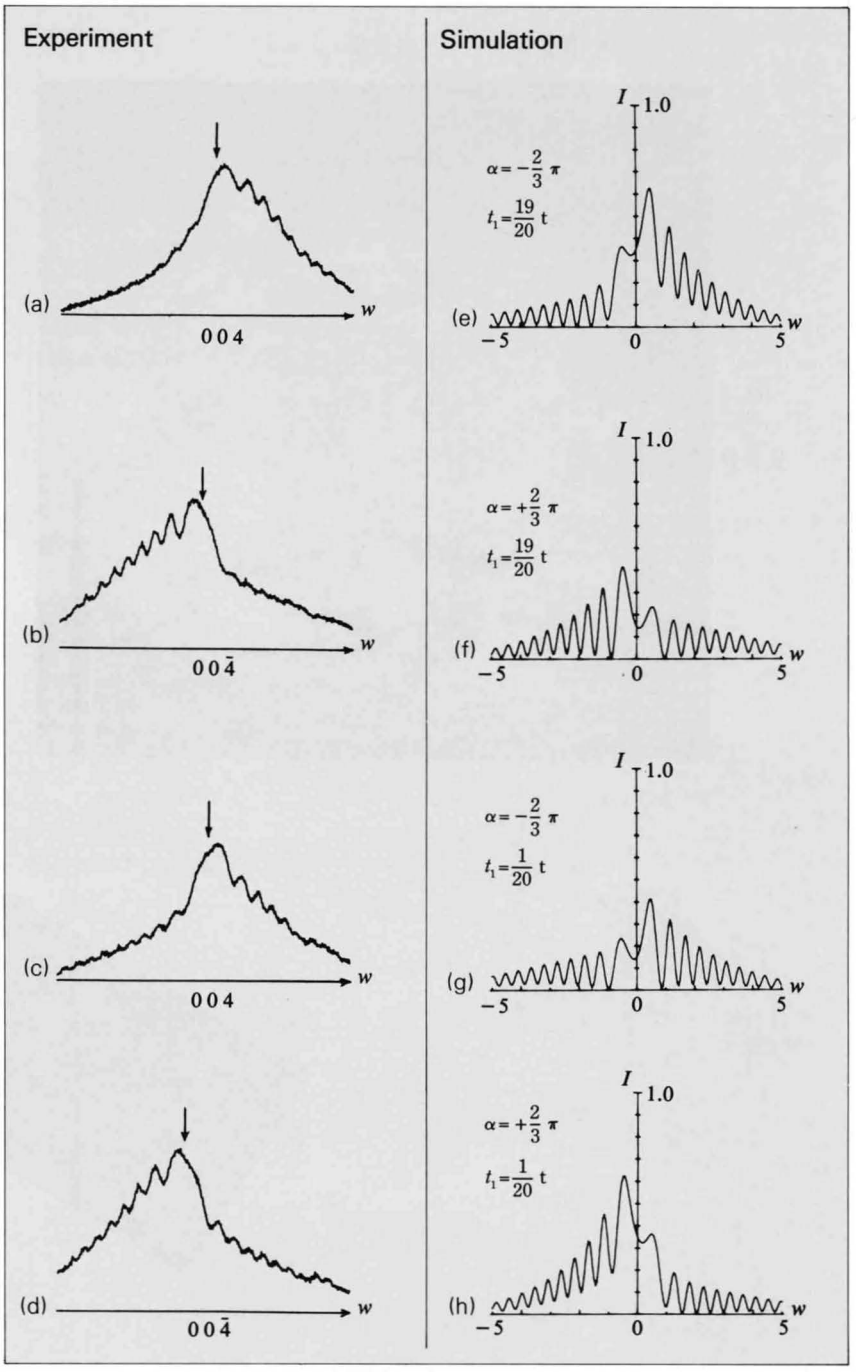

Microdensitometer charts of dark-field disks. Arrows indicate Bragg position.

Calculated rocking curves at $t=400$ nm and $\xi_g=166.6$ nm.

Observation of stacking faults using LACBED

Si [111] **100 kV**

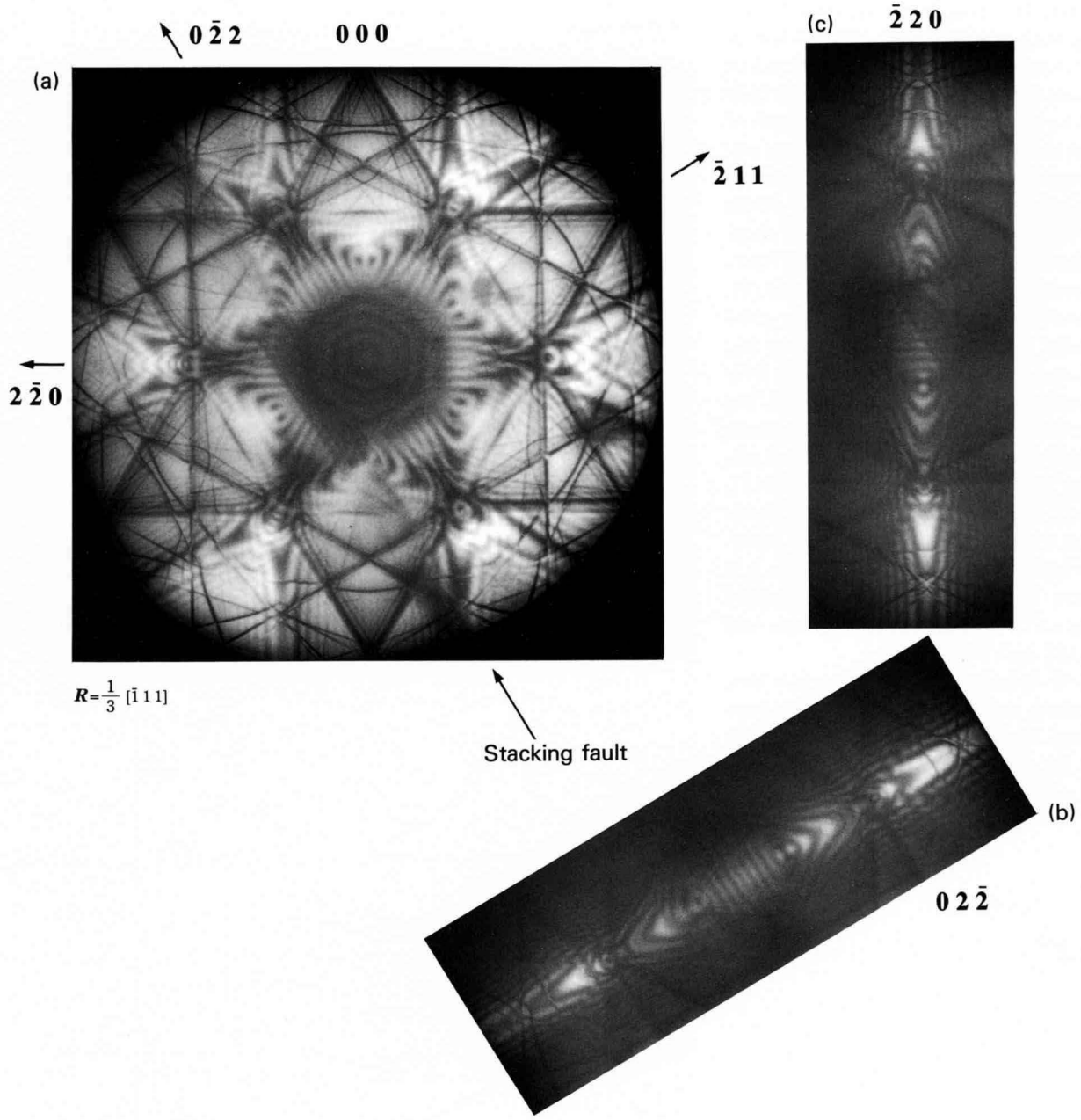

Photographs (a), (b) and (c) show LACBED patterns of a (111) Si film containing a stacking fault with a displacement vector $\boldsymbol{R}$ of the 1/3<111> type. In Photo (a), the image of the stacking fault, indicated by an arrow, and the CBED pattern are simultaneously recorded. As a result, the orientation of the fault is unambiguously identified. At the $02\bar{2}$ Bragg position, where $\alpha = 2\pi \boldsymbol{g}\cdot\boldsymbol{R} = 0$, the fault is seen to have lost its contrast. The same information is obtained from dark-field LACBED patterns. In the $02\bar{2}$ pattern (b), the fault has lost the contrast because of $\alpha = 0$, whereas in the $\bar{2}20$ pattern (c) it shows a definite contrast. The fact that $\alpha = 0$ for $\boldsymbol{g} = 02\bar{2}$ allows us to select the possible vectors of $\boldsymbol{R}$ to be $1/3[1\bar{1}\bar{1}]$, $1/3[\bar{1}11]$, $1/3[111]$ and $1/3[\bar{1}\bar{1}\bar{1}]$. Since the fault is tilted to the specimen surface, the vectors $1/3[111]$ and $1/3[\bar{1}\bar{1}\bar{1}]$ are rejected. The displacement vector $\boldsymbol{R}$ is determined as $1/3[1\bar{1}\bar{1}]$ or $1/3[\bar{1}11]$. The sign of the vector is left undetermined.

Si [110]

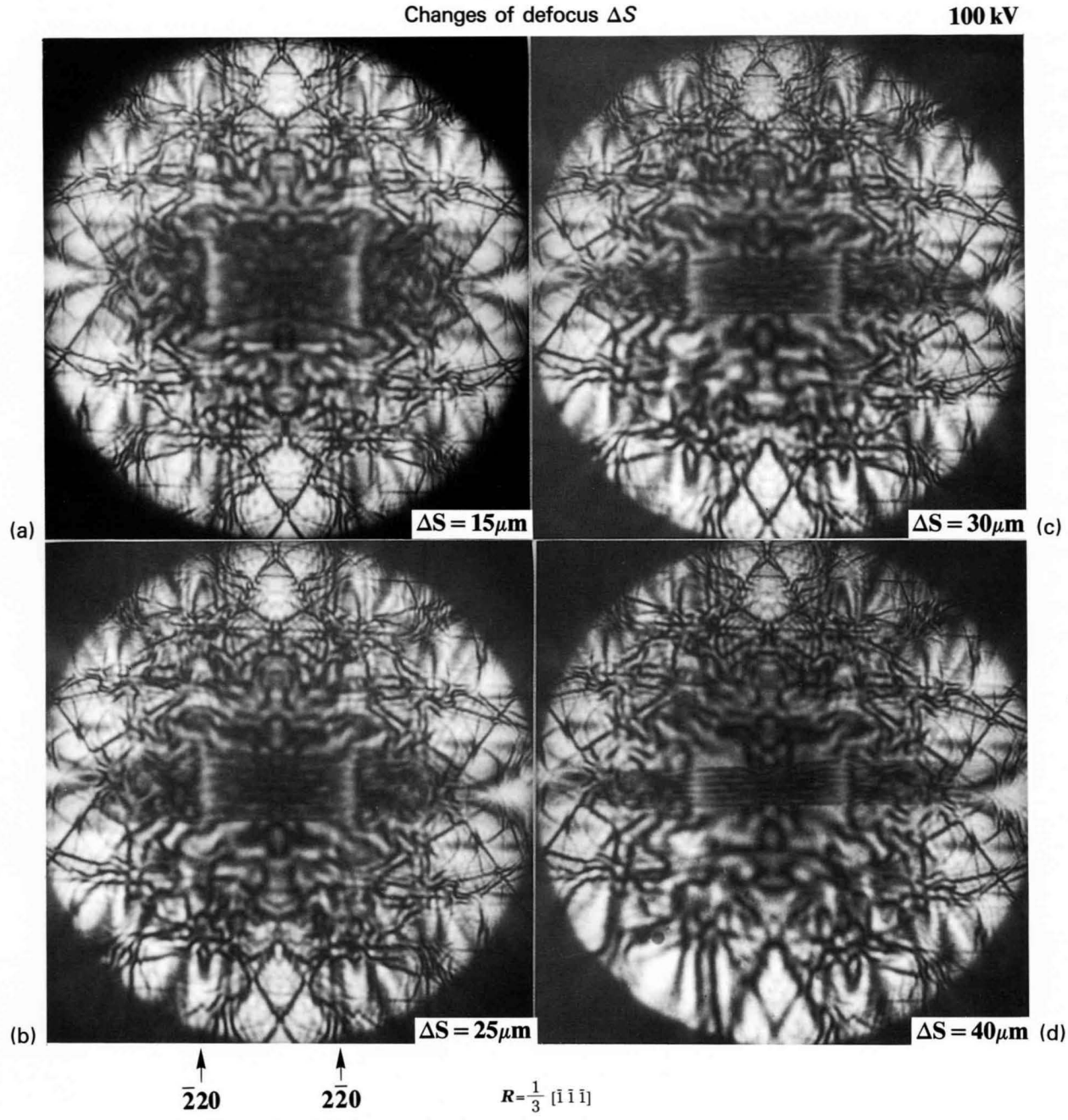

Photographs (a), (b), (c) and (d) show LACBED patterns taken from a (110) Si film containing a stacking fault of $\boldsymbol{R} = 1/3[\bar{1}\,\bar{1}\,\bar{1}]$ at defocus $\Delta S = 15$, 25, 30 and 40μm, respectively. When the amount of defocus is small, the fault is largely magnified. (In-focus CBED patterns, therefore, are regarded as images with a magnification of infinity.) The pattern due to the fault is difficult to recognize as an image (a), but the loss of a symmetry due to the fault is easily seen. With larger defocuses (c) and (d), the fault becomes to be seen as a usual microscope image, but the change of the symmetry on the fault is difficult to see. It is noted that the deterioration of the pattern is seen owing to the thickness variation in the illuminated specimen area.

Determination of the top and bottom of a stacking fault

CBED patterns from the edges of a stacking fault

The sense of tilt of a stacking fault can be determined by a simple CBED technique. One half of the incident beam illuminates the fault and the other half illuminates a perfect specimen area. Then, a half of the bright-field CBED pattern is affected by the fault and the other half is not. The expected results are illustrated in the diagrams for two senses of tilt of the fault and for three different focuses; (a) in-focus, (b) under-focus and (c) over-focus. The letters F and P indicate a faulted and a perfect pattern. These results are summarized in the table.

Photographs (c), (e) and (g) were taken from edge A of the fault in Photo (a) at the three different focuses. Photographs (d), (f) and (h) were taken from edge B at the three different focuses. Referring to the diagrams and the table, edge A was determined to be at the top surface and edge B at the bottom surface.

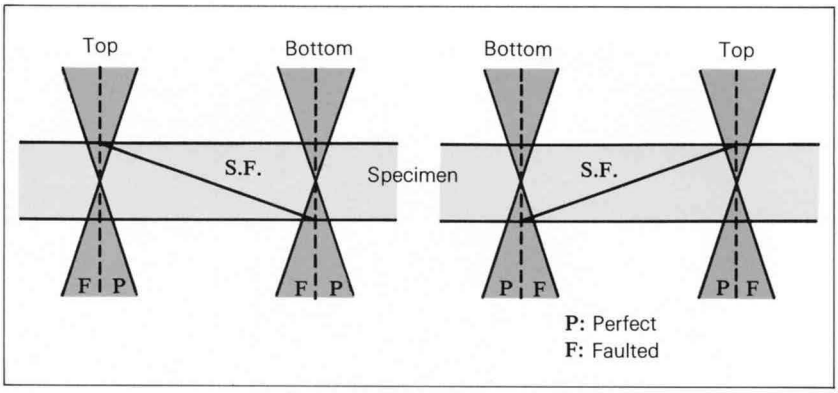

(a)

Incident beam is focused in the specimen (in-focus).

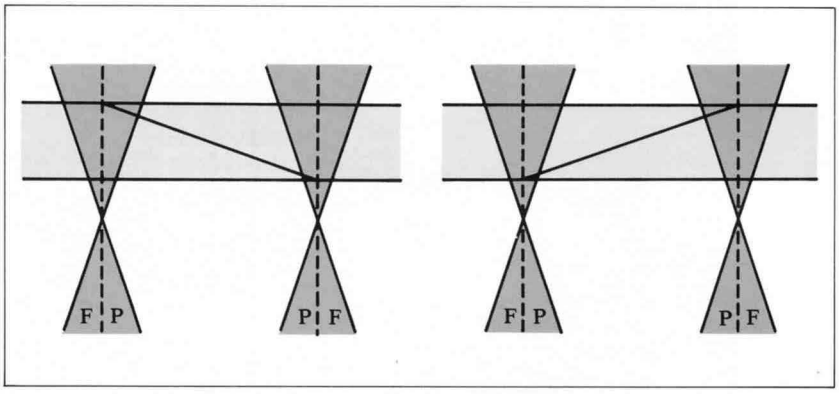

(b)

Incident beam is focused below the specimen (under-focus).

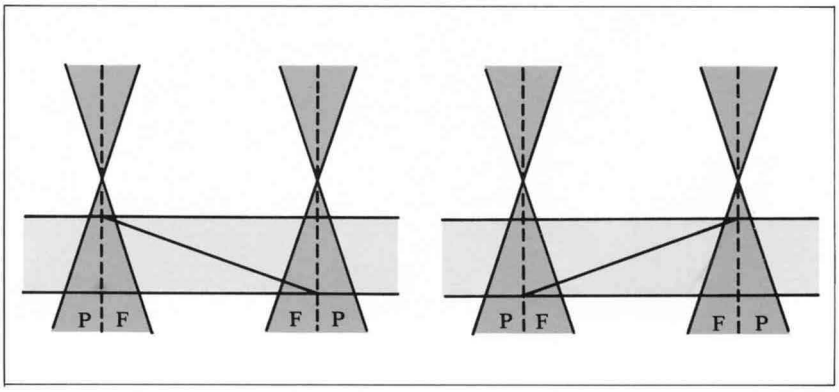

(c)

Incident beam is focused above the specimen (over-focus).

Focus				
	Top	Bottom	Bottom	Top
In-focus	FP	FP	PF	PF
Under-focus	FP	PF	FP	PF
Over-focus	PF	FP	PF	FP

Si [110]

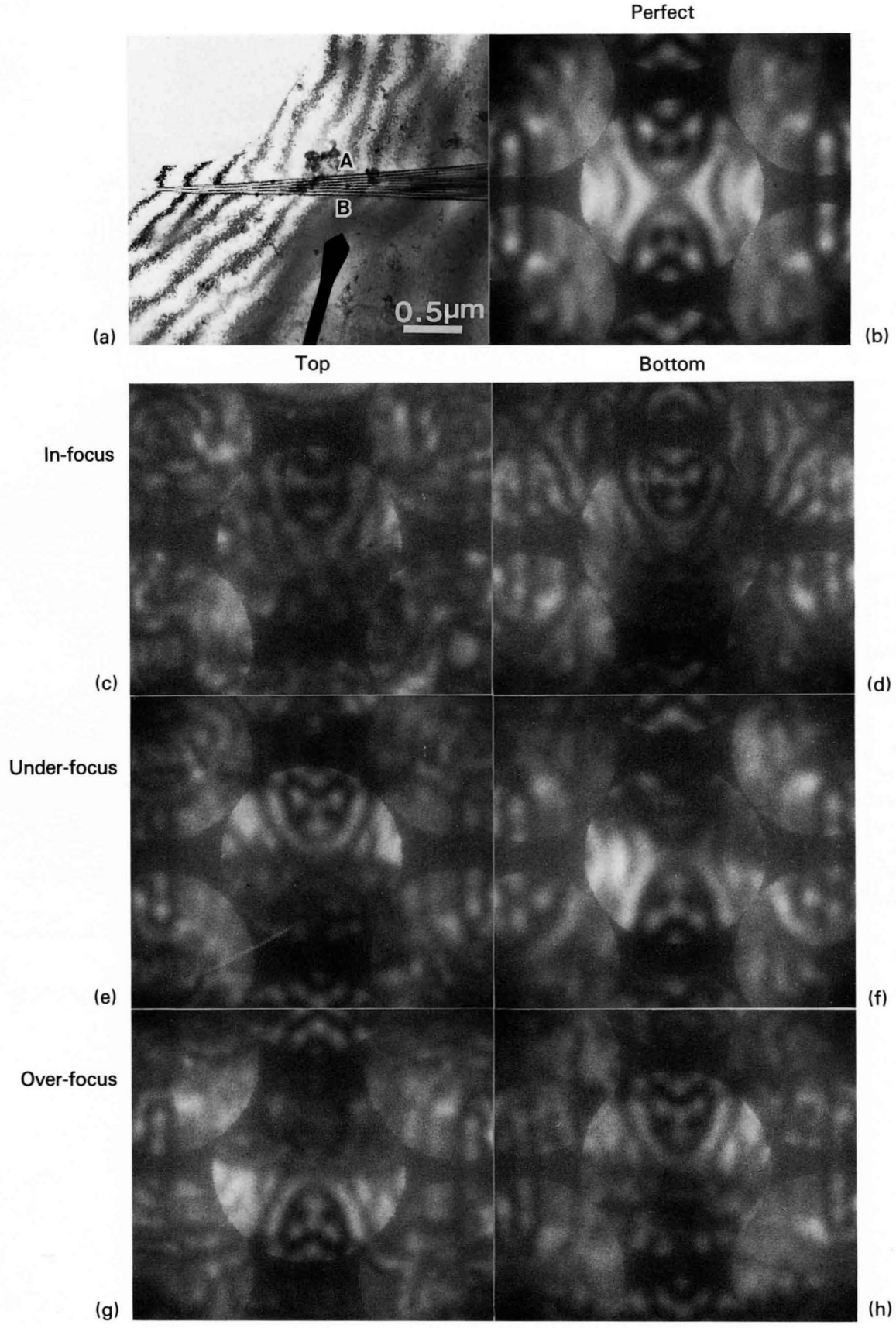
Perfect
A
B
0.5μm
(a)
(b)
Top
Bottom
In-focus
(c)
(d)
Under-focus
(e)
(f)
Over-focus
(g)
(h)

Determination of the displacement vector R using HOLZ reflections

Rocking curves were calculated for a HOLZ reflection by the two-beam dynamical theory. Thickness t was assumed as $t/\xi_g = 1/4.25$ (e.g. $t = 100$ nm and $\xi_g = 425$ nm) by considering usual experimental conditions. Figure (a) shows three pairs of rocking curves of the transmitted beam and a diffracted beam for $\alpha = 0$, $+(2/3)\pi$ and $-(2/3)\pi$ at $t_1 = (1/2)t$. The curve of the dark-field pattern for $\alpha = 0$ is symmetric about $w = 0$, and the curve of the bright-field pattern is almost symmetric, because of a small anomalous absorption effect. The principal peak of the curves are split into two peaks when $\alpha = \pm(2/3)\pi$. For $\alpha = -(2/3)\pi$, the peak intensity at $w > 0$ is larger than that at $w < 0$. For $\alpha = +(2/3)\pi$, the peak intensity at $w < 0$ is larger than that at $w > 0$. (The two peaks are expected to be the same for $\alpha = (1/2)\pi$.) The sense of asymmetry between the two peaks is characteristic of the sign of α, which permits the determination of the displacement vector.

It should be noted that the asymmetry of the peaks does not originate from the anomalous absorption effect but from the redistribution of the Bloch waves on two branches of the dispersion surface at the fault.

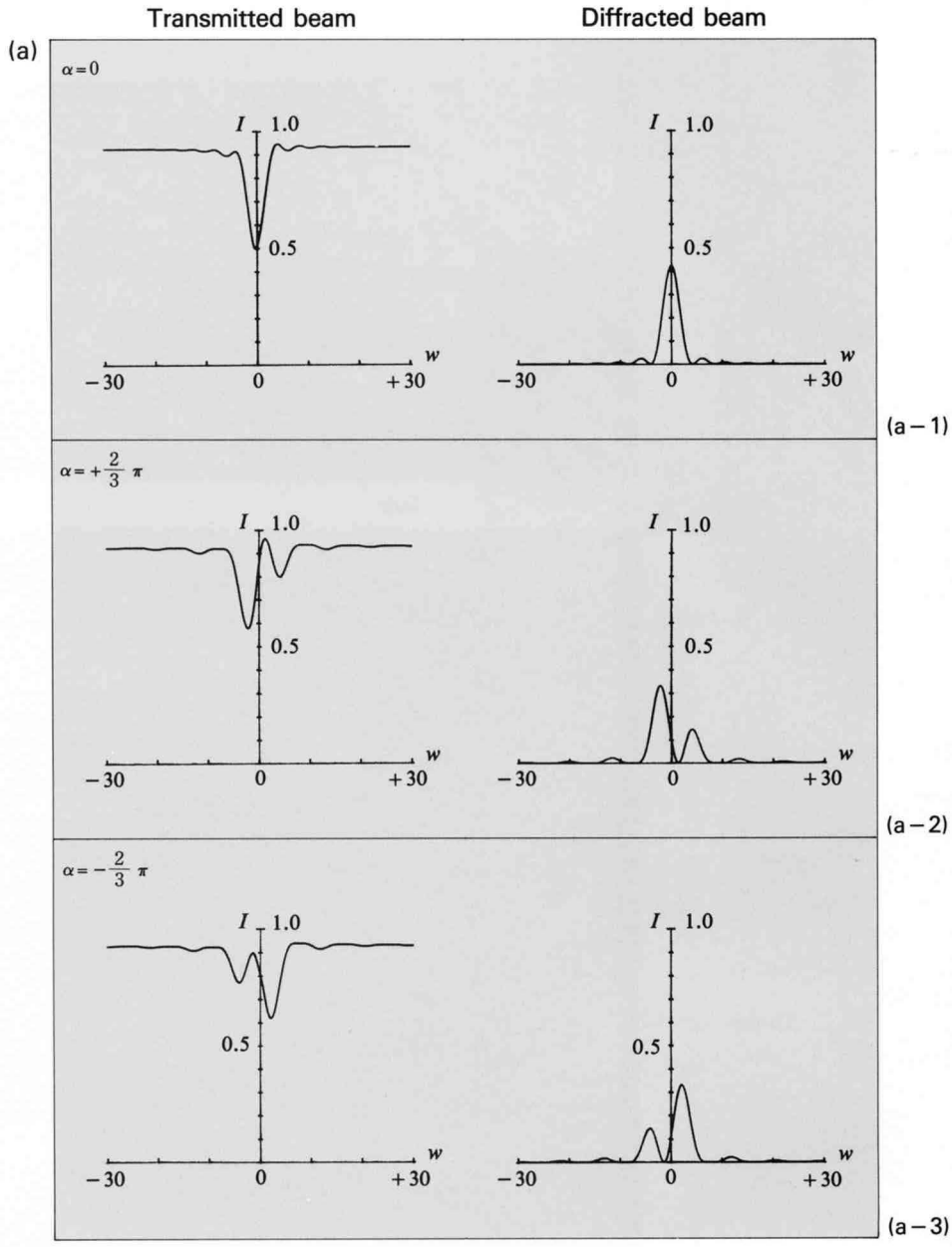

Calculated rocking curves at $\frac{t}{\xi_g} = \frac{1}{4.25}$ and $t_1 = \frac{1}{2}t$

Dependence on the depth of a stacking fault

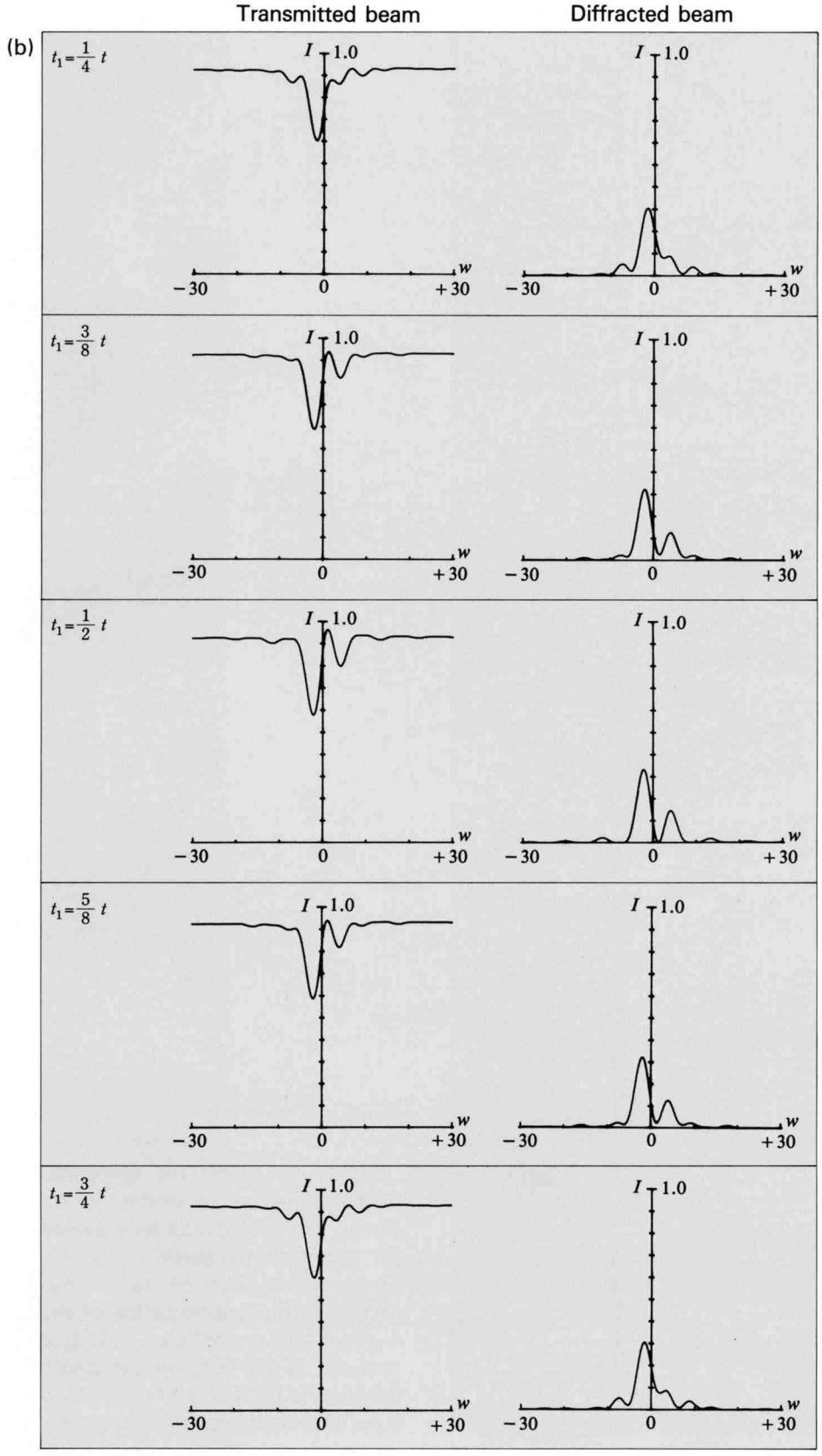

Calculated rocking curves at $\frac{t}{\xi_g}=\frac{1}{4.25}$ for $\alpha=+\frac{2}{3}\pi$

Figure (b) shows the fault-depth dependence of the rocking curves. The curves obtained at depths of the fault $(3/8)t \leqq t_1 \leqq (5/8)t$ show a definite splitting of the peak. The curves at $t_1 < (3/8)t$ and $t_1 > (5/8)t$ do not show a clear splitting and approach the curve for a perfect crystal. This fact indicates that the incident beam needs to illuminate a position around the middle of the fault to identify the fault.

Dependence on specimen thickness

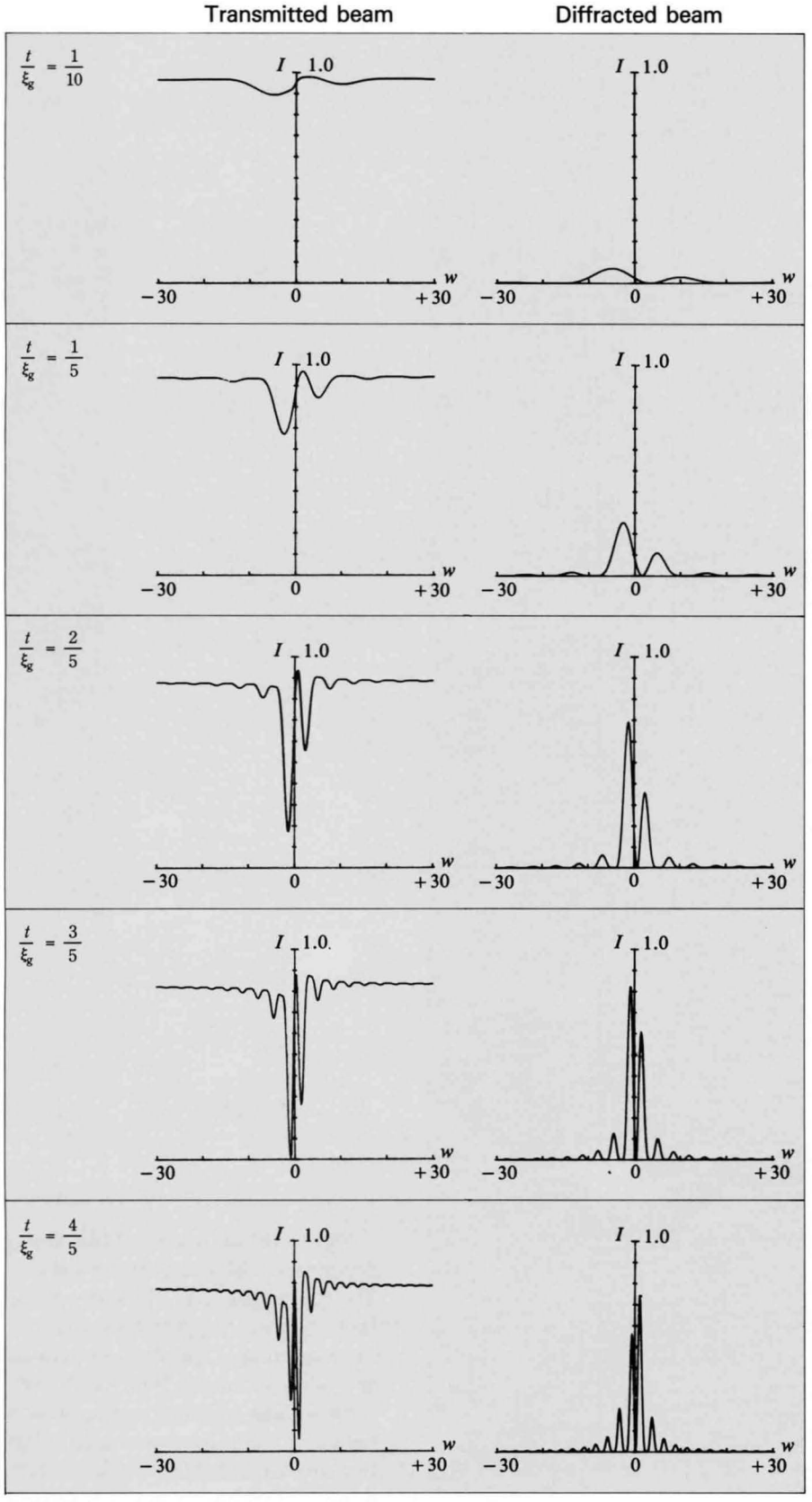

Calculated rocking curves at $t_1 = \frac{1}{2}\,t$ for $\alpha = +\frac{2}{3}\,\pi$

Figure (c) shows the specimen-thickness dependence of the rocking curves. Two clear peaks are obtained for specimen thickness $t/\xi_g \leqq 3/5$. This condition places no practical restriction to the determination of the displacement vector. That is, if ξ_g is assumed as 500 nm, the maximum thickness to be used is 300 nm, which is sufficiently thick for usual experiments. There is no restriction to thin specimens, in contrast to the electron-microscope-image method.

Si [334]

80 kV

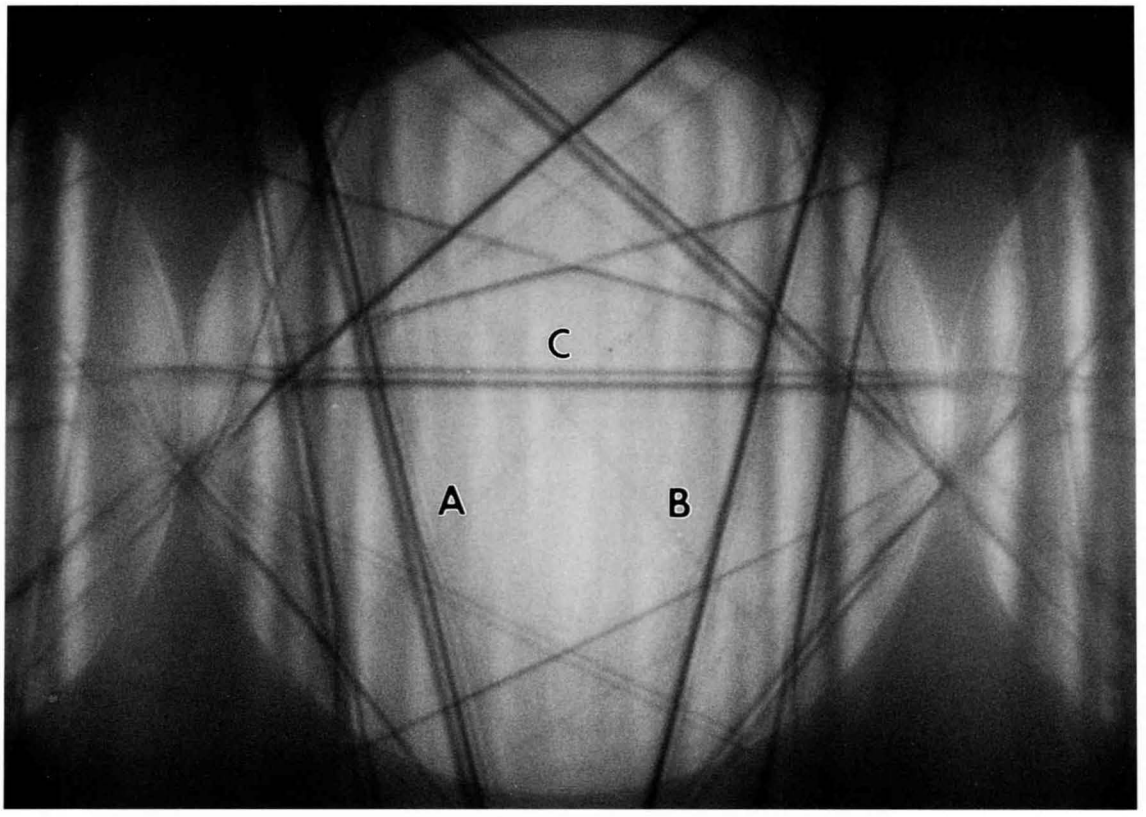

$2\bar{2}0$ 000 $\bar{2}20$

$\boldsymbol{R}=\frac{1}{3}[1\,\bar{1}\,\bar{1}]$

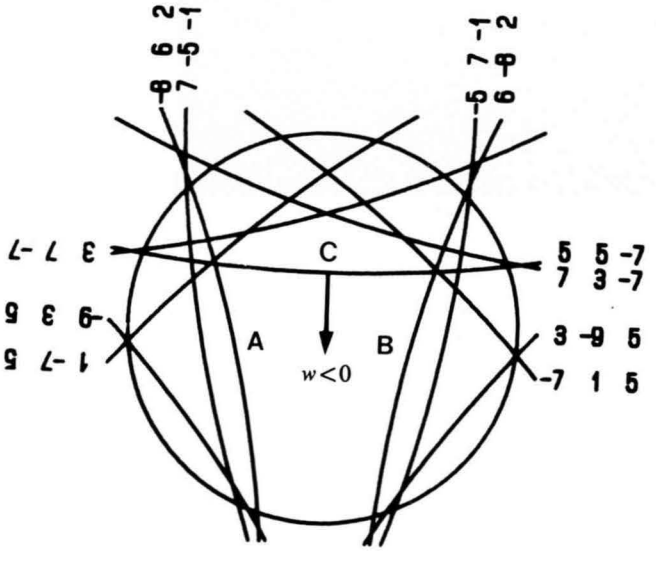

The photograph was taken at the [334] incidence from (111) Si containing a stacking fault with $\boldsymbol{R}=1/3[1\bar{1}\bar{1}]$. A simulation of HOLZ line geometry obtained by an arc (circle) approximation is shown, which provides an easy identification of the sign of excitation error w. The sign of w is positive inside arcs and negative outside them. From the simulation, the HOLZ lines A, B and C in the photograph are indexed as $\bar{8}62$, $6\bar{8}2$ and $55\bar{7}$. The values of α for the three reflections are $-(2/3)\pi$, 0, $+(2/3)\pi$. The HOLZ line profiles A, B and C show a good agreement with the calculated curves for $\alpha=-(2/3)\pi$, 0, $+(2/3)\pi$ (Fig. (a) on page 150), respectively.

Since the values of α including their signs can be determined for plural HOLZ lines, the displacement vector can uniquely be identified by the present method.

Dependence on stacking fault depth (experimental)

Si [3 3 2]

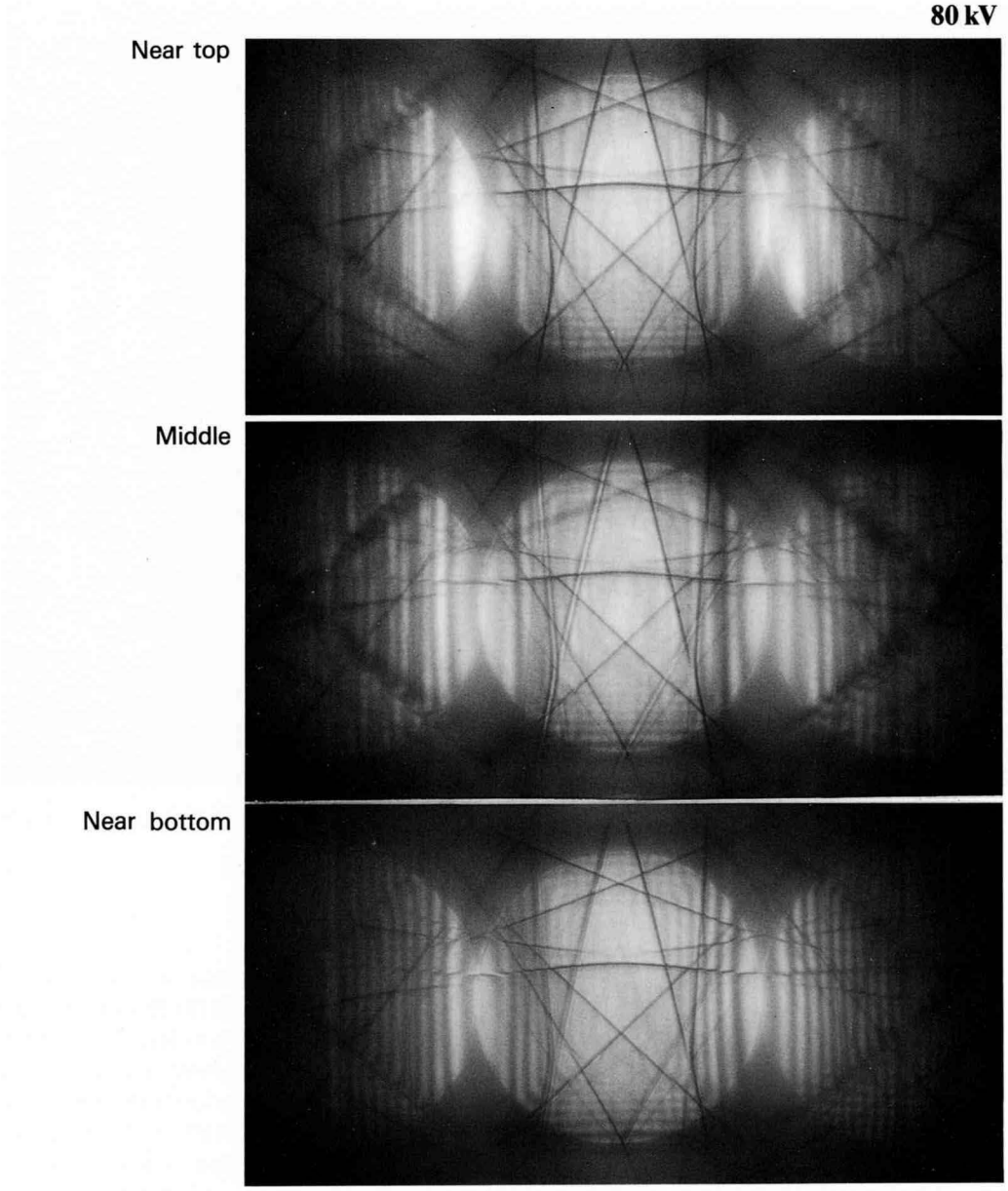

$$\boldsymbol{R}=\frac{1}{3}[\bar{1}\,\bar{1}\,\bar{1}]$$

HOLZ lines obtained from the middle of a stacking fault exhibit the best splitting, showing a good agreement with the theoretical prediction.

Hollow-cone beam technique

Si [3 3 1]

100 kV

Ordinary CBED pattern

Stacking fault

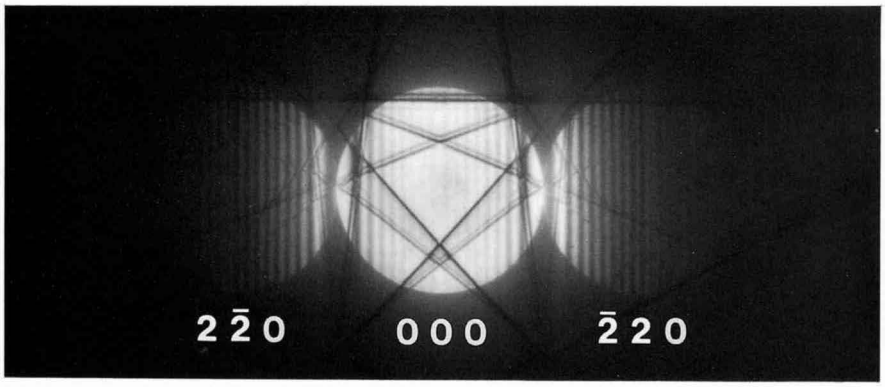

Hollow-cone beam pattern

Stacking fault

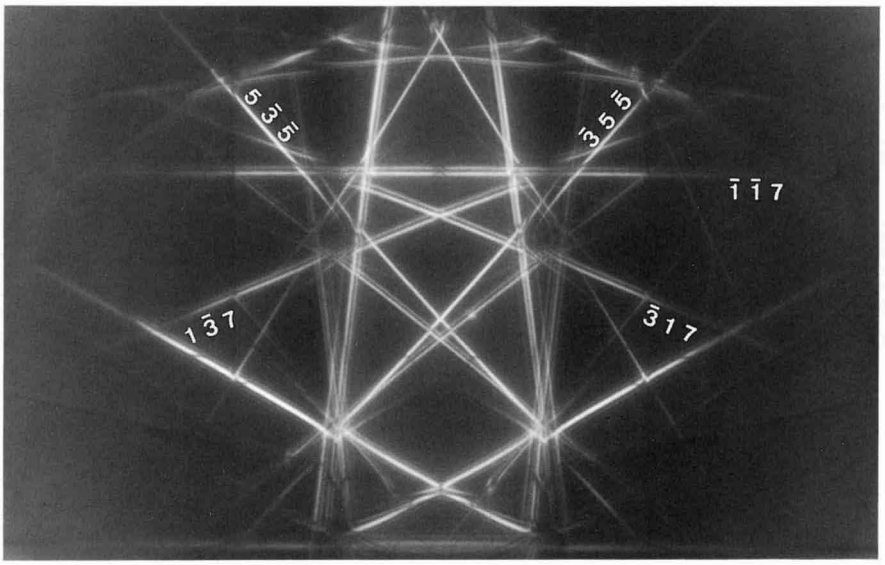

Perfect crystal

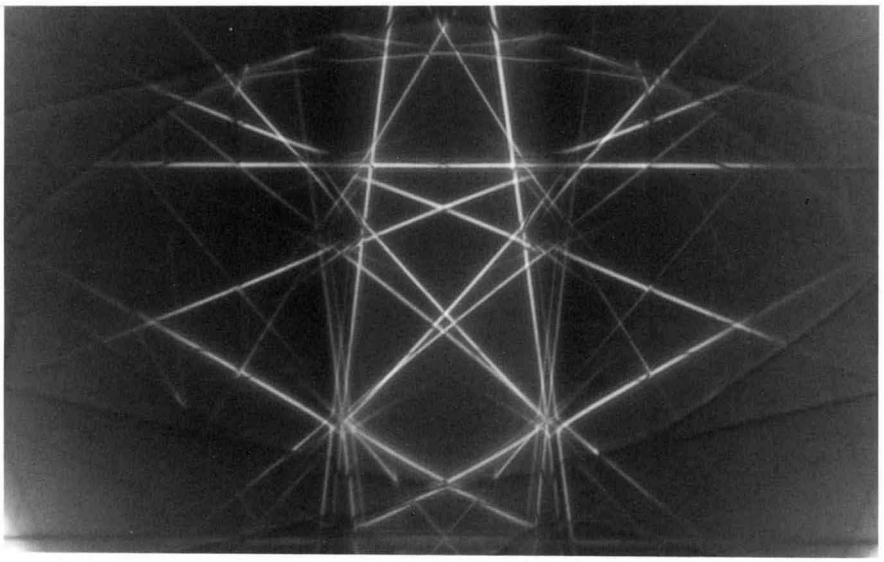

$$R = \frac{1}{3}[\bar{1}\,\bar{1}\,\bar{1}]$$

The hollow-cone beam technique makes the splitting of HOLZ lines clear over a wide angular range without strong background due to ZOLZ reflections.

Determination of displacement vectors of stacking faults

1) Si [3 3 1]

200 kV

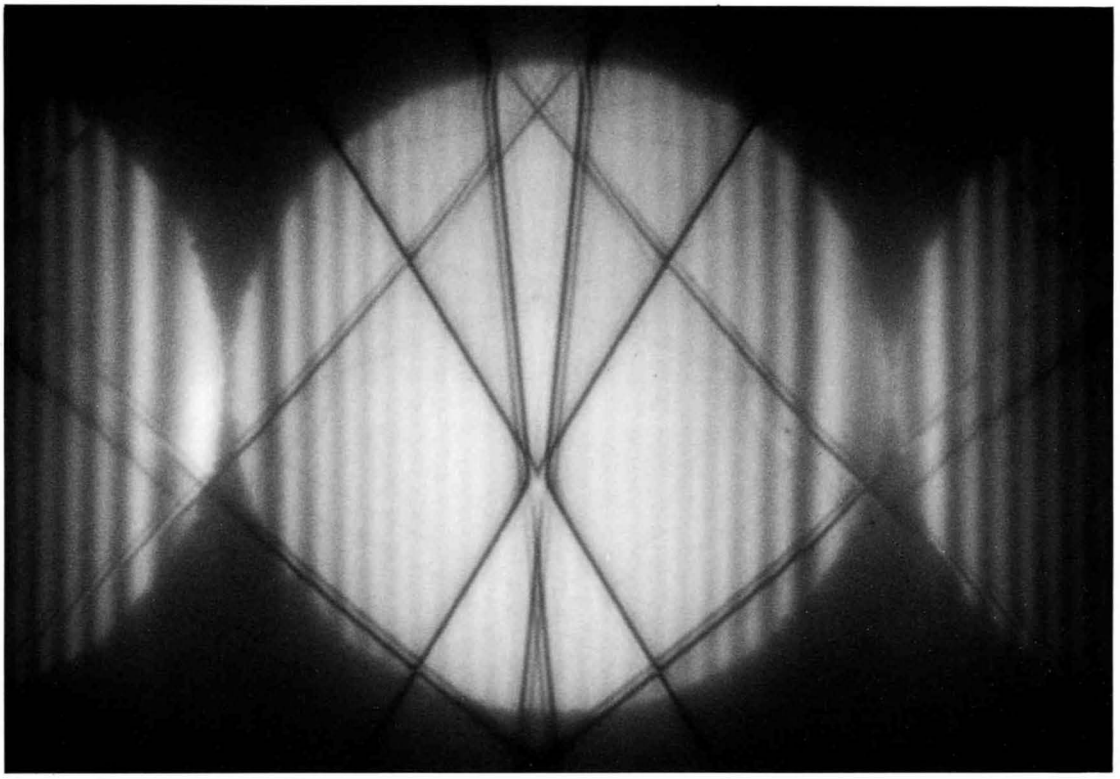

$\bar{2}\,2\,0$ 0 0 0 $2\,\bar{2}\,0$

Displacement vectors of stacking faults in Si

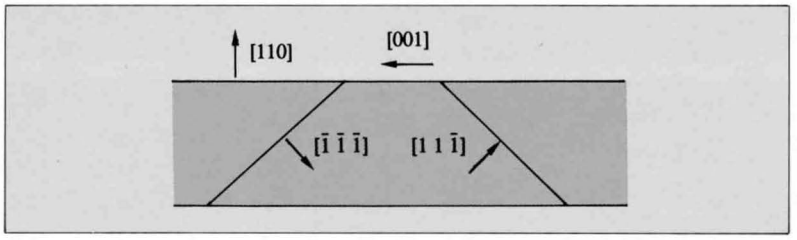

Geometrically allowed displacement vectors $\boldsymbol{R}$

$\boldsymbol{R}=\frac{1}{3}[111], \frac{1}{3}[\bar{1}\bar{1}\bar{1}], \frac{1}{3}[\bar{1}\bar{1}1], \frac{1}{3}[11\bar{1}]$

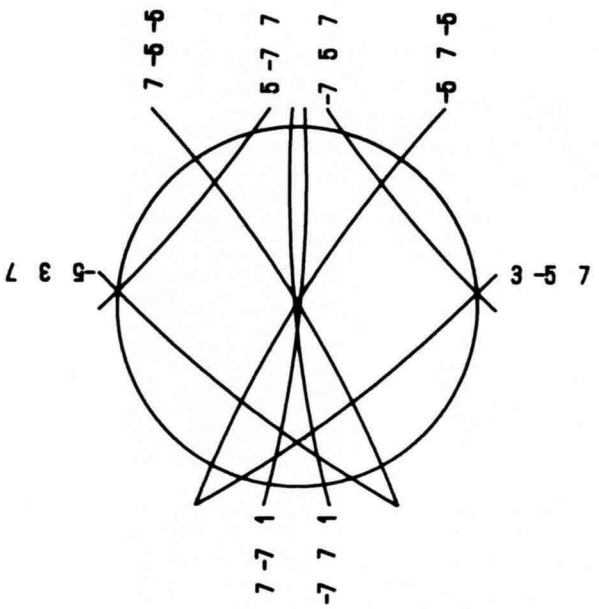

The bright-field pattern was taken from a (110) Si film containing a stacking fault at the [331] incidence and at an accelerating voltage of 200 kV. From the computer simulation, the observed HOLZ lines were indexed and the sign of w was determined for each line. It is seen that the $7\bar{5}\bar{5}$ and $\bar{5}7\bar{5}$ lines remain unsplit but the other lines are split. Allowed displacement vectors are given in the attached figure. The table lists experimental values of α for the eight reflections. The letter Y is given when the value of α calculated using a possible displacement vector agrees with the experimental value. The letter N is given when it does not agree.

g	α(exp.)	$\frac{1}{3}[111]$	$\frac{1}{3}[\bar{1}\bar{1}\bar{1}]$	$\frac{1}{3}[11\bar{1}]$	$\frac{1}{3}[\bar{1}\bar{1}1]$
$7\bar{7}1$	$-\frac{2}{3}\pi$	N	Y	Y	N
$\bar{7}71$	$-\frac{2}{3}\pi$	N	Y	Y	N
$\bar{5}7\bar{5}$	0	Y	Y	N	N
$7\bar{5}\bar{5}$	0	Y	Y	N	N
$\bar{5}37$	$+\frac{2}{3}\pi$	N	Y	N	N
$3\bar{5}7$	$+\frac{2}{3}\pi$	N	Y	N	N
$5\bar{7}7$	$+\frac{2}{3}\pi$	N	Y	N	N
$\bar{7}57$	$+\frac{2}{3}\pi$	N	Y	N	N

2) Si [3 1 1]

80 kV

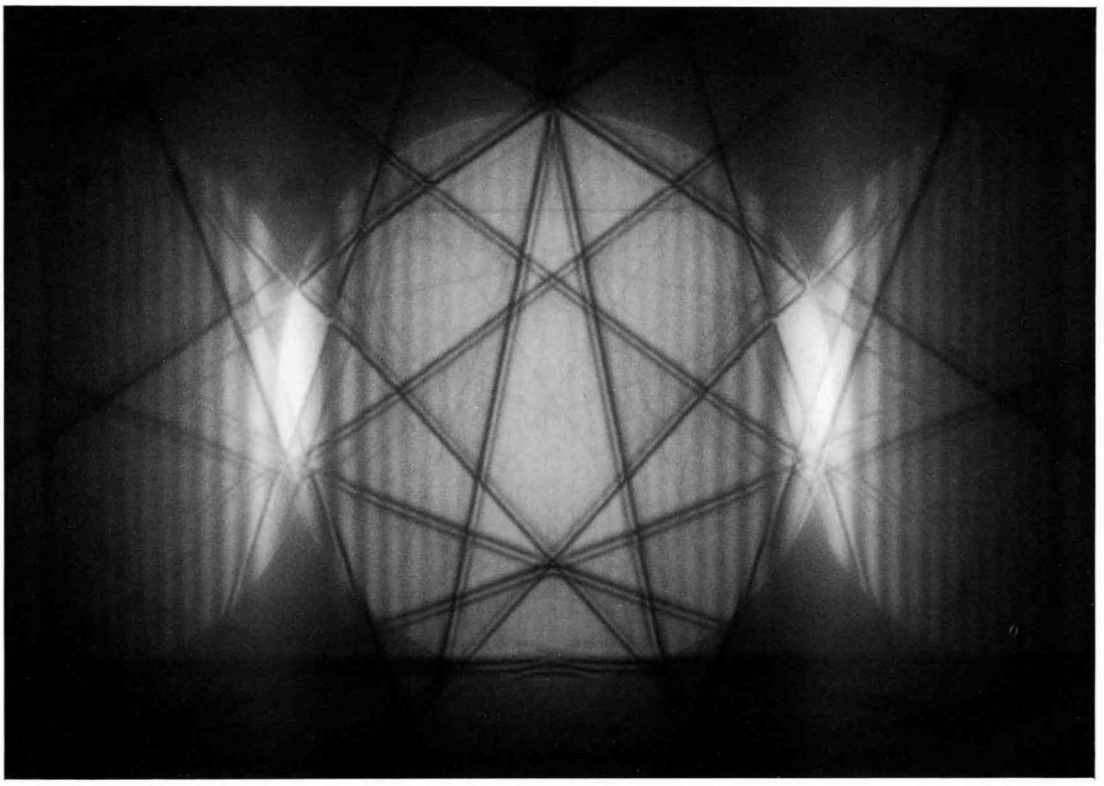

$0\bar{2}2$ 000 $02\bar{2}$

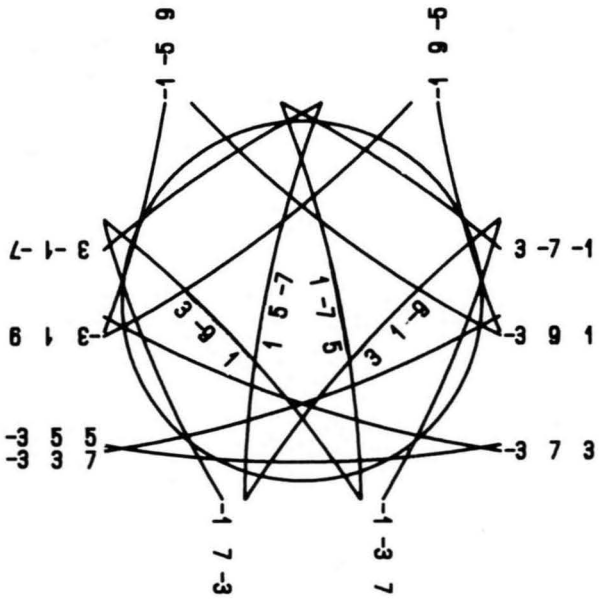

The determination of this displacement vector is left for readers' exercise.

g	α(exp.)	$\frac{1}{3}[111]$	$\frac{1}{3}[\bar{1}\bar{1}\bar{1}]$	$\frac{1}{3}[11\bar{1}]$	$\frac{1}{3}[\bar{1}\bar{1}1]$
$\bar{1}9\bar{5}$	0	Y	Y	N	N
$\bar{1}\bar{5}9$	0	Y	Y	Y	Y
$3\bar{1}\bar{7}$	$-\frac{2}{3}\pi$	N	Y	N	N
$3\bar{7}\bar{1}$	$-\frac{2}{3}\pi$	N	Y	N	N
$15\bar{7}$	$+\frac{2}{3}\pi$	N	Y	Y	N
$1\bar{7}5$	$+\frac{2}{3}\pi$	N	Y	Y	N
$\bar{3}19$	$-\frac{2}{3}\pi$	N	Y	N	Y
$\bar{3}91$	$-\frac{2}{3}\pi$	N	Y	Y	N
$\bar{3}73$	$-\frac{2}{3}\pi$	N	Y	N	Y
$\bar{3}37$	$-\frac{2}{3}\pi$	N	Y	Y	N
$\bar{1}\bar{3}7$	0	Y	Y	N	N
$\bar{1}7\bar{3}$	0	Y	Y	Y	Y
$3\bar{9}1$	$-\frac{2}{3}\pi$	N	Y	Y	N
$31\bar{9}$	$-\frac{2}{3}\pi$	N	Y	N	Y
$\bar{3}55$	$-\frac{2}{3}\pi$	N	Y	N	N

Thin specimen

Si [3 3 1]

80 kV

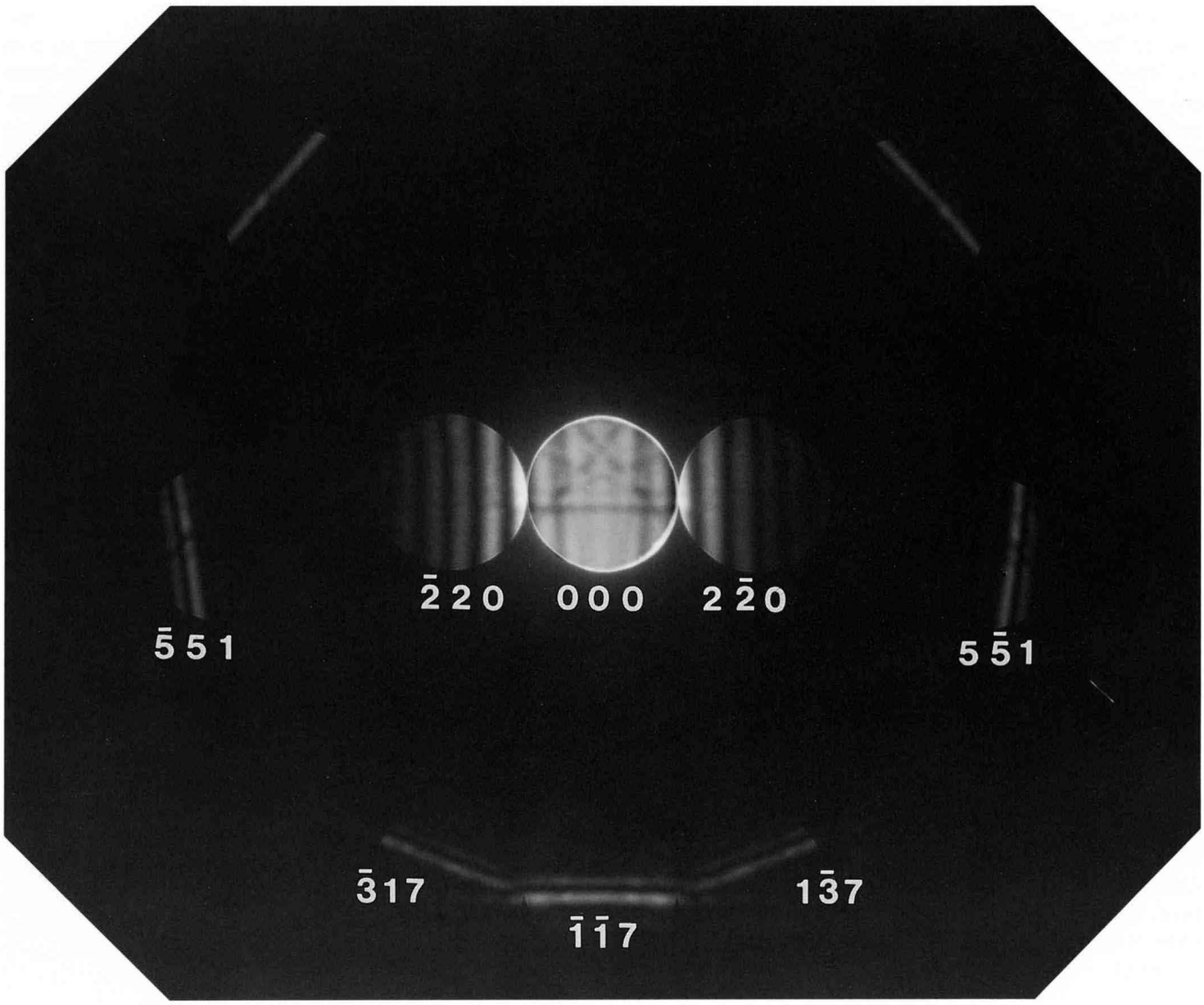

The CBED pattern was taken from a thin (about 40 nm) specimen area of (110) Si containing a stacking fault. The splittings of lines in HOLZ reflections are clearly seen. Note that the electron-microscope-image method does not allow easy identification of the displacement vector of a fault in such a thin specimen.

Dislocations

Carpenter and Spence [20] reported a method to identify the Burgers vector $\boldsymbol{b}$ of a dislocation. They observed additional fringes in intensity profiles of reflections with $\boldsymbol{g}\cdot\boldsymbol{b} \precsim 0$. They determined the vector $\boldsymbol{b}$ by finding a profile undisturbed by a dislocation or a reflection with $\boldsymbol{g}\cdot\boldsymbol{b}=0$. Cherns and Preston [23] have proposed an excellent method to determine the Burgers vector of a dislocation, in which the whole strain field of the dislocation is illuminated by a defocus convergent beam. When the incident beam illuminates a small specimen area around a dislocation, only the effect of local strain of the dislocation is observed. Defocus illumination or LACBED allows observing the whole strained area and identifying the Burgers vector. A defocus CBED pattern gives the intensity profile of a reflection as functions of the distance from a dislocation x and of excitation error w. The method [23] can use information obtained not only at $\boldsymbol{g}\cdot\boldsymbol{b}=0$ but also at $\boldsymbol{g}\cdot\boldsymbol{b}=n$ ($n \precsim 0$) for Burgers vector determination, while information obtained at $\boldsymbol{g}\cdot\boldsymbol{b} \precsim 0$ has been discarded in the traditional electron-microscope-image method except a few reports [a]. A defocus CBED pattern shows n nodes at the crossing region between a dislocation line and a reflection line when $\boldsymbol{g}\cdot\boldsymbol{b}=n$. The following studies of dislocations have fully been based upon their method. It should be emphasized that the relative sign of $\boldsymbol{g}\cdot\boldsymbol{b}=n$ is important for Burgers vector identification.

Figure (a) illustrates two defocus CBED modes. We adopt the left mode because the sense of an object shown by the arrow X is the same as that of a defocus CBED pattern (image) as shown by the arrows X_o and X_g. Figure (b) shows the side view of a specimen containing a dislocation and a column through which the electron beam runs. The atomic displacement $\boldsymbol{R}$ due to a general perfect dislocation in an infinite isotropic medium is written in the form

$$\boldsymbol{R}=\frac{1}{2\pi}\left[\boldsymbol{b}\Phi+\boldsymbol{b}_e\frac{\sin 2\Phi}{4(1-\nu)}+(\boldsymbol{b}\times\boldsymbol{u})\left\{\frac{1-2\nu}{2(1-\nu)}\ln r+\frac{\cos 2\Phi}{4(1-\nu)}\right\}\right] \quad (1)$$

where $\boldsymbol{b}$ is the Burgers vector, $\boldsymbol{b}_e$ is the edge component of $\boldsymbol{b}$, $\boldsymbol{u}$ is the unit vector of the dislocation line, r is the distance from the dislocation line, ν is Poisson's ratio and $\Phi=\phi-\gamma$. The atomic displacement due to a pure screw dislocation is expressed simply by the equation

$$\boldsymbol{R}=\frac{\boldsymbol{b}}{2\pi}\Phi \quad (2)$$

Reference

[a] Y. Ishida, H. Ishida, K. Kohra and H. Ichinose: *Phil. Mag.*, **42** (1980) 453.

►

Figure (c) shows defocus CBED patterns from an area containing a screw dislocation, computed by the two-beam dynamical theory using the Euler method for integration. The ratio between the thickness and extinction distance was given as $t/\xi_g=1/2$. The dislocation was assumed to be at the middle of the specimen, $y/t=1/2$. The absorption coefficients were assumed to be the same as those for stacking faults (see page 143). The ordinate and abscissa represent the excitation error w and the horizontal distance from the dislocation x/ξ_g. The dislocation lies parallel to the ordinate at $x=0$. A reflection line, the principal maximum of a reflection profile, lies parallel to the abscissa at $w=0$ for a perfect crystal.

For $\boldsymbol{g}\cdot\boldsymbol{b}=n=0$, the reflection line appears as a straight line without the influence of the dislocation. For $n=1$, the reflection line deviates from $w=0$ and splits into two lines near the dislocation, thus forming one node. For $n=2$, the reflection line splits into three, forming two nodes. When n is negative, the sense of deviation of the line from $w=0$ is opposite to that of positive n. The defocus CBED patterns for $n=1\sim6$ are given on page 162. Since the lowest order reflection is often far from the condition $t/\xi_g=1/2$ for a specimen thickness usually used, it exhibits a complicated profile and is not suitable for Burgers vector determination.

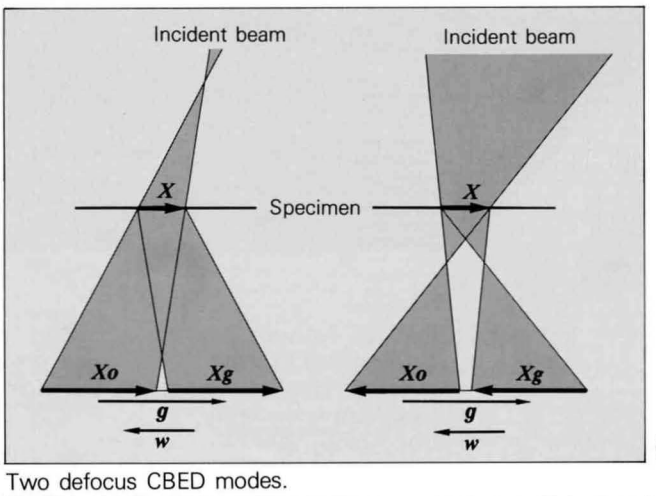

(a)

Two defocus CBED modes.

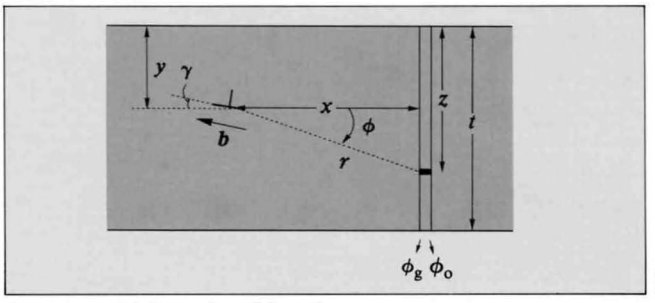

(b)

Crystal containing edge dislocation.

Determination of Burgers vectors of perfect dislocations

Simulations of a reflection line crossing a screw dislocation

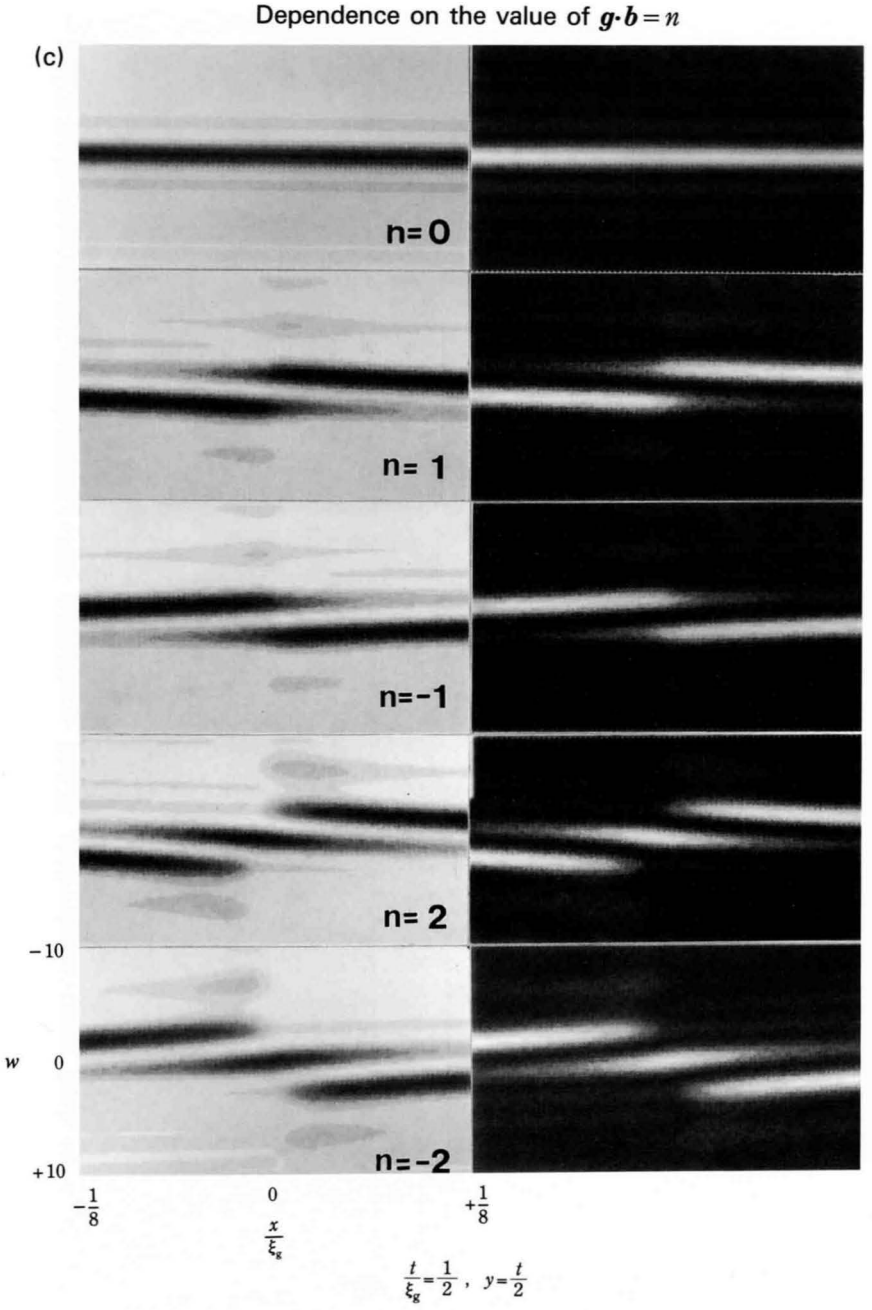

Left and right simulations are bright- and dark-field patterns, respectively.

Simulations of a reflection line crossing a screw dislocation

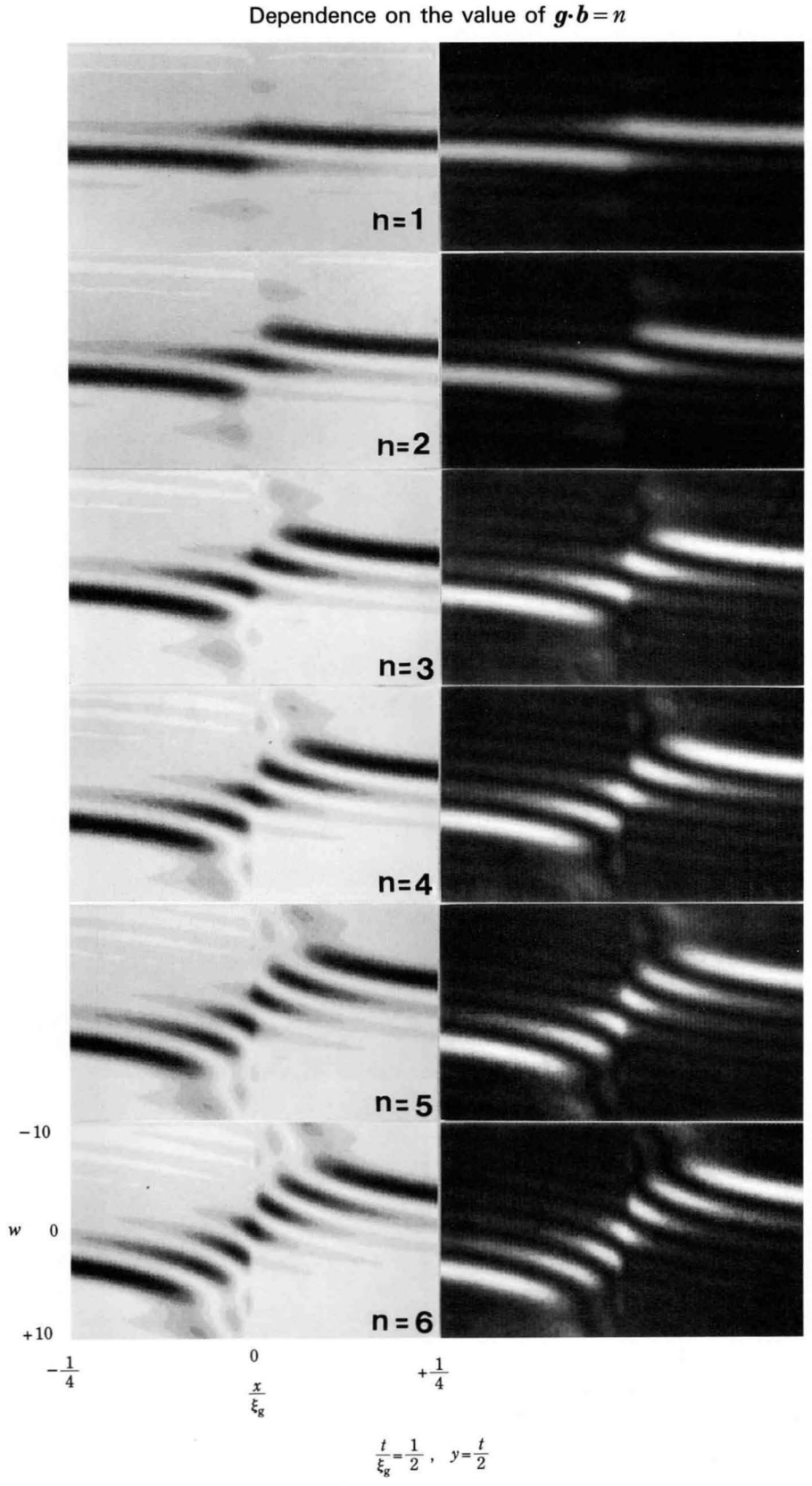

Dependence on dislocation depth

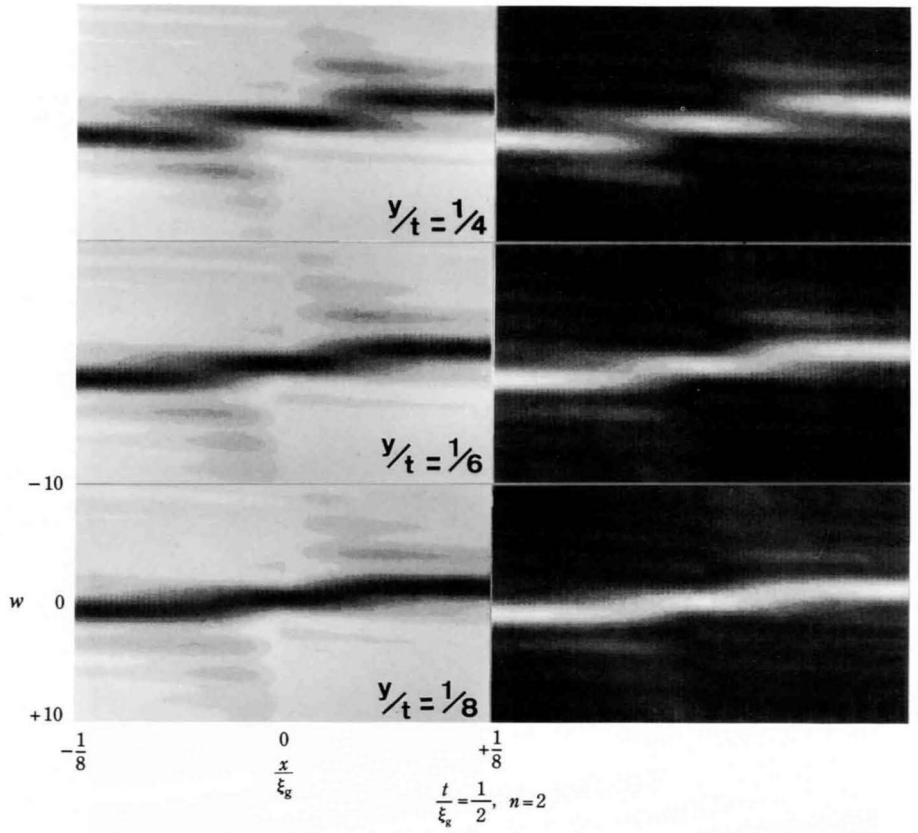

When a dislocation lies in the middle of a specimen, the splitting of a reflection line is seen best. The splitting is still clearly seen at a dislocation depth, $y/t = 1/4$, but becomes difficult to see at $y/t = 1/6$. This behaviour is analogous to that of a HOLZ reflection profile obtained from a stacking fault (see page 151).

If a dislocation lies at $1/4 \leqq y/t \leqq 3/4$ in an illuminated area, the Burgers vector can be safely determined even though it is oblique to the specimen surface.

Dependence on specimen thickness

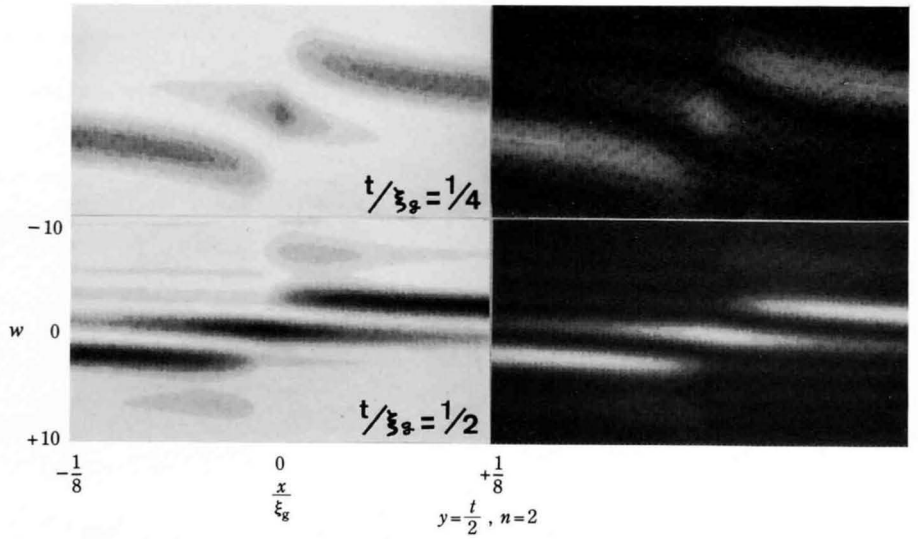

For thinner specimens, the deviation of a reflection line from $w = 0$ becomes larger, but the number of the nodes remains the same (see page 152).

Simulations of a reflection line crossing an edge dislocation

Dependence on the values of $\boldsymbol{g}\cdot\boldsymbol{b}=n$ and γ

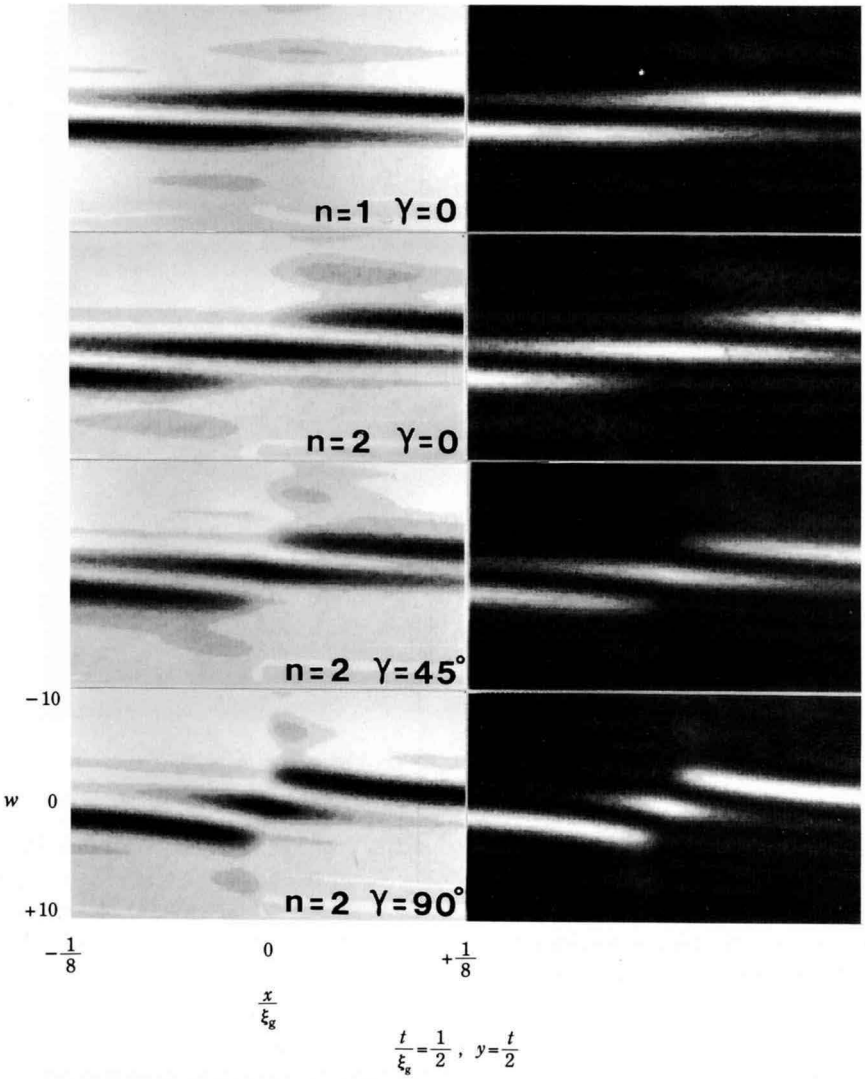

Defocus CBED patterns from an edge dislocation are very similar to those from a screw dislocation except a longer splitting in the horizontal direction x (see upper two figures). As the angle γ of the edge dislocation from the specimen surface (Fig. (b) on page 160) increases, the range of the splitting decreases as seen in the lower two figures.

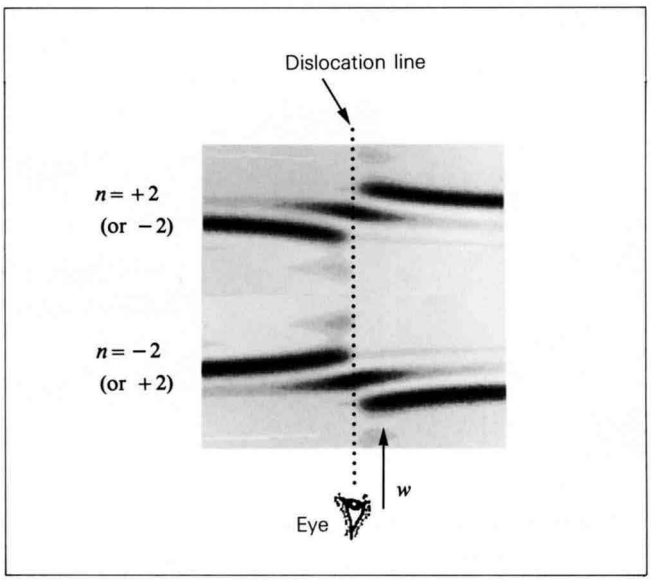

Burgers vector determination

1) Si

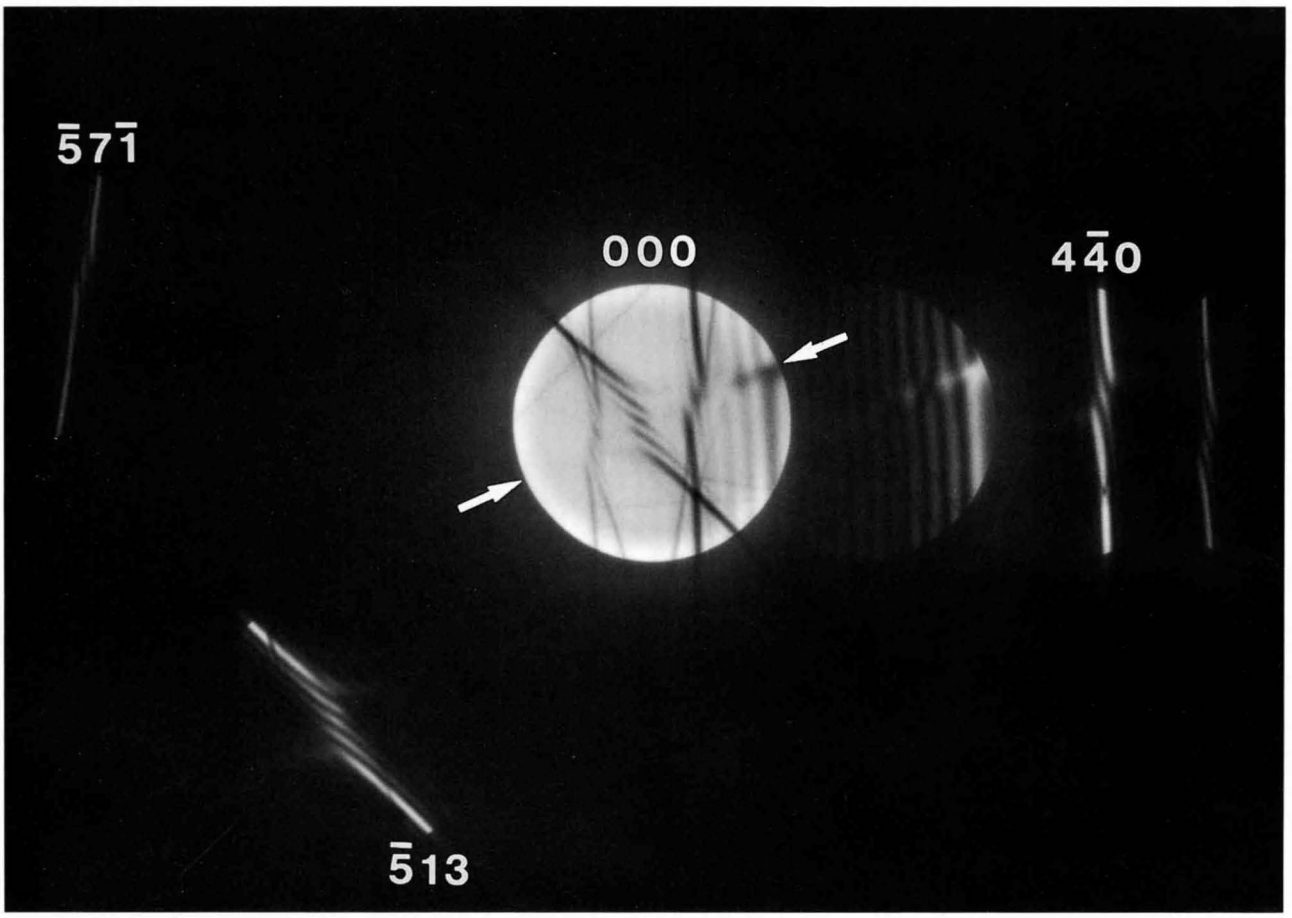

Illuminated specimen area: approx. 200 nm in diameter

$\boldsymbol{b}=[uvw]$

$\boldsymbol{g}$	$\boldsymbol{g}\cdot\boldsymbol{b}=n$
$4\bar{4}0$	$4u-4v=-2$
$\bar{5}13$	$-5u+v+3w=+4$
$\bar{5}7\bar{1}$	$-5u+7v-w=+2$

$\longrightarrow \boldsymbol{b}=\frac{1}{2}[\bar{1}01]$

For Burgers vector determination, it is not necessary to set a crystal at a particular zone axis, but at an orientation so that three linearly independent reflections are excited. The photo shows a defocus CBED pattern taken at such a crystal setting from an area containing a dislocation. We omit to use the lowest order reflection for the determination. The position of the dislocation line is indicated by the arrows. Let us write the Burgers vector $\boldsymbol{b}=[uvw]$. The $4\bar{4}0$, $\bar{5}13$ and $\bar{5}7\bar{1}$ reflections give values of $n=-2$, $+4$ and $+2$, respectively. The signs of n were determined relatively. By solving the linear system of equations, the Burgers vector was determined to be $\boldsymbol{b}=1/2[\bar{1}01]$. The (relative) sign of n is very important.

A practical method to determine the relative sign of n is illustrated in the figure on the opposite page. Look at a reflection line from a sense along the dislocation line (upward in the figure). Observe the sense of the bend of the reflection line with respect to the sense of the excitation error w. Regard one sense of bend as positive and the other as negative. We do not intend, here, to determine the sign of the Burgers vector.

It is noted that the dislocation of Si was assumed to be a perfect dislocation, because of a small separation of the two extended partials. The effect of the dissociation can be detected using a reflection satisfying $\boldsymbol{g}\cdot\boldsymbol{b}=0$ as will be seen later.

The Si specimens containing dislocations were supplied by Dr. I. Yonenaga and Prof. K. Sumino.

2) Al

80 kV

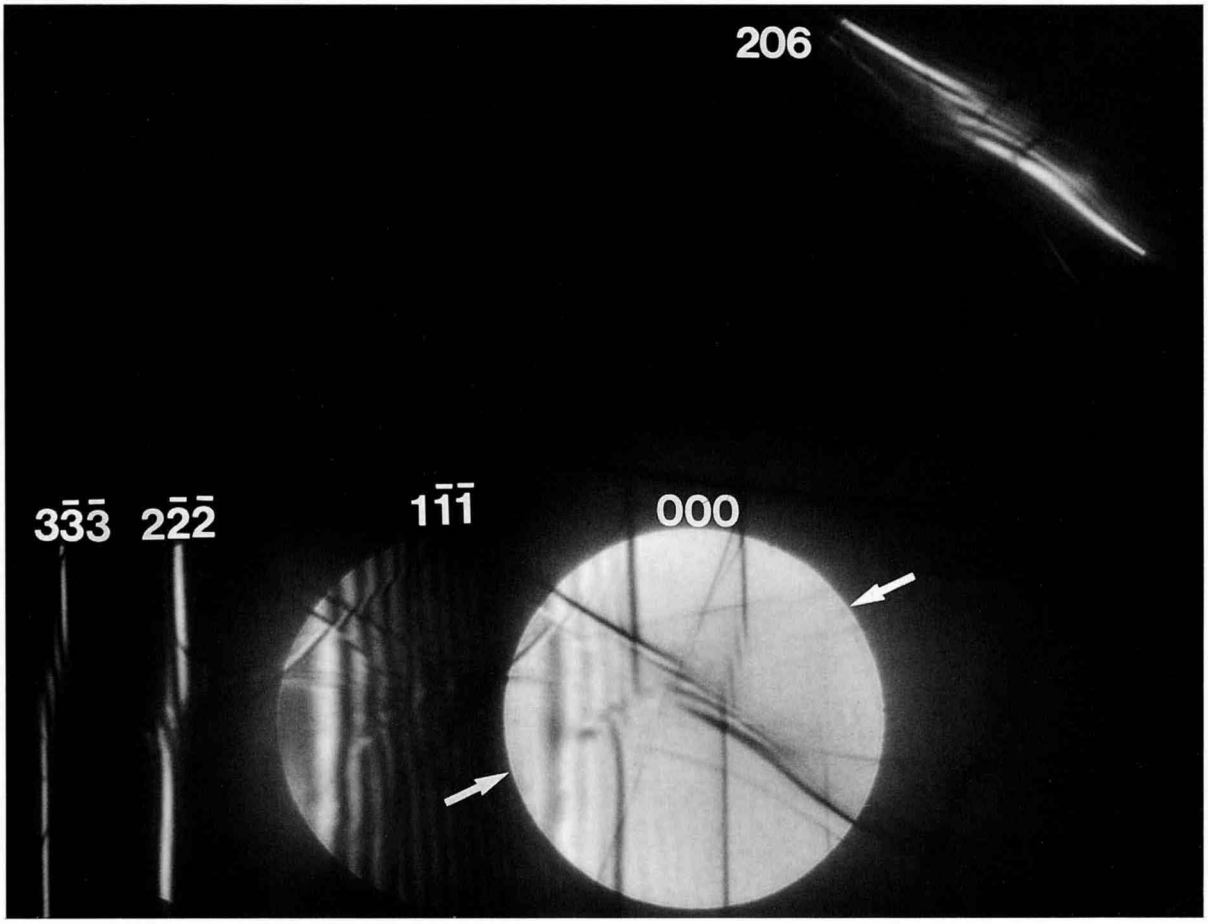

Illuminated specimen area: approx. 200 nm in diameter

$\boldsymbol{b}=\frac{1}{2}[u\,v\,w]$

$\boldsymbol{g}$	$\boldsymbol{g}\cdot\boldsymbol{b}=n$
$2\bar{2}\bar{2}$	$u-v-w=-2$
206	$u+3w=+3$

$\longrightarrow \boldsymbol{b}=\frac{1}{2}[011]$

Three reflection lines show splittings. As the $2\bar{2}\bar{2}$ and $3\bar{3}\bar{3}$ reflections are linearly dependent, we have only two equations to solve. We assume that the dislocation has a Burgers vector of the 1/2 <110> type. Then, we can determine the vector to be $\boldsymbol{b}=1/2[011]$.

3) Al

60 kV

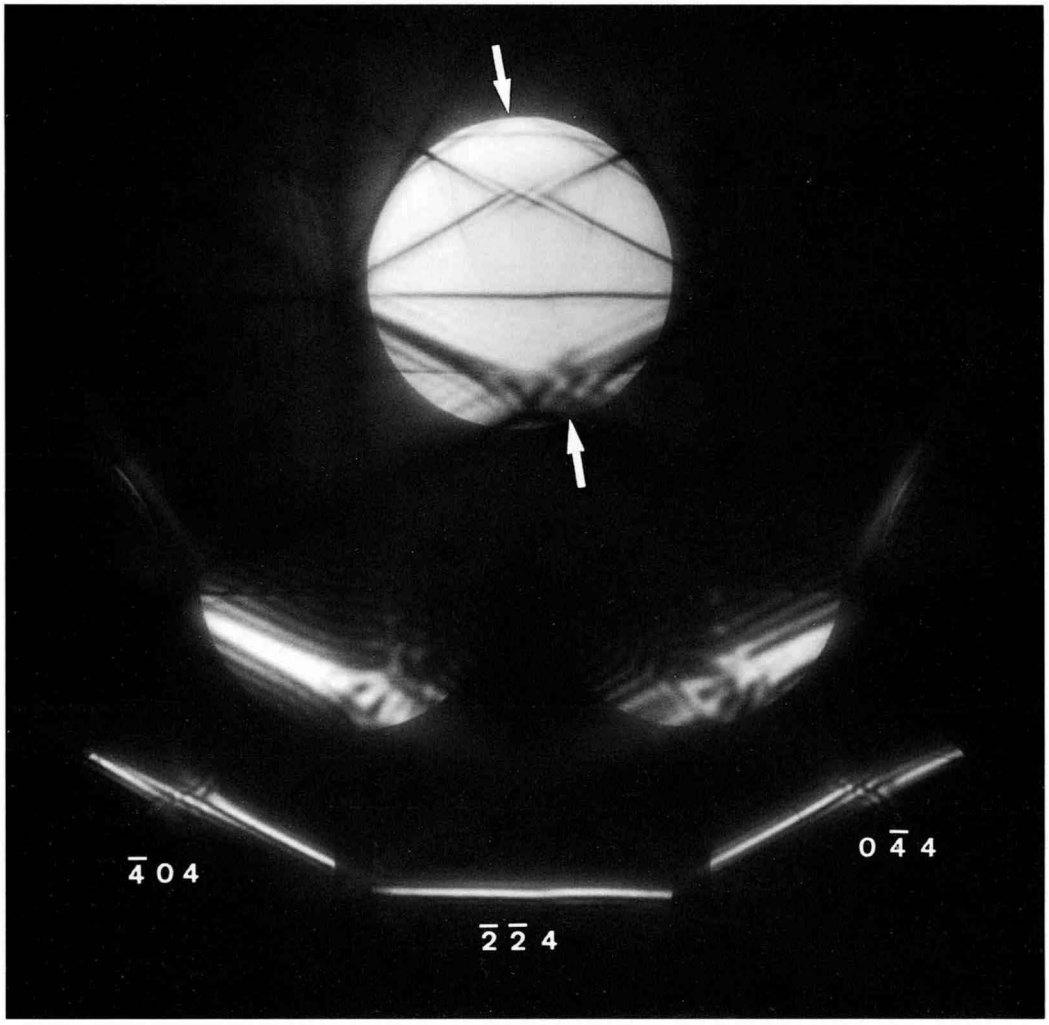

Illuminated specimen area: approx. 100 nm in diameter

$\boldsymbol{b}=\frac{1}{2}[u\,v\,w]$

$\boldsymbol{g}$	$\boldsymbol{g}\cdot\boldsymbol{b}=n$
$\bar{4}04$	$-2u+2w=+2$
$0\bar{4}4$	$-2v+2w=-2$
$\bar{2}\bar{2}4$	$-u-v+2w=0$

$\longrightarrow \boldsymbol{b}=\frac{1}{2}[\bar{1}10]$

The Burgers vector was assumed to be of the 1/2 <110> type.

Determination of Burgers vectors of partial dislocations

Simulations of a reflection line crossing a partial screw dislocation

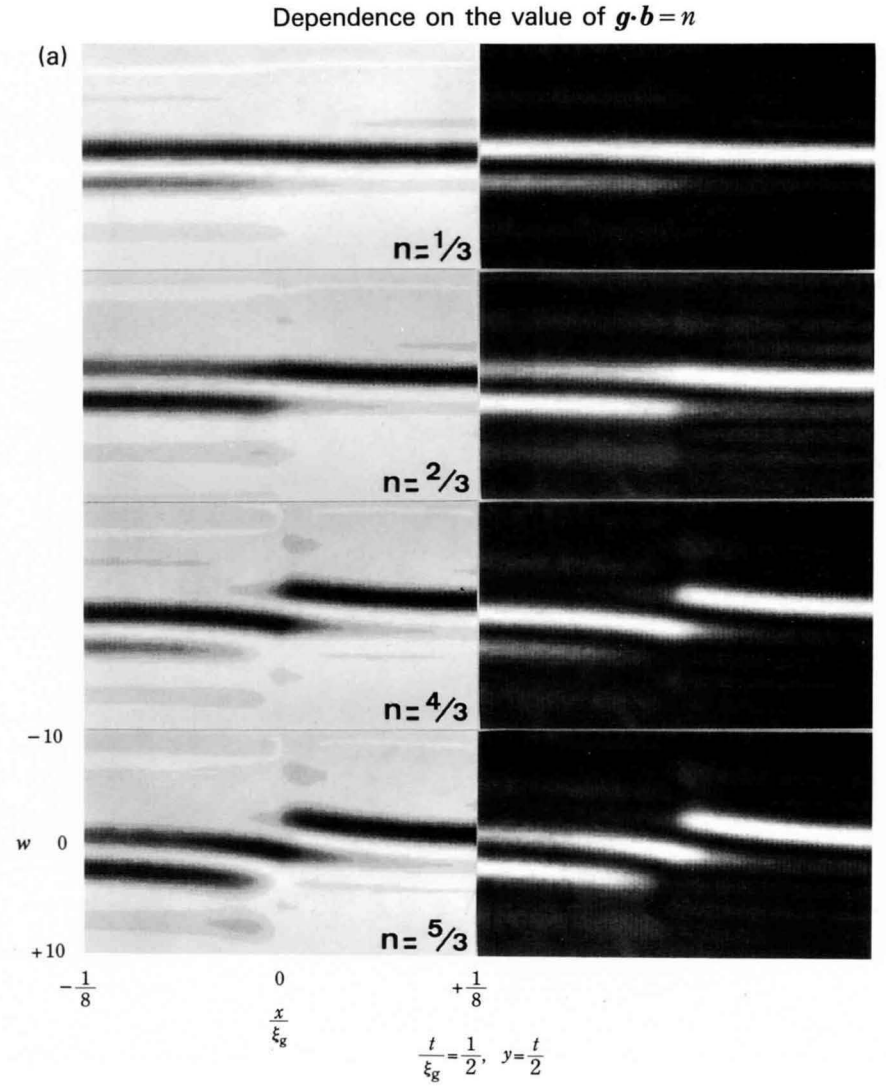

A partial dislocation has a Burgers vector which is not a lattice vector and is accompanied by a stacking fault at one side of it. In the case of face-centered cubic crystals, $n = \boldsymbol{g} \cdot \boldsymbol{b}$ takes values 0, $\pm 1/3$, $\pm 2/3$, ± 1, $\pm 4/3 \cdots$. Figure (a) shows computed CBED profiles of a reflection line crossing a partial dislocation and a stacking fault. The partial dislocation was assumed to be of the screw type for simplicity of calculation. The stacking fault was assumed to be present at $x<0$. Near the dislocation, the profiles for $n=N+1/3$ and $n=N+2/3$ (N: integer) are similar to that for $n=N$ of a perfect dislocation. With increasing x in the negative direction, the profiles become similar to those obtained from a stacking fault for $\alpha = 2\pi \boldsymbol{g} \cdot \boldsymbol{R} = \pm(2/3)\pi$ (compare with the profiles shown in the section

Photographs (a) and (b) show defocus CBED patterns taken from an about 250 nm diameter specimen area containing a stacking fault and a partial dislocation, shown in Photo (c). The $1\bar{1}\bar{5}$ and 008 reflection profiles are of $n=+5/3$ and $n=-8/3$, respectively. The low order 004 reflection is discarded, because the identification of n is difficult. The $11\bar{5}$ and $\bar{2}06$ reflection profiles are of $n=1$ and $n=-4/3$, respectively. From the three equations among four, the Burgers vector is determined to be $\boldsymbol{b} = 1/3[\bar{1}\bar{1}\bar{1}]$

Si

80 kV

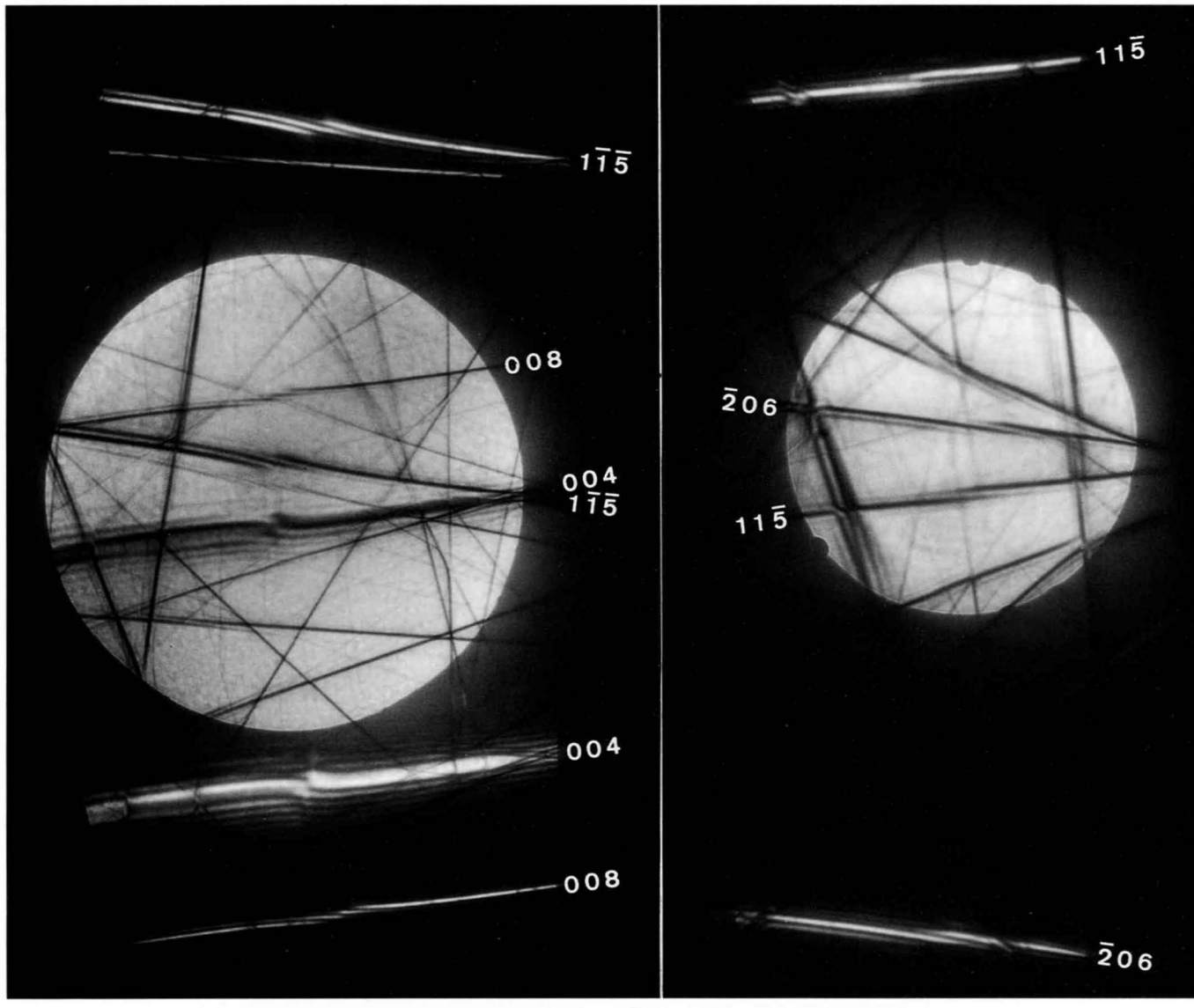

Illuminated specimen area: approx. 250 nm in diameter (a) (b)

$\boldsymbol{b}=[u\,v\,w]$

$\boldsymbol{g}$	$\boldsymbol{g}\cdot\boldsymbol{b}=n$
$1\bar{1}\bar{5}$	$u-v-5w=+\frac{5}{3}$
008	$8w=-\frac{8}{3}$
$11\bar{5}$	$u+v-5w=+1$
$\bar{2}06$	$-2u+6w=-\frac{4}{3}$

$\longrightarrow \boldsymbol{b}=\frac{1}{3}[\bar{1}\bar{1}\bar{1}]$

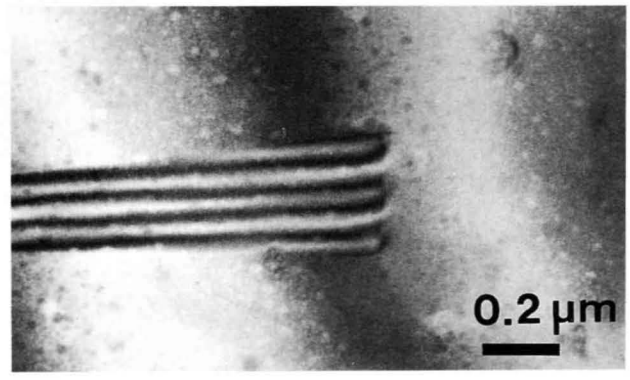

$\boldsymbol{b}=\frac{1}{3}[\bar{1}\bar{1}\bar{1}]$ (c)

Investigation of edge and mixed dislocations

Simulations of a reflection line crossing a 60° dislocation: Effect of $g \cdot b_e = p$ at $g \cdot b = 0$

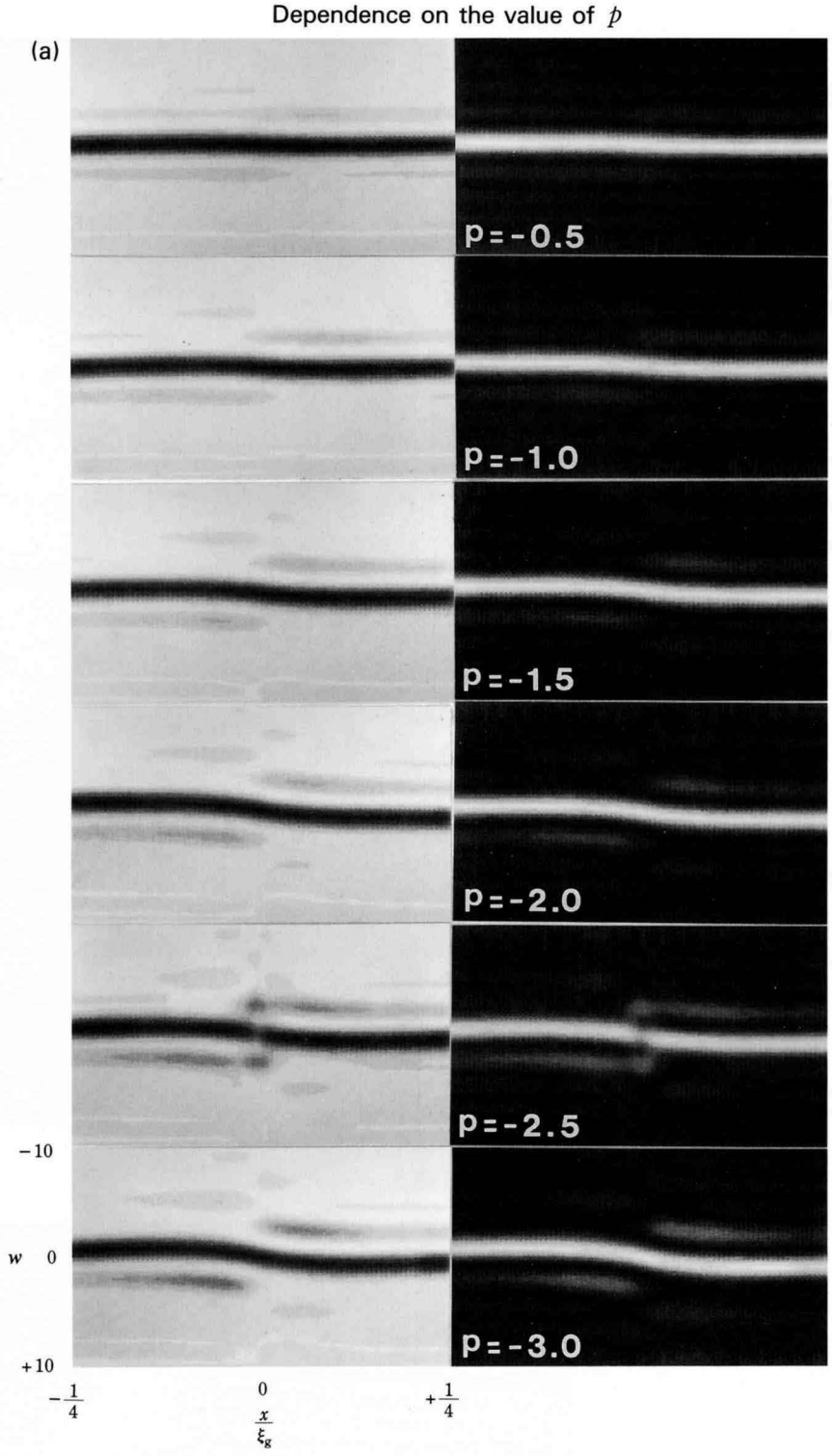

$\frac{t}{\xi_g}=\frac{1}{2}$, $y=\frac{t}{2}$, $n=0$, $m=0$, $\gamma=0°$

Dependence on the sign of p

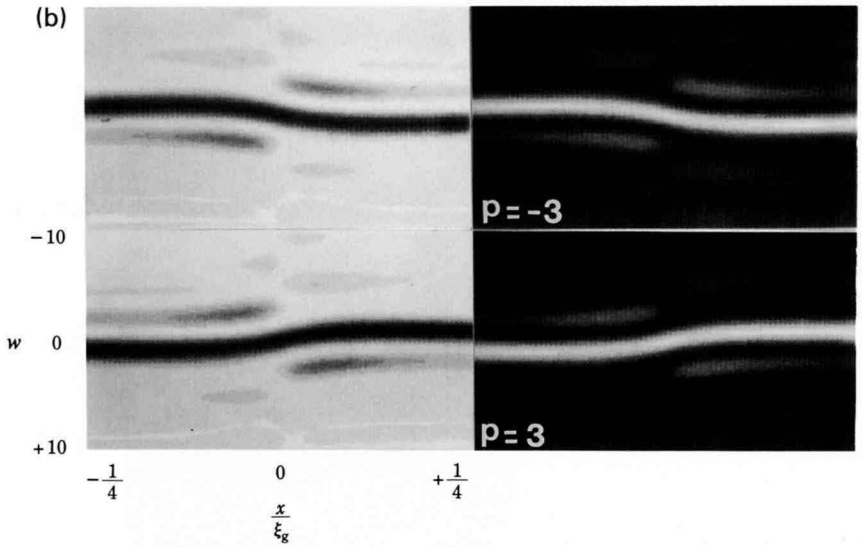

$\frac{t}{\xi_g}=\frac{1}{2}$, $y=\frac{t}{2}$, $n=0$, $m=0$, $\gamma=0°$

The condition $\boldsymbol{g}\cdot\boldsymbol{b}=0$ is not a sufficient condition for the invisibility of edge and mixed dislocations. The second and third terms of equation (1) on page 160 cause changes in the form of a reflection line. The second term, expresses the atomic displacements parallel to the slip plane and the third term the displacements perpendicular to the slip plane. It should be noted that the resultants of these displacements along the entire Burgers circuit are zero. The effect of the second term of $p=\boldsymbol{g}\cdot\boldsymbol{b}_e$ produces a bend similar to a kink in a reflection line. Figure (a), which was calculated for $\gamma=0°$, shows that the bend increases with the value of p. The sense of the bend becomes opposite when the sign of p is changed (Fig. (b)). When γ is increased for a definite value of p, the sense of the bend becomes opposite at $\gamma=45°$, as shown in Fig. (c).

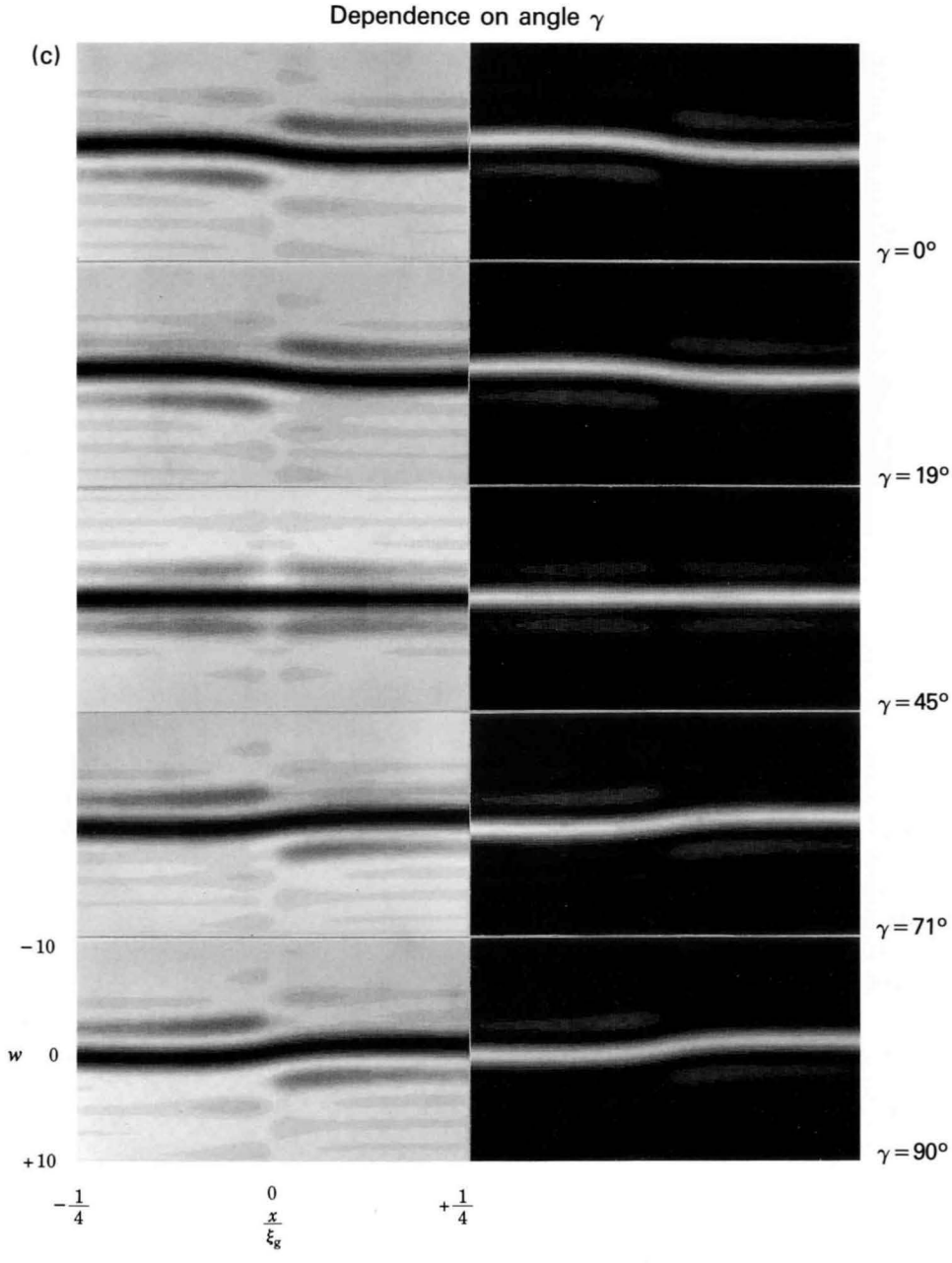

$\frac{t}{\xi_g}=\frac{1}{2}$, $y=\frac{t}{2}$, $n=0$, $m=0$, $p=-2$

Simulations of a reflection line crossing an edge dislocation: Effect of $\frac{1}{8}\, g\cdot b\times u=m$ at $g\cdot b=0$

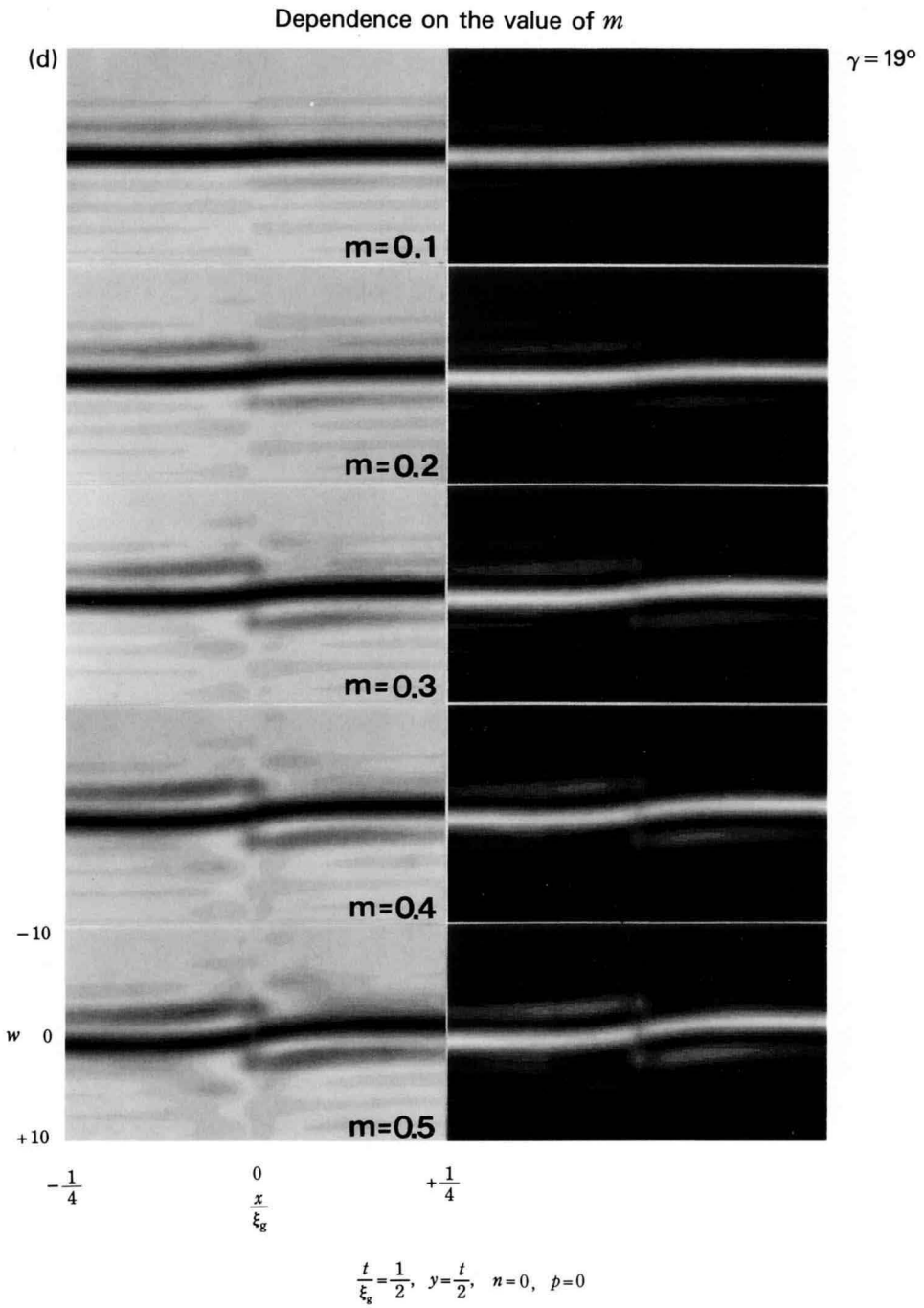

The effect of the third term, $m=1/8\ g\cdot b\times u$, causes a bend similar to that for p, but accompanied by stronger subsidiary maxima, as seen in Fig. (d). When the angle γ approaches 90°, the pattern becomes symmetric with respect to $x=0$ and $w=0$ (Figs. (e) and (f)). The sense of the bend becomes opposite when the sign of m is changed (Fig. (g)).

Dependence on the value of m

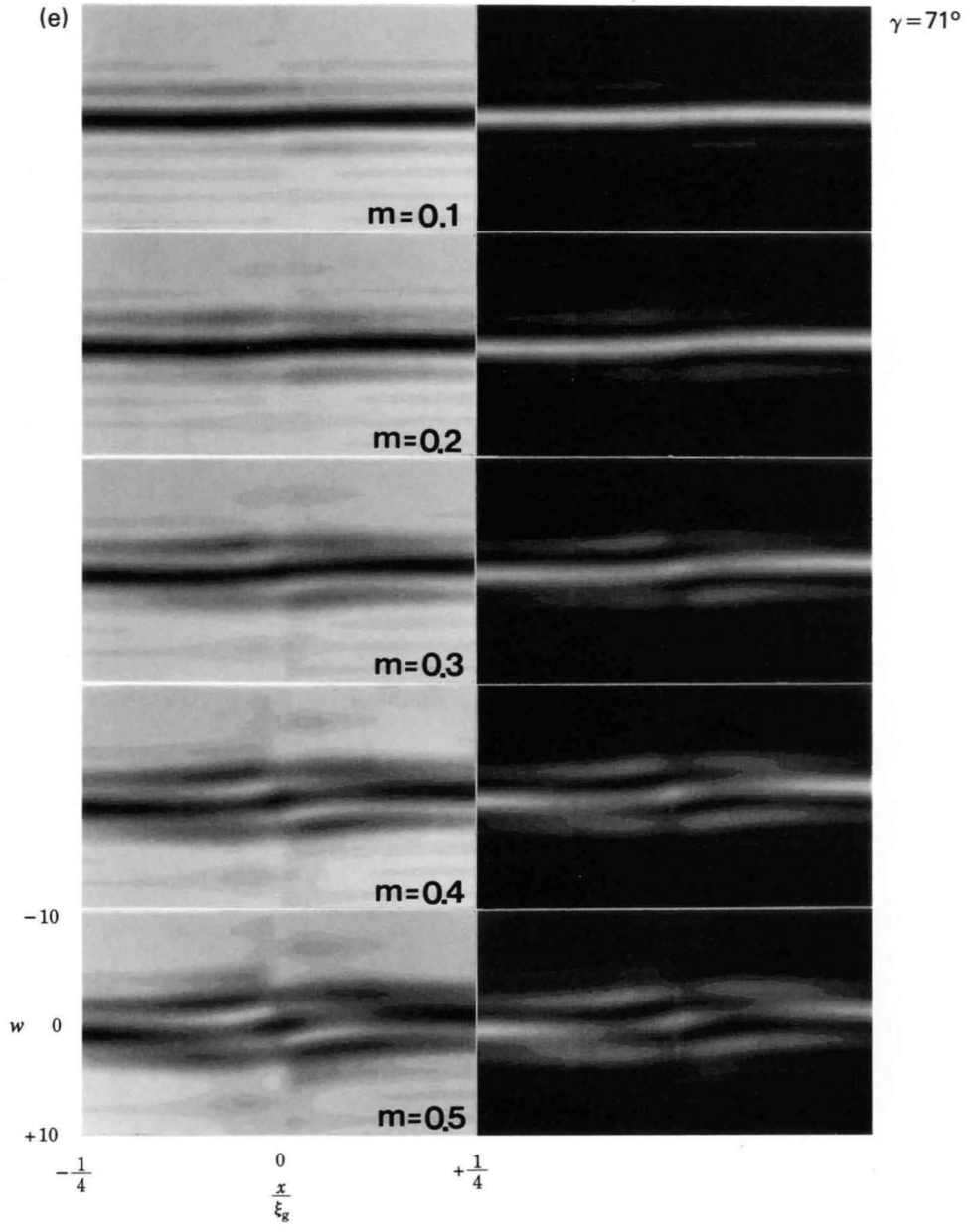

$\frac{t}{\xi_g}=\frac{1}{2}$, $y=\frac{t}{2}$, $n=0$, $p=0$

Dependence on the value of m

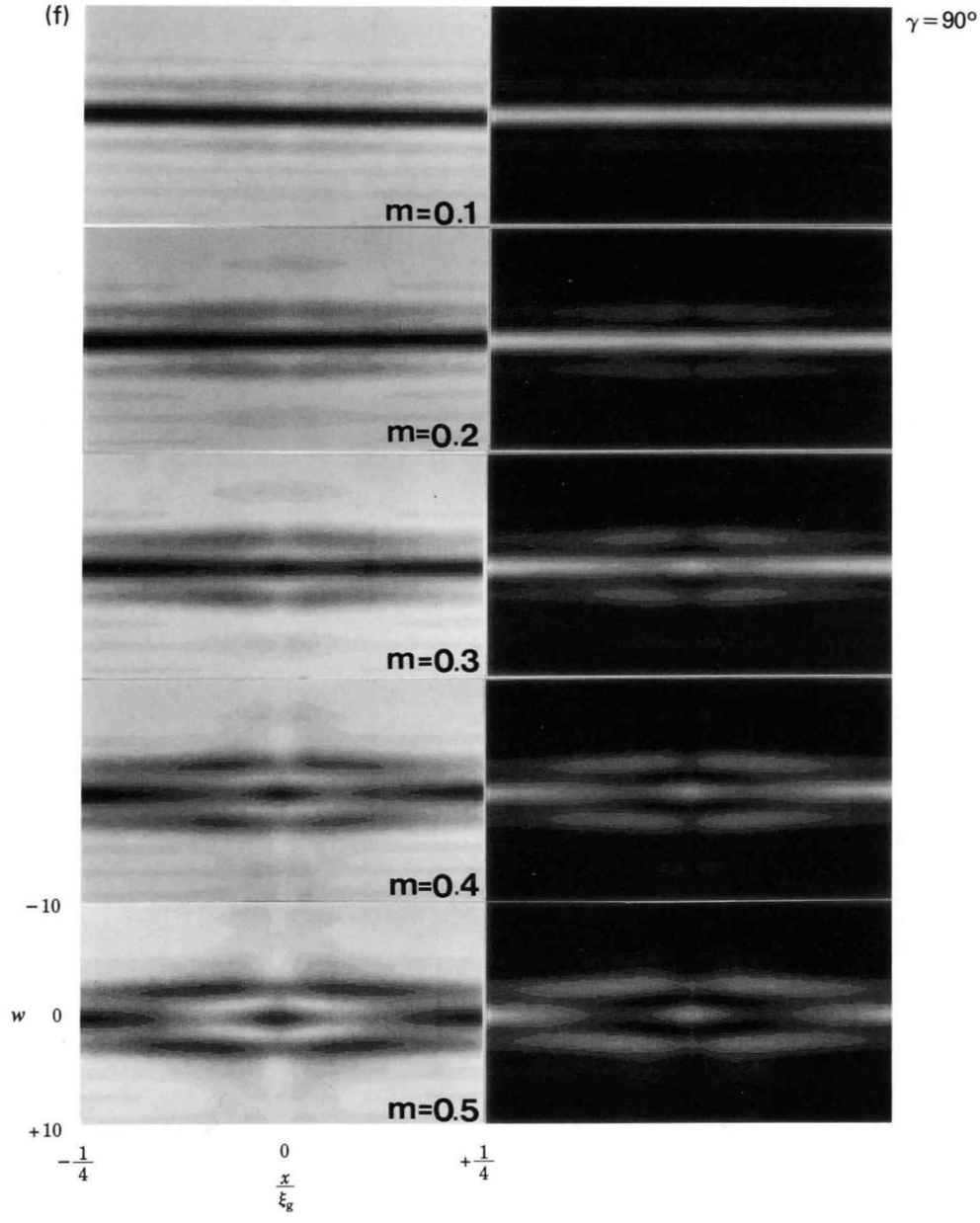

$\frac{t}{\xi_g}=\frac{1}{2}$, $y=\frac{t}{2}$, $n=0$, $p=0$

Dependence on the sign of m

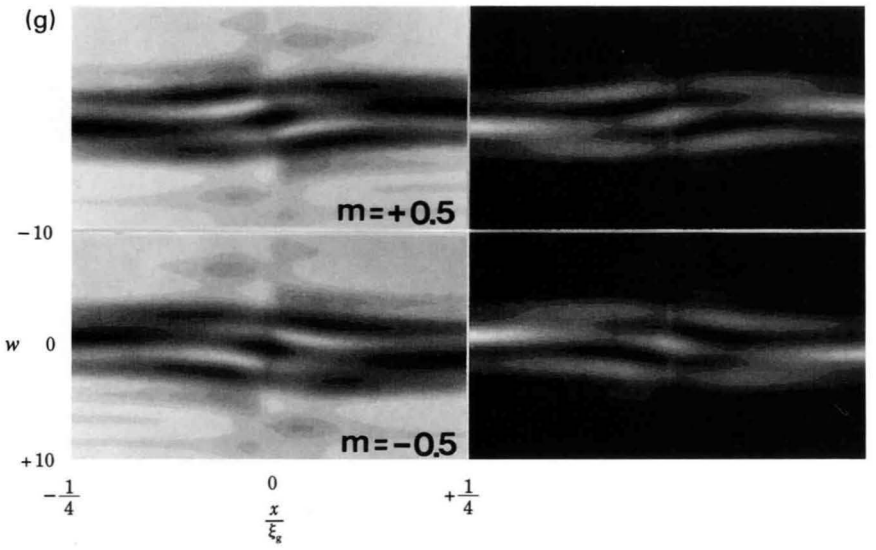

$\frac{t}{\xi_g}=\frac{1}{2}$, $y=\frac{t}{2}$, $n=0$, $p=0$, $\gamma=71°$

60° dislocation of Al 200 kV

Effect of $p = \boldsymbol{g}\cdot\boldsymbol{b}_e$

(a)

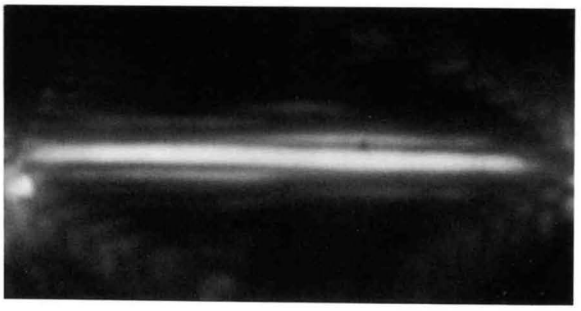

2 2 $\bar{4}$

$p = -1.5$
$m = 0$

$\boldsymbol{u}=\frac{1}{\sqrt{2}}[10\bar{1}]$, $\boldsymbol{b}=\frac{1}{2}[1\bar{1}0]$, $\boldsymbol{b}_e=\frac{1}{4}[1\bar{2}1]$, $n=0$, $\gamma=0°$

Photograph (a) is a $22\bar{4}$ dark-field pattern taken from a 60° dislocation of Al at the condition $\boldsymbol{g}\cdot\boldsymbol{b}=0$. The bend of the reflection line is caused by p, showing a qualitatively good agreement with the theoretical results (Fig. (a) on page 170).

Effect of $m = \frac{1}{8}\,\boldsymbol{g}\cdot\boldsymbol{b}\times\boldsymbol{u}$

(b)

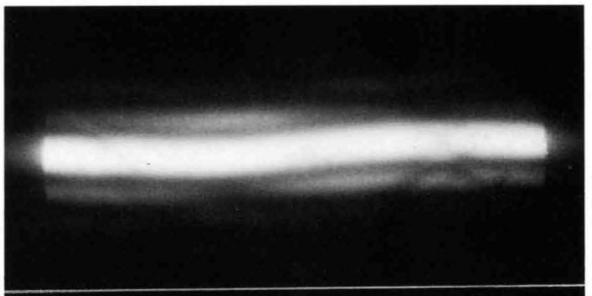

4 0 0

$p = 1.0$
$m = 0.177$

(c)

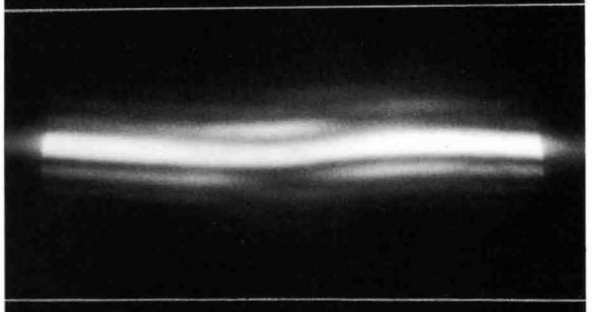

6 0 0

$p = 1.5$
$m = 0.265$

(d)

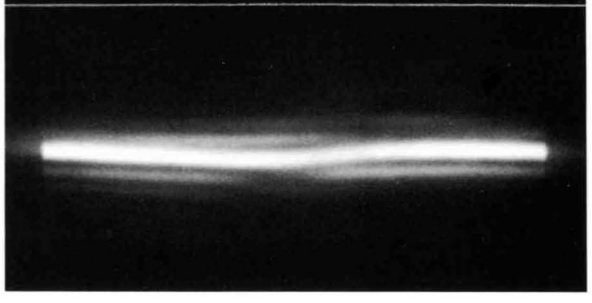

8 0 0

$p = 2.0$
$m = 0.354$

$\boldsymbol{u}=\frac{1}{\sqrt{2}}[\bar{1}10]$, $\boldsymbol{b}=\frac{1}{2}[0\bar{1}1]$, $\boldsymbol{b}_e=\frac{1}{4}[11\bar{2}]$, $n=0$, $\gamma=35°$

Photographs (b),(c) and (d) are 400, 600 and 800 dark-field patterns taken from a 60° dislocation of Al at the condition of $\boldsymbol{g}\cdot\boldsymbol{b}=0$. The values of p and m are written at each photo. The observed bend of the reflection line is almost due to m, because the effect of p at $\gamma=35°$ is very small (see Fig. (c) on page 172). It is seen that the bend increases as the value of m increases, showing a qualitatively good agreement with the theoretical results (Fig. (d) on page 173).

Determination of the Burgers vector of a dislocation loop

Figure (a) shows computed profiles of a reflection line crossing an edge dislocation dipole for $n = \pm 3$, $\boldsymbol{u}_1$, $\boldsymbol{u}_2$, $\boldsymbol{b}_1$ and $\boldsymbol{b}_2$ being shown in Fig. (b). In the computations the left dislocation was assumed to give a value of $n = +3$ and the right one $n = -3$. When the two dislocations consisting of the dipole are interchanged, the patterns are reversed with respect to the line of $w = 0$. The computed results are extensively applicable to a dislocation loop, by changing the sign of $\boldsymbol{u}_1$ (or $\boldsymbol{u}_2$).

Defocus CBED patterns can determine the Burgers vector of a dislocation loop, without observing the change of contrast of the loop by varying diffraction condition, which is necessary in the electron-microscope-image method. Figures (c) and (d) illustrate a dislocation loop whose Burgers vector is oblique to the incident beam. When the sense of a dislocation line $\boldsymbol{u}$ is defined as shown in Fig.(c), the Burgers vector of a dislocation loop is defined to be $\boldsymbol{b}$ as shown in Figs.(d)-(i) and (d)-(ii) for a vacancy type and an interstitial type using FS/RH convension. Schematic diagrams of a reflection line crossing

Simulations of a reflection line crossing a dislocation dipole

Dependence on the separation of a dipole

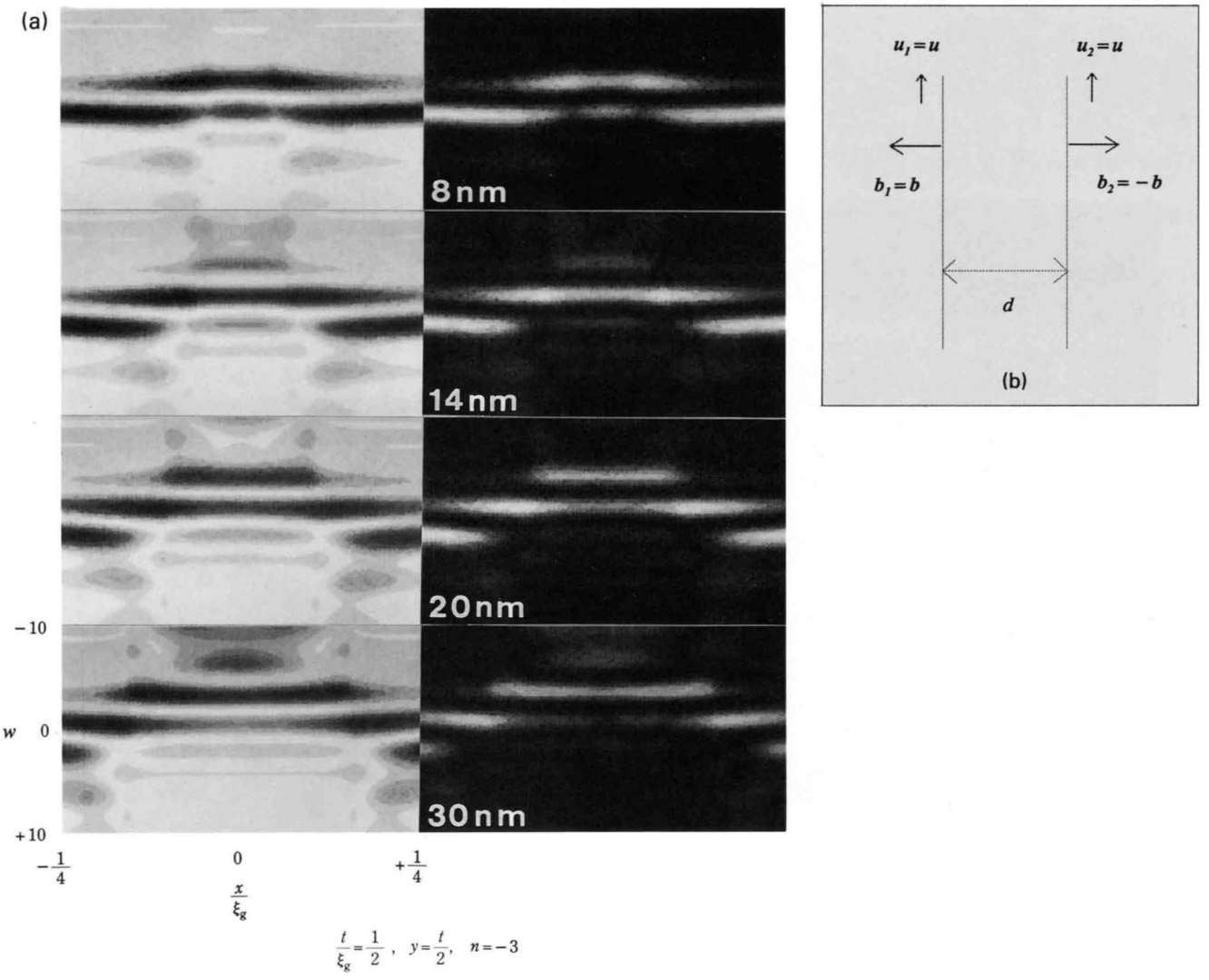

$\frac{t}{\xi_g} = \frac{1}{2}$, $y = \frac{t}{2}$, $n = -3$

a dislocation loop for $n = \boldsymbol{g}\cdot\boldsymbol{b} > 0$ and $n = \boldsymbol{g}\cdot\boldsymbol{b} < 0$ are shown in Fig.(e). The sense of the pattern with respect to a sense of w is opposite to each other between the cases of $n > 0$ and $n < 0$. The sign of n is determined absolutely. The Burgers vector $\boldsymbol{b}$ of the loop including its sense (vacancy type or interstitial type) can be determined from the values of $\boldsymbol{g}\cdot\boldsymbol{b}$ and their signs. The sign of $\boldsymbol{b}$ is determined in the present case in contrast to the case of dislocations (see page 165).

Photograph (a) was taken from a (111) Si film containing a dislocation loop with several ten nm in diameter. The $0\bar{4}4$ and $\bar{1}5\bar{3}$ reflections were found to have values of $n = +8/3$ and $-7/3$, respectively, where the outermost broad contrast was neglected. By assuming the Burgers vector to be of the $1/3\langle 111\rangle$ type, the Burgers vector of the loop was determined as $\boldsymbol{b} = 1/3[\bar{1}\bar{1}1]$ or an interstitial type. When more reflection lines crossing the loop are observed, more reliable determination is carried out. Decrease of the size of the loop makes difficult reliable determination. The identification of the sense of $\boldsymbol{b}$ for smaller loops is under study.

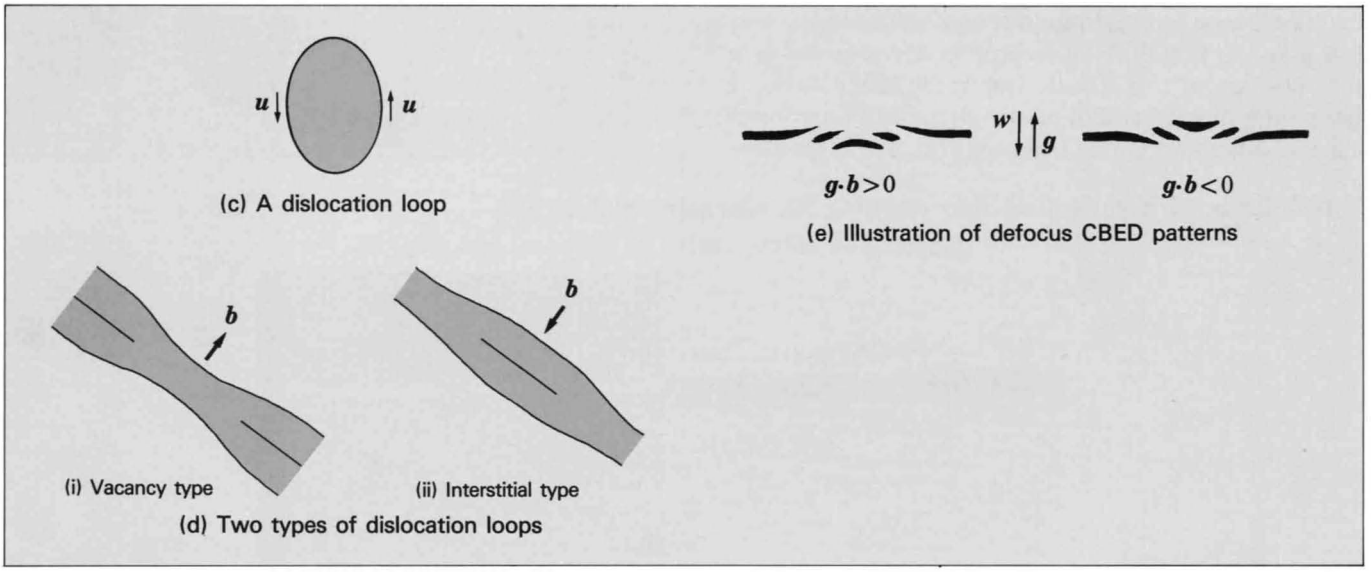

(c) A dislocation loop

(e) Illustration of defocus CBED patterns

(d) Two types of dislocation loops

Dislocation loop in Si **100 kV**

(a)

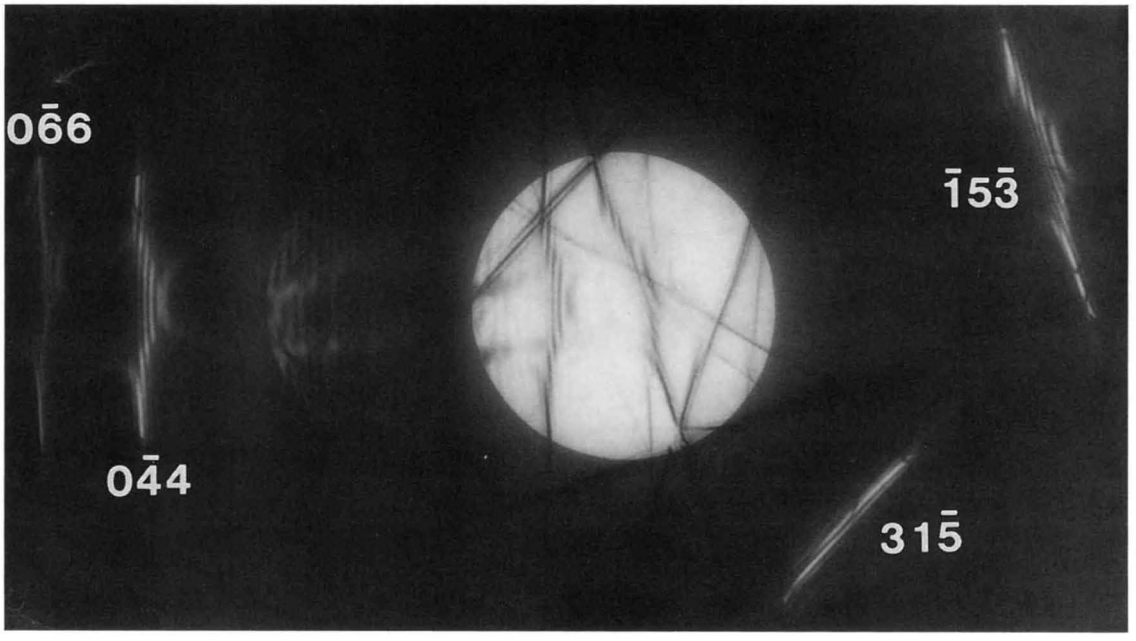

$0\bar{4}4 : n \cong +\frac{8}{3}$, $\bar{1}5\bar{3} : n \cong -\frac{7}{3}$, $\boldsymbol{b} = \frac{1}{3}[\bar{1}\bar{1}1]$

Investigation of extended dislocations

60° dislocation of Si extended into a 30° and an edge partial dislocation

In a face-centered cubic or diamond type crystal, a 60° dislocation with a Burgers vector of $\boldsymbol{b}=1/2<110>$ type can extend into two partial dislocations accompanied by a stacking fault (Fig.(a)):

$$1/2<110> \rightarrow 1/6<21\bar{1}> + 1/6<121>,$$

where one is a 30° partial dislocation and the other is an edge partial. The profile of a reflection line crossing an extended dislocation for $\boldsymbol{g}\cdot\boldsymbol{b}=n\neq 0$ is similar to that obtained from a perfect dislocation for the same n, as far as the separation is small. The profiles of reflection lines for $\boldsymbol{g}\cdot\boldsymbol{b}=0$ were computed for different values of $\boldsymbol{g}\cdot\boldsymbol{b}_1=n_1$ and $\boldsymbol{g}\cdot\boldsymbol{b}_2=n_2$ (Fig.(b)). These profiles are regarded as a superposition of two effects. One is the effect due to a dislocation dipole because of $n_1+n_2=n=0$, thus forming a subsidiary maximum (see page 178). The other is the effect due to a mixed dislocation because of a small extended width, forming a bend of the line (see page 170). The sense of the pattern is reversed when the operating reflection is reversed (Fig.(c)). The subsidiary maximum is clearer for an extended width, d, of 14 nm than for a width of 4 nm (Fig.(d)).

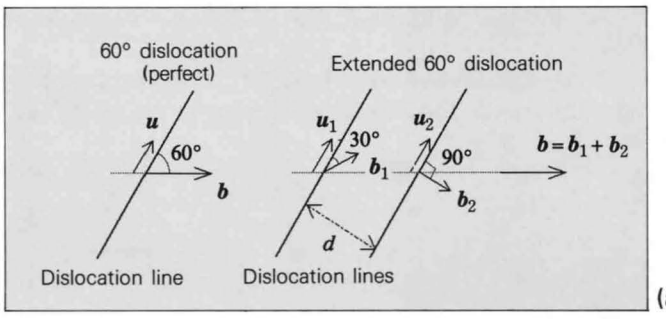

(a)

Simulations of a reflection line crossing an extended dislocation

Dependence on the values of $\boldsymbol{g}\cdot\boldsymbol{b}_1=n_1$ and $\boldsymbol{g}\cdot\boldsymbol{b}_2=n_2$

(b)

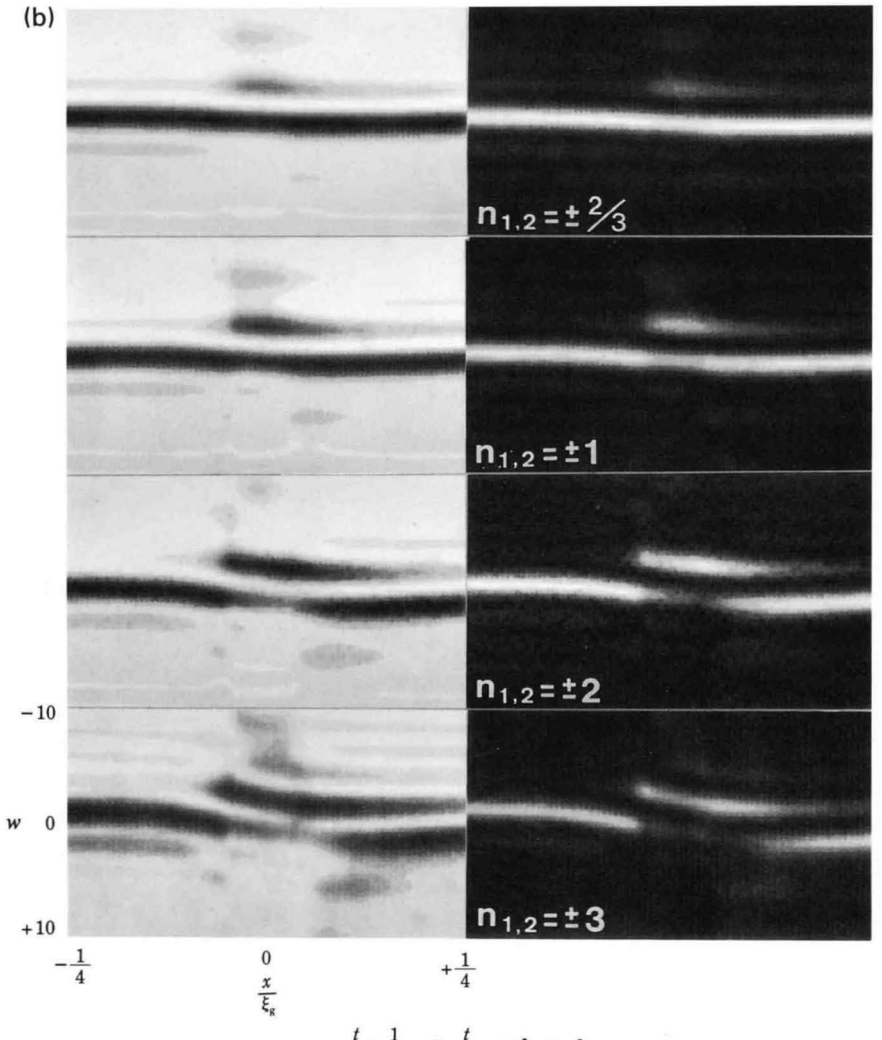

$\frac{t}{\xi_g}=\frac{1}{2}$, $y=\frac{t}{2}$, $\boldsymbol{g}\cdot\boldsymbol{b}=n=0$

Dependence on the signs of $\boldsymbol{g}\cdot\boldsymbol{b}_1 = n_1$ and $\boldsymbol{g}\cdot\boldsymbol{b}_2 = n_2$

(c)

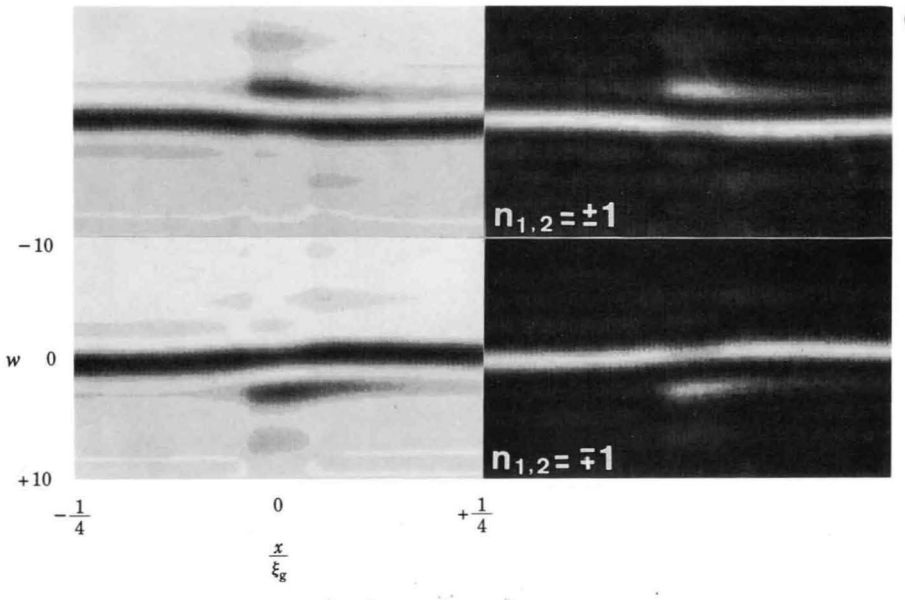

$\frac{t}{\xi_g} = \frac{1}{2}$, $y = \frac{t}{2}$, $\boldsymbol{g}\cdot\boldsymbol{b} = n = 0$, $d = 6$ nm

Dependence on the separation of two partials

(d)

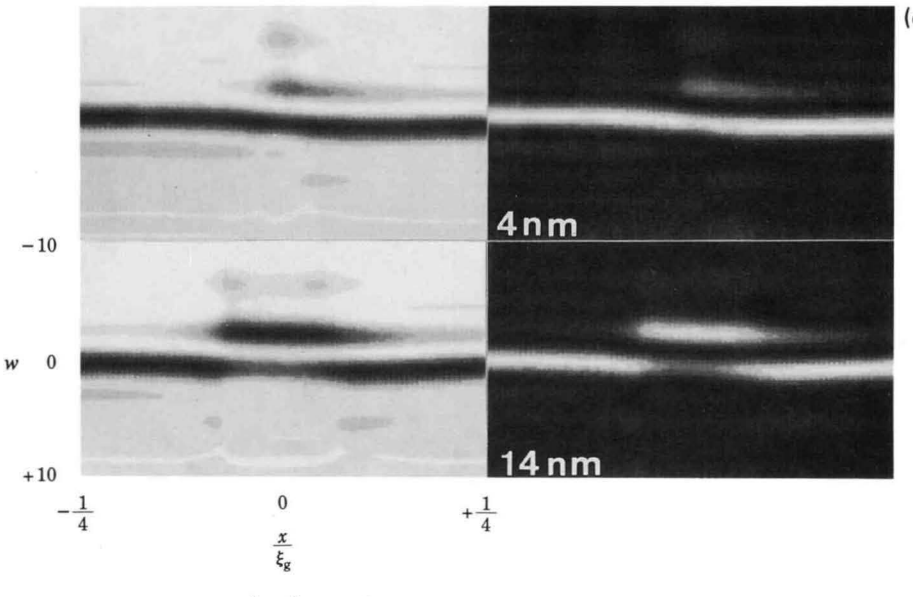

$\frac{t}{\xi_g} = \frac{1}{2}$, $y = \frac{t}{2}$, $\boldsymbol{g}\cdot\boldsymbol{b} = n = 0$, $\boldsymbol{g}\cdot\boldsymbol{b}_1 = n_1 = 1$, $\boldsymbol{g}\cdot\boldsymbol{b}_2 = n_2 = -1$

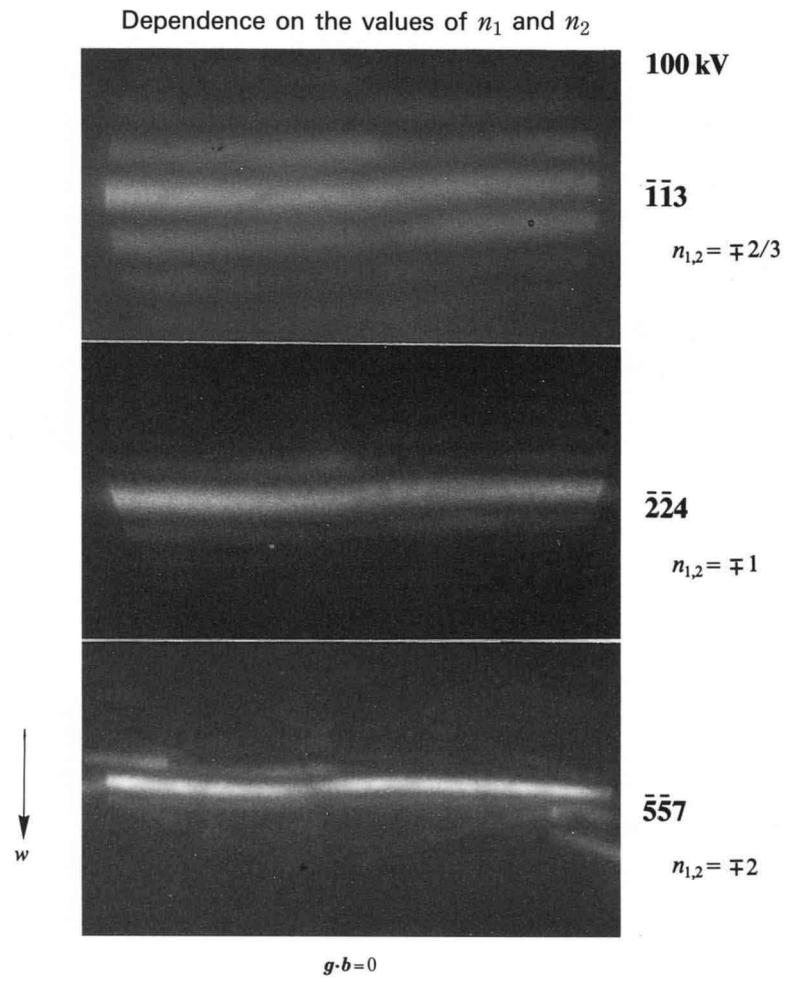

Defocus dark-field patterns taken from an extended 60° dislocation of Si at $\boldsymbol{g}\cdot\boldsymbol{b}=0$ for three values of $n_{1,2}$. Note that the profiles show a qualitative agreement with computed ones.

Dependence on the signs of n_1 and n_2

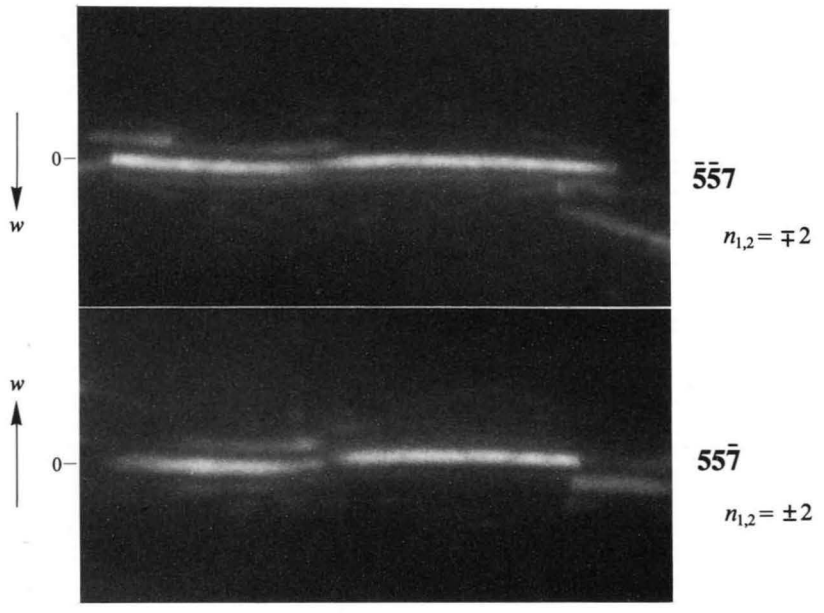

$\boldsymbol{g}\cdot\boldsymbol{b}=0$

$\boldsymbol{u}=\frac{1}{\sqrt{2}}[0\bar{1}1]$, $\boldsymbol{b}=\frac{1}{2}[1\bar{1}0]$, $\boldsymbol{b}_e=\frac{1}{4}[2\bar{1}\bar{1}]$, $\boldsymbol{b}_1=\frac{1}{6}[2\bar{1}\bar{1}]$, $\boldsymbol{b}_2=\frac{1}{6}[1\bar{2}1]$

Defocus dark-field patterns of the $\bar{5}\bar{5}7$ and $55\bar{7}$ reflections taken from an extended 60° dislocation of Si where $\boldsymbol{g}\cdot\boldsymbol{b}=0$.

Note that the pattern is reversed with respect to the line of $w=0$ when the operating reflection is reversed.

Screw dislocation of Si extended into two 30° dislocations

A screw dislocation with a Burgers vector of $\boldsymbol{b} = 1/2\langle 110\rangle$ type in a face-centered cubic or a diamond type crystal can extend into two 30° partials accompanied by a stacking fault (Fig.(a)). In the case of a screw dislocation, a reflection line giving $\boldsymbol{g}\cdot\boldsymbol{b} = 0$ is parallel to the dislocation line.

Photograph (a) was taken from an extended screw dislocation of Si at $\boldsymbol{g}\cdot\boldsymbol{b} = 0$, where the $\bar{4}22$ reflection line was superposed on the dislocation line. The reflection line is seen split in two lines. From the condition $\boldsymbol{g}\cdot\boldsymbol{b} = 0$ for the $\bar{4}22$ reflection, the Burgers vector of the perfect dislocation was found to be $1/2[01\bar{1}]$. The dislocation can dissociate in two ways:

$$1/2[01\bar{1}] \begin{cases} \rightarrow 1/6[\bar{1}2\bar{1}] + 1/6[11\bar{2}] \\ \rightarrow 1/6[\bar{1}1\bar{2}] + 1/6[12\bar{1}]. \end{cases}$$

The upper case gives values of $n_{1,2} = \pm 1$ and the lower case $n_{1,2} = \pm 1/3$.

Figure (b) shows a rocking curve for a perfect crystal as a reference. Figure (c) shows rocking curves from an extended screw dislocation for three different values of n_A ($= n_1$) and n_B ($= n_2$). Two partials are located at the positions A and B. The exact Bragg position is at the middle of two partials. Figure (d) shows the rocking curves for $n_A = +1$ and $n_B = -1$ ($n_{1,2} = \pm 1$) at three different Bragg settings with respect to the position of the extended dislocation. The profile of Photo (a) appears to have values of $n_{1,2} = \pm 1$, indicating the upper case of dissociation, because if $n_{1,2} = \pm 1/3$, the weaker peak should be much weaker than the observed one.

(a)

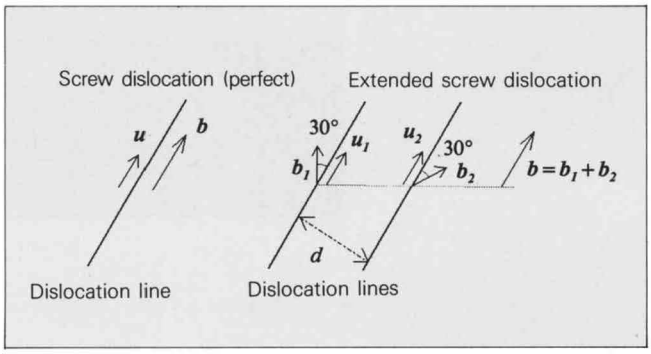

(a)

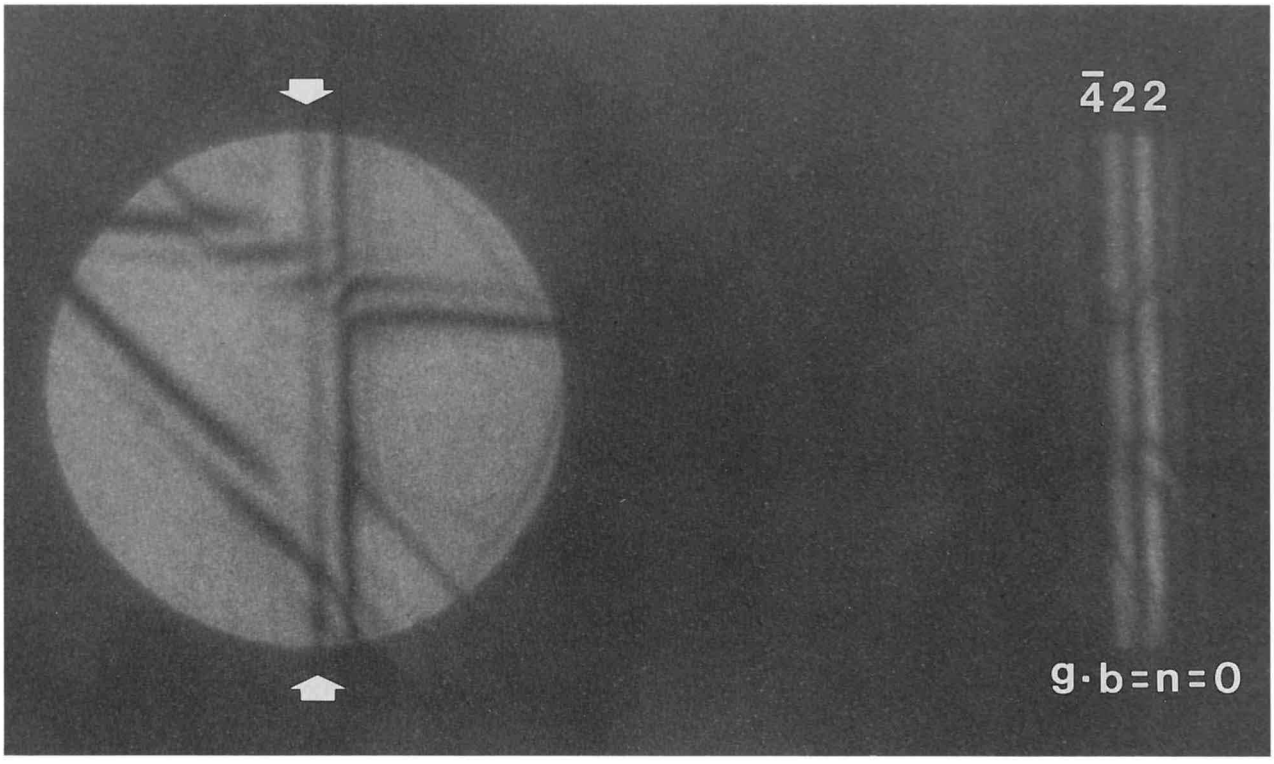

(b)

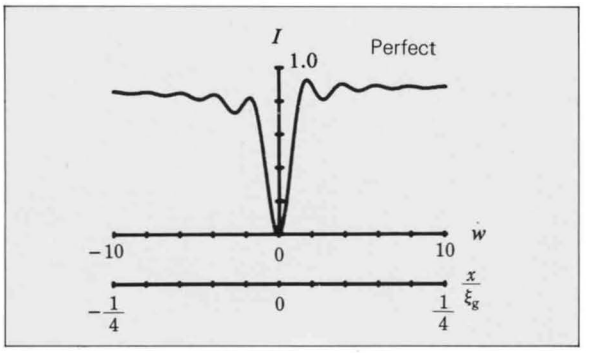

$\frac{t}{\xi_g}=\frac{1}{2}$

(c)

$g\cdot b_A=n_A=+1, \quad g\cdot b_B=n_B=-1$

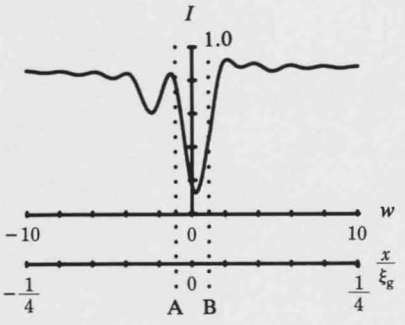

$n_A=+2, n_B=-2$

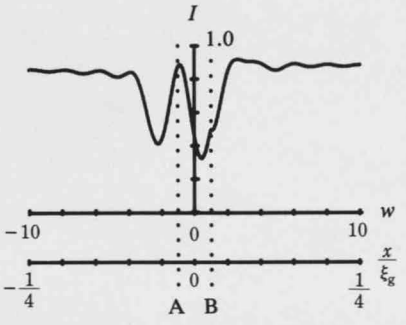

$n_A=+3, n_B=-3$

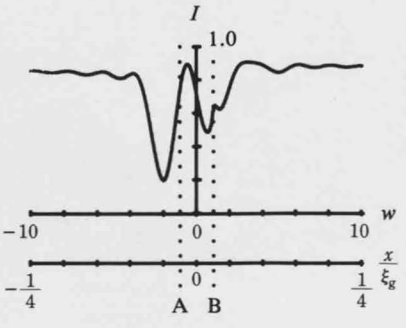

$\frac{t}{\xi_g}=\frac{1}{2}, \quad y=\frac{t}{2}, \quad g\cdot b=n=0$

(d)

$n_A=+1, \quad n_B=-1$

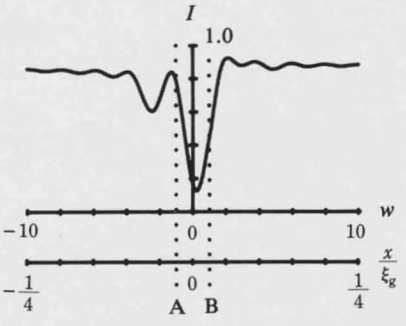

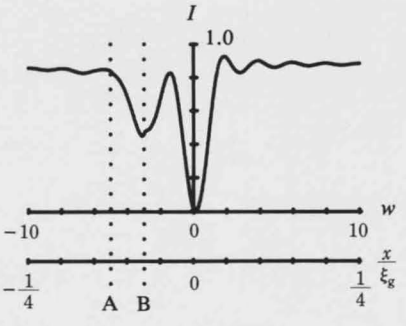

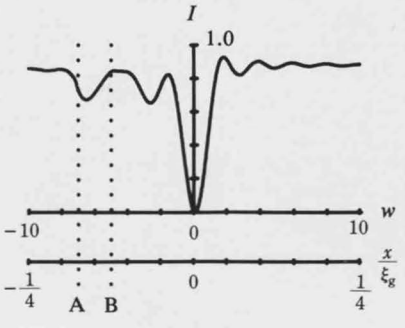

$\frac{t}{\xi_g}=\frac{1}{2}, \quad y=\frac{t}{2}, \quad g\cdot b=n=0$

Applications

Determination of Order Parameters

$Sr_2Ta_2O_7$

$Sr_2Ta_2O_7$ undergoes a second-order phase transition at 158°C from the high temperature phase belonging to a space group *Cmcm* to the low temperature phase belonging to $P2_1/m$. A series of Photos, (c) to (g), shows the temperature dependence of the bright-field CBED patterns. A vertical mirror symmetry exists in all the patterns. The horizontal mirror symmetry seen in Photo (c) gradually vanishes with decreasing temperature. The bright-field CBED patterns (a) and (b) were taken above and below the transition temperature. The intensities of the background a and the HOLZ lines b remain almost the same between Photos (a) and (b). The HOLZ line c is greatly different between the two photos. Thus, the HOLZ line b must be fundamental reflections and the line c must be a reflection directly related with the phase transition. The intensity of the line c was normalized by the intensities of the background a and the line b. The square of the normalized intensity was plotted as a function of temperature as shown in the diagram. It is seen that the value of the order parameter of the low temperature phase increases with decreasing temperature.

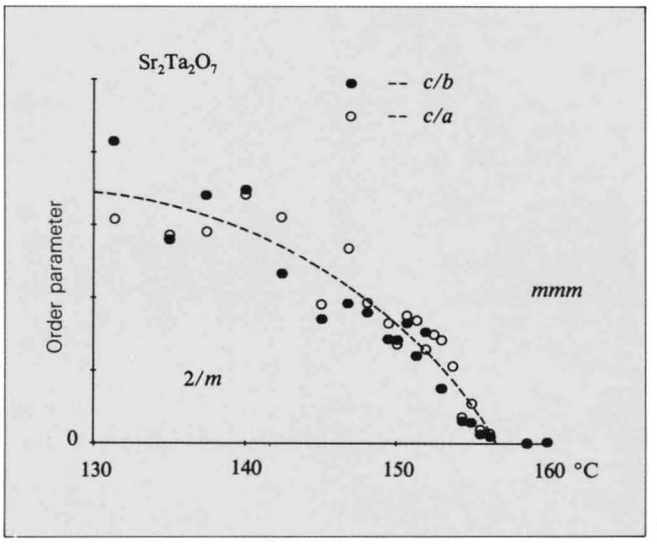

(a)

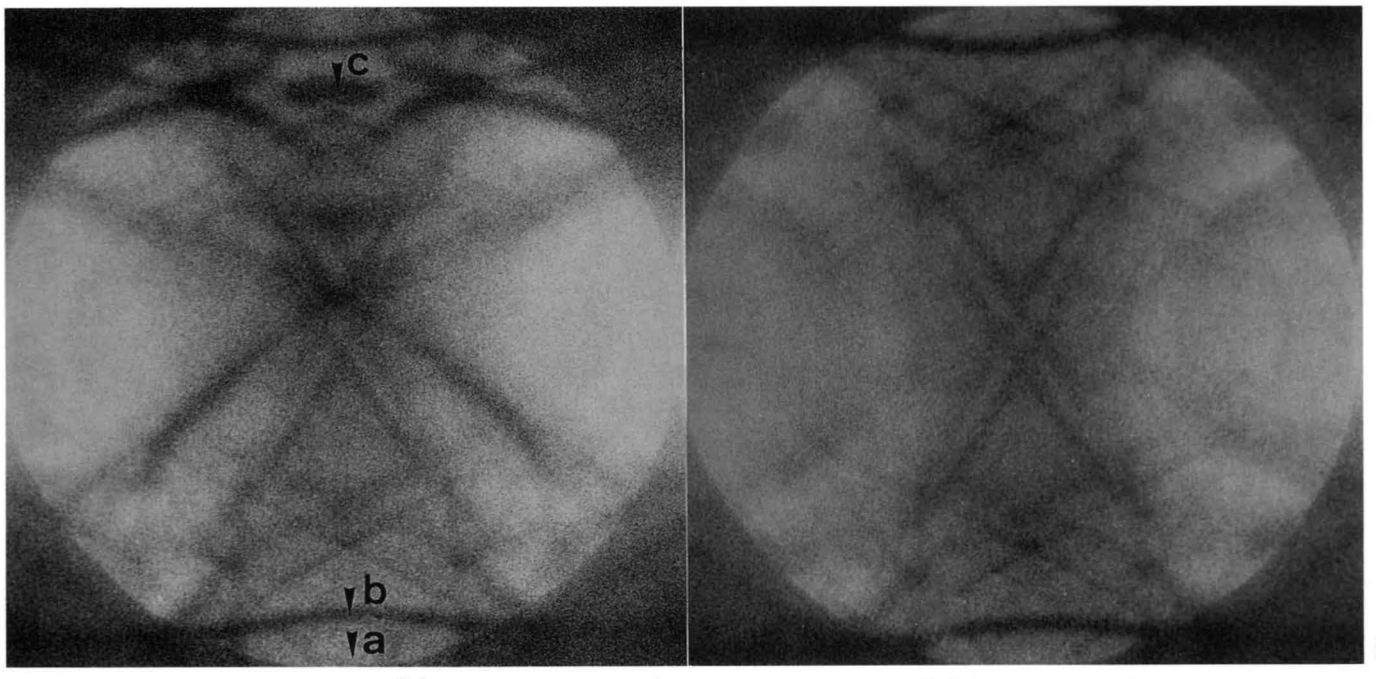

(a) (b)

Point group **2/*m***

Point group ***mmm***

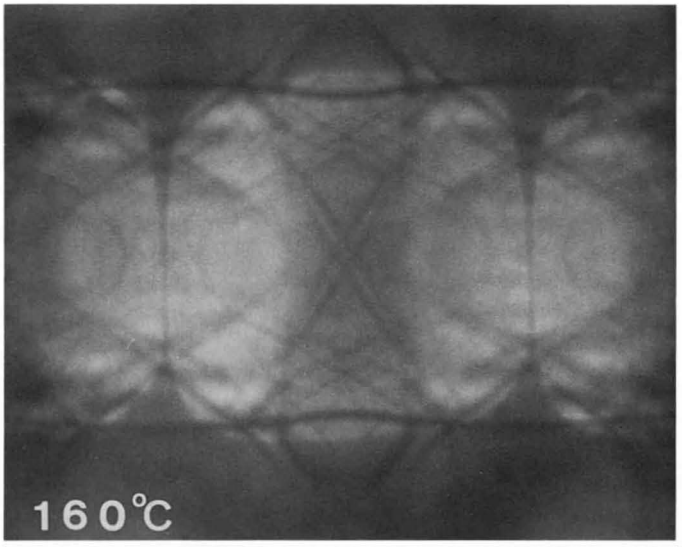

(c)

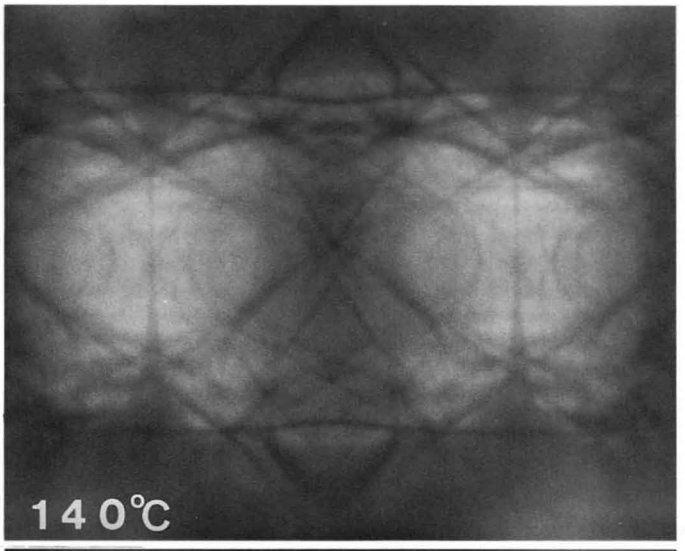

(f)

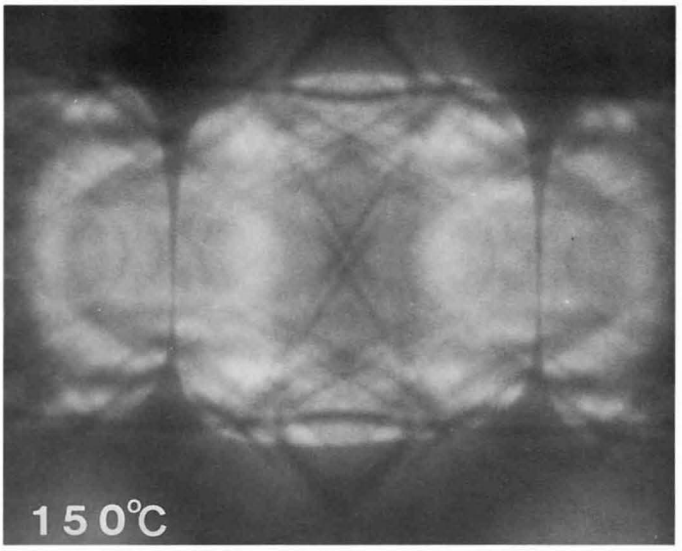

(d)

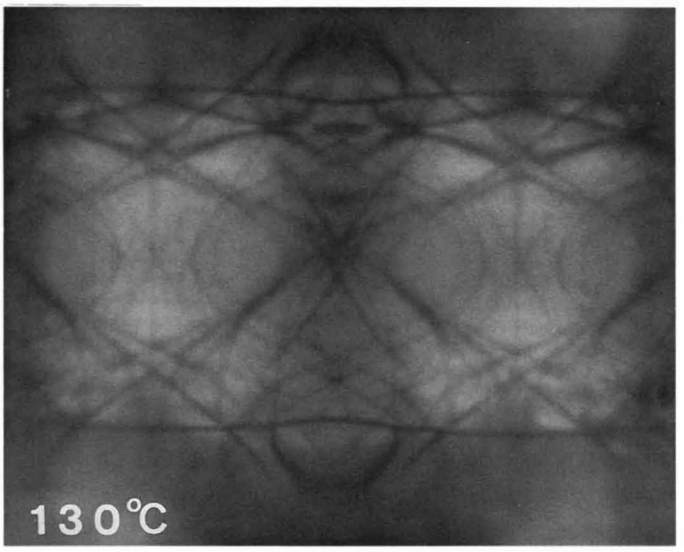

(g)

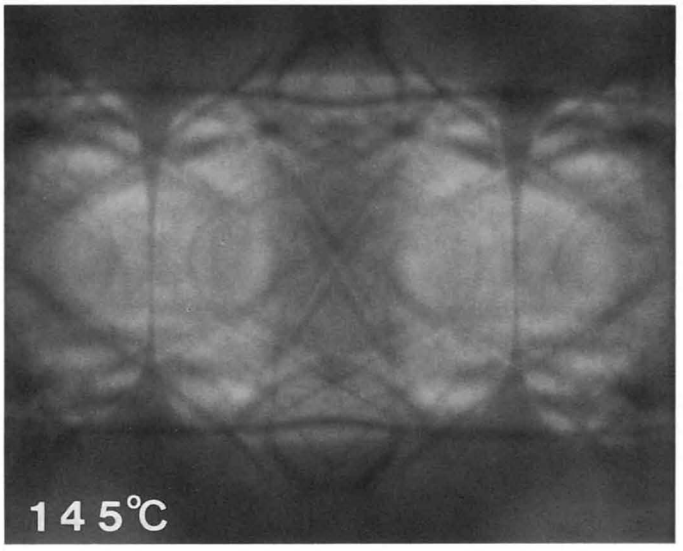

(e)

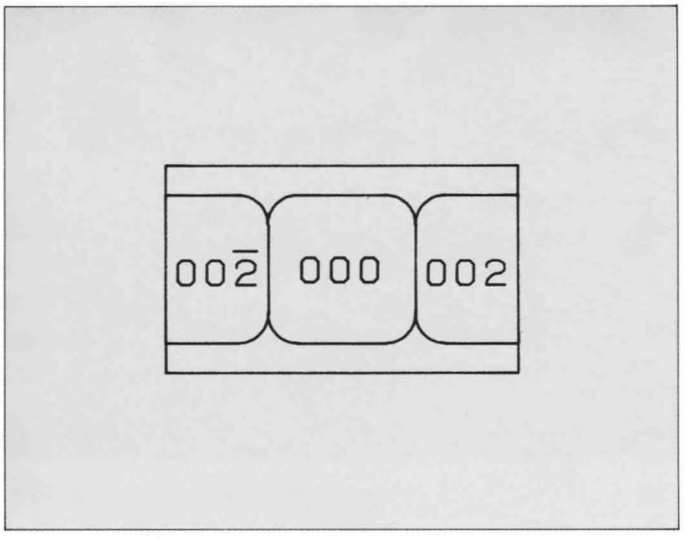

Observation of Domains

$Sr_2Ta_2O_7$

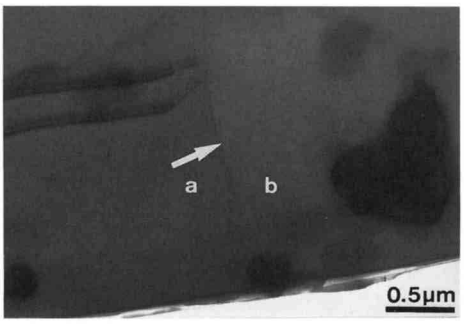

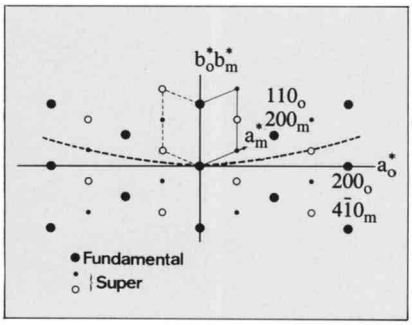

100 kV

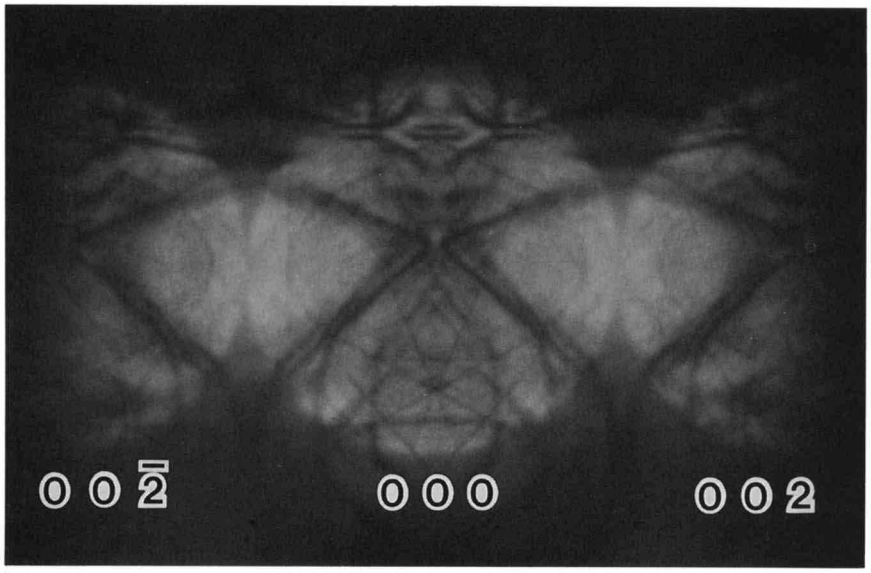

(a)

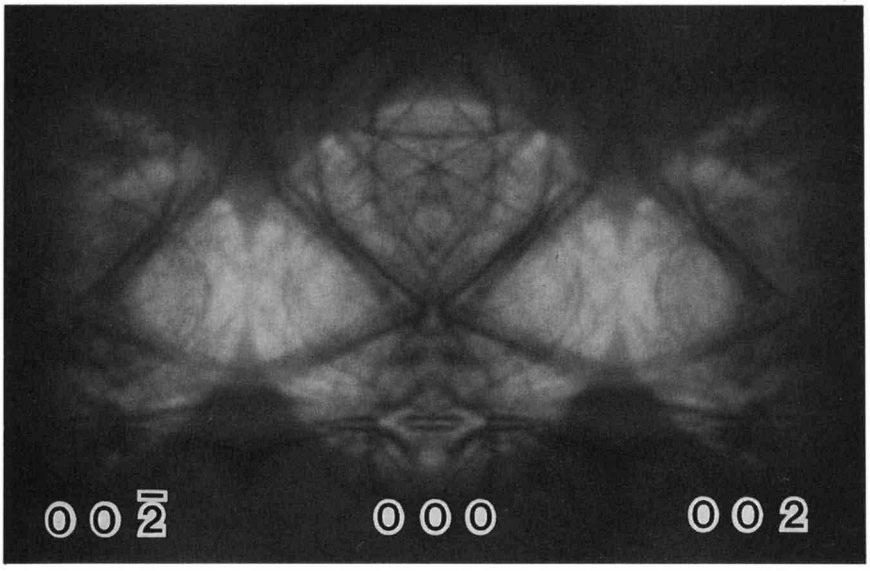

(b)

$Sr_2Ta_2O_7$

The electron micrograph of $Sr_2Ta_2O_7$, taken at an incidence parallel to the *b* axis, shows a contrast due to twin domains a and b. At this incidence, however, the contrast is very weak, because the ZOLZ reflections (fundamental) are common to both domains and only HOLZ reflections (superlattice) give difference between them. The diffraction spots in the a_o^*-b_o^* plane expected from the twin structure are depicted in the diagram. The reciprocal lattice cell drawn by the solid line corresponds to one domain and the cell drawn by the dotted line to the other domain.

The CBED patterns (a) and (b) were taken from the domains a and b, respectively. HOLZ lines appear with a strong contrast at opposite positions to each other between the two patterns. These patterns have revealed that the sense of the b_o^* axis of one domain is opposite to that of the other domain.

TaS_3 ➤

The CBED patterns (a), (b), (c) and (d) were taken at a common incidence respectively from the four domains a, b, c and d in the electron micrograph of TaS_3. The exactly excited reflections in (a) and (c) were found to have the same index, 0 16 0, although they show a little different patterns due to the difference of thickness. The exactly excited reflections in (b) and (d) show very similar patterns and have the same index, 0 $\overline{16}$ 0. These results have revealed that the sense of the *b* axes in the domains b and d is opposite to that in domains a and c, and that a certain displacement exists along the *b* direction between the domains a and c, and between the domains b and d.

TaS_3

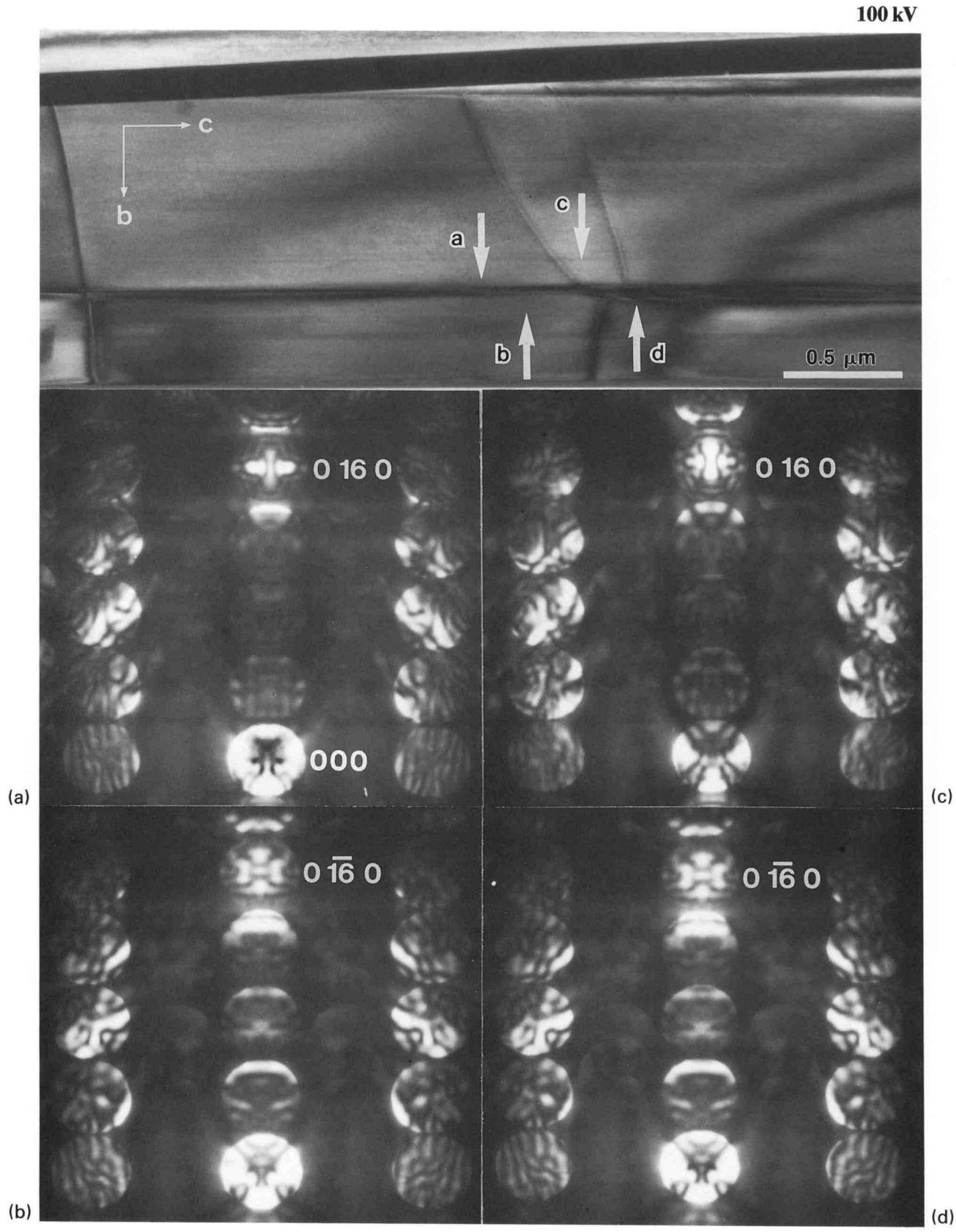
100 kV
c
b
a
c
b
d
0.5 μm
0 16 0
000
0 16 0
(a)
(c)
0 $\bar{1}\bar{6}$ 0
0 $\bar{1}\bar{6}$ 0
(b)
(d)

LACBED Patterns

Graphite (perfect) **[0 0 0 1]**

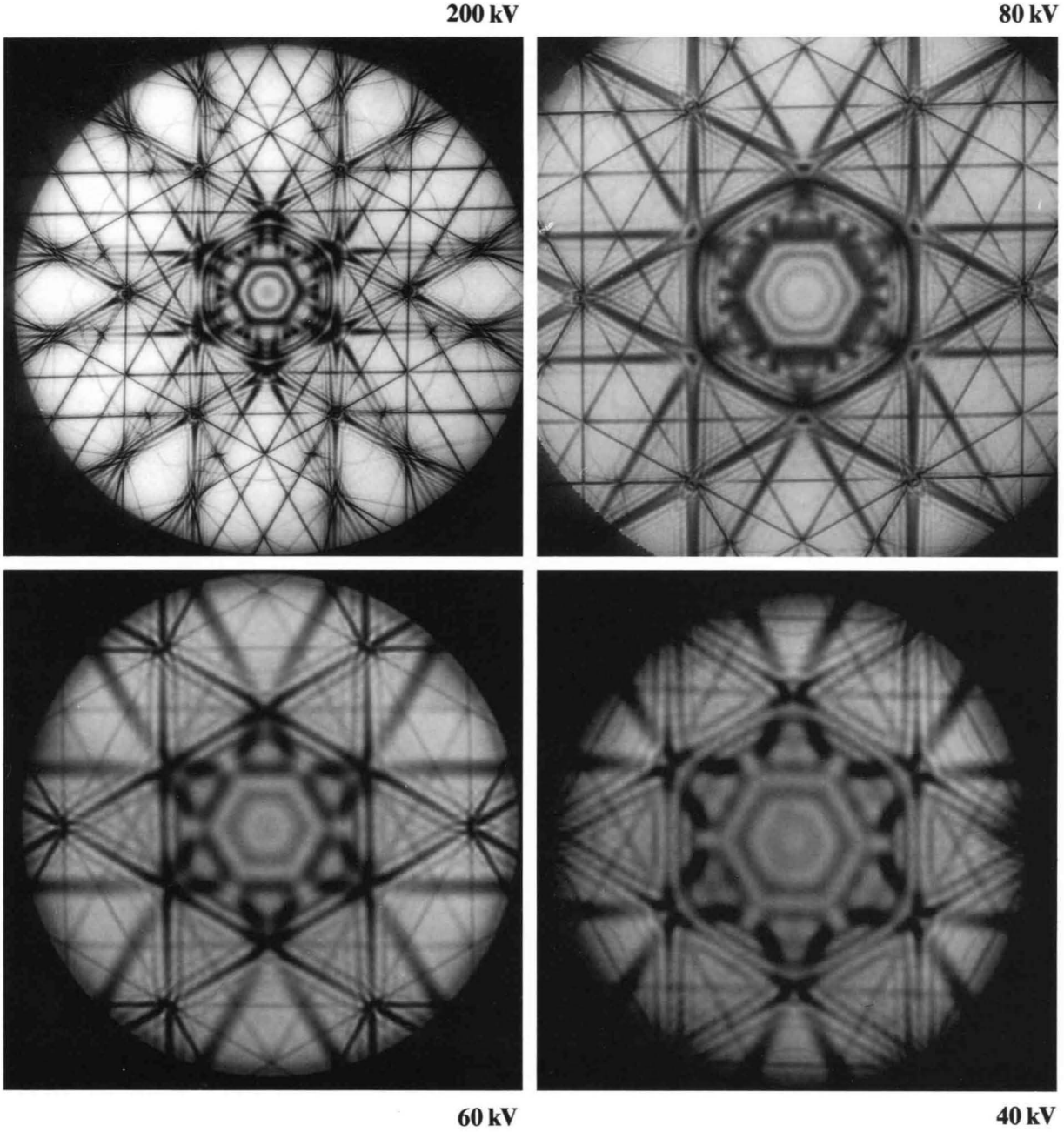

Bright-field LACBED patterns showing symmetries of 6*mm* taken from a perfect area of graphite at four different accelerating voltages with the camera length kept constant.

Graphite (stacking fault) [0 0 0 1]

200 kV

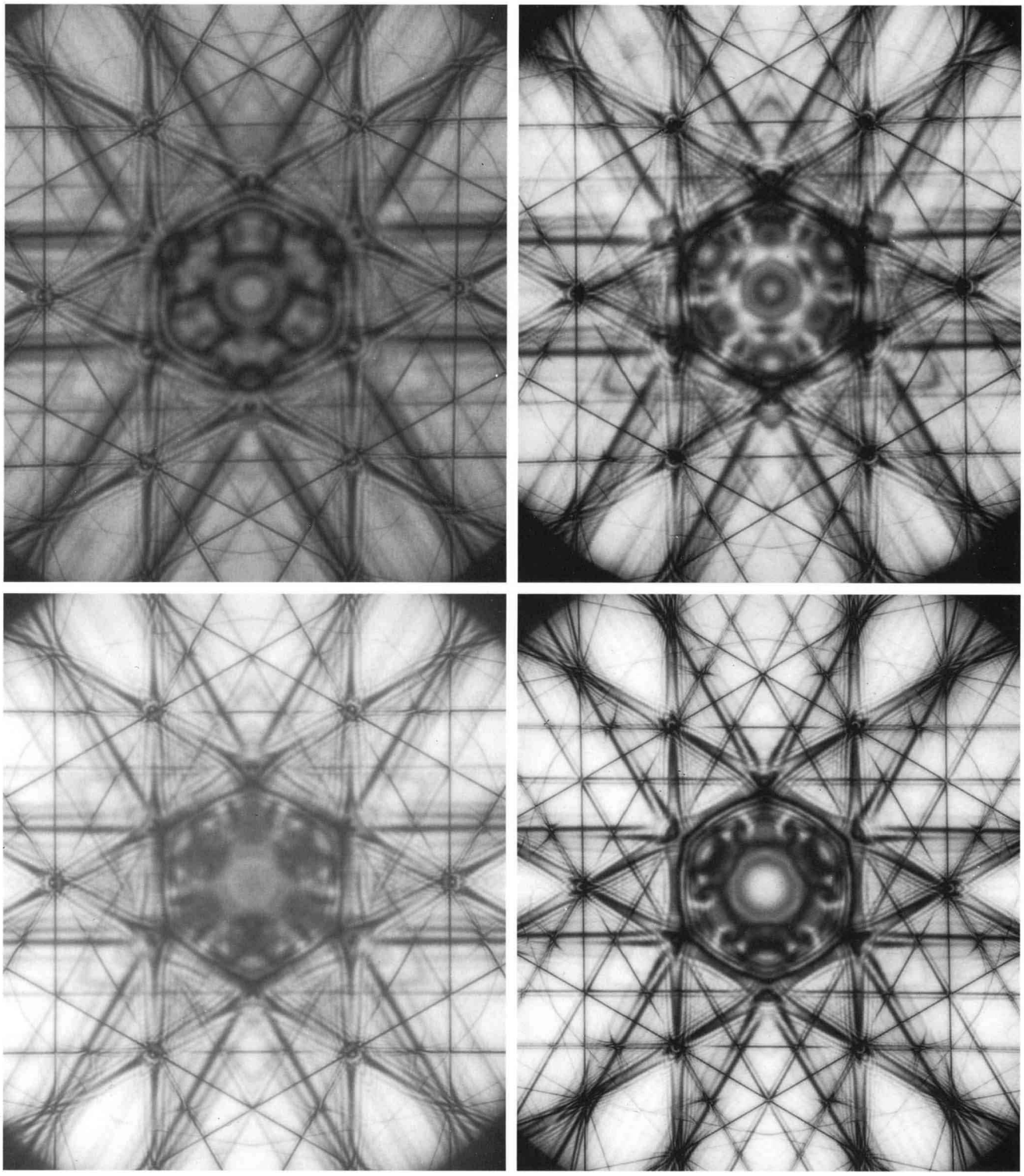

Bright-field LACBED patterns showing symmetries of 3*m* taken from four different areas containing stacking faults, the difference between the patterns being due to the numbers and positions of fault planes.

FeS_2 [001]

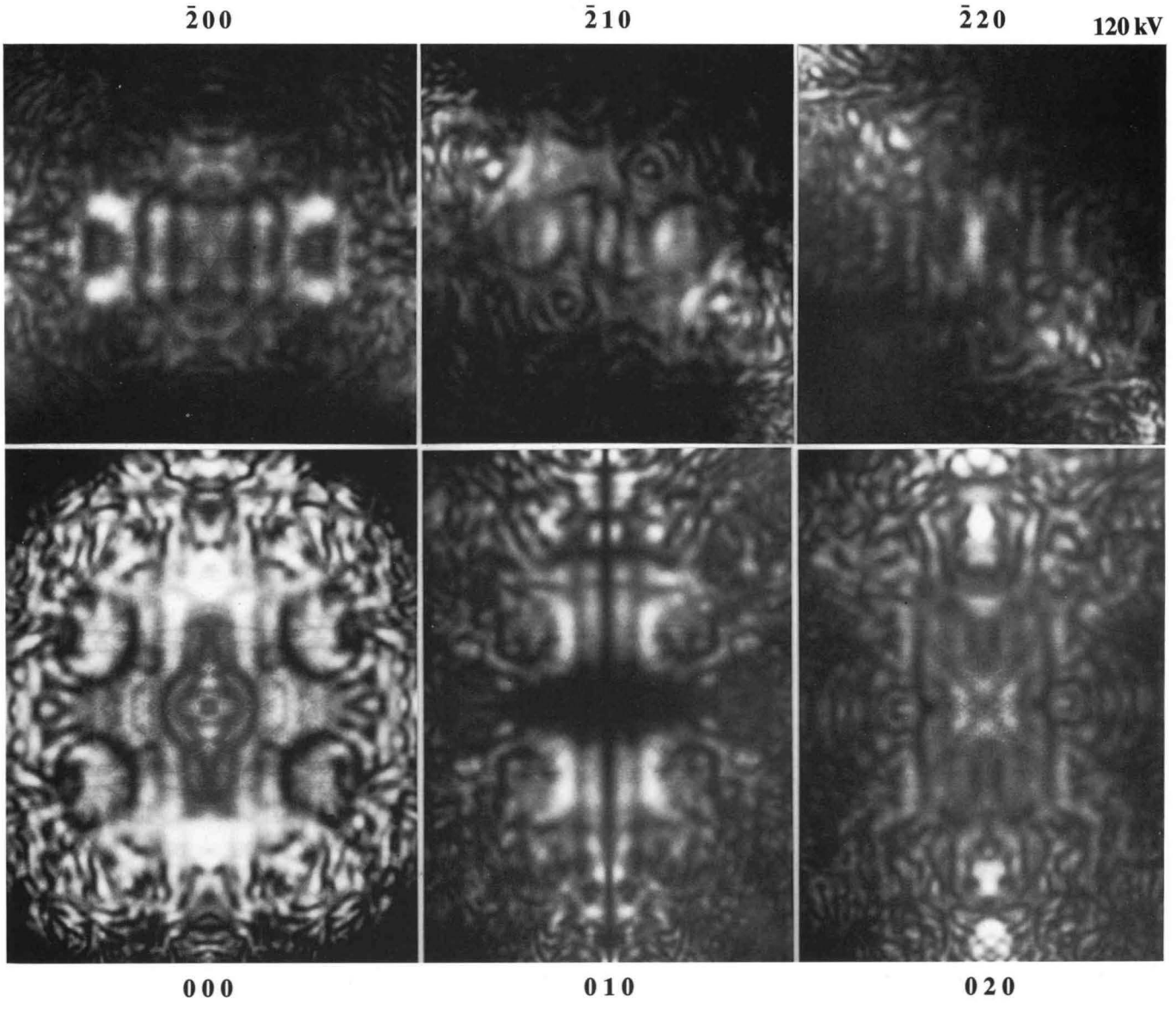

A set of LACBED patterns taken from FeS_2 at the [001] incidence.
GM lines due to a 2_1 screw axis and a *b*-glide plane are seen in the 0*k*0 (*k* = odd) patterns. Symmetries of 1_R and 2*mm* formed by ZOLZ and HOLZ interactions are clearly seen in the $\bar{2}10$ & $\bar{2}20$ patterns and in the other patterns, respectively.

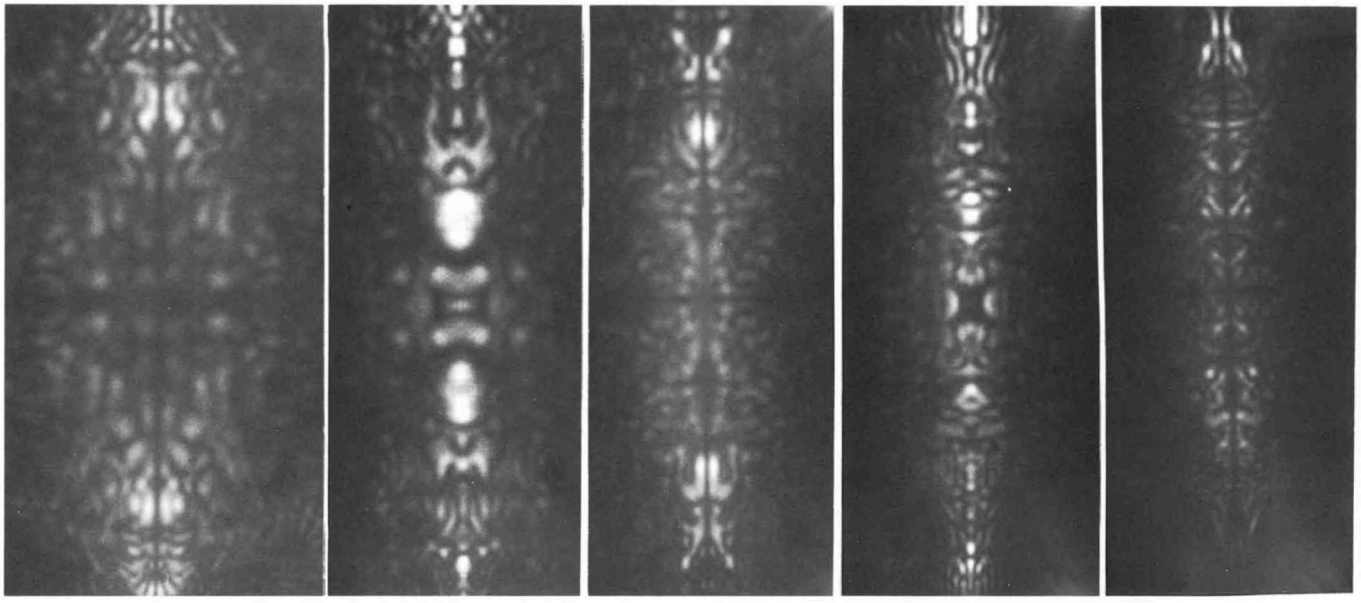

030 040 050 060 070

GaAs [10 1 0]

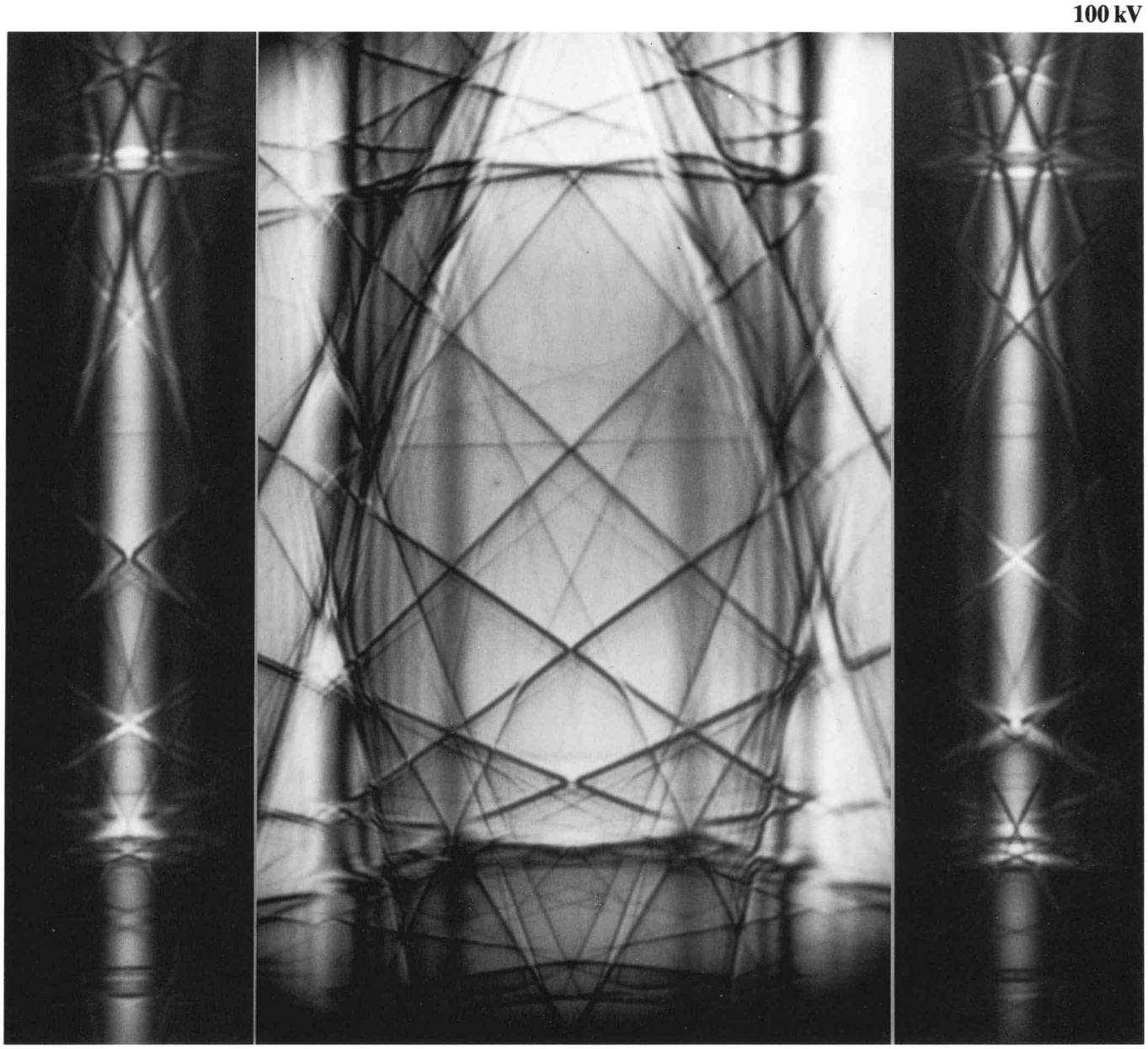

The 000, 002 and 00$\bar{2}$ LACBED patterns taken at the [10 1 0] incidence. The lack of a symmetry of 2_R is clearly seen over a wide angular range in the pair of patterns, 002 and 00$\bar{2}$.

Hollow-Cone Beam CBED Patterns

Graphite [0 0 0 1] **200 kV**

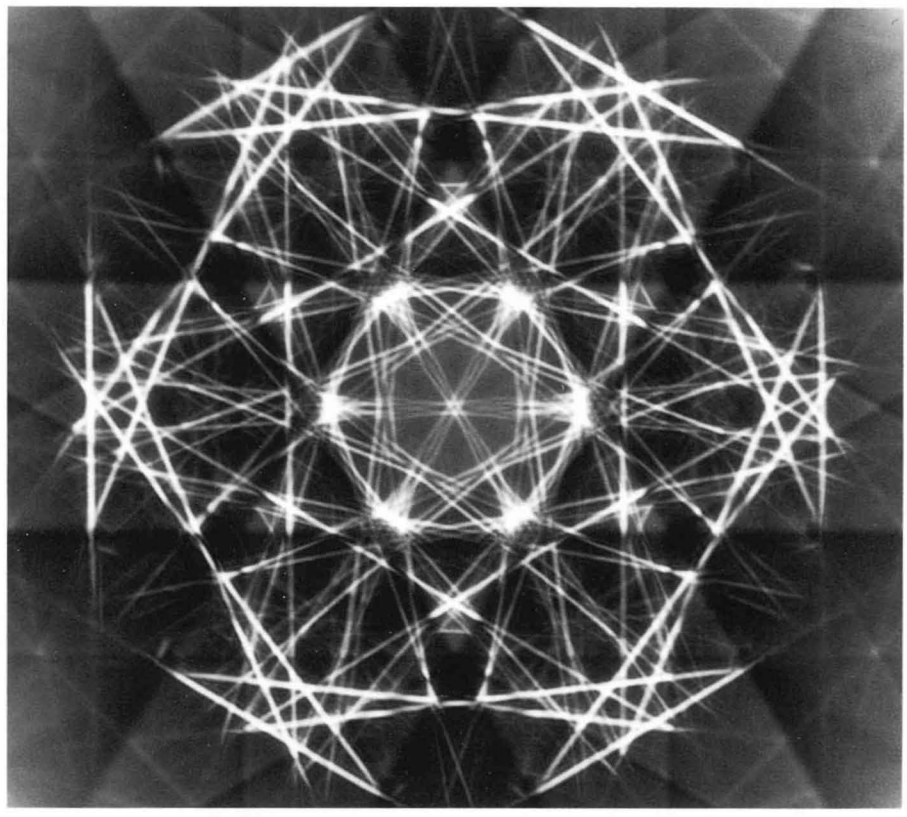

FOLZ

FeS_2 [0 0 1] **120 kV**

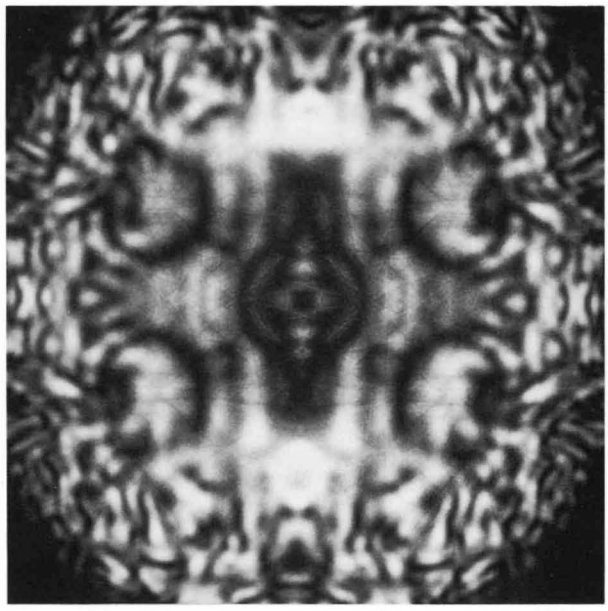

LACBED

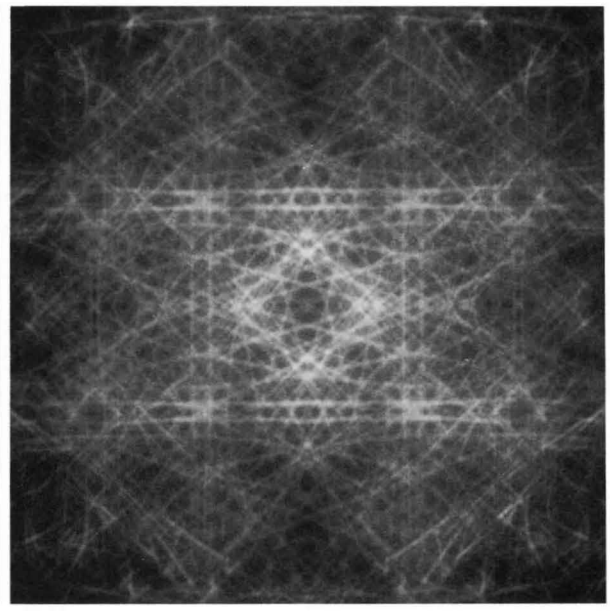

FOLZ

Note that symmetries due to HOLZ lines are clearly seen in the hollow-cone beam CBED patterns.

SiC-6H [0 0 0 1] FOLZ

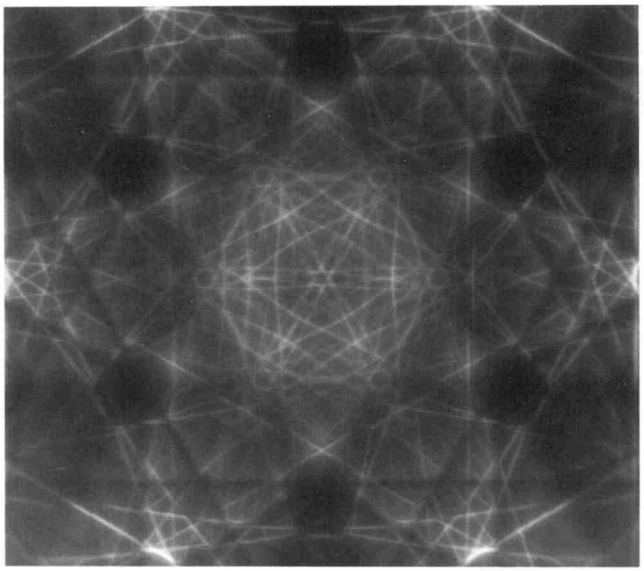

200 kV

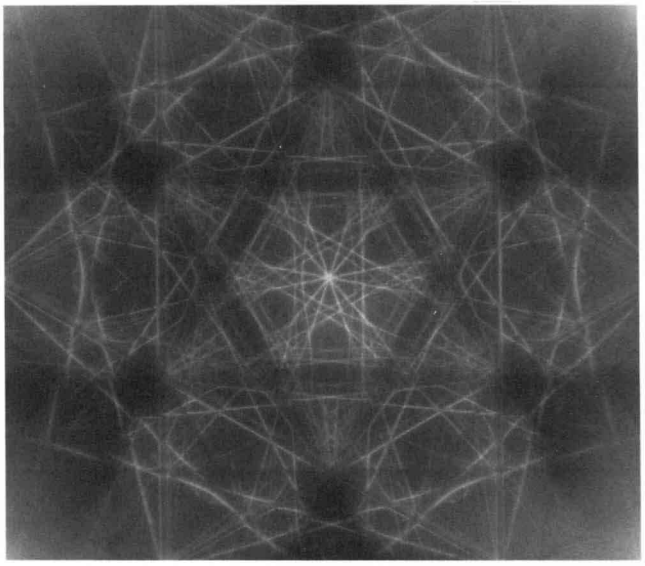

120 kV

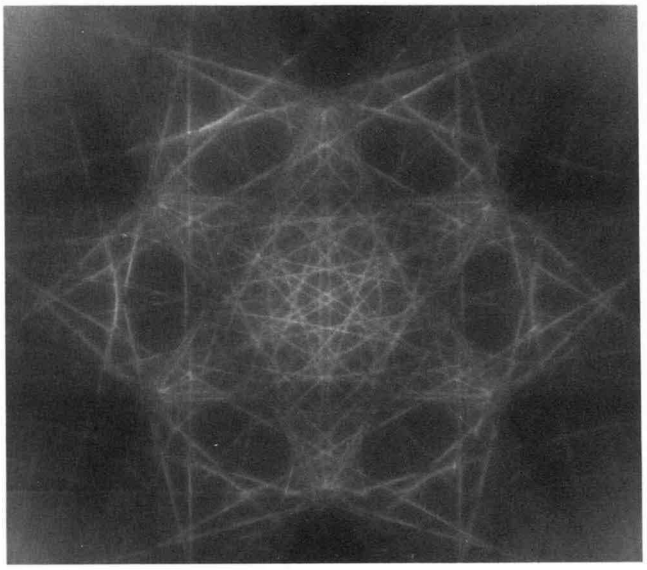

100 kV

SiC-6H [0 0 0 1] 200 kV

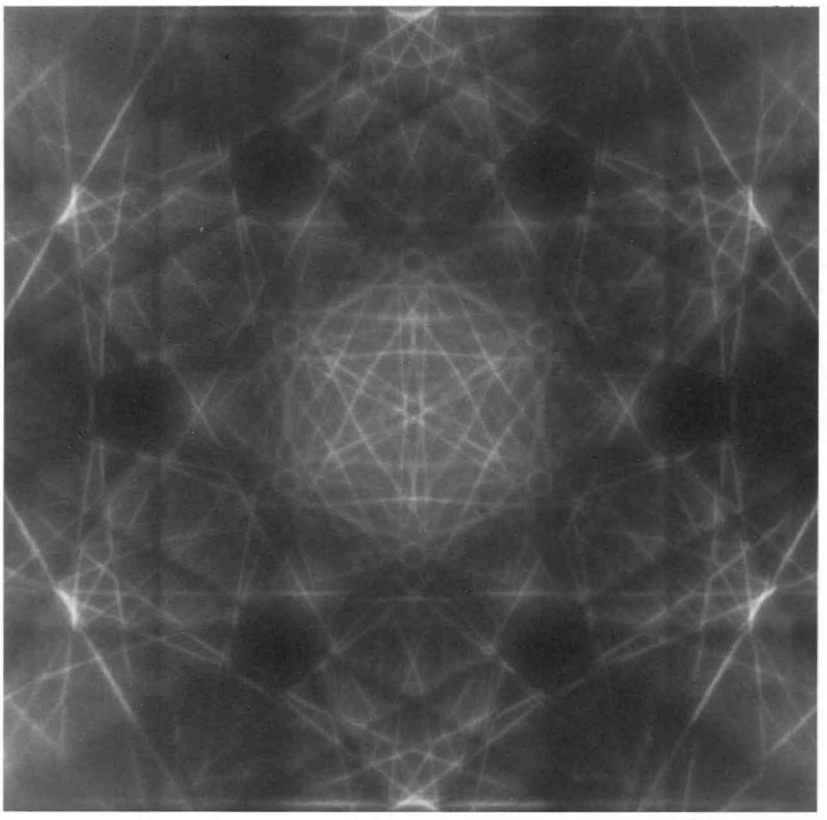

FOLZ

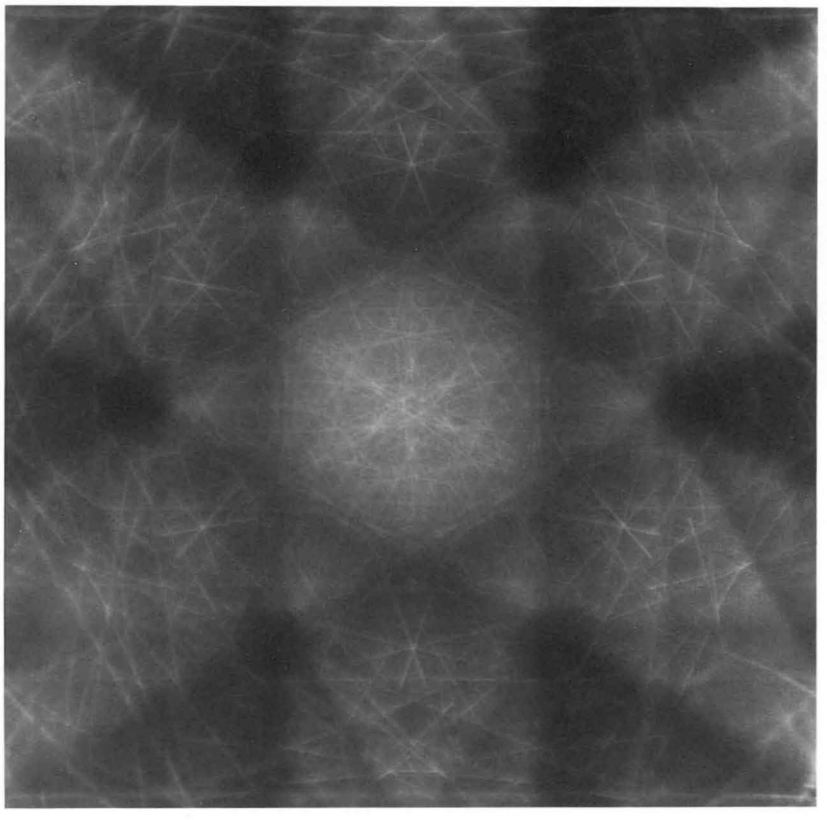

SOLZ

Si [1 1 1]

100 kV

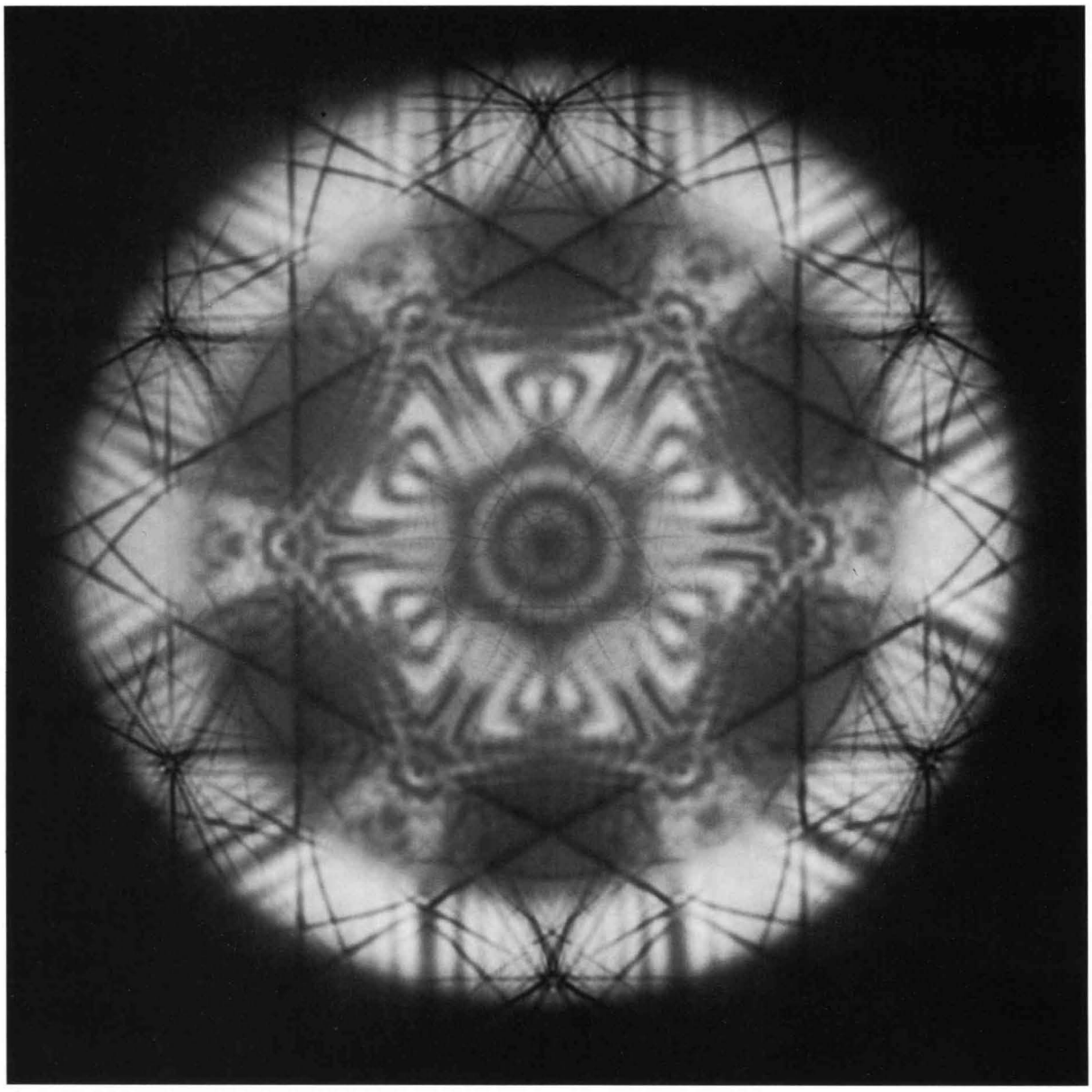

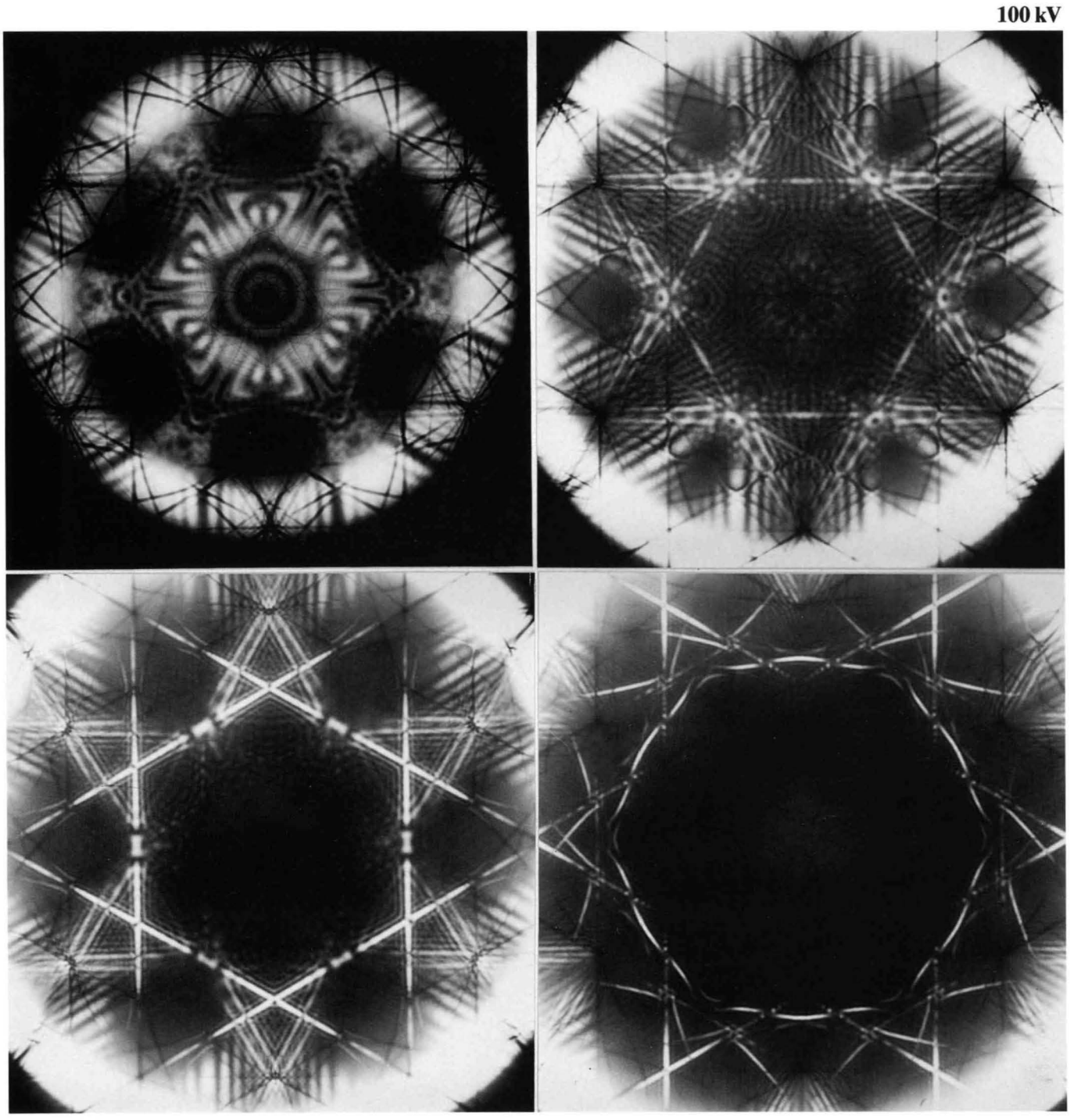

A series of hollow-cone beam CBED patterns taken from (111)Si at four different settings of the hollow-cone beam angle.

Appendices

Flow Charts

CBED pattern

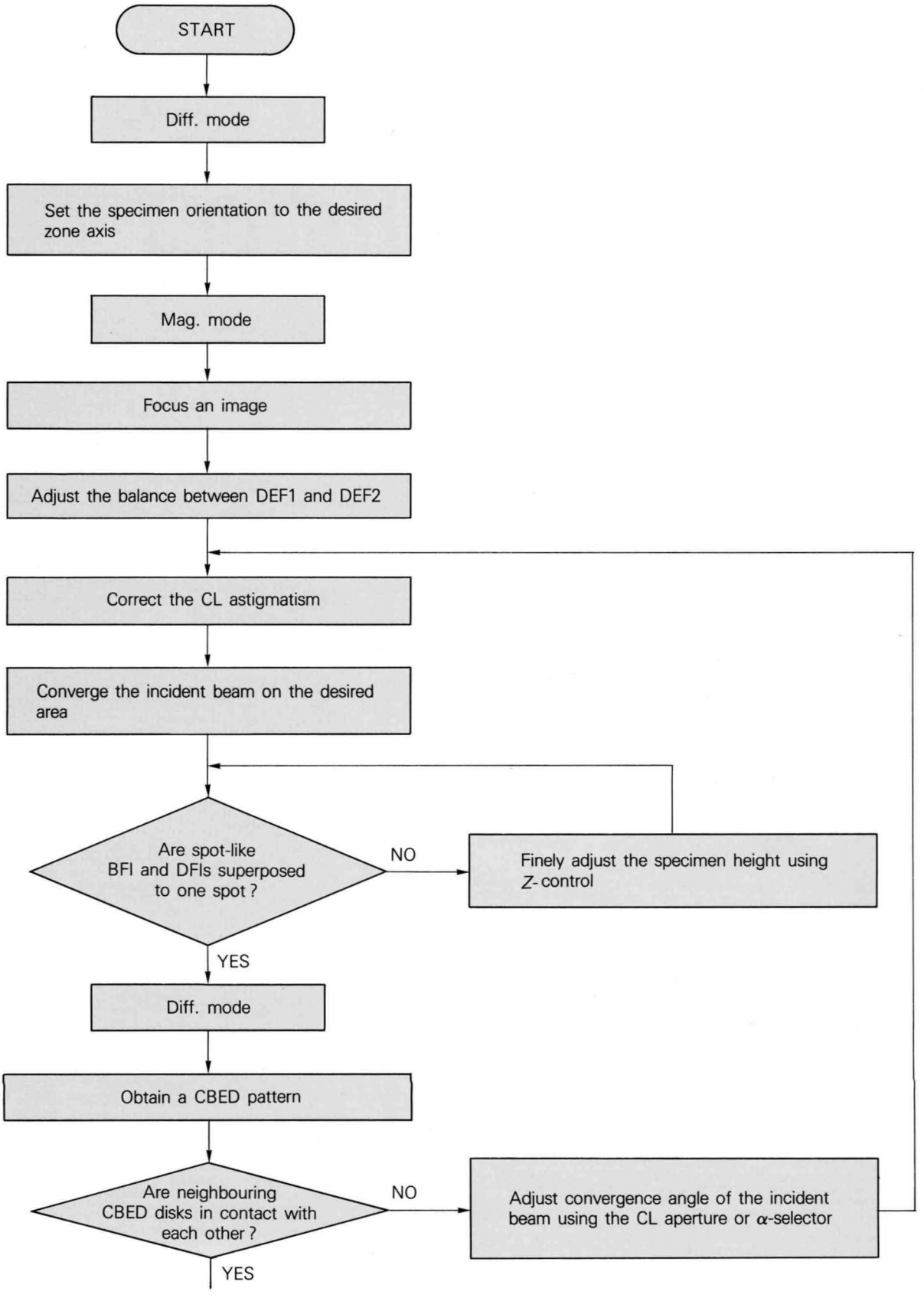

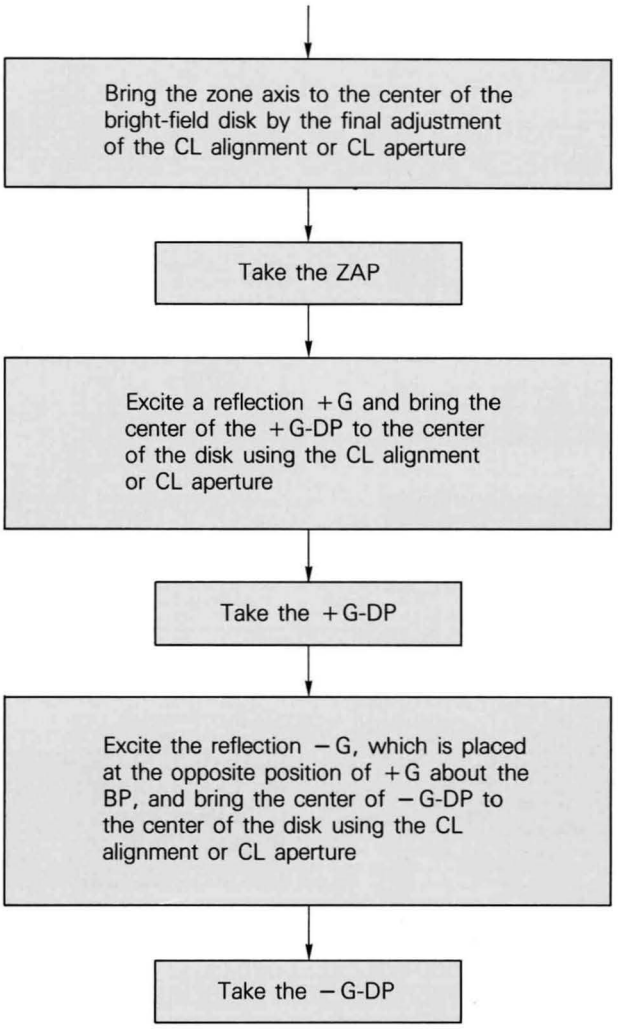
Bring the zone axis to the center of the bright-field disk by the final adjustment of the CL alignment or CL aperture
Take the ZAP
Excite a reflection +G and bring the center of the +G-DP to the center of the disk using the CL alignment or CL aperture
Take the +G-DP
Excite the reflection −G, which is placed at the opposite position of +G about the BP, and bring the center of −G-DP to the center of the disk using the CL alignment or CL aperture
Take the −G-DP

Large-angle CBED pattern (LACBED)

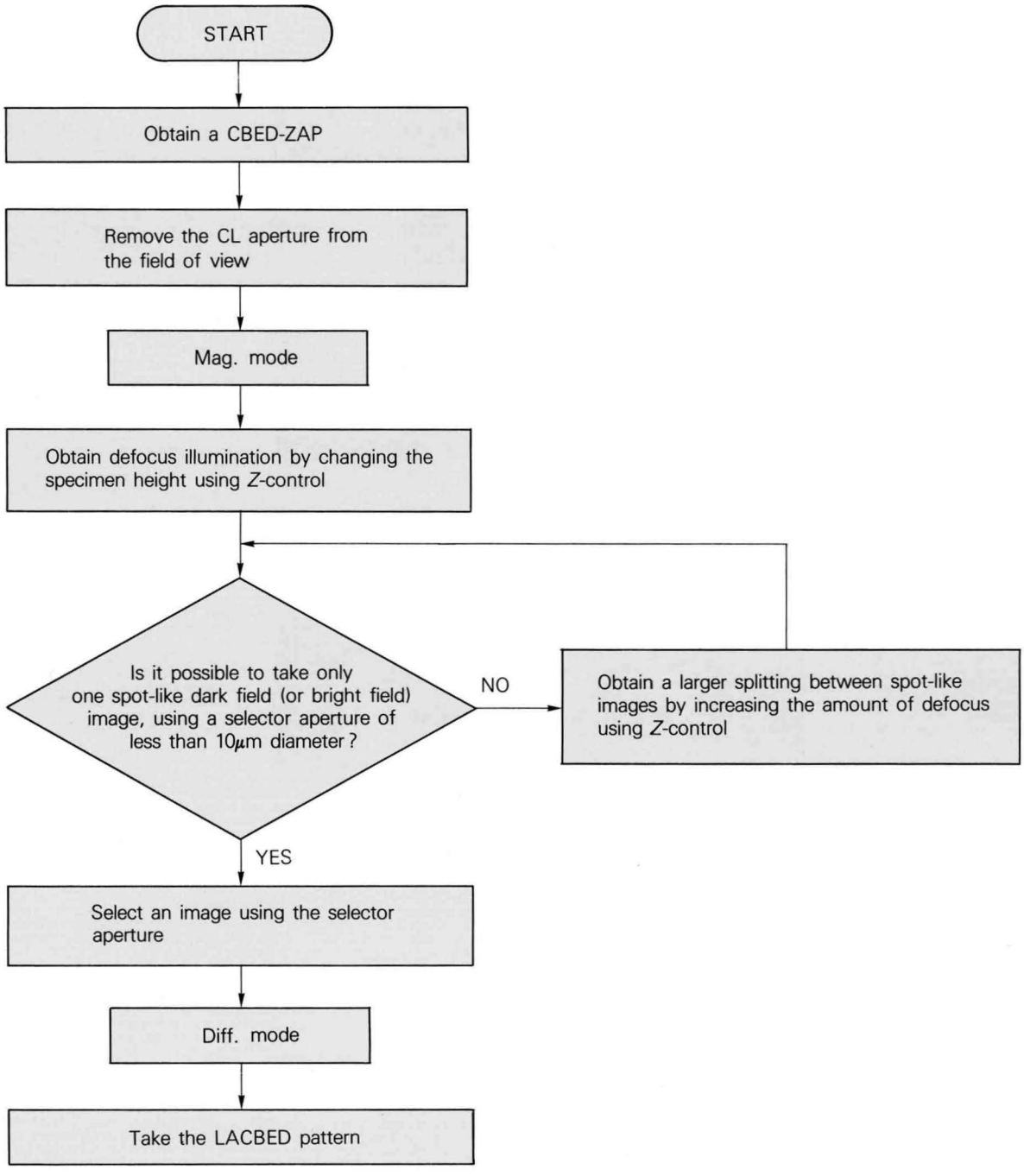

Reference

[a] M. Tanaka, R. Saito, K. Ueno and Y. Harada: *J. Electron Microsc.*, **29** (1980) 408.

Hollow-cone beam CBED (HCB-CBED) pattern

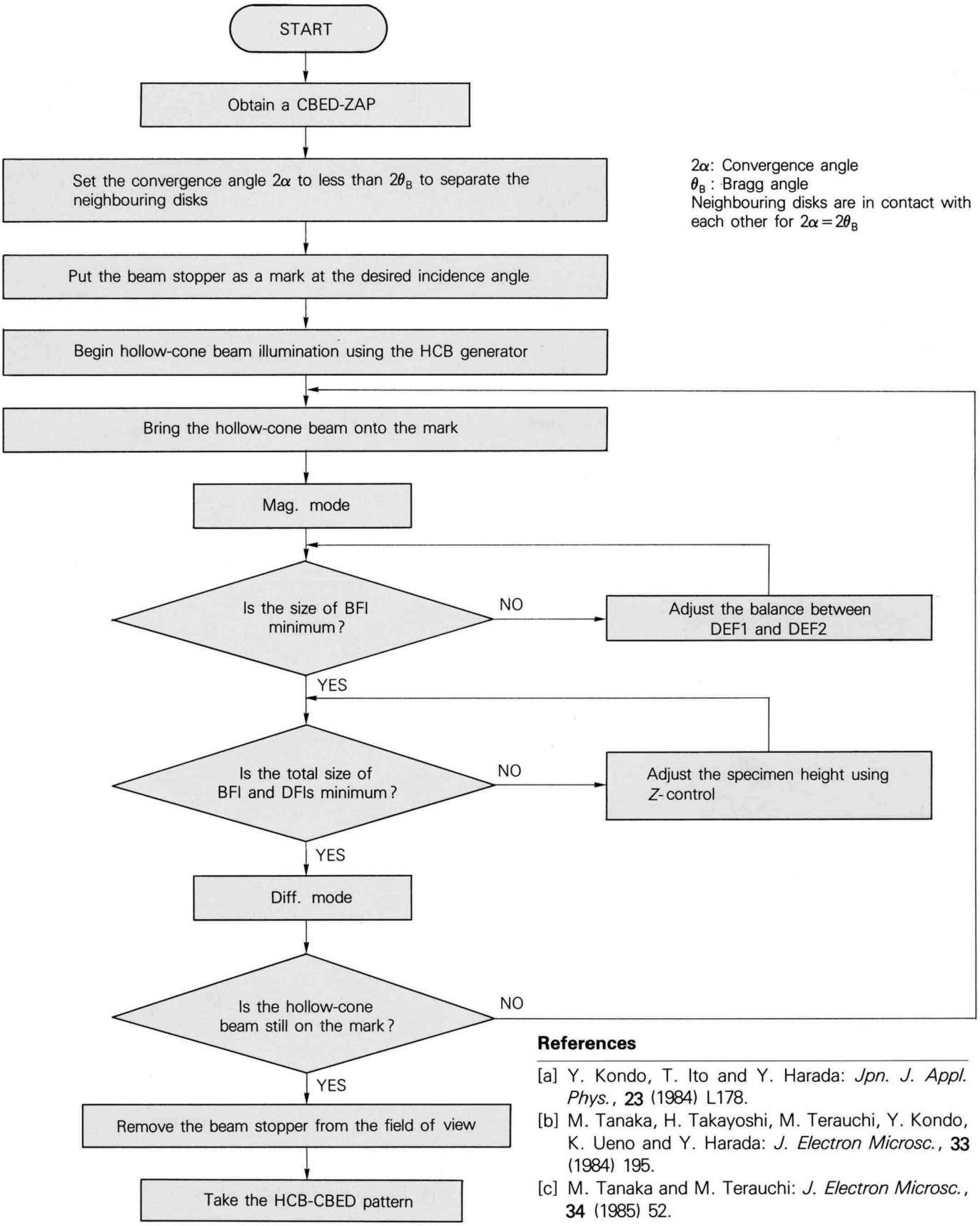

2α: Convergence angle
θ_B : Bragg angle
Neighbouring disks are in contact with each other for $2\alpha = 2\theta_B$

References

[a] Y. Kondo, T. Ito and Y. Harada: *Jpn. J. Appl. Phys.*, **23** (1984) L178.

[b] M. Tanaka, H. Takayoshi, M. Terauchi, Y. Kondo, K. Ueno and Y. Harada: *J. Electron Microsc.*, **33** (1984) 195.

[c] M. Tanaka and M. Terauchi: *J. Electron Microsc.*, **34** (1985) 52.

Many-beam LACBED pattern (MB-LACBED)

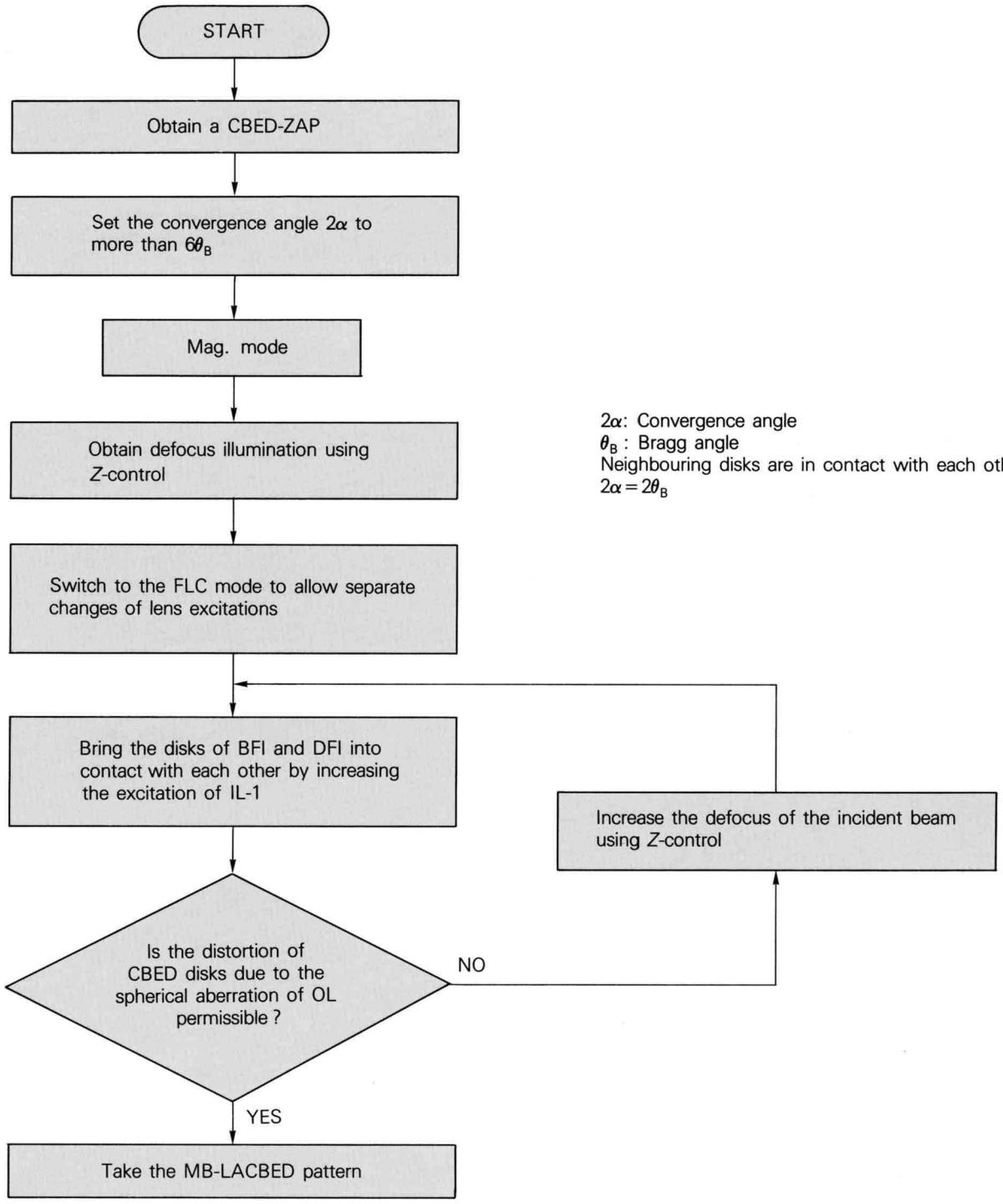

2α: Convergence angle
θ_B : Bragg angle
Neighbouring disks are in contact with each other for $2\alpha = 2\theta_B$

Reference

[a] M. Terauchi and M. Tanaka: *J. Electron Microsc.*, **34** (1985) 128.

Selected area CBED pattern (SA-CBED)

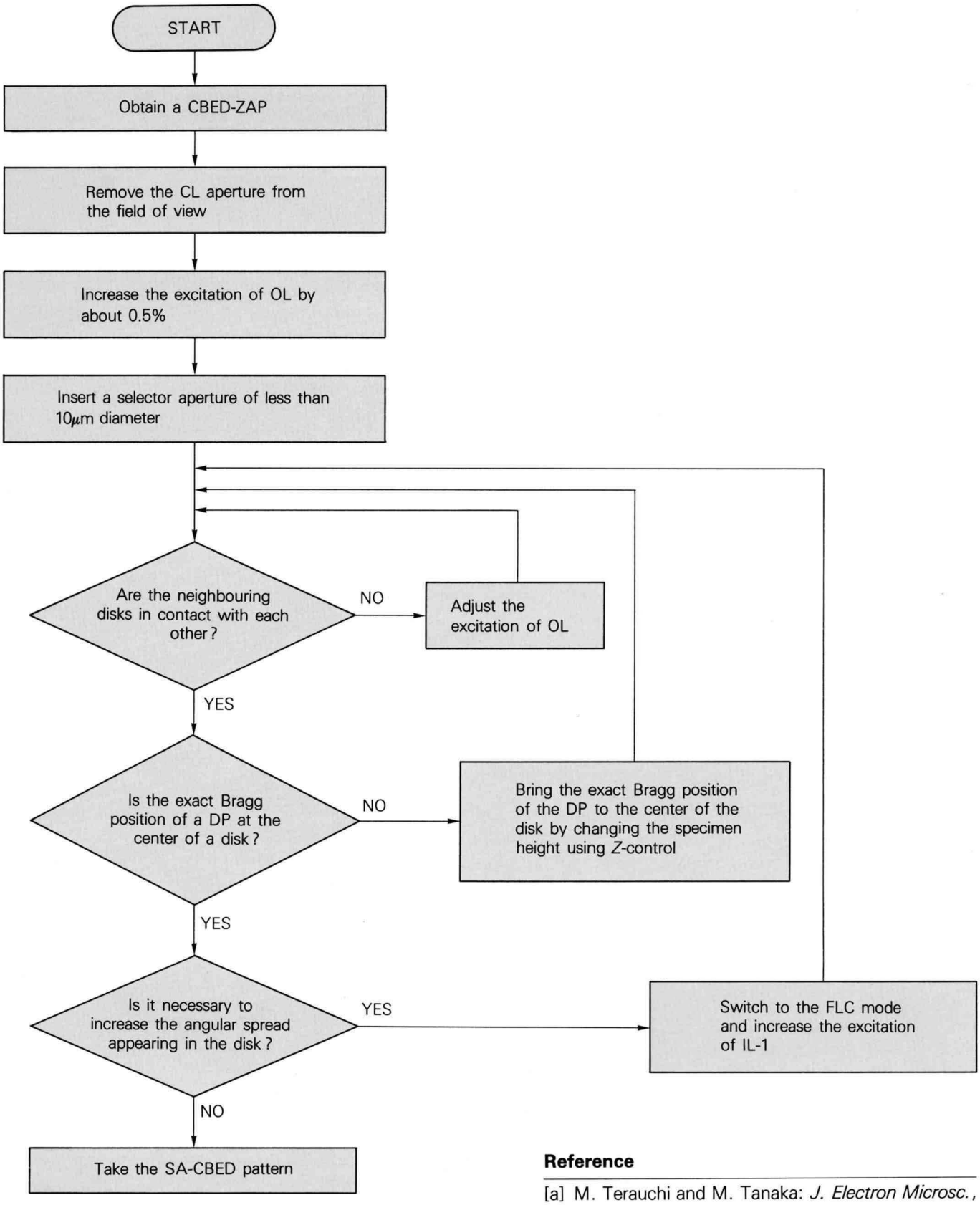

Reference

[a] M. Terauchi and M. Tanaka: *J. Electron Microsc.*, **34** (1985) 347.

Point-group determination

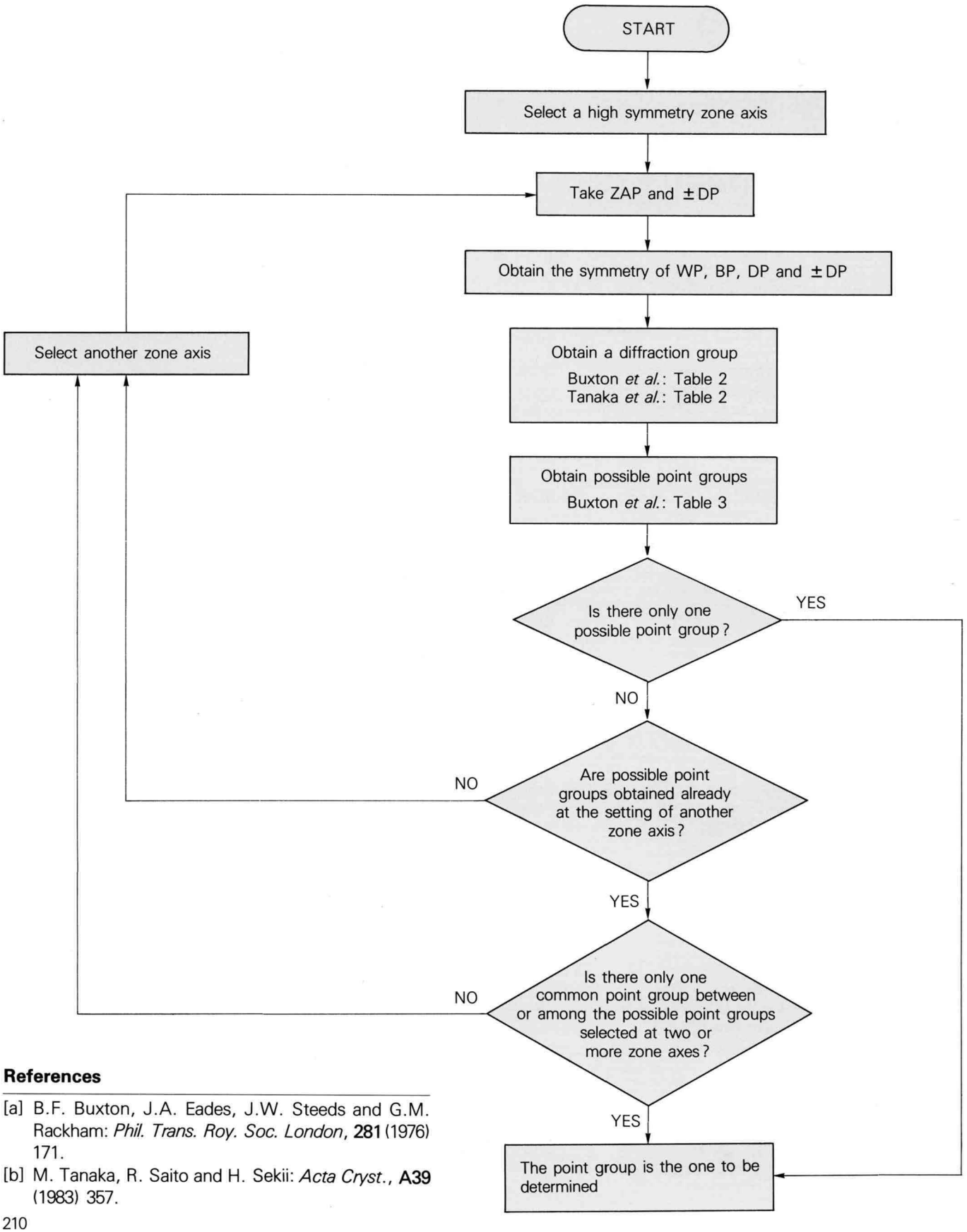

References

[a] B.F. Buxton, J.A. Eades, J.W. Steeds and G.M. Rackham: *Phil. Trans. Roy. Soc. London*, **281** (1976) 171.

[b] M. Tanaka, R. Saito and H. Sekii: *Acta Cryst.*, **A39** (1983) 357.

Space-group determination

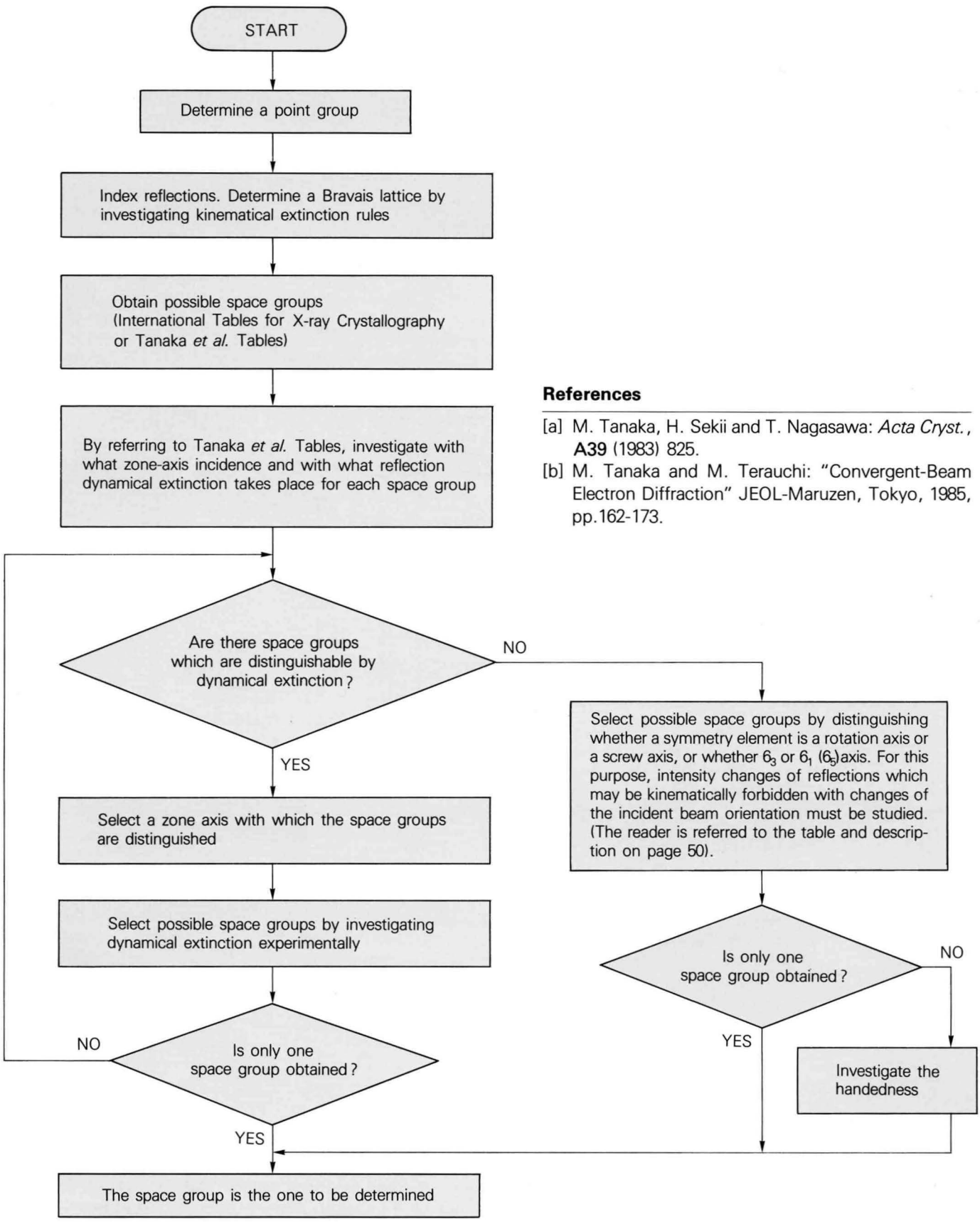

References

[a] M. Tanaka, H. Sekii and T. Nagasawa: *Acta Cryst.*, **A39** (1983) 825.

[b] M. Tanaka and M. Terauchi: "Convergent-Beam Electron Diffraction" JEOL-Maruzen, Tokyo, 1985, pp.162-173.

Determination of the displacement vector R of a stacking fault

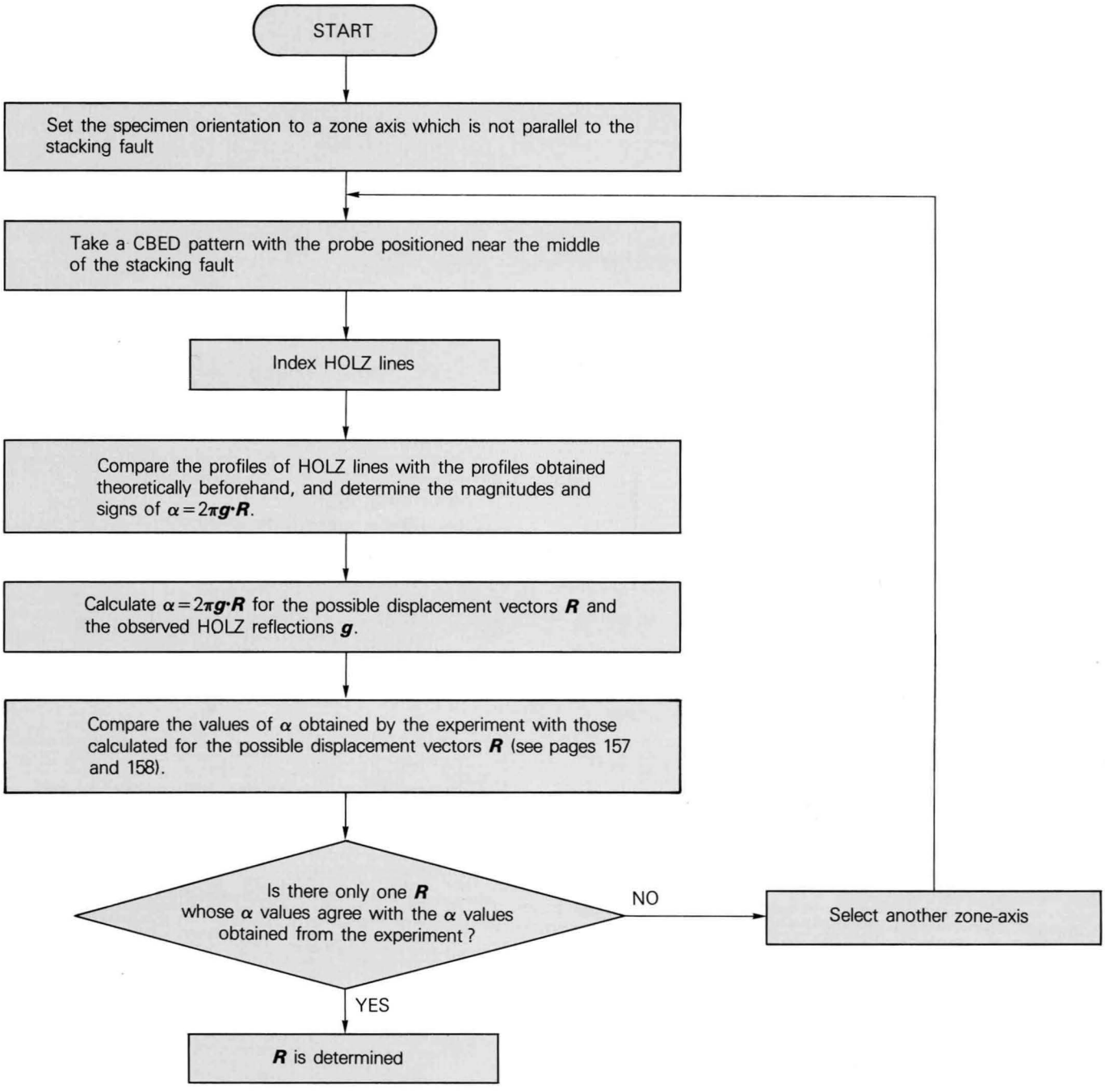

Reference

[a] M. Tanaka and T. Kaneyama: Proc. XIth Int. Congr. on Electron Microsc., Kyoto, 1986, p. 203.

References

[a] D. Cherns and A.R. Preston: Proc. XIth Int. Congr. on Electron Microsc., Kyoto, 1986, P. 721.

[b] M. Tanaka: *J. Electron Microsc.*, **35** (1986) 314.

Determination of the Burgers vector b of a dislocation

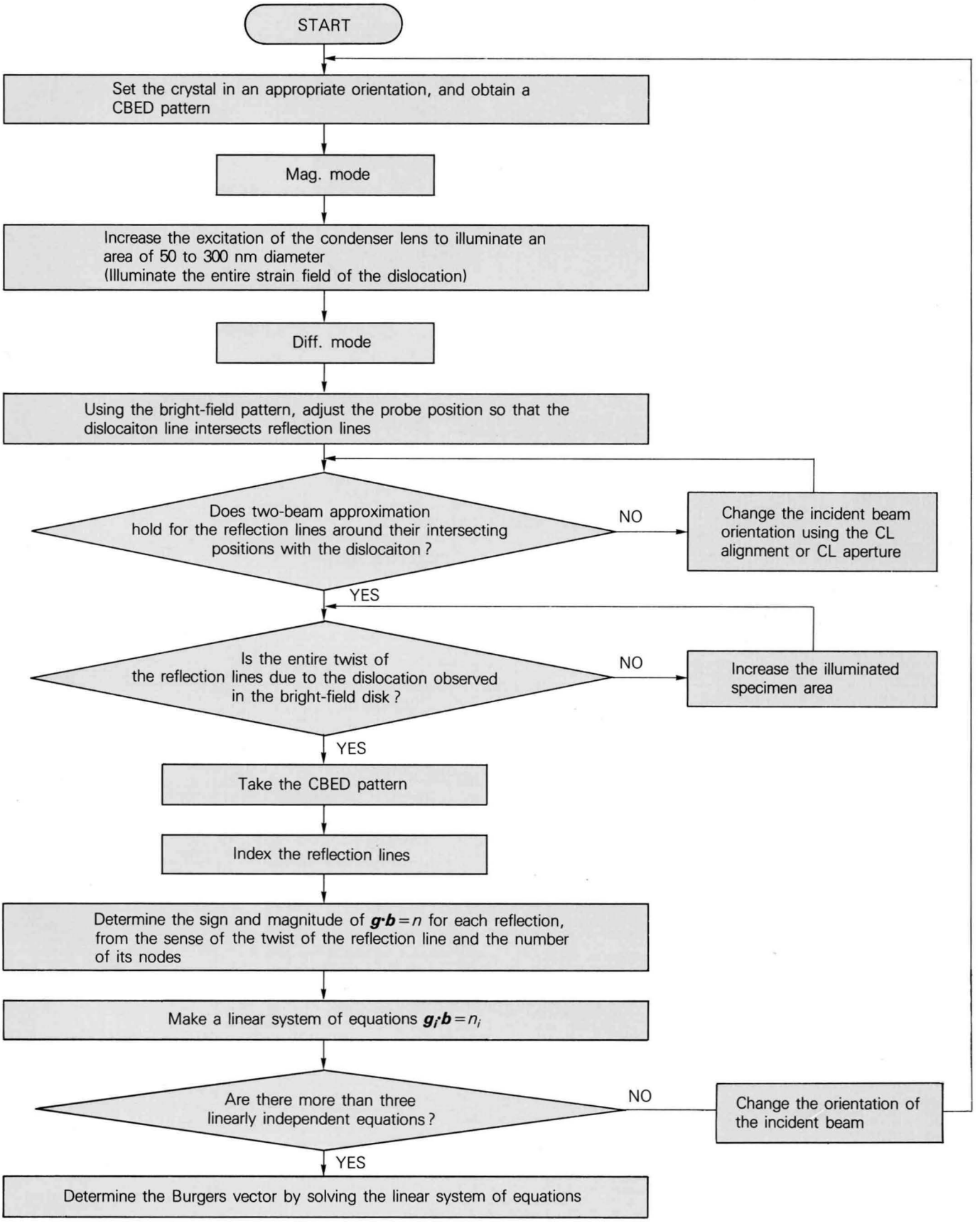

Tables of GM Lines in HOLZ Reflections for Space-Group

Point groups *m*, 2/*m*

Incident beam direction / Space group	[*u*0*w*]	
6 *Pm*		
7 *Pc*	$h0l_o$ *c*	A_h
8 *Cm*		
9 *Cc*	h_e0l_o *c*	A_h
10 *P*2/*m*		

Incident beam direction / Space group	[*u*0*w*]	
11 $P2_1/m$		
12 *C*2/*m*		
13 *P*2/*c*	$h0l_o$ *c*	A_h
14 $P2_1/c$	$h0l_o$ *c*	A_h
15 *C*2/*c*	h_e0l_o *c*	A_h

2nd setting : unique axis // b

Point group *mm*2 (I)

Incident beam direction / Space group	[100]		[010]		[001]		[0*vw*]		[*u*0*w*]	
25 *Pmm*2										
26 $Pmc2_1$	$h0l_o$ *c*	*A*			$h0l_o$ *c*	*A*			$h0l_o$ *c*	A_h
27 *Pcc*2	$h0l_o$ c_2	*A*	$0kl_o$ c_1	*A*	$0kl_o$ c_1 $h0l_o$ c_2	*A*	$0kl_o$ c_1	A_h	$h0l_o$ c_2	A_h
28 *Pma*2	h_o0l *a*	*A*			h_o0l *a*	*A*			h_o0l *a*	A_h
29 $Pca2_1$	h_o0l *a*	*A*	$0kl_o$ *c*	*A*	$0kl_o$ *c* h_o0l *a*	*A*	$0kl_o$ *c*	A_h	h_o0l *a*	A_h
30 *Pnc*2	$h0l_o$ *c*	*A*	$0kl$ $k+l=2n+1$ *n*	*A*	$0kl$ $k+l=2n+1$ *n* $h0l_o$ *c*	*A*	$0kl$ $k+l=2n+1$ *n*	A_h	$h0l_o$ *c*	A_h
31 $Pmn2_1$	$h0l$ $h+l=2n+1$ *n*	*A*			$h0l$ $h+l=2n+1$ *n*	*A*			$h0l$ $h+l=2n+1$ *n*	A_h
32 *Pba*2	h_o0l *a*	*A*	$0k_ol$ *b*	*A*	$0k_ol$ *b* h_o0l *a*	*A*	$0k_ol$ *b*	A_h	h_o0l *a*	A_h
33 $Pna2_1$	h_o0l *a*	*A*	$0kl$ $k+l=2n+1$ *n*	*A*	$0kl$ $k+l=2n+1$ *n* h_o0l *a*	*A*	$0kl$ $k+l=2n+1$ *n*	A_h	h_o0l *a*	A_h
34 *Pnn*2	$h0l$ $h+l=2n+1$ n_2	*A*	$0kl$ $k+l=2n+1$ n_1	*A*	$0kl$ $k+l=2n+1$ n_1 $h0l$ $h+l=2n+1$ n_2	*A*	$0kl$ $k+l=2n+1$ n_1	A_h	$h0l$ $h+l=2n+1$ n_2	A_h

Determination

Point group *mm*2 (II)

Space group \ Incident beam direction	[100]		[010]		[001]		[0*vw*]		[*u*0*w*]	
35 *Cmm*2 *ba*2										
36 *Cmc*2$_1$ *bn*2$_1$	h_e0l_o *c*	*A*			h_e0l_o *c*	*A*			h_e0l_o *c*	A_h
37 *Ccc*2 *nn*2	h_e0l_o c_2	*A*	$0k_el_o$ c_1	*A*	$0k_el_o$ c_1 h_e0l_o c_2	*A*	$0k_el_o$ c_1	A_h	h_e0l_o c_2	A_h
38 *Amm*2 *nc*2$_1$										
39 *Abm*2 *cc*2$_1$			$0k_ol_o$ *b*	*A*	$0k_ol_o$ *b*	*A*	$0k_ol_o$ *b*	A_h		
40 *Ama*2 *nn*2$_1$	h_o0l_e *a*	*A*			h_o0l_e *a*	*A*			h_o0l_e *a*	A_h
41 *Aba*2 *cn*2$_1$	h_o0l_e *a*	*A*	$0k_ol_o$ *b*	*A*	$0k_ol_o$ *b* h_o0l_e *a*	*A*	$0k_ol_o$ *b*	A_h	h_o0l_e *a*	A_h
42 *Fmm*2										
43 *Fdd*2 *dd*2$_1$	h_e0l_e $h_e+l_e=4n+2$ d_2	*A*	$0k_el_e$ $k_e+l_e=4n+2$ d_1	*A*	$0k_el_e$ $k_e+l_e=4n+2$ d_1 h_e0l_e $h_e+l_e=4n+2$ d_2	*A*	$0k_el_e$ $k_e+l_e=4n+2$ d_1	A_h	h_e0l_e $h_e+l_e=4n+2$ d_2	A_h
44 *Imm*2 *nn*2$_1$										
45 *Iba*2 *cc*2$_1$	h_o0l_o *a*	*A*	$0k_ol_o$ *b*	*A*	$0k_ol_o$ *b* h_o0l_o *a*	*A*	$0k_ol_o$ *b*	A_h	h_o0l_o *a*	A_h
46 *Ima*2 *nc*2$_1$	h_o0l_o *a*	*A*			h_o0l_o *a*	*A*			h_o0l_o *a*	A_h

Note: The meanings of the symbols A, A_h and A^* are referred to page 52.

Point group *mmm* (I)

Incident beam direction / Space group	[100]		[010]		[001]		[*uv*0]		[0*vw*]		[*u*0*w*]	
47 $P2/m2/m2/m$												
48 $P2/n2/n2/n$	$h0l$ $h+l=2n+1$ n_2 $hk0$ $h+k=2n+1$ n_3	A	$0kl$ $k+l=2n+1$ n_1 $hk0$ $h+k=2n+1$ n_3	A	$0kl$ $k+l=2n+1$ n_1 $h0l$ $h+l=2n+1$ n_2	A	$hk0$ $h+k=2n+1$ n_3	A_h	$0kl$ $k+l=2n+1$ n_1	A_h	$h0l$ $h+l=2n+1$ n_2	A_h
49 $P2/c2/c2/m$	$h0l_o$ c_2	A	$0kl_o$ c_1	A	$0kl_o$ c_1 $h0l_o$ c_2	A			$0kl_o$ c_1	A_h	$h0l_o$ c_2	A_h
50 $P2/b2/a2/n$	h_o0l a $hk0$ $h+k=2n+1$ n	A	$0k_ol$ b $hk0$ $h+k=2n+1$ n	A	$0k_ol$ b h_o0l a	A	$hk0$ $h+k=2n+1$ n	A_h	$0k_ol$ b	A_h	h_o0l a	A_h
51 $P2_1/m2/m2/a$	h_ok0 a	A	h_ok0 a	A			h_ok0 a	A_h				
52 $P2/n2_1/n2/a$	$h0l$ $h+l=2n+1$ n_2 h_ok0 a	A	$0kl$ $k+l=2n+1$ n_1 h_ok0 a	A	$0kl$ $k+l=2n+1$ n_1 $h0l$ $h+l=2n+1$ n_2	A	h_ok0 a	A_h	$0kl$ $k+l=2n+1$ n_1	A_h	$h0l$ $h+l=2n+1$ n_2	A_h
53 $P2/m2/n2_1/a$	$h0l$ $h+l=2n+1$ n h_ok0 a	A	h_ok0 a	A	$h0l$ $h+l=2n+1$ n	A	h_ok0 a	A_h			$h0l$ $h+l=2n+1$ n	A_h
54 $P2_1/c2/c2/a$	$h0l_o$ c_2 h_ok0 a	A	$0kl_o$ c_1 h_ok0 a	A	$0kl_o$ c_1 $h0l_o$ c_2	A	h_ok0 a	A_h	$0kl_o$ c_1	A_h	$h0l_o$ c_2	A_h
55 $P2_1/b2_1/a2/m$	h_o0l a	A	$0k_ol$ b	A	$0k_ol$ b h_o0l a	A			$0k_ol$ b	A_h	h_o0l a	A_h
56 $P2_1/c2_1/c2/n$	$h0l_o$ c_2 $hk0$ $h+k=2n+1$ n	A	$0kl_o$ c_1 $hk0$ $h+k=2n+1$ n	A	$0kl_o$ c_1 $h0l_o$ c_2	A	$hk0$ $h+k=2n+1$ n	A_h	$0kl_o$ c_1	A_h	$h0l_o$ c_2	A_h
57 $P2/b2_1/c2_1/m$	$h0l_o$ c	A	$0k_ol$ b	A	$0k_ol$ b $h0l_o$ c	A			$0k_ol$ b	A_h	$h0l_o$ c	A_h
58 $P2_1/n2_1/n2/m$	$h0l$ $h+l=2n+1$ n_2	A	$0kl$ $k+l=2n+1$ n_1	A	$0kl$ $k+l=2n+1$ n_1 $h0l$ $h+l=2n+1$ n_2	A			$0kl$ $k+l=2n+1$ n_1	A_h	$h0l$ $h+l=2n+1$ n_2	A_h
59 $P2_1/m2_1/m2/n$	$hk0$ $h+k=2n+1$ n	A	$hk0$ $h+k=2n+1$ n	A			$hk0$ $h+k=2n+1$ n	A_h				
60 $P2_1/b2/c2_1/n$	$h0l_o$ c $hk0$ $h+k=2n+1$ n	A	$0k_ol$ b $hk0$ $h+k=2n+1$ n	A	$0k_ol$ b $h0l_o$ c	A	$hk0$ $h+k=2n+1$ n	A_h	$0k_ol$ b	A_h	$h0l_o$ c	A_h

Point group *mmm* (II)

Incident beam direction / Space group	[100]		[010]		[001]		[$uv0$]		[$0vw$]		[$u0w$]	
61 $P2_1/b2_1/c2_1/a$	$h0l_o$ c h_ok0 a	A	$0k_ol$ b h_ok0 a	A	$0k_ol$ b $h0l_o$ c	A	h_ok0 a	A_h	$0k_ol$ b	A_h	$h0l_o$ c	A_h
62 $P2_1/n2_1/m2_1/a$	h_ok0 a	A	$0kl$ $k+l=2n+1$ n h_ok0 a	A	$0kl$ $k+l=2n+1$ n	A	h_ok0 a	A_h	$0kl$ $k+l=2n+1$ n	A_h		
63 $C2/m2/c2_1/m$	h_e0l_o c	A			h_e0l_o c	A					h_e0l_o c	A_h
64 $C2/m2/c2_1/a$	h_e0l_o c h_ok_o0 a	A	h_ok_o0 a	A	h_e0l_o c	A	h_ok_o0 a	A_h			h_e0l_o c	A_h
65 $C2/m2/m2/m$												
66 $C2/c2/c2/m$	h_e0l_o c_2	A	$0k_el_o$ c_1	A	$0k_el_o$ c_1 h_e0l_o c_2	A			$0k_el_o$ c_1	A_h	h_e0l_o c_2	A_h
67 $C2/m2/m2/a$	h_ok_o0 a	A	h_ok_o0 a	A			h_ok_o0 a	A_h				
68 $C2/c2/c2/a$	h_e0l_o c_2 h_ok_o0 a	A	$0k_el_o$ c_1 h_ok_o0 a	A	$0k_el_o$ c_1 h_e0l_o c_2	A	h_ok_o0 a	A_h	$0k_el_o$ c_1	A_h	h_e0l_o c_2	A_h
69 $F2/m2/m2/m$												
70 $F2/d2/d2/d$	h_e0l_e $h_e+l_e=4n+2$ d_2 h_ek_e0 $h_e+k_e=4n+2$ d_3	A	h_ek_e0 $h_e+k_e=4n+2$ d_3 $0k_el_e$ $k_e+l_e=4n+2$ d_1	A	$0k_el_e$ $k_e+l_e=4n+2$ d_1 h_e0l_e $h_e+l_e=4n+2$ d_2	A	h_ek_e0 $h_e+k_e=4n+2$ d_3	A_h	$0k_el_e$ $k_e+l_e=4n+2$ d_1	A_h	h_e0l_e $h_e+l_e=4n+2$ d_2	A_h
71 $I2/m2/m2/m$												
72 $I2/b2/a2/m$	h_o0l_o a	A	$0k_ol_o$ b	A	$0k_ol_o$ b h_o0l_o a	A			$0k_ol_o$ b	A_h	h_o0l_o a	A_h
73 $I2/b2/c2/a$	h_o0l_o c h_ok_o0 a	A	h_ok_o0 a $0k_ol_o$ b	A	$0k_ol_o$ b h_o0l_o c	A	h_ok_o0 a	A_h	$0k_ol_o$ b	A_h	h_o0l_o c	A_h
74 $I2/m2/m2/a$	h_ok_o0 a	A	h_ok_o0 a	A			h_ok_o0 a	A_h				

Point group 4/*m*

Incident beam direction / Space group	[100] [110]		[*uv*0]	
83 $P4/m$				
84 $P4_2/m$				
85 $P4/n$	$hk0$ $h+k=2n+1$ n	A	$hk0$ $h+k=2n+1$ n	A_h

Incident beam direction / Space group	[100] [110]		[*uv*0]	
86 $P4_2/n$	$hk0$ $h+k=2n+1$ n	A	$hk0$ $h+k=2n+1$ n	A_h
87 $I4/m$				
88 $I4_1/a$	h_0k_00 a	A	h_0k_00 a	A_h

Point group 4*mm*(I)

Incident beam direction / Space group	[100]		[001]		[110]		[*u*0*w*]*		[*uuw*]	
99 $P4mm$										
100 $P4bm$	h_00l a_2	A	$0k_0l$ b_1 h_00l a_2	A			h_00l a	A_h		
101 $P4_2cm$	$h0l_0$ c_2	A	$0kl_0$ c_1 $h0l_0$ c_2	A			$h0l_0$ c	A_h		
102 $P4_2nm$	$h0l$ $h+l=2n+1$ n_2	A	$0kl$ $k+l=2n+1$ n_1 $h0l$ $h+l=2n+1$ n_2	A			$h0l$ $h+l=2n+1$ n	A_h		
103 $P4cc$	$h0l_0$ c_{12}	A	$0kl_0$ c_{11} $h0l_0$ c_{12} $\underline{hhl_0}$ $\overline{h}hl_0$ c_2	A	hhl_0 c_2	A	$h0l_0$ c_1	A_h	hhl_0 c_2	A_h
104 $P4nc$	$h0l$ $h+l=2n+1$ n_2	A	$0kl$ $k+l=2n+1$ n_1 $h0l$ $h+l=2n+1$ n_2 $\underline{hhl_0}$ $\overline{h}hl_0$ c	A	hhl_0 c	A	$h0l$ $h+l=2n+1$ n	A_h	hhl_0 c	A_h
105 $P4_2mc$			$\underline{hhl_0}$ $\overline{h}hl_0$ c	A	hhl_0 c	A			hhl_0 c	A_h
106 $P4_2bc$	h_00l a_2	A	$0k_0l$ b_1 h_00l a_2 $\underline{hhl_0}$ $\overline{h}hl_0$ c	A	hhl_0 c	A	h_00l a	A_h	hhl_0 c	A_h
107 $I4mm$										
108 $I4cm$	h_00l_0 c_2	A	$0k_0l_0$ c_1 h_00l_0 c_2	A			h_00l_0 c	A_h		

*The symbol "a" in the column of [u0w] incidence is equivalent to the symbol "b" in the space groups of the first column.

Point group 4*mm* (II)

Incident beam direction / Space group	[100]		[001]		[110]		[$u0w$]		[uuw]	
109 $I4_1md$			$\underline{hhl}_e$ $\bar{h}hl_e$ $2h+l_e=4n+2$ d	A	hhl_e $2h+l_e=4n+2$ d	A			hhl_e $2h+l_e=4n+2$ d	A_h
110 $I4_1cd$	$h_0 0 l_0$ c_2	A	$0k_0l_0$ c_1 $h_0 0 l_0$ c_2 $\underline{hhl}_e$ $\bar{h}hl_e$ $2h+l_e=4n+2$ d	A	hhl_e $2h+l_e=4n+2$ d	A	$h_0 0 l_0$ c	A_h	hhl_e $2h+l_e=4n+2$ d	A_h

Point group $\bar{4}2m$

Incident beam direction / Space group	[100]		[001]		[110]		[$u0w$]*		[uuw]	
111 $P\bar{4}2m$										
112 $P\bar{4}2c$			$\underline{hhl}_o$ $\bar{h}hl_o$ c	A	hhl_o c	A			hhl_o c	A_h
113 $P\bar{4}2_1m$										
114 $P\bar{4}2_1c$			$\underline{hhl}_o$ $\bar{h}hl_o$ c	A	hhl_o c	A			hhl_o c	A_h
115 $P\bar{4}m2$										
116 $P\bar{4}c2$	$h0l_o$ c_2	A	$0kl_o$ c_1 $h0l_o$ c_2	A			$h0l_o$ c	A_h		
117 $P\bar{4}b2$	$h_o 0 l$ a_2	A	$0k_o l$ b_1 $h_o 0 l$ a_2	A			$h_o 0 l$ a	A_h		
118 $P\bar{4}n2$	$h0l$ $h+l=2n+1$ n_2	A	$0kl$ $k+l=2n+1$ n_1 $h0l$ $h+l=2n+1$ n_2	A			$h0l$ $h+l=2n+1$ n	A_h		
119 $I\bar{4}m2$										
120 $I\bar{4}c2$	$h_o 0 l_o$ c_2	A	$0k_o l_o$ c_1 $h_o 0 l_o$ c_2	A			$h_o 0 l_o$ c	A_h		
121 $I\bar{4}2m$										
122 $I\bar{4}2d$			$\underline{hhl}_e$ $\bar{h}hl_e$ $2h+l_e=4n+2$ d	A	hhl_e $2h+l_e=4n+2$ d	A			hhl_e $2h+l_e=4n+2$ d	A_h

*The symbol "a" in the column of [$u0w$] incidence is equivalent to the symbol "b" in the space groups of the first column.

Point group 4/*mmm*(I)

Incident beam direction / Space group	[100]		[001]		[110]		[$u0w$]*		[uuw]		[$uv0$]	
123 $P4/mmm$ $P4/m2/m2/m$												
124 $P4/mcc$ $P4/m2/c2/c$	$h0l_o$ c_{12}	A	$0kl_o$ c_{11} $h0l_o$ c_{12} $\underline{hhl_o}$ $\overline{h}hl_o$ c_2	A	hhl_o c_2	A	$h0l_o$ c_1	A_h	hhl_o c_2	A_h		
125 $P4/nbm$ $P4/n2/b2/m$	$hk0$ $h+k=2n+1$ n h_o0l a_2	A	$0k_ol$ b_1 h_o0l a_2	A	$hk0$ $h+k=2n+1$ n	A	h_o0l a	A_h			$hk0$ $h+k=2n+1$ n	A_h
126 $P4/nnc$ $P4/n2/n2/c$	$hk0$ $h+k=2n+1$ n_1 $h0l$ $h+l=2n+1$ n_{22}	A	$0kl$ $k+l=2n+1$ n_{21} $h0l$ $h+l=2n+1$ n_{22} $\underline{hhl_o}$ $\overline{h}hl_o$ c	A	$hk0$ $h+k=2n+1$ n_1 hhl_o c	A	$h0l$ $h+l=2n+1$ n_2	A_h	hhl_o c	A_h	$hk0$ $h+k=2n+1$ n_1	A_h
127 $P4/mbm$ $P4/m2_1/b2/m$	h_o0l a_2	A	$0k_ol$ b_1 h_o0l a_2	A			h_o0l a	A_h				
128 $P4/mnc$ $P4/m2_1/n2/c$	$h0l$ $h+l=2n+1$ n_2	A	$0kl$ $k+l=2n+1$ n_1 $h0l$ $h+l=2n+1$ n_2 $\underline{hhl_o}$ $\overline{h}hl_o$ c	A	hhl_o c	A	$h0l$ $h+l=2n+1$ n	A_h	hhl_o c	A_h		
129 $P4/nmm$ $P4/n2_1/m2/m$	$hk0$ $h+k=2n+1$ n	A			$hk0$ $h+k=2n+1$ n	A					$hk0$ $h+k=2n+1$ n	A_h
130 $P4/ncc$ $P4/n2_1/c2/c$	$hk0$ $h+k=2n+1$ n $h0l_o$ c_{12}	A	$0kl_o$ c_{11} $h0l_o$ c_{12} $\underline{hhl_o}$ $\overline{h}hl_o$ c_2	A	$hk0$ $h+k=2n+1$ n hhl_o c_2	A	$h0l_o$ c_1	A_h	hhl_o c_2	A_h	$hk0$ $h+k=2n+1$ n	A_h
131 $P4_2/mmc$ $P4_2/m2/m2/c$			$\underline{hhl_o}$ $\overline{h}hl_o$ c	A	hhl_o c	A			hhl_o c	A_h		
132 $P4_2/mcm$ $P4_2/m2/c2/m$	$h0l_o$ c_2	A	$0kl_o$ c_1 $h0l_o$ c_2	A			$h0l_o$ c	A_h				

*The symbol "a" in the column of [$u0w$] incidence is equivalent to the symbol "b" in the space groups of the first column.

Point group 4/*mmm*(II)

Incident beam direction / Space group	[100]		[001]		[110]		$[u0w]$*		$[uuw]$		$[uv0]$	
133 $P4_2/nbc$ $P4_2/n2/b2/c$	$hk0$ $h+k=2n+1$ n h_o0l a_2	A	$0k_ol$ b_1 h_o0l a_2 $\underline{h}hl_o$ $\overline{h}hl_o$ c	A	$hk0$ $h+k=2n+1$ n hhl_o c	A	h_o0l a	A_h	hhl_o c	A_h	$hk0$ $h+k=2n+1$ n	A_h
134 $P4_2/nnm$ $P4_2/n2/n2/m$	$hk0$ $h+k=2n+1$ n_1 $h0l$ $h+l=2n+1$ n_{22}	A	$0kl$ $k+l=2n+1$ n_{21} $h0l$ $h+l=2n+1$ n_{22}	A	$hk0$ $h+k=2n+1$ n_1	A	$h0l$ $h+l=2n+1$ n_2	A_h			$hk0$ $h+k=2n+1$ n_1	A_h
135 $P4_2/mbc$ $P4_2/m2_1/b2/c$	h_o0l a_2	A	$0k_ol$ b_1 h_o0l a_2 $\underline{h}hl_o$ $\overline{h}hl_o$ c	A	hhl_o c	A	h_o0l a	A_h	hhl_o c	A_h		
136 $P4_2/mnm$ $P4_2/m2_1/n2/m$	$h0l$ $h+l=2n+1$ n_2	A	$0kl$ $k+l=2n+1$ n_1 $h0l$ $h+l=2n+1$ n_2	A			$h0l$ $h+l=2n+1$ n	A_h				
137 $P4_2/nmc$ $P4_2/n2_1/m2/c$	$hk0$ $h+k=2n+1$ n	A	$\underline{h}hl_o$ $\overline{h}hl_o$ c	A	hhl_o c $hk0$ $h+k=2n+1$ n	A			hhl_o c	A_h	$hk0$ $h+k=2n+1$ n	A_h
138 $P4_2/ncm$ $P4_2/n2_1/c2/m$	$hk0$ $h+k=2n+1$ n $h0l_o$ c_2	A	$0kl_o$ c_1 $h0l_o$ c_2	A	$hk0$ $h+k=2n+1$ n	A	$h0l_o$ c	A_h			$hk0$ $h+k=2n+1$ n	A_h
139 $I4/mmm$ $I4/m2/m2/m$												
140 $I4/mcm$ $I4/m2/c2/m$	h_o0l_o c_2	A	$0k_ol_o$ c_1 h_o0l_o c_2	A			h_o0l_o c	A_h				
141 $I4_1/amd$ $I4_1/a2/m2/d$	h_ok_o0 a	A	$\underline{hhl}_e$ $\overline{h}hl_e$ $2h+l_e=4n+2$ d	A	h_ok_o0 a hhl_e $2h+l_e=4n+2$ d	A			hhl_e $2h+l_e=4n+2$ d	A_h	h_ok_o0 a	A_h
142 $I4_1/acd$ $I4_1/a2/c2/d$	h_ok_o0 a h_o0l_o c_2	A	$0k_ol_o$ c_1 h_o0l_o c_2 $\underline{hhl}_e$ $\overline{h}hl_e$ $2h+l_e=4n+2$ d	A	h_ok_o0 a hhl_e $2h+l_e=4n+2$ d	A	h_o0l_o c	A_h	hhl_e $2h+l_e=4n+2$ d	A_h	h_ok_o0 a	A_h

*The symbol "a" in the column of $[u0w]$ incidence is equivalent to the symbol "b" in the space groups of the first column.

Point groups $3m$, $\bar{3}m$

Incident beam direction / Space group	[0001]		[11$\bar{2}$0]		[1$\bar{1}$00]		[11$\bar{2}w$]		[1$\bar{1}$0w]	
156 $P3m1$										
157 $P31m$										
158 $P3c1$	$h\bar{h}0l_o$ $0h\bar{h}l_o$ $\bar{h}0hl_o$ c	A			$h\bar{h}0l_o$ c	A			$h\bar{h}0l_o$ c	A_h
159 $P31c$	$hh\overline{2h}l_o$ $h\overline{2h}hl_o$ $\overline{2h}hhl_o$ c	A	$hh\overline{2h}l_o$ c	A			$hh\overline{2h}l_o$ c	A_h		
160 $R3m$										
161 $R3c$	$h\bar{h}0l_o$ $0h\bar{h}l_o$ $\bar{h}0hl_o$ $h+l_o=3n$ c	A_h			$h\bar{h}0l_o$ $h+l_o=3n$ c	A_h			$h\bar{h}0l_o$ $h+l_o=3n$ c	A_h
162 $P\bar{3}1m$										
163 $P\bar{3}1c$	$hh\overline{2h}l_o$ $h\overline{2h}hl_o$ $\overline{2h}hhl_o$ c	A	$hh\overline{2h}l_o$ c	A			$hh\overline{2h}l_o$ c	A_h		
164 $P\bar{3}m1$										
165 $P\bar{3}c1$	$h\bar{h}0l_o$ $0h\bar{h}l_o$ $\bar{h}0hl_o$ c	A			$h\bar{h}0l_o$ c	A			$h\bar{h}0l_o$ c	A_h
166 $R\bar{3}m$										
167 $R\bar{3}c$	$h\bar{h}0l_o$ $0h\bar{h}l_o$ $\bar{h}0hl_o$ $h+l_o=3n$ c	A_h			$h\bar{h}0l_o$ $h+l_o=3n$ c	A_h			$h\bar{h}0l_o$ $h+l_o=3n$ c	A_h

Point groups 6*mm*, $\bar{6}m2$, 6/*mmm*

Incident beam direction / Space group	[0001]		[11$\bar{2}$0]		[1$\bar{1}$00]		[11$\bar{2}w$]		[1$\bar{1}$0w]	
183 $P6mm$										
184 $P6cc$	$h\bar{h}0l_o$ $0h\bar{h}l_o$ $\bar{h}0hl_o$ c_1 $hh\bar{2}hl_o$ $h\bar{2}hhl_o$ $\bar{2}hhhl_o$ c_2	A	$hh\bar{2}hl_o$ c_2	A	$h\bar{h}0l_o$ c_1	A	$hh\bar{2}hl_o$ c_2	A_h	$h\bar{h}0l_o$ c_1	A_h
185 $P6_3cm$	$h\bar{h}0l_o$ $0h\bar{h}l_o$ $\bar{h}0hl_o$ c	A			$h\bar{h}0l_o$ c	A			$h\bar{h}0l_o$ c	A_h
186 $P6_3mc$	$hh\bar{2}hl_o$ $h\bar{2}hhl_o$ $\bar{2}hhhl_o$ c	A	$hh\bar{2}hl_o$ c	A			$hh\bar{2}hl_o$ c	A_h		
187 $P\bar{6}m2$										
188 $P\bar{6}c2$	$h\bar{h}0l_o$ $0h\bar{h}l_o$ $\bar{h}0hl_o$ c	A			$h\bar{h}0l_o$ c	A			$h\bar{h}0l_o$ c	A_h
189 $P\bar{6}2m$										
190 $P\bar{6}2c$	$hh\bar{2}hl_o$ $h\bar{2}hhl_o$ $\bar{2}hhhl_o$ c	A	$hh\bar{2}hl_o$ c	A			$hh\bar{2}hl_o$ c	A_h		
191 $P6/mmm$										
192 $P6/mcc$	$h\bar{h}0l_o$ $0h\bar{h}l_o$ $\bar{h}0hl_o$ c_1 $hh\bar{2}hl_o$ $h\bar{2}hhl_o$ $\bar{2}hhhl_o$ c_2	A	$hh\bar{2}hl_o$ c_2	A	$h\bar{h}0l_o$ c_1	A	$hh\bar{2}hl_o$ c_2	A_h	$h\bar{h}0l_o$ c_1	A_h
193 $P6_3/mcm$	$h\bar{h}0l_o$ $0h\bar{h}l_o$ $\bar{h}0hl_o$ c	A			$h\bar{h}0l_o$ c	A			$h\bar{h}0l_o$ c	A_h
194 $P6_3/mmc$	$hh\bar{2}hl_o$ $h\bar{2}hhl_o$ $\bar{2}hhhl_o$ c	A	$hh\bar{2}hl_o$ c	A			$hh\bar{2}hl_o$ c	A_h		

Point group $m3$

Incident beam direction / Space group	[100]		[110]		[$uv0$]	
200 $Pm3$ $P2/m\bar{3}$						
201 $Pn3$ $P2/n\bar{3}$	$h0l$ $h+l=2n+1$ n_2 $hk0$ $h+k=2n+1$ n_3	A	$hk0$ $h+k=2n+1$ n_3	A	$hk0$ $h+k=2n+1$ n	A_h
202 $Fm3$ $F2/m\bar{3}$						
203 $Fd3$ $F2/d\bar{3}$	h_e0l_e $h_e+l_e=4n+2$ d_2 h_ek_e0 $h_e+k_e=4n+2$ d_3	A	h_ek_e0 $h_e+k_e=4n+2$ d_3	A	h_ek_e0 $h_e+k_e=4n+2$ d	A_h
204 $Im3$ $I2/m\bar{3}$						
205 $Pa3$ $P2_1/a\bar{3}$	$h0l_o$ c_2 h_ok0 a_3	A	h_ok0 a_3	A^*	h_ok0 a	A_h
206 $Ia3$ $I2_1/a\bar{3}$	h_o0l_o c_2 h_ok_o0 a_3	A	h_ok_o0 a_3	A	h_ok_o0 a	A_h

Point group $\bar{4}3m$

Incident beam direction / Space group	[100]*		[110]		[uuw]	
215 $P\bar{4}3m$						
216 $F\bar{4}3m$						
217 $I\bar{4}3m$						
218 $P\bar{4}3n$	h_okk , $h_o\bar{k}k$ n	A	hhl_o n	A	hhl_o n	A_h
219 $F\bar{4}3c$	$h_ok_ok_o$, $h_o\bar{k}_ok_o$ a	A	$h_oh_ol_o$ c	A	$h_oh_ol_o$ c	A_h
220 $I\bar{4}3d$	h_ekk $h_e\bar{k}k$ $2k+h_e=4n+2$ d	A	hhl_e $2h+l_e=4n+2$ d	A	hhl_e $2h+l_e=4n+2$ d	A_h

*The symbol "a" in the column of [100] incidence is equivalent to the symbol "c" in the space groups of the first column.

Point group $m3m$

Incident beam direction / Space group	[100]*		[110]		[$uv0$]		[uuw]	
221 $Pm\bar{3}m$ $P4/m\bar{3}2/m$								
222 $Pn\bar{3}n$ $P4/n\bar{3}2/n$	$h0l$ $h+l=2n+1$ n_{12} $hk0$ $h+k=2n+1$ n_{13} $h_o kk$, $h_o\bar{k}k$ n_2	A	$hk0$ $h+k=2n+1$ n_{13} hhl_o n_2	A	$hk0$ $h+k=2n+1$ n_1	A_h	hhl_o n_2	A_h
223 $Pm\bar{3}n$ $P4_2/m\bar{3}2/n$	$h_o kk$, $h_o\bar{k}k$ n	A	hhl_o n	A			hhl_o n	A_h
224 $Pn\bar{3}m$ $P4_2/n\bar{3}2/m$	$h0l$ $h+l=2n+1$ n_2 $hk0$ $h+k=2n+1$ n_3	A	$hk0$ $h+k=2n+1$ n_3	A	$hk0$ $h+k=2n+1$ n	A_h		
225 $Fm\bar{3}m$ $F4/m\bar{3}2/m$								
226 $Fm\bar{3}c$ $F4/m\bar{3}2/c$	$h_o k_o k_o$, $h_o\bar{k}_o k_o$ a	A	$h_o h_o l_o$ c	A			$h_o h_o l_o$ c	A_h
227 $Fd\bar{3}m$ $F4_1/d\bar{3}2/m$	$h_e 0 l_e$ $h_e+l_e=4n+2$ d_2 $h_e k_e 0$ $h_e+k_e=4n+2$ d_3	A	$h_e k_e 0$ $h_e+k_e=4n+2$ d_3	A	$h_e k_e 0$ $h_e+k_e=4n+2$ d	A_h		
228 $Fd\bar{3}c$ $F4_1/d\bar{3}2/c$	$h_e 0 l_e$ $h_e+l_e=4n+2$ d_2 $h_e k_e 0$ $h_e+k_e=4n+2$ d_3 $h_o k_o k_o$, $h_o\bar{k}_o k_o$ a	A	$h_o h_o l_o$ c $h_e k_e 0$ $h_e+k_e=4n+2$ d_3	A	$h_e k_e 0$ $h_e+k_e=4n+2$ d	A_h	$h_o h_o l_o$ c	A_h
229 $Im\bar{3}m$ $I4/m\bar{3}2/m$								
230 $Ia\bar{3}d$ $I4_1/a\bar{3}2/d$	$h_o k_o 0$ a_3 $h_o 0 l_o$ c_2 $h_e kk$, $h_e\bar{k}k$ $2k+h_e=4n+2$ d	A	hhl_e $2h+l_e=4n+2$ d $h_o k_o 0$ a_3	A	$h_o k_o 0$ a	A_h	hhl_e $2h+l_e=4n+2$ d	A_h

*The symbol "a" in the column of [100] incidence is equivalent to the symbol "c" in the space groups of the first column.

Computer Simulations

HOLZ line program

This program can simulate a HOLZ ring and HOLZ lines appearing in the bright-field and dark-field disks in the kinematical approximation for all the crystal systems and all the zone axes. HOLZ lines are drawn 1) by using arcs (HOLZ I) and 2) by solving Bragg equation (HOLZ II). The number of HOLZ lines in the dark-field disk G drawn by HOLZ II is twice that by HOLZ I, because the HOLZ lines excited not only from the bright-field but also from the dark-field G are drawn when using HOLZ II.

HOLZ ring

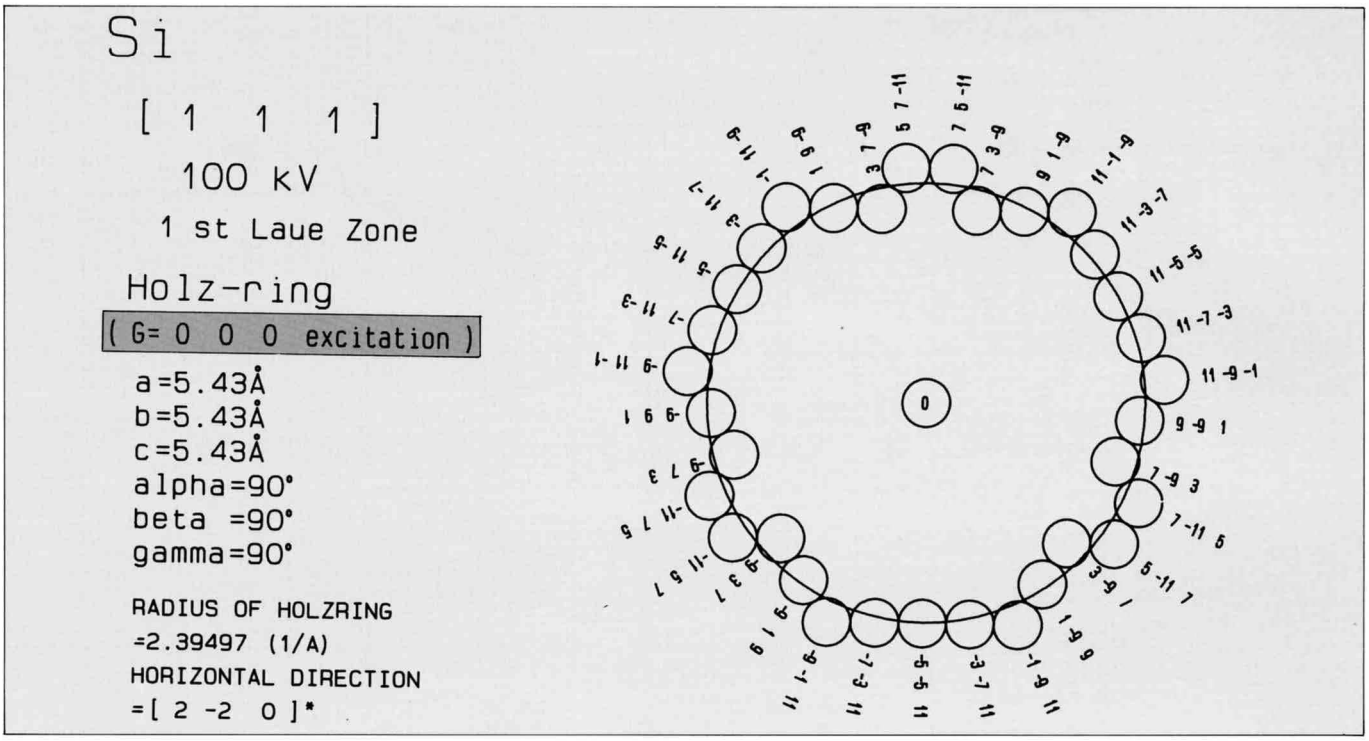

HOLZ lines: arc (circle) approximation

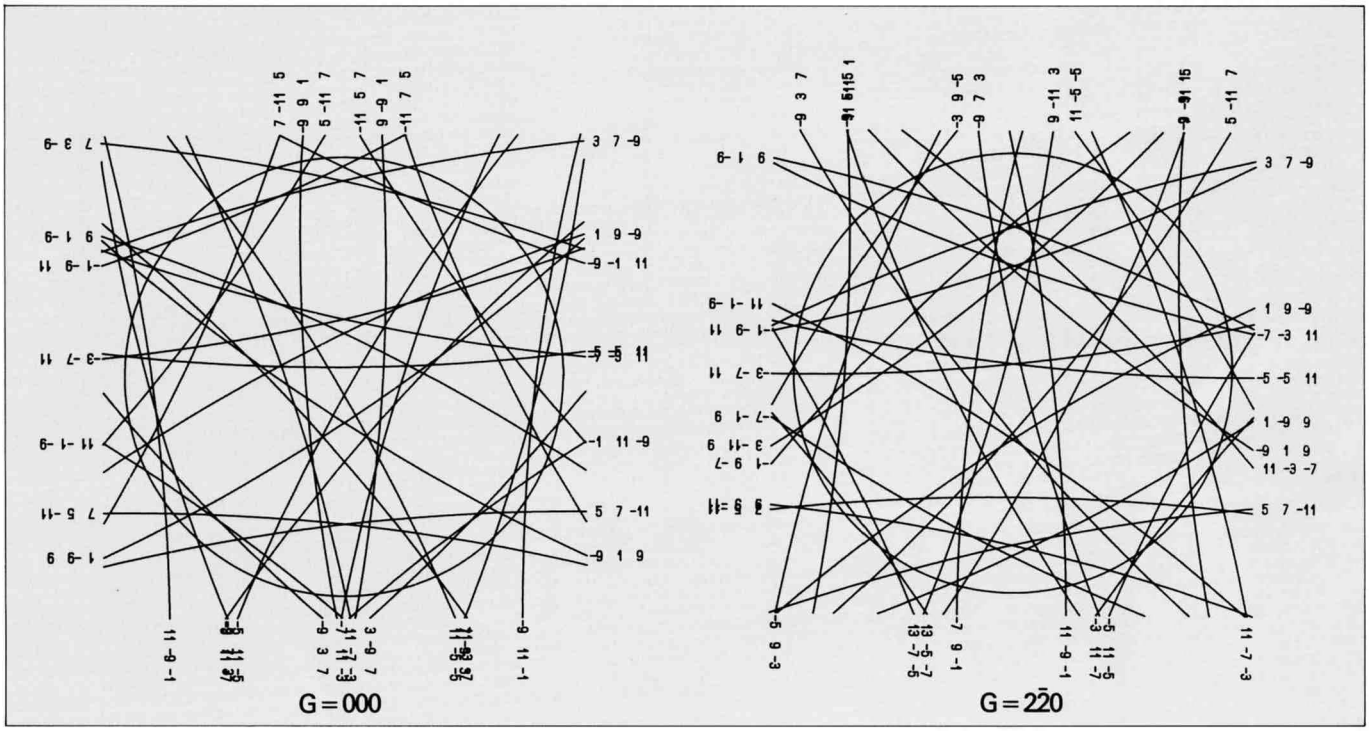

HOLZ I is used in determining reflection indices and the senses of excitation errors which are necessary in the identification of lattice defects, but has a low accuracy in reproducing the positions of reflection lines.

HOLZ II is recommended for use in the determination of the accelerating voltage and lattice parameters, but is not suitable for finding the signs of excitation errors.

Simulated patterns are printed out to a printer or a plotter. Subprograms of CHPR and CHPL are for printing out simulation patterns to a printer and a plotter, respectively.

HOLZ ring

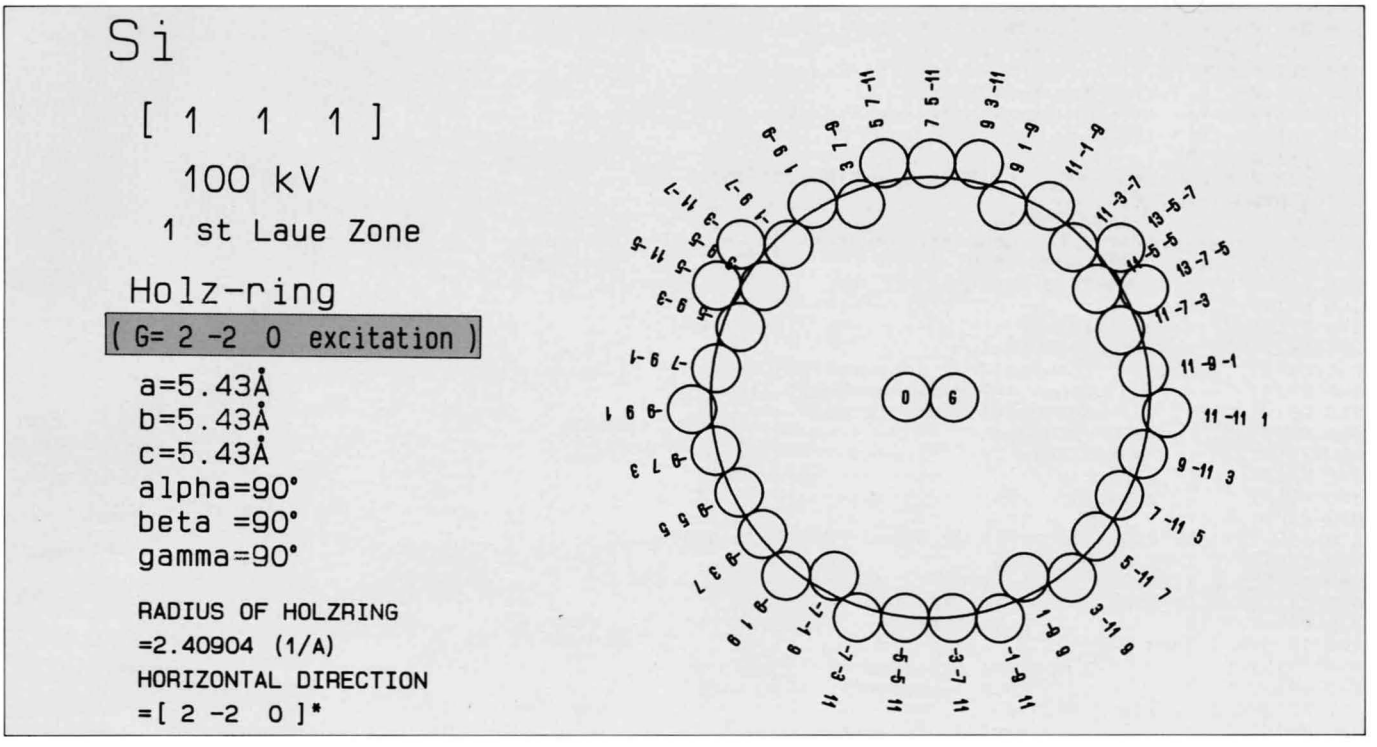

HOLZ lines: more accurate approximation

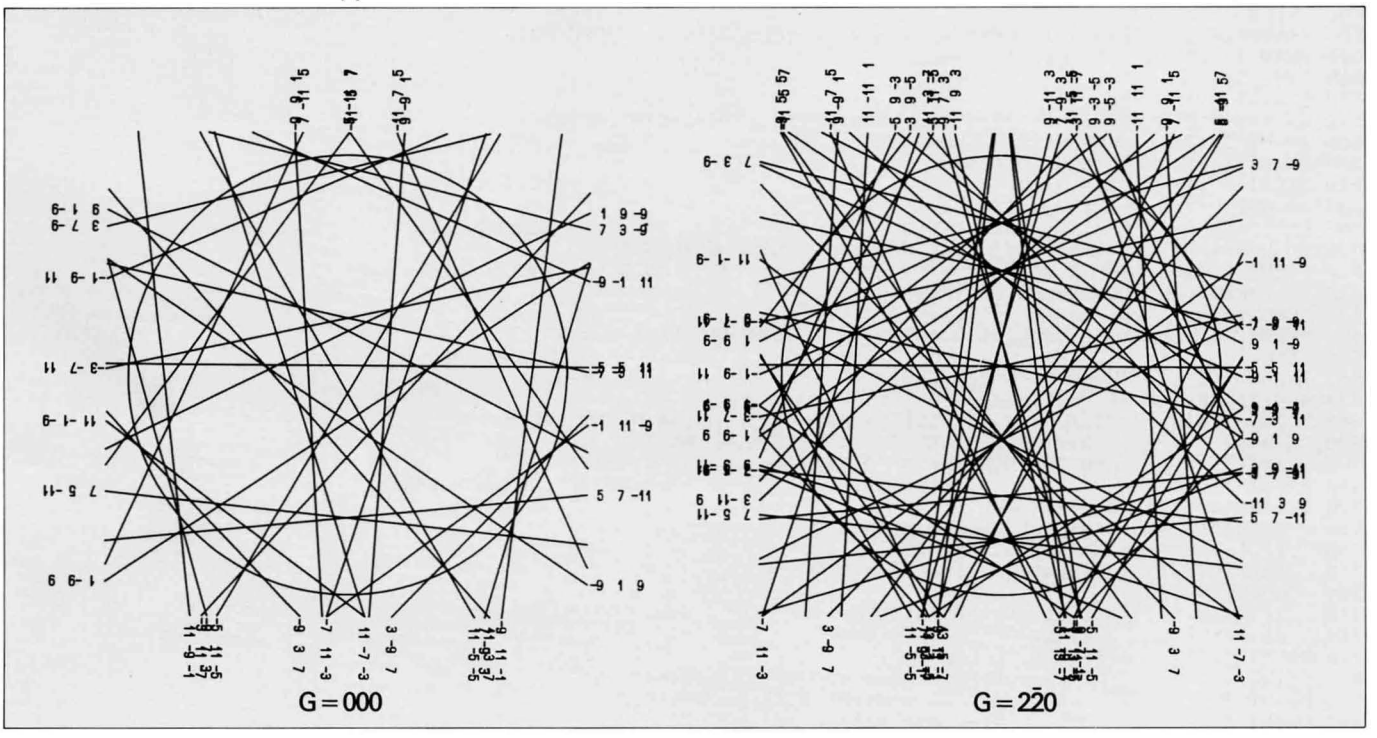

```
10 '  ***********************
20 '  ******* H O L Z *******
30 '  ***********************
40 CONSOLE 0,25,0,0
50 REM ***** definition of user function *****
60 DEF FNPARITY(X)=2*(X/2-INT(X/2))
70 DEF FNPRO(X1,X2,X3,Y1,Y2,Y3)=X1*Y1+X2*Y2+X3*Y3
80 DEF FNCS(X1,Y1,Z1,X2,Y2,Z2)=(X1*X2+Y1*Y2+Z1*Z2)/SQR((X1*X1+Y1*Y1+Z1*Z1)*(X2*X2+Y2*Y2+Z2*Z2))
90 DEF FNRL(H,K,L)=SQR((H*AST1)^2+(H*AST2+K*BST2+L*CST2)^2+(H*AST3+L*CST3)^2)
100 DEF FNXABC(H,K,L)=H*AST1+K*BST1+L*CST1
110 DEF FNYABC(H,K,L)=H*AST2+K*BST2+L*CST2
120 DEF FNZABC(H,K,L)=H*AST3+K*BST3+L*CST3
130 DEF FNPROX(X,Y,Z)=(UU*WW*X+VV*WW*Y-FA1*FA1*Z)/(FA1*FA2)
140 DEF FNPROY(X,Y,Z)=(VV*X-UU*Y)/FA1
150 DEF FNPROZ(X,Y,Z)=-(UU*X+VV*Y+WW*Z)/FA2
160 DEF FNL(X,Y,Z)=X*X+Y*Y+Z*Z
170 ' ***************************************
180 PAI#=3.14159265359#
190 OPTION BASE 1
200 DIM HCA(300),KCA(300),LCA(300),DISK(300),SO(25)
210 SCREEN 2,0:CLS 3
220 '
230 REM ************ data input ************
240 INPUT " (1)   SPECIMEN NAME                                    ";S$
250 PRINT " (2)   CRYSTAL SYSTEM"
260 PRINT "       cubic              ------------------ 1"
270 PRINT "       tetragonal         ------------------ 2"
280 PRINT "       rhombohedral"
290 PRINT "          (rhombohedral coordinates) --- 3"
300 PRINT "       hexagonal,trigonal,rhombohedral"
310 PRINT "          (hexagonal coordinates) ------ 4"
320 PRINT "       orthorhombic       ------------------ 5"
330 PRINT "       monoclinic         ------------------ 6"
340 PRINT "       triclinic          ------------------ 7"
350 PRINT "       diamond type       ------------------ 8"
360 INPUT "                                                        ";SYS
370 SYS=INT(ABS(SYS)):IF SYS>8 OR SYS=0 THEN GOTO 360
380 IF SYS=6 THEN GOSUB *SYS6
390 IF SYS=8 THEN 530
400 IF SYS=3 OR SYS=4 OR SYS=7 THEN 510
410 PRINT " (4)             primitive --------------- 1"
420 IF SYS=2 THEN 440
430 PRINT "                 face centered ----------- 2"
440 PRINT "                 body centered ----------- 3"
450 IF SYS=1 OR SYS=2 THEN 490
460 PRINT "                 A-base centered --------- 4"
470 PRINT "                 B-base centered --------- 5"
480 PRINT "                 C-base centered --------- 6"
490 INPUT "                                                  ";BRAV
500 BRAV=FIX(ABS(BRAV)):IF BRAV>6 OR BRAV=0 THEN GOTO 490 ELSE GOTO 540
510 BRAV=1            ' primitive
520 GOTO 540
530 BRAV=7
540 ON SYS GOSUB *SYS1,*SYS2,*SYS3,*SYS4,*SYS5,*SYS6,*SYS7,*SYS1
550 INPUT " (7)   ACCELERATING VOLTAGE                  E(kV) =";E
560 E=ABS(E):IF E=0 THEN GOTO 550
570 INPUT " (8)   ZONE AXIS                             U,V,W =";U,V,W
580 IF U*U+V*V+W*W=0 THEN GOTO 570
590 INPUT " (9)   EXCITE G-REFLECTION ? (y/n)                  ";GREF$
600 IF GREF$="n" OR GREF$="N" THEN HG=0:KG=0:LG=0:GOTO 660
610 INPUT " (10)  INDEX OF G                            H,K,L =";HG,KG,LG
620 IF FNPRO(U,V,W,HG,KG,LG)=0 THEN 660
630 BEEP
640 PRINT " reinput indices of G which is in the 0th Laue zone!"
650 INPUT "                                       H,K,L =";HG,KG,LG:GOTO 620
660 INPUT " (11)  ORDER OF LAUE ZONE                        N=";N
670 N=FIX(ABS(N)):IF N=0 THEN GOTO 660
680 PRINT " (12)  INDEX OF A REFLECTION ADJACENT TO THE DIRECT BEAM "
690 PRINT "        (THIS DETERMINES THE DIAMETER OF DISKS"
700 PRINT "        AND THE HORIZONTAL DIRECTION IN THE OUTPUT)"
710 INPUT "                                             H,K,L =";HAD,KAD,LAD
720 X(1)=HAD:Y(1)=KAD:Z(1)=LAD
730   IF HAD=0 AND KAD=0 AND LAD=0 THEN 750
740   IF 0=U*HAD+V*KAD+W*LAD THEN 760
750   BEEP:PRINT " reinput indices !" :GOTO 710
760  GOSUB *VECTOR
770   IF FNCS(X1,Y1,Z1,X2,Y2,Z2)=>0 THEN 790
780   X2=X2+X1:Y2=Y2+Y1:Z2=Z2+Z1:GOTO 770
790 PRINT " (13)  DIAMETER OF DISKS "
800 PRINT "          D=1 -- direct beam and above reflection "
810 PRINT "               are in contact with each other"
820 PRINT "          D<1 -- they are separated"
```

```
830 PRINT "          D>1 -- they overlap each other"
840 INPUT "                                                D=";DA
850   IF DA<0 THEN DA=-DA
860   IF DA=0 THEN DA=1
870 PRINT " (14)  Which do you want?"
880 PRINT "          HOLZ-ring ---------------------------------- 0"
890 PRINT "          HOLZ-line I (circle approximation) --------- 1"
900 PRINT "          HOLZ-line II(more accurate approximation) -- 2"
910 INPUT "                                              ";HLZ
920 OORG$="":OORG=999:HLZ=INT(ABS(HLZ)) MOD 3
930 IF HLZ=2 THEN GOTO 940 ELSE GOTO 990
940 IF GREF$="N" OR GREF$="n" THEN GOTO 990
950 INPUT "              O-disk(O) or G-disk(G)      ";OORG$
960 IF OORG$="O" OR OORG$="o" OR OORG$="G" OR OORG$="g" THEN GOTO 980
970 GOTO 950
980 IF OORG$="O" OR OORG$="o" THEN OORG=1 ELSE OORG=999
990   IF HLZ=0 THEN INTE=0:GOTO 1020
1000 INPUT "          number of step in HOLZ-line ";INTE
1010   INTE=ABS(INTE):IF INTE<10 THEN INTE=10
1020 PRINT :PRINT " (15)  Output to the PRINTER ----------------- 1"
1030 PRINT "                    PLOTTER ----------------- 2"
1040 INPUT "                                          ";PRPL
1050 PRPL=INT(ABS(PRPL)):IF PRPL>2 THEN GOTO 1040
1060 SP=0:IF PRPL=0 THEN GOTO 1040
1070      IF PRPL=1 THEN GOTO 1100
1080 INPUT "                    pen number 1-8 ";SP
1090 '************************************
1100 CLS 1:LOCATE 18,10 :PRINT "by  PHYS. DEPT. FAC OF SCI. TOHOKU UNIV."
1110 PRINT "                              T.KANEYAMA "
1120 GOSUB *ZONE
1130 '
1140 REM ********** construction of reciprocal lattice **********************
1150 DREA=SQR(1-COS(ALP)^2-COS(BET)^2-COS(GAM)^2+2*COS(ALP)*COS(BET)*COS(GAM))
1160 DREC=DREA*DREA/(SIN(ALP)*SIN(BET)*SIN(GAM))
1170 VOL=A*B*C*DREA : VOLST=1/VOL
1180 AST=B*C*SIN(ALP)/VOL:BST=C*A*SIN(BET)/VOL:CST=A*B*SIN(GAM)/VOL
1190 COA=(COS(BET)*COS(GAM)-COS(ALP))/(SIN(BET)*SIN(GAM))
1200 COB=(COS(GAM)*COS(ALP)-COS(BET))/(SIN(GAM)*SIN(ALP))
1210 COG=(COS(ALP)*COS(BET)-COS(GAM))/(SIN(ALP)*SIN(BET))
1220 SIA=DREA/(SIN(BET)*SIN(GAM)):SIB=DREA/(SIN(GAM)*SIN(ALP)):SIG=DREA/(SIN(ALP)*SIN(BET))
1230 S11ST=(BST*CST*SIA)^2:S22ST=(CST*AST*SIB)^2:S33ST=(AST*BST*SIG)^2
1240 S12ST=AST*BST*CST*CST*(COA*COB-COG):S23ST=AST*AST*BST*CST*(COB*COG-COA):S31ST=AST*BST*BST*CST*
     (COG*COA-COB)
1250 D=N*VOLST/SQR(S11ST*U*U+S22ST*V*V+S33ST*W*W+2*S12ST*U*V+2*S23ST*V*W+2*S31ST*W*U)
1260 A1=A:B1=B*COS(GAM):B2=B*DREA/SIN(BET):B3=B*(COS(ALP)-COS(BET)*COS(GAM))/SIN(BET):C1=C*COS(BET)
     :C3=C*SIN(BET)
1270 BST1=0:BST3=0:CST1=0
1280 AST1=1/A:AST2=(COS(ALP)*COS(BET)-COS(GAM))/(A*DREA*SIN(BET)):AST3=-COS(BET)/(A*SIN(BET)):BST2=SIN(BET)
     /(B*DREA):CST2=(COS(BET)*COS(GAM)-COS(ALP))/(C*DREA*SIN(BET)):CST3=1/(C*SIN(BET))
1290 ' ************************************************************************
1300 '
1310 UU=A1*U+B1*V+C1*W : VV=A2*U+B2*V+C2*W : WW=A3*U+B3*V+C3*W
1320 RD=FNRL(HAD,KAD,LAD)/2:DDA=DA*RD : DD=1.1*DDA
1330 '                  <*> 'DDA' is radius of disk
1340 FA1=SQR(UU*UU+VV*VV) : FA2=SQR(UU*UU+VV*VV+WW*WW)
1350 WN=SQR(1000*E*(1+9.788E-07*1000*E))/12.26:WN2=WN*WN
1360 '                  <*> 'WN' is wave number of electron beam
1370 RO=FNRL(HG/2,KG/2,LG/2):R=SQR(RO*RO-D*D+2*D*SQR(WN2-RO*RO))
1380 '                  <*> 'R' is radius of HOLZ-ring
1390 RR=SQR(RO*RO+2*D*SQR(WN2-RO*RO))
1400 IF UU*UU+VV*VV<.0001 THEN 1440
1410 X=FNPROX(FNXABC(HAD,KAD,LAD),FNYABC(HAD,KAD,LAD),FNZABC(HAD,KAD,LAD))
1420 Y=FNPROY(FNXABC(HAD,KAD,LAD),FNYABC(HAD,KAD,LAD),FNZABC(HAD,KAD,LAD))
1430 GOTO 1450
1440 X=FNXABC(HAD,KAD,LAD):Y=-FNYABC(HAD,KAD,LAD)
1450 CO=FNCS(1,0,0,X,Y,0):SI=FNCS(0,1,0,X,Y,0)
1460 '                  <*> 'CO' and 'SI' are direction cosign
1470 COAV12=SQR(1-FNCS(X1,Y1,Z1,X2,Y2,Z2)^2)
1480 LV1=FNRL(X1,Y1,Z1):NV1=2*(RR+DD+RO)/(LV1*COAV12)
1490 IF NV1<5 THEN NV1=5
1500 O1=0:O2=0:O3=0:I=0:V2=0:QQ=0:NQ1=0:NQ2=0:NQ3=0:NQ4=0
1510 WINXY=R+DDA*2.2
1520 IF R/DDA<10 THEN 1540
1530 WINXY=1.1*WINXY
1540 WINDOW (-WINXY,-WINXY)-(WINXY,WINXY)
1550 VIEW (205,5)-(595,395):CIRCLE(0,0),R
1560 IF GREF$="n" OR GREF$="N" THEN HGP=0:KGP=0:GOTO 1680
1570 IF UU*UU+VV*VV<.0001 THEN 1610
1580 HGPROI=FNPROX(FNXABC(HG/2,KG/2,LG/2),FNYABC(HG/2,KG/2,LG/2),FNZABC(HG/2,KG/2,LG/2))
1590 KGPROI=FNPROY(FNXABC(HG/2,KG/2,LG/2),FNYABC(HG/2,KG/2,LG/2),FNZABC(HG/2,KG/2,LG/2))
1600 GOTO 1620
1610 HGPROI=FNXABC(HG/2,KG/2,LG/2) : KGPROI=-FNYABC(HG/2,KG/2,LG/2)
```

```
1620 HGPRO=HGPROI*CO+KGPROI*SI:KGPRO=-HGPROI*SI+KGPROI*CO
1630 HGP=HGPRO:KGP=KGPRO:CIRCLE(HGPRO,KGPRO),DDA
1640 SX=MAP(-HGPRO,0)-3:SY=MAP(-KGPRO,1)-3
1650 PUT(SX,SY),KANJI(&H14F),OR
1660 SX=MAP(HGPRO,0)-3:SY=MAP(KGPRO,1)-3
1670 PUT(SX,SY),KANJI(&H147),OR
1680 CIRCLE(-HGPRO,-KGPRO),DDA
1690 CLS 1 : GOSUB *LABEL
1700 '
1710 ' ** searchig reciprocal lattice points **
1720 GOSUB *NEARZONE
1730 H=HN : K=KN : L=LN
1740 GOSUB *V1
1750 LL1=FNRL(H-HG/2,K-KG/2,L-LG/2):LL2=FNRL(H+HG/2,K+KG/2,L+LG/2)
1760 IF LL1=>RR+DDA AND LL2=>RR+DDA THEN  1790
1770 GOTO 1740
1780 '
1790 IF I=3 THEN 2030
1800 LL1=FNRL(H-HG/2,K-KG/2,L-LG/2):LL2=FNRL(H+HG/2,K+KG/2,L+LG/2)
1810 P=0:P1=0:P2=0
1820 IF LL1>RR-DDA AND LL1<RR+DDA THEN P1=1:GOTO 1850
1830 IF LL1<=RR-DDA THEN P1=2:GOTO 1850
1840 IF LL1>=RR+DDA THEN P1=3
1850 IF LL2>RR-DDA AND LL2<RR+DDA THEN P2=1:GOTO 1880
1860 IF LL2<=RR-DDA THEN P2=2:GOTO 1880
1870 IF LL2>=RR+DDA THEN P2=3
1880 IF P1=1 OR P2=1 THEN P=1:GOTO 1950
1890 IF P1=2 AND P2=2 THEN P=2:GOTO 1950
1900 P=3
1910 IF P1<>3 OR P2<>3 THEN 1940
1920 '
1930 IF P=3 AND O2<>0 THEN P=4
1940 IF P=4 THEN P4=P4+1
1950 ON P GOSUB *HOLZRING , *V2 , *MV1 , *V2
1960 IF P=1 THEN GOSUB *MV1
1970 IF P=3 AND O2=0 AND O1>NV1 THEN GOSUB *TV
1980 IF P=2 OR P=4 THEN GOTO 1740
1990 IF P=10 THEN 2030
2000 GOTO 1790
2010 ' ******************************************
2020 '
2030 IF O3=0 THEN 2190
2040 '
2050 ' ****** load the program for output ********
2060 COMMON S$,A,B,C,ALPH,BETA,GAMM
2070 COMMON U,V,W,E,N,GREF$,HG,KG,LG,HAD,KAD,LAD,OORG
2080 COMMON AST1,AST2,AST3,BST1,BST2,BST3,CST1,CST2,CST3
2090 COMMON HGP,KGP,CO,SI,DD,DDA,UU,VV,WW,FA1,FA2
2100 COMMON D,WN,WN2,R,HLZ,INTE,SP,O3,HCA(),KCA(),LCA(),DISK()
2110 COLOR 2:LOCATE 30,23:PRINT "HIT RETURN KEY":COLOR 0
2120 HRK$=INKEY$:IF HRK$="" THEN 2120
2130 CLS 3:LOCATE 30,12:PRINT "Now loading"
2140 ON PRPL GOTO 2150,2160
2150 CHAIN "CHPR"
2160 CHAIN "CHPL"
2170 ' ******************************************
2180 END
2190 LOCATE 40,3:BEEP:PRINT " You have no holz."
2200 END
2210 '
2220 '   ((((  sub routine  ))))
2230 '** data input **
2240 *SYS1 'cubic
2250 INPUT " (5)   LATTICE PARAMETERS (A°)              a=b=c= ";A
2260  B=A:C=A:ALP=PAI#/2:BET=PAI#/2:GAM=PAI#/2:ALPH=90:BETA=90:GAMM=90
2270 RETURN
2280 *SYS2 'tetragonal
2290 INPUT " (5)   LATTICE PARAMETERS (A°)                a=b= ";A
2300 INPUT "                                                c= ";C
2310  B=A:ALP=PAI#/2:BET=PAI#/2:GAM=PAI#/2:ALPH=90:BETA=90:GAMM=90
2320 RETURN
2330 *SYS3 'rhombohedral
2340 INPUT " (5)   LATTICE PARAMETERS (A°)              a=b=c= ";A
2350 INPUT " (6)                ANGLE (deg)  alpha=beta=gamma= ";ALPH
2360 B=A:C=A:ALP=ALPH*PAI#/180:BET=ALP:GAM=ALP:BETA=ALPH:GAMM=ALPH
2370 RETURN
2380 *SYS4 'hexagonal (trigonal,rhombohedral)
2390 INPUT " (5)   LATTICE PARAMETERS (A°)                a=b= ";A
2400 INPUT "                                                c= ";C
2410 INPUT "      rhombohedral ? (y/n)                        ";RH$
2420  B=A:ALP=PAI#/2:BET=PAI#/2:GAM=2*PAI#/3:ALPH=90:BETA=90:GAMM=120
2430 RETURN
```

```
2440 *SYS5 'orthorhombic
2450 INPUT " (5)   LATTICE PARAMETERS (A° )                    a= ";A
2460 INPUT "                                                   b= ";B
2470 INPUT "                                                   c= ";C
2480 ALP=PAI#/2:BET=PAI#/2:GAM=PAI#/2:ALPH=90:BETA=90:GAMM=90
2490 RETURN
2500 *SYS6 'monoclinic
2510 INPUT " (3)      UNIQUE AXIS,B or C ?                       ";UNIQ$
2520 IF UNIQ$="B" OR UNIQ$="b" OR UNIQ$="C" OR UNIQ$="c" THEN 2540
2530 GOTO 2510
2540 PRINT " (4)          primitive -------------- 1"
2550 IF UNIQ$="b" OR UNIQ$="B" THEN 2580
2560 PRINT "              B-base centered -------- 2"
2570 GOTO 2590
2580 PRINT "              C-base centered -------- 3"
2590 INPUT "                                                   ";BRAV
2600 INPUT " (5)   LATTICE PARAMETERS (A° )                    a= ";A
2610 INPUT "                                                   b= ";B
2620 INPUT "                                                   c= ";C
2630 IF UNIQ$="c" OR UNIQ$="C" THEN 2660
2640 INPUT " (6)                ANGLE (deg)              beta= ";BETA:GAMM=90
2650 GOTO 2670
2660 INPUT " (6)                ANGLE (deg)             gamma= ";GAMM:BETA=90
2670 ALP=PAI#/2:BET=BETA*PAI#/180:GAM=GAMM*PAI#/180:ALPH=90
2680 IF BRAV=2 THEN BRAV=5
2690 IF BRAV=3 THEN BRAV=6
2700 RETURN 550
2710 *SYS7 'tricrinic
2720 INPUT " (5)   LATTICE PARAMETERS (A° )                    a= ";A
2730 INPUT "                                                   b= ";B
2740 INPUT "                                                   c= ";C
2750 INPUT " (6)                ANGLE (deg)             alpha= ";ALPH
2760 INPUT "                                             beta= ";BETA
2770 INPUT "                                            gamma= ";GAMM
2780 ALP=ALPH*PAI#/180:BET=BETA*PAI#/180:GAM=GAMM*PAI#/180
2790 RETURN
2800 '
2810 *LABEL ' ** labeling **
2820 LOCATE 2,2:PRINT S$:PRINT
2830 PRINT "  [";U;" ";V;" ";W;"]":PRINT
2840 PRINT "     "E;"kV":PRINT
2850 PRINT "  ";N;
2860 IF N>3 THEN 2910
2870 ON N GOTO 2880,2890,2900
2880 PRINT "st Laue Zone":GOTO 2920
2890 PRINT "nd Laue Zone":GOTO 2920
2900 PRINT "rd Laue Zone":GOTO 2920
2910 PRINT "th Laue Zone"
2920 PRINT
2930 IF GREF$="n" OR GREF$="N" THEN 2960
2940 PRINT " G reflection :"
2950 PRINT "     (";HG;" ";KG;" ";LG;")"
2960 PRINT :PRINT "  a =";A;"(A)":PRINT "  b =";B;"(A)":PRINT "  c =";C;"(A)"
2970 PRINT "  alpha,beta,gamma ":PRINT "  =";ALPH;",";BETA;",";GAMM;"(deg)"
2980 PRINT : PRINT " Radius of N-th Laue Zone"
2990 PRINT "  =";R;"(1/A)"
3000 PRINT " Horizontal Direction"
3010 PRINT "  = [";HAD;",";KAD;",";LAD;"]*"
3020 RETURN
3030 '
3040 *ZONE'* seach the reciprocal lattice point allowed by extinction rule *
3050 NZNE=1
3060 FOR H=-NZNE TO NZNE
3070 FOR K=-NZNE TO NZNE
3080 FOR L=-NZNE TO NZNE
3090 IF U*H+V*K+W*L=N THEN 3140
3100 NEXT:NEXT:NEXT
3110 NZNE=NZNE+2
3120 IF NZNE>=15 THEN GOTO 3160
3130 GOTO 3060
3140 HN=H:KN=K:LN=L
3150 RETURN
3160 PRINT " cannot find N-th laue zone"
3170 PRINT " indices of reciprocal lattice point in the N-th Laue zone"
3180 INPUT "                                              h,k,l=";H,K,L
3190 IF FNPRO(H,K,L,U,V,W)=N THEN 3140
3200 PRINT "  reinput indices":GOTO 3180
3210 '
3220 *NEARZONE
3230 NRLO=FNRL(HN,KN,LN)
3240 FOR NHN1=-1 TO 1
3250 FOR NHN2=-1 TO 1
```

```
3260 IF NHN1=0 AND NHN2=0 THEN GOTO 3330
3270 H=HN+X1*NHN1+X2*NHN2
3280 K=KN+Y1*NHN1+Y2*NHN2
3290 L=LN+Z1*NHN1+Z2*NHN2
3300 NRL1=FNRL(H,K,L)
3310 IF NRL1>=NRL0 THEN GOTO 3330
3320 HN=H:KN=K:LN=L:GOTO *NEARZONE
3330 NEXT:NEXT
3340 RETURN
3350 '
3360 *V2
3370 GOSUB *V1
3380 LL1=FNRL(H-HG/2,K-KG/2,L-LG/2)
3390 LL2=FNRL(H+HG/2,K+KG/2,L+LG/2)
3400 IF LL1>RR+DDA AND LL2>RR+DDA THEN 3420
3410 GOTO 3370
3420 H=H+X2*(-1)^I:K=K+Y2*(-1)^I:L=L+Z2*(-1)^I:O1=0:O2=0
3430 RETURN
3440 *MV1
3450 H=H-X1*(-1)^I:K=K-Y1*(-1)^I:L=L-Z1*(-1)^I:O1=O1+1
3460 RETURN
3470 *V1
3480 H=H+X1*(-1)^I : K=K+Y1*(-1)^I : L=L+Z1*(-1)^I
3490 RETURN
3500 *TV
3510 I=I+1
3520 H=H+(P4+1)*X2*(-1)^I : K=K+(P4+1)*Y2*(-1)^I : L=L+(P4+1)*Z2*(-1)^I
3530 IF FNRL(H-HG/2,K-KG/2,L-LG/2)<=RR+DDA THEN 3590
3540 LL1=FNRL(H-HG/2,K-KG/2,L-LG/2):LL2=FNRL(H+HG/2,K+KG/2,L+LG/2)
3550 IF LL1<=RR+DDA AND LL2<=RR+DDA THEN 3590
3560 IF NORI>NV1*2 THEN O3=O3+1:P=10:RETURN
3570 NORI=NORI+1:GOSUB *MV1
3580 GOTO 3530
3590 O1=0:O2=0:P=2:P4=0:NORI=0
3600 RETURN
3610 '
3620 *VECTOR' ** calculate two seaching vector **
3630 FOR I=1 TO 25
3640 READ SO(I):NEXT I
3650 X=U:Y=V:Z=W:GOSUB *SOS:U=X:V=Y:W=Z
3660 X(2)=V*Z(1)-W*Y(1):Y(2)=W*X(1)-U*Z(1):Z(2)=U*Y(1)-V*X(1)
3670 FOR J=1 TO 2
3680 X=X(J):Y=Y(J):Z=Z(J)
3690 GOSUB *SOS
3700 X(J)=X:Y(J)=Y:Z(J)=Z
3710 NEXT J
3720 *VECTOR2
3730 X1A=X(1):Y1A=Y(1):Z1A=Z(1)
3740 X2A=X(2):Y2A=Y(2):Z2A=Z(2)
3750 LV1=FNL(X1A,Y1A,Z1A)
3760 LV2=FNL(X2A,Y2A,Z2A)
3770 FOR V1=-2 TO 2
3780 X(2)=X2A+X(1)*V1:Y(2)=Y2A+Y(1)*V1:Z(2)=Z2A+Z(1)*V1
3790       X=X(2):Y=Y(2):Z=Z(2):GOSUB *SOS:X(2)=X:Y(2)=Y:Z(2)=Z
3800   IF LV2>FNL(X(2),Y(2),Z(2)) THEN GOTO 3740
3810 NEXT V1
3820 X(2)=X2A:Y(2)=Y2A:Z(2)=Z2A
3830 '
3840 X1A=X(1):Y1A=Y(1):Z1A=Z(1)
3850 LV1=FNL(X1A,Y1A,Z1A)
3860 LV2=FNL(X2A,Y2A,Z2A)
3870 FOR V2=-2 TO 2
3880 X(1)=X1A+X(2)*V2:Y(1)=Y1A+Y(2)*V2:Z(1)=Z1A+Z(2)*V2
3890       X=X(1):Y=Y(1):Z=Z(1):GOSUB *SOS:X(1)=X:Y(1)=Y:Z(1)=Z
3900   IF LV1>FNL(X(1),Y(1),Z(1)) THEN GOTO 3840
3910 NEXT V2
3920 X(1)=X1A:Y(1)=Y1A:Z(1)=Z1A
3930 X1=X(1):Y1=Y(1):Z1=Z(1):X2=X(2):Y2=Y(2):Z2=Z(2)
3940 RETURN
3950 '
3960 DATA 2,3,5,7,11,13,17,19,23,29,31,37,41,43
3970 DATA 47,53,59,61,67,71,73,79,83,89,97
3980 *SOS
3990 FOR I=1 TO 6
4000 XX=X-SO(I)*INT(X/SO(I)):YY=Y-SO(I)*INT(Y/SO(I))
4010 ZZ=Z-SO(I)*INT(Z/SO(I))
4020 IF XX=0 AND YY=0 AND ZZ=0 THEN GOTO 4030 ELSE GOTO 4040
4030 X=X/SO(I):Y=Y/SO(I):Z=Z/SO(I):SO2=1:GOTO 4000
4040 NEXT I
4050 IF X>16 OR Y>16 OR Z>16 THEN 4070 ELSE RETURN
4060 '
4070 FOR I=7 TO 12
```

```
4080 XX=X-SO(I)*INT(X/SO(I)):YY=Y-SO(I)*INT(Y/SO(I))
4090 ZZ=Z-SO(I)*INT(Z/SO(I))
4100 IF XX<>0 OR YY<>0 OR ZZ<>0 THEN 4120
4110 X=X/SO(I):Y=Y/SO(I):Z=Z/SO(I):SO2=1:GOTO 4080
4120 NEXT I
4130 IF X>40 OR Y>40 OR Z>40 THEN 4150 ELSE RETURN
4140 '
4150 FOR I=13 TO 25
4160 XX=X-SO(I)*INT(X/SO(I)):YY=Y-SO(I)*INT(Y/SO(I))
4170 ZZ=Z-SO(I)*INT(Z/SO(I))
4180 IF XX<>0 OR YY<>0 OR ZZ<>0 THEN 4200
4190 X=X/SO(I):Y=Y/SO(I):Z=Z/SO(I):SO2=1:GOTO 4160
4200 NEXT I
4210 IF X=0 AND Y=0 THEN Z=SGN(Z):RETURN
4220 IF Y=0 AND Z=0 THEN X=SGN(X):RETURN
4230 IF Z=0 AND X=0 THEN Y=SGN(Y):RETURN
4240 RETURN
4250 '
4260 ' ** extinction rule **          AL=0:allowed    AL#0:forbidden
4270 *DIAMOND
4280 IF 1=FNPARITY(H+K) OR 1=FNPARITY(K+L) THEN 4320
4290 IF 1=FNPARITY(H) THEN 4310
4300 IF 1=FNPARITY((H+K+L)/2) THEN 4320
4310 AL=0:RETURN
4320 AL=1:RETURN
4330 *I ' body centered
4340 AL=FNPARITY(H+K+L)
4350 RETURN
4360 *P ' primitive
4370 AL=0
4380 RETURN
4390 *F ' face centered
4400 AL=FNPARITY(H+K)+FNPARITY(K+L)
4410 RETURN
4420 *A ' A-base centered
4430 AL=FNPARITY(K+L)
4440 RETURN
4450 *B ' B-base centered
4460 AL=FNPARITY(H+L)
4470 RETURN
4480 *C ' C-base centered
4490 AL=FNPARITY(H+K)
4500 RETURN
4510 *RHOMBO ' rhombohedral (hexagonal coodinates)
4520 AL=3*((-H+K+L)/3-INT((-H+K+L)/3))
4530 RETURN
4540 '
4550 *HOLZRING ' ** draw HOLZRING pattern **
4560 O1=0 : O2=O2+1
4570 ON BRAV GOSUB *P,*F,*I,*A,*B,*C,*DIAMOND
4580 IF RH$="Y" OR RH$="y" THEN GOSUB *RHOMBO
4590 IF AL<>0 THEN 4790
4600 O3=O3+1
4610 HCA(O3)=H : KCA(O3)=K : LCA(O3)=L
4620 IF O3=0 OR O3=1 THEN 4640
4630 IF (HCA(O3)-HCA(1))^2<.1 AND (KCA(O3)-KCA(1))^2<.1 AND (LCA(O3)-LCA(1))^2<.1 AND I=2 THEN
     P=10:GOTO 4790
4640 DISK(O3)=1
4650 IF P1<>1 THEN DISK(O3)=0:RETURN
4660 IF P2=1 THEN DISK(O3)=2
4670 IF UU*UU+VV*VV<.0001 THEN 4710
4680 XI=FNPROX(FNXABC(H-HG/2,K-KG/2,L-LG/2),FNYABC(H-HG/2,K-KG/2,L-LG/2),FNZABC(H-HG/2,K-KG/2,L-LG/2))
4690 YI=FNPROY(FNXABC(H-HG/2,K-KG/2,L-LG/2),FNYABC(H-HG/2,K-KG/2,L-LG/2),FNZABC(H-HG/2,K-KG/2,L-LG/2))
4700 GOTO 4720
4710 XI=FNXABC(H-HG/2,K-KG/2,L-LG/2):YI=-FNYABC(H-HG/2,K-KG/2,L-LG/2)
4720 X=XI*CO+YI*SI:Y=-XI*SI+YI*CO:CIRCLE(X,Y),DDA
4730 SHKL$=STR$(O3):LHKL=LEN(SHKL$)
4740 SX=MAP(X,0)-3:SY=MAP(Y,1)-3
4750 FOR I1=1 TO LHKL
4760 MHKL$=MID$(SHKL$,I1,1):MHKL=ASC(MHKL$)+256
4770 PUT (SX-4*LHKL+8*(I1-1),SY),KANJI(MHKL),OR
4780 NEXT I1
4790 RETURN
4800 '
4810 END
```

CHPR

```
10 REM FILE NAME "CHPR"
20 '  *** output HOLZ for printer ***
30 '
40 '  This program will be chained from program "HOLZ" and ·····
```

```
50 '    (1)get hard-copy of CRT screen
60 '    (2)print out Miller indices' list of excited reflections.
70 '
80 CONSOLE ,,0
90 DEF FNPRO(X1,X2,X3,Y1,Y2,Y3)=X1*Y1+X2*Y2+X3*Y3
100 DEF FNRL(H,K,L)=SQR((H*AST1)^2+(H*AST2+K*BST2+L*CST2)^2+(H*AST3+L*CST3)^2)
110 DEF FNXABC(H,K,L)=H*AST1+K*BST1+L*CST1
120 DEF FNYABC(H,K,L)=H*AST2+K*BST2+L*CST2
130 DEF FNZABC(H,K,L)=H*AST3+K*BST3+L*CST3
140 DEF FNPROX(X,Y,Z)=(UU*WW*X+VV*WW*Y-FA1*FA1*Z)/(FA1*FA2)
150 DEF FNPROY(X,Y,Z)=(VV*X-UU*Y)/FA1
160 DEF FNPROZ(X,Y,Z)=-(UU*X+VV*Y+WW*Z)/FA2
170 DEF FNL(X,Y,Z)=X*X+Y*Y+Z*Z
180 '
190 I=0 :HGPRO=HGP:KGPRO=KGP: CLS 3
200 IF HLZ=0 THEN GOSUB *HOLZRING2
210 XX1=DD*1.05
220 XX4=-XX1:XX5=-XX1:XX8=XX1:YY2=-XX1:YY3=-XX1:YY6=XX1:YY7=XX1
230 INDX=4*DD/240 : INDY=28*DD/240
240 XY1=-DD*5/3-INDY/2
250 XY4=XY1:XY5=-XY1-2.1*INDY:XY8=XY5
260 NQ1=0:NQ4=0:NQ5=0:NQ8=0
270 ON HLZ GOSUB *HOLZ,*HOLZ2
280 GOSUB *POUT:CLS 3
290 PRINT " (14)  Which do you want?"
300 PRINT "           HOLZRING ------------------------------ 0"
310 PRINT "           HOLZ I (circle approximation) --------- 1"
320 PRINT "           HOLZ II(more accurate approximation) -- 2"
330 PRINT "               E    N    D          ---------------- 3"
340 INPUT "                                        ";HLZ
350 OORG=999
360 HLZ=INT(ABS(HLZ)):IF HLZ>3 THEN GOTO 340
370 IF HLZ=2 THEN GOTO 380 ELSE GOTO 430
380 IF GREF$="N" OR GREF$="n" THEN GOTO 430
390 INPUT "                0-disk(0) or G-disk(G) ";OORG$
400 IF OORG$="0" OR OORG$="o" OR OORG$="G" OR OORG$="g" THEN GOTO 420
410 GOTO 390
420 IF OORG$="0" OR OORG$="o" THEN OORG=1 ELSE OORG=999
430 IF HLZ=3 THEN 660
440 IF HLZ=0 THEN 470
450 INPUT "          number of step in HOLZ line ";INTE
460 INTE=ABS(INTE) :IF INTE<10 THEN INTE=10
470 PRINT " (15)  Output to the PRINTER ----------------- 1"
480 PRINT "                     PLOTTER ----------------- 2"
490 INPUT "                                        ";PRPL
500 PRPL=INT(ABS(PRPL)):IF PRPL>2 THEN GOTO 490
510 IF PRPL=0 THEN GOTO 490
520 IF PRPL=1 THEN CLS 1:GOTO 200
530 INPUT "                        pen number 1-8  ";SP
540 SP=INT(ABS(SP)):IF SP>8 THEN GOTO 530
550 CLS 1:COLOR 2:PRINT "    Ready the plotter"
560 COMMON S$,A,B,C,ALPH,BETA,GAMM
570 COMMON U,V,W,E,N,GREF$,HG,KG,LG,HAD,KAD,LAD,OORG
580 COMMON AST1,AST2,AST3,BST1,BST2,BST3,CST1,CST2,CST3
590 COMMON HGP,KGP,CO,SI,DD,DDA,UU,VV,WW,FA1,FA2
600 COMMON D,WN,WN2,R,HLZ,INTE,SP,O3,HCA(),KCA(),LCA(),DISK()
610 PRINT:PRINT "  Hit return key to start":COLOR 0
620 HRK$=INKEY$:IF HRK$="" THEN 620
630 CLS 1:LOCATE 30,10:PRINT "Now loading"
640 CHAIN "CHPL"
650 GOTO 200
660 CLS 1:END
670 '
680 *LABEL ' ** labeling **
690 LOCATE 2,2:PRINT S$:PRINT
700 PRINT "  ["U" "V" "W"]":PRINT
710 PRINT "     "E;"kV":PRINT
720 PRINT "  ";N;
730 IF N>3 THEN 780
740 ON N GOTO 750,760,770
750 PRINT "st Laue Zone":GOTO 790
760 PRINT "nd Laue Zone":GOTO 790
770 PRINT "rd Laue Zone":GOTO 790
780 PRINT "th Laue Zone"
790 PRINT
800 IF GREF$="n" OR GREF$="N" THEN 830
810 PRINT " G reflection :"
820 PRINT "     ("HG" "KG" "LG")"
830 PRINT :PRINT "  a ="A"(A)":PRINT "  b ="B"(A)":PRINT "  c ="C"(A)"
840 PRINT "  alpha,beta,gamma ":PRINT "  ="ALPH","BETA","GAMM"(deg)"
850 PRINT : PRINT " Radius of HOLZ-ring"
860 PRINT "  =";R;"(1/A)"
```

```
870 PRINT " Horizontal Direction"
880 PRINT "  = [";HAD;",";KAD;",";LAD;"]*"
890 RETURN
900 '
910 *HOLZ'** draw K-M line by circle approximation **
920 WINDOW (-DD,-DD)-(DD,DD):VIEW (200,80)-(440,320)
930 CIRCLE(0,0),DDA
940 IF R/DDA>100 THEN GOTO *HOLZ100
950 FOR IJ=1 TO 03-1
960 IF DISK(IJ)=0 THEN 1080
970 H=HCA(IJ):K=KCA(IJ):L=LCA(IJ)
980 WINDOW (-DD,-DD)-(DD,DD):VIEW (200,80)-(440,320)
990 IF UU*UU+VV*VV<.0001 THEN 1030
1000 XI=FNPROX(FNXABC(H-HG/2,K-KG/2,L-LG/2),FNYABC(H-HG/2,K-KG/2,L-LG/2),FNZABC(H-HG/2,K-KG/2,L-LG/2))
1010 YI=FNPROY(FNXABC(H-HG/2,K-KG/2,L-LG/2),FNYABC(H-HG/2,K-KG/2,L-LG/2),FNZABC(H-HG/2,K-KG/2,L-LG/2))
1020 GOTO 1040
1030 XI=FNXABC(H-HG/2,K-KG/2,L-LG/2):YI=-FNYABC(H-HG/2,K-KG/2,L-LG/2)
1040 X=XI*CO+YI*SI:Y=-XI*SI+YI*CO:CIRCLE(-X,-Y),R
1050 WINDOW (-DD*8/3,-DD*5/3)-(DD*8/3,DD*5/3)
1060 VIEW (0,0)-(639,399)
1070 GOSUB *INDEXING
1080 NEXT IJ
1090 RETURN
1100 *HOLZ100
1110 IF INTE=0 THEN INTE=10
1120 ANGRAN=SQR(2)*DD/R:SANG=2*ANGRAN/INTE
1130 FOR IJ=1 TO 03-1
1140 IN=0:INA=0
1150 IF DISK(IJ)=0 THEN 1700
1160 H=HCA(IJ):K=KCA(IJ):L=LCA(IJ)
1170 WINDOW (-DD,-DD)-(DD,DD):VIEW (200,80)-(440,320)
1180 IF UU*UU+VV*VV<.0001 THEN 1220
1190 XI=FNPROX(FNXABC(H-HG/2,K-KG/2,L-LG/2),FNYABC(H-HG/2,K-KG/2,L-LG/2),FNZABC(H-HG/2,K-KG/2,L-LG/2))
1200 YI=FNPROY(FNXABC(H-HG/2,K-KG/2,L-LG/2),FNYABC(H-HG/2,K-KG/2,L-LG/2),FNZABC(H-HG/2,K-KG/2,L-LG/2))
1210 GOTO 1230
1220 XI=FNXABC(H-HG/2,K-KG/2,L-LG/2):YI=-FNYABC(H-HG/2,K-KG/2,L-LG/2)
1230 X=XI*CO+YI*SI:Y=-XI*SI+YI*CO
1240 IF X=0 THEN 1280
1250 T=ATN(Y/X)*180/PAI#+90*(1-ABS(X)/X)
1260 T=T-360*(INT((T+360)/360)-1)
1270 P=INT((T+45)/90):P=P-4*INT(P/4):GOTO 1300
1280 IF Y>0 THEN T=90:P=1:GOTO 1300
1290 T=270:P=3
1300 FU1=R*R-(X+DD)*(X+DD):FU2=R*R-(X-DD)*(X-DD)
1310 FU3=R*R-(Y+DD)*(Y+DD):FU4=R*R-(Y-DD)*(Y-DD)
1320 ON P+1 GOTO 1330,1390,1450,1510
1330 KXS=-X+SQR(FU3):KYS=DD:KXL=-X+SQR(FU4):KYL=-DD:ANGSL=-1
1340 IF KXS>DD  THEN KXS=DD :KYS=-Y-SQR(FU1)
1350 IF KXS<-DD THEN KXS=-DD:KYS=-Y+SQR(FU2)
1360 IF KXL>DD  THEN KXL=DD :KYL=-Y+SQR(FU1)
1370 IF KXL<-DD THEN KXL=-DD:KYL=-Y-SQR(FU2)
1380 GOTO 1570
1390 KXS=DD:KYS=-Y+SQR(FU1):KXL=-DD:KYL=-Y+SQR(FU2):ANGSL=1
1400 IF KYS>DD  THEN KXS=-X-SQR(FU3):KYS=DD
1410 IF KYS<-DD THEN KXS=-X+SQR(FU4):KYS=-DD
1420 IF KYL>DD  THEN KXL=-X+SQR(FU3):KYL=DD
1430 IF KYL<-DD THEN KXL=-X-SQR(FU4):KYL=-DD
1440 GOTO 1570
1450 KXS=-X-SQR(FU3):KYS=DD:KXL=-X-SQR(FU4):KYL=-DD:ANGSL=1
1460 IF KXS>DD  THEN KXS=DD :KYS=-Y+SQR(FU1)
1470 IF KXS<-DD THEN KXS=-DD:KYS=-Y-SQR(FU2)
1480 IF KXL>DD  THEN KXL=DD :KYL=-Y-SQR(FU1)
1490 IF KXL<-DD THEN KXL=-DD:KYL=-Y+SQR(FU2)
1500 GOTO 1570
1510 KXS=DD:KYS=-Y-SQR(FU1):KXL=-DD:KYL=-Y-SQR(FU2):ANGSL=-1
1520 IF KYS>DD  THEN KXS=-X+SQR(FU3):KYS=DD
1530 IF KYS<-DD THEN KXS=-X-SQR(FU4):KYS=-DD
1540 IF KYL>DD  THEN KXL=-X-SQR(FU3):KYL=DD
1550 IF KYL<-DD THEN KXL=-X+SQR(FU4):KYL=-DD
1560 '
1570 PSET(KXS,KYS)
1580 FOR ANG=-ANGRAN TO ANGRAN STEP SANG
1590 ANGLE=T*PAI#/180+ANG*ANGSL
1600 XPLOT=R*COS(ANGLE)-X:YPLOT=R*SIN(ANGLE)-Y
1610 IF ABS(XPLOT)>DD OR ABS(YPLOT)>DD THEN 1630
1620 LINE -(XPLOT,YPLOT):IN=1
1630 NEXT ANG
1640 IF IN=0 THEN 1700
1650 LINE -(KXL,KYL)
1660 '
1670 WINDOW (-DD*8/3,-DD*5/3)-(DD*8/3,DD*5/3)
1680 VIEW (0,0)-(639,399)
```

```
1690 GOSUB *INDEXING
1700 NEXT IJ
1710 RETURN
1720 '
1730 *INDEXING ' ** index on the K-M pattern **
1740 IF X=0 AND Y>0 THEN P=3 : GOTO *SEP
1750 IF X=0 AND Y<0 THEN P=7 : GOTO *SEP
1760 IF X>0 AND Y=0 THEN P=4 : GOTO *SEP
1770 IF X<0 AND Y=0 THEN P=1 : GOTO *SEP
1780 RAT=Y/X
1790 IF RAT>-1 AND RAT<0 AND X<0 THEN P=1 : GOTO *SEP
1800 IF RAT<=-1          AND X<0 THEN P=2 : GOTO *SEP
1810 IF RAT>=1           AND X>0 THEN P=3 : GOTO *SEP
1820 IF RAT>0  AND RAT<1 AND X>0 THEN P=4 : GOTO *SEP
1830 IF RAT>-1 AND RAT<0 AND X>0 THEN P=5 : GOTO *SEP
1840 IF RAT<=-1          AND X>0 THEN P=6 : GOTO *SEP
1850 IF RAT>=1           AND X<0 THEN P=7 : GOTO *SEP
1860 IF RAT>0  AND RAT<1 AND X<0 THEN P=8 : GOTO *SEP
1870 BEEP:RETURN
1880 *SEP
1890 IF HLZ=2 THEN 1930
1900 FU1=R*R-(X+DD)*(X+DD):FU2=R*R-(X-DD)*(X-DD):FU3=R*R-(Y+DD)*(Y+DD):FU4=R*R-(Y-DD)*(Y-DD)
1910 ON P GOSUB *P1,*P2,*P3,*P4,*P5,*P6,*P7,*P8
1920 GOTO 1940
1930 GOSUB *SEP2
1940 ON Q GOSUB *Q1,*Q2,*Q3,*Q4,*Q5,*Q6,*Q7,*Q8
1950 RETURN
1960 *SEP2
1970 ON P GOTO 1980,2050,2120,1980,2190,2120,2050,2190
1980 EKS=KXS:WAI=KYS '                    P=1,4
1990 IF ABS(WAI)<DD THEN GOTO 2020
2000 IF EKS<0 THEN Q=6 ELSE Q=7
2010 RETURN
2020 EKS=KXL:WAI=KYL
2030 IF EKS>0 THEN Q=2 ELSE Q=3
2040 RETURN
2050 EKS=KXS:WAI=KYS '                    P=2,7
2060 IF ABS(EKS)<DD THEN GOTO 2090
2070 IF WAI>0 THEN Q=8 ELSE Q=1
2080 RETURN
2090 EKS=KXL:WAI=KYL
2100 IF WAI<0 THEN Q=4 ELSE Q=5
2110 RETURN
2120 EKS=KXL:WAI=KYL '                    P=3,6
2130 IF ABS(EKS)<DD THEN GOTO 2160
2140 IF WAI<0 THEN Q=4 ELSE Q=5
2150 RETURN
2160 EKS=KXS:WAI=KYS
2170 IF WAI>0 THEN Q=8 ELSE Q=1
2180 RETURN
2190 EKS=KXL:WAI=KYL '                    P=5,8
2200 IF ABS(WAI)<DD THEN GOTO 2230
2210 IF EKS>0 THEN Q=2 ELSE Q=3
2220 RETURN
2230 EKS=KXS:WAI=KYS
2240 IF EKS<0 THEN Q=6 ELSE Q=7
2250 RETURN
2260 '
2270 *P1
2280 IF FU4<0 THEN 2320
2290 EKS=-X-FU4^.5:IF ABS(EKS)>DD THEN 2320
2300 IF EKS>=0 THEN Q=2 ELSE Q=3
2310 RETURN
2320 EKS=-X-FU3^.5:IF EKS>0 THEN Q=7 ELSE Q=6
2330 RETURN
2340 *P2
2350 IF FU1<0 THEN 2390
2360 WAI=-Y+FU1^.5:IF ABS(WAI)>DD THEN 2390
2370 IF WAI<0 THEN Q=1 ELSE Q=8
2380 RETURN
2390 WAI=-Y+FU2^.5:IF WAI=<0 THEN Q=4 ELSE Q=5
2400 RETURN
2410 *P3
2420 IF FU2<0 THEN 2460
2430 WAI=-Y+FU2^.5: IF ABS(WAI)>DD THEN 2460
2440 IF WAI<=0 THEN Q=4 ELSE Q=5
2450 RETURN
2460 WAI=-Y+FU1^.5:IF WAI<0 THEN Q=1 ELSE Q=8
2470 RETURN
2480 *P4
2490 IF FU4<0 THEN 2530
2500 EKS=-X+FU4^.5:IF ABS(EKS)>DD THEN 2530
```

```
2510 IF EKS>0 THEN Q=2 ELSE Q=3
2520 RETURN
2530 EKS=-X+FU3^.5:IF EKS>0 THEN Q=7 ELSE Q=6
2540 RETURN
2550 *P5
2560 IF FU3<0 THEN 2600
2570 EKS=-X+FU3^.5:IF ABS(EKS)>DD THEN 2600
2580 IF EKS>0 THEN Q=7 ELSE Q=6
2590 RETURN
2600 EKS=-X+FU4^.5:IF EKS>0 THEN Q=2 ELSE Q=3
2610 RETURN
2620 *P6
2630 IF FU2<0 THEN 2670
2640 WAI=-Y-FU2^.5:IF ABS(WAI)>DD THEN 2670
2650 IF WAI<0 THEN Q=4 ELSE Q=5
2660 RETURN
2670 WAI=-Y-FU1^.5:IF WAI<0 THEN Q=1 ELSE Q=8
2680 RETURN
2690 *P7
2700 IF FU1<0 THEN 2740
2710 WAI=-Y-FU1^.5:IF ABS(WAI)>DD THEN 2740
2720 IF WAI<0 THEN Q=1 ELSE Q=8
2730 RETURN
2740 WAI=-Y-FU2^.5:IF WAI<0 THEN Q=4 ELSE Q=5
2750 RETURN
2760 *P8
2770 IF FU3<0 THEN 2810
2780 EKS=-X-FU3^.5:IF ABS(EKS)>DD THEN 2810
2790 IF EKS>0 THEN Q=7 ELSE Q=6
2800 RETURN
2810 EKS=-X-FU4^.5:IF EKS>0 THEN Q=2 ELSE Q=3
2820 RETURN
2830 '
2840 *POUT ' ** print out **
2850 LPRINT
2860 IF HLZ=0 THEN 3040
2870 IF N=>4 THEN 2890
2880 ON N GOTO 2900,2910,2920
2890 LPRINT "  *"S$"    ["U""V""W"]    "N"th zone    "E"kV":GOTO 2930
2900 LPRINT "  *"S$"    ["U""V""W"]     1 st zone    "E"kV":GOTO 2930
2910 LPRINT "  *"S$"    ["U""V""W"]     2 nd zone    "E"kV":GOTO 2930
2920 LPRINT "  *"S$"    ["U""V""W"]     3 rd zone    "E"kV"
2930 IF GREF$="n" OR GREF$="N" THEN 2990
2940 '
2950 IF OORG=1 THEN 2960 ELSE 2970
2960 LPRINT "      0 0 0 disk";:GOTO 2980
2970 LPRINT "     ";HG;KG;LG;"disk";
2980 LPRINT " (";HG;KG;LG;"excitation )":GOTO 3000
2990 LPRINT "      0 0 0 disk"
3000 LPRINT "       a =";A;"A";" ,b =";B;"A";" ,c =";C;"A"
3010 LPRINT "       alpha,beta,gamma=";ALPH;",";BETA;",";GAMM;"deg"
3020 LPRINT "     Radius of HOLZ-ring =";R;"(1/A)"
3030 LPRINT "     Horizontal Direction = [";HAD;",";KAD;",";LAD;"]*"
3040 COPY 3
3050 LPRINT "   * indices list *"
3060 JI=FIX((O3-1)/3)+1
3070 FOR IJ=1 TO JI
3080 IF IJ+JI>O3-1 THEN 3120
3090 IF IJ+JI*2>O3-1 THEN 3110
3100 LPRINT IJ"-"" ("HCA(IJ)","KCA(IJ)","LCA(IJ)")", IJ+JI"-"" ("HCA(IJ+JI)","KCA(IJ+JI)","LCA(IJ+JI)")",
     IJ+JI*2"-"" ("HCA(IJ+JI*2)","KCA(IJ+JI*2)","LCA(IJ+JI*2)")":GOTO 3130
3110 LPRINT IJ"-"" ("HCA(IJ)","KCA(IJ)","LCA(IJ)")", IJ+JI"-"" ("HCA(IJ+JI)","KCA(IJ+JI)","LCA(IJ+JI)")"
     :GOTO 3130
3120 LPRINT IJ"-"" ("HCA(IJ)","KCA(IJ)","LCA(IJ)")"
3130 NEXT IJ
3140 RETURN
3150 '
3160 *HOLZRING2 '** draw HOLZRING pattern **
3170 WINXY=R+DDA*2.2
3180 IF R/DDA<10 THEN 3200
3190 WINXY=1.1*WINXY
3200 WINDOW (-WINXY,-WINXY)-(WINXY,WINXY)
3210 VIEW (205,5)-(595,395):CIRCLE(0,0),R
3220 IF GREF$="n" OR GREF$="N" THEN 3270
3230 SX=MAP(-HGPRO,0)-3:SY=MAP(-KGPRO,1)-3
3240 PUT(SX,SY),KANJI(&H14F)
3250 SX=MAP(HGPRO,0)-3:SY=MAP(KGPRO,1)-3
3260 PUT(SX,SY),KANJI(&H147)
3270 CIRCLE(HGPRO,KGPRO),DDA : CIRCLE(-HGPRO,-KGPRO),DDA
3280 GOSUB *LABEL
3290 FOR J=1 TO O3-1
3300 H=HCA(J) : K=KCA(J) : L=LCA(J)
```

```
3310 IF DISK(J)=0 THEN 3440
3320 IF UU*UU+VV*VV<.0001 THEN 3360
3330 XI=FNPROX(FNXABC(H-HG/2,K-KG/2,L-LG/2),FNYABC(H-HG/2,K-KG/2,L-LG/2),FNZABC(H-HG/2,K-KG/2,L-LG/2))
3340 YI=FNPROY(FNXABC(H-HG/2,K-KG/2,L-LG/2),FNYABC(H-HG/2,K-KG/2,L-LG/2),FNZABC(H-HG/2,K-KG/2,L-LG/2))
3350 GOTO 3370
3360 XI=FNXABC(H-HG/2,K-KG/2,L-LG/2):YI=-FNYABC(H-HG/2,K-KG/2,L-LG/2)
3370 X=XI*CO+YI*SI:Y=-XI*SI+YI*CO:CIRCLE(X,Y),DDA
3380 SHKL$=STR$(J):LHKL=LEN(SHKL$)
3390 SX=MAP(X,0)-3:SY=MAP(Y,1)-3
3400 FOR I1=1 TO LHKL
3410 MHKL$=MID$(SHKL$,I1,1):MHKL=ASC(MHKL$)+256
3420 PUT (SX-4*LHKL+8*(I1-1),SY),KANJI(MHKL),OR
3430 NEXT I1
3440 NEXT J
3450 RETURN
3460 '
3470 *Q1
3480 IF NQ1+NQ8>66 THEN BEEP:RETURN
3490 NQ1=NQ1+1 : XX1=XX1+INDX
3500 IF NQ1-3*INT(NQ1/3)<>1 THEN 3520
3510 XY1=XY1-2*INDX+INDY : XX1=XX1+INDX/2
3520 LINE(DD,WAI)-(XX1,WAI) : LINE(XX1,WAI)-(XX1,XY1)
3530 LINE(XX1,XY1)-(1.8*DD,XY1)
3540 LOCATE 67+4*(NQ1-1-3*INT((NQ1-1)/3)),INT((NQ1-1)/3):PRINT IJ
3550 XY1=XY1+INDX
3560 RETURN
3570 *Q2
3580 IF NQ1+NQ8>66 THEN BEEP:RETURN
3590 NQ1=NQ1+1 : XX1=XX1+INDX : YY2=YY2-INDX
3600 IF NQ1-3*INT(NQ1/3)<>1 THEN GOTO 3620
3610 XY1=XY1-2*INDX+INDY : XX1=XX1+INDX/2 : YY2=YY2-INDX
3620 LINE(EKS,-DD)-(EKS,YY2) : LINE(EKS,YY2)-(XX1,YY2)
3630 LINE(XX1,YY2)-(XX1,XY1) : LINE(XX1,XY1)-(1.8*DD,XY1)
3640 LOCATE 67+4*(NQ1-1-3*INT((NQ1-1)/3)),INT((NQ1-1)/3):PRINT IJ
3650 XY1=XY1+INDX
3660 RETURN
3670 *Q3
3680 IF NQ4+NQ5>66 THEN BEEP:RETURN
3690 NQ4=NQ4+1 : XX4=XX4-INDX : YY3=YY3-INDX
3700 IF NQ4-3*INT(NQ4/3)<>1 THEN GOTO 3720
3710 XY4=XY4-2*INDX+INDY : XX4=XX4-INDX/2 : YY3=YY3-INDX
3720 LINE(EKS,-DD)-(EKS,YY3) : LINE(EKS,YY3)-(XX4,YY3)
3730 LINE(XX4,YY3)-(XX4,XY4) : LINE(XX4,XY4)-(-1.8*DD,XY4)
3740 LOCATE 1+4*(NQ4-1-3*INT((NQ4-1)/3)),INT((NQ4-1)/3):PRINT IJ
3750 XY4=XY4+INDX
3760 RETURN
3770 *Q4
3780 IF NQ4+NQ5>66 THEN BEEP:RETURN
3790 NQ4=NQ4+1 : XX4=XX4-INDX
3800 IF NQ4-3*INT(NQ4/3)<>1 THEN 3820
3810 XY4=XY4-2*INDX+INDY : XX4=XX4-INDX/2
3820 LINE(-DD,WAI)-(XX4,WAI) : LINE(XX4,WAI)-(XX4,XY4)
3830 LINE(XX4,XY4)-(-1.8*DD,XY4)
3840 LOCATE 1+4*(NQ4-1-3*INT((NQ4-1)/3)),INT((NQ4-1)/3):PRINT IJ
3850 XY4=XY4+INDX
3860 RETURN
3870 *Q5
3880 IF NQ4+NQ5>66 THEN BEEP:RETURN
3890 NQ5=NQ5+1 : XX5=XX5-INDX
3900 IF NQ5-3*INT(NQ5/3)<>1 THEN 3920
3910 XY5=XY5-4*INDX-INDY : XX5=XX5-INDX/2
3920 LINE(-DD,WAI)-(XX5,WAI) : LINE(XX5,WAI)-(XX5,XY5)
3930 LINE(XX5,XY5)-(-1.8*DD,XY5)
3940 LOCATE 1+4*(NQ5-1-3*INT((NQ5-1)/3)),22-INT((NQ5-1)/3):PRINT IJ
3950 XY5=XY5+INDX
3960 RETURN
3970 *Q6
3980 IF NQ4+NQ5>66 THEN BEEP:RETURN
3990 NQ5=NQ5+1 : XX5=XX5-INDX : YY6=YY6+INDX
4000 IF NQ5-3*INT(NQ5/3)<>1 THEN GOTO 4020
4010 XY5=XY5-4*INDX-INDY : XX5=XX5-INDX/2 : YY6=YY6+INDX
4020 LINE(EKS,DD)-(EKS,YY6) : LINE(EKS,YY6)-(XX5,YY6)
4030 LINE(XX5,YY6)-(XX5,XY5) : LINE(XX5,XY5)-(-1.8*DD,XY5)
4040 LOCATE 1+4*(NQ5-1-3*INT((NQ5-1)/3)),22-INT((NQ5-1)/3):PRINT IJ
4050 XY5=XY5+INDX
4060 RETURN
4070 *Q7
4080 IF NQ1+NQ8>66 THEN BEEP:RETURN
4090 NQ8=NQ8+1 : XX8=XX8+INDX : YY7=YY7+INDX
4100 IF NQ8-3*INT(NQ8/3)<>1 THEN GOTO 4120
4110 XY8=XY8-4*INDX-INDY : XX8=XX8+INDX/2 : YY7=YY7+INDX
4120 LINE(EKS,DD)-(EKS,YY7) : LINE(EKS,YY7)-(XX8,YY7)
```

```
4130 LINE(XX8,YY7)-(XX8,XY8) : LINE(XX8,XY8)-(1.8*DD,XY8)
4140 LOCATE 67+4*(NQ8-1-3*INT((NQ8-1)/3)),22-INT((NQ8-1)/3):PRINT IJ
4150 XY8=XY8+INDX
4160 RETURN
4170 *Q8
4180 IF NQ1+NQ8>66 THEN BEEP:RETURN
4190 NQ8=NQ8+1 : XX8=XX8+INDX
4200 IF NQ8-3*INT(NQ8/3)<>1 THEN 4220
4210 XY8=XY8-4*INDX-INDY : XX8=XX8+INDX/2
4220 LINE(DD,WAI)-(XX8,WAI) : LINE(XX8,WAI)-(XX8,XY8)
4230 LINE(XX8,XY8)-(1.8*DD,XY8)
4240 LOCATE 67+4*(NQ8-1-3*INT((NQ8-1)/3)),22-INT((NQ8-1)/3):PRINT IJ
4250 XY8=XY8+INDX
4260 RETURN
4270 '
4280 *HOLZ2
4290 FOR I=0 TO 1
4300 IF I=OORG THEN GOTO 4780
4310 WINDOW (-DD,-DD)-(DD,DD):VIEW (200,80)-(440,320)
4320 CIRCLE(0,0),DDA
4330 FOR IJ=1 TO 03-1
4340 IF DISK(IJ)=I THEN GOTO 4760
4350 WINDOW (-DD,-DD)-(DD,DD):VIEW (200,80)-(440,320)
4360 H=HCA(IJ):K=KCA(IJ):L=LCA(IJ)
4370 IF UU*UU+VV*VV<.0001 THEN 4410
4380 XI=FNPROX(FNXABC(H,K,L),FNYABC(H,K,L),FNZABC(H,K,L))
4390 YI=FNPROY(FNXABC(H,K,L),FNYABC(H,K,L),FNZABC(H,K,L))
4400 GOTO 4420
4410 XI=FNXABC(H,K,L):YI=-FNYABC(H,K,L)
4420 X=XI*CO+YI*SI:Y=-XI*SI+YI*CO
4430 IF I=0 THEN 4450
4440 IF ABS(FNPRO(X,Y,0,HGPRO,KGPRO,0))<.0001 THEN 4760
4450 IN=0:INA=0:KXS=0:KYS=0:KXL=0:KYL=0
4460 GG=X*X+Y*Y+D*D
4470 GOSUB *BRAGGSL
4480 PSET (KXS,KYS)
4490 IF X=0 THEN 4510
4500 IF ABS(Y/X)<1 THEN 4580
4510 FOR II=0 TO INTE
4520 KX=-DD+2*II*DD/INTE+HGPRO*(-1)^I
4530 GOSUB *BRAGG1
4540 IF BR=0 THEN 4560
4550 GOSUB *PLOT
4560 NEXT II
4570 GOTO 4710
4580 FOR II=0 TO INTE
4590 KY=-DD+2*II*DD/INTE+KGPRO*(-1)^I
4600 GOSUB *BRAGG2
4610 IF BR=0 THEN 4630
4620 GOSUB *PLOT
4630 NEXT II
4640 GOTO 4710
4650 *PLOT
4660 KX=KX-HGPRO*(-1)^I:KY=KY-KGPRO*(-1)^I
4670 IF ABS(KX)>DD OR ABS(KY)>DD THEN IN=0 ELSE IN=1
4680 IF IN=0 THEN RETURN
4690 LINE -(-KX,-KY):INA=1
4700 RETURN
4710 IF INA=0 THEN 4760
4720 LINE -(KXL,KYL)
4730 WINDOW (-DD*8/3,-DD*5/3)-(DD*8/3,DD*5/3)
4740 VIEW (0,0)-(639,399)
4750 GOSUB *INDEXING
4760 NEXT IJ
4770 IF GREF$="N" OR GREF$="n" THEN 4790
4780 NEXT I
4790 RETURN
4800 '
4810 *BRAGG1
4820 AA=4*(Y*Y+D*D)
4830 BB=2*(2*KX*X*Y-GG*Y)
4840 CC=4*(X*X+D*D)*KX*KX-4*GG*X*KX+GG*GG-4*D*D*WN2
4850 DDD=BB*BB-AA*CC:BR=1:IF DDD<0 THEN BR=0 :GOTO 4870
4860 KY=(-BB-ABS(Y)/Y*SQR(DDD))/AA
4870 RETURN
4880 *BRAGG2
4890 AA=4*(X*X+D*D)
4900 BB=2*(2*KY*X*Y-GG*X)
4910 CC=4*(Y*Y+D*D)*KY*KY-4*GG*Y*KY+GG*GG-4*D*D*WN2
4920 DDD=BB*BB-AA*CC:BR=1:IF DDD<0 THEN BR=0 :GOTO 4940
4930 KX=(-BB-ABS(X)/X*SQR(DDD))/AA
4940 RETURN
```

```
4950 '
4960 *BRAGGSL
4970 FOR BSL=1 TO 2
4980 IF X=0 THEN 5000
4990 IF ABS(Y/X)<1 THEN 5160
5000 KX=DD*(-1)^BSL+HGPRO*(-1)^I
5010 GOSUB *BRAGG1
5020 KX=KX-HGPRO*(-1)^I:KY=KY-KGPRO*(-1)^I
5030 IF ABS(KY)>DD THEN IN=0 ELSE IN=1
5040 IF IN=1 THEN 5130
5050 FOR J=1 TO 2
5060 KY=DD*(-1)^J+KGPRO*(-1)^I
5070 GOSUB *BRAGG2
5080 KX=KX-HGPRO*(-1)^I:KY=KY-KGPRO*(-1)^I
5090 IF ABS(KX)>DD THEN IN=0 ELSE IN=1
5100 IF IN=1 THEN 5130
5110 NEXT J
5120 BEEP:RETURN 4760
5130 ON BSL GOTO 5140,5150
5140 KXS=-KX:KYS=-KY:GOTO 5320
5150 KXL=-KX:KYL=-KY:GOTO 5320
5160 KY=DD*(-1)^BSL+KGPRO*(-1)^I
5170 GOSUB *BRAGG2
5180 KX=KX-HGPRO*(-1)^I:KY=KY-KGPRO*(-1)^I
5190 IF ABS(KX)>DD THEN IN=0 ELSE IN=1
5200 IF IN=1 THEN 5290
5210 FOR J=1 TO 2
5220 KX=DD*(-1)^J+HGPRO*(-1)^I
5230 GOSUB *BRAGG1
5240 KX=KX-HGPRO*(-1)^I:KY=KY-KGPRO*(-1)^I
5250 IF ABS(KY)>DD THEN IN=0 ELSE IN=1
5260 IF IN=1 THEN 5290
5270 NEXT J
5280 BEEP:RETURN 4760
5290 ON BSL GOTO 5300,5310
5300 KXS=-KX:KYS=-KY:GOTO 5320
5310 KXL=-KX:KYL=-KY
5320 NEXT BSL
5330 RETURN
```

CHPL

```
10 REM FILE NAME "CHPL"
20 '  *** output HOLZ for X-Y Plotter Roland DXY-990 ***
30 '
40 '     This program will be chained from program "HOLZ" and
50 ' draw Holzring and Holzlines (circle approximation and exact Bragg's
60 ' equation) on the x-y plotter.
70 '
80 CONSOLE ,,0
90 DEF FNPRO(X1,X2,X3,Y1,Y2,Y3)=X1*Y1+X2*Y2+X3*Y3
100 DEF FNRL(H,K,L)=SQR((H*AST1)^2+(H*AST2+K*BST2+L*CST2)^2+(H*AST3+L*CST3)^2)
110 DEF FNXABC(H,K,L)=H*AST1+K*BST1+L*CST1
120 DEF FNYABC(H,K,L)=H*AST2+K*BST2+L*CST2
130 DEF FNZABC(H,K,L)=H*AST3+K*BST3+L*CST3
140 DEF FNPROX(X,Y,Z)=(UU*WW*X+VV*WW*Y-FA1*FA1*Z)/(FA1*FA2)
150 DEF FNPROY(X,Y,Z)=(VV*X-UU*Y)/FA1
160 DEF FNPROZ(X,Y,Z)=-(UU*X+VV*Y+WW*Z)/FA2
170 DEF FNL(X,Y,Z)=X*X+Y*Y+Z*Z
180 PAI#=3.14159265359#
190 '
200 I=0 :HGPRO=HGP:KGPRO=-KGP
210 DDSC=FIX(DD*1E+06)/10000!
220 HGPRO=FIX(HGPRO*1E+06)/1E+06:KGPRO=FIX(KGPRO*1E+06)/1E+06
230 PLDDA=FIX(DDA*1E+06)/10000!:PLDD=FIX(DD*1E+06)/10000!:PLR=100*R
240 DDA=FIX(DDA*1E+06)/1E+06
250 CLS 1:LOCATE 33,12:PRINT "plotting"
260 IF HLZ=0 THEN GOSUB *HOLZRING2
270 ON HLZ GOSUB *HOLZ,*HOLZ2
280 GOSUB *LABEL
290 CLS 3
300 PRINT " (14)  Which do you want?"
310 PRINT "          HOLZRING ------------------------------ 0"
320 PRINT "          HOLZ I (circle approximation) --------- 1"
330 PRINT "          HOLZ II(more accurate approximation) -- 2"
340 PRINT "              E    N    D        ---------------- 3"
350 INPUT "                                          ";HLZ
360 OORG=999
370 HLZ=INT(ABS(HLZ)):IF HLZ>3 THEN GOTO 350
380 IF HLZ=2 THEN GOTO 390 ELSE GOTO 440
390 IF GREF$="N" OR GREF$="n" THEN GOTO 440
400 INPUT "               O-disk(O) or G-disk(G) ";OORG$
```

```
410 IF OORG$="O" OR OORG$="o" OR OORG$="G" OR OORG$="g" THEN GOTO 430
420 GOTO 400
430 IF OORG$="O" OR OORG$="o" THEN OORG=1 ELSE OORG=999
440 IF HLZ=3 THEN 670
450 IF HLZ=0 THEN 480
460 INPUT "             number of step in HOLZ line ";INTE
470 INTE=ABS(INTE) :IF INTE<10 THEN INTE=10
480 PRINT " (15)  Output to the PRINTER ----------------- 1"
490 PRINT "                     PLOTTER ----------------- 2"
500 INPUT "                                              ";PRPL
510 PRPL=FIX(ABS(PRPL)):IF PRPL>2 THEN GOTO 500
520 IF PRPL=0 THEN GOTO 500
530 IF PRPL=2 THEN GOTO 640
540 CLS 1:COLOR 2:PRINT "    Ready the printer"
550 COMMON S$,A,B,C,ALPH,BETA,GAMM
560 COMMON U,V,W,E,N,GREF$,HG,KG,LG,HAD,KAD,LAD,OORG
570 COMMON AST1,AST2,AST3,BST1,BST2,BST3,CST1,CST2,CST3
580 COMMON HGP,KGP,CO,SI,DD,DDA,UU,VV,WW,FA1,FA2
590 COMMON D,WN,WN2,R,HLZ,INTE,SP,O3,HCA(),KCA(),LCA(),DISK()
600 PRINT:PRINT "  Hit return key to start":COLOR 0
610 HRK$=INKEY$:IF HRK$="" THEN 610
620 CLS 1:LOCATE 30,10:PRINT "Now loading"
630 CHAIN "CHPR"
640 INPUT "                     pen number 1-8   ";SP
650 SP=FIX(ABS(SP)):IF SP>8 THEN GOTO 640
660 GOTO 250
670 CLS 1:END
680 '
690 *LABEL ' ** labeling **
700 LPRINT "IN;DF;SP";SP;";"
710 LPRINT "IP0,0,4000,7200;IW;"
720 LPRINT "SC0,100,0,180;"
730 LPRINT "PU;PA5,165;SI0.54,0.8;LB";S$;CHR$(3)
740 LPRINT "PA10,150;SI0.33,0.5;LB[";U;V;W;"]";CHR$(3)
750 LPRINT "PA15,138;SI0.33,0.5;LB";E;"kV";CHR$(3)
760 LPRINT "PA12,128;SI0.26,0.4;LB";N;
770   IF N>3 THEN GOTO 820
780    ON N GOTO 790,800,810
790  LPRINT "st";:GOTO 830
800  LPRINT "nd";:GOTO 830
810  LPRINT "rd";:GOTO 830
820  LPRINT "th";:GOTO 830
830 LPRINT " Laue Zone";CHR$(3)
840 'LPRINT "PA10,116;SI0.32,0.5;LBG=";HG;KG;LG;CHR$(3)
850 IF HLZ<>0 THEN GOTO 870
860 LPRINT "PA10,115;SI0.32,0.5;LBHolz-ring";CHR$(3):GOTO 900
870 IF OORG<>1 THEN GOTO 890
880 LPRINT "PA10,115;SI0.3,0.5;LB";0;0;0;"disk";CHR$(3):GOTO 900
890 LPRINT "PA10,115;SI0.3,0.5;LB";HG;KG;LG;"disk";CHR$(3)
900 LPRINT "PA5,106;SI0.2,0.4;LB( G=";HG;KG;LG;" excitation )";CHR$(3)
910 LPRINT "PA12,96;SI0.26,0.39;LBa=";CHR$(8);A;CHR$(8);CHR$(3);";CS7;LB";CHR$(80);CHR$(3);"CS;"
920 LPRINT "PA12,89;LBb=";CHR$(8);B;CHR$(8);CHR$(3);";CS7;LB";CHR$(80);CHR$(3);";CS;"
930 LPRINT "PA12,82;LBc=";CHR$(8);C;CHR$(8);CHR$(3);";CS7;LB";CHR$(80);CHR$(3);";CS;"
940 LPRINT "PA12,75;LBalpha=";CHR$(8);ALPH;CHR$(8);CHR$(3);"CS8;LB";CHR$(95);CHR$(3);"CS;"
950 LPRINT "PA12,68;LBbeta =";CHR$(8);BETA;CHR$(8);CHR$(3);"CS8;LB";CHR$(95);CHR$(3);"CS;"
960 LPRINT "PA12,61;LBgamma=";CHR$(8);GAMM;CHR$(8);CHR$(3);"CS8;LB";CHR$(95);CHR$(3);"CS;"
970 LPRINT "PA12,50;SI0.2,0.3;LBRADIUS OF HOLZRING";CHR$(3)
980 LPRINT "PA12,43;LB=";CHR$(8);R;"(1/A)";CHR$(3)
990 LPRINT "PA12,36;LBHORIZONTAL DIRECTION";CHR$(3)
1000 LPRINT "PA12,29;LB=[";HAD;KAD;LAD;"]";CHR$(3)
1010 LPRINT "CP0,0.3;SI0.13,0.2;LB*";CHR$(3)
1020 LPRINT "SP0;"
1030 RETURN
1040 '
1050 *HOLZRING2 '** draw HOLZRING pattern **
1060 LPRINT "IN;DF;PS4;SP";SP;";"
1070 WINXY=R+6*DDA:WINXY=FIX(WINXY*1E+06)/1E+06
1080 SR=DDA/(2*WINXY)*50
1090    IF SR<1.3 THEN SR=1.3:WINXY=1.2*R
1100    IF SR>3 THEN SR=3:WINXY=R+4*DDA
1110 IF WINXY/DDA>200 THEN PLDA=FIX(WINXY*50)/10000! ELSE PLDA=DDA
1120 LPRINT "IP4000,860,10000,6860;IW;"
1130 LPRINT "SC";-WINXY;",";WINXY;",";-WINXY;",";WINXY;";"
1140 LPRINT "SR";.4*SR;",";SR;";"
1150 LPRINT "PU;PA0,0;CI";R;";"
1160 IF GREF$="n" OR GREF$="N" THEN 1230
1170 LPRINT "PU;PA";HGPRO;",";KGPRO;";CI";PLDA;";" '         G-disk
1180 LL=SQR(HGPRO^2+KGPRO^2)
1190 X=FIX(DDA*HGPRO/LL*1E+06)/1E+06:Y=FIX(DDA*KGPRO/LL*1E+06)/1E+06
1200 'LPRINT "PR";X;",";Y;";DI";HGPRO;",";KGPRO;";"
1210 'LPRINT "CP1,-0.25;LB";HG;KG;LG;CHR$(3)
1220 LPRINT "DI;CP-0.5,-0.25;LBG";CHR$(3)
```

```
1230 LPRINT "PU;PA";-HGPRO;",";-KGPRO;";CI";PLDA;";" '       0-disk
1240 'LPRINT "DI;CP-2.5,-0.25;LBO 0 0";CHR$(3)
1250 LPRINT "DI;CP-0.5,-0.25;LBO";CHR$(3)
1260 FOR J=1 TO 03-1
1270 H=HCA(J) : K=KCA(J) : L=LCA(J)
1280 IF DISK(J)=0 THEN 1410
1290 IF UU*UU+VV*VV<.0001 THEN 1330
1300 XI=FNPROX(FNXABC(H-HG/2,K-KG/2,L-LG/2),FNYABC(H-HG/2,K-KG/2,L-LG/2),FNZABC(H-HG/2,K-KG/2,L-LG/2))
1310 YI=FNPROY(FNXABC(H-HG/2,K-KG/2,L-LG/2),FNYABC(H-HG/2,K-KG/2,L-LG/2),FNZABC(H-HG/2,K-KG/2,L-LG/2))
1320 GOTO 1340
1330 XI=FNXABC(H-HG/2,K-KG/2,L-LG/2):YI=-FNYABC(H-HG/2,K-KG/2,L-LG/2)
1340 X=XI*CO+YI*SI:Y=XI*SI-YI*CO
1350 X=FIX(X*1E+06)/1E+06:Y=FIX(Y*1E+06)/1E+06
1360 LPRINT "PU;PA";X;",";Y;";CI";PLDA;";"
1370 LL=SQR(X*X+Y*Y)
1380 X=FIX(DDA*X/LL*1E+06)/1E+06:Y=FIX(DDA*Y/LL*1E+06)/1E+06
1390 LPRINT "PR";X;",";Y;";DI";X;",";Y;";"
1400 LPRINT "CP1,-0.25;LB";H;K;L;CHR$(3)
1410 NEXT J
1420 LPRINT "SP0;"
1430 RETURN
1440 '
1450 *INDEXING ' ** index on the K-M pattern **
1460 LPRINT "IW;"
1470 IF X=0 AND Y>0 THEN Q=3 : GOTO *SEP
1480 IF X=0 AND Y<0 THEN Q=2 : GOTO *SEP
1490 IF X>0 AND Y=0 THEN Q=4 : GOTO *SEP
1500 IF X<0 AND Y=0 THEN Q=1 : GOTO *SEP
1510 RAT=Y/X
1520 IF RAT>-1 AND RAT<0 AND X<0 THEN Q=1 : GOTO *SEP
1530 IF RAT<=-1          AND X<0 THEN Q=2 : GOTO *SEP
1540 IF RAT>=1           AND X>0 THEN Q=3 : GOTO *SEP
1550 IF RAT>0  AND RAT<1 AND X>0 THEN Q=1 : GOTO *SEP
1560 IF RAT>-1 AND RAT<0 AND X>0 THEN Q=4 : GOTO *SEP
1570 IF RAT<=-1          AND X>0 THEN Q=3 : GOTO *SEP
1580 IF RAT>=1           AND X<0 THEN Q=2 : GOTO *SEP
1590 IF RAT>0  AND RAT<1 AND X<0 THEN Q=4 : GOTO *SEP
1600 BEEP:RETURN
1610 *SEP
1620 GOSUB *SEP2
1630 DIX=FIX(100*COS(P*PAI#/2))/100:DIY=FIX(100*SIN(P*PAI#/2))/100
1640 LPRINT "DI";DIX;",";DIY;";"
1650 'LPRINT "DI";COS(P*PAI#/2);",";SIN(P*PAI#/2);";"
1660 ON P+1 GOTO 1670,1680,1690,1700
1670 LPRINT "PA";DDSC;",";WAI;";":GOTO 1710
1680 LPRINT "PA";EKS;",";DDSC;";":GOTO 1710
1690 LPRINT "PA";-DDSC;",";WAI;";":GOTO 1710
1700 LPRINT "PA";EKS;",";-DDSC;";"
1710 LPRINT "CP0.5,-0.25;LB";H;K;L;CHR$(3)
1720 RETURN
1730 *SEP2
1740 ON Q GOTO 1750,1790,1830,1870
1750 EKS=KXL:WAI=KYL '                    Q=1
1760 IF ABS(WAI)<PLDD THEN GOTO 1780
1770 P=3:RETURN
1780 EKS=KXS:WAI=KYS:P=1:RETURN
1790 EKS=KXS:WAI=KYS '                    Q=2
1800 IF ABS(EKS)<PLDD THEN GOTO 1820
1810 P=0:RETURN
1820 EKS=KXL:WAI=KYL:P=2:RETURN
1830 EKS=KXL:WAI=KYL '                    Q=3
1840 IF ABS(EKS)<PLDD THEN GOTO 1860
1850 P=2:RETURN
1860 EKS=KXS:WAI=KYS:P=0:RETURN
1870 EKS=KXS:WAI=KYS '                    Q=4
1880 IF ABS(WAI)<PLDD THEN GOTO 1900
1890 P=1:RETURN
1900 EKS=KXL:WAI=KYL:P=3:RETURN
1910 '
1920 *HOLZ
1930 LPRINT "IN;DF;PS4;PA;SI0.12,0.25;SP";SP;";"
1940 LPRINT "IP4300,1400,9400,6500;"
1950 LPRINT "IW100,100,11000,7500;"
1960 LPRINT "SC";-DDSC;",";DDSC;",";-DDSC;",";DDSC;";"
1970 ANGRAN=SQR(2)*DD/R:SANG=ANGRAN/INTE
1980 LPRINT "PU0,0;CI";PLDDA;",1;"
1990 FOR IJ=1 TO 03-1
2000 LPRINT "IW4300,1100,9900,6700;"
2010 IN=0:INA=0
2020 H=HCA(IJ):K=KCA(IJ):L=LCA(IJ)
2030 IF DISK(IJ)=0 THEN 2900
2040 IF UU*UU+VV*VV=.0001 THEN 2080
```

```
2050 XI=FNPROX(FNXABC(H-HG/2,K-KG/2,L-LG/2),FNYABC(H-HG/2,K-KG/2,L-LG/2),FNZABC(H-HG/2,K-KG/2,L-LG/2))
2060 YI=FNPROY(FNXABC(H-HG/2,K-KG/2,L-LG/2),FNYABC(H-HG/2,K-KG/2,L-LG/2),FNZABC(H-HG/2,K-KG/2,L-LG/2))
2070 GOTO 2090
2080 XI=FNXABC(H-HG/2,K-KG/2,L-LG/2):YI=-FNYABC(H-HG/2,K-KG/2,L-LG/2)
2090 X=XI*CO+YI*SI:Y=XI*SI-YI*CO
2100 IF X=0 THEN 2150
2110 T=ATN(Y/X)*180/PAI#+90*(1-ABS(X)/X)
2120 ' T=T-360*(INT((T+360)/360)-1)
2130 T=T+360:T=T MOD 360
2140 P=INT((T+45)/90):P=P-4*INT(P/4):GOTO 2170
2150 IF Y>0 THEN T=90:P=1:GOTO 2170
2160 T=270:P=3
2170 FU1=R*R-(X+DD)*(X+DD):FU2=R*R-(X-DD)*(X-DD)
2180 FU3=R*R-(Y+DD)*(Y+DD):FU4=R*R-(Y-DD)*(Y-DD)
2190 ON P+1 GOTO 2200,2340,2480,2620
2200 ANGSL=-1
2210    IF FU3=>0 THEN GOTO 2240
2220    IF X=>0 THEN KXS=-2*DD:GOTO 2250
2230    IF X<0 THEN KXS=2*DD:GOTO 2250
2240 KXS=-X+SQR(FU3):KYS=DD
2250    IF FU4=>0 THEN GOTO 2280
2260    IF X=>0 THEN KXL=-2*DD:GOTO 2290
2270    IF X<0 THEN KXL=2*DD:GOTO 2290
2280 KXL=-X+SQR(FU4):KYL=-DD
2290 IF KXS>DD  THEN KXS=DD :KYS=-Y-SQR(FU1)
2300 IF KXS<-DD THEN KXS=-DD:KYS=-Y+SQR(FU2)
2310 IF KXL>DD  THEN KXL=DD :KYL=-Y+SQR(FU1)
2320 IF KXL<-DD THEN KXL=-DD:KYL=-Y-SQR(FU2)
2330 GOTO 2760
2340 ANGSL=1
2350    IF FU1=>0 THEN 2380
2360    IF Y=>0 THEN KYS=-2*DD:GOTO 2390
2370    IF Y<0 THEN KYS=2*DD:GOTO 2390
2380 KXS=DD:KYS=-Y+SQR(FU1)
2390    IF FU2=>0 THEN 2420
2400    IF Y=>0 THEN KYL=-2*DD:GOTO 2430
2410    IF Y<0 THEN KYL=2*DD:GOTO 2430
2420 KXL=-DD:KYL=-Y+SQR(FU2)
2430 IF KYS>DD  THEN KXS=-X-SQR(FU3):KYS=DD
2440 IF KYS<-DD THEN KXS=-X+SQR(FU4):KYS=-DD
2450 IF KYL>DD  THEN KXL=-X+SQR(FU3):KYL=DD
2460 IF KYL<-DD THEN KXL=-X-SQR(FU4):KYL=-DD
2470 GOTO 2760
2480 ANGSL=1
2490    IF FU3=>0 THEN 2520
2500    IF X=>0 THEN KXS=-2*DD:GOTO 2530
2510    IF X<0 THEN KXS=2*DD:GOTO 2530
2520 KXS=-X-SQR(FU3):KYS=DD
2530    IF FU4=>0 THEN 2560
2540    IF X=>0 THEN KXL=-2*DD:GOTO 2570
2550    IF X<0 THEN KXL=2*DD:GOTO 2570
2560 KXL=-X-SQR(FU4):KYL=-DD
2570 IF KXS>DD  THEN KXS=DD :KYS=-Y+SQR(FU1)
2580 IF KXS<-DD THEN KXS=-DD:KYS=-Y-SQR(FU2)
2590 IF KXL>DD  THEN KXL=DD :KYL=-Y-SQR(FU1)
2600 IF KXL<-DD THEN KXL=-DD:KYL=-Y+SQR(FU2)
2610 GOTO 2760
2620 ANGSL=-1
2630    IF FU1=>0 THEN 2660
2640    IF Y=>0 THEN KYS=-2*DD:GOTO 2670
2650    IF Y<0 THEN KYS=2*DD:GOTO 2670
2660 KXS=DD:KYS=-Y-SQR(FU1)
2670    IF FU2=>0 THEN 2700
2680    IF Y=>0 THEN KYL=-2*DD:GOTO 2710
2690    IF Y<0 THEN KYL=2*DD:GOTO 2710
2700 KXL=-DD:KYL=-Y-SQR(FU2)
2710 IF KYS>DD  THEN KXS=-X+SQR(FU3):KYS=DD
2720 IF KYS<-DD THEN KXS=-X-SQR(FU4):KYS=-DD
2730 IF KYL>DD  THEN KXL=-X-SQR(FU3):KYL=DD
2740 IF KYL<-DD THEN KXL=-X+SQR(FU4):KYL=-DD
2750 '
2760 KXS=FIX(KXS*1E+06)/10000!:KYS=FIX(KYS*1E+06)/10000!
2770 KXL=FIX(KXL*1E+06)/10000!:KYL=FIX(KYL*1E+06)/10000!
2780 LPRINT "PU;PA";KXS;",";KYS;";"
2790 FOR ANG=-ANGRAN TO ANGRAN STEP SANG
2800 ANGLE=T*PAI#/180+ANG*ANGSL
2810 XPLOT=R*COS(ANGLE)-X:YPLOT=R*SIN(ANGLE)-Y
2820 IF ABS(XPLOT)>DD OR ABS(YPLOT)>DD THEN 2850
2830 XPLOT=INT(XPLOT*1E+06)/10000!:YPLOT=INT(YPLOT*1E+06)/10000!
2840 LPRINT "PD";XPLOT;",";YPLOT;";":IN=1
2850 NEXT ANG
2860 IF IN=0 THEN 2900
```

```
2870 LPRINT "PD";KXL;",";KYL;";PU;"
2880 '
2890 GOSUB *INDEXING
2900 NEXT IJ
2910 LPRINT "SPO;"
2920 RETURN
2930 '
2940 *HOLZ2
2950 LPRINT "IN;DF;PS4;PA;SI0.12,0.25;SP";SP;";"
2960 LPRINT "IP4300,1400,9400,6500;"
2970 LPRINT "IW4300,1100,9900,6700;"
2980 LPRINT "SC";-DDSC;",";DDSC;",";-DDSC;",";DDSC;";"
2990 LPRINT "PUO,0;CI";PLDDA;",1;"
3000 FOR I=0 TO 1
3010 IF I=OORG THEN GOTO 3480
3020 FOR IJ=1 TO 03-1
3030 LPRINT "IW4300,1100,9900,6700;"
3040 IF DISK(IJ)=I THEN GOTO 3460
3050 H=HCA(IJ):K=KCA(IJ):L=LCA(IJ)
3060 IF UU*UU+VV*VV<.0001 THEN 3100
3070 XI=FNPROX(FNXABC(H,K,L),FNYABC(H,K,L),FNZABC(H,K,L))
3080 YI=FNPROY(FNXABC(H,K,L),FNYABC(H,K,L),FNZABC(H,K,L))
3090 GOTO 3110
3100 XI=FNXABC(H,K,L):YI=-FNYABC(H,K,L)
3110 X=XI*CO+YI*SI:Y=XI*SI-YI*CO
3120 IF I=0 THEN 3140
3130 IF ABS(FNPRO(X,Y,0,HGPRO,KGPRO,0))<.0001 THEN 3460
3140 IN=0:INA=0:KXS=0:KYS=0:KXL=0:KYL=0
3150 GG=X*X+Y*Y+D*D
3160 GOSUB *BRAGGSL
3170 KXS=FIX(KXS*1E+06)/10000!:KYS=FIX(KYS*1E+06)/10000!
3180 KXL=FIX(KXL*1E+06)/10000!:KYL=FIX(KYL*1E+06)/10000!
3190 LPRINT "PU;PA";KXS;",";KYS;";"
3200 IF X=0 THEN 3220
3210 IF ABS(Y/X)<1 THEN 3290
3220 FOR II=0 TO INTE
3230 KX=-DD+2*II*DD/INTE+HGPRO*(-1)^I
3240 GOSUB *BRAGG1
3250 IF BR=0 THEN 3270
3260 GOSUB *PLOT
3270 NEXT II
3280 GOTO 3430
3290 FOR II=0 TO INTE
3300 KY=-DD+2*II*DD/INTE+KGPRO*(-1)^I
3310 GOSUB *BRAGG2
3320 IF BR=0 THEN 3340
3330 GOSUB *PLOT
3340 NEXT II
3350 GOTO 3430
3360 *PLOT
3370 KX=KX-HGPRO*(-1)^I:KY=KY-KGPRO*(-1)^I
3380 IF ABS(KX)>DD OR ABS(KY)>DD THEN IN=0 ELSE IN=1
3390 IF IN=0 THEN RETURN
3400 KX=FIX(KX*1E+06)/10000!:KY=FIX(KY*1E+06)/10000!
3410 LPRINT "PD";-KX;",";-KY;";":INA=1
3420 RETURN
3430 IF INA=0 THEN 3460
3440 LPRINT "PD";KXL;",";KYL;";PU;"
3450 GOSUB *INDEXING
3460 NEXT IJ
3470 IF GREF$="N" OR GREF$="n" THEN 3490
3480 NEXT I
3490 LPRINT "SPO;":RETURN
3500 '
3510 *BRAGG1
3520 AA=4*(Y*Y+D*D)
3530 BB=2*(2*KX*X*Y-GG*Y)
3540 CC=4*(X*X+D*D)*KX*KX-4*GG*X*KX+GG*GG-4*D*D*WN2
3550 DDD=BB*BB-AA*CC:BR=1:IF DDD<0 THEN BR=0 :GOTO 3570
3560 KY=(-BB-ABS(Y)/Y*SQR(DDD))/AA
3570 RETURN
3580 *BRAGG2
3590 AA=4*(X*X+D*D)
3600 BB=2*(2*KY*X*Y-GG*X)
3610 CC=4*(Y*Y+D*D)*KY*KY-4*GG*Y*KY+GG*GG-4*D*D*WN2
3620 DDD=BB*BB-AA*CC:BR=1:IF DDD<0 THEN BR=0 :GOTO 3640
3630 KX=(-BB-ABS(X)/X*SQR(DDD))/AA
3640 RETURN
3650 '
3660 *BRAGGSL
3670 FOR BSL=1 TO 2
3680 IF X=0 THEN 3700
```

```
3690 IF ABS(Y/X)<1 THEN 3860
3700 KX=DD*(-1)^BSL+HGPRO*(-1)^I
3710 GOSUB *BRAGG1
3720 KX=KX-HGPRO*(-1)^I:KY=KY-KGPRO*(-1)^I
3730 IF ABS(KY)>DD THEN IN=0 ELSE IN=1
3740 IF IN=1 THEN 3830
3750 FOR J=1 TO 2
3760 KY=DD*(-1)^J+KGPRO*(-1)^I
3770 GOSUB *BRAGG2
3780 KX=KX-HGPRO*(-1)^I:KY=KY-KGPRO*(-1)^I
3790 IF ABS(KX)>DD THEN IN=0 ELSE IN=1
3800 IF IN=1 THEN 3830
3810 NEXT J
3820 RETURN 3460
3830 ON BSL GOTO 3840,3850
3840 KXS=-KX:KYS=-KY:GOTO 4020
3850 KXL=-KX:KYL=-KY:GOTO 4020
3860 KY=DD*(-1)^BSL+KGPRO*(-1)^I
3870 GOSUB *BRAGG2
3880 KX=KX-HGPRO*(-1)^I:KY=KY-KGPRO*(-1)^I
3890 IF ABS(KX)>DD THEN IN=0 ELSE IN=1
3900 IF IN=1 THEN 3990
3910 FOR J=1 TO 2
3920 KX=DD*(-1)^J+HGPRO*(-1)^I
3930 GOSUB *BRAGG1
3940 KX=KX-HGPRO*(-1)^I:KY=KY-KGPRO*(-1)^I
3950 IF ABS(KY)>DD THEN IN=0 ELSE IN=1
3960 IF IN=1 THEN 3990
3970 NEXT J
3980 RETURN 3460
3990 ON BSL GOTO 4000,4010
4000 KXS=-KX:KYS=-KY:GOTO 4020
4010 KXL=-KX:KYL=-KY
4020 NEXT BSL
4030 RETURN
```

Language	: N88BASIC (86) COMPILER
DOS	: MS-DOS
Computer	: NEC PC-9801
Printer	: NEC PC-PR201
Plotter	: ROLAND DXY-990

Kikuchi-line program

This program enables simulating Kikuchi-line maps for all the crystal systems and for an arbitrary orientation of a crystal. Simulated patterns are printed out to a printer or a plotter. The Kikuchi lines are drawn in four different widths or four different colors according to the spacings of lattice planes. This program has the following commands:

1) magnify/demagnify the angular range
2) rotate the pattern
3) shift the pattern
4) index/search the pole (zone axis)
5) index the Kikuchi line
6) calculate the angle between two poles (zone axes)

Output 1

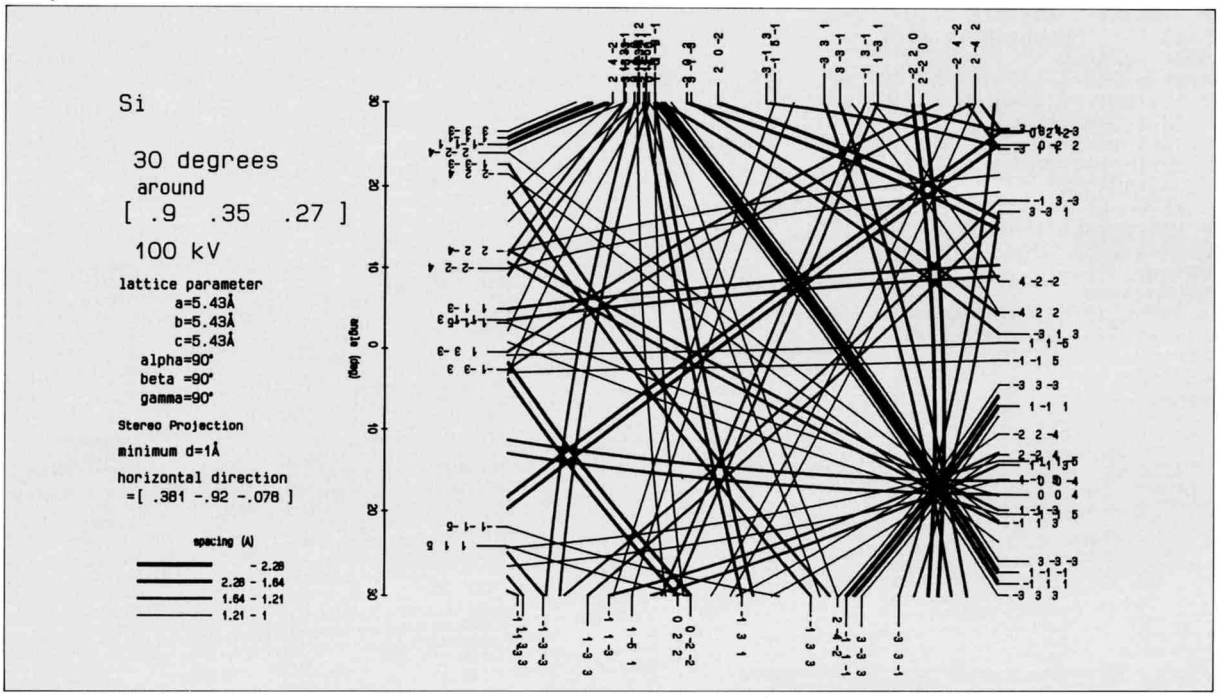

Output 2

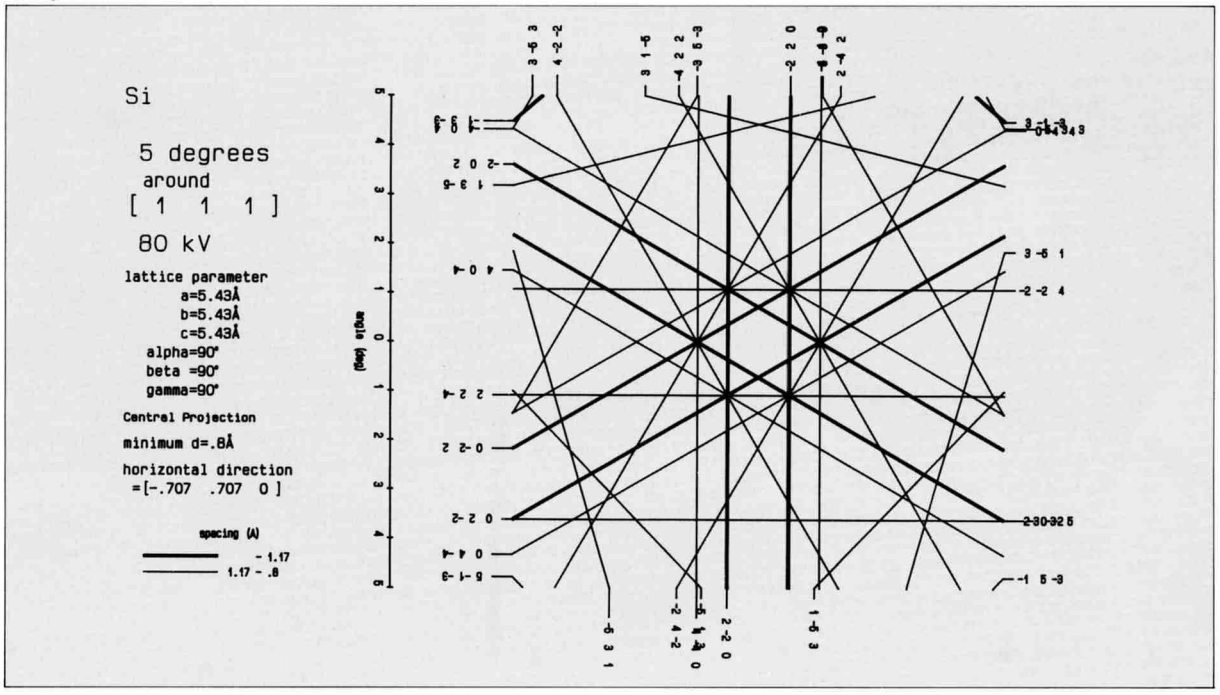

```
10 '*********************************
20 '***                           ***
30 '***   KIKUCHI PATTERN ver.5   ***
40 '***        1988. 2.10 (Wed)   ***
50 '***                           ***
60 '*********************************
70 '
80 DEFINT H-L,N
90 DIM HA(1000),KA(1000),LA(1000),IHKL$(1500),RLA(1000)
100 DIM XPLS(1500),YPLS(1500),XPLE(1500),YPLE(1500)
110 DIM XPL(300),YPL(300),XPLL(300),YPLL(300),SYS$(8),BRAV$(7)
120 DIM IG%(33),IGR%(33),IGR2%(33),IG2%(33),IG3%(33),IG4%(33)
130 CONSOLE ,,0,0:SCREEN 3,1:KEY ON:STOP ON:CLS 3:PI=3.14159
140 ON STOP GOSUB *STRP
150 GOSUB *FUNCTION
160 GOSUB *RDAT
170 GOSUB *INDAT
180 GOSUB *CONSTANT
190 GOSUB *KIKUCHI
200 GOSUB *COMMAND
210 END
220 ' ## DATA ##
230 DATA " cubic               "," hexagonal ,trigonal "
240 DATA " rhombohedral        "," tetragonal          "
250 DATA " orthorhombic        "," monoclinic          "
260 DATA " triclinic           "," < diamond type >    "
270 DATA " primitive           "," body centered       "
280 DATA " face centered       "," A-base centered     "
290 DATA " B-base centered     "," C-base centered     "
300 DATA " < diamond type >    "
310 DATA 10,10,0,0,192,0,0,240,0,0,120,0,0,126,0,0,-32705,0,0,-16353
320 DATA 0,0,-32737,0,0,15,0,0,14,0,0,4,0,0
330 DATA 10,10,0,0,-16129,0,0,-16129,0,0,-16129,0,0,-16129,0,0,-16129,0,0
340 DATA -16129,0,0,-16129,0,0,-16129,0,0,-16129,0,0,-16129,0,0
350 DATA 10,10,0,0,8,0,0,28,0,0,60,0,0,126,0,0,254,0,0,127,0,0
360 DATA -32737,0,0,-32761,0,0,-16381,0,0,-16384,0,0
370 '
380 ' ## subroutines ##
390 '
400 *STRP
410 RETURN
420 *FUNCTION ' define user functions
430 DEF FNPRO(X1,Y1,Z1,X2,Y2,Z2)=X1*X2+Y1*Y2+Z1*Z2
440 DEF FNL(X,Y,Z)=X*X+Y*Y+Z*Z
450 DEF FNSCPR(A,B,C,D,E,F)=(A*D+B*E+C*F)/SQR((A*A+B*B+C*C)*(D*D+E*E+F*F))
460 DEF FNXCOD(U,V,W)=U*AX+V*BX+W*CX
470 DEF FNYCOD(U,V,W)=U*AY+V*BY+W*CY
480 DEF FNZCOD(U,V,W)=U*AZ+V*BZ+W*CZ
490 DEF FNXICOD(U,V,W)=U*AIX+V*BIX+W*CIX
500 DEF FNYICOD(U,V,W)=U*AIY+V*BIY+W*CIY
510 DEF FNZICOD(U,V,W)=U*AIZ+V*BIZ+W*CIZ
520 DEF FNXCODS(H,K,L)=H*AXS+K*BXS+L*CXS
530 DEF FNYCODS(H,K,L)=H*AYS+K*BYS+L*CYS
540 DEF FNZCODS(H,K,L)=H*AZS+K*BZS+L*CZS
550 DEF FNPROX(X,Y,Z)=(UU*WW*X+VV*WW*Y-FA1*FA1*Z)/(FA1*FA2)
560 DEF FNPROY(X,Y,Z)=(-VV*X+UU*Y)/FA1
570 DEF FNPROZ(X,Y,Z)=(UU*X+VV*Y+WW*Z)/FA2
580 DEF FNPROIX(X,Y,Z)=(UU*WW*X-FA2*VV*Y+FA1*UU*Z)/(FA1*FA2)
590 DEF FNPROIY(X,Y,Z)=(VV*WW*X+FA2*UU*Y+FA1*VV*Z)/(FA1*FA2)
600 DEF FNPROIZ(X,Y,Z)=(-FA1*X+WW*Z)/FA2
610 DEF FNEVOD(X)=X-2*INT(X/2)
620 RETURN
630 *REC.L
640 RL=(H*AXS+K*BXS+L*CXS)^2+(H*AYS+K*BYS+L*CYS)^2
650 RL=RL+(H*AZS+K*BZS+L*CZS)^2:RL=SQR(RL)
660 RETURN
670 '   ****  extinction rule  ****
680 '     forbidden - - - AL=0 , allowed - - - AL=1
690 *P ' ** primitive
700     AL=1:RETURN
710 *I ' ** body center
720     AL=FNEVOD(H+K+L+1):RETURN
730 *F ' ** face center
740     AL1=FNEVOD(H+K+1):AL2=FNEVOD(K+L+1)
750     AL=INT((AL1+AL2)/2):RETURN
760 *A ' ** A-base center
770     AL=FNEVOD(K+L+1):RETURN
780 *B ' ** B-base center
790     AL=FNEVOD(L+H+1):RETURN
800 *C ' ** C-base center
810     AL=FNEVOD(H+K+1):RETURN
820 *D ' ** diamond
```

```
830      AL1=FNEVOD(H+K+1):AL2=FNEVOD(K+L+1):AL=INT((AL1+AL2)/2)
840            IF AL=0 OR FNEVOD(H)=1 THEN RETURN
850     AL3=FNEVOD((H+K+L)/2+1):AL=INT((AL1+AL2+AL3)/3):RETURN
860 *R ' ** rhombohedral
870     AL=(-H+K+L+1)-3*INT((-H+K+L+1)/3):AL=FNEVEOD(AL):RETURN
880 '
890 *RDAT
900  FOR I=1 TO 8:  READ SYS$(I):NEXT
910  FOR I=1 TO 7:  READ BRAV$(I):NEXT
920  FOR I=0 TO 33: READ IG%(I):NEXT
930  FOR I=0 TO 33: READ IGR%(I):NEXT
940  FOR I=0 TO 33: READ IGR2%(I):NEXT
950 RETURN
960 *INDAT '  data input
970   GOSUB *DAT1: GOSUB *DAT2: GOSUB *DAT5: GOSUB *DAT6: GOSUB *DAT7
980   GOSUB *DAT8: GOSUB *DAT9: GOSUB *DAT10: GOSUB *DAT11
990   GOSUB *DAT12: GOSUB *DAT13: GOSUB *CONF.INDAT
1000 RETURN
1010 *DAT1
1020   PRINT " Specimen name "
1030   PRINT "    (within 15 characters)";TAB(29);:INPUT S$
1040   S1$=S$:S$="":FOR I=1 TO 15:S$=S$+MID$(S1$,I,1):NEXT
1050 RETURN
1060 *DAT2
1070 PRINT " Crystal system"
1080   FOR I=1 TO 8:PRINT "   ";SYS$(I);" - ";I:NEXT
1090   PRINT TAB(29);:INPUT SYS
1100   SYS=INT(ABS(SYS)):IF SYS=0 OR SYS>8 THEN 1090
1110   GOSUB *DAT3: GOSUB *DAT4
1120 RETURN
1130 *DAT3
1140   IF SYS=8 THEN BRAV=7:RETURN
1150 PRINT " Lattice type"
1160   FOR I=1 TO 6:PRINT "   ";BRAV$(I);" - ";I:NEXT
1170   PRINT TAB(29);:INPUT BRAV
1180   BRAV=INT(ABS(BRAV)):IF BRAV=0 OR BRAV>6 THEN 1170
1190 RETURN
1200 *DAT4
1210   ON SYS GOSUB *SYS1,*SYS2,*SYS3,*SYS4,*SYS5,*SYS6,*SYS7,*SYS1
1220 A=ABS(A):B=ABS(B):C=ABS(C)
1230 IF A*B*C*ALP*BET*GAM=0 THEN 1210
1240 RETURN
1250 *DAT5
1260 PRINT " Accelerating voltage (kV)";TAB(29);:INPUT E
1270   IF E<=0 THEN 1260
1280 RETURN
1290 *DAT6
1300 PRINT " Zone axis  u,v,w";TAB(29);:INPUT U,V,W
1310   IF FNL(U,V,W)=0 THEN 1300
1320 RETURN
1330 *DAT7
1340 PRINT " Horizontal direction u,v,w";TAB(29);:INPUT XO,YO,ZO
1350   IF FNL(XO,YO,ZO)=0 THEN 1340
1360   IF ABS(FNSCPR(U,V,W,XO,YO,ZO))>.9999 THEN 1340
1370 RETURN
1380 *DAT8
1390 PRINT " minimum limit of spacing (A)";TAB(29);:INPUT DMIN
1400   DMIN=ABS(DMIN):IF DMIN=0 THEN 1390
1410 RDMIN=1/DMIN:RETURN
1420 *DAT9
1430 PRINT " Projection"
1440   PRINT "     central  - - - - C or c"
1450   PRINT "     stereo - - - - - S or s"
1460   PRINT TAB(29);:INPUT PRJ$
1470   IF PRJ$="" THEN PRJ$="C"
1480   IF PRJ$="C" OR PRJ$="c" THEN PRJ=1 :GOTO 1510
1490   IF PRJ$="S" OR PRJ$="s" THEN PRJ=2 :GOTO 1510
1500   GOTO 1460
1510   PRINT "        line - - L or l":PRINT "        curve  - C or c"
1520   PRINT TAB(29);:INPUT PRJLC$
1530   IF PRJLC$="" THEN PRJLC$="L"
1540   IF PRJLC$="L" OR PRJLC$="l" THEN PRJLC=1 :GOTO 1570
1550   IF PRJLC$="C" OR PRJLC$="c" THEN PRJLC=2 :GOTO 1570
1560   GOTO 1520
1570   IF PRJ=1 AND ANGRAN>60 THEN GOSUB *DAT10
1580   IF PRJ=2 AND ANGRAN>90 THEN GOSUB *DAT10
1590 RETURN
1600 *DAT10
1610 PRINT " Angular range ";
1620 IF PRJ=1 THEN PRINT "(max 60 deg)"; ELSE PRINT "(max 90 deg)";
1630 PRINT TAB(29);:INPUT ANGRAN
1640   ANGRAN=ABS(ANGRAN):IF ANGRAN<.01 THEN ANGRAN=10
```

```
1650   IF PRJ=1 AND ANGRAN>60 THEN 1630
1660   IF PRJ=2 AND ANGRAN>90 THEN 1630
1670 RETURN
1680 *DAT11
1690 PRINT " Step number of lines (std. setting 10) ";TAB(29);:INPUT INTE
1700   INTE=INT(ABS(INTE))
1710   IF INTE<10 THEN INTE=10
1720   IF INTE>100 THEN INTE=100
1730 RETURN
1740 *DAT12
1750   PRINT " Output"
1760   PRINT "          CRT - - - - C":PRINT "          plotter - - P"
1770   PRINT TAB(29);:INPUT PRPL$
1780   IF PRPL$="" THEN PRPL$="C"
1790   IF PRPL$="C" OR PRPL$="c" THEN PRPL=1:GOTO 1820
1800   IF PRPL$="P" OR PRPL$="p" THEN PRPL=2:GOTO 1820
1810   GOTO 1770
1820 RETURN
1830 *DAT13
1840   PRINT " Grouping number of reflections";TAB(29);:INPUT NIL
1850   NIL=INT(ABS(NIL)):IF NIL>4 THEN 1840
1860        IF NIL=1 OR NIL=0 THEN NIL=1:RETURN
1870   PRINT "           by color  - - - c":PRINT "          by thickness  - t"
1880   PRINT TAB(29);:INPUT COWI$
1890      IF COWI$="" THEN COWI$="C"
1900      IF COWI$="c" OR COWI$="C" THEN COWI=1:GOTO 1930
1910      IF COWI$="t" OR COWI$="T" THEN COWI=2:GOTO 1930
1920       GOTO 1880
1930   PRINT "     Boundary set"
1940   PRINT "                 auto - - a":PRINT "               manual - m"
1950   PRINT TAB(29);:INPUT AUMANU$
1960      IF AUMANU$="" THEN AUMANU$="A"
1970      IF AUMANU$="A" OR AUMANU$="a" THEN AUMANU$="A":RETURN
1980      IF AUMANU$="M" OR AUMANU$="m" THEN AUMANU$="M":GOTO 2000
1990   GOTO 1950
2000 '    * manual boundary set *
2010   PRINT TAB(11);"input boundary spacings (A)"
2020   FOR I=1 TO NIL-1
2030    PRINT TAB(19);I;"-->";I+1;:INPUT ":";BOUND(I):NEXT
2040   FOR I=1 TO NIL-1:FOR J=1 TO I:BOU=BOUND(I)
2050    IF BOUND(J)<BOU THEN BOUND(I)=BOUND(J):BOUND(J)=BOU
2060   NEXT:NEXT
2070 RETURN
2080 *SYS1 '     cubic <diamond>
2090   PRINT " Lattice constant";
2100   PRINT TAB(23);:INPUT "a (A) ";A:B=A:C=A
2110   ALP=PI/2:BET=ALP:GAM=ALP:ALPH=90:BETA=90:GAMM=90
2120 RETURN
2130 *SYS2 '     hexagonal ,trigonal
2140   PRINT " Lattice constant";
2150   PRINT TAB(23);:INPUT "a (A) ";A :B=A
2160   PRINT TAB(23);:INPUT "c (A) ";C
2170   ALP=PI/2:BET=ALP:GAM=2*PI/3:ALPH=90:BETA=90:GAMM=120
2180 RETURN
2190 *SYS3 '     rhombohedral
2200   PRINT "     rhombohedral coordinates -- 1"
2210   PRINT "     hexagonal coordinates ----- 2"
2220   PRINT TAB(33);:INPUT;RHOMB
2230   RHOMB=INT(ABS(RHOMB))
2240   IF RHOMB=0 OR RHOMB>2 THEN 2220
2250   IF RHOMB=2 THEN GOTO *SYS2
2260   PRINT " Lattice constant";
2270   PRINT TAB(23);:INPUT "a (A) ";A :B=A:C=A
2280   PRINT TAB(18);:INPUT "alpha (deg)";ALPH :BETA=ALPH:GAMM=ALPH
2290   ALP=ALPH*PI/180:BET=ALP:GAM=ALP
2300 RETURN
2310 *SYS4 '     tetragonal
2320   PRINT " Lattice constant";
2330   PRINT TAB(23);:INPUT "a (A) ";A :B=A
2340   PRINT TAB(23);:INPUT "c (A) ";C
2350   ALP=PI/2:BET=ALP:GAM=ALP:ALPH=90:BETA=90:GAMM=90
2360 RETURN
2370 *SYS5 '     orthorhombic
2380   PRINT " Lattice constant";
2390   PRINT TAB(23);:INPUT "a (A) ";A
2400   PRINT TAB(23);:INPUT "b (A) ";B
2410   PRINT TAB(23);:INPUT "c (A) ";C
2420   ALP=PI/2:BET=ALP:GAM=ALP:ALPH=90:BETA=90:GAMM=90
2430 RETURN
2440 *SYS6 '     monoclinic
2450   PRINT " Lattice constant";
2460   PRINT TAB(23);:INPUT "a (A) ";A
```

```
2470   PRINT TAB(23);:INPUT "b (A) ";B
2480   PRINT TAB(23);:INPUT "c (A) ";C
2490   PRINT TAB(18);:INPUT "beta  (deg)";BETA
2500   PRINT TAB(18);:INPUT "gamma (deg)";GAMM
2510   ALPH=90:ALP=ALPH*PI/180:BET=BETA*PI/180:GAM=GAMM*PI/180
2520 RETURN
2530 *SYS7 '     triclinic
2540   PRINT " Lattice constant"
2550   PRINT TAB(23);:INPUT "a (A) ";A
2560   PRINT TAB(23);:INPUT "b (A) ";B
2570   PRINT TAB(23);:INPUT "c (A) ";C
2580   PRINT TAB(18);:INPUT "alpha (deg)";ALPH
2590   PRINT TAB(18);:INPUT "beta  (deg)";BETA
2600   PRINT TAB(18);:INPUT "gamma (deg)";GAMM
2610   ALP=ALPH*PI/180:BET=BETA*PI/180:GAM=GAMM*PI/180
2620 RETURN
2630 *CONF.INDAT
2640 CLS 3
2650 PRINT "1. Specimen name";TAB(37);S$
2660 PRINT "2.  Crystal system";TAB(37);SYS$(SYS)
2670 PRINT "3.  Lattice type";TAB(37);BRAV$(BRAV)
2680 PRINT "4.  Lattice constant";
2690 PRINT TAB(36);" a ,b ,c =";A;B;C;"(A)"
2700 PRINT TAB(25);" alpha ,beta ,gamma =";ALPH;BETA;GAMM;"(deg)"
2710 PRINT "5.  Accelerating voltage";SPC(12);" E       =";E;"(kV)"
2720 UP=FIX(U*1000)/1000:VP=FIX(V*1000)/1000:WP=FIX(W*1000)/1000
2730 PRINT "6.  Zone axis";SPC(23);" [u,v,w] = [";UP;VP;WP;"]"
2740    X01=FIX(X0*1000)/1000:Y01=FIX(Y0*1000)/1000:Z01=FIX(Z0*1000)/1000
2750 PRINT "7.  Horizontal direction             [u,v,w] = [";X01;Y01;Z01;"]"
2760 PRINT "8.  minimum limit of spacing        ";DMIN;"(A)"
2770 PRINT "9.  Projection ";TAB(36);
2780    IF PRJ=1 THEN PRINT " Central "; ELSE PRINT " Stereographic ";
2790    PRINT "projection";
2800    IF PRJLC=1 THEN PRINT "( line )" ELSE PRINT "( curve )"
2810 PRINT "10. Angular range ";TAB(36);FIX(ANGRAN*100)/100;"(deg)"
2820 PRINT "11. Step number of lines";TAB(36);INTE
2830 PRINT "12. Output";TAB(36);
2840    IF PRPL=1 THEN PRINT " CRT " ELSE PRINT " Plotter "
2850 PRINT "13. Grouping number of reflections";TAB(36);NIL
2860    IF NIL=1 THEN 2940
2870 PRINT TAB(37)
2880 IF COWI=1 THEN PRINT "color"; ELSE PRINT "thickness";
2890 PRINT " change ";
2900    IF AUMANU$="A" THEN PRINT " ( auto )":GOTO 2940
2910     PRINT:PRINT TAB(37);"< boundary >"
2920     FOR I=1 TO NIL-1
2930     PRINT TAB(35);I;"-->";I+1;":";BOUND(I):NEXT
2940 PRINT:PRINT " If some data must be altered, input number.";
2950 PRINT "  Else enter 0 to start ."
2960 PRINT TAB(35);:INPUT WRONGDATA$
2970 IF WRONGDATA$="" THEN 2960
2980    IF WRONGDATA$="E" OR WRONGDATA$="e" THEN END
2990 WRONGNUM=VAL(WRONGDATA$)
3000    IF WRONGNUM=0 THEN GOTO 3070
3010    IF WRONGNUM>13 THEN 2960
3020    IF WRONGNUM>7 THEN 3050
3030 ON WRONGNUM GOSUB *DAT1,*DAT2,*DAT3,*DAT4,*DAT5,*DAT6,*DAT7
3040 GOTO 3060
3050 ON WRONGNUM-7 GOSUB *DAT8,*DAT9,*DAT10,*DAT11,*DAT12,*DAT13
3060 GOTO *CONF.INDAT
3070 CLS 1:RETURN
3080 *CHDATA
3090   GOSUB *CONF.INDAT: GOSUB *REC
3100 RETURN
3110 *AUTISTP
3120 AUMANU$="AL"
3130  DMAX=1/RLA(N):DSTEP=2*(DMAX-DMIN)/(NIL*(NIL+1))
3140  FOR I=1 TO NIL-1:BOUND(NIL-I)=DMIN+I*(I+1)/2*DSTEP:NEXT
3150 RETURN
3160 *REC
3170  RECAL=0
3180    IF SYS<>SYS1 THEN RECAL=1
3190    IF BRAV<>BRAV1 THEN RECAL=1
3200    IF A1<>A OR B1<>B OR C1<>C THEN RECAL=1
3210    IF ALPH1<>ALPH OR BETA1<>BETA OR GAMM1<>GAMM THEN RECAL=1
3220    IF E1<>E THEN RECAL=1
3230    IF DMIN1>DMIN THEN RECAL=1
3240        UU=FNXCOD(U,V,W):VV=FNYCOD(U,V,W):WW=FNZCOD(U,V,W)
3250  XA1=UU1:YA1=VV1:ZA1=WW1:XA2=UU:YA2=VV:ZA2=WW
3260  GOSUB *CALAN:ANG10=CANGL:IF ANGRAN1*1.05<ANG10+ANGRAN THEN RECAL=1
3270 RETURN
3280 *CALAN
```

```
3290  RL1=XA1*XA1+YA1*YA1+ZA1*ZA1
3300  RL2=XA2*XA2+YA2*YA2+ZA2*ZA2
3310  COBR=FNPRO(XA1,YA1,ZA1,XA2,YA2,ZA2)
3320  COBR2=COBR*COBR/(RL1*RL2)
3330  IF ABS(COBR2)>.5 THEN 3350
3340  TAS=SQR(ABS(1/COBR2-1)):CANGL=ATN(TAS*SGN(COBR))*180/PI:GOTO 3380
3350  YZ=YA1*ZA2-ZA1*YA2:ZX=ZA1*XA2-XA1*ZA2:XY=XA1*YA2-YA1*XA2
3360  SIBR2=(YZ*YZ+ZX*ZX+XY*XY)/(RL1*RL2)
3370  TAS=SQR(ABS(SIBR2/(1-SIBR2))):CANGL=ATN(TAS*SGN(COBR))*180/PI
3380 CANGL=CANGL+360:CANGL=CANGL-180*INT(CANGL/180)
3390 IF SGN(COBR)=1 THEN 3400 ELSE IF CANGL=0 THEN CANGL=180
3400 RETURN
3410 *TEXTC
3420 LOCATE 3, 0:PRINT S$
3430 LOCATE 1, 1:PRINT FIX(ANGRAN*100)/100;"degrees"
3440 LOCATE 4, 2:PRINT "around"
3450 UP=FIX(U*1000)/1000:VP=FIX(V*1000)/1000:WP=FIX(W*1000)/1000
3460 LOCATE 1, 3:PRINT "[";UP;VP;WP;"]"
3470 LOCATE 2, 4:PRINT E;"kV"
3480 LOCATE 1, 5:PRINT "a =";A;"A"
3490 LOCATE 1, 6:PRINT "b =";B;"A"
3500 LOCATE 1, 7:PRINT "c =";C;"A"
3510 LOCATE 1, 8:PRINT "alpha =";ALPH;"deg"
3520 LOCATE 1, 9:PRINT "beta  =";BETA;"deg"
3530 LOCATE 1,10:PRINT "gamma =";GAMM;"deg"
3540 LOCATE 0,11:IF PRJ=1 THEN PRINT "central"; ELSE PRINT "stereographic";
3550 PRINT " projection "
3560 LOCATE 0,12:PRINT "horizontal direction"
3570   XO1=FIX(XO*1000)/1000:YO1=FIX(YO*1000)/1000:ZO1=FIX(ZO*1000)/1000
3580 LOCATE 1,13:PRINT "= [";XO1;YO1;ZO1;"]"
3590 LOCATE 1,14:PRINT "minimum d =";DMIN;"A"
3600 RETURN
3610 *WID
3620 IF NIL=1 THEN RETURN
3630   BOUND(NIL)=DMIN:BOU1$="spacing (A)":LBOU=LEN(BOU1$)
3640   IF PRPL=1 THEN 3680
3650    LPRINT "PU";-XYMAX*220;",";-XYMAX*80;";SI0.18,0.25;DI1,0;CP-3,0;";
3660    LPRINT "LB";BOU1$;CHR$(3);
3670   GOTO 3720
3680   WINDOW (0,0)-(639,399):VIEW (0,0)-(639,399)
3690     FOR J=1 TO LBOU
3700        MBOU$=MID$(BOU1$,J,1):MBOU=ASC(MBOU$)+256
3710     PUT (40+8*J,310),KANJI(MBOU):NEXT
3720    FOR I=NIL TO 1 STEP -1
3730        BOUN1$=STR$(BOUND(NIL-I)):BOUN2$=STR$(BOUND(NIL-I+1))
3740         IF BOUND(NIL-I  )=0 THEN BOUN1$="      "
3750         IF BOUND(NIL-I+1)=0 THEN BOUN2$="      "
3760          BOU1$="" : BOU2$=""
3770     FOR J=1 TO 5
3780     BOU1$=BOU1$+MID$(BOUN1$,J,1):BOU2$=BOU2$+MID$(BOUN2$,J,1):NEXT
3790          SCL$=BOU1$+" -"+BOU2$
3800   ON PRPL GOTO 3810,3930
3810 '* CRT *
3820 CL(0)=7:CL(1)=5:CL(2)=2:CL(3)=1:LSCL=LEN(SCL$):SST=(NIL-I)*20
3830   ON COWI GOTO 3840,3850
3840      LINE (10,330+SST)-(50,330+SST),CL(NIL-I):GOTO 3890
3850           IF NIL=2 AND I=2 THEN I2=3 ELSE I2=I
3860        FOR J=0 TO I2-1
3870           LINE (10,330+SST+J)-(50,330+SST+J)
3880        NEXT
3890        FOR J=1 TO LSCL
3900           MSCL$=MID$(SCL$,J,1):MSCL=ASC(MSCL$)+256
3910           PUT (50+8*J,326+SST),KANJI(MSCL)
3920        NEXT J :GOTO 4030
3930 '*plotter*
3940           WWXY=XYMAX/(6.5/2.4)
3950           IF NIL=2 AND I=2 THEN I2=3 ELSE I2=I
3960        FOR J=1 TO I2
3970         IF COWI=1 THEN LPRINT "SP";NIL-I2+1;";";
3980         XYME=-(XYMAX*87+WWXY*J)-XYMAX*7*(NIL-I)
3990         LPRINT "PU";-XYMAX*250;",";XYME;";PD";-XYMAX*220;",";XYME;";PU;";
4000         IF COWI=1 THEN GOTO 4020
4010        NEXT
4020        LPRINT "SI0.1,0.2;DI1,0;CP1,-0.25;LB";SCL$;CHR$(3);
4030    NEXT
4040 RETURN
4050 *TEXT
4060 LPRINT "IN;DF;SP1;IP0,0,4000,7200;IW;SC0,100,0,180"
4070 LPRINT "PU;PA10,160;SI0.26,0.4;LB";S$;CHR$(3)
4080 LPRINT "PA10,145;SI0.20,0.4;LB";FIX(ANGRAN*100)/100;"degrees";CHR$(3)
4090 LPRINT "PA15,138;SI0.20,0.35;LBaround";CHR$(3)
4100 UP=FIX(U*1000)/1000:VP=FIX(V*1000)/1000:WP=FIX(W*1000)/1000
```

```
4110 LPRINT "PA10,131;SI0.20,0.4;LB[";UP;CHR$(9);VP;CHR$(9);WP;"]";CHR$(3)
4120 LPRINT "PA10,121;SI0.20,0.4;LB";E;"kV";CHR$(3)
4130 LPRINT "PA10,113;SI0.15,0.25;LBlattice parameter";CHR$(3)
4140 LPRINT "PA25,108;LBa=";CHR$(8);A;CHR$(8);CHR$(3);
4150    LPRINT "CS7;LB";CHR$(80);CHR$(3);"CS;"
4160 LPRINT "PA25,103;LBb=";CHR$(8);B;CHR$(8);CHR$(3);
4170    LPRINT "CS7;LB";CHR$(80);CHR$(3);"CS;"
4180 LPRINT "PA25,98;LBc=";CHR$(8);C;CHR$(8);CHR$(3);
4190    LPRINT "CS7;LB";CHR$(80);CHR$(3);"CS;"
4200 LPRINT "PA25,93;CP-4,0;LBalpha=";CHR$(8);ALPH;CHR$(8);CHR$(3);
4210    LPRINT "CS8;LB";CHR$(95);CHR$(3);"CS;"
4220 LPRINT "PA25,88;CP-4,0;LBbeta =";CHR$(8);BETA;CHR$(8);CHR$(3);
4230    LPRINT "CS8;LB";CHR$(95);CHR$(3);"CS;"
4240 LPRINT "PA25,83;CP-4,0;LBgamma=";CHR$(8);GAMM;CHR$(8);CHR$(3);
4250    LPRINT "CS8;LB";CHR$(95);CHR$(3);"CS;"
4260 LPRINT "PA10,76;SI0.13,0.2;";
4270    IF PRJ=1 THEN LPRINT "LBCentral "; ELSE LPRINT "LBStereo ";
4280    LPRINT "Projection ";CHR$(3)
4290 LPRINT "PA10,69;SI0.15,0.25;LBminimum d=";CHR$(8);DMIN;CHR$(8);CHR$(3);
4300    LPRINT "CS7;LB";CHR$(80);CHR$(3);"CS;"
4310 LPRINT "PA10,62;SI0.15,0.25;LBhorizontal direction";CHR$(3);
4320   X01=FIX(X0*1000)/1000:Y01=FIX(Y0*1000)/1000:Z01=FIX(Z0*1000)/1000
4330 LPRINT "PA10,57;SI0.12,0.25;LB =[";X01;Y01;Z01;"]";CHR$(3);
4340 LPRINT "SP0;"
4350 RETURN
4360 *CONSTANT ' calculate constants for calculation
4370 WN=SQR(1000*E*(1+9.788E-07*1000*E))/12.26 :WN2=WN*WN ' ** wave number
4380 COA=COS(ALP):COB=COS(BET):COG=COS(GAM)
4390 SIA=SIN(ALP):SIB=SIN(BET):SIG=SIN(GAM)
4400 DREA=SQR(1-COA*COA-COB*COB-COG*COG+2*COA*COB*COG):VOL=A*B*C*DREA
4410 AX=A:AY=0:AZ=0
4420 BX=B*COG:BY=DREA*B/SIB:BZ=B*(COA-COB*COG)/SIB
4430 CX=C*COB:CY=0:CZ=C*SIB
4440 AXS=1/A:AYS=(COA*COB-COG)/(A*DREA*SIB):AZS=-COB/(A*SIB)
4450 BXS=0:BYS=SIB/(B*DREA):BZS=0
4460 CYS=(COB*COG-COA)/(C*DREA*SIB):CXS=0:CZS=1/(C*SIB)
4470 '   above coordinates construct matrix
4480 '          AX  BX  CX          AXS  BXS  CXS
4490 '     A = AY  BY  CY      B = AYS  BYS  CYS
4500 '          AZ  BZ  CZ          AZS  BZS  CZS
4510 D=AX*BY*CZ+AZ*BX*CY+CX*AY*BZ-(CX*BY*AZ+AX*CY*BZ+CZ*BX*AY)
4520 AIX=BY*CZ-BZ*CY : AIY=-AY*CZ+AZ*CY : AIZ=AY*BZ-AZ*BY
4530 BIX=-BX*CZ+BZ*CX : BIY=AX*CZ-AZ*CX : BIZ=-AX*BZ+AZ*BX
4540 CIX=BX*CY-BY*CX : CIY=-AX*CY+AY*CX : CIZ=AX*BY-AY*BX
4550 AIX=AIX/D : AIY=AIY/D : AIZ=AIZ/D
4560 BIX=BIX/D : BIY=BIY/D : BIZ=BIZ/D
4570 CIX=CIX/D : CIY=IC2/D : CIZ=CIZ/D
4580 '   above coordinates construct inversion matrix
4590 '              AIX  BIX  CIX
4600 '     INV(A) = AIY  BIY  CIY        A*(INV(A)) = I
4610 '              AIZ  BIZ  CIZ
4620 UU=FNXCOD(U,V,W)                          '  ** [uu,vv,ww] represents
4630 VV=FNYCOD(U,V,W)                          '     incident beam direction
4640 WW=FNZCOD(U,V,W)                          '     in real space.
4650 FA1=SQR(UU*UU+VV*VV):FA2=SQR(UU*UU+VV*VV+WW*WW)
4660 MAXKXY=WN*SIN(ANGRAN*PI/180)              '  ** max. kx,ky
4670 MAXKZ=WN*COS(ANGRAN*PI/180)               '  ** max. kz
4680 ON PRJ GOTO 4710,4730                     '  ** angle at the corner
4690 '                        **  ANGLEMAX(rad) is muximum angle at the corner.
4700 '                        **  XYMAX is muximum value of x,y in graph
4710  ANGLEMAX=ATN(SQR(2)*TAN(ANGRAN*PI/180))     '  * for central proj.
4720     XYMAX=WN*TAN(ANGRAN*PI/180):GOTO 4750
4730  ANGLEMAX=2*ATN(SQR(2*(TAN(ANGRAN*PI/360))^2))' for stereographic proj.
4740     XYMAX=2*WN*TAN(ANGRAN*PI/360):GOTO 4750
4750 ZMAX=1.1*(WN-WN*COS(ANGLEMAX))            '  ** muximum z consider
4760 ANGSTEP=ANGRAN/INTE
4770   XPR=FNXCOD(X0,Y0,Z0):YPR=FNYCOD(X0,Y0,Z0):ZPR=FNZCOD(X0,Y0,Z0)
4780   GOSUB *PRJ :XHORI=XPR:YHORI=YPR
4790 CO=FNSCPR(1,0,0,XHORI,YHORI,0)
4800 SI=FNSCPR(0,1,0,XHORI,YHORI,0) '** CO and SI determine horiz. direction
4810 GOSUB *HORDIR
4820 RETURN
4830 *HORDIR
4840 XX=WN:YY=0:ZZ=0:X=1:Y=0:Z=0
4850 GOSUB *CALZONE2:X0=X3:Y0=Y3:Z0=Z3
4860 RETURN
4870 '
4880 *PRJ
4890   IF FA1<.001 THEN 4920
4900   XJ=FNPROX(XPR,YPR,ZPR):YJ=FNPROY(XPR,YPR,ZPR):ZJ=FNPROZ(XPR,YPR,ZPR)
4910      GOTO 4940
4920   IF SGN(WW)=1 THEN RETURN
```

```
4930   XJ=-XPR:YJ=YPR:ZJ=-ZPR
4940 XPR=XJ:YPR=YJ:ZPR=ZJ: RETURN
4950 '
4960 *KIKUCHI
4970 SCREEN 3,1:CONSOLE 0,25:CLS 3:COLOR 2
4980 LOCATE 33,12:PRINT " calculating ":COLOR 0
4990    SYS1=SYS:BRAV1=BRAV
5000    A1=A:B1=B:C1=C:ALPH1=ALPH:BETA1=BETA:GAMM1=GAMM
5010    E1=E:U1=U:V1=V:W1=W:UU1=UU:VV1=VV:WW1=WW
5020    DMIN1=DMIN:ANGRAN1=ANGRAN:NIL1=NIL
5030 HJ=0:KJ=0:LJ=0:N=0
5040 GOSUB *CLIO
5050    IF ALCLI=0 THEN 5070
5060    LJ=LJ+1:GOTO 5040
5070    LJ=0:KJ=KJ+1:GOSUB *CLIL
5080    IF ALCLI=0 THEN 5100
5090    GOTO 5040
5100    LJ=0:KJ=0:HJ=HJ+1:GOSUB *CLILK
5110    IF ALCLI=0 THEN GOTO 5130
5120    GOTO 5040
5130 GOSUB *SORTING
5140 RETURN
5150 *CLIL
5160    ALCLI=0
5170    FOR LIJ=0 TO 2
5180    FOR HI=-1 TO 1 STEP 2
5190    FOR KI=-1 TO 1 STEP 2
5200    FOR LI=-1 TO 1 STEP 2
5210         H=HI*HJ:K=KI*KJ:L=LI*LIJ :GOSUB *REC.L
5220            IF RL<=RDMIN THEN ALCLI=1:RETURN
5230    NEXT:NEXT:NEXT:NEXT
5240 RETURN
5250 *CLILK
5260    ALCLI=0
5270    FOR LIJ=0 TO 1
5280    FOR KIJ=0 TO 2
5290    FOR HI=-1 TO 1 STEP 2
5300    FOR KI=-1 TO 1 STEP 2
5310    FOR LI=-1 TO 1 STEP 2
5320         H=HI*HJ:K=KI*KIJ:L=LI*LIJ :GOSUB *REC.L
5330            IF RL<=RDMIN THEN ALCLI=1:RETURN
5340    NEXT:NEXT:NEXT:NEXT:NEXT
5350 RETURN
5360 *CLIO
5370    ALCLI=0
5380    FOR HI=-1 TO 1 STEP 2
5390            IF HJ=0 AND HI=1 THEN 5480
5400    FOR KI=-1 TO 1 STEP 2
5410            IF KJ=0 AND KI=1 THEN 5470
5420    FOR LI=-1 TO 1 STEP 2
5430            IF LJ=0 AND LI=1 THEN 5460
5440         H=HI*HJ:K=KI*KJ:L=LI*LJ
5450      GOSUB *REC.L: IF RL<=RDMIN THEN ALCLI=1:GOSUB *KIKU
5460    NEXT
5470    NEXT
5480    NEXT
5490 RETURN
5500 *KIKU
5510 ON BRAV GOSUB *P,*I,*F,*A,*B,*C,*D,*R
5520    IF AL=0 THEN RETURN
5530    IF H*H+K*K+L*L=0 THEN RETURN
5540     XI=FNXCODS(H,K,L):YI=FNYCODS(H,K,L):ZI=FNZCODS(H,K,L)
5550     XPR=XI:YPR=YI:ZPR=ZI
5560 GOSUB *PRJ
5570     X=XPR:Y=YPR:Z=ZPR
5580         COPS=FNSCPR(0,0,1,X,Y,Z):GG=XI*XI+YI*YI+ZI*ZI
5590         RY=SQR(WN2-GG/4) : RX=RY*COPS
5600    ANG=180:GOSUB *ELLIPSE:IF INAREA=0 THEN 5620 '     ** out of area
5610 GOSUB *CHIND: N=N+1:HA(N)=H:KA(N)=K:LA(N)=L:RLA(N)=RL:RETURN
5620 RETURN
5630 *CHIND
5640 FOR IJ=1 TO N
5650 IF H=HA(IJ) THEN 5670
5660 NEXT : RETURN
5670 IF K<>KA(IJ) THEN 5660
5680 IF L<>LA(IJ) THEN 5660
5690 RETURN 5620
5700 '
5710 *ELLIPSE '  ** reference ellipse --> reference circle --> projection
5720    ANGL=ANG*PI/180
5730    XX1=-RX*COS(ANGL):YY1=RY*SIN(ANGL) '       ** ref. ellipse
5740    RXY1=RY*RY-(XX1*XX1+YY1*YY1):IF RXY1<0 THEN RXY1=0
```

```
5750            IF ANG=>90 AND ANG<=270 THEN 5770
5760    ZZ1=WN+SQR(RXY1):GOTO 5780
5770    ZZ1=WN-SQR(RXY1):GOTO 5780
5780    XXYY=X*X+Y*Y:IF XXYY=0 THEN GOTO 5830
5790    XX=(X*XX1-Y*YY1)/SQR(XXYY)+X/2
5800    YY=(X*YY1+Y*XX1)/SQR(XXYY)+Y/2
5810    ZZ=ZZ1+Z/2
5820    GOTO 5860
5830    XX=XX1+X/2
5840    YY=YY1+Y/2
5850    ZZ=ZZ1+Z/2   '                  ** (XX,YY,ZZ) is on the ref. circle
5860    INAREA=1:IF ZZ>ZMAX THEN INAREA=0:RETURN
5870 '*Projection
5880    ON PRJ GOTO 5890,5910
5890     XX=XX*WN/(WN-ZZ):YY=YY*WN/(WN-ZZ) ' *center
5900    RETURN
5910     XX=XX*2*WN/(2*WN-ZZ):YY=YY*2*WN/(2*WN-ZZ)' *stereo
5920 RETURN
5930 '
5940 *COMMAND
5950 IF PRPL=2 THEN GOSUB *PLOTWAIT
5960 GOSUB *PLOTTING
5970 *COMIN
5980 ON STOP GOSUB *STRP
5990   ON KEY GOSUB *F1,*F2,*F3,*F4,*F5,*F6,*F7,*F8,*F9,*F10
6000   ON HELP GOSUB *HLP
6010  HLP=0:ST=1:KEY ON:HELP ON:GOSUB *HLP
6020  HFK$=INKEY$:GOTO 6020
6030 RETURN
6040 *FMEN
6050 FOR J=1 TO 10
6060 FU$=" f."+STR$(J)+" "
6070 FU$=MID$(FU$,1,3)+MID$(FU$,5,2)
6080    COLOR 4:PRINT FU$:PRINT
6090 NEXT J
6100 COLOR 0
6110  LOCATE 7,0 :PRINT ": change data "
6120  LOCATE 7,2 :PRINT ": magnify "
6130  LOCATE 7,4 :PRINT ": rotate "
6140  LOCATE 7,6 :PRINT ": shift "
6150  LOCATE 7,8 :PRINT ": pole indices "
6160  LOCATE 7,10:PRINT ": line indices "
6170  LOCATE 7,12:PRINT ": angle between ":PRINT "          two poles "
6180  LOCATE 7,14:PRINT ": hard copy "
6190  LOCATE 7,16:PRINT ": plotter "
6200  LOCATE 7,18:PRINT ": end "
6210  LOCATE 0,20:COLOR 4:PRINT " Select function key "
6220  PRINT " type [HELP]         ":PRINT "      for input data "
6230 COLOR 0:RETURN
6240 *HLP
6250 COLOR 0:CLS 1:HLP=HLP+1:HLP=FNEVOD(HLP)
6260 IF HLP=0 THEN GOSUB *FMEN :RETURN
6270 GOSUB *TEXTC
6280 COLOR 4:PRINT:PRINT " Select function key "
6290               PRINT " type [HELP]          "
6300               PRINT "   for function menu "
6310 COLOR 0:RETURN
6320 *F1
6330    SCREEN 3,1:CLS 3:KEY OFF:HELP OFF
6340    GOSUB *CHDATA
6350    GOSUB *REC
6360    GOSUB *CONSTANT
6370       IF RECAL=1 THEN GOSUB *KIKUCHI
6380    GOSUB *PLOTTING
6390 RETURN *COMIN
6400 *F2
6410   CLS 1:CONSOLE 1,24:LOCATE 1,0
6420 COLOR 0:PRINT " command ";:COLOR 4:PRINT " Magnify ":COLOR 0
6430    KEY OFF:HELP OFF
6440    GOSUB *MAG
6450       IF MAG$="R" OR MAG$="r" THEN  6500
6460    GOSUB *CONSTANT
6470    GOSUB *REC
6480       IF RECAL=1 THEN GOSUB *KIKUCHI
6490    GOSUB *PLOTTING
6500 CONSOLE 0,24:CLS 1:RETURN *COMIN
6510 *F3
6520   CLS 1:CONSOLE 1,24:LOCATE 1,0
6530 COLOR 0:PRINT " command ";:COLOR 4:PRINT " Rotation ":COLOR 0
6540    KEY OFF:HELP OFF
6550    GOSUB *ROT
6560       IF RANG=0 THEN 6580
```

```
6570    GOSUB *PLOTTING
6580 CONSOLE 0,24:CLS 1:RETURN *COMIN
6590 *F4
6600   CLS 1:CONSOLE 1,24:LOCATE 1,0
6610 COLOR 0:PRINT " command ";:COLOR 4:PRINT " Shift ":COLOR 0
6620    KEY OFF:HELP OFF
6630    GOSUB *SHIFT
6640       IF TRAN$="R" OR TRAN$="r" THEN 6690
6650    GOSUB *CONSTANT
6660    GOSUB *REC
6670       IF RECAL=1 THEN GOSUB *KIKUCHI
6680    GOSUB *PLOTTING
6690 CONSOLE 0,24:CLS 1:RETURN *COMIN
6700 *F5
6710   CLS 1:CONSOLE 1,24:LOCATE 1,0
6720 COLOR 0:PRINT " command ";:COLOR 4:PRINT " Pole ":COLOR 0
6730    HFK=5:KEY OFF:HELP OFF
6740    GOSUB *POLE
6750 CONSOLE 0,24:CLS 1:RETURN *COMIN
6760 *F6
6770   CLS 1:CONSOLE 1,24:LOCATE 1,0
6780 COLOR 0:PRINT " command ";:COLOR 4:PRINT " Reflection ":COLOR 0
6790    CLS 1:KEY OFF:HELP OFF
6800    GOSUB *REF
6810 CONSOLE 0,24:CLS 1:RETURN *COMIN
6820 *F7
6830   CLS 1:CONSOLE 1,24:LOCATE 1,0
6840 COLOR 0:PRINT " command ";:COLOR 4:PRINT " Angle ":COLOR 0
6850    HFK=7:CLS 1:KEY OFF:HELP OFF
6860    GOSUB *CA
6870 CONSOLE 0,24:CLS 1:RETURN *COMIN
6880 *F8
6890    CLS 1:KEY OFF:HELP OFF
6900    GOSUB *TEXTC
6910    COPY 3 : CLS 1
6920 RETURN *COMIN
6930 *F9
6940    KEY OFF:HELP OFF
6950    GOSUB *PLOTWAIT
6960 RETURN *COMIN
6970 *PLOTWAIT
6980 COLOR 0:CLS 1:PRINT " command ";:COLOR 4:PRINT " Plotter ":PRINT:COLOR 0
6990 COLOR 2:PRINT " * Set plotter *":COLOR 0:PRINT
7000      PRINT " Pen  No. 1"
7010      IF NIL=1 OR COWI=2 THEN 7030
7020      PRINT "    - No.";NIL
7030      PRINT " will be used."
7040 IF COWI=2 THEN 7100
7050   PRINT:PRINT " recommendable color"
7060      PRINT "     Pen 1 : Black":IF NIL=1 THEN 7100
7070      PRINT "     Pen 2 : Brown":IF NIL=2 THEN 7100
7080      PRINT "     Pen 3 : Blue ":IF NIL=3 THEN 7100
7090      PRINT "     Pen 4 : Green"
7100 PRINT:PRINT "  Pen speed ( cm/sec ) "
7110 INPUT "            =";VS:VS=ABS(VS)
7120 IF VS=0 THEN 7100
7130 IF VS<1 THEN VS=1
7140 IF VS>127 THEN VS=127
7150 CLS 1:PRINT :PRINT " Hit any key to start ":PRINT
7160 PRINT "  ( no indices [N] )"
7170 PRINT "  (   cancel [C]   )"
7180 HAK$=INKEY$:RMD=RND:IF HAK$="" THEN 7180
7190 IF HAK$="c" OR HAK$="C" THEN RETURN *COMIN
7200 PRPL=2:IF HAK$="n" OR HAK$="N" THEN NINDEX=1 ELSE NINDEX=0
7210 CLS 1:LOCATE 5,12:COLOR 2:PRINT "Plotting":COLOR 0
7220 GOSUB *PLOTTING:PRPL=1
7230 RETURN
7240 *F10
7250    CLS 1:KEY OFF:HELP OFF
7260    PRINT "Are you sure":PRINT " to terminate":PRINT " this program ";
7270    INPUT "(y/n)";HFK$
7280    IF HFK$="Y" OR HFK$="y" THEN HFK$="E" ELSE HFK$=""
7290 IF HFK$="E" THEN SCREEN 3,1:CLS 3 :END
7300 CLS 1:RETURN *COMIN
7310 *MAG
7320 CLS 1:LOCATE 0,3
7330 COLOR 4:PRINT "1";
7340 COLOR 0:PRINT "change ":PRINT " angular range "
7350 COLOR 4:PRINT "2";
7360 COLOR 0:PRINT "center and angular ":PRINT " range by cursor "
7370 COLOR 4:PRINT "3";
7380 COLOR 0:PRINT "center by cursor and ":PRINT " input angular range "
```

```
7390 COLOR 4:PRINT "4";
7400 COLOR 0:PRINT "input center and ":PRINT " angular range "
7410 COLOR 0:PRINT
7420 COLOR 4:PRINT "R";
7430 COLOR 0:PRINT "Return to ":PRINT " function menu"
7440 COLOR 0:INPUT "                    ";MAG$
7450    IF MAG$="R" OR MAG$="r" THEN RETURN
7460    MAG=VAL(MAG$) : MAG=INT(ABS(MAG))
7470    IF MAG=0 OR MAG>4 THEN 7440
7480 CLS 1:ON MAG GOSUB *RA,*CC,*CI,*II
7490 RETURN
7500 *RA
7510    LOCATE 0,3 : PRINT "present angular range "
7520    PRINT "  =";ANGRAN;"deg."
7530    PRINT : PRINT "angular range (deg)"
7540            INPUT "     =";ANGRANRA
7550    ANGRANRA=ABS(ANGRANRA)
7560     IF PRJ=1 AND ANGRANRA>60 THEN 7530
7570     IF PRJ=2 AND ANGRANRA>90 THEN 7530
7580     IF ANGRANRA<.01 THEN RETURN *MAG
7590    ANGRAN=ANGRANRA
7600 RETURN
7610 *CC
7620    XP0=0:YP0=0
7630    LOCATE 0,3:PRINT "determine center pole"
7640   GOSUB *POINTER
7650    IF A$="E" OR A$="e" THEN RETURN *MAG
7660    XM1=ZAX0:YM1=ZAY0:GOSUB *F257:XP0=XM1:YP0=YM1
7670   GOSUB *CALZONE:UC1=X3:VC1=Y3:WC1=Z3'     ** zone axis at center
7680    CLS 1:LOCATE 0,3:PRINT "zone axis"
7690    PRINT " at the center is"
7700    PRINT " [";UZA;VZA;WZA;"]"
7710    PRINT : PRINT "determine angular range"
7720    PRINT " by cursor "
7730    GOSUB *POINTER:XM2=ZAX0:YM2=ZAY0 '   ** another z.a. for angle range
7740    IF A$<>"E" AND A$<>"e" THEN GOTO 7760
7750   GOSUB *F257E:RETURN *MAG
7760    UUC=FNXCOD(UC1,VC1,WC1):VVC=FNYCOD(UC1,VC1,WC1):WWC=FNZCOD(UC1,VC1,WC1)
7770    ZAX0=XM2:ZAY0=YM2
7780   GOSUB *CALZONE
7790    UZA1=X3:VZA1=Y3:WZA1=Z3 '        ** zone axis on side-line of screen
7800    UUS=FNXCOD(X3,Y3,Z3):VVS=FNYCOD(X3,Y3,Z3):WWS=FNZCOD(X3,Y3,Z3)
7810   XA1=UUC:YA1=VVC:ZA1=WWC:XA2=UUS:YA2=VVS:ZA2=WWS
7820   GOSUB *CALAN :ANGRANRA=CANGL
7830    IF ANGRANRA>.01 THEN ANGRAN=ANGRANRA
7840    U=UC1:V=VC1:W=WC1
7850 RETURN
7860 *CI
7870  XP0=0:YP0=0
7880    LOCATE 0,3:PRINT "determine center pole"
7890   GOSUB *POINTER
7900    IF A$="E" OR A$="e" THEN RETURN *MAG
7910    XM0=ZAX0:YM0=ZAY0 '       ** zone axis at centere
7920   GOSUB *CALZONE
7930    U=X3:V=Y3:W=Z3:UP=UZA:VP=VZA:WP=WZA
7940    CLS 1:LOCATE 0,3:PRINT "zone axis"
7950    PRINT " at the center is
7960    PRINT " [";UP;VP;WP;"]"
7970    PRINT : PRINT "determine angular range"
7980    INPUT " angle range (deg) =";ANGRANRA
7990    ANGRANRA=ABS(ANGRANRA)
8000     IF PRJ=1 AND ANGRANRA>60 THEN 7980
8010     IF PRJ=2 AND ANGRANRA>90 THEN 7980
8020     IF ANGRANRA<.01 THEN GOSUB *TYC:RETURN *MAG
8030   ANGRAN=ANGRANRA
8040 RETURN
8050 *II
8060    LOCATE 0,3
8070    PRINT " Zone axis  u,v,w ":INPUT "  ";UII,VII,WII
8080     IF UII^2+VII^2+WII^2=0 THEN RETURN *MAG
8090    PRINT " angular range (deg) ":INPUT "  ";ANGRANRA
8100    ANGRANRA=ABS(ANGRANRA)
8110     IF PRJ=1 AND ANGRANRA>60 THEN 8090
8120     IF PRJ=2 AND ANGRANRA>90 THEN 8090
8130    IF ANGRANRA<.01 THEN RETURN *MAG
8140    U=UII:V=VII:W=WII:ANGRAN=ANGRANRA
8150 RETURN
8160 *ROT
8170 COLOR 0:LOCATE 0,3
8180    PRINT "rotation angle (deg)"
8190    INPUT "      =";RANG:RANGL=RANG*PI/180
8200    CO1=CO*COS(RANGL)+SI*SIN(RANGL)
```

```
8210    SI1=-CO*SIN(RANGL)+SI*COS(RANGL)
8220  CO=CO1:SI=SI1:GOSUB *HORDIR
8230 RETURN
8240 *SHIFT
8250 LOCATE 0,2:COLOR 4:PRINT "1";
8260 COLOR 0:PRINT "determine center":PRINT " by cursor "
8270 COLOR 4:PRINT "2";
8280 COLOR 0:PRINT "input x-angle  ":PRINT "  and y-angle  "
8290 COLOR 0:PRINT:COLOR 4:PRINT "R";
8300 COLOR 0:PRINT "Return to    ":PRINT " function menu"
8310         INPUT "                  ";TRAN$
8320    IF TRAN$="R" OR TRAN$="r" THEN RETURN
8330    TRAN=VAL(TRAN$):TRAN=INT(ABS(TRAN))
8340    IF TRAN=0 OR TRAN>2 THEN 8310
8350   ON TRAN GOTO *TRAN1,*TRAN2
8360 *TRAN1
8370            CLS 1:XP0=0:YP0=0
8380    LOCATE 0,3:PRINT "determine center pole"
8390    GOSUB *POINTER:XP0=ZAX0:YP0=ZAY0
8400    IF A$="E" OR A$="e" THEN TRAN$="E" : GOTO *SHIFT
8410    GOSUB *CALZONE:U=X3:V=Y3:W=Z3
8420 RETURN
8430 *TRAN2
8440     CLS 1 : LOCATE 0,2 : PRINT "input angle (deg)"
8450    INPUT " x-direction =";TRX0
8460            IF ABS(TRX0)>89 THEN GOTO 8450
8470    INPUT " y-direction =";TRY0
8480            IF ABS(TRY0)>89 THEN GOTO 8470
8490    IF TRX0=0 AND TRY0=0 THEN CLS 1:TRAN$="R": GOTO *SHIFT
8500    TRX=TRX0*PI/180:TRY=TRY0*PI/180
8510            STRX=SIN(TRX):STRY=SIN(TRY)
8520            STR2=SQR(1-STRX*STRX*STRY*STRY)
8530    XX=WN*STRX*SQR(1-STRY*STRY)/STR2
8540    YY=WN*STRY*SQR(1-STRX*STRX)/STR2
8550    ZZ=SQR(WN2-(XX*XX+YY*YY))
8560    GOSUB *CALZONE2:U=X3:V=Y3:W=Z3
8570 RETURN
8580 *POLE
8590 LOCATE 0,3
8600 COLOR 4:PRINT "1";
8610 COLOR 0:PRINT "index the pole ":PRINT
8620 COLOR 4:PRINT "2";
8630 COLOR 0:PRINT "search the pole ":PRINT
8640 COLOR 4:PRINT "3";
8650 COLOR 0:PRINT "calculate the angle "
8660         PRINT " between two poles ":PRINT
8670 COLOR 4:PRINT "R";
8680 COLOR 0:PRINT "Return to ":PRINT " function menu"
8690 COLOR 0:INPUT "                  ";PO$
8700            IF PO$="R" OR PO$="r" THEN RETURN
8710    PO=VAL(PO$):PO=INT(ABS(PO)):IF PO=0 OR PO>4 THEN 8690
8720    CLS 1: ON PO GOSUB *SI,*FP,*CA
8730 CLS 1:GOTO *POLE
8740 *SI
8750  XP0=0:YP0=0
8760    GOSUB *POINTER
8770            XP0=ZAX0:YP0=ZAY0
8780            IF A$="E" THEN RETURN
8790    GOSUB *CALZONE
8800    LOCATE 1,5:PRINT "pole :"
8810 PRINT "  [";UZA;VZA;WZA;"]          "
8820 GOSUB *TYC:GOTO 8760
8830 *FP
8840 CLS 1:LOCATE 0,12:PRINT " for END ":PRINT "  input  0,0,0"
8850 LOCATE 0,3 : PRINT "input index"
8860  INPUT " U,V,W =";UX,VX,WX
8870  IF UX^2+VX^2+WX^2 =0 THEN :RETURN
8880  GET (XP,YP)-STEP(9,9),IG2%
8890  GOSUB *TYC
8900  XPR=FNXCOD(UX,VX,WX):YPR=FNYCOD(UX,VX,WX):ZPR=FNZCOD(UX,VX,WX)
8910  SLEN=SQR(XPR*XPR+YPR*YPR+ZPR*ZPR)
8920  GOSUB *PRJ :X=XPR:Y=YPR:Z=ZPR
8930  X1=(CO*X+SI*Y)*WN/SLEN : Y1=(-SI*X+CO*Y)*WN/SLEN : Z1=Z*WN/SLEN
8940  X1=-X1 : Y1=Y1 : Z1=WN-Z1
8950 ON PRJ GOTO 8960,8980
8960   X2=X1*WN/(WN-Z1):Y2=Y1*WN/(WN-Z1) ' ** central
8970 GOTO 8990
8980   X2=X1*2*WN/(2*WN-Z1):Y2=Y1*2*WN/(2*WN-Z1) ' ** stereo
8990    IF ABS(X2)<=XYMAX AND ABS(Y2)<=XYMAX THEN CLS 1:GOTO 9040
9000        LOCATE 0,6:COLOR 2:PRINT " out of area ":COLOR 0
9010        LOCATE 0,8 :PRINT " HIT RETURN KEY"
9020        HIR$=INKEY$:IF HIR$="" THEN 9020
```

```
9030     GOTO *FP
9040         XP=MAP(X2,0):YP=MAP(Y2,1)
9050     GET (XP,YP)-STEP(9,9),IG2%:PUT (XP,YP),IG%,OR
9060     LOCATE 0,6:PRINT " Zone axis "
9070               PRINT "  [";UX;VX;WX;"]":PRINT "  is indicated."
9080     LOCATE 0,10 :PRINT " HIT RETURN KEY"
9090     HIR$=INKEY$:IF HIR$="" THEN 9090
9100     PUT (XP,YP),IG2%,AND:GOTO *FP
9110 RETURN
9120 *CA
9130 LOCATE 0,3
9140 PRINT:COLOR 4:PRINT "1";:COLOR 0:PRINT "two poles by cursor "
9150 PRINT:COLOR 4:PRINT "2";:COLOR 0:PRINT "one pole by cursor "
9160   PRINT "   onother by index "
9170       COLOR 4:PRINT "3";:COLOR 0:PRINT "two poles by indices "
9180 PRINT:PRINT:COLOR 4:PRINT "R";:COLOR 0:PRINT "Return to  "
9190 PRINT " function menu  ":INPUT "                  ";CA3$
9200      IF CA3$="R" OR CA3$="r" THEN RETURN
9210      CA3=VAL(CA3$):CA3=INT(ABS(CA3))
9220   IF CA3=0 OR CA3>4 THEN 9190
9230 ON CA3 GOTO *TPC,*OCOI,*TPI
9240 *TPC
9250 CLS 1:XPO=0:YPO=0
9260   GOSUB *POINTER
9270     IF A$="E" THEN RETURN
9280     GOSUB *F257:XPO=ZAXO:YPO=ZAYO
9290   GOSUB *CALZONE:UZA1=UZA:VZA1=VZA:WZA1=WZA
9300     XX1=XX:YY1=YY:ZZ1=ZZ
9310   GOSUB *POINTER
9320     IF A$="E" THEN GOSUB *F257E:RETURN
9330     XPO=ZAXO:YPO=ZAYO
9340   GOSUB *CALZONE:UZA2=UZA:VZA2=VZA:WZA2=WZA
9350     XX2=XX:YY2=YY:ZZ2=ZZ
9360 XA1=XX1:YA1=YY1:ZA1=ZZ1:XA2=XX2:YA2=YY2:ZA2=ZZ2
9370 GOSUB *CALAN : ANG=CANGL:ANG=FIX(ANG*100)/100
9380   CLS 1:LOCATE 0,5:PRINT " angle between "
9390   PRINT " [";UZA1;VZA1;WZA1;"]"
9400   PRINT "       and":PRINT " [";UZA2;VZA2;WZA2;"]"
9410   PRINT " is ";ANG;"degrees"
9420 PRINT:PRINT " Hit return key"
9430 A$=INKEY$ : IF A$="" THEN 9430
9440 GOSUB *TYC:GOSUB *F257E:CLS 1:GOTO 9260
9450 *OCOI
9460 CLS 1:XPO=0:YPO=0
9470   GOSUB *POINTER
9480       IF A$="E" THEN RETURN
9490   XPO=ZAXO:YPO=ZAYO :GOSUB *CALZONE :XX1=XX:YY1=YY:ZZ1=ZZ
9500   UZA1=UZA:VZA1=VZA:WZA1=WZA
9510   CLS 1:LOCATE 0,5:PRINT "arrowed pole is"
9520   PRINT " [";UZA;VZA;WZA;"]"
9530   LOCATE 0,8:PRINT "another pole "
9540   INPUT " u,v,w =";UX,VX,WX
9550   IF UX^2+VX^2+WX^2=0 THEN GOSUB *TYC:RETURN
9560   XPR=FNXCOD(UX,VX,WX):YPR=FNYCOD(UX,VX,WX):ZPR=FNZCOD(UX,VX,WX)
9570   SLEN=SQR(XPR*XPR+YPR*YPR+ZPR*ZPR)
9580   GOSUB *PRJ :X=XPR:Y=YPR:Z=ZPR
9590   XX2=CO*X+SI*Y : YY2=-SI*X+CO*Y : ZZ2=Z
9600 XA1=XX1:YA1=YY1:ZA1=ZZ1:XA2=XX2:YA2=YY2:ZA2=ZZ2
9610 GOSUB *CALAN :ANG=CANGL:ANG=FIX(ANG*100)/100
9620   CLS 1:LOCATE 0,5:PRINT " angle between "
9630   PRINT "    [";UZA1;VZA1;WZA1;"]"
9640   PRINT "  and [";UX;VX;WX;"]"
9650   PRINT " is ";ANG;"degrees"
9660 PRINT:PRINT "  Hit return key"
9670 A$=INKEY$ : IF A$="" THEN 9670
9680 GOSUB *TYC:CLS 1:GOTO 9470
9690 *TPI
9700 CLS 1:LOCATE 0,15:PRINT " for END ":PRINT "  input 0,0,0"
9710   LOCATE 0,5:PRINT "  one pole "
9720   INPUT "  u,v,w =";UX1,VX1,WX1
9730   IF UX1^2+VX1^2+WX1^2=0 THEN RETURN
9740   XPR=FNXCOD(UX1,VX1,WX1):YPR=FNYCOD(UX1,VX1,WX1):ZPR=FNZCOD(UX1,VX1,WX1)
9750   GOSUB *PRJ :XA1=XPR:YA1=YPR:ZA1=ZPR
9760   LOCATE 0,8:PRINT "  another pole "
9770   INPUT "  u,v,w =";UX2,VX2,WX2
9780            IF UX2^2+VX2^2+WX2^2=0 THEN RETURN
9790   XPR=FNXCOD(UX2,VX2,WX2):YPR=FNYCOD(UX2,VX2,WX2):ZPR=FNZCOD(UX2,VX2,WX2)
9800   GOSUB *PRJ :XA2=XPR:YA2=YPR:ZA2=ZPR
9810 GOSUB *CALAN : ANG=CANGL:ANG=FIX(ANG*100)/100
9820   CLS 1:LOCATE 0,5:PRINT " angle between "
9830   PRINT "    [";UX1;VX1;WX1;"]"
9840   PRINT "  and [";UX2;VX2;WX2;"]"
```

```
9850   PRINT " is ";ANG;"degrees"
9860 PRINT:PRINT "HIT RETURN KEY"
9870 A$=INKEY$:IF A$="" THEN 9870
9880 CLS 1:GOTO *TPI
9890 RETURN
9900 *REF
9910   GOSUB *MENUR
9920   XR=195:YR=195
9930   GET (XR,YR)-STEP(9,9),IG2%
9940 AREF$=INKEY$:AREF=VAL(AREF$)
9950 IF AREF$="" THEN 9940
9960 IF AREF$=" " THEN GOSUB *REFSEARCH:GOSUB *MENUR:GOTO 9940
9970 IF AREF=5 THEN 9940
9980 ON AREF GOSUB *TY1R,*TY2R,*TY3R,*TY4R,,*TY6R,*TY7R,*TY8R,*TY9R
9990 IF AREF$="E" OR AREF$="e" THEN GOSUB *TYER:RETURN
10000 GOTO 9940
10010 *MENUR
10020 CLS 1 : LOCATE 0,3 : PRINT " Push ten key"
10030 LOCATE 0,10
10040 PRINT " space  :  get "
10050 PRINT
10060 PRINT "   E    :  end "
10070 PRINT
10080 PRINT "ten key : cursor control"
10090 RETURN
10100 *TY2R
10110   IF YR=390 THEN RETURN
10120   PUT (XR,YR),IG2%,AND
10130   IF XR=0 THEN YR=YR+5:GOTO 10160
10140   IF XR=390 THEN YR=YR+5:GOTO 10160
10150   YR=390
10160   GET (XR,YR)-STEP(9,9),IG2%:PUT (XR,YR),IGR%,OR
10170 RETURN
10180 *TY4R
10190   IF XR=0 THEN RETURN
10200   PUT (XR,YR),IG2%,AND:IF YR=0 THEN XR=XR-5:GOTO 10230
10210   IF YR=390 THEN XR=XR-5:GOTO 10230
10220   XR=0
10230   GET (XR,YR)-STEP(9,9),IG2%:PUT (XR,YR),IGR%,OR
10240 RETURN
10250 *TY6R
10260   IF XR=390 THEN RETURN
10270   PUT (XR,YR),IG2%,AND:IF YR=0 THEN XR=XR+5:GOTO 10300
10280   IF YR=390 THEN XR=XR+5:GOTO 10300
10290   XR=390
10300   GET (XR,YR)-STEP(9,9),IG2%:PUT (XR,YR),IGR%,OR
10310 RETURN
10320 *TY8R
10330   IF YR=0 THEN RETURN
10340   PUT (XR,YR),IG2%,AND:IF XR=0 THEN YR=YR-5:GOTO 10370
10350   IF XR=390 THEN YR=YR-5:GOTO 10370
10360   YR=0
10370   GET (XR,YR)-STEP(9,9),IG2%:PUT (XR,YR),IGR%,OR
10380 RETURN
10390 *TY1R
10400   PUT (XR,YR),IG2%,AND :XR=0:YR=390
10410   GET (XR,YR)-STEP(9,9),IG2%:PUT (XR,YR),IGR%,OR
10420 RETURN
10430 *TY3R
10440   PUT (XR,YR),IG2%,AND :XR=390:YR=390
10450   GET (XR,YR)-STEP(9,9),IG2%:PUT (XR,YR),IGR%,OR
10460 RETURN
10470 *TY7R
10480   PUT (XR,YR),IG2%,AND :XR=0:YR=0
10490   GET (XR,YR)-STEP(9,9),IG2%:PUT (XR,YR),IGR%,OR
10500 RETURN
10510 *TY9R
10520   PUT (XR,YR),IG2%,AND :XR=390:YR=0
10530   GET (XR,YR)-STEP(9,9),IG2%:PUT (XR,YR),IGR%,OR
10540 RETURN
10550 *TYER
10560   PUT (XR,YR),IG2%,AND
10570 RETURN
10580 *REFSEARCH
10590   IF XR=0   THEN CASE=1:GOTO 10640
10600   IF XR=390 THEN CASE=2:GOTO 10640
10610   IF YR=0   THEN CASE=3:GOTO 10640
10620   IF YR=390 THEN CASE=4:GOTO 10640
10630 RETURN
10640   ON CASE GOTO 10650,10680,10710,10740
10650           SYR1=-MAP(YR+9,3):SYR2=-MAP(YR,3)
10660           SXR1=-XYMAX*1.01:SXR2=-XYMAX*.99
```

```
10670   GOTO 10770
10680           SYR1=-MAP(YR+9,3):SYR2=-MAP(YR,3)
10690           SXR1=XYMAX*.99:SXR2=XYMAX*1.01
10700   GOTO 10770
10710           SXR1=MAP(XR,2):SXR2=MAP(XR+9,2)
10720           SYR1=XYMAX*.99:SYR2=XYMAX*1.01
10730   GOTO 10770
10740           SXR1=MAP(XR,2):SXR2=MAP(XR+9,2)
10750           SYR1=-XYMAX*1.01:SYR2=-XYMAX*.99
10760   GOTO 10770
10770   FOR JSER=1 TO NSER
10780           XPS=XPLS(JSER):YPS=YPLS(JSER)
10790           XPE=XPLE(JSER):YPE=YPLE(JSER)
10800         IF XPS<=SXR1 OR XPS=>SXR2 THEN 10840
10810         IF YPS<=SYR1 OR YPS=>SYR2 THEN 10840
10820   GOSUB *SHREF1
10830         IF A$="e" OR A$="E" THEN RETURN
10840         IF XPE<=SXR1 OR XPE=>SXR2 THEN 10880
10850         IF YPE<=SYR1 OR YPE=>SYR2 THEN 10880
10860   GOSUB *SHREF2
10870         IF A$="e" OR A$="E" THEN RETURN
10880   NEXT JSER
10890 RETURN
10900 *SHREF1
10910   XR1=XPE:YR1=YPE:GOTO 10940
10920 *SHREF2
10930   XR1=XPS:YR1=YPS:GOTO 10940
10940   XR0=MAP(XR1,0):YR0=MAP(-YR1,1)
10950           IF XR0<11 OR YR0<11 THEN 10980
10960   GET (XR0,YR0)-STEP(9,9),IG3%:PUT (XR0,YR0),IG%,OR
10970  GOTO 10990
10980   GET (XR0-10,YR0-10)-STEP(9,9),IG3%:PUT (XR0-10,YR0-10),IGR2%,OR
10990   CLS 1:LOCATE 0,3:PRINT "     index "
11000   PRINT " h,k,l =";IHKL$(JSER)
11010   PRINT:PRINT "Hit space key":PRINT "  for next index"
11020   PRINT:PRINT "Hit key [E]":PRINT "  for end "
11030   A$=INKEY$ : IF A$="" THEN GOTO 11030
11040   IF A$=" " THEN 11070
11050   IF A$="e" OR A$="E" THEN 11070
11060   GOTO 11030
11070  IF XR0<11 OR YR0<11 THEN 11100
11080   PUT (XR0,YR0),IG3%,AND
11090  GOTO 11110
11100   PUT (XR0-10,YR0-10),IG3%,AND
11110 RETURN
11120 *SORTING
11130 FOR I=1 TO N
11140    FOR J=1 TO I
11150    RRR=RLA(J):HH=HA(J):KK=KA(J):LL=LA(J)
11160    IF RLA(J)=>RLA(I) THEN 11190
11170    RLA(J)=RLA(I):HA(J)=HA(I):KA(J)=KA(I):LA(J)=LA(I)
11180    RLA(I)=RRR:HA(I)=HH:KA(I)=KK:LA(I)=LL
11190    NEXT
11200 NEXT
11210 RETURN
11220 *STRP2
11230 RETURN *STRP1
11240 *PLOTTING
11250    IF AUMANU$="M" THEN 11270
11260 GOSUB *AUTISTP
11270 NSER=0
11280 ON STOP GOSUB *STRP2
11290 STOP ON
11300 ON PRPL GOTO 11310 , 11370
11310 ' ** C R T **
11320   CONSOLE ,,0,0 : SCREEN 3,1 : CLS 3
11330   XYMX=1.05263*XYMAX
11340   WINDOW (-XYMX,-XYMX)-(XYMX,XYMX)
11350   VIEW (210,0)-(609,399)
11360 GOTO 11470
11370 ' ** plotter **
11380   SCXY=FIX(XYMAX*1E+06)/10000
11390   ORGX=7100:ORGY=3900:IPXY=2600
11400   IPXMIN=4300:IPXMAX=9900:IPYMIN=1100:IPYMAX=6700
11410   IPXMIN=ORGX-IPXY:IPXMAX=ORGX+IPXY
11420   IPYMIN=ORGY-IPXY:IPYMAX=ORGY+IPXY
11430 LPRINT "IN;DF;PS4;PA;SI0.1,0.2;SP1;VS";VS;";"
11440 LPRINT "IP";IPXMIN;",";IPYMIN;",";IPXMAX;",";IPYMAX;";"
11450 LPRINT "IW";IPXMIN;",";IPYMIN;",";IPXMAX;",";IPYMAX;";"
11460 LPRINT "SC";-SCXY;",";SCXY;",";-SCXY;",";SCXY;";"
11470 '** CURVE OR LINE
11480 ON PRJLC GOTO *AP.LINE , *CURVE
```

```
11490 '
11500 *AP.LINE '                    ** line approx.
11510 FOR J=1 TO N
11520     H=HA(J):K=KA(J):L=LA(J)
11530   IF RLA(J)>1/DMIN THEN GOTO 11830
11540     XPR=FNXCODS(H,K,L):YPR=FNYCODS(H,K,L):ZPR=FNZCODS(H,K,L)
11550   GG=XPR*XPR+YPR*YPR+ZPR*ZPR
11560     GOSUB *PRJ: XJ=XPR:YJ=YPR:ZJ=ZPR
11570   X=XJ*CO+YJ*SI:Y=-XJ*SI+YJ*CO:Z=ZJ '         ** reciprocal lattice point
11580           COPS=FNSCPR(0,0,1,X,Y,Z)
11590           RY=SQR(WN2-GG/4) : RX=RY*COPS
11600   ANG=180:STOP STOP:GOSUB *ELLIPSE :STOP ON
11610           IF INAREA=0 THEN GOTO 11830
11620           IF ABS(X)<.0001 THEN GOTO *XEQ0
11630           IF ABS(Y)<.0001 THEN GOTO *YEQ0
11640   XL(1)=-Y/X*(XYMAX-YY)+XX  :YL(1)=XYMAX
11650           XYL2(1)=XL(1)^2+YL(1)^2
11660   XL(2)=-Y/X*(-XYMAX-YY)+XX :YL(2)=-XYMAX
11670           XYL2(2)=XL(2)^2+YL(2)^2
11680   YL(3)=-X/Y*(XYMAX-XX)+YY  :XL(3)=XYMAX
11690           XYL2(3)=XL(3)^2+YL(3)^2
11700   YL(4)=-X/Y*(-XYMAX-XX)+YY :XL(4)=-XYMAX
11710           XYL2(4)=XL(4)^2+YL(4)^2
11720   FOR IJ=1 TO 4
11730    FOR IJ2=1 TO IJ
11740             XLA=XL(IJ2):YLA=YL(IJ2):XYLA=XYL2(IJ2)
11750    IF XYL2(IJ)=>XYL2(IJ2) THEN 11790
11760             XL(IJ2)=XL(IJ):XL(IJ)=XLA
11770             YL(IJ2)=YL(IJ):YL(IJ)=YLA
11780             XYL2(IJ2)=XYL2(IJ):XYL2(IJ)=XYLA
11790   NEXT:NEXT
11800   XPL(0)=XL(1):YPL(0)=YL(1):XPL(1)=XL(2):YPL(1)=YL(2)
11810   IF ABS(XPL(1))>XYMAX OR ABS(YPL(1))>XYMAX THEN GOTO 11830
11820 STOP STOP:GOSUB *PLOT :STOP ON
11830 NEXT J
11840 STOP STOP:GOSUB *SCALE :GOSUB *WID :STOP ON
11850   IF PRPL=2 THEN STOP STOP:GOSUB *TEXT :LPRINT "SP0;":STOP ON:RETURN
11860   WINDOW (-XYMX,-XYMX)-(XYMX,XYMX):VIEW (210,0)-(609,399)
11870 RETURN
11880 *XEQ0
11890   XL(1)=XYMAX:YL(1)=YY
11900   XL(2)=-XYMAX:YL(2)=YY
11910 GOTO 11800
11920 *YEQ0
11930   XL(1)=XX:YL(1)=XYMAX
11940   XL(2)=XX:YL(2)=-XYMAX
11950 GOTO 11800
11960 '
11970 *CURVE
11980 FOR J=1 TO N
11990     H=HA(J):K=KA(J):L=LA(J)
12000   IF RLA(J)>1/DMIN THEN GOTO 12380
12010     XPR=FNXCODS(H,K,L):YPR=FNYCODS(H,K,L):ZPR=FNZCODS(H,K,L)
12020   GG=XPR*XPR+YPR*YPR+ZPR*ZPR
12030     GOSUB *PRJ: XJ=XPR:YJ=YPR:ZJ=ZPR
12040 X=XJ*CO+YJ*SI:Y=-XJ*SI+YJ*CO:Z=ZJ '         ** reciprocal lattice point
12050   COPS=FNSCPR(0,0,1,X,Y,Z)
12060   RY=SQR(WN2-GG/4) : RX=RY*COPS
12070   ANG=180:STOP STOP:GOSUB *ELLIPSE :STOP ON
12080           IF INAREA=0 THEN GOTO 12380
12090 STOP STOP
12100 ANG=30:GOSUB *ELLIPSE :IF INAREA=0 THEN 12120
12110     SANG=0:EANG=360:GOTO 12250
12120 ANG=60:GOSUB *ELLIPSE :IF INAREA=0 THEN 12140
12130     SANG=30:EANG=330:GOTO 12250
12140 ANG=90:GOSUB *ELLIPSE :IF INAREA=0 THEN 12160
12150     SANG=60:EANG=300:GOTO 12250
12160 ANG=120:GOSUB *ELLIPSE :IF INAREA=0 THEN 12180
12170     SANG=90:EANG=270:GOTO 12250
12180 ANG=150:GOSUB *ELLIPSE :IF INAREA=0 THEN 12200
12190     SANG=120:EANG=240:GOTO 12250
12200 ANG=170:GOSUB *ELLIPSE :IF INAREA=0 THEN 12220
12210     SANG=150:EANG=210:GOTO 12250
12220 ANG=178:GOSUB *ELLIPSE :IF INAREA=0 THEN 12240
12230     SANG=170:EANG=190:GOTO 12250
12240     SANG=178:EANG=182
12250 STOP ON:NP=0:IN=0:CIRS=0:CIRE=0:XPL(0)=0:YPL(0)=0
12260   FOR ANG=SANG TO EANG STEP ANGSTEP
12270    STOP STOP:GOSUB *ELLIPSE:STOP ON
12280    IF ABS(XX)>XYMAX THEN INAREA=0 : GOTO 12310
12290    IF ABS(YY)>XYMAX THEN INAREA=0 : GOTO 12310
12300    IF INAREA=1 THEN GOTO 12340
```

```
12310    IF IN=0 THEN XPL(0)=XX:YPL(0)=YY:GOTO 12360
12320    IF IN=1 THEN STOP STOP:GOSUB *PLOT:STOP ON
12330    XPL(0)=XX:YPL(0)=YY:GOTO 12360
12340       NP=NP+1:IN=1:XPL(NP)=XX:YPL(NP)=YY
12350                   XPL(NP+1)=XX:YPL(NP+1)=YY
12360   NEXT ANG
12370    IF NP>0 THEN CIRE=1:STOP STOP:GOSUB *PLOT:STOP ON
12380 NEXT J
12390 STOP STOP:GOSUB *SCALE :GOSUB *WID:STOP ON
12400 ON STOP GOSUB *STRP
12410   IF PRPL=2 THEN GOSUB *TEXT:LPRINT "SPO;":RETURN
12420   WINDOW (-XYMX,-XYMX)-(XYMX,XYMX):VIEW (210,0)-(609,399)
12430 RETURN
12440 *STRP1
12450 ON STOP GOSUB *STRP
12460   IF PRPL=2 THEN LPRINT "PU;SPO;":RETURN
12470   WINDOW (-XYMX,-XYMX)-(XYMX,XYMX):VIEW (210,0)-(609,399)
12480 RETURN
12490 *PLOT
12500   IF PRJLC=1 THEN NP=0:GOTO 12570
12510   XPL(NP+1)=XX:YPL(NP+1)=YY
12520   IF XPL(0)=0 AND YPL(0)=0 THEN CIRS=1
12530   IF CIRS=0 THEN GOSUB *SPOINT
12540   IF CIRE=0 THEN GOSUB *EPOINT
12550   IF CIRS=1 THEN XPL(0)=XPL(1):YPL(0)=YPL(1)
12560   IF CIRE=1 THEN XPL(NP+1)=XPL(NP):YPL(NP+1)=YPL(NP)
12570   NSER=NSER+1
12580   IHKL$(NSER)=STR$(H)+" "+STR$(K)+" "+STR$(L)
12590   XPLS(NSER)=XPL(0):YPLS(NSER)=YPL(0)
12600   XPLE(NSER)=XPL(NP+1):YPLE(NSER)=YPL(NP+1)
12610   COL=1 : IF NIL=1 THEN 12660
12620   FOR JI=NIL-1 TO 1 STEP -1
12630     IF 1/RLA(J)>BOUND(JI) THEN COL=NIL-JI+1
12640   NEXT
12650 ON COWI GOTO *CCHAN, *WCHAN
12660 *CCHAN
12670 COL=NIL-COL+1
12680   ON PRPL GOTO 12690,12820
12690 '* C R T *
12700 IF COL>4 THEN 12760
12710 ON COL GOTO 12720,12730,12740,12750
12720     COL=7:GOTO 12770
12730     COL=5:GOTO 12770
12740     COL=2:GOTO 12770
12750     COL=1:GOTO 12770
12760     COL=1
12770   FOR JNP=0 TO NP
12780     LINE (XPL(JNP),-YPL(JNP))-(XPL(JNP+1),-YPL(JNP+1)),COL
12790   NEXT
12800  NP=0:IN=0:XPL(0)=0:YPL(0)=0
12810 RETURN
12820 '* Plotter *
12830   FOR JNP=0 TO NP+1
12840       XPL(JNP)=FIX(XPL(JNP)*1E+06)/10000
12850       YPL(JNP)=FIX(YPL(JNP)*1E+06)/10000
12860   NEXT
12870 LPRINT "SP";COL;";VS";VS;";"
12880   FOR JNP=0 TO NP+1
12890       LPRINT "PA";XPL(JNP);",";YPL(JNP);";PD;";
12900   NEXT
12910   LPRINT "PU;"
12920  IF NINDEX=0 THEN GOSUB *INDEXING
12930       NP=0:IN=0:XPL(0)=0:YPL(0)=0
12940 RETURN
12950 '
12960 *WCHAN
12970 ON PRPL GOTO 12980 , 13160
12980 ' * C R T *
12990 WXY0=XYMAX/391
13000 IF NIL=2 AND COL=2 THEN COL=3
13010 FOR JCOL=1 TO COL
13020           WXY=WXY0*(2*JCOL-COL-1)
13030   SJNP=0:EJNP=NP
13040   IF XPL(0)=XPL(1) AND YPL(0)=YPL(1) THEN SJNP=1
13050   IF XPL(NP)=XPL(NP+1) AND YPL(NP)=YPL(NP+1) THEN EJNP=NP-1
13060   FOR JNP=SJNP TO EJNP
13070           WX0=YPL(JNP+1)-YPL(JNP)
13080           WY0=-XPL(JNP+1)+XPL(JNP)
13090           WWXY=SQR(WX0*WX0+WY0*WY0)
13100           WX=WX0*WXY/WWXY:WY=WY0*WXY/WWXY
13110    LINE (XPL(JNP)+WX,-YPL(JNP)-WY)-(XPL(JNP+1)+WX,-YPL(JNP+1)-WY)
13120   NEXT
```

```
13130 NEXT JCOL
13140       NP=0:IN=0:XPL(0)=0:YPL(0)=0
13150 RETURN
13160 ' * plotter *
13170       WXYO=XYMAX/(650/1.2)
13180 IF NIL=2 AND COL=2 THEN COL=3
13190 FOR JCOL=1 TO COL
13200           WXY=WXYO*(2*JCOL-COL-1)
13210   FOR JNP=0 TO NP
13220           WXO=YPL(JNP+1)-YPL(JNP)
13230           WYO=-XPL(JNP+1)+XPL(JNP)
13240           WWXY=SQR(WXO*WXO+WYO*WYO)
13250           WX=WXO*WXY/WWXY : WY=WYO*WXY/WWXY
13260     XPLL(JNP)=XPL(JNP)+WX
13270     YPLL(JNP)=YPL(JNP)+WY
13280     XPLL(JNP)=FIX(XPLL(JNP)*1E+06)/10000
13290     YPLL(JNP)=FIX(YPLL(JNP)*1E+06)/10000
13300   NEXT
13310     XPLL(NP+1)=XPL(NP+1)+WX
13320     YPLL(NP+1)=YPL(NP+1)+WY
13330     XPLL(NP+1)=FIX(XPLL(NP+1)*1E+06)/10000
13340     YPLL(NP+1)=FIX(YPLL(NP+1)*1E+06)/10000
13350   FOR JNP=0 TO NP+1
13360     IJNP=FNEVOD(JCOL):JJNP=ABS((NP+1)*IJNP-JNP)
13370     LPRINT "PA";XPLL(JJNP);",";YPLL(JJNP);";PD;";
13380   NEXT
13390   LPRINT "PU;"
13400 NEXT JCOL
13410     XPL(0)=FIX(XPL(0)*1E+06)/10000
13420     YPL(0)=FIX(YPL(0)*1E+06)/10000
13430     XPL(NP+1)=FIX(XPL(NP+1)*1E+06)/10000
13440     YPL(NP+1)=FIX(YPL(NP+1)*1E+06)/10000
13450   IF NINDEX=0 THEN GOSUB *INDEXING
13460       NP=0:IN=0:XPL(0)=0:YPL(0)=0
13470 RETURN
13480 *SCALE
13490   IF ANGRAN=>60 THEN ANGSCALE=20:GOTO *SCALING
13500   IF ANGRAN=>30 THEN ANGSCALE=10:GOTO *SCALING
13510   IF ANGRAN=>15 THEN ANGSCALE= 5:GOTO *SCALING
13520   IF ANGRAN=> 6 THEN ANGSCALE= 2:GOTO *SCALING
13530   IF ANGRAN=> 3 THEN ANGSCALE= 1:GOTO *SCALING
13540   IF ANGRAN=> 1.5 THEN ANGSCALE= .5:GOTO *SCALING
13550   IF ANGRAN=> 1 THEN ANGSCALE= .2:GOTO *SCALING
13560   IF ANGRAN=> .5 THEN ANGSCALE= .1:GOTO *SCALING
13570   IF ANGRAN<.5 THEN RETURN
13580 *SCALING
13590 ON PRPL GOTO 13600,13810
13600 ' ** C R T **
13610 WINDOW (0,0)-(639,399)
13620 VIEW (0,0)-(639,399)
13630 FOR SCI=0 TO ANGRAN STEP ANGSCALE
13640  FOR IJ=-1 TO 1 STEP 2
13650      SCJ=SCI*IJ
13660   ON PRJ GOTO 13670,13680
13670           Y=WN*TAN(SCJ*PI/180):GOTO 13690
13680           Y=2*WN*TAN(SCJ*PI/360)
13690           YSCJ=199+Y*190/XYMAX
13700           LINE (205,199)-(205,YSCJ):LINE (202,YSCJ)-(208,YSCJ)
13710           SSCJ$=STR$(ABS(SCJ)):LSCJ=LEN(SSCJ$):IF LSCJ>4 THEN LSCJ=4
13720         FOR J=1 TO LSCJ
13730           MSCJ$=MID$(SSCJ$,J,1):MSCJ=ASC(MSCJ$)+256
13740           PUT (190-8*(LSCJ-J),YSCJ-4),KANJI(MSCJ),OR
13750         NEXT J
13760  NEXT IJ
13770 NEXT SCI
13780 WINDOW (-XYMX,-XYMX)-(XYMX,XYMX)
13790 VIEW (210,0)-(609,399)
13800 RETURN
13810 ' * plotter *
13820    LPRINT "SP1;IW;SI0.18,0.25;PU";-XYMAX*150;",0;DI0,-1;";
13830    LPRINT "CP-5,-2.2;LBangle (deg)";CHR$(3);";PU";-XYMAX*150;",0;";
13840 FOR J=1 TO 100
13850 ANGJ=J*ANGSCALE:IF ANGJ>ANGRAN THEN ANGJ=ANGJ-ANGSCALE:GOTO 13870
13860 NEXT
13870 FOR SCJ=-ANGJ TO ANGJ STEP ANGSCALE
13880   ON PRJ GOTO 13890,13900
13890           Y=WN*TAN(SCJ*PI/180):GOTO 13910
13900           Y=2*WN*TAN(SCJ*PI/360)
13910           LPRINT "PA";-XYMAX*150;",";Y*100;";YT;";
13920           LPRINT "PU;SI0.1,0.2;CP-1.8,-1;LB";ABS(SCJ);CHR$(3);
13930           LPRINT "PU";-XYMAX*150;",";Y*100;";PD";
13940 NEXT
```

```
13950 LPRINT "PU;PA;DI1,0;"
13960 RETURN
13970 *SPOINT ' * calculate start point *
13980   XPL1=XPL(0):YPL1=YPL(0):XPL2=XPL(1):YPL2=YPL(1)
13990   GOSUB *SEPOINT:XPL(0)=XSL:YPL(0)=YSL
14000 RETURN
14010 *EPOINT ' * calculate end point *
14020   XPL2=XPL(NP):YPL2=YPL(NP):XPL1=XPL(NP+1):YPL1=YPL(NP+1)
14030   GOSUB *SEPOINT:XPL(NP+1)=XSL:YPL(NP+1)=YSL
14040 RETURN
14050 *SEPOINT ' * calculate start and end point
14060   IF XPL1>XYMAX AND YPL1>XYMAX THEN CASE=1:GOTO 14140
14070   IF XPL1>XYMAX AND ABS(YPL1)<XYMAX THEN CASE=2:GOTO 14140
14080   IF XPL1>XYMAX AND YPL1<-XYMAX THEN CASE=3:GOTO 14140
14090   IF ABS(XPL1)<XYMAX AND YPL1>XYMAX THEN CASE=4:GOTO 14140
14100   IF ABS(XPL1)<XYMAX AND YPL1<-XYMAX THEN CASE=5:GOTO 14140
14110   IF XPL1<-XYMAX AND YPL1>XYMAX THEN CASE=6:GOTO 14140
14120   IF XPL1<-XYMAX AND ABS(YPL1)<XYMAX THEN CASE=7:GOTO 14140
14130   IF XPL1<-XYMAX AND YPL1<-XYMAX THEN CASE=8
14140  ON CASE GOTO 14150,14220,14240,14310,14330,14350,14420,14440
14150 XSL1=XYMAX:YSL1=YPL1+(YPL1-YPL2)*(XYMAX-XPL1)/(XPL1-XPL2)
14160 YSL2=XYMAX:XSL2=XPL1+(XPL1-XPL2)*(XYMAX-YPL1)/(YPL1-YPL2)
14170       RXSL1=XSL1*XSL1+YSL1*YSL1
14180       RXSL2=XSL2*XSL2+YSL2*YSL2
14190       XSL=XSL1:YSL=YSL1
14200       IF RXSL1>RXSL2 THEN XSL=XSL2:YSL=YSL2:RETURN
14210 RETURN
14220 XSL=XYMAX:YSL=YPL1+(YPL1-YPL2)*(XYMAX-XPL1)/(XPL1-XPL2)
14230 RETURN
14240 XSL1=XYMAX:YSL1=YPL1+(YPL1-YPL2)*(XYMAX-XPL1)/(XPL1-XPL2)
14250 YSL2=-XYMAX:XSL2=XPL1-(XPL1-XPL2)*(XYMAX+YPL1)/(YPL1-YPL2)
14260       RXSL1=XSL1*XSL1+YSL1*YSL1
14270       RXSL2=XSL2*XSL2+YSL2*YSL2
14280       XSL=XSL1:YSL=YSL1
14290       IF RXSL1>RXSL2 THEN XSL=XSL2:YSL=YSL2:RETURN
14300 RETURN
14310 YSL=XYMAX:XSL=XPL1+(XPL1-XPL2)*(XYMAX-YPL1)/(YPL1-YPL2)
14320 RETURN
14330 YSL=-XYMAX:XSL=XPL1-(XPL1-XPL2)*(XYMAX+YPL1)/(YPL1-YPL2)
14340 RETURN
14350 XSL1=-XYMAX:YSL1=YPL1-(YPL1-YPL2)*(XYMAX+XPL1)/(XPL1-XPL2)
14360 YSL2=XYMAX:XSL2=XPL1+(XPL1-XPL2)*(XYMAX-YPL1)/(YPL1-YPL2)
14370       RXSL1=XSL1*XSL1+YSL1*YSL1
14380       RXSL2=XSL2*XSL2+YSL2*YSL2
14390       XSL=XSL1:YSL=YSL1
14400       IF RXSL1>RXSL2 THEN XSL=XSL2:YSL=YSL2:RETURN
14410 RETURN
14420 XSL=-XYMAX:YSL=YPL1-(YPL1-YPL2)*(XYMAX+XPL1)/(XPL1-XPL2)
14430 RETURN
14440 XSL1=-XYMAX:YSL1=YPL1-(YPL1-YPL2)*(XYMAX+XPL1)/(XPL1-XPL2)
14450 YSL2=-XYMAX:XSL2=XPL1-(XPL1-XPL2)*(XYMAX+YPL1)/(YPL1-YPL2)
14460       RXSL1=XSL1*XSL1+YSL1*YSL1
14470       RXSL2=XSL2*XSL2+YSL2*YSL2
14480       XSL=XSL1:YSL=YSL1
14490       IF RXSL1>RXSL2 THEN XSL=XSL2:YSL=YSL2:RETURN
14500 RETURN
14510 '
14520 *INDEXING
14530   IF CIRS=1 OR CIRE=1 THEN GOTO *INDCIR
14540   ON 1+FNEVOD(INT(RND*100)) GOTO *INDS,*INDE
14550 *INDS ' * index at start point *
14560   XIND=XPL(0):YIND=YPL(0) ' * start point *
14570   IF ABS(XYMAX*100-ABS(YIND))<.01 THEN GOTO 14600
14580   IF XIND>0 THEN PIND=1 ELSE PIND=3
14590 GOTO *POSIND
14600   IF YIND>0 THEN PIND=2 ELSE PIND=4
14610 GOTO *POSIND
14620   XIND=XPL(NP+1):YIND=YPL(NP+1) ' * end point *
14630   IF ABS(XYMAX*100-ABS(YIND))<.01 THEN 14660
14640   IF XIND>0 THEN PIND=1 ELSE PIND=3
14650 GOTO *POSIND
14660   IF YIND>0 THEN PIND=2 ELSE PIND=4
14670 GOTO *POSIND
14680 *INDE ' * index at end point *
14690   XIND=XPL(NP+1):YIND=YPL(NP+1) ' * end point *
14700   IF ABS(XYMAX*100-ABS(YIND))<.01 THEN GOTO 14730
14710   IF XIND>0 THEN PIND=1 ELSE PIND=3
14720 GOTO *POSIND
14730   IF YIND>0 THEN PIND=2 ELSE PIND=4
14740 GOTO *POSIND
14750   XIND=XPL(0):YIND=YPL(0) ' * start point *
14760   IF ABS(XYMAX*100-ABS(YIND))<.01 THEN 14790
```

```
14770   IF XIND>0 THEN PIND=1 ELSE PIND=3
14780 GOTO *POSIND
14790   IF YIND>0 THEN PIND=2 ELSE PIND=4
14800 GOTO *POSIND
14810 *INDCIR '          * at the case of Kikuchi line being circle *
14820   IF CIRE=0 THEN CIRS=0:RETURN
14830   XIND=XPL(0):YIND=YPL(0)
14840   IF CIRS=0 THEN GOTO *INDCIR2
14850   XYIND=SQR(XIND^2+YIND^2)
14860   XINDA=FIX(XIND/XYIND*1E+06)/10000
14870   YINDA=FIX(YIND/XYIND*1E+06)/10000
14880   LPRINT "IW;PU";XIND;",";YIND;";"
14890   LPRINT "DI";YINDA*II;",";-XINDA*II;";CP-5,.5;"
14900      CIRS=0:CIRE=0:GOTO *INDEX
14910 *INDCIR2
14920   IF XYMAX*100-ABS(YIND)>.01 AND XIND>0 THEN PIND=1:GOTO *POSIND
14930   IF XYMAX*100-ABS(XIND)>.01 AND YIND>0 THEN PIND=2:GOTO *POSIND
14940   IF XYMAX*100-ABS(YIND)>.01 AND XIND<0 THEN PIND=3:GOTO *POSIND
14950   IF XYMAX*100-ABS(XIND)>.01 AND XIND<0 THEN PIND=4:GOTO *POSIND
14960 *POSIND ' ** pen move --> draw bar(-) --> set direction of index **
14970   LPRINT "IW;" '                    * release draw limit
14980   LPRINT "PA";XIND;",";YIND;";" '      * move to indexing position
14990     RAN=INT(RND*100):RAN=1+RAN-3*INT(RAN/3) '* set length of bar(-)
15000   BAR=RAN*FIX(XYMAX/25*1E+06)/10000 ' * length of bar
15010 ON PIND GOTO 15020,15050,15080,15110
15020 ' * position 1 *
15030   LPRINT "PD;PR";BAR;",0;PU;DI1,0;" ' * draw bar and set direction
15040 GOTO *INDEX
15050 ' * position 2 *
15060   LPRINT "PD;PR0,";BAR;";PU;DI0,1;"
15070 GOTO *INDEX
15080 ' * position 3 *
15090   LPRINT "PD;PR";-BAR;",0;PU;DI-1,0;"
15100 GOTO *INDEX
15110 ' * position 4 *
15120   LPRINT "PD;PR0,";-BAR;";PU;DI0,-1;"
15130 GOTO *INDEX
15140 *INDEX
15150   LPRINT "CP1.0,-0.25;" '                    ,       character origin set
15160   LPRINT "LB";H;K;L;CHR$(3) ' index
15170   LPRINT "IW";IPXMIN;",";IPYMIN;",";IPXMAX;",";IPYMAX;";" ' limit set
15180   LPRINT "SC";-SCXY;",";SCXY;",";-SCXY;",";SCXY;";" '          scaling
15190   LPRINT "PA;" '                                  absolute pen control
15200 RETURN
15210 *POINTER ' ** cursor control **
15220   GOSUB *MENU
15230   XP0=MAP(XP0,0):YP0=MAP(YP0,1)
15240   XP=XP0:YP=YP0
15250   GET (XP,YP)-STEP(9,9),IG2%: PUT (XP,YP),IG%,OR
15260   A$=INKEY$:AIN=VAL(A$)
15270   IF A$="" THEN 15260
15280   IF AIN=5 THEN GOTO 15260
15290  ON AIN GOSUB *TY1,*TY2,*TY3,*TY4,,*TY6,*TY7,*TY8,*TY9
15300   IF AIN<>0 THEN GOTO 15260
15310   IF A$=" " THEN GOTO *GETPOINT
15320   IF A$="S" OR A$="s" THEN GOSUB *TYS
15330   IF A$="Q" OR A$="q" THEN GOSUB *TYQ
15340   IF A$="E" OR A$="e" THEN GOSUB *TYC:A$="E":RETURN
15350   GOTO 15260
15360 *GETPOINT
15370   ZAX0=MAP(XP,2):ZAY0=MAP(YP,3)
15380 RETURN
15390 '
15400 *CALZONE ' calculete zone axis from a point in Kikuchi pattern
15410    ZAY0=-ZAY0 '      CRT-case
15420    PLEN=SQR(ZAX0*ZAX0+ZAY0*ZAY0) ' ** (ZAX0,ZAY0) is in Kikuchi pattern
15430   ON PRJ GOTO 15440,15480
15440      TAS=PLEN/WN  ' ** central
15450   ZZ=WN*(1-1/SQR(1+TAS*TAS))
15460   XX=(WN-ZZ)*ZAX0/WN:YY=(WN-ZZ)*ZAY0/WN
15470  GOTO 15510
15480      TAS=PLEN/(2*WN) : TAS2=TAS*TAS ' ** stereo
15490   ZZ=2*WN*TAS2/(1+TAS2)
15500   XX=(2*WN-ZZ)*ZAX0/(2*WN):YY=(2*WN-ZZ)*ZAY0/(2*WN)
15510   XX=-XX:YY=-YY:ZZ=WN-ZZ '     ** (XX,YY,ZZ) is on the reference sphere
15520  *CALZONE2
15530   X1=CO*XX-SI*YY:Y1=SI*XX+CO*YY:Z1=ZZ:X2=X1:Y2=Y1:Z2=Z1:SGW=SGN(WW)
15540   IF FA1<.001 THEN X2=SGW*X2:Y2=Y2:Z2=SGW*Z2:GOTO 15560
15550    X2=FNPROIX(X1,Y1,Z1):Y2=FNPROIY(X1,Y1,Z1):Z2=FNPROIZ(X1,Y1,Z1)
15560    X3=FNXICOD(X2,Y2,Z2):Y3=FNYICOD(X2,Y2,Z2):Z3=FNZICOD(X2,Y2,Z2)
15570   XYZ3=SQR(X3*X3+Y3*Y3+Z3*Z3)
15580   X3=X3/XYZ3:Y3=Y3/XYZ3:Z3=Z3/XYZ3 ' ** calculated zone axis
```

```
15590   UZA=FIX(X3*1000)/1000:VZA=FIX(Y3*1000)/1000:WZA=FIX(Z3*1000)/1000
15600 RETURN
15610 *MENU
15620 LOCATE 0,12
15630   PRINT " space  : get ":PRINT "   E     : end(cancel)":PRINT
15640   PRINT "ten key : cursor control":PRINT
15650   PRINT "   Q     : quick ":PRINT "   S     : slow  "
15660 RETURN
15670 *TY4 ' left
15680   PUT (XP,YP),IG2%,AND:XP=XP-ST:IF XP<10 THEN XP=XP+ST
15690   GET (XP,YP)-STEP(9,9),IG2%:PUT (XP,YP),IG%,OR
15700 RETURN
15710 *TY2 ' down
15720   PUT (XP,YP),IG2%,AND:YP=YP+ST:IF YP>389 THEN YP=YP-ST
15730   GET (XP,YP)-STEP(9,9),IG2%:PUT (XP,YP),IG%,OR
15740 RETURN
15750 *TY6 ' right
15760   PUT (XP,YP),IG2%,AND:XP=XP+ST:IF XP>389 THEN XP=XP-ST
15770   GET (XP,YP)-STEP(9,9),IG2%:PUT (XP,YP),IG%,OR
15780 RETURN
15790 *TY8 ' up
15800   PUT (XP,YP),IG2%,AND:YP=YP-ST:IF YP<10 THEN YP=YP+ST
15810   GET (XP,YP)-STEP(9,9),IG2%:PUT (XP,YP),IG%,OR
15820 RETURN
15830 *TY1 ' left-down
15840   GOSUB *TY2:GOSUB *TY4 :RETURN
15850 *TY3 ' right-down
15860   GOSUB *TY6:GOSUB *TY2 :RETURN
15870 *TY9 ' right-up
15880   GOSUB *TY8:GOSUB *TY6 :RETURN
15890 *TY7 ' left-up
15900   GOSUB *TY4:GOSUB *TY8 :RETURN
15910 *TYQ ' speed up
15920   IF ST=>1 THEN ST=ST+1 ELSE ST=ST*2
15930   IF ST>10 THEN ST=ST-1
15940 RETURN
15950 *TYS ' speed down
15960   IF ST>1 THEN ST=ST-1 ELSE ST=ST/2
15970   IF ST<.125 THEN ST=.125
15980 RETURN
15990 *TYC ' cursor clear
16000   PUT (XP,YP),IG2%,AND:GET (XP,YP)-STEP(9,9),IG2%
16010 RETURN
16020 *F257
16030 FOR IJ=0 TO 33:IG4%(IJ)=IG2%(IJ):NEXT
16040 XP01=XP:YP01=YP
16050 RETURN
16060 *F257E
16070 PUT (XP01,YP01),IG4%,AND
16080 RETURN
```

Language	: N88BASIC (86) COMPILER
DOS	: MS-DOS
Computer	: NEC PC-9801
Printer	: NEC PC-PR201
Plotter	: ROLAND DXY-990

Thickness determination program

This method of specimen thickness determination is based upon the method of Kelly *et al.* This program computes ten sets of specimen thickness, extinction distance and the fourth power of a correlation coefficient, when the measured distance between the bright-field disk and a dark-field disk, L_0, and those between the exact Bragg position and each of successive minima, L_i, are used as input data. When the correlation coefficients have a similar value for a few thicknesses, the thickness exhibiting a reasonable extinction distance is selected as the correct one.

Reference

[a] P.M. Kelly, A. Jostsons, R.G. Blake and J.G. Napier: *phys. stat. sol.*, **(a) 31** (1975) 771.

Input data

```
        Calculation of foil thickness
          by T.Kaneyama,M.Terauchi and M.Tanaka, Dept of Phys., Fac. of Science, Tohoku
        Univ.
             ( refs. P.M.Kelly  et al.: phys. stat. sol. (a):31(1975)771
                    M.Tanaka and M.Terauchi:Convergent-Beam Electron Diffraction(1985)
                     JEOL-Mruzen, P.38-39 )
        1)Accelerating voltage (kV)? 62.8
        2)Lattice paramater      a,b,c(A) =? 5.43,5.43,5.43
                  alpha,beta,gamma(deg) =? 90,90,90
        3)Index of G (h,k,l) ? 2,-2,0
        4)Number of data Li ? 4
        5)Distance between O and G reflection  L 0 =? 1
        6)Distances between successive subsidiary minima
                       and the exact Bragg position of G
          L 1 =? 0.0798
          L 2 =? 0.180
          L 3 =? 0.261
          L 4 =? 0.343
```

Output

n1:	Thickness(A)	Extinction distance(A)	Fourth power of correlation coef.
1:	T= 877.5	GSI= 2120.6	r^4= 0.4251
2:	T= 1073.3	GSI= 642.6	r^4= 0.9974
3:	T= 1228.7	GSI= 448.3	r^4= 0.9852
4:	T= 1362.2	GSI= 360.1	r^4= 0.9766
5:	T= 1481.6	GSI= 308.0	r^4= 0.9716
6:	T= 1590.9	GSI= 272.8	r^4= 0.9685
7:	T= 1692.5	GSI= 247.1	r^4= 0.9664
8:	T= 1787.8	GSI= 227.4	r^4= 0.9651
9:	T= 1878.0	GSI= 211.7	r^4= 0.9641
10:	T= 1963.8	GSI= 198.7	r^4= 0.9634

Illustration

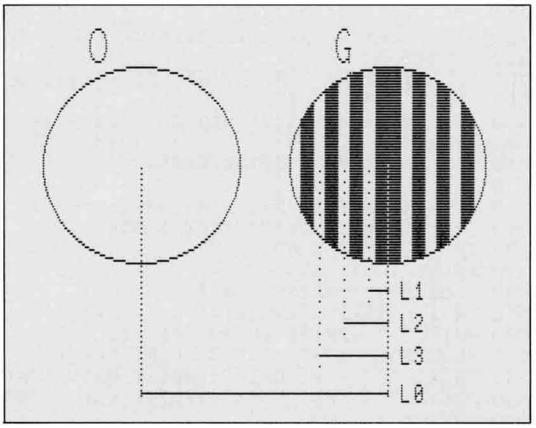

```
10 REM file name 'Thickness'
20 SCREEN 0,0:CLS 3
30 COLOR 4:PRINT " Calculation of foil thickness ":COLOR 0
40 PRINT "   by T.Kaneyama,M.Terauchi and M.Tanaka, Dept of Phys., Fac. of Science, Tohoku Univ."
50 CONSOLE 3,4,0,0
60 PRINT "       ( refs. P.M.Kelly  et al.: phys. stat. sol. (a):31(1975)771"
70 PRINT "       M.Tanaka and M.Terauchi:Convergent-Beam Electron Diffraction(1985) JEOL-Maruzen, P.38-39 )"
80 GOSUB *SML
90 OPTION BASE 1
100 DIM T(100),S(100),SN(100),X(100),Y(100),TA(100),SA(100),XA(100),YA(100)
110 DIM TT(10),GS(10),R(10)
120 INPUT "1)Accelerating voltage (kV)";E
130       INPUT "2)Lattice paramater     a,b,c(A) =";A,B,C
140 INPUT "           alpha,beta,gamma(deg) =";ALPH,BETA,GAMM
150       INPUT "3)Index of G (h,k,l) ";H,K,L
160 '
170 PI=3.14159
180 LAM=12.26/SQR(1000*E*(1+9.788E-07*1000*E))
190 ALP=ALPH*PI/180 : BET=BETA*PI/180 : GAM=GAMM*PI/180
200 SIA=SIN(ALP):SIB=SIN(BET):SIG=SIN(GAM)
210 COA=COS(ALP):COB=COS(BET):COG=COS(GAM)
220 S11=B*B*C*C*SIA^2:S22=A*A*C*C*SIB^2:S33=A*A*B*B*SIG^2
230 S12=A*B*C*C*(COA*COB-COG):S23=A*A*B*C*(COB*COG-COA)
240 S13=A*B*B*C*(COG*COA-COB):VC=A*B*C*SQR(1-COA^2-COB^2-COG^2+2*COA*COB*COG)
250 D2=S11*H*H+S22*K*K+S33*L*L+2*S12*H*K+2*S23*K*L+2*S31*L*H
260 D=VC/SQR(D2)
270       INPUT "4)Number of data Li ";ND
280       INPUT "5)Distance between 0 and G reflection  L 0 =";T2
290       PRINT "6)Distances between successive subsidiary minima "
300       PRINT "                 and the exact Bragg position of G"
310 FOR I=1 TO ND
320 PRINT "  L";I;"=";:INPUT T(I)
330 S(I)=LAM*T(I)/(D^2*T2)
340 NEXT I
350 CONSOLE 0,25
360 '
370 CLS 1
380 PRINT "n1:  Thickness(A)      Extinction       Fourth power of"
390 PRINT "                       distance(A)      correlation coef."
400 FOR I=1 TO 10
410  N(1)=I : X(1)=1/I^2 : Y(1)=(S(1)/I)^2
420  XT=X(1):YT=Y(1):SXT=X(1)^2:XYT=X(1)*Y(1)
430 '
440   FOR J=2 TO ND
450      N(J)=N(J-1)+1
460      X(J)=1/N(J)^2
470      Y(J)=(S(J)/N(J))^2
480      XT=XT+X(J) : YT=YT+Y(J) : SXT=SXT+X(J)^2 : XYT=XYT+X(J)*Y(J)
490   NEXT J
500     MX=XT/ND : MY=YT/ND :SX2=0:SY2=0
510   FOR J=1 TO ND
520      SX2=SX2+(X(J)-MX)^2 : SY2=SY2+(Y(J)-MY)^2
530   NEXT J
540   SX2=SX2/ND : SY2=SY2/ND
550 '
560  TT=(XT*XYT-YT*SXT)/(XT^2-ND*SXT) :  TT(I)=1/SQR(ABS(TT))
570  GG=-(XT*YT-ND*XYT)/(XT^2-ND*SXT)
580 IF GG<>0 THEN 600
590 PRINT :GOTO 660
600   GS(I)=1/SQR(ABS(GG))
610  R(I)=-GG*SQR(SX2/SY2)
620 PRINT" " :PRINT USING "##";I;
630 PRINT ":   T=";:PRINT USING "#####.#";TT(I);
640 PRINT "        GSI=";:PRINT USING "#####.#";GS(I);
650 PRINT "        r^4=";:PRINT USING "##.####";R(I)^4
660 NEXT I
670 CLS 2
680 PRINT :INPUT " 7)OUTPUT TO THE PRINTER ?(y/n)";PR$
690 IF PR$="N" OR PR$="n" THEN END
700 LPRINT "n1:  Thickness(A)      Extinction       Fourth power of"
710 LPRINT "                       distance(A)      correlation coef."
720 FOR I=1 TO 10
730 IF GS(I)=0 AND R(I)=0 THEN PRINT :GOTO 780
740 LPRINT" ":LPRINT USING "##";I;
750 LPRINT ":   T=";:LPRINT USING "#####.#";TT(I);
760 LPRINT "        GSI=";:LPRINT USING "#####.#";GS(I);
770 LPRINT "        r^4=";:LPRINT USING "##.####";R(I)^4
780 NEXT I
790 ''
800 END
810 *SML
```

```
820 WINDOW (0,0)-(199,149)
830 VIEW (139,0)-(499,199)
840 CIRCLE (49,79),40:CIRCLE (149,79),40
850 LINE (144,53)-(144,106):LINE (139,53)-(139,105)
860 LINE (134,54)-(134,103):LINE (129,56)-(129,102)
870 LINE (124,59)-(124,99) :LINE (119,62)-(119,96)
880 LINE (114,67)-(114,92) :LINE (154,53)-(154,106)
890 LINE (159,53)-(159,105):LINE (164,54)-(164,103)
900 LINE (169,56)-(169,102):LINE (174,59)-(174,101)
910 LINE (179,62)-(179,97) :LINE (184,68)-(184,92)
920 PAINT (149,79),7:PAINT (137,79),7:PAINT (127,79),7:PAINT (117,79),7
930 PAINT (161,79),7:PAINT (171,79),7:PAINT (181,79),7
940 LINE (149,79)-(149,144),0
950 LINE (49,79)-(49,144),4,,&H5555:LINE (149,79)-(149,144),4,,&H5555
960 LINE (141.5,79)-(141.5,118),6,,&H2222:LINE (131.5,79)-(131.5,127),6,,&H2222
970 LINE (121.5,79)-(121.5,136),6,,&H2222:LINE (49,142)-(149,142),4
980 LINE (141.5,114)-(149,114),6
990 LINE (131.5,123)-(149,123),6:LINE (121.5,132)-(149,132),6
1000 PUT (49,55),KANJI(&H234F) : PUT (229,55),KANJI(&H2347)
1010 PUT (279,187),KANJI(&H14C),,2,0 :PUT (289,187),KANJI(&H130),,2,0
1020 PUT (279,149),KANJI(&H14C),,2,0 :PUT (289,149),KANJI(&H131),,2,0
1030 PUT (279,161),KANJI(&H14C),,2,0 :PUT (289,161),KANJI(&H132),,2,0
1040 PUT (279,173),KANJI(&H14C),,2,0 :PUT (289,173),KANJI(&H133),,2,0
1050 RETURN
```

Language : N88BASIC (86) COMPILER
DOS : MS-DOS
Computer : NEC PC-9801
Printer : NEC PC-PR201

Simulations of reflection lines crossing various types of dislocations

This program simulates the profiles of reflections crossing a screw, an edge, a mixed and a partial dislocation, a dislocation dipole and an extended dislocation.

Specification

```
programs : AUTOEXEC.BAT
           BATCH   .BAT
           CONTROL .EXE
           DIS-S   .EXE
           DIS-M   .EXE
           DIS-MP  .EXE
           DIS2-SF .EXE
           PICTURE .EXE
           PATTRN-5.DAT

language : N88BASIC(86) COMPILER

DOS      : MS-DOS

computer : NEC PC-9801

printer  : NEC PC-PR201

********** provisos **********

   Notes for the use of other computers and printers.

      1. All the programs written in BASIC must be compiled in advance
         because of batch processing upon MS-DOS.
      2. The alternation of codes in the subroutine *PRN. in PICTURE.BAS
         may be required for other printers.
      3. The alternation of the standard dot patterns in PATTRN-5.DAT
         may be required for other printers.
```

Flow chart

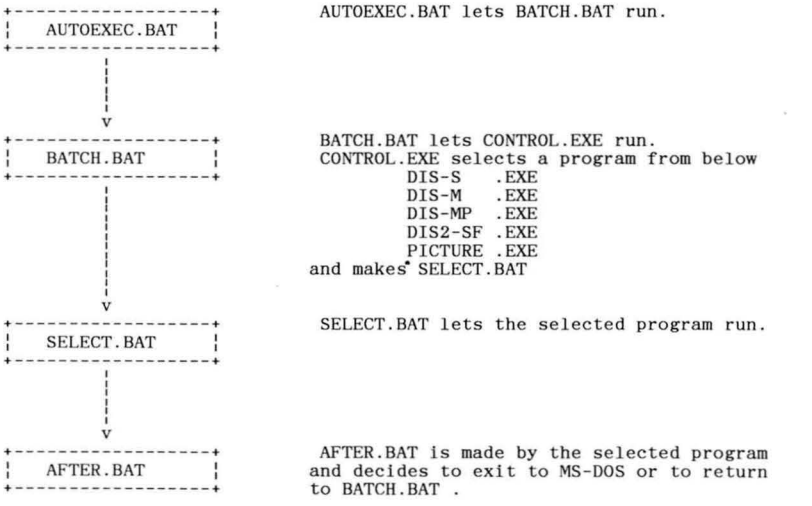

Function of each program

```
CONTROL .EXE          Selection of the program to run

DIS-S   .EXE          Calculation of the rocking curves around
                      the screw dislocation

DIS-M   .EXE          Calculation of the rocking curves around
                      the mixed or edge dislocation

DIS-MP  .EXE          Calculation of the rocking curves around
                      the partial dislocation(screw,mixed & edge)

DIS2-SF .EXE          Calculation of the rocking curves around
                      the dislocation dipole or extended dislo-
                      cation

PICTURE .EXE          Printing out the rocking curves to a dot
                      printer NEC PC-PR201
                       Image processing ;
                             magnifying and interpolation
                             filtering
                             enhancement

PATTRN-5.DAT          Data file of the standard dot patterns
```

CONTROL

```
ready CONTROL (ver. 1.4)

     CONTROL selects a compiled program working on MS-DOS.

     Input the number.


          1  Calculation of the rocking curves around a dislocation

          2  Printing out the rocking curves

          3  Exit to MS-DOS


     Calculation around single dislocation

          1  Screw dislocation
          2  Mixed or edge dislocation
          3  Partial dislocation( screw , mixed & edge )

     Calculation around a dislocation pair

          4  Dislocation dipole or extended dislocation
```

DIS-S

```
 ready  DIS-S

        This program calculates the rocking curves
              around the screw dislocation.

************** Provisos **********************************************

    1.  The dislocation is assumed to be parallel to the surface.

    2.  2-beam & column approximations of the dynamical theory are used.

    3.  Euler's method is used for the integration along depth direction.

    4.  Length is in unit of angstrom.

    5.  Excitation error W is dimensionless.

**********************************************************************


                                  1  Start calculation.
                                  2  Return to CONTROL.
                                                      1
        Set a disket for data file to drive b:

              1  Open new data file.

              2  Append to old file.

                                      1

        Input the file name of the data file.
                                      test-s


 1  Reflection vector g  = -2   2   0
 2  Burgers vector     b  =  .5  -.5   0

  Value of n = g·b   -2

 3  Thickness of the specimen      500
 4  Depth of the dislocation       250
 5  Mean extinction distance                  1000
 6  Extinction distance for the reflection    1000
 7  Mean absorption distance                  20000
 8  Absorption distance for the reflection    20000
 9  Range of the excitation error W (minimum) -10
10                                 (maximum)  10
11  Range of distance from the dislocation (minimum) -125
12                                 (maximum)  125
13  Total number of calculation points along the excitation error axis  45
14  Total number of calculation points along the distanse axis          79
15  Total number of slabs perpendicular to the depth direction          250

                      Are all parameters right ?
                                1  Yes.
                                2  No.
```


CONTROL

```
ready CONTROL (ver. 1.4)

     CONTROL selects a compiled program working on MS-DOS.

     Input the number.


          1  Calculation of the rocking curves around a dislocation

          2  Printing out the rocking curves

          3  Exit to MS-DOS
```


PICTURE

```
ready PICTURE

          This program prints out
             the rocking curves to a dot printer
                 using PRINTONE .


          PRINTONE ( ver. 4.1 on May 12th,1987  by S.Ito )
            is an image processing program
            to magnify-interpolate, enhance & filter


                                  1  Print out.
                                  2  Return to CONTROL.
                                                      1

com: Set the disket with the data file to drive B:
     Input the file name.
you: test-s
com: Set a printer.(dot printer PC-PR201)
     Have the data already been processed by PICTURE ?
        1) Yes.
        2) No.
you: 2
com: Select an output mode.
        1) Printer.
        2) FD file.
        3) Both printer & FD file.
you: 1
com: How wide is the FORM-PAPER ?
        1)  10 inches (80 columns)
        2)  17 inches (136 columns)
you: 1
com: Do you use standard dot patterns ?
        1) Yes.
        2) No.
you: 1
com: Is the background color black or white ?
        1) Black.
        2) White.
you: 2
com: Three functions are prepared;
        magnification, filtering and enhancement.

com: Input the magnifying power.
                ( 1, 2  or  3 )
you: 3
com: Input the order of interpolation.
                ( 1, 2 , 3 , 4 , 5  or  6 )
you: 2
com: Input an enhancement function.
             (1,2,3,4 in the right-side figures.)
you: 1
com: Do you start processing ?
        1) Yes.
        2) Return to title page.
you: 1
com: Now computing.  Don't disturb.
```

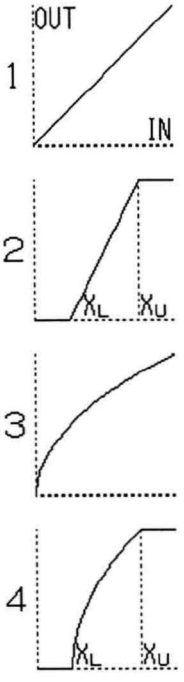

Flow chart of calculation

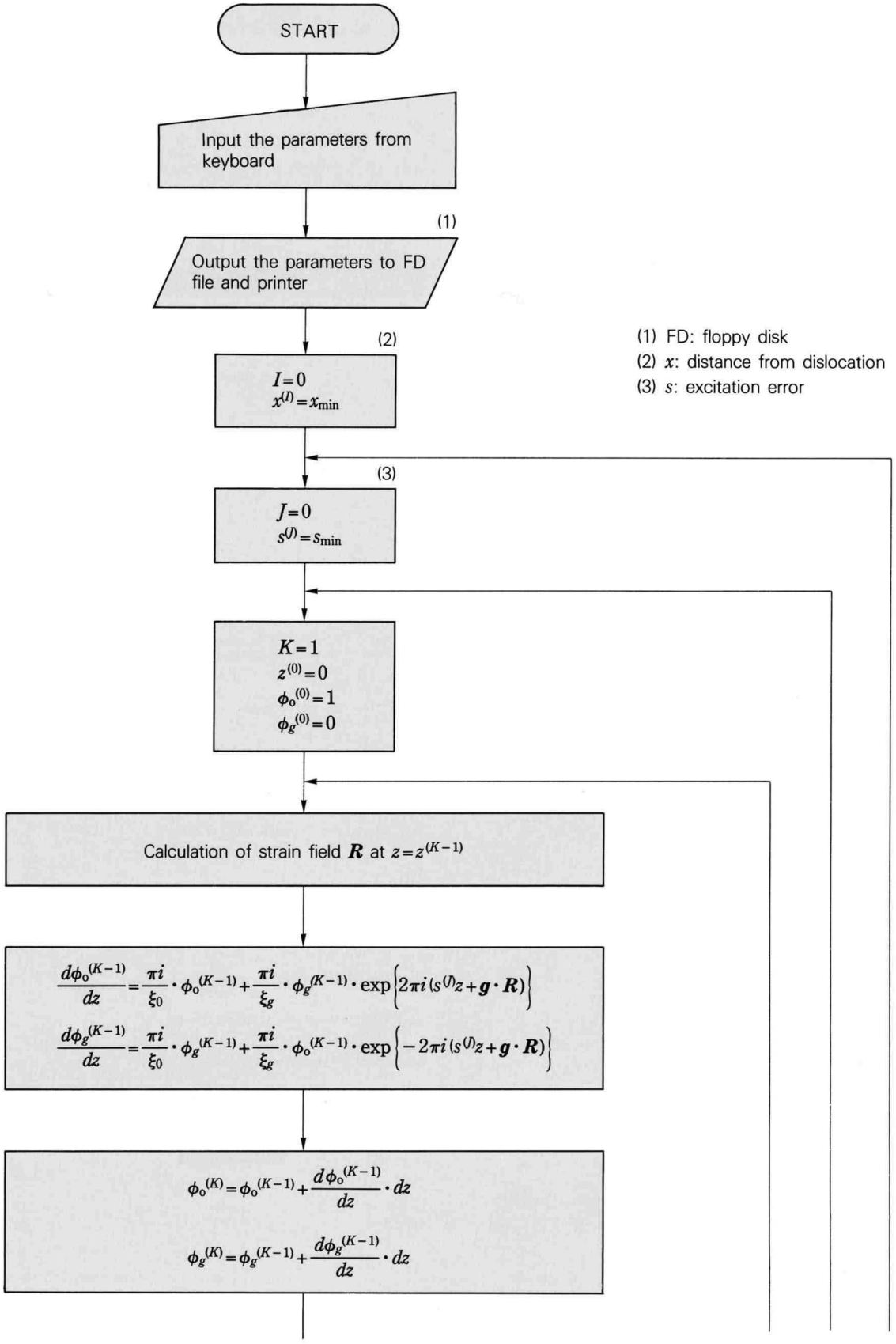

(1) FD: floppy disk
(2) x: distance from dislocation
(3) s: excitation error

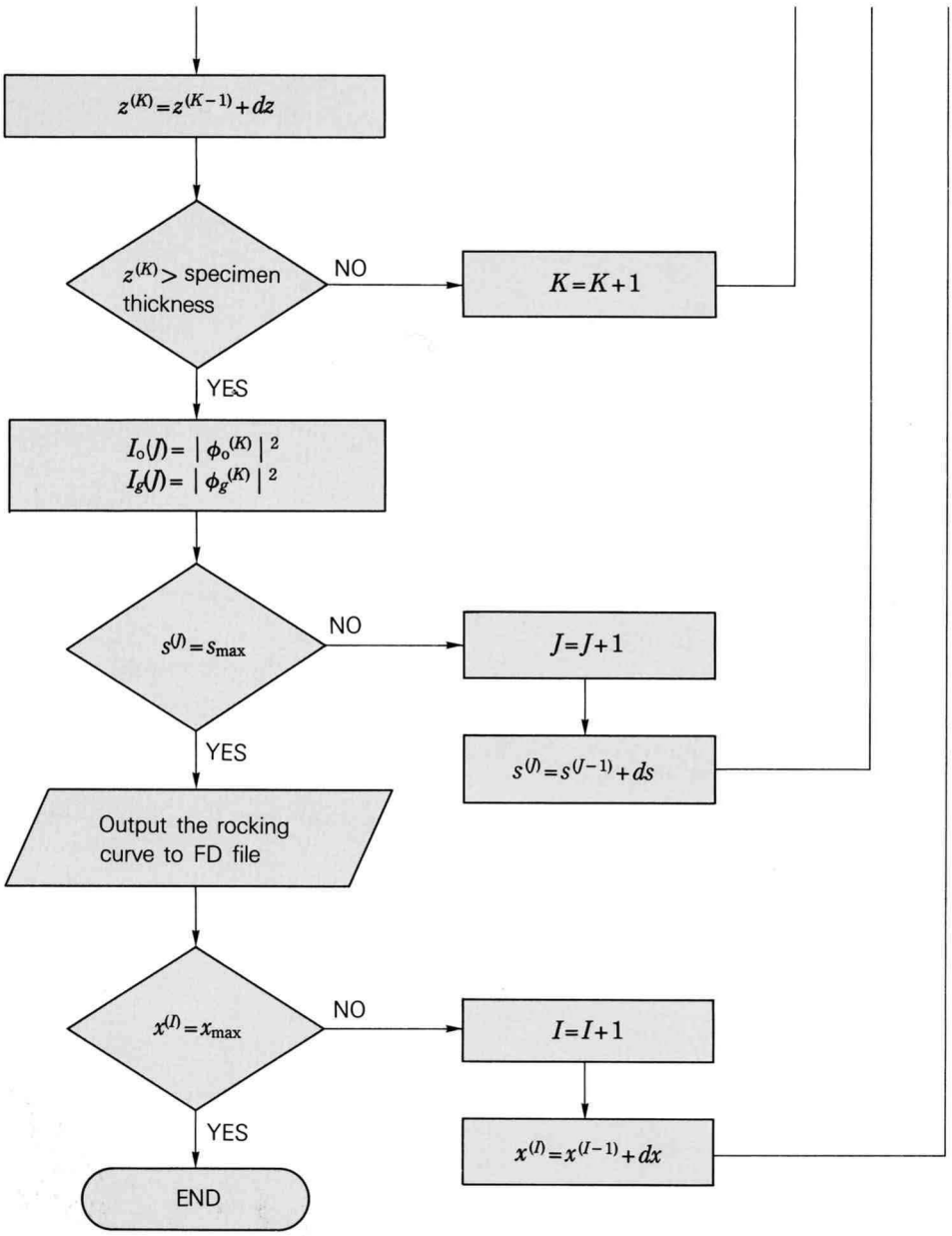
$z^{(K)}=z^{(K-1)}+dz$
$z^{(K)}$ > specimen thickness
NO
$K=K+1$
YES
$I_o(J)=|\phi_o^{(K)}|^2$
$I_g(J)=|\phi_g^{(K)}|^2$
$s^{(J)}=s_{max}$
NO
$J=J+1$
$s^{(J)}=s^{(J-1)}+ds$
YES
Output the rocking curve to FD file
$x^{(I)}=x_{max}$
NO
$I=I+1$
$x^{(I)}=x^{(I-1)}+dx$
YES
END

Input data

```
file name   test-s

********** assumptions for calculation ************************************

Rocking curves around the screw dislocation.
The dislocation is assumed to be parallel to the surface.
2-beam & column approximations of the dynamical theory are used.
Euler's method is used for the integration along depth direction.
Length is in unit of angstrom.
Excitation error W is dimensionless.

********** parameters used for calculation ********************************

Reflection vector g  = -2   2   0
Burgers vector    b  =  .5  -.5   0
Value of n = g·b   -2
Thickness of the specimen     500
Depth of the dislocation      250
Mean extinction distance                    1000
Extinction distance for the reflection      1000
Mean absorption distance                    20000
Absorption distance for the reflection      20000
Range of the excitation error W (minimum) -10
                                (maximum)  10
Range of distance from the dislocation (minimum) -125
                                       (maximum)  125
Total number of calculation points along the excitation error axis  45
Total number of calculation points along the distanse axis          79
Total number of slabs perpendicular to the depth direction          250

********** image processing data *****************************************

          magnification  3 times
          2nd order interpolation

********** printing mode **************************************************

 135 * 237 pixcels / original : 45 * 79 pixcels
 background color : white
 type 1 enhancement curve
```

Output

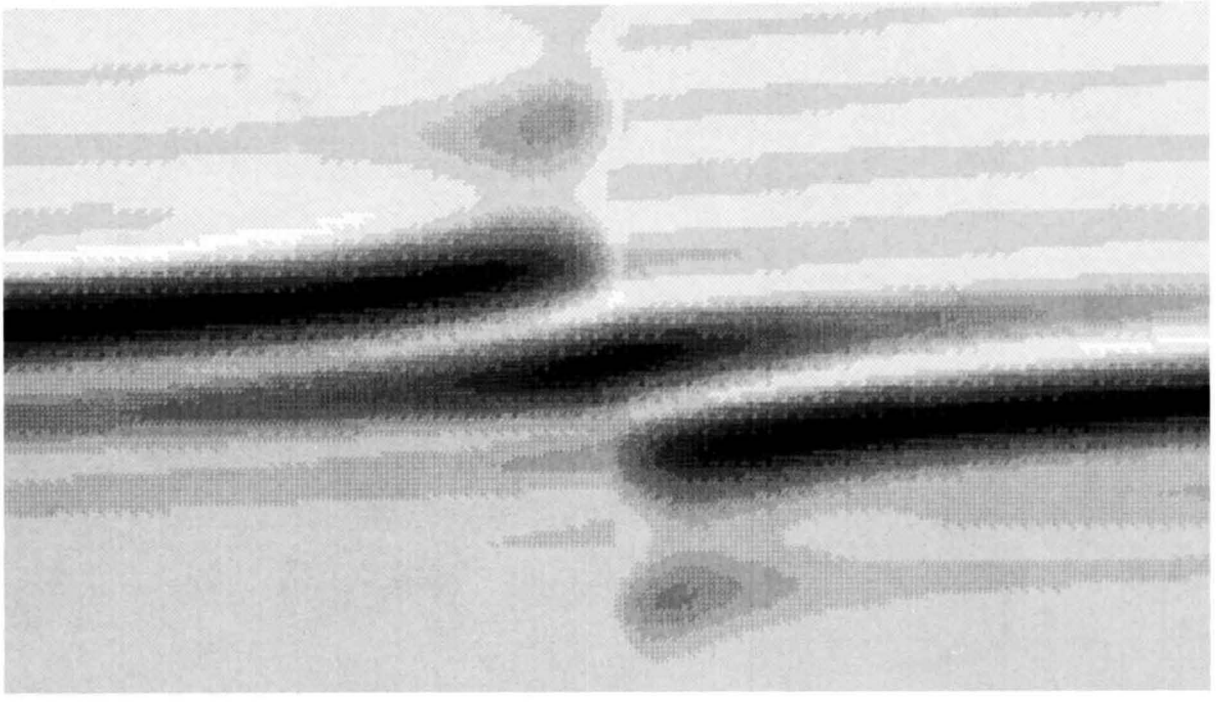

Dynamical calculations

Flow chart

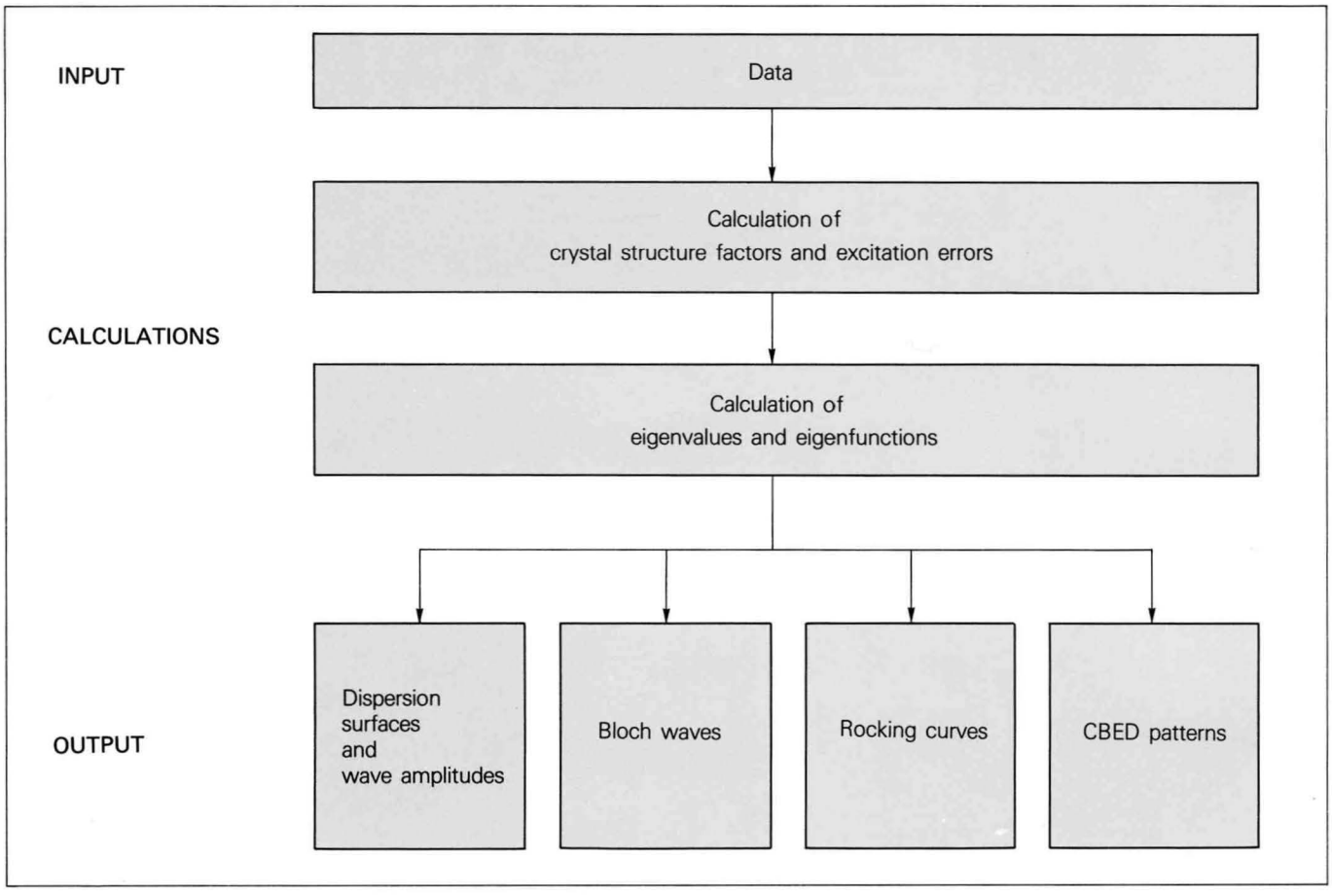

Dispersion surfaces and wave amplitudes

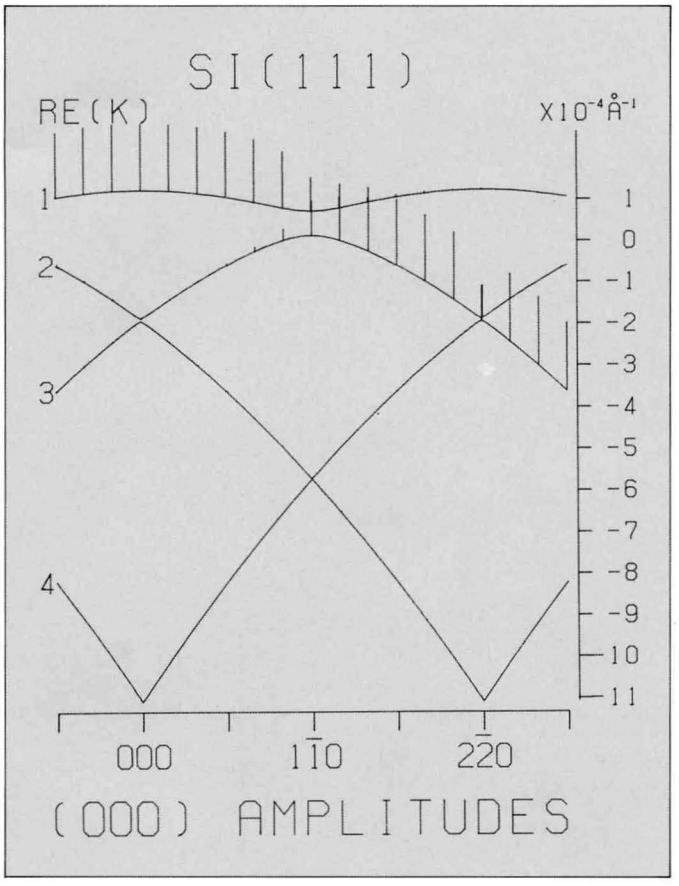

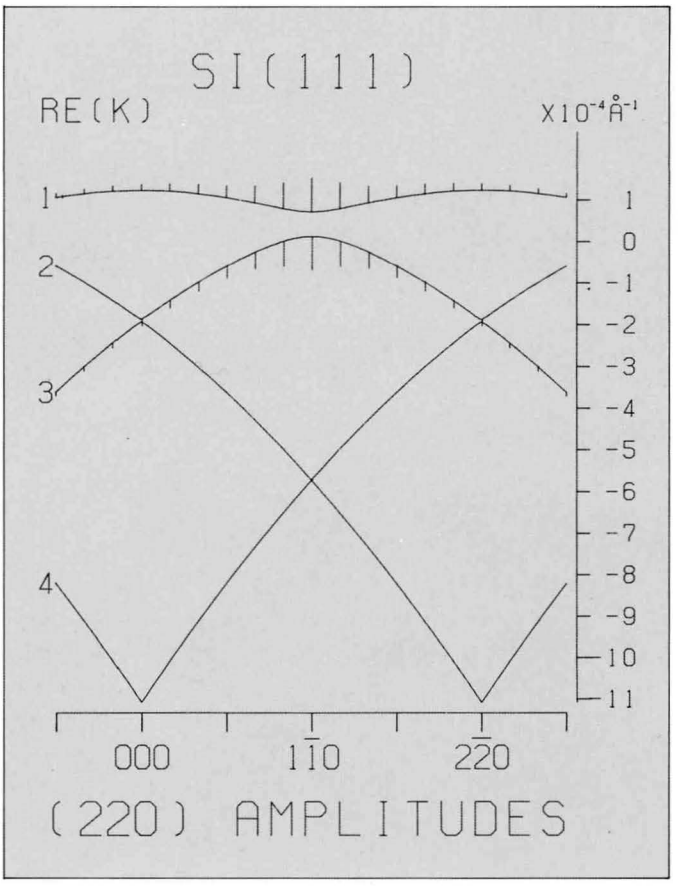

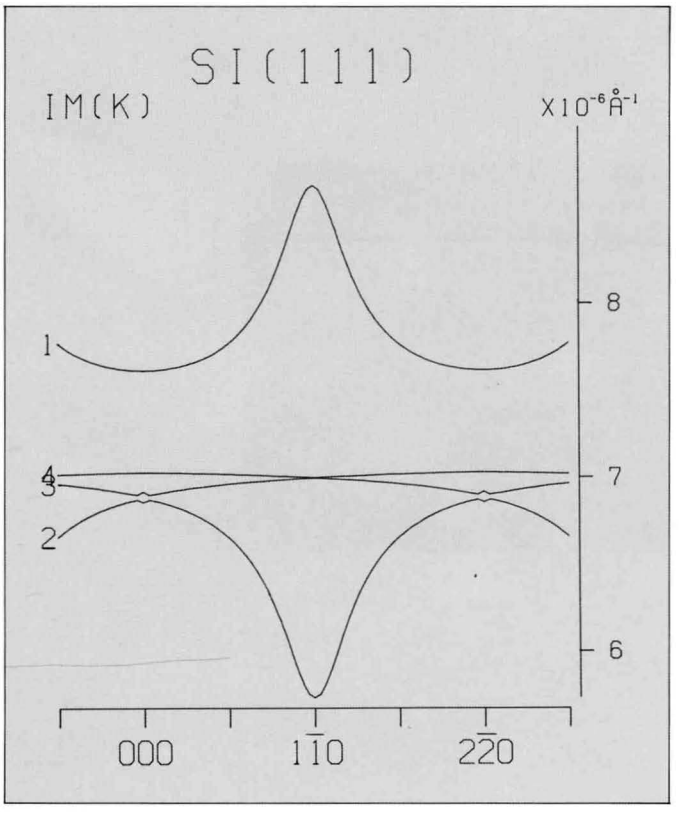

Si [1 1 1]

$2\bar{2}0$ excitation
Accelerating voltage: 100kV
$h\bar{h}0$ systematic reflections: 10 beams
Thickness: 156.0 nm
Absorption: $\frac{\xi_o}{\xi'_o} = \frac{1}{20}$, $\frac{\xi_g}{\xi'_g} = \frac{1}{20}$

Bloch waves

Si [111]

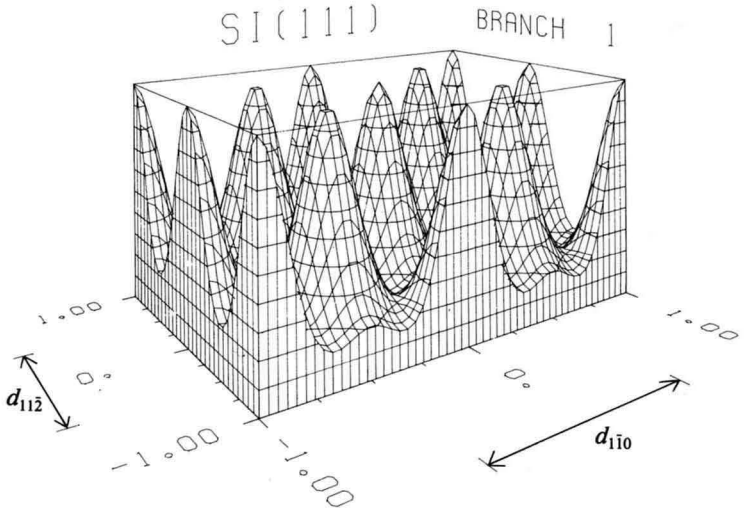

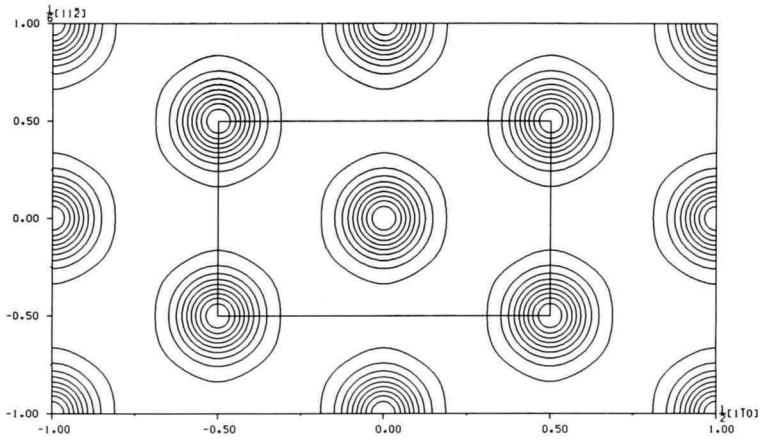

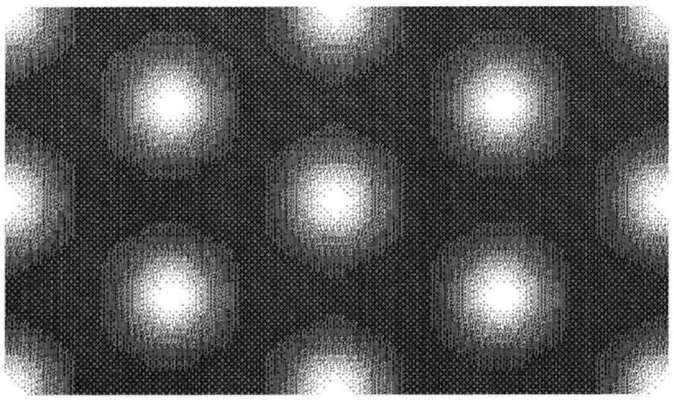

Zone-axis incidence
Accelerating voltage: 100kV
19 ZOLZ beams
Absorption: $\frac{\xi_o}{\xi'_o} = \frac{1}{20}$, $\frac{\xi_g}{\xi'_g} = \frac{1}{20}$

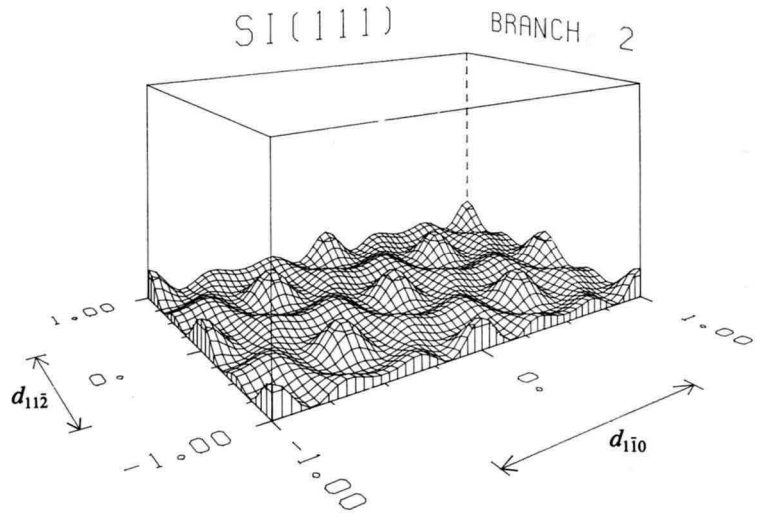
SI(111) BRANCH 2
1.00
0.
-1.00
-1.00
0.
1.00
$d_{11\bar{2}}$
$d_{1\bar{1}0}$

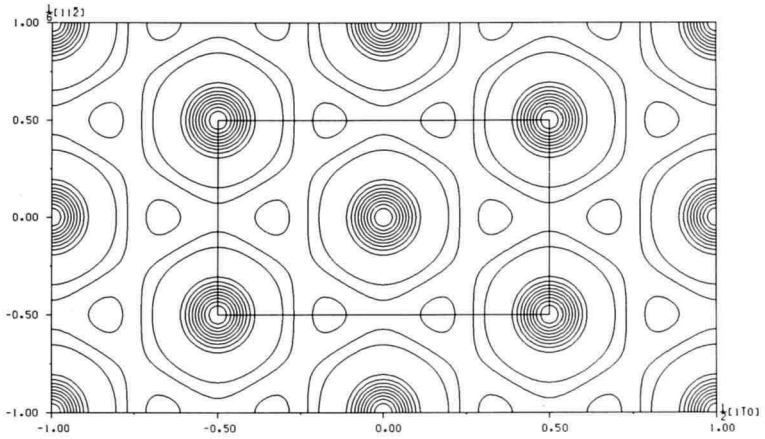
1.00
0.50
0.00
-0.50
-1.00
-1.00
-0.50
0.00
0.50
1.00

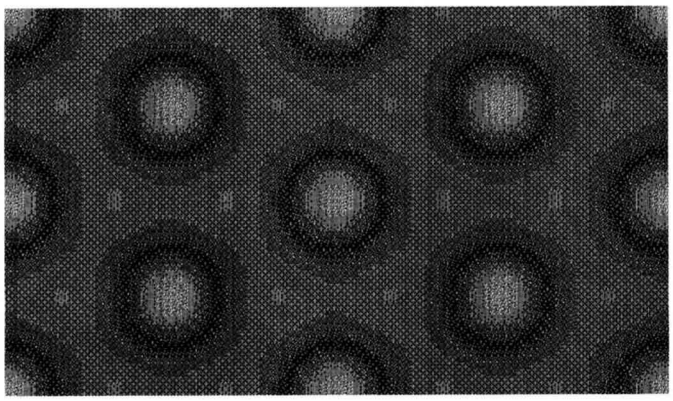

Rocking curves

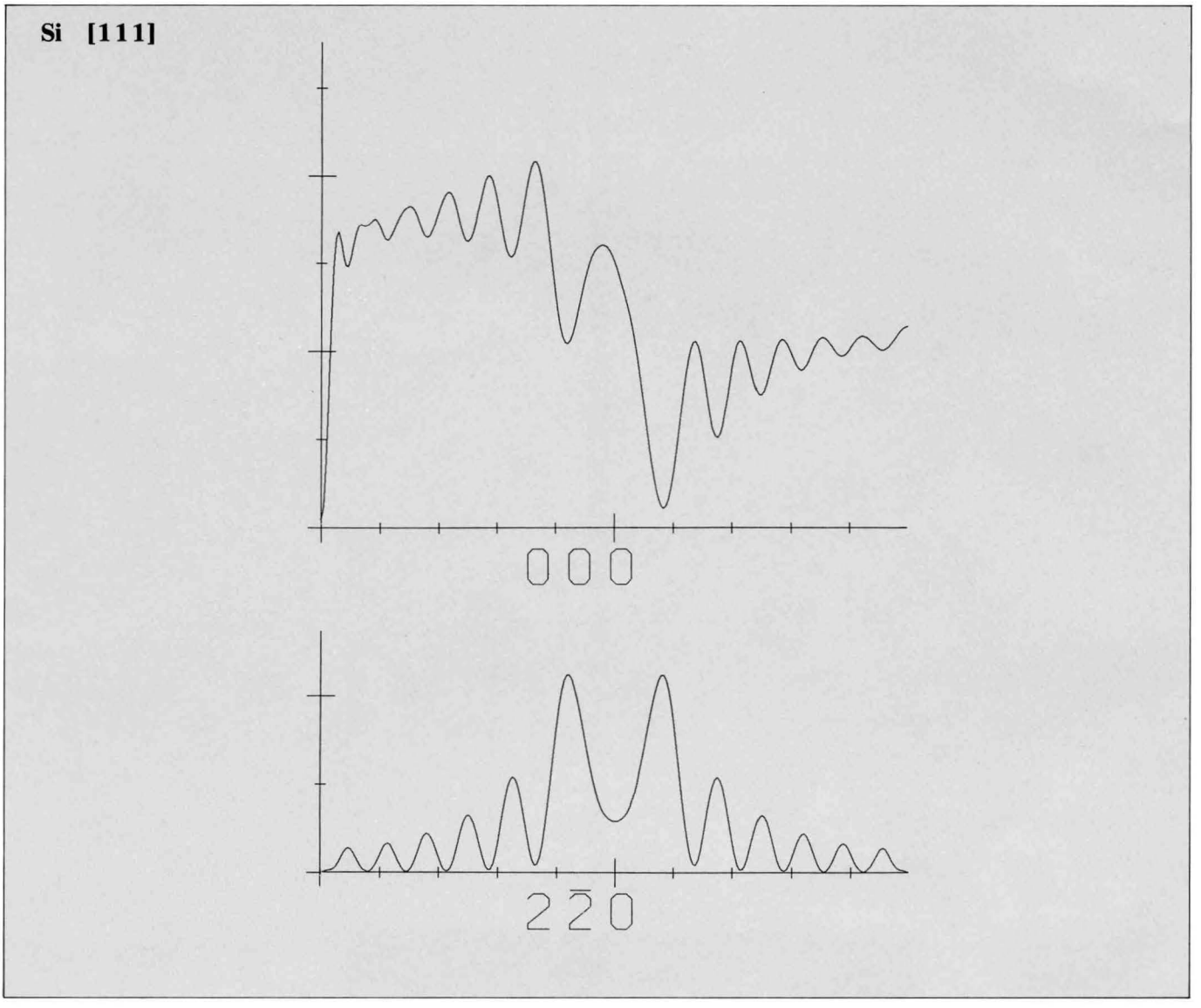

2$\bar{2}$0 excitation
Accelerating voltage: 100kV
$h\bar{h}0$ systematic reflections: 10 beams
Thickness: 156.0 nm
Absorption: $\frac{\xi_g}{\xi'_g} = \frac{1}{20}$

CBED pattern

Si [111], 000 disk

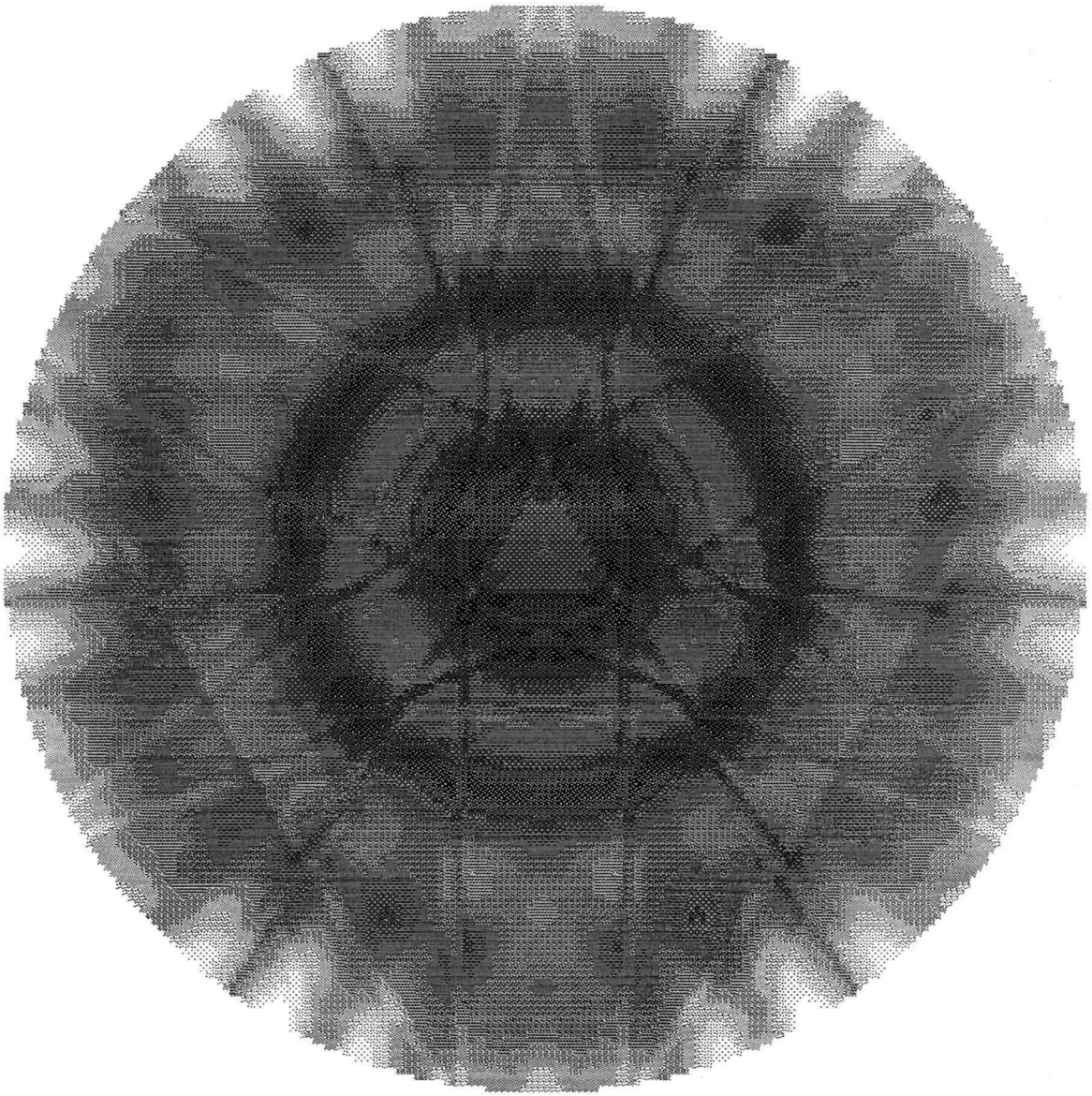

Zone-axis incidence
Accelerating voltage: 100kV
19 ZOLZ and 11 HOLZ beams
Thickness: 156.0 nm
Absorption: $\frac{\xi_g}{\xi'_g} = \frac{1}{20}$

181 * 181 pixcels
type 3 enhancement curve / gamma-coef. = .5

Reciprocal-Space Lines Corresponding to CBED Disks

The larger the reflection index, the longer the reciprocal-space line projected in the corresponding disk. In the disk, the excitation error changes along the direction of the reflection vector (direction h in the present figure) and remains the same along the direction perpendicular to the reflection vector (direction k). Everywhere in the bright-field disk, the excitation error is zero.

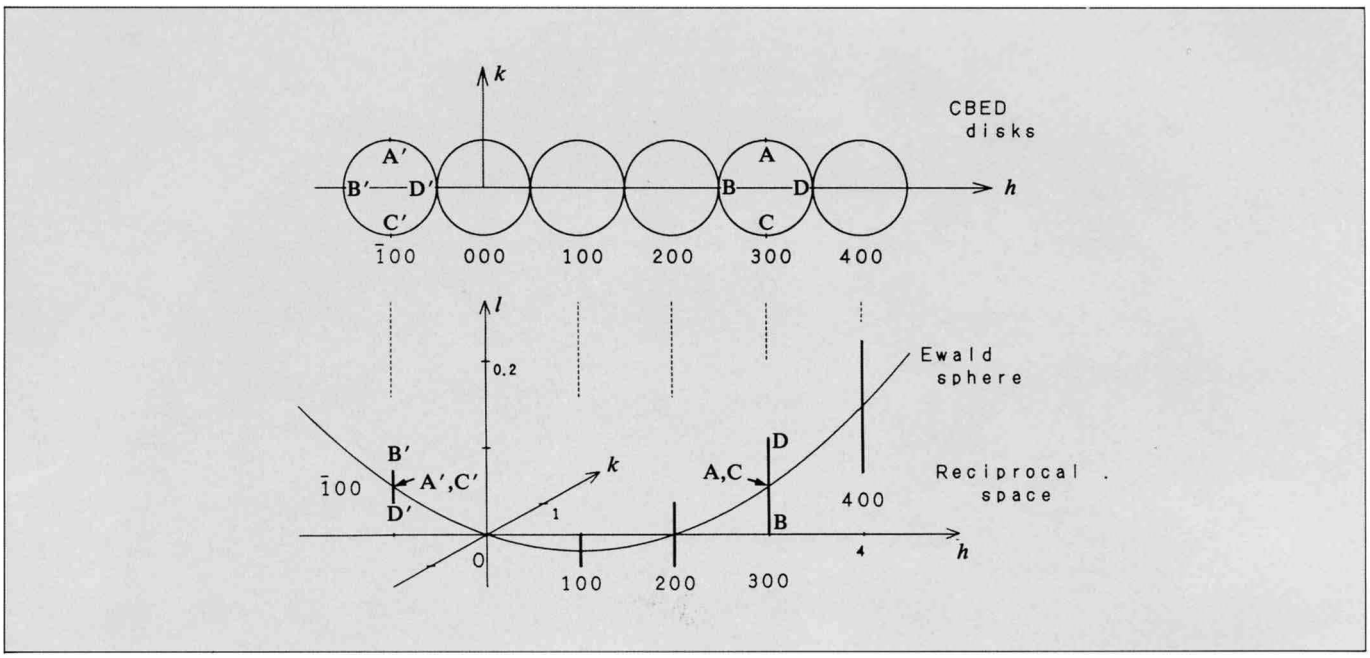

Elimination of Specimen Contamination

Today's electron microscopes are usually equipped with a dry evacuation system and have a clean vacuum of better than 6×10^{-5} Pa. The amount of dirt coming directly from the microscope itself is less important than before, as long as an anticontamination trap for specimens is used.

Specimen contamination occurs due to the surface migration and pile-up of previously stuck hydrocarbons and other types of dirt towards the area illuminated by the electron beam. Thus, preparation of clean specimens is needed above all things. However, we often encounter the need to observe insufficiently clean specimens. Practical elimination of specimen contamination is carried out in the following ways:

1) When the specimen is observed at about 150°C using a specimen heating stage, contamination decreases due to the desorption of stuck molecules.
2) When the specimen is observed at the Liq.N_2 temperature using a specimen cooling stage, contamination also decreases due to the suppression of surface migration of dirt.

However, observation is not always possible at high and low temperatures, since it must often be conducted at varying temperatures.

3) The most practical and convenient technique to eliminate contamination is the use of a beam shower. When an indication of contamination is noticed during observation, strong electron illumination should be given for more than 5 minutes by removing the condenser aperture. Contamination is then definitely reduced.
4) Contamination is more reliably reduced by a technique of heating the specimen up to 150°C for about half an hour on a furnace in a vacuum evaporation device. This is the best way known by us at present.
5) Another possible technique is the slight etching of the surfaces by sputtering light ions of He at a low accelerating voltage of about 500 V for a few minutes, using an ion sputtering device for SEM specimen preparation.

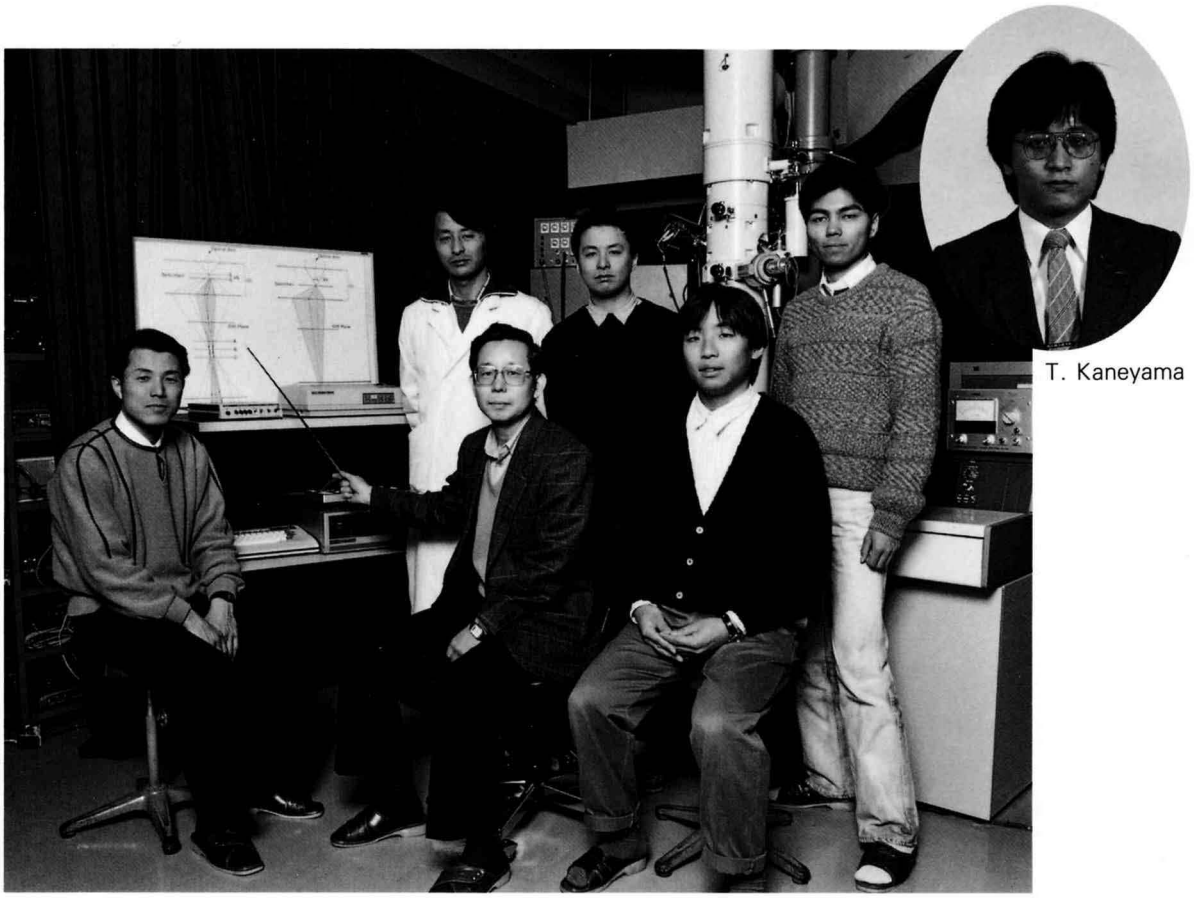

T. Kaneyama

F. Sato M. Terauchi A. Ishikawa S. Ito
M. Tanaka K. Tsuda

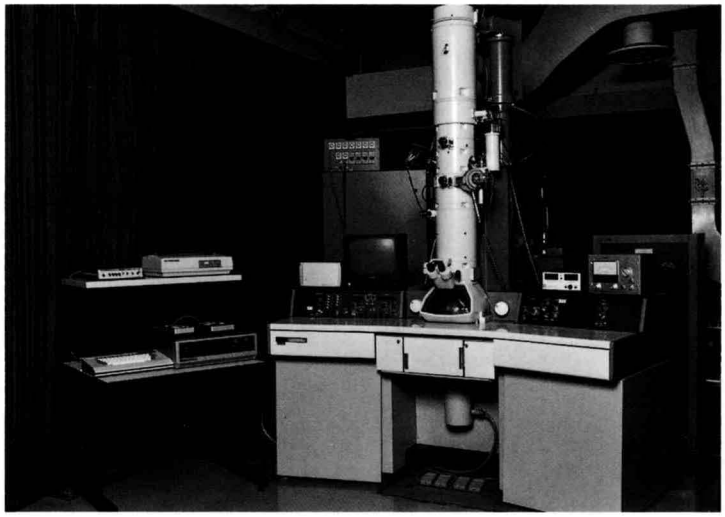

JEM-2000 FX with TV system